

The Effect of Aging on Binder Properties of Porous Asphalt Concrete

E.T. HAGOS

De Invloed van Veroudering op de Eigenschappen van het Bindmiddel in Zeer Open Asfaltbeton

PROEFSCHRIFT

ter verkrijging van de graad van doctor
aan de Technische Universiteit Delft,
op gezag van de Rector Magnificus Prof. dr. ir. J.T. Fokkema
voorzitter van het College voor Promoties,
in het openbaar te verdedigen op
maandag 27 oktober 2008 om 10:00 uur

door

Eyassu Tesfamariam HAGOS

Master of Science in Road and Transportation Engineering,
IHE/TU Delft, The Netherlands

geboren te Axum, Ethiopia

Dit proefschrift is goedgekeurd door de promotor:
Prof. dr. ir. A.A.A. Molenaar

Copromotor
Ir. M.F.C. van de Ven

Samenstelling promotiecommissie:

Rector Magnificus	Technische Universiteit Delft, voorzitter
Prof. dr. ir. A.A.A. Molenaar	Technische Universiteit Delft, promotor
Ir. M.F.C. van de Ven	Technische Universiteit Delft, copromotor
Prof. A.C. Collop, B.Eng., PhD., DSc.	University of Nottingham
Prof. K.J. Jenkins, BSc., MSc., PhD.	University of Stellenbosch
Prof. dr. S.J. Picken	Technische Universiteit Delft
Dr. ir. R. Hofman	Rijkswaterstaat, DVS
Dr. ir. Z. Su	ESHA Group bv, R&D
Prof. ir. A.F. van Tol	Technische Universiteit Delft, reserve lid

Published and distributed by:
Eyassu T. Hagos
Email: eyasu_tesfa@yahoo.com, e.t.hagos@tudelft.nl

Section of Road and Railway Engineering
Faculty of Civil Engineering and Geosciences
Delft University of Technology
P.O. Box 5048
2600 GA, Delft
The Netherlands

ISBN 978-90-8570-331-0

Printing: Wohrmann Print Service, Zutphen (The Netherlands)

© 2008 Eyassu Tesfamariam Hagos.

All rights reserved. No part of this publication may be reproduced, stored in a retrieval system or transmitted in any form or by any means, electronic, mechanical, photocopying, recording, or otherwise without the prior permission of the proprietor.

I dedicate this dissertation to my parents – my late father Tesfamariam Hagos, who has always been curious to see me achieve a milestone in education, and my mother Tafessech Gebremariam, who gave me the inner strength in all my commitments.

Acknowledgements

The research presented in this dissertation was conducted at the Road and Railway Engineering section in the Faculty of Civil Engineering and Geo-Sciences at the Delft University of Technology. The research was funded by the University, the Dr. ir. Cornelis Lely Stichting (CLS) organization and partly by the Road and Hydraulic Engineering Division of Rijkswaterstaat, the Dutch Ministry of Transport, Public Works, and Water Management (formerly DWW – currently Dienst Verkeer en Scheepvaart DVS). In addition, most of the material testing was performed at DVS laboratory. I wish to extend my sincere gratitude to these organizations for their sponsorship and support.

I wish to extend my gratitude for the support offered by organizations and individuals, without their help it would have been practically not possible to realize the outcomes of this research. I express my unreserved and sincere appreciation to Jeroen Besamusca and Johan Villerius from Kuwait Petroleum (Q8) for providing the bitumen samples that I used in the study and for their kind cooperation. I thank Peter Bontrup, the General Manager of Bestone, for supplying aggregates for the research and for his interest in the subject. My appreciation goes to Jan Voskuilen who was instrumental for all the arrangements and coordination to get the materials needed for my research. I would also like to thank him for his unreserved and prompt help for all my technical questions and cooperation requests. I would like to express my gratitude to the organizations that offered me help in sharing their experience and knowledge. I appreciate, in particular, the support from Gerard van Ling from ATLAS materials, W.M. Bos from TNO Den Helder, and Jan Scholten (MSc.) and Jan Korenstra from KRATON Polymers bv.

I am really grateful to DVS (formerly DWW) laboratory staff who were kind enough to offer their support in every way possible. In particular, I appreciate the full support of Ing. Dave van Vliet who was organizing and facilitating my testing programs in addition to fully taking the responsibility to perform the chemical characterization tests, Ljerka Nardelli-Jercic who kindly cooperated to perform part of my rheological tests, and I extend my thanks to Paul Kuijper, J.P.C.M. van der Aa, and everyone whom I enjoyed having a cup of coffee with in the coffee room at DVS for their encouragements and support.

I would also like to appreciate the help offered by the Road and Railway Engineering staff members. My sincere appreciation goes to Ir. Lambert

Houben for his contributions to my work that he offered without any reservations. I express my appreciation to the head of our laboratory Abdol Miradi for his kind cooperation in all matters involving laboratory testing and administrative issues. For their part in helping plan and execute my lab experiments, I would also like to say thank you to our laboratory staff – Marco Poot, Jan Moraal, Robin van Dijk, Jan Willem Bientjes, and Radjan Khedoe. I am very grateful to Milliyon Fekade Woldekidan who took his time to run the ABAQUS finite element program to provide additional information for my project. Additionally, I would like to thank the secretariat of our section Jacqueline Barnhoorn and Sonja van den Bos for their essential contributions to my work.

Finally, I would like to acknowledge the support of friends and colleagues who contributed in various ways to this thesis. I would like to mention here the support from Alemgena Araya Alene and his family, Kibreab Ghebremichael (PhD) and his family, and my relatives in Amsterdam – Belaynesh Tareke, Elsa and Eleni Kidane. I also would like to take this opportunity to thank all colleagues in the section of Road and Railway Engineering for their warm friendship, which I will definitely miss a lot.

Eyassu Tesfamariam Hagos
Delft, September 2008

Summary

The aim of this study was to characterize the effect of binder aging on the performance of Porous Asphalt (PA) pavement layers. Aging is believed to be an important factor in relation to PA durability. To realise the objective two approaches were employed, which are the investigation of laboratory aged binders and binders recovered from field specimens. The laboratory aging methods employed were the standard binder aging method for short and long term bitumen aging and a new aging protocol for the aging of a PA mixture. The short term aging of bitumen was conducted using the Rotating Thin Film Oven Test (RTFOT) and the Rotating Cylinder Aging Test (RCAT) was used for long term aging. A new mixture aging protocol was proposed to simulate field aging of PA in a more realistic way by combining the major environmental factors involved in field aging, which are temperature, UV light, and humidity (moisture). For this a weatherometer was used. Samples from the field were extracted from the emergency lane (EL) and the trafficked lane or slow lane (SL). The field specimens were cored from a road section immediately after construction and from sections with 1, 3, 7, and 12 years service period.

In order to understand the effect of aging, rheological and chemical tests were conducted on the binders recovered from field cores and on binders that were subjected to laboratory aging. Accordingly, various rheological tests including conventional empirical tests such as the penetration and the ring and ball tests were performed. The fundamental tests carried out included complex shear modulus and phase angle determination of the binders at different temperatures ranging from -10°C to 50°C using the Dynamic Shear Rheometer (DSR), fatigue tests at intermediate temperature (20°C) using the DSR, and low temperature tests using the Direct Tension Test (DTT) and Bending Beam Rheometer (BBR).

Before recovering the binder for rheological and chemical characterization, repeated load Indirect Tension Tests (ITT) were performed to determine the resilient modulus of the PA materials coming from road sections of different age. Finally, the viscoelastic properties of the laboratory and field binders/mastics were modelled using Prony series with the intention for use as input in Finite Element Modelling (FEM). A limited number of finite element runs were conducted to determine the stress condition in the binder/mastic in an effort to address the implications of aging on the mixture performance.

The chemical characterization of binders was conducted using two analytical tools: Infrared spectroscopy and Gel-permeation chromatography. The former tool is useful in identifying the development of the functional groups responsible for oxidation during the process of aging. The latter is important to characterise the molecular weight distribution of the binder, which changes due to the aging effect. In addition to the analytical tools, the vanadium content of the laboratory and field binders was determined to bridge the missing information on the binder properties of the field materials. This information was crucial in order to minimize uncertainties in the interpretation of test results arising from differences in the binder's origin or source.

It has been shown that the low temperature properties of the bitumen are significantly influenced by the effect of aging. Using the penetration and softening point data it was possible to show that aging increases the "critical" temperature, this is the temperature at which the binder starts to behave brittle, of the binder significantly even to temperatures above 0°C. Similarly, the DTT results have shown that aging reduces the strain level to failure and that it strongly reduces the stress relaxation behaviour. It also implies that the sensitivity to damage (cracking) of the aged materials has been increased due to aging.

The binder fatigue tests revealed that the accumulation of damage in the field materials is higher than the damage accumulation in unaged bitumen. On the other hand, the laboratory aged binders have shown a better fatigue life than the reference, unaged, bitumen. Care should therefore be taken in making use of information from laboratory aged binder tests to draw conclusions related to PA performance.

Combining the results mentioned above clearly indicates that aging has a pronounced effect on the initiation and propagation of ravelling. Although the traffic induced stresses in the mortar, as calculated by means of the FE model, seem not to be affected by aging, the combined effects of temperature and traffic induced stresses as they occur in winter time, the reduced relaxation and healing capacity as well as the lower fracture resistance because of aging all point to a potential high risk of ravelling due to aging.

The research findings of both the rheological and chemical investigations show that the laboratory aging of the binder does not simulate 7 and 12 years of field aging. The new proposed aging method simulated more years of binder aging in the field than the standard aging method, but it still could not adequately simulate long term field aging of PA. The chemical characterization of the binders has revealed that the rate of aging of the emergency lane binders is lower than the slow (trafficked) lane according to analysis based on the sum of the characteristic peak areas using a kinetic approach. The aging of the upper and lower part of the field materials has not shown significant differences. The new aging protocol seems a promising aging protocol to simulate field aging although it has only predicted less than 3 years of field aging. An amendment to the aging protocol has been suggested to improve aging in the weatherometer.

Samenvatting

Het doel van deze studie was om het effect te bepalen van de veroudering van het bitumineuze bindmiddel op het gedrag van zeer open asfaltbeton (ZOAB). Er wordt over het algemeen aangenomen dat de duurzaamheid van ZOAB sterk afhangt van de mate van veroudering. Ten behoeve van het onderzoek zijn daarom proeven uitgevoerd op in het laboratorium verouderde bindmiddelen en op bindmiddelen die teruggewonnen zijn uit proefstukken welke uit de weg zijn genomen. Voor de veroudering van de bitumineuze bindmiddelen in het laboratorium zijn standaard procedures gebruikt, te weten de "Rotating Thin Film Oven Test" (RTFOT) voor het simuleren van de "korte termijn" veroudering en de "Rotating Cylinder Aging Test" (RCAT) voor simulatie van het "lange termijn" verouderingsgedrag. Ook is een nieuwe verouderingsmethode toegepast op ZOAB mengsels die in het laboratorium zijn vervaardigd. Met deze nieuwe methode werd beoogd het verouderingsproces zoals dat in werkelijkheid optreedt, zo goed mogelijk te simuleren door de ZOAB proefstukken bloot te stellen aan de gecombineerde invloed van temperatuur, UV licht en vocht. Hiervoor is een "weatherometer" gebruikt.

De proefstukken uit de weg komen uit de vluchtstrook en de zwaarst belaste strook van een pas aangelegd wegvak en van 1, 3, 7 en 12 jaar oude wegsecties.

Het effect van veroudering op de eigenschappen van de bitumen uit de in het laboratorium vervaardigde en uit de weg genomen proefstukken is bepaald met behulp van rheologische en chemische proeven. Niet alleen eenvoudige rheologische proeven ter bepaling van de penetratie en het verwekingspunt zijn uitgevoerd, maar ook zijn met behulp van een "dynamic shear rheometer" (DSR) de complexe glijdingsmodulus en de fasehoek tussen belasting en verplaatsing bepaald als functie van de temperatuur (variërend tussen -10°C en 50°C) en de lastfrequentie. Daarnaast zijn met behulp van de DSR vermoeiingsproeven bij 20°C uitgevoerd. Met de Direct Tension Test (DTT) en de Bending Beam Rheometer, zijn rheologische karakteriseringen bij lage temperaturen uitgevoerd.

Het rheologisch gedrag is vervolgens gemodelleerd met Prony series die weer gebruik zijn als invoer voor eindige elementen berekeningen. Een beperkt aantal van deze berekeningen is uitgevoerd om het effect van veroudering te kunnen bepalen op de in een ZOAB mengsel door het verkeer opgewekte spanningen.

Voordat de bitumen van de proefstukken welke uit de weg zijn genomen werd teruggewonnen, is van de proefstukken de stijfheidsmodulus als functie van belastingtijd en temperatuur bepaald. Dit is gedaan met behulp van de indirecte trekproef.

Voor de chemische karakterisering van de bindmiddelen is gebruik gemaakt van "Infrared spectroscopy" (IR) en "Gel-permeation chromatography" (GPC). De IR techniek is gebruikt om de verandering in geaardheid en hoeveelheid van die functionele groepen te bepalen die verantwoordelijk zijn voor de tijdens de veroudering optredende oxidatie. De GPC techniek is gebruikt om de verdeling van de moleculair gewichten te bepalen van de in de bindmiddelen aanwezige componenten. Deze verdeling verandert als gevolg van veroudering. Daarnaast is het vanadium gehalte bepaald van de in het laboratorium verouderde bindmiddelen en de bindmiddelen die zijn teruggewonnen uit kernen uit de weg. Op basis van deze informatie is geconcludeerd dat de tussen de diverse bindmiddelen gevonden verschillen naar alle waarschijnlijkheid niet veroorzaakt werden door een verschil in herkomst van de bindmiddelen.

Het onderzoek heeft aangetoond dat de eigenschappen van de bitumina bij lage temperaturen sterk beïnvloed zijn door de opgetreden veroudering. Met behulp van de penetratie- en verwekingspuntbepalingen kon worden vastgesteld dat de zgn kritische temperatuur, dit is de temperatuur waarbij het bindmiddel zich bros begint te gedragen, tot boven 0°C kan stijgen. Verder hebben de DTT proeven aangetoond dat de rek bij breuk alsook het vermogen tot spanningsrelaxatie sterk afneemt ten gevolge van veroudering. Dit alles geeft aan dat door veroudering de gevoeligheid van de bindmiddelen voor scheurvorming sterk toeneemt. De vermoeiingsproeven toonden aan dat de schade-ontwikkeling bij bitumina die in de weg zijn verouderd groter is dan bij niet verouderde bitumen. Daartegenover staat dat het vermoeiingsgedrag van de bitumina die in het laboratorium zijn verouderd beter is dan dat van niet verouderde bitumen. Dit geeft aan dat men toch wel op moet passen met het trekken van conclusies over de duurzaamheid van ZOAB welke zijn gebaseerd op vermoeiing van in het lab verouderde bitumina.

Alle resultaten overziend kan worden geconcludeerd dat veroudering een duidelijk effect heeft op het ontstaan en de ontwikkeling van rafeling (steenverlies) van ZOAB. Weliswaar nemen de verkeerslastspanningen in het bindmiddel, zoals die bepaald zijn met de eindige elementen berekeningen, niet toe tgv veroudering, maar de temperatuurspanningen welke zich gedurende de winter ontwikkelen wel. De stijfheid is door veroudering immers toegenomen. Verder is door veroudering het relaxatie- en zelfherstellend vermogen afgenomen. Dit alles leidt tot de conclusie dat veroudering van het bindmiddel resulteert in een sterk vergrote kans op rafeling.

De resultaten van het rheologische en chemische onderzoek tonen aan dat de verouderingsprocedures die in het laboratorium zijn gebruikt, niet in staat zijn om de veroudering te simuleren zoals die zich in werkelijkheid 7 - 12 jaar na

aanleg manifesteert. Met de nieuwe verouderingsmethode konden weliswaar meer jaren praktijk veroudering worden gesimuleerd dan met de standaard laboratorium technieken, maar een simulatie van 7 – 12 jaar praktijk veroudering werd niet gerealiseerd. De chemische karakterisering toonde aan dat het bindmiddel dat teruggewonnen is uit kernen genomen uit de vluchtstrook minder verouderd is dan het bindmiddel dat is teruggewonnen uit kernen genomen uit de rechter rijstrook. Verder is gebleken dat er geen significant verschil in veroudering is tussen bindmiddel afkomstig uit de bovenste helft van kernen en dat afkomstig van de onderste helft. Ondanks het feit dat het nieuwe verouderingsprotocol slechts 3 jaar praktijk veroudering simuleert, kan worden geconcludeerd dat het een veelbelovende techniek is zeker als het te volgen protocol wordt aangepast.

Table of Contents

Summary	ix
Table of Contents	xv
1 Introduction	1
1.1 General Introduction	1
1.2 Porous Asphalt Performance Characteristics	3
1.2.1 Functional Aspects of Porous Asphalt	3
1.2.2 Understanding the Ravelling of PA	10
1.3 Research Description	13
1.4 Research Problem, Objectives, and Scope	14
1.4.1 Problem Description	14
1.4.2 Research Objectives	15
1.4.3 Scope of the Research	15
1.5 Organization of the Dissertation	15
1.6 References	16
2 Literature Review on Aging	19
2.1 Ravelling Distress in Porous Asphalt (PA)	19
2.1.1 Binder Age Hardening	19
2.1.2 Effects of Moisture	28
2.1.3 Summary	33
2.2 Simulation of Binder Aging	34
2.2.1 Aging of the Binder	34
2.2.2 Aging of Asphalt Mixtures	44
2.2.3 Summary	49
2.3 Durability and Chemical Composition of Binders	50
2.3.1 Aging effect on Chemical Composition	50
2.3.2 Influence of Mineral Aggregates on Aging	54
2.3.3 Indicators of Compositional Changes	56
2.3.4 Summary	58
2.4 Prediction of Binder Durability	59
2.4.1 Empirical Approach	59

2.4.2	Aging Prediction using the Kinetic Approach	60
2.5	Effect of Binder Film Thickness on Aging	62
2.5.1	Effect of Polymer Modification.....	63
2.5.2	Effect of Filler on Mastic Characteristics	66
2.5.3	Effect of Fibres on Aging.....	70
2.5.4	Summary.....	72
2.6	The Dutch Experience on Porous Asphalt	73
2.7	Summary of the Literature Review	76
2.8	References	78
3	The Research Methodology.....	83
3.1	Introduction	83
3.2	Lessons from Literature Review	84
3.3	The Research Approach	85
3.3.1	The Research Topics	85
3.3.2	The Research Method.....	93
3.4	References	99
4	Materials and Methods.....	101
4.1	Laboratory Binder Aging Test	101
4.1.1	Short Term Aging (STA).....	101
4.1.2	Long Term Aging (LTA).....	102
4.2	Preparation of Porous Asphalt Specimens	102
4.2.1	Specimens for Aging Protocol 1 and 2	102
4.2.2	Specimens for Aging Protocol 3.....	104
4.3	Weatherometer Aging of Porous Asphalt	106
4.3.1	Accelerated Weathering Test.....	106
4.3.2	Background on Weathering Factors.....	108
4.3.3	The Aging of Asphalt Mixtures Produced in the Laboratory	119
4.4	Field Asphalt Core Specimens	123
4.4.1	Field Specimens	124
4.4.2	Bitumen Recovery	127
4.5	Porous Asphalt Mixture Assessment	131
4.5.1	Composition of Asphalt Mixtures.....	131
4.5.2	CT-scan and Thin-film Analysis	134
4.5.3	Thin-Film Sections of Field Materials	141
4.6	Asphalt Mixture Test Results	142
4.6.1	Repeated Load Indirect Tensile Test (RLITT)	142

4.7 Bitumen Rheology Tests	149
4.7.1 Penetration and Softening point.....	150
4.7.2 The Bending Beam Rheometer (BBR).....	150
4.7.3 The Direct Tensile Test (DTT).....	152
4.7.4 Dynamic Shear Rheometer (DSR).....	153
4.7.5 Fatigue Test.....	155
4.8 References	157
5 Effect of aging on Rheological and Mechanical Characteristics.....	159
5.1 Penetration and Softening Point	159
5.2 The Bending Beam Rheometer (BBR)	165
5.2.1 BBR Data Fitting	165
5.2.2 Test Results and Analysis.....	167
5.2.3 Prediction of Relaxation Modulus.....	171
5.2.4 The Effect of Aging on Damage Susceptibility	173
5.3 The Direct Tensile Test (DTT)	175
5.3.1 DTT Test Output	175
5.3.2 Analysis of DTT Test Results.....	176
5.3.3 Effect of aging on Binder Low Temperature Performance	183
5.3.4 Prediction of Time Dependant Modulus from DTT test	185
5.4 Dynamic Shear Rheometer (DSR)	188
5.4.1 DSR Test Principles.....	188
5.4.2 Modeling Bitumen Viscoelasticity.....	191
5.4.3 Characterization of Bitumen Materials	193
5.4.4 Binder Fatigue.....	203
5.5 Modelling of Bituminous Materials	212
5.5.1 Bitumen Viscoelastic Properties.....	212
5.5.2 Modelling of Test Data	217
5.5.3 Finite Element Modelling.....	226
5.6 Findings and Summary	234
5.6.1 In relation to Low Temperature Properties.....	234
5.6.2 In relation to Laboratory/Field Binder Aging Properties.....	236
5.6.3 General Discussion	237
5.7 References	239
6 Chemical Characterization	243
6.1 Vanadium Content	243
6.2 Infrared Spectroscopy	246
6.2.1 Principles of Infrared (IR) Spectroscopy	248

6.2.2	The ATR/FTIR Spectrometry	252
6.2.3	Materials and Testing Method	253
6.2.4	IR Spectrum Quantitative Analysis	254
6.3	Gel-Permeation Chromatography (GPC)	272
6.3.1	The Principles of GPC.....	272
6.3.2	Molecular Weight Distribution (MWD)	273
6.3.3	Sample Preparation and Testing.....	275
6.3.4	Test Data and Interpretation	277
6.4	Relationship between Rheology and Molecular Structure	297
6.5	Summary and Findings	299
6.5.1	In relation to Infrared Spectrometer Test Results.....	299
6.5.2	In relation to Molecular Weight Distribution	300
6.6	Reference	301
1	Conclusions and Recommendations	303
1.1	Main conclusions	303
1.2	Recommendations	305
	Appendix.....	307
	Appendix A:	309
	Results of RLITT for Asphalt Specimens from the Field	309

Abbreviations

AFS	asphaltene formation susceptibility
AI	aging index
AP	aging protocol (e.g. AP3 = aging protocol 3)
AS	asphaltenes
ASTM	American society for testing and materials
ATR-FTIR	attenuated total refraction – Fourier transform infrared
AU	Absorbance unit
BBR	bending beam rheometer
BRRC	Belgian road research centre
BST	black surface temperature
BTDC	bitumen test data chart
CA	carbonyl area (area under the C=O peak)
CAM model	Christensen-Anderson-Marasteanu model
CIE	international commission on illumination
CEN	the European committee for standardization
CROW	the national information and technology platform for infrastructure, traffic, transport, and public space in the Netherlands
CT-scan	computed tomography scan (x-ray tomography)
DAC	dense asphalt concrete
dBA	decibels (a measure of sound)
DER	dissipated energy ratio
DI	ductility index
DIN	the German institute for standardization (Deutsches Institut für Normung e.V.)
DRI	Danish road institute
DSR	dynamic shear rheometer
DTT	direct tensile test
DWW	road and hydraulic engineering institute (Rijkswaterstaat) DVS – a new name for DWW
EL (SH)	emergency lane (shoulder)
EVA	ethylene-vinyl acetate polymer (plastomer)
EVT	equivalent viscous temperature
FEM	finite element modelling
GMM	generalized Maxwell model

GPC	gel-permeation chromatography
GRFT /MGRFT	(modified) German rotating flask test
GVM	generalised Voigt model
HiPAT	high pressure aging test
HMA	hot mix asphalt
HS	hardening susceptibility
HU	Hounsfield units
IC	Gaestel index
IPG	innovatie program geluid (noise innovation program)
IRE	internal reflection element
ISO	international organization for standardization
ITT	indirect tensile test
KNMI	Koninklijk (Royal) Netherlands meteorological inistitute
Lab	Laboratory
LMS/MMS/SMS	large / medium / small molecular sizes
LTA	long term aging
LTOA	long term oven aging (asphalt mixture)
LZ	lower zone
Mastic	bitumen + filler
Mortar	bitumen + sand fractions + filler
MATLAB	a programming language for scientific and engineering computations (MA Trix LAB oratory)
MWD	molecular weight distribution
NEN	Dutch standardization institute (het nationale normalisatie-instituut)
NL	Netherlands
NMR	nuclear magnetic resonance
NRTFOT	nitrogen rolling thin film oven test
PA / PH	peak area / peak height
PA	porous asphalt (In Dutch: ZOAB = zeer open asphalt beton)
PAC	porous asphalt concrete
PAN	polyacrilonitrile fibre
PATTI	pneumatic adhesion tensile testing instrument
PAV	pressure aging vessel
PDA	photodiode array
PDI	polydispersity index – relative spread of molecular weights
Pen	penetration test/value
PMB	polymer modified bitumen
POV	pressure oxidation vessel

Q8	Kuwait petroleum
RAW	Dutch standard specification for the civil engineering sector (RAW Bepalingen)
RCAT	rotating cylinder aging test
RH	humidity
RI	refractive index
Rijkswaterstaat	Ministry of Transport, Public Works and Water Management in the Netherlands (RWS)
RILEM	international union of laboratories and experts in construction materials, systems and structures
RLITT	repeated load indirect tensile test
RMITT	resilient modulus indirect tensile test
RMR	resilient modulus ratio
RTFOT	rolling thin film oven test
SARA	saturates, asphaltenes, resins, aromatics
SBS	styrene-butadiene-styrene polymer (elastomer)
SEC	size exclusion chromatography
SHRP	strategic highway research program
SL	slow lane (trafficked lane)
SLPA	single layer porous asphalt
STA	short term aging
STD	standard deviation
STOA	short term oven aging (asphalt mixture)
Temp	temperature
TFOT	thin film oven test
THF	tetrahydrofuran solvent (C_4H_8O) used in GPC test
TLPA	two layer porous asphalt
TSR	retained tensile strength
TTS	time-temperature superposition
TU Delft	Delft University of technology
UTM	universal testing machine
UV light	ultraviolet light/radiation
UZ	upper zone
VIS light	visible light/spectrum
VMS	Von-Mises stress
WLF model	William-Landel-Ferry model / Arrhenius model /

1 Introduction

1.1 General Introduction

In the Netherlands, Porous Asphalt (PA) surface courses (in Dutch Zeer Open Asphalt Beton or ZOAB) are extensively used as a surfacing layer on motorways. A major reason for this widespread use is that they provide a significant reduction of the noise level produced by car and truck tyres at speeds higher than 50 km/h. They are relatively cheap and effective solutions for the reduction of traffic noise compared to other noise reducing options such as noise barriers. Because of the high population density, people live very close to the main roads in the Netherlands and the need to reduce traffic noise is of paramount importance. In 2007, approximately 70% of the main road network has been surfaced with porous asphalt and the coverage is still increasing. Figure 1.1 shows the use of porous asphalt on main roads in the Netherlands since 1987.

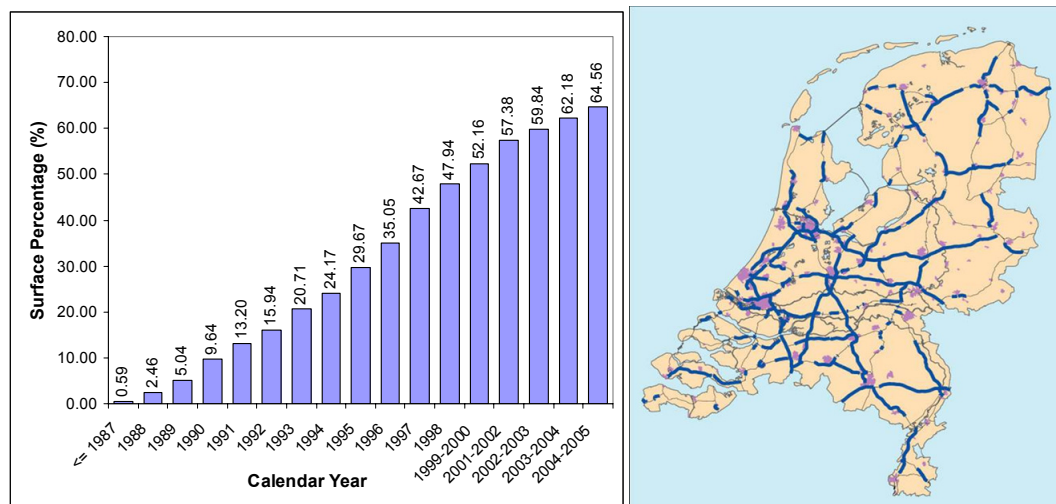


Figure 1.1: Growth of porous asphalt surfaces on the main roads in the Netherlands

Despite the advantage of porous asphalt in reducing noise, there are associated disadvantages due to its high voids content (20-27%). Disadvantages of the open-graded asphalt layer include premature clogging of the voids reducing their potential to absorb noise, higher sensitivity to the damaging effect of traffic and climate, winter maintenance problems, necessity for high quality aggregate because of skid resistance requirements, and higher construction cost compared to dense asphalt concrete. Table 1.1 shows the advantages and disadvantages of the use of PA as a surface course compared to dense asphalt wearing courses.

Table 1.1: Characteristics and Relative Advantages of Porous and Dense Asphalt

	Porous asphalt mixture (single layer PA 0/16)	Continuously-graded dense asphalt mixture
Mean service life	10 - 12 yrs	15 - 20 yrs
Air voids	> 20 %	3 - 5 %
Gradation	Uniform/Open-graded	Continuously-graded
Common defect types	Ravelling/Stripping, Cracking (fatigue/thermal)	Rutting (deformation) Surface Cracking
<u>Advantages:</u>	<ul style="list-style-type: none"> • Reduced traffic noise • Reduced spray and splash from traffic tyres • Prevention of aquaplaning • Safety: <ul style="list-style-type: none"> - improved skid resistance - improved head-light glare - no permanent deformation 	<ul style="list-style-type: none"> • Impermeable – Lower susceptibility to water damage • Higher bearing capacity • Less sensitive to binder aging
<u>Disadvantages:</u>	<ul style="list-style-type: none"> • Higher construction cost • Lower structural contribution • Demand for higher quality aggregate • Premature clogging of voids • Winter maintenance problem 	<ul style="list-style-type: none"> • Do not contribute to noise reduction • Spray and splash, and aquaplaning problems likely • Permanent deformation (rutting) due to heavy traffic loading

With regard to safety, porous asphalt generally provides a good skid resistance because of a relatively dry road surface during wet conditions (Table 1.1). However, this assertion should be critically evaluated, because:

1. After construction, the aggregate surfaces are covered by thin bitumen film causing the so-called 'bitu-planing' when braking suddenly, which implies that the pavement can only acquire a good skid resistance after the binder film wears out which could take 3-6 months for unmodified and up to 18 months for modified binders (Swart 1997).
2. Users tend to consume the "safety factor" (improved skid resistance and better visibility of a porous asphalt pavement) by adopting high speeds and relatively small head tail distances during wet weather conditions.

3. When the pavement starts to ravel, the loose aggregate particles may result in windscreen damage.

1.2 Porous Asphalt Performance Characteristics

This section deals with the functional aspects of Porous Asphalt (PA) and the factors influencing PA performance during production and service period. Moreover, the effect of environmental factors on the aging process and binder properties is discussed.

1.2.1 Functional Aspects of Porous Asphalt

Porous Asphalt Characteristics

Factors such as aggregate characteristics, mix design, construction variables, and the environment play a major role in pavement performance. Asphalt mixtures constructed with the same type of binder quality can, therefore, have large differences in performance and serviceability depending on these factors. The void content in asphalt mixtures, as a design variable, can be cited as one of the factors affecting performance all other variables remaining equal. In Figure 1.2, a Two Layer Porous Asphalt (TLPA) with 0/16 and 0/8 aggregate matrix in the bottom and top layer, respectively, is shown. The TLPA with 0/8 chipping size (thickness 30 mm) as top layer has the advantage of reducing traffic noise to 4-6 dB(A) compared to 2-3 dB(A) reduction by Single Layer Porous Asphalt (SLPA) (thickness 50 mm). Additional advantage of TLPA includes reduced clogging problems of the PA surfacing layer (DWW report 1997).

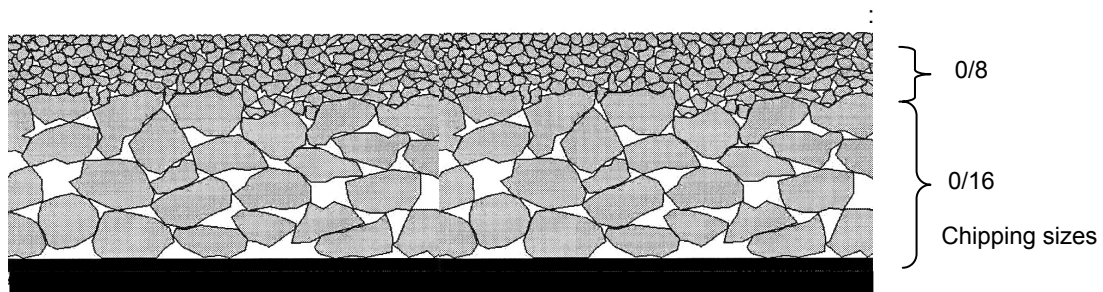


Figure 1.2: Two layer porous asphalt.

The primary cause of excessive aging of the binder in PA is attributed to high permeability, high voids content, and relatively thin binder coating of the aggregate particles (Kandhal and Chakraborty 1996). Dense asphalt mixtures with air voids content of 3 – 5% are considered impermeable compared to PA mixtures with air voids of 20 – 27% (Table 1.2, Figure 1.3, and Figure 1.4). In dense mixtures, the binder film thickness covering the aggregates is thicker; as a result, only the surface of the top layer is influenced by the effect of aging. Choquet (1994) showed that the properties of bitumen recovered from the lower part of dense asphalt pavement were almost unchanged whereas the binder recovered closer to the road surface (within 5mm thickness) showed significant changes with regard to physical properties and generic composition. Other researchers reported similar results. Fonsceca and Witczak (1996) found

that the deeper the point within the dense asphalt mixture, the lower the binder viscosity is at a given temperature and aging period.

In the case of porous asphalt mixtures the effect of aging (binder hardening) was observed over the entire thickness of the pavement layer. This is mainly due to easy entry of oxygen, light and water into the pavement structure causing changes in the properties of the binder (Francken et al (1997)). This can be explained by the fact that the voids in a porous asphalt surface layer are interconnected and the relatively thin binder film thickness (estimated mastic thickness of 0.45 mm, Mo et al. 2007) coating the aggregates. Exposure to environmental factors (air, UV light, water) results in oxidation of the binder throughout the thickness of the PA layer. In addition, the mixture is exposed to easy ingress of water. The major disadvantage of porous asphalt is, therefore, a durability problem (sensitivity of the mixture to traffic and climatic loading) because of high rate of aging of the binding material as a result of environment influences and the damaging effect of water. The durability aspect of PA is further discussed in the next sections of this chapter.

Table 1.2: Typical mixture composition of dense and porous asphalt mixtures

Mixture	Aggregate % by weight			Binder* (%)
	Stone	Sand	Filler	
Dense Asphalt Concrete (DAC)	56	36	8	6
Porous Asphalt (PA - 0/16)	80	16	4	4.5
	Mixture composition % by Volume			
	V_a	V_b	V_v	VMA
DAC	83	13	4	17
PA (0/16)	70	8	22	30
Remark: V_a is volume percentage of aggregates (stones + sand + filler), V_b is volume percentage of bitumen, V_v is volume percentage of voids, and VMA is voids in mineral aggregates ($VMA = V_b + V_v$). *NB: The binder content is expressed as a percentage by mass on 100% aggregates.				

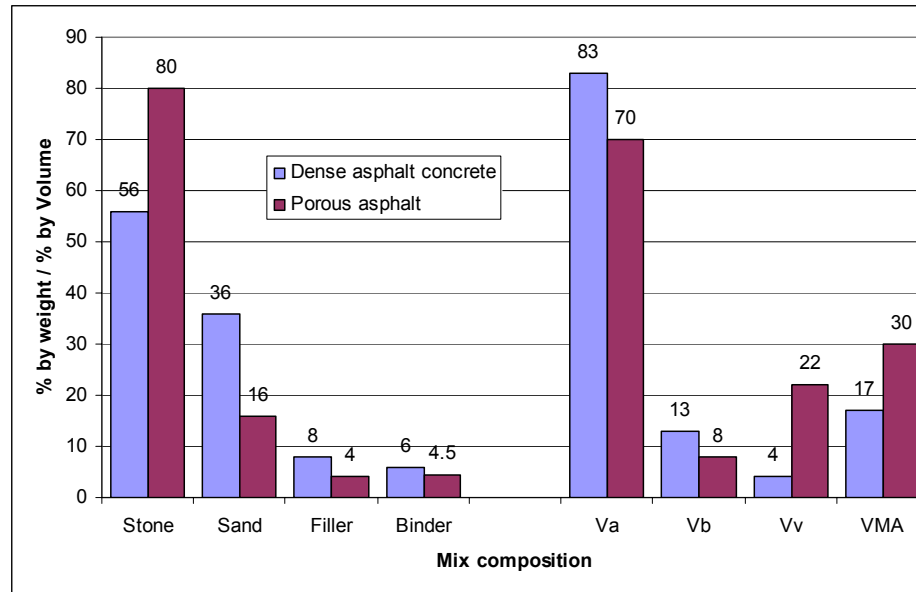


Figure 1.3: Dense Asphalt Concrete (DAC) and Porous Asphalt (PA) mixture composition

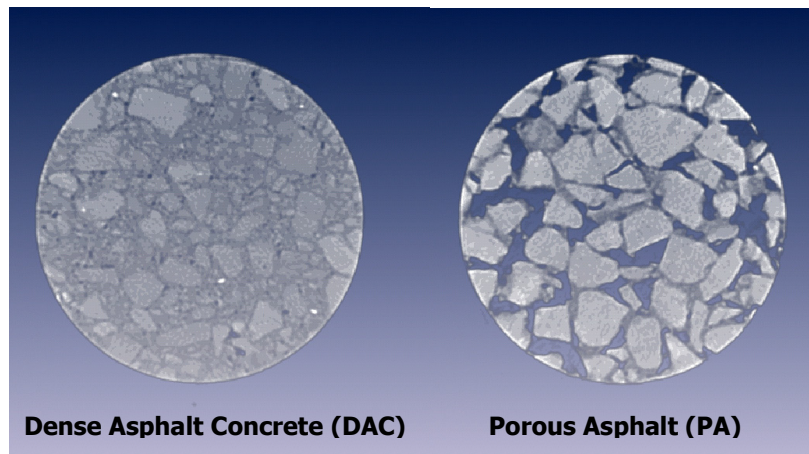


Figure 1.4: Cross-sections of dense asphalt concrete and porous asphalt (X-ray CT scans)

PA Performance

PA is susceptible to ravelling (loss of aggregates from the pavement surface) due to traffic and climatic influences. Ravelling is the dominating damage type observed on PA surfacings because of the high voids content of the mixture (Figure 1.5). In addition to ravelling, surface cracking is also regularly observed. The ravelling of the PA surface decreases the noise reducing potential of the pavement layer and threatens the technical durability of the surface layer (early maintenance is required). Given the fact that the traffic intensity on the Dutch motorways is very high, a PA surface should have a longer service life to reduce interruption of traffic flow because of maintenance operations. In other words, there is a high demand for durable PA surface courses.

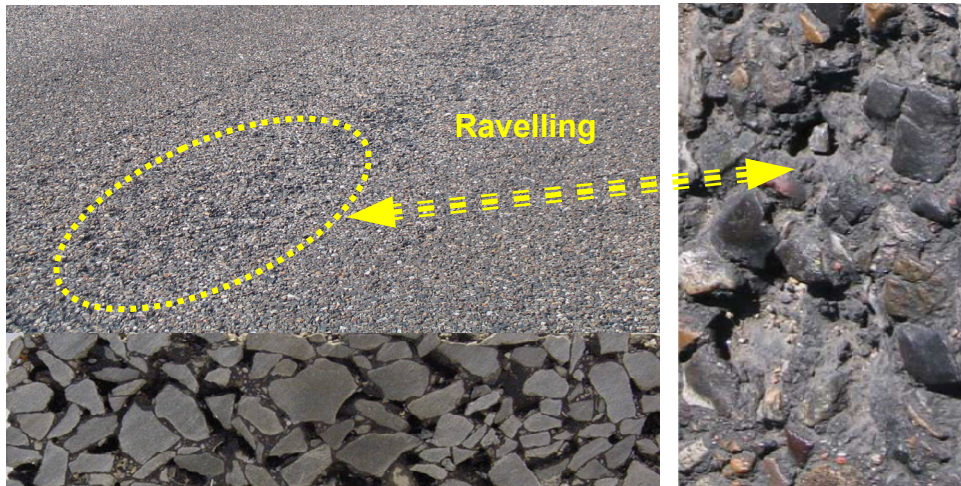


Figure 1.5: Loss of stones (ravelling) of PA surfacing layer

The average service period of porous asphalt in the Netherlands is 10-12 years, which is about 5 years less than the minimum “design” life of dense asphalt. Some good performing PA roads could have up to 16 years of service; on the other hand at curves where traffic imposes high torsion/shear stresses and sections of the road with bad performance because of poor workmanship during construction, as a result of fuel leakage or other related factors, the lifetime of porous asphalt could be sometimes as low as 4 years. The variation in the deterioration level of PA with respect to time is much wider than dense mixtures as illustrated in Figure 1.7. Maintenance intervention is usually performed when the ravelled area of the PA pavement reaches 40%. The emergency lane (road shoulder) also experiences ravelling (although it is not trafficked) because of environmental impacts – temperature variation, oxidation, water damage, and so forth – which subject the pavement to stresses and strains and hence damage, limiting its service life to a maximum of 20 years. Figure 1.6 shows a schematic representation of the service life of porous asphalt with and without the effect of traffic loading; it is an interpretation of data presented in a report by Verra et al. (2003) and Voskuilen et al. (2004) on the conditions of PA in the Netherlands. The figure shows that the effect of aging results in a dramatic change of the bitumen properties (Pen, T_{ring} & ball) in the first few years of the pavement life.

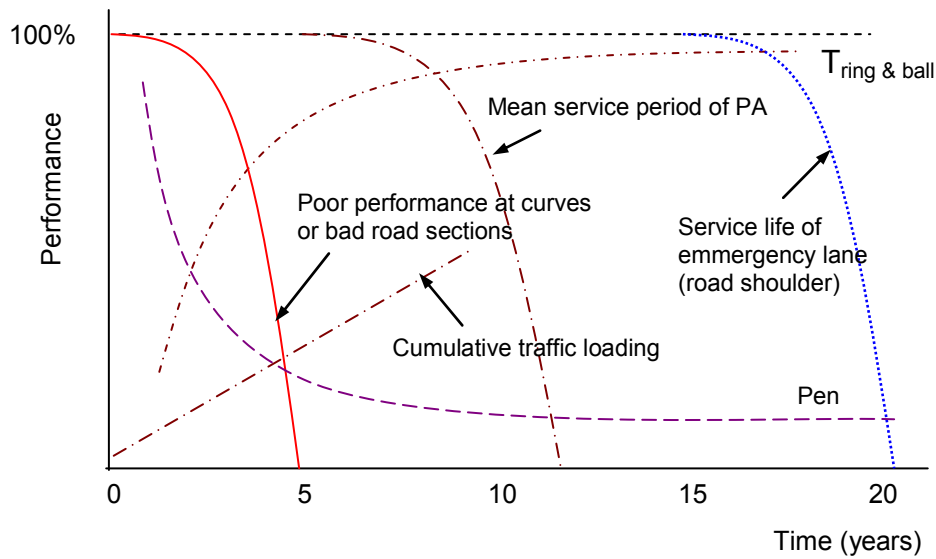


Figure 1.6: Schematic description of the performance of porous asphalt at curves, shoulder, and straight road sections and the change in binder property with time.

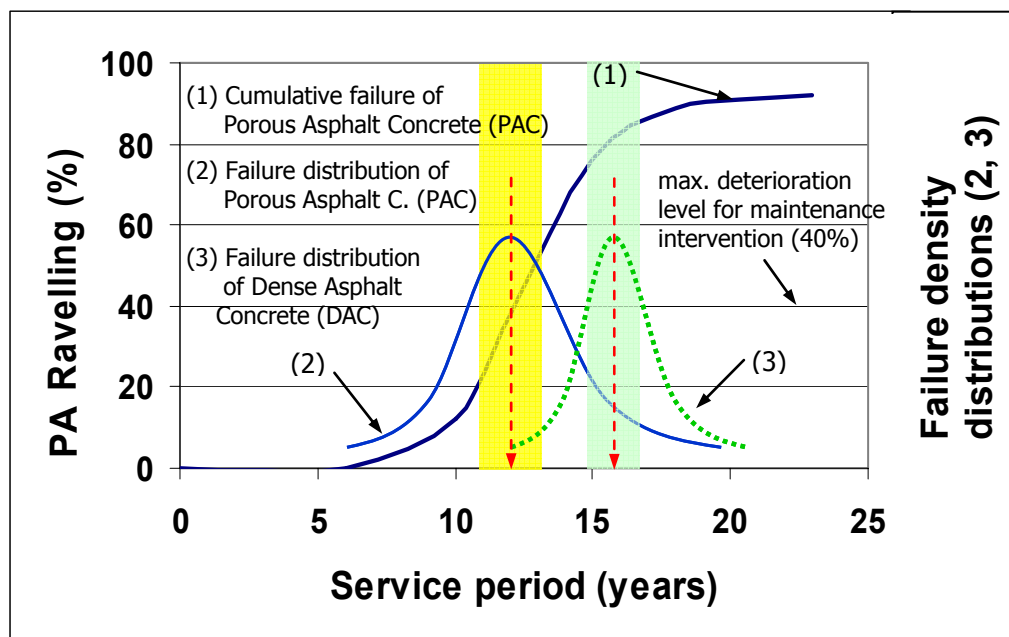


Figure 1.7: Schematic plot of PA performance relative to dense asphalt

From experience, the initiation of ravelling on PA surfacings is on average 4 to 5 years. The deterioration of the pavement is very fast once ravelling is initiated (Figure 1.7). In Figure 1.6, it can be observed that a service life of 4 years corresponds to bad performing pavement sections and/or road sections at curves, and sections without traffic (the emergency lane) could last for 20 yrs.

The service life of PA is determined by the sensitivity to ravelling of the asphalt mixture and the intensity of traffic loading. Considering the ever increasing traffic volume in the Netherlands, it is clear that the durability of open graded

asphalt mixtures needs to be addressed for sustainable and cost effective noise reduction applications of the PA layer.

Effect of Workmanship on PA Performance

In addition to the influence of environmental factors and traffic loadings, the performance of porous asphalt during its service period depends on the workmanship during production and laying. According to Molenaar et al. (2006), premature ravelling of PA is related to the quality of the construction. Variations in the mixture composition during construction contribute to early occurrence of ravelling. Variations in the mixture composition of PA are a result of:

1. variations during the production of the asphalt mixture;
2. segregation of the aggregates and dripping off of the bituminous material during transportation and laying of the mixture.

Molenaar et al. (2006) observed variation in asphalt composition along the cross-section (horizontally along the width of the paving direction), longitudinal direction, and the thickness of newly laid asphalt. These problems arise from poor quality control practices during construction. The factors related to production, construction, and service on the performance of PA are described below:

Construction phase

The following are some examples of poor workmanship during production of the asphalt mixture contributing to reduced performance of PA pavements:

a. Production

- The first problem arises if the binder is over or under heated during the production of the asphalt mixture. Excessive amount of volatile components of the binder will be lost during this phase especially if the mixing temperature is high which would have subsequent effect on the performance of the asphalt mixture. Mixing at very high temperature during the production of the asphalt mixture greatly degrades the binder, particularly if it contains polymers, causing durability problems when the pavement is open to traffic. On the other hand, an asphalt mixture produced below the proper mixing temperature can have a reduced quality as a result of inadequate coating of the aggregates by bitumen and can result in compaction difficulty contributing to poor performance of the pavement.
- Another reason for poor performance might be the effect of agglomeration of the filler during mixing or production. If the limited amount of filler in porous asphalt is not sufficiently dispersed in the binder during production, it is likely to cause failure in the pavement because of loss of stiffening potential of the filler that contributes to the resistance to ravelling of PA.

- The use of dusty aggregates and an excessive quantity of “own” filler in the mixture can contribute to poor PA performance.

b. Transportation

- Drainage of the bituminous mortar due to gravitational forces might occur during the transportation of the asphalt mixture from the asphalt production plant to the job site and during the early years (first 1-2 years) in service. This happens especially if the bitumen content in the mixture is too high. Thus, the use of appropriate binder grade, drainage inhibitors such as fibres, and appropriate concentration of filler in bitumen will contribute to reduce the problem.

c. Laying

- Segregation can be a major problem during the laying process of porous asphalt. Segregation can occur when the truck is emptied in the hopper and when the mixture is spread by the auger (Molenaar et al. 2006).
- A sharp decline in temperature of the asphalt mixture during construction is a significant factor to consider because it may critically affect the compaction of the asphalt mixture and thus the performance of the pavement. Segregation and compaction problems occur if the continuity of the supply of asphalt mixture to the construction site is not regular causing the paving operation to proceed at variable pace or temporarily stop to wait for material supply; the effect is a sharp drop in the temperature of the mixture resulting in compaction problems and unevenness in the road surface and texture. Compaction has a significant effect on the performance of PA (Molenaar et al. 2006).
- Crushing of aggregates should be avoided during the compaction stage to produce a good quality PA pavement. Aggregate crushing is likely in PA since high stresses are concentrated at the point to point contact of the stone matrix.

Service Period

Because of hardening of the binder, porous asphalt is especially susceptible to ravelling. Two types of ravelling can be distinguished (Molenaar and Molenaar 2002):

1. Short-term ravelling, caused in the first 3 years of the pavement's service life,
2. Long-term ravelling, occurring in an average service life of 10-12 years.

Long-term ravelling is believed to be explained by a combination of the following:

- a. Slow gravity segregation of the mastic in the asphalt layer, driven by the yearly temperature cycle, reduces the content of mastic in the upper part of the asphalt layer.

- b. The effect of rain water entering the bitumen/aggregate interface, causing gradual stripping and loss of the interface strength (adhesion),
- c. Aging of the binder, limiting the self-healing potential of the bitumen/aggregate interface.

The noise reduction potential of porous asphalt is affected to a great extent by the loss of aggregates (ravelling) from the pavement surface.

1.2.2 Understanding the Ravelling of PA

The sensitivity to ravelling of PA is already known for a long time and has been subject to investigation. From a qualitative point of view, the reasons and causes of the ravelling failure are clear, quantification of the factors involved however seems to be a complex task and no clear cut solutions to solve or control the ravelling problem are available yet. However, it is apparent that the adhesive and cohesive characteristics of the porous surface courses are of prime importance in relation to PA performance.

With adhesive characteristics those characteristics are meant which are responsible for the adhesion between aggregates and the bituminous mortar. With cohesive characteristics those characteristics are meant which are responsible for the cohesion in the bituminous mortar (filler + fine sand fraction + bitumen). Because of the very open nature of porous surface courses (>20% voids most of which are interconnected), the cohesive and adhesive characteristics of these mixtures are strongly influenced by the effects of water and aging (hardening of the bituminous mortar due to the effects of oxygen, UV radiation, temperature, etc.).

Studying the PA mixture at macro level does not provide sufficient insight into the underlying problems. Hence, studies at mezzo and micro level are necessary to understand the damage mechanisms and to develop solutions that will enhance the ravelling resistance of porous asphalt mixtures (refer to Figure 3.2 in section 3.3). Research on the adhesive and cohesive characteristics of asphalt mixtures is a complex task because of the large number of variables involved and because the underlying processes are complex. Research on this topic should combine the expertise of civil and chemical engineers as well as engineers in physics and material science. It was therefore decided to split the research into two parts. Part one should focus on the cohesive aspects while part two should deal with adhesive aspects. This project is dealing with the cohesive characteristics, and is mainly associated to age hardening of the binder.

Table 1.3 shows dominant factors influencing the adhesion and cohesion of the bituminous mortar.

Table 1.3: Factors influencing the cohesion and adhesion bond in PA

Factors	Dominant effect
Weather Conditions: <ul style="list-style-type: none"> - Temperature - UV light - Moisture 	Age hardening – cohesion Degradation – cohesion Stripping – adhesion
Effect of additives: <ul style="list-style-type: none"> - Polymer modified bitumen - Fibres 	Increase binder film thickness, Improved aging behaviour – cohesion Reduces drainage of mastic – improves cohesion
Bitumen source and content: <ul style="list-style-type: none"> - Bitumen content - Type and source of bitumen 	Film thickness – cohesion – adhesion Rate of aging – cohesion
Effect of filler: <ul style="list-style-type: none"> - Filler type and concentration 	Aging/drainage/strength – cohesion (addition of hydrated lime improves bonding and delays aging – adhesion and cohesion)
Effect of aggregate type: <ul style="list-style-type: none"> - Aggregate type 	Compatibility with binder – adhesion Mineral composition, specific surface → bonding
Additional factors: <ul style="list-style-type: none"> - Winter maintenance - Addition of salt - Traffic: leakage of oil, fuel, etc... 	
<i>Remark:</i> <i>Moisture is believed to contribute to the change in properties of the bituminous mortar because of the possibility of diffusion of water molecules into the binder.</i>	

Mechanisms of ravelling failure in PA

The mechanism of ravelling failure in PA is understood as damage caused by high levels of stress and/or strain in the system due to traffic and environmental actions. Figure 1.8 shows the stress levels in the bituminous mortar of a PA mixture before and after the application of traffic load. Stress levels are very high at the aggregate contact points as a result of the wheel loading. The bituminous mortar binding the PA stone matrix is believed to be subjected to tensile, compressive and/or shear forces, which are absorbed by the binding material (mortar) depending on its ability to resist or relax stress. In the process of stress development, the material is subject to damage which is accumulated till the occurrence of ravelling. The horizontal tensile stress in the

upper few millimeters of the PA layer is estimated to reach a maximum value of 3 MPa (Tolman and van Gorkum 1997), which is in agreement with recent modelling work of PA at TU Delft (Woldekidan 2006, Huurman et al. 2007). The ability of the material to resist stress or fatigue (i.e. damage under repeated loading) depends on the performance of the bitumen/mortar. Thus, the resistance to damage development and healing capacity can be regarded as important performance indicators of the binder especially at low temperatures where the expected damage is usually high. Damage is mainly manifested in terms of (micro) crack development in the binding material. Once ravelling is initiated, the rate of ravelling increases at a much higher speed for two main reasons:

1. There will be lack of side support for stones in the neighbourhood;
2. Stresses will be transferred to the remaining contact points causing progressive loss of stones from the surface.

The effect of aging results in hardening of the bitumen which alters the creep and relaxation behaviour of the binder and its failure properties.

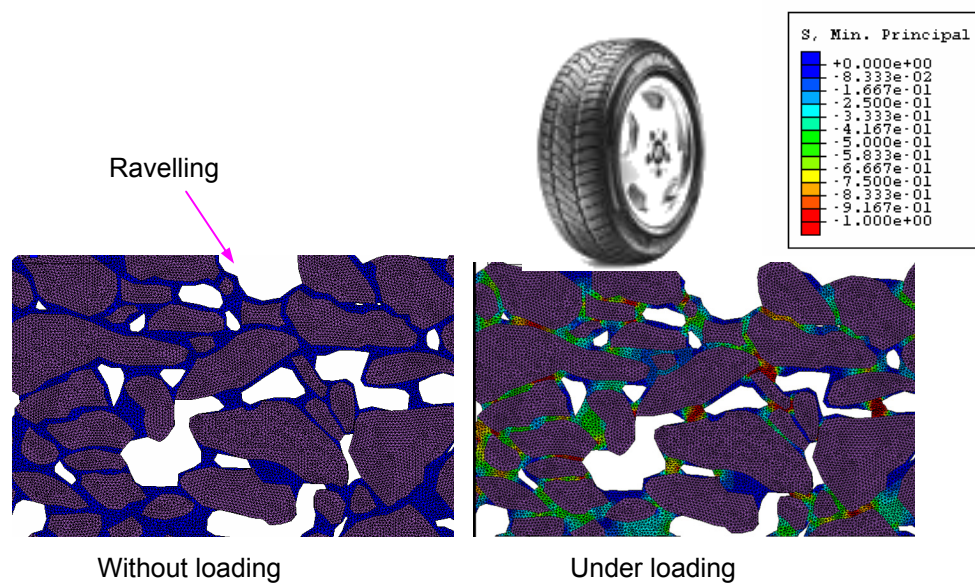


Figure 1.8: The effect of loading on a PA structure (Huurman et al. 2007)

PA performance is also influenced by the effect of freeze and thaw actions during the winter period. Freeze and thaw effects occur during low temperature periods when the ability of the binding material to sustain large strains is hindered and its healing potential is low. The ravelling of PA on the emergency lanes (road shoulders without traffic) may explain the contribution of climatic actions (thermal effect due to rise and drop in temperature and freeze and thaw actions) to damage development in the mixture. It is assumed that the effect of freeze and thaw is indirectly taken into account by studying recovered bitumen samples from field specimens.

The effect of binder aging can be summarized as follows:

- In PA mixtures, the bituminous mortar is subjected to:
 - shear,
 - tension, and/or
 - compression.

⇒ This implies that the strength and relaxation behaviour of the binder are important.
- Effect of aging:
 - Increases the stiffness of the binder
 - Increase in storage modulus (increment in strength)
 - Decrease in loss modulus (reduced viscous flow)

This implies a change in

- creep and relaxation properties
- failure behaviour (energy to failure)
- fatigue life & healing potential

Low temperature:

- Failure at low strains (susceptibility to fracture due to brittleness).
- Rate of energy dissipation.

Intermediate Temperature:

- Fatigue: energy loss per load cycle, i.e. rate of damage development.
- Decrease in healing potential.

Thus, low temperature characterization and fatigue performance of the binder are core subjects in the assessment of the effect of aging in relation to cohesive failure of the mortar/mastic in PA.

1.3 Research Description

As mentioned before, porous asphalt surface layers are sensitive to the damaging action of climate and traffic. The main reason for maintenance is ravelling (the loss of aggregates from the surface) and to some extent surface cracking. 70% of the yearly maintenance costs of PA surface courses are related to ravelling and approximately 80 million Euros per year is needed to repair damage due to ravelling. There is a high demand to reduce the maintenance needs of PA not only to reduce the maintenance costs but also to minimize disruption to traffic flow. In this regard, much attention has been given to address durability problem of porous asphalt in order to achieve longer pavement life.

Ravelling is a failure type that develops because of the fact that the induced stresses are higher than the strength of the material, which is related either to the cohesive strength of the mortar (binder), the adhesive bond between the mortar and the aggregates or a combination of both. The durability of the

pavement surface depends on the magnitude of these bond strengths, the degree to which they are influenced by moisture and aging, the mixture composition, and last but not least the degree of compaction and the magnitude of stress imposed on the pavement (Molenaar 2000). Because of the high rate of aging of the bitumen in porous asphalt pavement layers, loss of cohesive and/or adhesive bonds occur, resulting in ravelling.

The purpose of this research is to investigate the effects of aging on the physical (both rheological and mechanical properties) and chemical properties of bitumen. It is believed that the understanding of the aging process and the change in the fundamental bitumen properties will contribute to the understanding and improvement of the resistance to ravelling of porous asphalt.

1.4 Research Problem, Objectives, and Scope

1.4.1 Problem Description

The lower service life of a PA layer due to ravelling (the loss of aggregates from the surface layer) is, as stated before, a major concern. Aging of the binder (bituminous mortar) is believed to be a major contributor to poor performance of PA. The focus of the aging study as performed in this research project is on the effect of weathering actions on the cohesive failure of the binding material (Figure 1.9). The cohesive strength of PA is influenced by the aging of the bituminous mortar, which results in hardening of the binding material due to climatic factors, i.e. interaction with the environment (oxidation) which is a complex process involving the effects of temperature, exposure to UV radiation, and water/rain. Aging results in hardening of the binder resulting in brittle behaviour of the material at low temperatures.

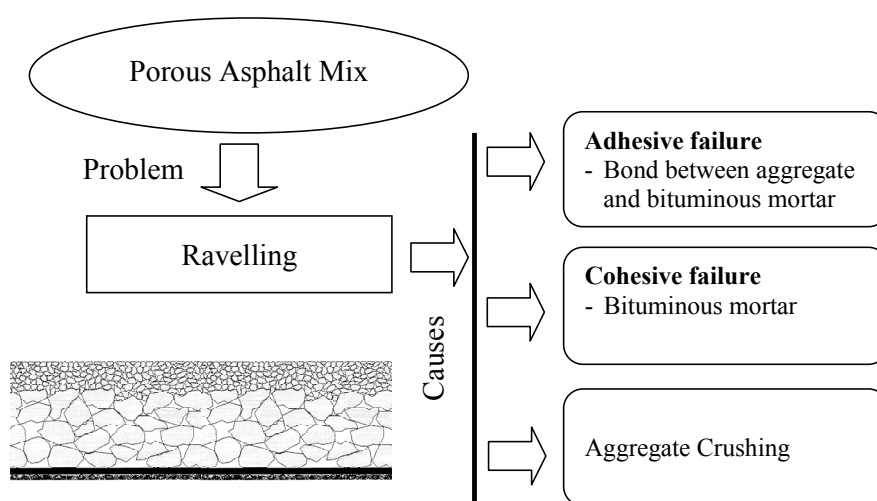


Figure 1.9: Factors contributing to ravelling failure in PA pavement layer

1.4.2 Research Objectives

The aim of this study is to understand the effect of environmental influences on the aging of the binder (bituminous mortar) and its effect on the ravelling of PA. The study focuses on binder aging which is considered as the main reason for durability concerns of PA. The main objective of the study is to understand the effect of binder age hardening on the performance of the binder. The theme of this study is limited to the effect of aging on the cohesive binder properties and the implications to PA performance. The intention of the aging project is mainly the understanding of the effects of the aging processes on the rheological and chemical properties of the binder and the implications to ravelling of a PA mixture.

The goals of the aging research can be summarized as follows:

- Understanding the aging of the binder and its effect on cohesive properties of PA concrete.
- Material modelling of the behaviour of bitumen / bituminous mortar for use as input in Finite Element modelling of PA concrete.

1.4.3 Scope of the Research

The scope of this project is to investigate the effects of aging of PA on the physical and chemical properties of the binder and the implications to ravelling of PA surface courses. The research concentrates on the characterization of the binding material in relation to the effects of environmental factors influencing the age hardening of the bitumen. To understand the effect of aging on mixture resilient modulus, tests are to be performed on asphalt mixtures. Moreover, the research intends to provide binder properties as input parameters in the modelling of the mixture performance using FEM (Finite Element Method). The modelling of the asphalt mixture at mezzo level (i.e. inhomogeneous material modelling, in which the aggregates, voids and mortar are modelled separately) is not part of this research. To sum up, the effects of aging on the initiation and progression of ravelling due to traffic and environmental influences are to be analyzed and understood in this research.

1.5 Organization of the Dissertation

This report consists of 7 chapters structured in such a way that a detailed clarification of the research based on the outlined methodology. In chapter 1, a general introduction is presented with the description of PA characteristics and performance, main objectives and the scope of the study. Chapter 2 presents a literature review on aging of bitumen. This chapter is a state of the art report on the aging and the effects of aging on the physical and chemical properties of bitumen. In chapter 3, the research methodology is presented based on the objective of the study and the literature review. In Chapter 4, the materials and testing methods are described. The effect of aging on rheological and mechanical performance of bitumen is discussed in chapter 5. This chapter also includes the modelling of the viscoelastic properties of mastic including limited

simulations of traffic loading on PA using Finite Element Modelling (FEM). The chemical characterization of binders is presented in chapter 6. The last chapter, chapter 7, provides conclusions and recommendations based on analyses and discussions of the results of the study.

1.6 References

Choquet, F. S., and Verhasselt, A. F. (1994). "Aging of bitumens: From the road to the laboratory and vice versa." *Strategic Highway Research Program (SHRP) and Traffic Safety on Two Continents*. Swedish Road and Transport Research Institute, pp. 194-213.

DWW (1997). "De "European Conference on Asphalt"." *Rep. No. W-DWW-97-058*, Ministrie van Verkeer en Waterstaat, Rijkswaterstaat, Dienst Weg- en Waterbouwkunde (RWS, DWW), Delft, The Netherlands.

Fonsceca, O. A., and Witczak, M. W. (1996). "A Prediction Methodology for the Dynamic Modulus of In-Place Aged Asphalt Mixtures." *Association of Asphalt Paving Technologists (AAPT)*, 65.

Francken, L., Vanelstraete, A., and Verhasselt, A. (1997). "Long term aging of pure and modified bitumen: Influence on the rheological properties and relation with the mechanical performance of asphalt mixtures." 1259-1278.

Hofman, R., Wieringen, J. B. M., and Visser, J. C. (2005). "Noise Innovation Program IPG: Two-Layer Porous Asphalt for use on the Dutch Main." *Inter-Noise Congress and Exposition on Noise Control Engineering*. Rio de Janiro, Brazil.

Huurman, R. M., Mo, L. T., Woldekidan, M. F., and Medani, T. O. (2007). "Advanced pavement analysis technique." *9th Conference on Asphalt Pavements for Southern Africa*.

IPG (2002). "Noise Innovation Program, Road Traffic (The IPG Program)." *Rep. No. DWW 2002-073*, Rijkswaterstaat, Road and Hydraulic Engineering Institute (DWW). The Netherlands.

Kandhal, P. S., and Chakraborty, S. (1996). "Effect of Asphalt Film Thickness on Short and Long-Term Aging of Asphalt Paving Mixtures." *Transportation Research Record*, (No. 1535), 83.

Mo, L. T., Huurman, R. M., Wu, S. P., and Molenaar, A. A. A. (2007). "Investigation into stress states in porous asphalt concrete on the basis of FE-modelling." *Finite element in analysis and design*, 43(4), 333-343.

Molenaar, A. A. A. (2000). "Pavement Design II: Structural Design of Flexible Pavements." *Rep. No. Lecture Notes TRE 070/98/1*, Delft University of Technology, Delft.

Molenaar, A. A. A., Meekerkerk, A. J. J., Miradi, A., and van der Steen, T. (2006). "Performance of Porous Asphalt." *Association of Asphalt Paving Technologists (AAPT)*, Vol. 75 (CD).

Molenaar, J. L. M., and Molenaar, A. A. A. (2002). "An Investigation into the Contribution of Bituminous Binder to the Resistance to Raveling of Porous Asphalt." *Euroasphalt and Eurobitumen Congress*, Barcelona.

Swart, J. H. (1997). "Experience with porous asphalt in the Netherlands." *European conference on porous asphalt*. Madrid.

Tolman, F., and van Gorkum, F. (1997). "A model for the mechanical durability of porous asphalt." *European conference on porous asphalt*. Madrid.

Verra, N., Bol, M. v. d., and Gaarkeuken, B. (2003). "De levensduur van ZOAB." *Rep. No. DWW-2003-066*, Road and Hydraulic Engineering Institute (DWW).

Voskuilen, J. L. M., Tolman, F., and Rutten, E. (2004). "Do modified porous asphalt mixtures have a longer service life?". *Euroasphalt and Eurobitumen Congress*, Vienna.

Woldekidan, M. F. (2006). "Performance study of C-Fix in PAC using a 2D Finite Element Model.", *MSc thesis*. Technical University of Technology (TU Delft).

2 Literature Review on Aging

In this chapter the results of a literature survey into the aging of bituminous binders and mixtures is presented. As mentioned in the Introduction, aging is known to change the characteristics of bituminous materials such as stiffness, strength, fracture, toughness, and relaxation. Although this research is focussed on the cohesive properties of binders, mastics, and mortars, some attention is also placed on the adhesive characteristics of the aggregate-binder system. This is done because in practice cohesive and adhesive failure are closely related and it is quite often not easy to differentiate whether aggregate loss (ravelling) is due to one of them or a combination.

2.1 Ravelling Distress in Porous Asphalt (PA)

Ravelling of PA surface layers occurs due to various factors. During the construction phase, factors related to the quality or work (i.e. workmanship, weather conditions, etc.) have significant influence on the subsequent performance of the pavement. Those factors include the influence of temperature during mixing and laying of the asphalt mixture and lack of compaction. In addition, factors related to the mixture composition such as insufficient or excessive bitumen content and/or amount of fines contribute to poor performance. Because of high voids content, PA mixtures are sensitive to ravelling due to accelerated rate of “age hardening” of the bituminous mortar.

2.1.1 Binder Age Hardening

The Effect of Aging

The effect of asphalt mixture aging can be classified in two major groups: short- and long-term aging (Roberts et al. 1996).

Short Term Aging (STA): STA involves the loss of volatiles and oxidation of the bitumen during the construction phase. The first significant hardening of the binder takes place in the mixing facility during hot mix asphalt production where heated aggregate and binder is mixed. Two processes take place, oxidation and loss of volatile components. Age

hardening of the binder continues, although at a much slower rate, while the hot asphalt mixture is processed through a storage silo, transported to a paving site, laid and compacted.

Long Term Aging (LTA): LTA refers to the oxidation of the bitumen during the service life of the asphalt mixture. Age hardening continues at a slower rate for the first 2-3 years. Thereafter, the rate of hardening further decreases and longer time periods are required to discern the changes in rheological properties of the binder during its service period.

The following factors have been reported to contribute to age hardening of the binder during mixing and/or in service (Roberts et al. 1996):

- a. Oxidation: Oxidation is the reaction of oxygen with the binder, the rate depending on the character of the bitumen (source) and the temperature.
- b. Volatilisation: Volatilisation is the evaporation of the light fractions from binders and is primarily a function of temperature. It is usually not a significant factor contributing to long term aging in the pavement.
- c. Polymerisation: Polymerisation is a combination of like molecules to form larger molecules, resulting in a progressive hardening. At low temperatures the rate of association is considered slow as a result of higher viscosity of the binder (Peterson 2000).
- d. Thixotropy: Thixotropy (Steric Hardening) is a progressive hardening due to the formation of a structure within the binder over a period of time, which can be destroyed to a degree by reheating and working the material.
- e. Synersis: Synersis is an oxidation reaction in which the thin oily liquids are excluded to the surface of the binder film. With the elimination of these oily constituents, the binder becomes harder.
- f. Separation: Separation (exudation) is the removal of the oily constituents, resins, or asphaltenes from the bitumen caused by absorption into some porous aggregates.

Significant aging takes place during short term aging where the binder is subject to high temperature during production of the asphalt mixture. During the short term aging of the bitumen, both oxidation and volatilization processes take place. The hardening of the binder during the service period of the pavement (long term aging) is mainly due to oxidation. The long term aging process of an asphalt pavement depends on the prevailing environmental conditions and the type and origin of the binder. The aging process is influenced by the type of asphalt mixture; for example, a higher rate of aging is expected in a porous asphalt mixture compared to dense asphalt. In a study conducted by Choquet¹ (1991) the effect of aging over the entire thickness of a porous asphalt pavement layer was observed, indicating the severity of aging in highly porous mixtures. The reason is attributed to the high amount of voids in porous asphalt that allows access to oxygen and water, resulting in changes

¹ Source: Franken et al. 1997.

in the binder property over the whole thickness within relatively shorter period of time. As a result, substantial rheological changes take place such as a decrease in penetration, an increase in 'softening point', and an increase in viscosity of the binder due to age hardening. According to Franken et al. (1997) practical experimental studies on a number of porous asphalt sites indicate that the original 70/100 bitumen displayed penetration of less than 25 dmm and a softening point (ring and ball temperature) higher than 60°C after 3 years of service, which could contribute to brittle behaviour of the binder and sensitivity to ravelling.

Figure 2.1 shows a general trend of the effect of aging during production (short term) and service period (long term) on the viscosity ratio (ratio of the aged to un-aged binder viscosity). The change in viscosity ratio shown in Figure 2.1 is typical for aging of dense asphalt mixtures. Figure 2.2 shows the effects of temperature and exposure time to aging on the viscosity ratio and penetration of a bitumen sample aged using the Thin Film Oven Test (TFOT) method (Ishai 1996).

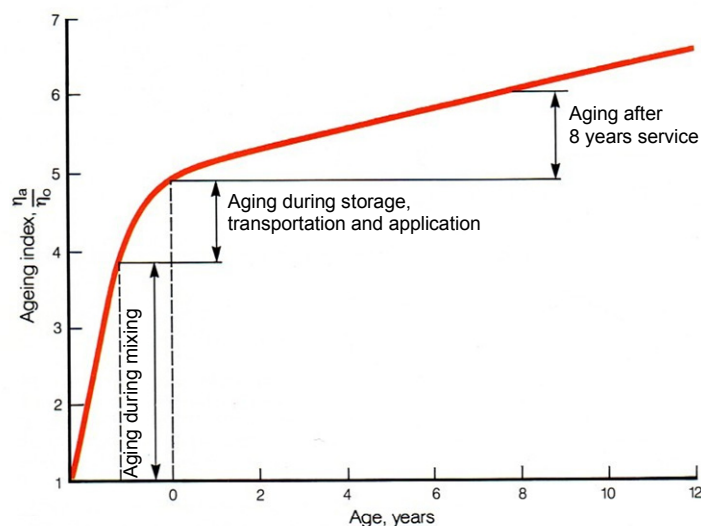


Figure 2.1: Effect of short and long term aging of the binder on viscosity ratio with aging period (Source: Shell Bitumen Handbook, 1990).

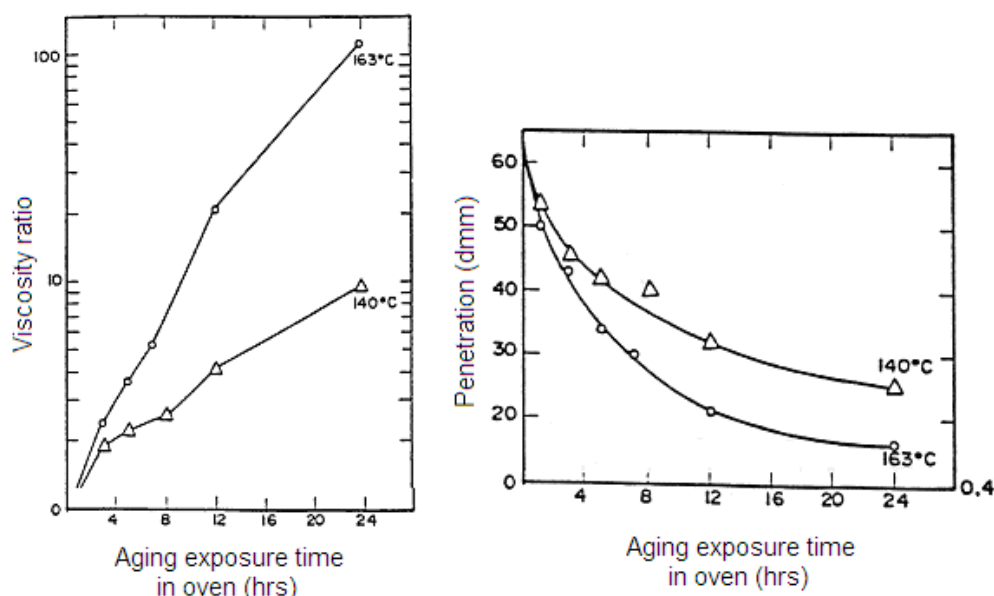


Figure 2.2: Left: Change in viscosity ratio (virgin) with aging time. Right: Change in Penetration with aging time (Source Ishai 1996).

Some general criteria were established by some researchers to limit the effect of aging on the performance of binders. For example, a penetration of less than 10 dmm and a ductility of less than 20 cm, measured at 25°C, were established to be the limits at which pavements start to show cracking. However, these criteria could be misleading because cracking, either due to thermal effects or traffic, will only occur when the stresses in the material exceed the strength. The strength and stiffness of a binder not only depends on the degree of aging but also on the temperature and loading time (Anderson et al. 1994). In general, empirical properties such as penetration, ductility, and softening point cannot provide accurate measures of the changes in the bitumen property because of the following reasons:

1. they are one-point measurements that can not give adequate representation of the original or the change after aging of the complex nature of bitumen viscoelastic properties, and
2. they are empirical in nature, which indicates that they cannot accurately nor simply be related to any fundamental rheological property of the binder.

A number of models have been developed and reported by different researchers to predict the changes in binder properties (such as penetration, softening point, and viscosity) with time. Some examples are given in Equation 2.1 through Equation 2.3. The validity of these empirical models for porous asphalt binder performance has not been proven. The empirical equations are based on a large number of binders recovered from actual pavements over a period of 10 years (COST333 1999, Dauzats et al. 1988). The expressions for long-term effects of aging on the penetration and ring and ball (softening point) with time are:

$$Pen(t) = 11.9925 - 1.2578 \cdot \sqrt{t} + 0.3322 \cdot Pen(0) - 2.9965 \cdot V_v \cdot X(t) + 0.765 \cdot Pen(0) \cdot X(t) \quad (2.1)$$

$$T_{RB}(t) = 64.448 + 1.5755 \cdot \sqrt{t} + 0.2531 \cdot Pen(0) + 0.5518 \cdot V_v \quad (2.2)$$

$$X(t) = \frac{1}{(\sqrt{t} + 1)} \quad (2.3)$$

Where:

- t = number of months that the binder has been in place in the pavement,
 $Pen(0)$ = penetration at 25°C of the original bitumen [dmm],
 $Pen(t)$ = penetration at 25°C of the aged bitumen [dmm],
 $T_{RB}(t)$ = softening point temperature of the aged binder [°C],
 V_v = voids content in the mixture [%].

It has been recognized in different studies that the oxidation susceptibility of binders not only depends on the source of the original binder and the mixture variables like voids content but also on the yearly atmospheric cycle (i.e. temperature variation, rain/water, UV light and so on). Anderson et al (1994) and other researchers have reported that environmental conditions such as seasonal and daily pavement temperatures strongly affect the aging rate of binders. The sensitivity of binder aging rate to temperature is binder specific; that is, binders from different sources could have different aging dependencies. The degree of aging of bitumen can also be related to the energy of the solar influx that depends on the cut-off angle of the sun radiation.

Aging Indicators

Aging Indicators for Binders: The extent of age hardening of fresh bitumen materials can be quantified in terms of penetration (% Retained Penetration), change in softening point, mass loss (STA, short term aging), or viscosity (Aging Index) as follows (Roberts et al. 1996):

$$\% \text{ Retained Penetration} = \frac{\text{Penetration of aged binder}}{\text{Penetration of original binder}} \times 100 \quad (2.4)$$

$$\begin{aligned} \text{Change in Ring and Ball Temperature, } \Delta T_{RB} &= T_2 - T_1 \\ \left(\begin{array}{l} T_1 = \text{ring and ball temperature of un-aged binder} \\ T_2 = \text{ring and ball temperature of aged binder} \end{array} \right) \end{aligned} \quad (2.5)$$

$$\text{Mass loss / gain} = \text{weight of STA bitumen} - \text{weight of fresh bitumen} \quad (2.6)$$

$$\text{Aging Index (AI)} = \frac{\text{Viscosity of aged binder}}{\text{Viscosity of original binder}} \quad (2.7)$$

Equation 2.4, 2.5 and 2.7 are indices used to evaluate the susceptibility of

binders to aging. The indices are usually employed in specifications to set a limit to the level of deterioration in asphalt pavements. Short term aging is simulated in the laboratory at high temperature (163°C) which is similar to the production temperature in reality. The aging process during the service life of the pavement occurs at low temperatures (maximum of 50 - 60°C) while, the long term aging in the laboratory is conducted at relatively higher temperature (90-100°C). This leads to differences in the aging process, which might not be representative to the long term aging of binders in the field.

For conventional binders, higher values of the aging index (AI) indicate a high degree of bitumen aging (hardening). In most cases, the aging indices in specifications describe binder aging requirements at a temperature of 60°C (viscosity) and 25°C (penetration) to indicate the relative performance at high and intermediate pavement temperatures. The absolute viscosity at 60°C of aged material was reported to be a useful parameter for characterizing long-term age hardening characteristics and to distinguish the durability of binders of different type or origin (Bell et al. 1994). According to Isaccson and Lu (1999), the aging index (Equation 2.7) may be used for pure bitumen and certain modified binders exhibiting no significant changes in the polymer aging. The aging process of polymer modified binders is discussed in more detail in section 2.3.1.

It is important to note that these indices of aging vary with the pavement structure, location, and mixture type, which is the reflection of the effect of environment, binder source and asphalt mixture type. That is, all other factors remaining constant, oxidation progression in dense and porous asphalt greatly differ for the same grade of bitumen or type of binder because of the very open nature (high void content) of porous asphalt. Apart from empirical methods, fundamental properties such as stiffness are also used to describe the effect of binder aging over wider spectrum of temperatures including low temperatures corresponding to cracking temperatures (Anderson et al. 1994).

Aging of binders is also related to the change in binder chemical composition. Binders exposed to age-hardening (RTFOT, PAV tests) show an increase in the so called Gaestel Index (IC), an interpretation of the chemical composition of the binder that explains its internal colloidal structure (Ishai et al. 1988). The Gaestel Index is discussed further in 2.3.3. The Gaestel Index (IC) is expressed as the ratio of the asphaltenes and saturates to aromatics and resins as given in Equation 2.8.

$$IC = \frac{\text{Asphaltenes} + \text{Saturates}}{\text{Aromatics} + \text{Resins}} \quad (2.8)$$

An example of the effect of age hardening is shown in Figure 2.3 through a relationship between the viscosity ratio (Aging Index) and Gaestel Index (IC) before and after aging. The changes in the binder characteristic due to aging

resulted in a shift of the line.

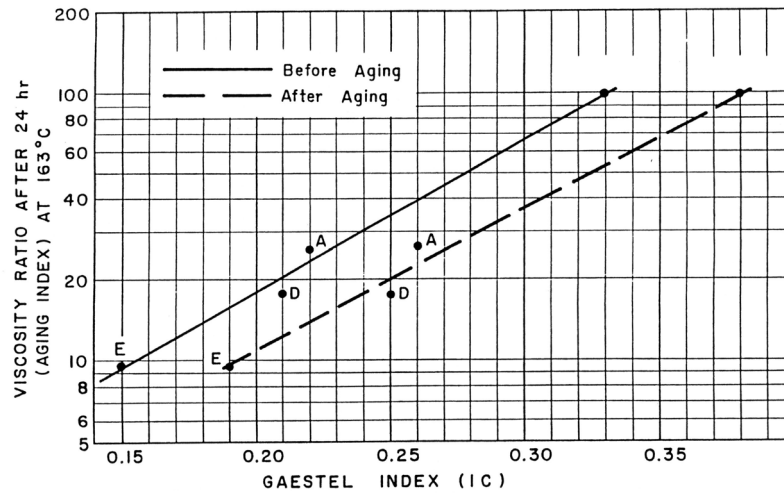


Figure 2.3: An example of the effect of binder aging with a plot of the viscosity ratio (AI) as a function of Gaestel Index (IC) (Source Ishai 1996).

The aging process can also be explained by the changes in fundamental rheological properties of bitumen, such as complex modulus and phase angle as a function of frequency. For plain (un-modified) bitumen, aging increases the complex modulus and decreases the phase angle over a range of frequencies, indicating that the aged bitumen becomes more elastic. By elastic, it is meant that the binder loses its viscous characteristics and shows increase in stiffness. For modified binders, changes in viscoelasticity are dependant on the frequency considered since the phase angle master curve shows unique behaviour towards the low frequency region as shown in Figure 2.4 for modified binder before and after the aging process (Isaccson and Lu 1999). Aging results in a change of the rheology of the binder and thus the rheological index² (R) and also temperature dependency (t_c , the frequency at which the two tangent lines fitting the complex modulus mastercurve data intersect), as indicated in Figure 2.4. The change in R indicates that aging can not only be represented by a shift factor along the logarithmic time scale because such shift does not take into consideration the change in shape of the complex modulus (G^*) and the phase angle (δ) master curve (Anderson et al. 1994).

² Rheological Index R is defined as the difference between the glassy modulus and the dynamic complex modulus at the cross over frequency ω_c ($\omega_c = 1/t_c$) of the complex modulus master curve and t_c is the corresponding loading time (Bahia et al. 2001).

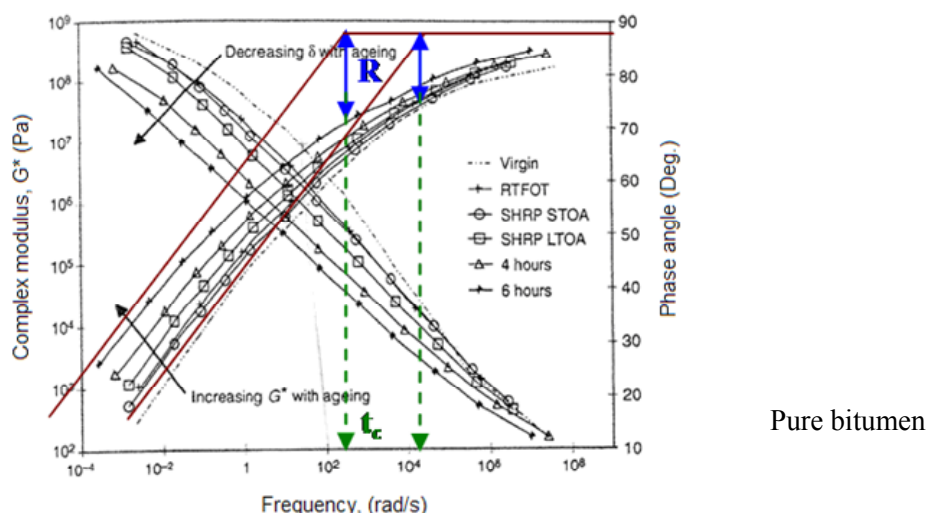


Figure 2.4: top: Complex modulus and phase angle master curve of pure bitumen before aging, and after short term (STOA), and long term oxidative aging (LTOA).

Aging Indicators for Asphalt Mixtures: Bell et al. (1994) utilized the ratio of the aged resilient modulus to the unaged resilient modulus as an aging indicator for asphalt mixtures.

The ratio of the slopes (or intercept) of the creep curve ($\log \epsilon$ versus $\log t$), which is referred to as the “Ductility Index”, before and after oxidation was used by Kumar & Goetz (1997) as an indicator for the aging of asphalt mixtures (Equation 2.10).

$$\text{Resilient Modulus Ratio (RMR)} = \frac{\text{Resilient Modulus after aging}}{\text{Resilient Modulus before aging}} \times 100\% \quad (2.9)$$

$$\text{Ductility Index (DI)} = \frac{m_1}{m_0} \quad (2.10)$$

Where:

- RMR = Resilient Modulus Ratio (Indirect Tensile and Triaxial compression Test),
- DI = ratio of the slope or intercept of a creep curve (non-destructive compression test) of aged to unaged mixture,
- m_0 = the slope (or intercept) of a creep curve for unaged mixture,
- m_1 = the slope (or intercept) of a creep curve for aged mixture.

According to Airey et al (2003), aging of bituminous binder is manifested, in general, as an increase in the stiffness modulus (or viscosity), while water damage is generally manifested as a loss of cohesion in the mixture and/or loss of adhesion in the bitumen and aggregate interface (i.e., stripping). It implies that moisture decreases the stiffness modulus of the mixture.

A summary of commonly used aging indicators for both binders and asphalt mixtures is given in Table 2.1.

Table 2.1: Summary of Aging Indicators Used to Describe Changes in Binder Property

	<i>Aging Indicators</i>
Binders	<p><i>Rheology:</i></p> <ol style="list-style-type: none"> 1. Retained Penetration (%) 2. Change in Softening Point ($\Delta T_{RB} = T_{RB} - T_{RB}$) 3. Mass loss (short term aging) 4. Aging Index / Viscosity Ratio (AI) 5. Complex modulus, G^* and phase angle, δ as a function of frequency, ω 6. *Shift in critical (cracking) temperature (t_c) <p><i>Mechanical:</i></p> <ol style="list-style-type: none"> 7. *Tensile/Creep strength (stiffness), $S(t)$ and m-value <p><i>Chemical:</i></p> <ol style="list-style-type: none"> 8. Gaestel Index (IC) 9. *Increment in carbonyl + sulfoxide area (Infra-red spectra test) 10. *Change in Molecular weight distribution (GPC test)
Asphalt Mixtures	<ol style="list-style-type: none"> 1. Resilient Modulus ratio 2. Ductility Index (DI) 3. Cantabro Test: Change in mass loss

NB: *Some of the aging indicators have also been discussed in other sections of the report.

Summary

- Two types of aging are prevalent in asphalt mixtures: short term and long term aging. Short term aging is considered causing the loss of volatiles and oxidation during production, transportation, laying and compaction of the asphalt mixture. Long term aging is predominantly the continuation of the oxidation process during the service life of the asphalt pavement.
- Environmental effects and the action of traffic are responsible for ravelling of porous asphalt. Environmental effects cause aging of the binder due to reaction with the atmospheric air resulting in hardening of the binder and the action of water that weakens the bond between binder and aggregate resulting in stripping of the stones. The ravelling of the surface of porous asphalt is further exacerbated by the action of traffic.
- Aging changes the rheological, mechanical, and chemical properties of the binder. The changes in property of the binder and asphalt mixture can be quantified by means of aging indicators. Aging indicators commonly used in practice are either empirical parameters describing change in binder property, fundamental properties designating change in the viscoelastic behaviour of the binder or a measure of the change of binder chemical composition indicating the change in colloidal structure after aging.

2.1.2 Effects of Moisture

Adhesive and Cohesive bonds

The modes of failure in bitumen/aggregate systems are adhesive and/or cohesive. If the aggregate is clean and dry and the asphalt mixture is effectively impermeable, then the mode of failure depends on the binder film thickness, rheological properties, and the nature of the aggregate (Figure 2.6). In the presence of water, the failure mode will likely be a loss of adhesion caused by stripping of the bitumen (mortar) from the aggregate. Several mechanisms of disbonding can be identified (Read and Whiteoak 2003):

1. Displacement: Retraction of bitumen along the surface of the aggregate due to introduction of water to the bitumen/aggregate system. The displacement theory relates to the thermodynamic equilibrium of the three-phase bitumen-aggregate-water system.
2. Detachment: Separation of the bitumen and the aggregate when a thin film of water or dust exists between the bitumen and aggregates. The bitumen film can easily be peeled from the aggregate surface since no adhesive bond exists. No obvious break in the surface of the bitumen film is apparent.
3. Film Rapture: This type of disbonding occurs when water penetrates through the bitumen film to reach the aggregate surface at sharp aggregate edges where the film is the thinnest. The speed with which the water can penetrate and detach the bitumen film will depend on the viscosity of the bitumen, the nature of the aggregate surface, the thickness of the bitumen film, and the presence of filler and other components such as surface active agents.
4. Blistering and Pitting: If the temperature of the bitumen in a pavement increases, the viscosity of the bitumen will be reduced. If this is associated with a recent rainfall, the bitumen may creep up the edges of water droplets to form a blister. If the temperature is increased, the blister will expand, leaving a pit which may allow access for water to the aggregate surface (Figure 2.5).
5. Hydraulic Scouring: Hydraulic scouring occurs in the wearing course and is caused by the action of vehicle tyres on a saturated pavement surface. The action of a passing traffic tyre pressurizes the water into and pumps it out of the voids inducing a compression-tension cycle in the mixture, which may result in debonding of the bitumen from the aggregate.
6. Pore Pressure: In poorly compacted or open mixtures water can be trapped as the material is compacted by traffic causing pore water pressure to build up by subsequent traffic after the mixture has become effectively impermeable. This may result in loss of bond due to channels created around the bitumen/aggregate interface. Higher temperatures acting on the entrapped water result in expansive stresses accelerating water migration and de-bonding. Low temperatures may lead to the formation of ice which is equally destructive.

7. Chemical Disbonding: Diffusion of water through the bitumen film causes the aggregate surface to adopt a negative surface charge against slightly negatively charged bitumen. This results in two negatively charged surfaces to be in contact resulting in a net repulsion. As more water is attracted to the aggregate surface, disbonding of the bitumen film will be the result.

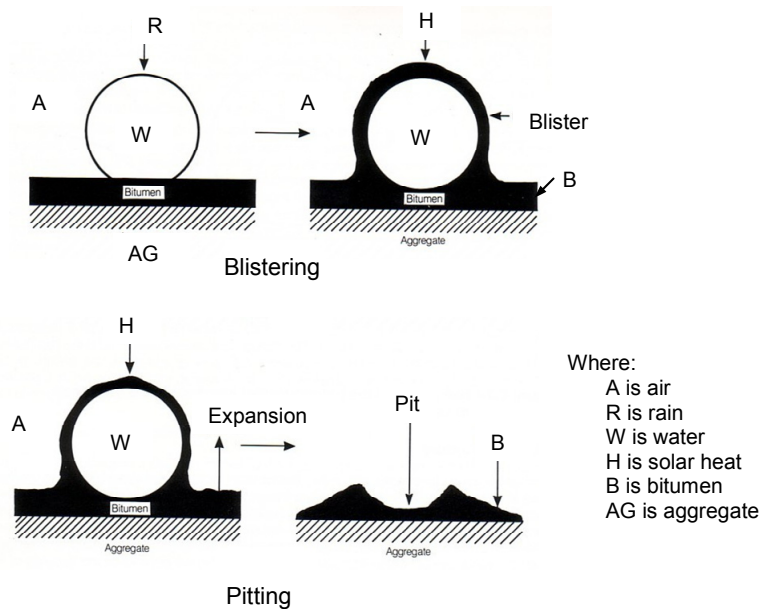


Figure 2.5: Formation of blisters and pits in a bituminous material (Source: Shell bitumen handbook, 2003)

The damaging effect of water with respect to the adhesion and cohesion properties of binders has recently been investigated by Konitpong and Bahia (2003). Their findings have shown that moisture damage could be manifested in binders as stripping (adhesive failure) or the loss of stability to resist traffic induced stress (cohesive failure).

The most important failure modes of asphalt mixtures according to Bell et al. 1994 are:

- diffusion of water into the asphalt film or through cracks in the asphalt film,
- separation of the bond at the interface,
- failure of the binder, and
- crushing of the aggregate.

In general, failure in asphalt mixtures can be categorized into two:

- *Adhesive failure*: In general, stripping in asphalt mixtures can be defined as an adhesive failure caused by the de-bonding of the asphalt film from the aggregate surface as a result of the damaging effect of water. Water can infiltrate into the binder-aggregate interface to eventually strip the binder from the aggregate. This could happen due to the higher affinity of most aggregates to water than to bitumen. Aggregate types with a high content of

silicon oxide, e.g. Quartz and granite, i.e. acidic aggregates, are more difficult to coat with bitumen than basic aggregates such as basalt or diabase (Read and Whiteoak 2003).

The aggregate surface charges in an asphalt mixture are considered important since the adhesive capacity of the aggregates is a function of their chemical composition. In addition, the grain size, shape and texture of the aggregates play a role. The phenomenon of stripping of the bitumen in the presence of water can be related to the surface charges. Since water balances the surface charge more than bitumen does, it leads to the separation of the bitumen from the aggregate surface in favour of water (Read and Whiteoak 2003).

- *Cohesive failure:* Water can also affect the cohesive properties of the binder resulting in a severe reduction in integrity and strength of the mixture. Cohesive failure may be attributed to the following factors:
 - Hardening of the binder leading to brittle behaviour of the material. The hardening effect could also result in adhesive failure due to stress reconfiguration in the system.
 - Softening of the binder because of the presence of water.

It is difficult to answer the question – what is the dominant damage indicator in porous asphalt concrete? PA is a mixture that allows easy access of water into the mixture. The permeability of PA, however, is so high that it will easily lose water as well. Given the fact that ravelling is a typical surface related defect type (potholes due to stone loss has seldom been reported in PA) one could hypothesize that traffic and environmentally (thermally) induced stresses, together with age hardening, are the main causes of ravelling. Moisture will certainly affect the deterioration process, but is not considered to be the main reason for the ravelling of PA.

Testing Methods for Cohesion and Adhesion

An asphalt mixture derives its strength from the adhesive and/or cohesive bond strengths of the binder (bituminous mortar) and the interlocking or frictional resistance of the aggregates. The adhesive strength of the bituminous mortar will be maximized if a strong bond exists between the aggregates and the binder. In the presence of a strong adhesive bond, the failure of the mixture should occur in the bituminous mortar due to either softening or cracking of the binder (assuming the breaking of aggregates rarely occurs). If the adhesive bond strength is poor, the failure will occur at the aggregate-mortar interface, resulting in premature failure of the mixture, i.e. stripping (Konitpong and Bahia 2003).

For a detailed description of tests used to determine adhesive strength, i.e. static immersion test, dynamic immersion test, chemical immersion test, immersion mechanical tests, immersion trafficking tests, and coating tests,

reference can be made to the Shell Bitumen Handbook (Read and Whiteoak 2003, Bitval report 2006).

Konitpong and Bahia (2003) suggested the use of the modified Pneumatic Adhesion Tensile Testing Instrument (PATTI) device for the evaluation of the adhesion properties of binders in binder-aggregate systems exposed to water (ASTM D 4541, "Pull-Off Strength of coatings using Portable Adhesion Tester"). In performing the test with the PATTI apparatus, pressure is applied to pull-off the bitumen film placed between the aggregate surface and the pull stub. When the applied pressure exceeds the cohesive strength of the binder or the adhesive strength of the binder-aggregate interface, failure of the specimen will occur (Figure 2.6). The pressure at failure is recorded and converted into pull-off tensile strength. The advantages of the PATTI device are that it allows:

1. the use of an aggregate surface,
2. conditioning of the specimen in water, and
3. observing the failure surface to define adhesive versus cohesive failure.

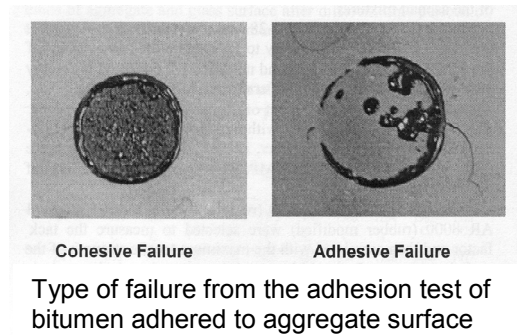
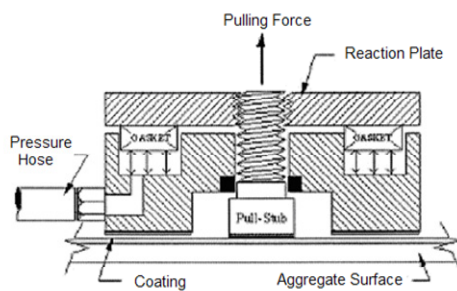


Figure 2.6: left: Schematic of the PATTI device, right: Example of cohesive and adhesive failure in the PATTI test (Source: Konitpong and Bahia 2003)

A Thin Film Tackiness Test, which can be performed in a rheometer is suggested for measuring Tackiness (a measure of cohesion) properties of asphalt binders. The Tack factor (C_T), defined as the work required to produce separation of an adhesive, is determined. The test consists of two circular parallel plates with an adhesive filling the space between the plates (Figure 2.7). Force is applied to pull the plates apart; the tackiness is thus the resistance of the adhesive determined at the rate of separation of the plates. The tack factor represents the energy of separation (w = "work of cohesion" i.e. area under the force versus time curve) of the adhesive joint which can be calculated using Equation 2.11:

$$w = \frac{1}{A} \int F \cdot v \, dt = d \cdot \int \sigma \cdot d\varepsilon \quad (2.11)$$

where:

- w = work or energy,
 F = the force applied,
 A = the contact area of adhesive joint,

v = the speed of plate separation.
 t = the measuring time,
 d = the specimen thickness,
 σ = applied stress, and
 $d\varepsilon$ = change in strain.

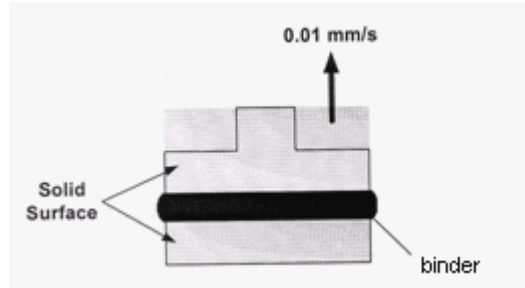


Figure 2.7: Adhesive joint - measurement of tackiness in rheometer (Source: Konitpong and Bahia 2003).

The relationship between the stress and the time during which the distance between the plates increased from d_0 to d_1 is given in Equation 2.12.

$$\sigma \cdot t = \frac{3\eta a^2}{4} \left(\frac{1}{d_0^2} - \frac{1}{d_1^2} \right) \quad (2.12)$$

where:

σ = the stress applied,
 t = the duration,
 η = the viscosity of adhesive,
 a = the radius of specimen,
 d_0 = the initial thickness of adhesive layer, and
 d_1 = the thickness after time interval t .

According to Lytton 2004, the bond strength greatly depends on the binder film thickness (Figure 2.8). Adhesive fracture dominates at thinner binder film thicknesses and cohesive fracture is the dominant failure type at thicker film thicknesses. However, it should also be noted that temperature and loading speed influences the behaviour of failure.

The effect of water is dependent on the binder's potential to adsorb water on its surface and absorb into its interior through diffusion. The presence of water in the binder reduces the material strength. As the binder ages, the temperature at which the material becomes brittle increases, which implies that the susceptibility to cracking increases. The aging of the binder, thus, reduces the low temperature performance of PA as a result of brittle behaviour of the binder. The healing potential of the material is also believed to be reduced by aging.

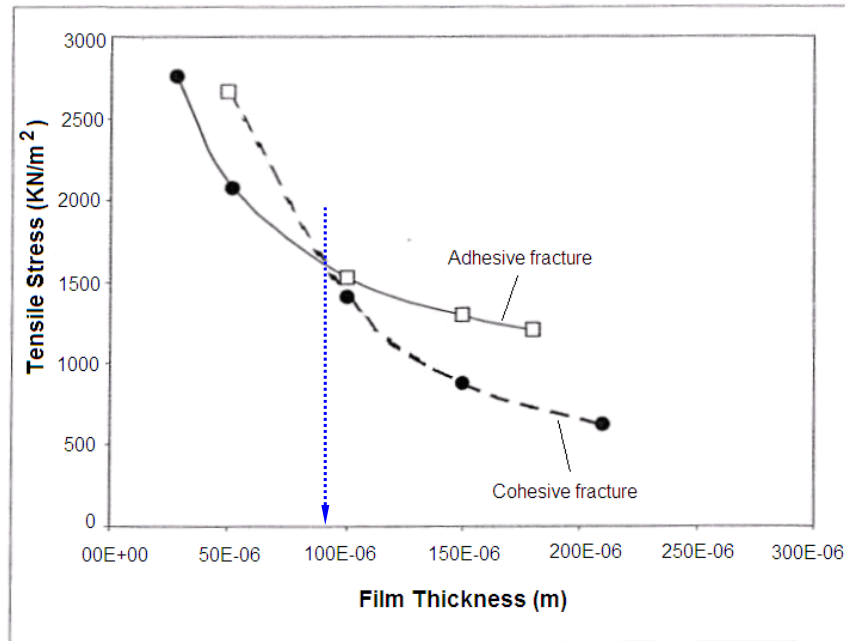


Figure 2.8: Tensile stress versus binder film thickness - constant stress conditions (Lytton 2004)

For a given aggregate a hard binder once adhered is more resistant against stripping than a soft binder as more energy is required for water to displace the binder (Heslop and Catt 1997). Equation 2.12 shows that the stress required to pull apart the sandwiched binder sample in the tackiness test is related to the viscosity and the thickness of the binder sample. Hence, it can be said that viscosity and film thickness are important factors associated with the performance of porous asphalt as both factors have a role to play with regard to the influence of water (de-bonding) and aging (hardness) of the binder.

To reduce the effects of water damage on the adhesive bondage of a porous asphalt mixture, middle sort filler (bitumen number BN 56-62) with a minimum of 25% hydrated lime is suggested to be used in PA. Hydrated lime enhances durability of the asphalt mixture, improving its resistance to stripping (water damage).

2.1.3 Summary

- Ravelling in asphalt mixtures is caused either by cohesive failure of the binder, adhesive failure (stripping of the binder from the aggregate), the crushing of the aggregate, or a combination of these failures.
- Adhesive failure is largely attributed to damage caused by the effect of water and cohesive failure is caused when the stress levels in the binder/mortar are exceeded. Diffusion of water into the binder increases the chance of cohesive failure due to the “softening” of the binder. Hardening of the binder may improve the resistance to the damaging effect of water on its adhesive strength, but will increase the possibility of load related damage (cracking) of the binding material.

- The hardening of the binder due to aging increases the temperature at which the material starts to behave brittle. As will be shown in chapter 5, hardening of the binder results in an increase in strength but a decrease in strain at failure. Ultimately, however, the strength will also decrease.
- The effects of aging and moisture on the cohesive and adhesive properties of binders can be assessed using different testing techniques. The PATTI and Tackiness test methods are recent techniques used for determining the adhesive and cohesive properties of binders. These test methods were not used in this research for two main reasons: 1) the PATTI test is not available at the laboratories of Road and Railway Engineering (Technical University of Delft) and DWW (Rijkswaterstaat – Road and Hydraulic Engineering Institute) and 2) the DSR equipment at the DWW laboratory that was used in this research program does not allow conducting tackiness test at constant rate of displacement.

2.2 Simulation of Binder Aging

Laboratory tests have been developed to simulate bitumen aging both for the short and long term aging; the most common techniques are: (1) increasing the temperature, (2) decreasing the bitumen film thickness, (3) increasing the bitumen surface area exposed to oxygen, (4) increasing air flow, and (5) application of pressure. In general, binder aging techniques can be classified into two major groups: (1) oven tests, and (2) pressure oxidation tests (Anderson et al. 1994).

However, it is not only the binder, but also the binder-aggregate interaction that should be taken into consideration in the aging process. The nature of the aggregate will have an effect on the aging rate and adhesive bonding which might play an important role in the durability of the pavement. Depending on the aggregate type (mineralogical nature of the aggregate and surface characteristics), the aging performance of the same binder mixed with different aggregate can differ due to the mineral contents of the aggregate surface, adsorption properties of the aggregate, and orientation of the polar molecules in the binder in the vicinity of the binder-mineral surface interface. The effect of binder-aggregate interaction is discussed in section 2.2.2.

2.2.1 Aging of the Binder

Durability of a wearing course is affected by binder age hardening both during the construction phase and service period; therefore, simulation of aging needs to take account of these effects. In order to accelerate the aging process in the laboratory in a realistic way, understanding the mechanism of aging in the field is essential. Aging is predominantly caused by oxidative aging, which is an irreversible process, where oxygen from the environment has to diffuse physically into the binder before it chemically reacts with the binder components resulting in hardening. Temperature serves two purposes during the aging process: 1) it softens the bitumen and increases the diffusion rate, and

2) it accelerates the chemical reaction. Based on the aging process, two alternative mechanisms are, therefore, used to accelerate aging: 1) reducing the film thickness and 2) accelerating the diffusion of air/oxygen into the binder film under pressure (Anderson et al. 1994).

Laboratory tests which are carried out to simulate the two types of aging, i.e. aging occurring during construction (short-term) and in service (long-term), are discussed here after.

Short-Term Binder Aging

Short-term aging occurs during the construction phase and is primarily due to oxidation and the loss of volatile components during asphalt mixture production. A number of laboratory tests are available to simulate the loss of volatiles and oxidation that take place whilst mixing, transporting, and laying the asphalt. These tests are specified for all types of binders although validation is required for polymer-modified binders.

According to Parmeggiani (2000), the mechanisms of the two reactions in short term aging are:

⟨⟨ *First Reaction (Loss of Volatiles)*

The first reaction comprises the loss of volatiles (through evaporation) and reflects the volatility of bituminous binders. Less volatile binders (with low mass loss) will be less susceptible to change in their rheological properties and are therefore more stable than highly volatile binders. Hence, the loss of volatiles reflects two things: a degree of imbalance in the binder composition and fuming of the binder.

Second Reaction (Oxidation)

Several possible types of chemical reactions occur during the “oxidation” process as direct consequences of the extent of the first reaction. A stable binder exhibits a smaller loss of volatiles, which consequently reflects a lower degree of oxidation and therefore less hardening of the binder. ⟩⟩

Parmeggiani stated that a degree of imbalance and fuming of the binder are reflected as a result of loss of volatiles. There could be a chance of fuming of the binder due to mixing at a very high temperature but not necessarily due to loss of volatiles. Indeed, a greater loss of volatiles is expected when the mixing of asphalt is performed at high temperatures. The second statement regarding the degree of imbalance is not clearly defined; but the loss of volatiles in itself simply results in a binder hardening.

According to Zupanick and Baselice (1997), the overall mass change in short term aging of bitumen depends on two competing phenomena. A portion of the sample volatilizes (i.e. volatilization of oily components), causing the sample to loose mass, and oxygen reacts with the sample (oxidation), causing the sample

to gain mass. The net sum of these two effects determines whether the sample has an overall mass gain or an overall mass loss.

The chemical changes taking place during the oxidation process are discussed in section 2.3. The tests used to simulate the short term aging are presented below:

1. The Thin Film Oven Test (TFOT; ASTM D 1754, EN 12607-2)

The Thin Film Oven Test is a standard binder test used for measuring the combined effects of heat and air on a film of bituminous binder. The primary purpose of the test is to simulate the degree of aging of bituminous binder during mixing in an asphalt mixing plant. In the test, a thin film of bitumen is placed in a pan, which is held in a convection oven at 163°C for 5 hours. The effect of hardening is determined on the basis of the change in mass (expressed as a percentage) and/or as a change in the bituminous binder's characteristics such as penetration (EN1426), softening point (EN 1427) or dynamic viscosity (EN 12596) before and after oven aging.

2. The Rolling Thin Film Oven Test (RTFOT; ASTM D 2872, EN 12607-1)

The Rolling Thin Oven Test (Figure 2.9) is used as a standard test under the SHRP binder specification to simulate aging in hot-mix asphalt plant. The aging test is conducted by placing 50 g of bitumen in cylindrical bottles that have an opening at one end (there are 8 bottles in total). The bottles are placed in oven at 163°C for 75 min (85 min in the case of SHRP specification). The bottles rotate in a carousel, and fresh hot air is periodically injected into the bottles. The percent mass loss is determined. The effect of hardening is, as in the TFOT aging, determined on the basis of the change in mass loss (expressed as a percentage) and/or as a change in the binder property, such as penetration (EN1426), softening point (EN 1427) or dynamic viscosity (EN 12596), before and after oven aging.

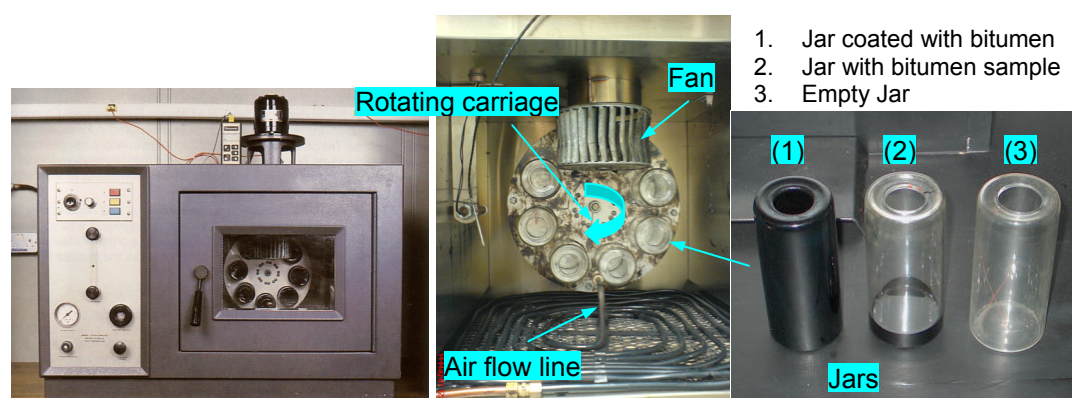


Figure 2.9: The Rotating Thin Film Oven Testing (RTFOT) equipment (left) and Jars for holding sample (right)

The test conditions of the RTFOT were chosen to give results comparable with those of the TFOT. However, studies indicate that the RTFOT is about 10%

more severe than the TFOT and thus will typically volatilize more binder components (Zupanick and Baseline, 1997). In the RTFOT test, the rolling effect exposes fresh bitumen surface resulting in lower skin formation compared to TFOT test.

- **Modified RTFOT Procedure:**

The difference in viscosity of bitumen materials at the aging temperature (163°C) results in a variation in the exposure of fresh material during RTFOT testing. In other words, the test is not conducted at equiviscous temperature (EVT), which implies that the RTFOT procedure does not provide equivalent oxidation conditions for materials with viscosity (or consistency) differences, such as pure bitumen and PMB (Polymer Modified Bitumen). A material with a high consistency will flow slower in a rolling bottle under the influence of gravity whereas a material with low consistency will flow promptly. In the case of the highly viscous material (PMB), less fresh surface is exposed to air during the rotation of the bottles, and thus less oxidative hardening occurs. The opposite is true with low consistency binders according to Oliver and Tredrea (1997).

In order to use the RTFOT procedure for materials with different consistencies (viscosity), a modified RTFOT was suggested. A set of steel rods (127 mm long by 6.4 mm in diameter) was introduced inside each of the rolling bottles (Bahia et al. 1998) to ensure uniform aging of binders. As the bottle rotates, so does the rod, constantly exposing fresh film of binder on the interior bottle walls. A roller (rod) with equal length as the RTFOT bottles and with screwed thread was used by Oliver and Tredrea (1997) to “screw” the binder towards the back wall of the bottle in order to prevent spilling of the binder sample. However, studies conducted to determine the effect of the metal rods on short-term aging revealed that the steel rods did not improve aging of modified and unmodified binders (Bahia et al. 1998, ETG 2000). The method has not been successful and is seldom used.

- **The Nitrogen Rolling Thin Film Oven Test (NRTFOT)**

A modified short-term aging suggested by Parmeggiani (2000) on the RTFOT testing method takes into account the physical and chemical reaction occurring during simulation of asphalt production which involves two reactions: i.e. evaporation and oxidation. Significant mass transfer processes and chemical reactions occurring during RTFOT testing comprise evaporation (Reaction 1: Loss of volatiles) followed by oxidation (Reaction 2: mostly increase of mass) of the bitumen; the combined effect of which results in hardening of the bitumen. The test is called Nitrogen Rolling Thin Oven Test (NRTFOT) which suggests the replacement of blowing of hot air on the samples during RTFOT by an inert gas Nitrogen in order to make an assessment of the extent of evaporation of the lighter molecules (volatiles) during asphalt production. This test method is developed to enable the determination of the extent of each process (i.e. evaporation and oxidation) taking place in the short-term. On the other hand,

the test can be used to distinguish the sensitivity of different binders to aging as the loss of oily components is a crucial element in the subsequent performance of the binder.

3. The German Rotating Flask Test (GRFT; DIN 52016)

The German Rotating Flask Test was developed in Germany as an alternative to the TFOT and RTFOT. It was developed to provide simpler dynamic test equipment that enables a short term aging of binders including modified binders. The perceived advantage of the GRFT equipment is that it is a dynamic conditioning test method that intends to avoid skin formation and separation (segregation) of the polymer that normally occurs during testing in static type testing methods (TFOT, PAV). In some references the GRFT has been reported as a test method that could be related to RCAT testing method and possibly be used for long term aging as the PAV and RCAT aging methods. The PAV and RCAT aging methods will be discussed latter on in this chapter.

In the GRFT, 100g of bitumen is placed in a spherical flask. This flask is tilted, submerged in a 165°C oil bath as shown in Figure 2.10. The test is run for 150 min. The flask rotates at a speed of 20 rpm while 500 cc/min of air passes through the flask. The test is conducted in a closed vessel, which allows control of the type and volume of gas that comes in contact with the binder. The rotation of the vessel turns the sample over during the aging process, maintains a representative binder film, and prevents skin formation. The test is conducted in an oil bath, which allows rapid sample heating and eliminates the radiant heating problems associated with some ovens. The test apparatus can be modified to permit collection of volatilized components. Comparison with the RTFOT and TFOT suggest that the GRFT is roughly one-third as severe as the other tests in producing volatiles, which means less aging (Airey 2003).

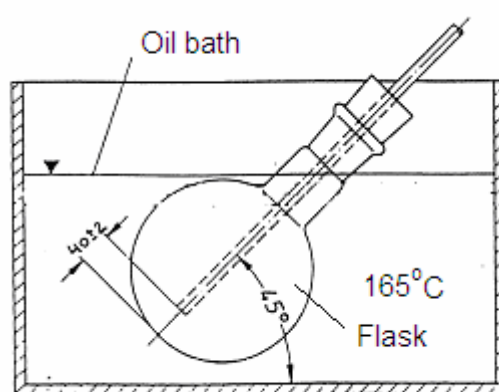


Figure 2.10: The German Rotating Flask Test (GRFT) setup

- Modified German Rotating Flask Test (MGRFT)

The purpose of the modified apparatus is to age more material while maintaining the same degree of aging of the material as that of the RTFOT

method. A 200 g binder sample is placed in a 2000 ml flask attached to a rotary evaporator for 210 min at 165°C, with 2000 ml/min air being supplied continuously. The flask is rotated at 20 rpm and may contain steel balls inside to expose fresh binder film during aging. A comparison of the RTFOT and MGRFT aging methods on plain and modified bitumen showed good agreement with an exception in the level of mass loss. According Ramaiah et al. 2004, the mass loss in the RTFOT aging was a bit higher than in the GRFT Method.

Long-Term Binder Aging

After short-term aging, bituminous binders are subject to field (natural) aging during their service life under the prevailing climatic conditions of the road location. This second stage aging process is a very important factor in the long-term behaviour of bituminous mixtures and in the development of their performance characteristics (Francken et al 1997). Long-term aging occurs primarily due to the oxidation of an asphalt mixture in service. Long-term aging is defined as a slow oxidation (aging) process that the binder undergoes as a result of interaction with the environment or air. A number of tests were developed to simulate the oxidation process in the longer-term with the purpose to “rank” binders, which include:

1. The Pressure Aging Vessel (PAV, SHRP test method B-005, EN 14769)

This is a SHRP aging method used to simulate the oxidation process that takes place during the service life of the pavement. The binder is firstly aged for short term using either TFOT or RTFOT (SHRP standard test) method. In the standard PAV test (Figure 2.11) 50 g of binder is poured into preheated 140 mm diameter pan (the binder film thickness will be approximately 3.2 mm) and is placed in a shelf rack with a capacity of 10 pans. The temperature of the aging vessel is maintained at either 85°C (PAV 85), 90°C (PAV 90), 100°C (PAV 100), or 110°C (PAV 110) and at a pressure of 2.1 MPa during the aging process that is run for 20 hours. Aging temperatures below 100°C are generally recommended in order to achieve similar chemical changes as in field aging. The HiPAT (High Pressure Aging Test) is another long term testing method which is performed using the PAV equipment at a lower operating temperature and a longer aging time. The HiPAT aging test is conducted at 85°C for 65 hours under 2.1 MPA air pressure.

For a constant temperature, aging with application of different pressures will result in different degrees of hardening of the binder. In fact, the rate of increase in binder aging is not only pressure dependant, but also geometry, temperature and time dependant according to Domke et al. (1997 and 1999). According to the study by Domke et al. (1997), identical aging results were obtained on PAV and POV (Pressure Oxidation Vessel) aged samples subjected to the same aging conditions. Similar to the PAV aging test, the POV aging test also predicts long-term aging of binders. The difference between the PAV and POV tests is the heating mechanism. The POV test is conducted in a stainless

steel reactor immersed in a temperature-controlled water-triethylene glycol bath. Inside the POV, a rack with a capacity of holding 40 trays of 5.50 cm diameter is put in-place. In each of the trays 7.6 g of bitumen is placed which will expose a binder film thickness of about 3.2 mm for aging.

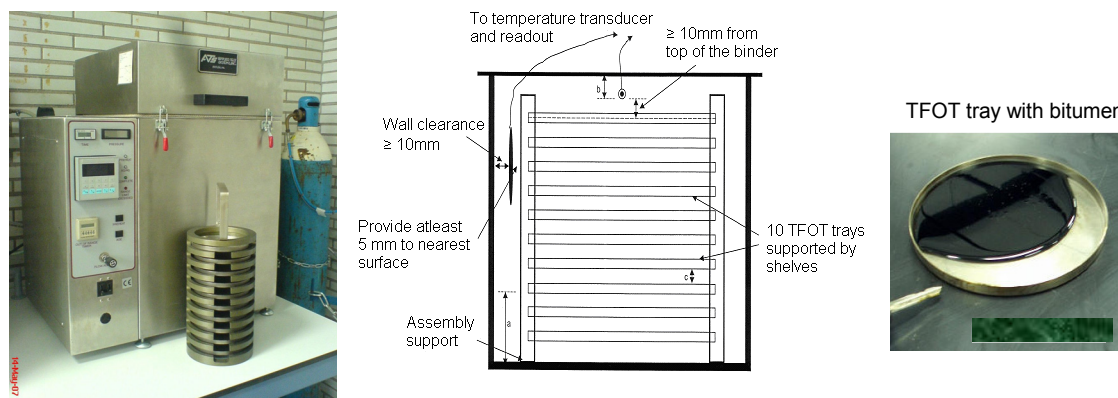


Figure 2.11: left: the PAV aging apparatus, right: Tray assembly inside the PAV

The PAV aging method accelerates the binder aging without destroying the integrity of the binder. The aging of bituminous materials according to this procedure was introduced to model field aging and predict performance. Researchers debate that accelerated aging tests conducted at elevated temperature above the actual pavement temperatures may result in a change of binder properties different from reality. A major criticism of researchers to the PAV aging technique is that it is a static test and the diffusion of oxygen is inhomogeneous leading to differences in aging between the surface and the bulk of the sample (according to Verhasselt (2002)). He showed that polymer migration occurs in the PAV aging of PMB materials by investigating the top and bottom parts of the aged specimens. Nevertheless, it is possible that the aging process in the road is also similar to the static aging which substantiates the PAV aging procedure for simulating long term aging.

2. The Rotating Cylinder Aging Test (RCAT)

The Rotating Cylinder Aging Test (RCAT), Figure 2.12, is an accelerated aging test developed by the Belgian Road Research Center (BRRC) to simulate both the short and the long-term aging of binders. The test is dynamic, aging of binder is uniform, and the amount of aged binder is sufficient for further testing to characterize the bitumen. Despite the long duration of testing, which is a major disadvantage, it has the advantage of monitoring the development of aging on the properties of the binder at various intervals of time (reaction time) during the testing process. Another major advantage of the RCAT test is that it is possible to combine short-term (RTFOT-type) aging test and long-term (PAV-type) aging for the same sample and with the same equipment, which reduces intermediary sample handling operations (Verhasselt 2002). The long term test procedure using the RCAT method produced good correlation with recovered binder samples from porous asphalt pavement according to Mes 2003. This

may be explained by the relatively slow aging process, prevention of skin formation and uniform aging of the binder compared to PAV aging which is also conducted at the same temperature.

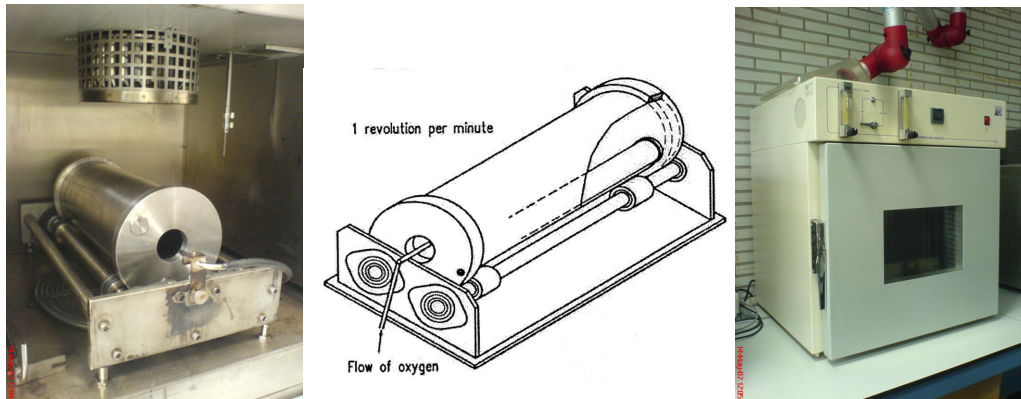


Figure 2.12: RCAT device for accelerated aging of bituminous binders

The RCAT aging procedure is as follows (Draft standard CEN TC336 WG3):

- 500-550 g of binder is poured into a stainless steel cylinder.
- The cylinder is rotated at a rate of 1 rpm for long term aging
- A stainless steel roller with groove is inserted to press and distribute about 3mm thick binder film against the inner wall of the cylinder to constantly expose fresh surface and homogenizing the binder sample.
- A constant flow rate of 4.5 l/h of oxygen enriches and renews the atmosphere inside the cylinder
- The recommended operating temperature is 85°C, but a temperature of 90°C may be preferred to reduce the test duration.
- The duration of the test is 240 h at 85°C or 144 h at 90°C.

When using the RCAT for short-term aging simulation, the cylinder is set at 5 rpm (instead of 15 rpm in RTFOT method), an air inflow rate of 4 liters/min, and the test is run for 235 ± 5 min (4 hours) at 163°C temperature for an equivalent degree of aging as in RTFOT (Verhasselt 2002).

Table 2.2 summarizes the aging methods discussed with regard to short term aging and long term aging of binders.

A study conducted by Mes (2003) at the Dutch Road and Hydraulic Engineering Institute (DWW) indicated important findings with respect to aging techniques employed to simulate the binder aging process in porous asphalt. The study was performed on bitumen materials recovered from the road and aged in the laboratory. The molecular weight vs penetration and molecular weight vs viscosity plots of the binder recovered from the road matches with the material aged under the procedure RTFOT+RCAT and showed some difference with the RTFOT+PAV material (refer to Figure 2.13 and Figure 2.14). In addition, the viscosity versus carbonyl (Ketones) area plot of the field and RTFOT+RCAT materials showed the same trend of aging

process. This provided the basis for the selection of the RCAT aging procedure in this research in addition to the advantage it offers in handling the material during aging.

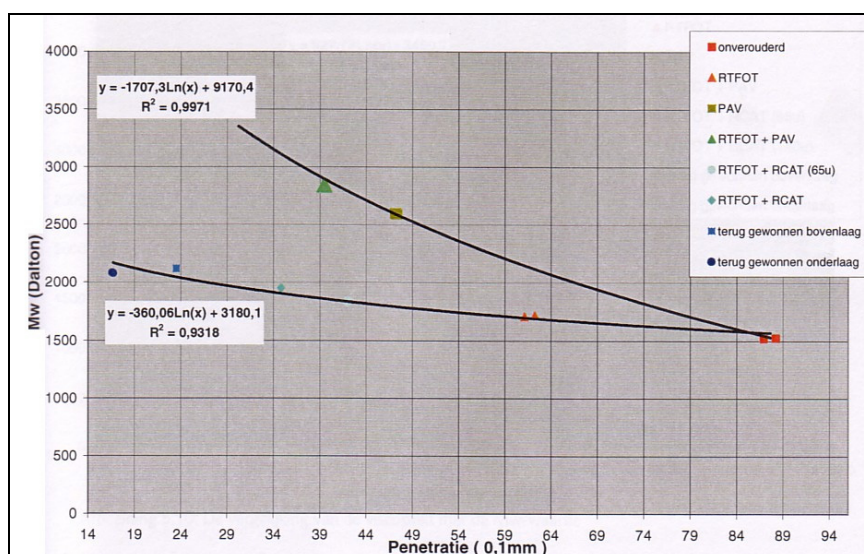


Figure 2.13: Penetration-Molecular weight plot of different binder aging protocols (Mes 2003)

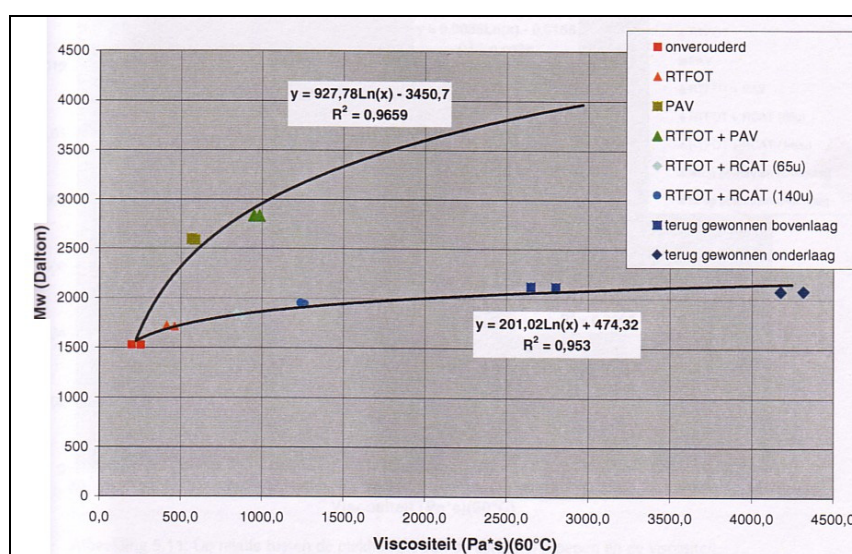


Figure 2.14: Viscosity-Molecular weight plot of different binder aging protocols (Mes 2003)

NB: The meaning of the Dutch words in Figure 2.13 and Figure 2.14 are given below.

Onverouderd	=	unaged bitumen.
RTFOT	=	Rolling Thin Film Oven Test
RCAT	=	Rotating Cylinder Aging Test
RCAT (65u / 140u)	=	long term aging using RCAT for 65/140 hours.
PAV	=	Pressure Aging Test
Terug gewonnen bovenlaag	=	recovered bitumen from upper zone of PA cored from the field.
Terug gewonnen onderlaag	=	recovered bitumen from lower zone of PA cored from the field.

Table 2.2: Summary of binder aging test methods

Test method	Temperature (°C)	Duration (min / hr)	Sample size (g)	Film thickness (mm)	Other features	Standard
<i>Short-term aging</i>						
1. Thin Film Oven Test (TFOT)	163	5 hr	50	3.2	--	EN 12607-2
2. Rolling Thin Film Oven Test (RTFOT)	163	75 min	35 x 8 bottles	1.25	15 rpm, air flow 4 l/min	EN 12607-1
3. Rotating Cylinder Aging Test (RCAT)	163	235 min	500 - 550	--	5 rpm, air flow 4 l/min	NEN-EN 15323 (Draft)
4. German Rotating Flask Test (MGRFT)	165	150 min	100	--	flask rotation 20 rpm	DIN 52016
Modified* German Rotating Flask Test	165	210 min	200	--	flask rotation 20 rpm	DIN 52016
<i>Long-term aging</i>						
1. Pressure Aging Vessel Test (PAV), [POV]	90	20 hr			2.1 MPa pressure	EN-14769 (SHRP B-005)
2. High Pressure Aging Test (HiPAT)	85	65 hr	50	3.2	2.1 MPa pressure	BRRC method
3. Rotating Cylinder Aging Test (RCAT)	85 / 90	240 / 144 hr	500 - 550	2.0	1 rpm, 4.5 l/hr Oxygen	DIN 52016
4. Modified German Rotating Flask Test	85	65 hr	200	--	flask rotation 20 rpm	New method -
5. Weatherometer aging *	60	1000 hr	PA mixture	4.5% bitumen	Temp. +UV+humidity (refer to section 4.3.3)	Simulation of field conditions
Combinations of light (UV), moisture (humidity, RH), and temperature						

* Refer to section 4.3.3 for the weatherometer aging protocol.

2.2.2 Aging of Asphalt Mixtures

The field aging process of bitumen is influenced by the nature of the aggregate. Hence it seems rational to perform long-term binder aging in the presence of mineral matter (i.e. filler, sand, and stone) or as mixture aging.

Asphalt Mixture Aging

Short and long term aging procedures were developed under the SHRP-A-003A project (Bell et al. 1994).

Loose Mixture

The SHRP procedure for Short-Term Oven Aging (STOA) requires that loose mixtures be heated (aged) in a forced draft oven for 4 hours at 135°C prior to compaction with the condition that they be stirred and turned every hour. This was found to represent the condition during mixing and placing and also represents less than 2 years in service for dense mixtures.

Compacted Mixture

The Long-Term Oven Aging (LTOA) procedure requires that the mixture, previously subjected to STOA, be compacted and reintroduced in an oven at 85°C for additional 120 hours.

Table 2.3: Summary of aging tests on asphalt mixture

<i>Type of Test</i>	<i>Standard Conditions</i>	<i>Reference</i>
1. Short-term Oven Aging (STOA) (loose mixture)	135°C, 4 hr	SHRP B-003
2. Long-term Oven Aging (LTOA) (compacted mixture)	85°C, 120 hr	SHRP B-003

A study on asphalt mixtures was conducted at the Nottingham Centre for Pavement Engineering (NCPE) – University of Nottingham, to investigate the combined effects of oxidation and water conditioning on the performance of the asphalt mixtures. It was shown that the binders recovered from the aged asphalt mixtures had similar rheological properties (complex shear modulus and phase angle, G^* and δ) whereas the mixtures showed difference in performance. The variation in mixture performance was mainly attributed to the damaging effect of water on the asphalt mixture specimens during aging. The difference in the retained resilient modulus test was related to the level of adhesive damage (Airey et al. 2003). The damaging effect of water could have an adverse effect not only on the adhesion but also cohesion of the binder. The equipment that was developed at NCPE for this study is shown in Figure 2.15.

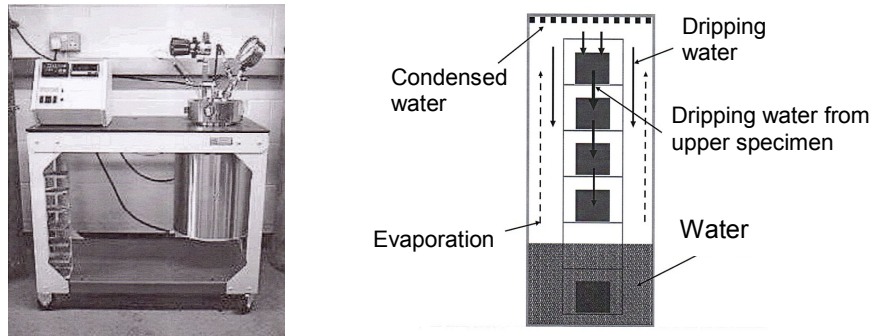


Figure 2.15: Asphalt mixture pressure aging / moisture conditioning apparatus (left) with setup for conditioning of samples inside the vessel (right) (Source: Airey et al. 2003).

Experiences in Materials Aging Methods

It is understood that “natural aging” is a complex process involving many factors such as environmental conditions, mixture type, and binder-aggregate interaction. The standard simulation of aging in the laboratory is performed under the influence of temperature and pressure which differs from the aging conditions in reality. Moreover, the loss of aggregates from the pavement surface is not only a result of the aging of the binder but also the stripping effect of water. In order to conduct more realistic aging tests, an approach of binders aging involving environmental factors, i.e. temperature, UV light, and moisture, is necessary to consider. Aging in a weatherometer is thought to be a rational way for investigating the sensitivity of porous asphalt to combined effects of environmental factors to determine changes in the binder’s adhesive and cohesive properties. To acquire fundamental understanding of accelerated weathering of materials, visits were made to a number of companies with the experience in the weathering of materials.

Visit to TNO: (Netherlands Organization for Applied Scientific research)

Visit to TNO at Den Helder was conducted on 16th December 2003 to share experiences with regard to aging methods of materials. Studies related to the use of paints as protection of metals against corrosion are performed at TNO, which involves the study of the effects of aging. The objective of the visit was to get a broader understanding of the principles in the process of aging and the methods for the simulation of materials aging. The explanation about the aging studies being conducted at TNO was given by Ing. W M Bos.

The importance of studying the aging of materials and problems associated with deterioration in performance of materials arising from aging was discussed. First and foremost, the simulation of the complex process of aging in the field would be significant to characterize how materials perform in reality under the influence of different factors. For this reason, aging studies conducted at TNO are carried out both outdoors (weathering used as reference) and in the laboratory. Samples are exposed to outside weathering by placing them in plates at an orientation of 45°C. Regular studies are conducted to evaluate the effect of the complex process involving the action of rain/water, light exposure, and temperature cycles in the field. Similarly, accelerated

weathering tests are performed in the laboratory to demonstrate the effects of weathering using artificial rainwater, i.e. water including chemical components (electrolytes) present in rainwater, absorption of UV light comparable to actual sunshine duration and intensity, and consideration of other factors such as chemical action. From the data obtained from the field and laboratory aging processes, relationships are established to understand the behaviour of materials and take actions to enhance their performance.

Although the processes involving the deterioration of materials at TNO due to aging are different from asphalt mixtures, the principles to simulate the effects of aging seem to be similar. The end result of a simulation is to replicate changes in the property of materials due to the aging process. The aging in asphalt mixtures involves short term aging during production which is not relevant in the case of metals that are protected by paintings. Conversely, the reaction of external components with metals through electrons transfer does not occur during the aging of asphalt mixtures. Nevertheless, in all cases, weathering contributes to the deterioration or change in property of materials which is an important condition to adopt methods and principles to simulate complex aging processes in the field.

Visit to ATLAS Materials: ATLAS Materials was visited to study weathering techniques and discuss possibilities for the use of weathering equipment for the aging of bituminous materials and asphalt mixtures. ATLAS Materials Testing Technology BV is a company specialized in weathering techniques of materials. The firm is located in Lochem (Netherlands) and has full laboratory testing facilities for testing materials durability. Materials are exposed to aging under different aging protocols that combine the influences of light, temperature, and water (moisture). The manager of ATLAS Materials at Lochem, Ing. Gerard van Ling, explained in detail the principles of weathering, instruments used for this technique, and the company's experience in simulating the weathering of materials both accelerated techniques and outdoor weathering involving natural/environmental conditions. Among other things, he explained that the choice of the type of UV light should match with the material's sensitivity to degradation and must be related to the real (applicable) process in the field. Different materials have different absorption capacity for a certain wavelength of light, which need to be predicted to select the appropriate type of UV lamp to conduct simulation tests. The ATLAS equipment for aging (weathering) of materials can also combine the effects of moisture and temperature cycles, which occur in real life.

The SOLAR Simulation testing equipment (SC Series) seems a very feasible option for weathering of bitumen, bituminous mortar, or asphalt mixtures. It has a fully controllable climatic chamber capable of simulating the weathering of specimens with testing conditions similar to the natural environment (field aging). Samples can be placed horizontally at a desired distance from the light

source to vary the intensity of the light / irradiation. The equipment is shown in Figure 2.16.



SC600 Solar Simulation Chamber

Full Function climatic chamber with additional simulation of the global sunlight spectra. Economic alternative to large solar simulation equipments. With a capacity of 600 l, the test chamber is designed for testing medium-sized components.

Features

- . Radiation source: Metal Halide Lamp, 1 x 2500 Watt
- . Chamber volume: 800x800x965 mm (WxDxH)
- . Filter system: Outdoor/Indoor
- . Irradiance: 800 to 1500 W/m²
- . Spectral distribution: Global radiation, 280-3000 nm (Base: CIE No.85; Share: DIN 75220)
- . Temperature ranges: w/ irradiation -20 °C to 100 °C, w/o irradiation -30 °C to 100 °C
- . Heating rate 4.0 K/min
- . Cooling rate 2.5 K/min

Figure 2.16: SC600 Solar simulation chamber

The second type of testing apparatus applicable for binders/bituminous mortar is a very compact one that can be used to perform quick durability tests with sunlight simulation, in combination with temperature and water (wetting) effect features. In the SUNTEST instrument (Figure 2.17), samples are placed horizontally exposed to long term influence of light and heat. This equipment can also be used for small scale routine laboratory applications to determine the extent of material degradation under simulated weathering conditions.

According to Ing. van Ling, the aging time of materials in the weathering apparatus to achieve the level of aging in the field depends on the material type. As a general rule, an accelerated aging by a factor of 20 to 30 relative to natural weathering is anticipated. This assertion is based on the aging behaviour of different materials such as polymers and paintings. The aging of a 10-12 yr old PA pavement would require about 1000 hours of aging in a weatherometer if only the sunshine hours that contribute to the aging in the field are considered. This is consistent with the weather data that has been analysed to come up with the aging protocol of PA mixture in the weatherometer (refer to section 4.3). Other factors such as increasing the aging temperature and the selection of the appropriate UV lamp that will have the most influence on the degradation of binders will facilitates the aging process or shorten the aging time. However, care should be taken to accelerate aging in a manner consistent with the aging process in reality.



SUNTEST XLS/XLS+ Tabletop Xenon Exposure Systems

The SUNTEST XLS/XLS+ system is an affordable xenon instrument in a table-top design for conducting accelerated lightfastness and photostability testing.

Features

- . Two models: manual XLS and fully automated XLS+
- . XLS+ offers full micro-processor control and simple test programming
- . Light source: 2200 watt air cooled xenon arc lamp
- . Total exposure area: 980 cm² (144 in²)
- . Temperature range: BST 30 °C to 90 °C
- . Controlled irradiance
- . Measurement and display of chamber temperature
- . Unique chamber design for better distribution of the ultraviolet radiation
- . Low cost operation

Figure 2.17: SUNTEST XLS/XLS+ tabletop xenon exposure system

The visit to ATLAS was very valuable in terms of understanding weathering techniques involving the combined effects of different factors to simulate the complex nature of aging in the reality. Accelerated weathering test methods are essential to determine and improve performance of materials exposed to environmental degradation. Hence, such weathering equipment was recommended to perform durability test of binders and asphalt mixtures to study materials aging behaviour. Based on the functionality of the weathering equipment, the climate chamber (Weatherometer) was recommended to conduct asphalt aging tests in this study and future researches.

Visit to KRATON Polymers Bv: KRATON Polymers BV was visited to look at their laboratory facilities especially the weatherometer apparatus used for aging polymer modified binders (Figure 2.18). KRATON Polymers BV produces polymers used to enhance the performance capabilities of a wide spectrum of end products and applications, among which is the modification of bitumen for road application.



a)



b)

Features:

- Light source: 6500 Watt water cooled xenon arc lamp
- Total exposure area: 11,000 cm² (1,705 in²)
- Temperature range: 40°C to 110°C
- Humidity range: 10 to 100% RH
- Water spray: specimen and rack
- Controlled irradiance upto 1sun levels
- Conforms to many automotive test methods

Figure 2.18: a) The Ci65a Xenon weatherometer apparatus available at KRATON b) Set-up of samples around UV light in Ci65a weatherometer (Source: ATLAS Material).

The visit to the laboratory was accompanied by valuable discussions with KRATON staff, namely: Mr. Erik Jan Scholten (MSc.), and Mr. Jan Korenstra mainly on the weatherometer apparatus and its possible use for aging of binders used in road application. The firm uses the Ci65a xenon weatherometer to conduct accelerated aging test by subjecting samples to combined effects of temperature, UV light, humidity, and water spray to simulate environmental aging conditions. The samples are placed in vertical and inclined positions and rotate around a UV light positioned in the centre. Thin film binder samples are coated on plates for aging as shown in Figure 2.18b. KRATON makes use of the weatherometer to age binder samples modified with up to 12% polymer, which are used for roofing and other applications. These binder samples have much lower temperature susceptibility compared to unmodified and polymer modified binders used in the road application (< 7% modification). For unmodified binders, the vertical and inclined positions are not suitable because of the low viscosity of the binder at temperatures higher than 50°C. Hence, the aging mechanism needs to be modified to avoid draining of the binder during aging. Aging at low temperatures is disadvantageous since the aging time would be too long to achieve the same aging conditions as the long term aging of the binder in the field.

2.2.3 Summary

- During asphalt production (short term aging) the binder loses considerable mass (depending on the binder type) due to the loss of volatiles that alter the original binder properties. The sensitivity of different binders to aging can be distinguished by the loss of oily components during the short term aging, which is crucial to the subsequent performance of the binder.
- A dynamic binder aging test allows uniform aging (homogenous diffusion of oxygen) to take place. This could be important for polymer modified binders that tend to segregate during static aging. The RCAT aging protocol is a dynamic aging test used for long term binder aging. RCAT requires longer aging time than PAV (a static type of aging test) to conduct the test.
- Studies indicate that the aging behaviour of binders recovered from a porous asphalt pavement comply with binders aged using the RTFOT+RCAT procedure which supports the preference for RCAT aging method for PA. This implies that although the long term aging test using PAV reflects the static nature of the binder aging in the field it may not be a realistic aging method for PA.
- The MGRF test is suggested for use in the short term aging of bitumen to minimize material handling problems during testing. The RCAT aging method has the same advantage in addition to combining the short-term and long-term aging.
- A weatherometer that combines the effects of temperature, UV light, and humidity/moisture during aging seems a practical aging protocol to simulate field aging conditions of PA.

2.3 Durability and Chemical Composition of Binders

A durable binder can be described as having acceptable initial properties to contribute to pavement performance and with good aging behaviour in service. When a thin binder film in PA is exposed to atmospheric air (oxygen), oxidation reaction takes place that changes the chemical composition of the binder. Oxidation is an irreversible chemical reaction and is considered to be the dominant aging process during the service life (Kandhal and Chakraborty 1996).

The most important mechanism of age hardening is the change in the chemical composition of the binder molecules because of a reaction with the atmospheric oxygen both during asphalt production and during the service life of the pavement (Parmeggiani 2000). Binder durability is determined by the physical properties of the binder, which is a function of the chemical composition. An understanding of the chemical factors affecting physical properties is thus fundamental to understand the factors influencing asphalt durability.

2.3.1 Aging effect on Chemical Composition

Three fundamental composition-related factors govern the changes that could cause binder hardening in pavements (Peterson 2000):

1. Loss of oily components of the binder either by volatility (during short term aging) or absorption by porous aggregates in the asphalt mixture.
2. Changes in chemical composition of the binder molecules from reaction with atmospheric oxygen (oxidation – long term aging).
3. Molecular structuring that produces thixotropic effects (steric hardening).

Oxidation of unmodified bitumen

In dealing with binder durability, a major factor that must be addressed is the change that takes place in the chemical composition of the binder as a result of oxidative aging. Two approaches are used to describe the compositional nature of bitumen in view of their rheological behaviour, these are:

- Multiple-Phase System (Traditional Approach)

The traditional approach is based on the bitumen functional groups that are generally referred to as saturates, aromatics (non-polar), resins (polar aromatics), and asphaltenes (Figure 2.19). The bitumen is considered to comprise a semi solid phase consisting of asphaltenes, which is covered by a protective layer of polar aromatics (resins), which are dispersed in a liquid phase consisting of the lower molecular weight aromatics and saturates. The chemical bonding that holds the hydrocarbon molecules together when the material is subjected to heat or shear stress results in the viscoelastic characteristics of the bitumen (Gubler et al. 1999).

- Single-Phase System (SHRP Approach)

To describe the compositional nature of bitumen, SHRP introduced (SHRP-A-367 report) the assertion that bitumen is a continuous, homogeneous material whose flow characteristics and performance are based on molecular size distribution and the polar forces holding the molecules together. The molecular size distribution determines the basic rheological behaviour of the bitumen. The strength and distribution of the polar forces holding the molecules together determines the viscoelastic behaviour of bitumen when temperature or loading conditions change.

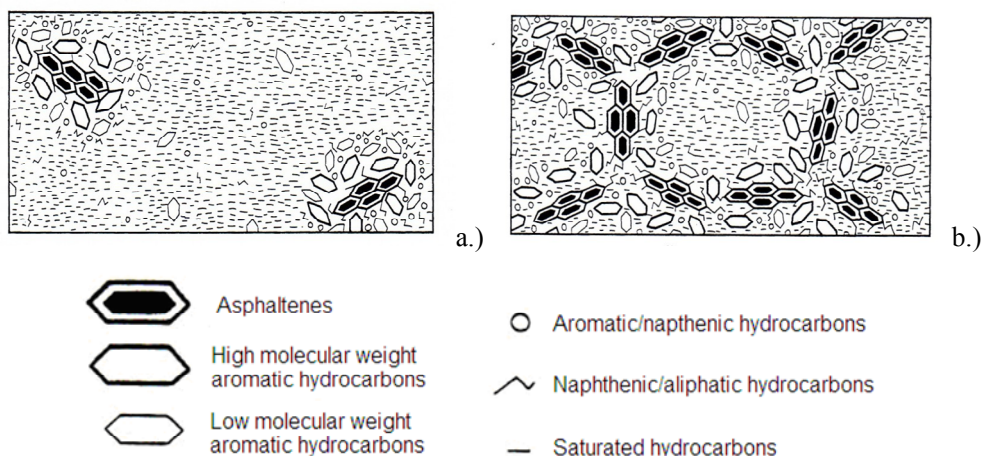


Figure 2.19: Schematic representation of SOL type and GEL type bitumen (Source: Read and Whiteoak 2003).

It has been widely recognized that a proper balance of chemical components is an important factor for the durability of binders. Bitumen is a complex mixture of organic molecules that vary widely in composition from non-polar saturated hydrocarbons to highly polar, highly condensed, aromatic ring systems. Although bitumen molecules are composed predominantly of carbon and hydrogen, most molecules contain one or more of the so-called heteroatoms: nitrogen, sulphur and oxygen together with trace amounts of metals, principally vanadium and nickel. The heteroatoms often impart functionality and polarity to the molecules, their presence may make a large contribution to the differences in physical properties among binders from different sources (Peterson 2000). Bitumen is considered as a dispersion of strongly associated polar molecules in a solvating medium composed of less polar bitumen molecules. Because polar molecules associate together, polar oxidation products greatly alter the state of dispersion of binder components, thus changing the mobility and, therefore, the chemical reactivity of binder molecules and its susceptibility to oxidation (Peterson and Harnsberger 1998).

In general, compositional change of bitumen during oxidative aging results in a development of polar fractions from non-polar components. This was also observed in a study conducted by Christopher et al. (1999) who reported that oxidation of bitumen causes the naphthene (non-polar) aromatics to form polar

aromatics (resins), and the polar aromatics to form asphaltenes; while saturates are considered to be non-reactive (Figure 2.20). Ishai et al. (1988) also reported, using a colloidal model (Gaestel Index, *IC*) that characterizes the chemical composition and colloidal structure of binders, that the saturate fraction remain unchanged (as shown in Figure 2.24), while the asphaltene content increases significantly at the expense of both the polar and naphthene-aromatics which decrease with aging. It is suggested that increasing the saturate fraction might limit reactive components in the bitumen and improve the resistance of the material to aging (Ishai et al. 1988).

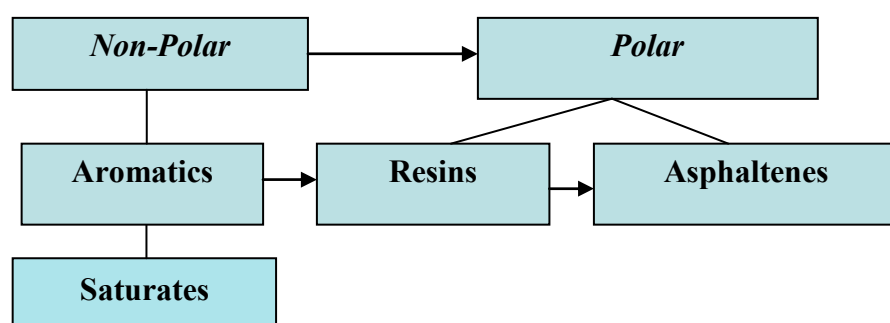


Figure 2.20: Schematic diagram showing movement of binder components towards more polar fractions

Analysis of the functional groups of a binder indicates that ketones and sulfoxides are the two major oxidation products formed during oxidative aging; anhydrides and carboxylic acids are also formed but in smaller amounts (Plancher et al. 1976). Figure 2.21 shows the chemical functionality in virgin bitumen molecules or formed due to oxidative aging.

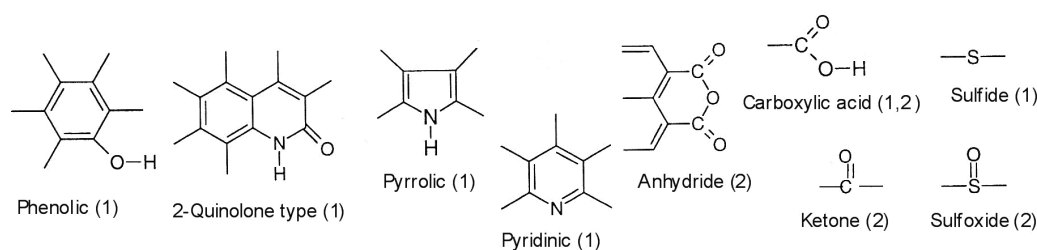


Figure 2.21: Chemical functionality in virgin bitumen molecules (1) or formed on oxidative aging (2) (Source: Peterson 2000)

According to Bell and Sosnovske (1994), bitumen aging is a complicated set of events involving oxidation at the molecular level and structuring at inter-molecular level. The two products of oxidation, i.e. ketones/carbonyl ($C=O$) and sulfoxides ($S=O$) (refer to Figure 2.21 and Figure 2.22), are formed by a slow oxidation reaction of the benzylic carbon during the reaction. Laboratory binder aging methods indicate that the ratio of ketones to sulfoxides formed and the rate of age hardening are dependant on the temperature and applied pressure (Bell and Sosnovske 1994; Peter and Harnsberger 1998), which shows the need to interrelate the laboratory aging techniques and field aging

conditions. Figure 2.22 shows the increase in the formation of ketones and sulfoxides as a function of aging time.

More severe oxidation produces carboxylic anhydrides and small amounts of other highly oxidized species. Further oxidative aging reduces structuring of the binder molecules, which implies that the rate of aging decreases with time at any given temperature. As temperature increase the amount of molecular structuring decreases resulting in an increase in reactivity and rate of oxidation (Bell and Sosnovske 1994). At much extended aging (severe oxidation) extreme hardening of the binder might occur. Hence, the way binder aging is simulated in the laboratory (accelerated aging) should be conducted in a manner that avoids severe aging that often occurs at elevated temperatures. Severe aging does not represent real aging in the field.

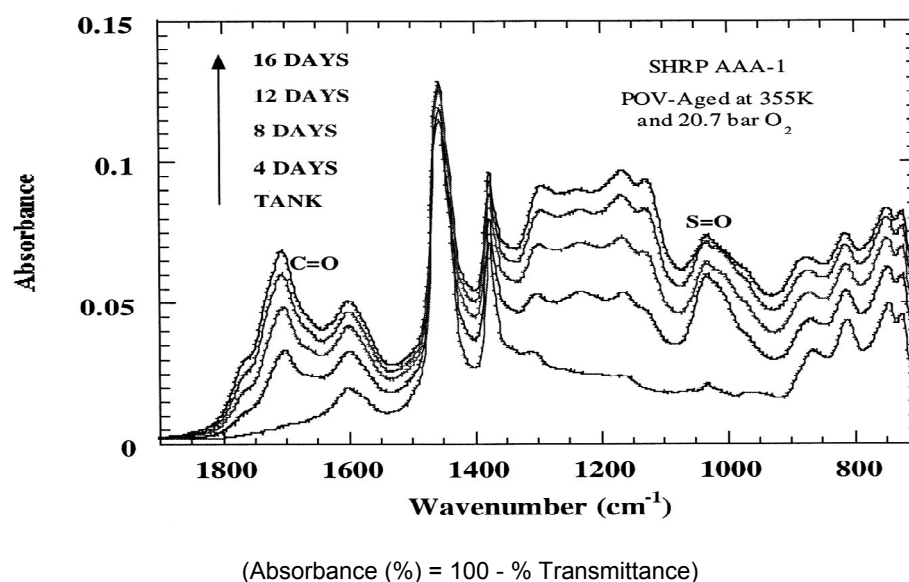


Figure 2.22: FTIR spectrum showing increase in carbonyl/ketone (1700 cm^{-1}) and Sulfoxide (1030 cm^{-1}) formation with aging (Source: Dome and et al, 1997).

Because ketones and sulfoxides are the major oxidation products, their sum indicates the relative degree of oxidation in binders. Sensitivity to oxidation is generally related to the sulphur content present. The rate of ketone formation decreases and sulfoxide formation increases for binders with higher sulphur content. Ketone concentration due to oxidation is strongly related to the increase in viscosity of the binder. Higher amount of ketones appear to be formed at the expense of sulfoxides at higher temperatures and ketone formation rate decreases with increasing viscosity (Peter and Harnsberger 1998).

The amount of hetro-atoms in bitumen varies between less than 1% and 5% depending on the source of the bitumen. High vanadium content is generally present in binders with high amount of hetro-atoms. According to Bell and Sosnovske 1994, severe hardening (aging) of binders could result from the

presence of high vanadium content because of its likely role as catalyst for oxidation.

Oxidation of Polymer Modified Binders (PMBs)

The rheological change of modified binders is dependant on a combined effect of bitumen oxidation (aging) and polymer degradation, which varies with the types of bitumen and polymer as well as the polymer content. From literature it is known that the accelerated aging of PMBs results in degradation (break-up) of the polymer (Isaccson and Lu 1999; Khalid and Walsh 1997). Thus, simulation of long term aging at elevated temperatures might not represent the “natural aging” process in real life due to the effect of apparent degradation of PMBs. Breakdown or degradation of the polymer upon aging reduces the number of large polymer molecules, and consequently reduce the effectiveness of the polymer to effectively modify the bitumen rheological properties (Isaccson and Lu 1999). On the other hand, breaking down of the polymer is believed to produce a reduction in viscosity which partially balances the hardening of the base bitumen thus enhancing resistance to age hardening.

The effect of polymer breakdown or degradation upon oxidative aging of modified binders (modified with EVA (plastomer) and SBS (elastomer) type of polymers) was verified in the study conducted by Khalid and Walsh (1997). They reported that the RTFOT short term aging of the PMB binder resulted in more aging than the long term aging, which is inconsistent with the principles of the respective tests. The two aging tests represent aging in a newly laid pavement and LTA after about 10 year service life respectively. The inconsistency in aging might be explained by the degradation of the polymer upon aging. An increasing content of functional groups as a result of polymer degradation may also change bitumen polarity and molecular association; as a result, the compatibility (micro structure) between polymer and bitumen might also be changed (Isaccson and Lu 1999).

2.3.2 Influence of Mineral Aggregates on Aging

The influence of interaction of binders with mineral aggregates during the oxidation process has been a subject of research. The role of aggregates in influencing the aging mechanism comes mainly from their influence, either physically or chemically, on the highly polar components of the binder. A literature survey by Anderson et al. (1994) indicates that aggregates, depending on their mineral composition, may have a dual role in binder oxidation: 1.) they may work as catalysts promoting the formation of the oxidation products in the low polar generic fractions (saturates and naphthalene aromatics), or 2.) they may absorb the highly polar fractions making them less oxidizable. Adsorption of the highly polar fractions isolates them at the mineral surface inhibiting their reaction with oxygen and, at the same time, reduces their catalytic effect in promoting the oxidation of saturates and naphthalene aromatics.

The rate and degree of chemical reaction between the binder and aggregates depends not only on the type of binder, but also on the surface charge of aggregates. The surface charge of aggregates is related to their chemical composition and crystalline structure. In general, aggregates with increased silica dioxide content (aggregates containing more than 65% silica, SiO_2 , are termed as acidic) cause an increase in polarity of the stone surface and reduce adhesion. Siliceous aggregates, usually termed as “acidic” aggregates (such as quartz, granite, and porphyry), are negatively charged at the surface while calcareous aggregate (which are described as “basic” such as calcite and basalt) are positively charged at the surface (Su 1996). Aggregates with the least adsorption of highly polar fractions (e.g. Quartzite) exhibit the greatest catalytic effect in asphalt oxidation, those showing the largest adsorption (e.g. Limestone) exhibited the smallest catalytic effect (Anderson et al. 1994; Read and Whiteoak 2003). A SHRP report (SHRP-A-341) indicates that the presence of mineral matter (filler, sand and aggregates) delays the increase of the viscosity of binders upon aging compared to bulk bitumen aging for equivalent aging times. This difference in viscosity is thought to have been caused by the aggregate particles holding some of the oxidative functional groups that prevent formation of viscosity build-up. The difference in diffusion process between the bulk bitumen and bitumen/aggregate systems may also contribute to this end.

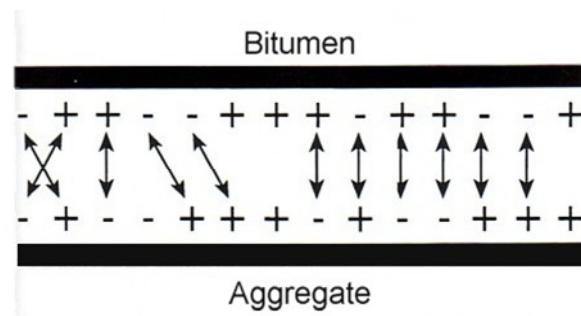


Figure 2.23: Chemical interaction between bitumen / aggregate system

The adhesion of the binder to the aggregate must be maintained for enhanced performance of the pavement. The chemistry between the bitumen and aggregate interface leads to bonding interactions that influence the ultimate adhesive strength. The polar functionalities present at the contact between the asphalt film and the aggregate surface adhere to the surface through electrostatic forces, hydrogen bonding, or van der Waals interactions. The adhesion of bitumen to the aggregate surface is dependant on the types of functionalities at the interface and on their ability to bond strongly to the surface (Figure 2.23). The resistance of the bond to environmental factors, particularly the intrusion of water, is essential for maintaining long pavement life. Water may attack the binder-aggregate bond by seeping through cracks in the binder and competing for the active sites on the aggregate or by being present in aggregate pores and diffusing into the interface. Once water enters in the bond formations with the aggregate constituents, the binder functional groups (such as carboxylic acid and phenolic) combine with alkali metals

present on the aggregate surface to form water-soluble salts. These bitumen-aggregate bonds are ionic bonds that weaken or solubilize over time with exposure to moisture (Curtis et al. 1993).

2.3.3 Indicators of Compositional Changes

A proper compositional and chemical analysis of binders before and after aging can provide significant information in terms of the aging sensitivity or age-hardening behaviour of binders. Binders exposed to age-hardening (RTFOT, PAV tests) show an increase in the so called Gaestel Index (IC), an expression of the chemical composition of the binder that explains its internal colloidal structure (Ishai et al. 1988; Ishai 1996). The Gaestel Index is given in Equation 2.13.

$$IC = \frac{\text{Asphaltenes} + \text{Saturates}}{\text{Aromatics} + \text{Resins}} \quad (2.13)$$

The use of the colloidal structure model for the compositional analysis implies that major changes in the initial, rheological, and aging properties of the binder are expressed by the creation of new levels of colloidal stability compatible with the new structure of the binder. It is believed that the relationship between asphalt colloidal stability characteristics and age hardening, molecular weight distribution, rheological behaviour, and other physical properties of the binder, may provide meaningful explanation of the long term aging behaviour of the binder; it may also provide a tool for a better prediction of asphalt durability or performance in the field (Ishai et al. 1988).

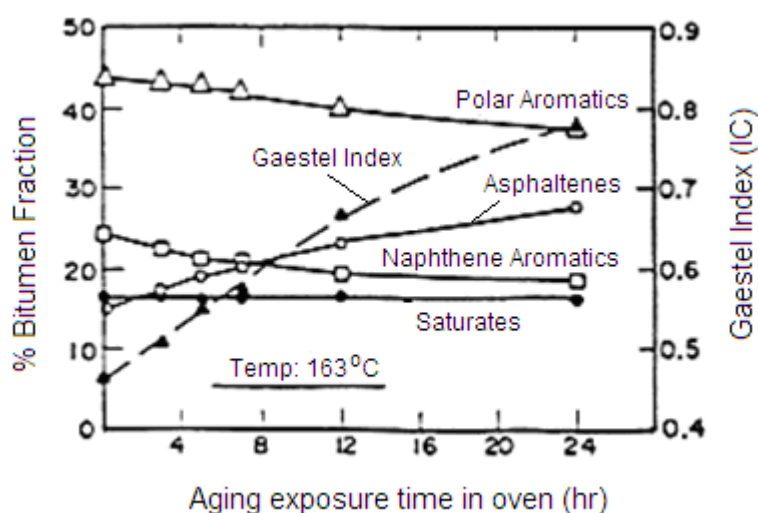


Figure 2.24: Changes in functional groups of bitumen during aging (Source: Ishai 1996).

An increase in IC after age-hardening is mainly due to an increase in the polar functional groups (the asphaltene content) and a decrease in the polar aromatics and non-polar (naphthene) aromatics functional groups (Figure 2.12, Figure 2.24). Hence, a change in the colloidal structure after long-term aging as expressed by the IC ratio may reflect the level of aging sensitivity of different

types of binders. Oxidative aging also causes an increase in the viscosity of the binder. Domke et al. (1997) showed that the logarithm of the viscosity ($\ln \eta$) varies linearly with the carbonyl area (ketone) determined by Fourier Transform Infrared spectroscopy test (FTIR). The slope of this line is designated as the Hardening Susceptibility (HS), which indicates the degree of binder aging. The value of the HS is found to be pressure dependant but not strongly dependent on oxidation temperature lower than 100°C (Domke et al. 1997). The expression of HS is given in Equation 2.14:

$$HS = \frac{d(\ln \eta)}{d(\%AS)} \frac{d(\%AS)}{dCA} = \frac{d(\ln \eta)}{dCA} \quad (2.14)$$

where:

HS	=	Hardening Susceptibility,
CA	=	carbonyl area (area under the C=O peak at wavenumber 1700 cm ⁻¹ of the infrared spectra of bitumen),
η	=	viscosity,
$\%AS$	=	the amount of asphaltenes present in the asphalt,
$d(\ln \eta)/d(\%AS)$	=	change in viscosity with respect to asphaltene content,
$d(\%AS)/dCA$	=	asphaltene formation susceptibility (AFS).

The asphaltene formation susceptibility (AFS) indicates the susceptible of the binder to the formation of asphaltenes due to the oxidation process.

Changes in molecular weight distribution and carbonyl formation as a result of binder oxidation (age hardening) can be determined from Gel-Permeation Chromatography (GPC) and Infra-red spectrum (FTIR) tests respectively. Nuclear Magnetic Resonance (NMR) is also one among many other types of chemical tests helpful to quantify the chemical composition of materials. The GPC and IR test methods are considered for use as a research tool in this study and are discussed in more detail here after.

Gel-Permeation Chromatography

The Gel Permeation Chromatography (GPC) is generally used to characterise the molecular weight distribution of binders. It is an analytical method that provides essential information on the molecular weight distribution of original and aged binders. Aging results in a shift towards the higher molecular weight as shown in Figure 2.25. Oxidative aging causes formation of more polar molecules at the expense of the lower weight molecules. Figure 2.25 shows the molecular weight distribution before and after aging of bitumen recovered from PA pavement.

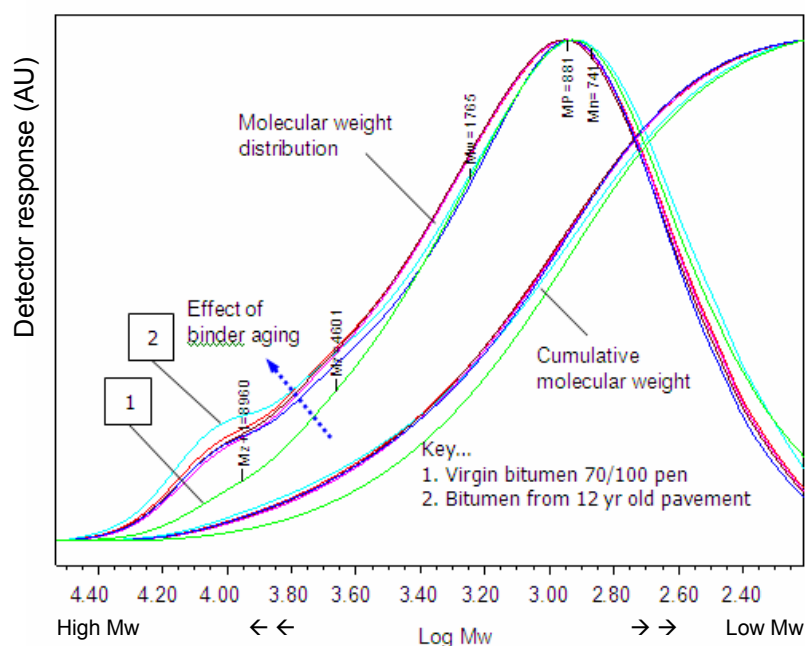


Figure 2.25: GPC test result of molecular weight distribution of binders before and after aging.

Infra-red Spectroscopy (FTIR)

Binder oxidation causes formation of functional groups which are characterized by the growth in the infra red carbonyl and sulfoxide peaks. The infra red absorption at 1700 cm^{-1} represents carbonyl formation (C=O) and at 1030 cm^{-1} represents sulfoxide formation (S=O), which are characteristic of chemical bonds formed by the oxidation process (refer to Figure 2.21). It should be noted, however, that the growth of carbonyl and sulfoxide formation represent only the major portion of the spectral change during oxidation (Domke et al. 1997). The increase in the area under the carbonyl (ketone) and sulfoxide peaks are usually used to describe the degree of binder aging.

2.3.4 Summary

- Oxidation is an irreversible chemical process that changes the molecular composition of binders increasing the binder hardness or stiffness. Compositional change due to oxidative aging results in the transformation of components from non-polar to more polar fractions. The formation of polar products alters the state of dispersion of the binder chemical components which also change the chemical reactivity because of change in the mobility of the molecules.
- The presence of hetro-atoms in bitumen contributes to the difference in physical properties and their aging behaviour. Binders from different sources have different amounts of hetro-atoms. The presence of vanadium in higher quantity is also considered to be indicator for susceptibility of binders to oxidation.

- The fraction of saturates is considered non-reactive in the process of oxidative reaction, hence, increasing this fraction in the binder composition might provide a means to improve the resistance to aging of bitumen.
- Ketones also known as carbonyl (C = O) and sulfoxides (S = O) are the two major functional groups formed during oxidative aging; they are recognized by their characteristic peaks at 1700 cm⁻¹ and 1030 cm⁻¹ wave number in the IR spectrum respectively. The formation of ketones and sulfoxides increases as a function of aging period and the sum of area under the IR peaks can be used as an indication for relative sensitivity of binders to oxidative aging.
- Aging of PMB is dependent on oxidation of the bitumen and degradation (breakdown) of the polymer. The breakdown of polymer molecules upon aging reduces the number of large polymer molecules reducing the effectiveness of the polymer to modify the binder properties; but may contribute to delay the aging of the binder.
- Aggregates, depending on their mineral composition, may have a dual role in binder oxidation: 1) as a catalyst promoting the formation of the oxidation products (ketones and sulfoxides) in the low polar generic fractions, 2) they may absorb the highly polar fractions making them less oxidizable. The adhesion of bitumen to the aggregate surface is dependent on the types of functionalities at the interface and their ability to bond strongly to the surface.
- The colloidal structure (chemical composition) of the binder indicates the balance of the binder compositional components which can be used as an indication of the stability of the binder. The Gaestel Index (IC) is the measure used as colloidal stability indicator. The GPC and IR tests are useful testing methods to indicate the chemical changes caused by oxidative aging of binders and provide both qualitative and quantitative data in determining the extent of age hardening.

2.4 Prediction of Binder Durability

2.4.1 Empirical Approach

Mathematically, the changes in the physical properties, which have been known to affect pavement performance, follow a hyperbolic function with time and approach a definite limit as time increases. The equation that expresses the age hardening of bitumen in the road can be expressed by Equation 2.15 (Roberts et al. 1996):

$$\Delta Y = \frac{t}{a + bt} \quad \Rightarrow \quad \frac{t}{\Delta Y} = a + bt \quad (2.15)$$

Where:

ΔY = change in binder property (such as pen and viscosity) with time t or the difference between the zero-life value and the value at any significant time,

t	=	time,
a	=	constant, the intercept of the equation line on the ordinate,
b	=	slope of the equation line,
$1/b$	=	ultimate change of property (limiting value of change) at infinite time.

This simple model does not seem to adequately predict the binder aging behaviour with time due to the complexity of the changes in binder property as a result of age hardening. The susceptibility of bituminous binders and polymer-modified bitumen (PMB) to hardening is not the same under accelerated laboratory aging (short and long term aging) and the field aging conditions.

2.4.2 Aging Prediction using the Kinetic Approach

It is assumed that the service life of an asphalt surfacing course can be extended if the aging resistance behaviour of the binder is enhanced. The kinetic approach can be used as a tool to assess the effectiveness of binder modification to improve the aging behaviour of the bitumen. The kinetic approach is a method used to predict the rate of change of binder properties due to accelerated aging in the laboratory or the aging of the binder in asphalt pavements. With this approach, developments in binder characteristics such as penetration, softening point (ring and ball temperature, T_{RB}), viscosity, and asphaltenes content can be described effectively.

A one-dimensional diffusion model resulted in best fits for reaction indicators such as asphaltene content (AS), and softening point (T_{RB}) for tests performed below 100°C. Equation 2.16 is the corresponding equation (Verhasselt and Choquet 1997; Verhasselt 2000):

$$\alpha^n = \left[\frac{S_t - S_0}{S_f - S_0} \right]^n = \left(\frac{dS_t}{dS_\infty} \right)^n = k \times t \quad (2.16)$$

Where:

α	=	the extent of reaction,
S_0	=	values of the signal or indicator S at times $t = 0$,
S_t	=	values of the signal or indicator S at times $t = t$,
S_f	=	values of the signal or indicator S at the end of the reaction,
k	=	the reaction constant,
n	=	aging coefficient, $n = 2$ for tests performed below 100°C and $n \approx 3/2$ for tests performed above 100°C.

Equation 2.16 can be reduced to a more practical equation (Equation 2.17):

$$\begin{aligned}
\frac{dS_t^n}{dS_\infty^n} &= k \cdot t &\Rightarrow & dS_t^n = (dS_\infty^n \cdot k) \cdot t \\
&&\Rightarrow & dS_t^n = K \cdot t &\text{Where: } K = (dS_\infty^n \cdot k) \\
&&\Rightarrow & dS_t = S_t - S_0 = (K \cdot t)^{1/n} \\
&&\Rightarrow & S_t = S_0 + (K \cdot t)^r &\text{Where: } r = 1/n
\end{aligned}$$

$$S_t = S_0 + (K^r \times t^r) \quad (2.17)$$

Where:

K = overall reaction constant,
 r = $1/n$.

When K results from an aging test performed at a given temperature T , it may be recommended to specify it with an index, K_T . When overall reaction constants, K_T , are known for different test temperatures, the activation energy (E) can be calculated from these values by applying the Arrhenius equation (Equation 2.18):

$$K_T = A \times e^{-E/RT} \quad (2.18)$$

Where:

K_T = overall reaction constant of aging at temperature T ,
 A = a constant (frequency factor),
 E = activation energy
 (E ranges between 68,500 and 86,400 KJ.°K/mole),
 R = perfect gas constant (8.314 J.K⁻¹mol⁻¹),
 T = absolute temperature (°K).

Because of the activation energy, equal time of aging at various temperatures will contribute in different ways to the aging of the binder. As a result of temperature variations in the field, the total in-service aging will be the sum of a series of partial aging processes in which the contribution of a particular temperature will depend on the time of exposure. The sum of the partial aging is equivalent to an identical aging obtained at a certain constant temperature, T_k , called “*annual kinetic mean temperature*”. Note that higher temperatures contribute the most to binder aging, which implies that most of the aging can be said to happen during summer periods.

The activation energy is a very important parameter to correlate the laboratory aging processes with the field aging. Knowing the activation energy and the kinetic mean temperature (T_k), extrapolation of the overall reaction constants

determined in the laboratory to field conditions is possible. These extrapolated constants are corrected using Equation 2.19.

$$K_{actual} = G \times P \times R \times K_{extrapolated} \quad (2.19)$$

Where:

K_{actual}	=	reaction constant in the field.
G	=	correction factor to account for the type of gas used in the test, e.g. for RCAT test $G = K_{air} / K_{oxygen}$.
P	=	correction factor to account for the pressure used in the test, $P = P_{air} / P_{test}$.
R	=	correction factor for the rotation rate of the type of test conducted.
$K_{extrapolated}$	=	reaction constant for a given exposure temperature.

Various laboratory tests using RCAT aging have yielded values for these factors to be on average $G = 0.57$, $P = 1$, and $R = 0.88$, which means that K_{actual} roughly equals $0.5 \times K_{extrapolated}$ (Verhasselt and Choquet 1997; Verhasselt 2000).

2.5 Effect of Binder Film Thickness on Aging

Achieving thicker binder film thickness is believed to result in stronger resistance to oxidation, resulting in delayed hardening and improved fatigue resistance. The reason, according to Heslope and Catt 1997, is that a thick binder film keeps binder hardening to a minimum because of longer time required for oxygen to penetrate the thicker binder film. Binder film thickness plays an important role in the oxidation process of the bitumen since oxidation is a chemical process that is a function of the diffusion of oxygen, which varies with the consistency or viscosity of the binder. Temperature and pressure are factors that affect the rate of diffusion of oxygen (in service) and thus the aging rate (Anderson et al. 1994). Fick's law of diffusion could be applied to determine the rate of diffusion of oxygen into the binder film (Equation 2.20). The rate of diffusion decreases with thicker binder films; in other words, longer time is required for oxygen to diffuse.

$$J = \begin{cases} -D \cdot \frac{dc}{dx} & \rightarrow \text{one dimensional} \\ -D \cdot \nabla c & \rightarrow \text{two dimensional} \end{cases} \quad (\text{Fick's law of diffusion}) \quad (2.20)$$

Where:

Fick's law as applied to oxygen-bitumen system,

J	=	diffusion of oxygen [mol/m ² s].
D	=	diffusion coefficient of oxygen in bitumen [m ² /s].
c	=	the concentration of oxygen in bitumen [mol/m ³].

x = concentration gradient for diffusion of oxygen (thickness of binder film).

In general, thicker binder films produce mixtures that are flexible and durable, whereas thin films are likely to produce mixtures that are brittle (at low temperature), tend to crack and ravel excessively, retard pavement performance and reduce useful service life. In view of this, increasing the binder content is believed to increase the durability of the binder and the asphalt mixture (Heslop and Catt 1997). Despite its positive side, however, care should be taken to increase the binder content in PA for two main reasons: 1. the limited amount of filler will probably restrict the need to increase the binder content because of likely drainage problems, and 2. the voids content of the mixture may be reduced as a result of increase in binder film thickness.

2.5.1 Effect of Polymer Modification

The main purpose of modifying bitumen with polymer is to improve the binder properties. The proportion of the viscous and elastic components of the binder determines the viscoelastic properties of the binder over a wide range of temperatures and loading conditions. The viscoelastic properties of the binder can be influenced by the modification of the binder to attain enhanced properties.

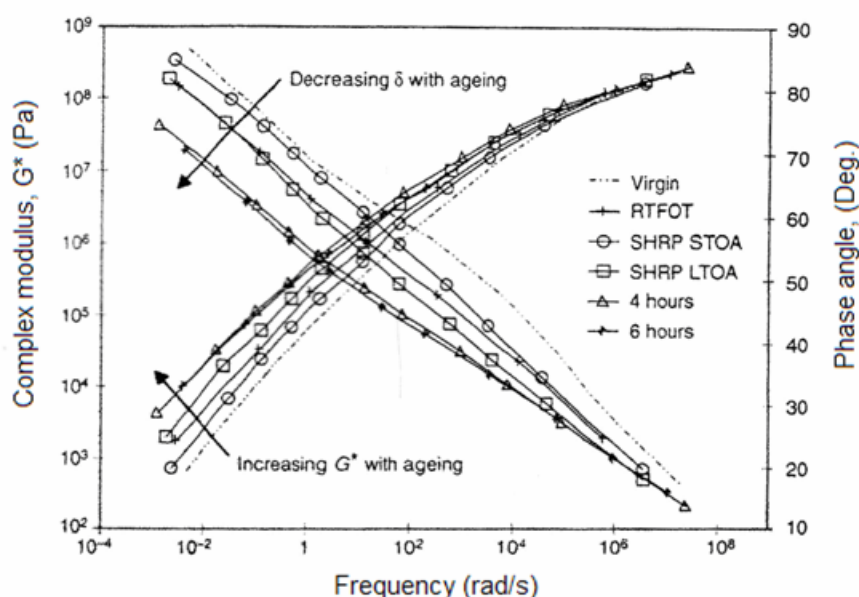
The use of Polymer Modified Bitumen (PMB) in PA is recommended since coating of the aggregates with relatively thicker binder film can be achieved with the modified binder. The temperature susceptibility of the bitumen is reduced by the addition of the polymer. PMB also improves the binder's resistance to aging. Similarly, fibres are believed to contribute to the durability of PA. The advantage of fibre application in PA is discussed in detail in Section 2.5.3.

It is assumed that the cohesive properties of the binder and/or adhesive properties of the binder/aggregate system can be improved with a thicker binder film. This also implies improved resistance to ravelling of the porous asphalt mixture. The mechanism of aging in PMB is explained by the degradation (breaking-down) of the polymer to smaller molecules counteracting the hardening process of the binder (Isaccson and Lu 1999). However, according to Heslop and Catt 1997 the effectiveness of the polymer in modifying the binder is regarded as reduced by the degradation.

Khalid et al (1998) determined porous asphalt mixture performance using a Cantabro test in which mixtures with modified binders showed better performance. His performance rating was in the order of SBS bitumen, EVA bitumen, and plane bitumen.

The effect of aging can also be studied through the changes in the rheological properties of the binder. In a dynamic shear test (DSR), the effect of aging

results in an increase in the complex modulus and a decrease in the phase angle indicating that the aged binder becomes more elastic³. For modified binders, change in elasticity is dependent on the frequency considered. Figure 2.26 and Figure 2.27 reveal differences in the complex modulus master curves for SBS modified bitumen compared to EVA modified bitumen. The difference is more apparent in the phase angle master curve. The observed difference can be explained by the degradation of the SBS polymer during the oxidation process.



Key:

- Virgin = virgin bitumen
- RTFOT = short term bitumen aging (Rotating Thin Film Oven Test)
- STOA = short term oven aging of asphalt mixture (SHRP spec.)
- LTOA = long term oven aging of asphalt mixture (SHRP spec.)
- 4 hours = aging time of 4 hours, and
- 6 hours = aging time of 6 hours

Figure 2.26: Complex modulus and phase angle master curve of EVA modified binder (Khalid et al. 1998).

³ By elastic, it is meant that the material increase in storage modulus upon aging. At solid state (at the glassy modulus) the material is considered elastic, which does not necessarily mean flexible but hard and probably brittle.

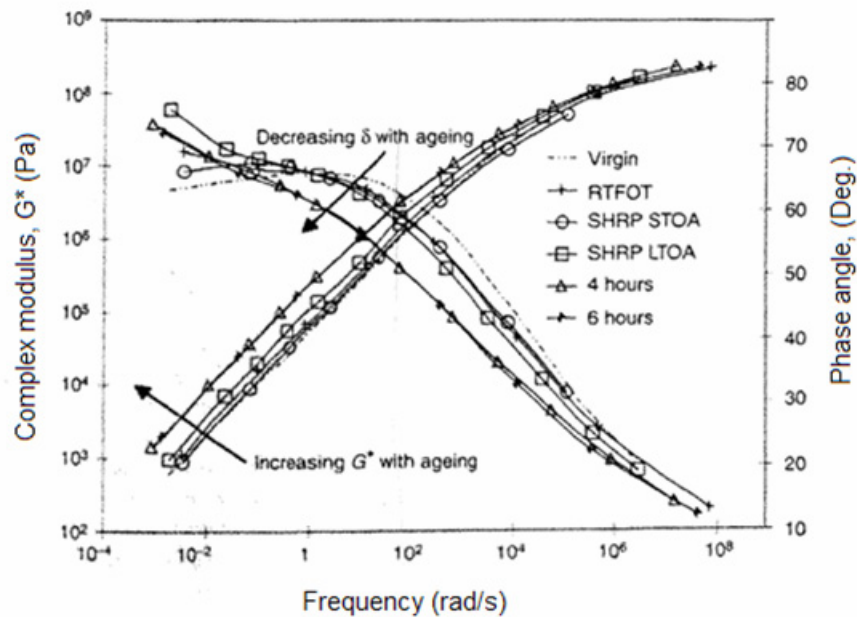


Figure 2.27: Complex modulus and phase angle master curve of SBS modified binder (Khalid et al. 1998).

As mentioned earlier, studies indicate that oxidation degrades the polymer in PMB's (Isaccson and Lu 1999; Wegan and Brule 1999). For SBS bitumen, oxidation increases the viscosity of the base bitumen, which forms the bulk of the binder, and causes break-down of the SBS polymer. Polymer degradation produces a reduction in viscosity which partially balances the hardening of the base bitumen (Oliver and Tredrea 1997). In the case of EVA bitumen, the polymer network seems to partially disintegrate during oxidation because of weaker compatibility between the EVA chains and the oxidised base bitumen molecules. The fact that the EVA network is not fully destroyed during the oxidation process is an indication of a remaining cohesion (Mouillet et al. 2003). In general, it can be said that the application of a PMB retards the hardening process and/or enhances the binder's resistance to oxidation due to a thicker binder film around aggregates which is possible because of increased viscosity/consistency of the binder through modification. From the aging behaviour of the SBS and EVA polymers, it seems that the application of SBS modified bitumen can improve the aging behaviour of PA.

Increased viscosity of the binder may not be the only factor that should be considered to evaluate the performance of modified binders. After undergoing aging, the change in property of the modified binder, either an SBS or EVA modified bitumen, can be determined by the use of molecular size distribution before and after aging using Gel-Permeation Chromatography (GPC) tests to assess the effect of oxidation on the molecular structure of the materials. Similarly, the infrared (IR) spectroscopy test can provide the material's response to absorption of infrared light, which can be used to understand the changes in the functional groups of the binder as a result of aging. A research

recently conducted by Mouillet et al (2003) used a newly developed aging cell that is combined with FTIR spectroscopy, which appears to be a very effective tool to observe and study the chemical microstructure changes of unmodified bitumen and PMB during the aging process.

2.5.2 Effect of Filler on Mastic Characteristics

The filler, as one of the ingredients in bituminous mixtures, plays a major role in the behaviour of the asphalt mixture. Filler (fines) influence pavement performance in different ways (Kandhal et al. 1998):

1. Depending on the particle size, fines can act as filler or an extender of the binder.
2. Fillers have considerable effect in stiffening the binder influencing the pavement performance including its fracture behaviour and resistance to permanent deformation.

Since fillers in binders behave as extenders with the effect of increasing the stiffness of the binder film around the aggregates, they might help in improving the resistance to ravelling.

The change in the binder property depends on the following factors (Kavusi and Hicks 1997):

1. Type of filler (e.g. limestone, quartzite, etc...).
2. Nature of filler (e.g. its physio-chemical property, i.e. acidic/basic nature).
3. Concentration of filler in the mixture.

The micro structure of bitumen asphalt system is shown in Figure 2.28.

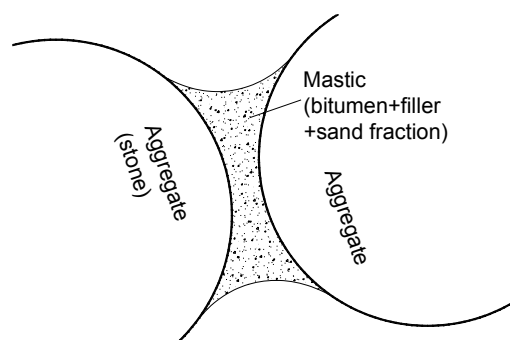


Figure 2.28: Micro-structure of the bitumen aggregate system

As far as oxidation and hardening of binders is concerned, fillers influence the asphalt binder by at least two mechanisms. Fillers, in the same way as the aggregates and sand, act as a catalyst and enhance oxidation or hinder diffusion and prevent reaction with oxygen, which reduces oxidative aging (Gubler et al. 1999). According to the study by Gubler et al. 1999, fillers might influence the aging of a binder by promoting oxidation or side reactions such as dehydration or polymerization. This effect was observed by the change in the aging index and some rheological indicators in the presence and absence of the mineral

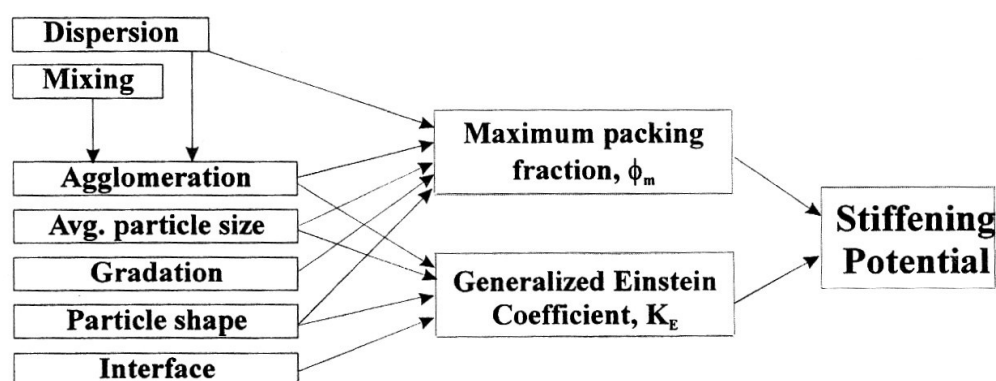
filler. On the other hand, the presence of mineral filler may retard the aging (oxidation) process by hindering the diffusion of oxygen into the mastic.

Type and Nature of Filler

The type and nature of filler especially material passing no. 200 (75 μm) appeared to have an effect on the properties and performance of binders. Studies indicate that the nature of the filler, i.e. its acidic or basic nature, may influence the aging behaviour of asphalt mixtures. The fines vary in gradation, particle shape, surface area, void content, mineral composition, and physiochemical properties, which influence in different ways the properties of an asphalt mixture and its aging resistance (Kandhal et al. 1998). Besides, the interaction between the filler and binder has an effect on the mechanical properties of mixtures by influencing the workability, compaction characteristics, voids in the mixture (binder film thickness in the case of porous asphalt), stiffness and strength (Kavusi and Hicks 1997). For these reasons it is important to characterise the fines.

A study by Kandhal et al. (1998) indicated that the effect of filler (P200 material, i.e. percentage passing sieve size 0.075 mm) in stiffening binders appears to be high. The smaller the size of P200 (especially at D10, which refers to the particle diameter corresponding to 10% pass in the particle size distribution curve) the more the binder is being modified and/or extended and thus increases the stripping resistance of an asphalt mixture. Similarly, Shashidhar et al. (1999) showed that the stiffening effect of fillers increases with increasing amount of material below 10 μm particle size. Kandhal et al. (1998) also reported that the fineness of the P200 material (as described by D10) has a significant effect on the retained tensile strength (TSR). TSR increases as the P200 becomes finer, i.e. D10 decreases. It appears that very fine size P200 at 10 percent passing level is stiffening the filler-asphalt binder or mastic and increases the resistance to stripping. In other words, finer fillers have more absorptivity potential in binders and thus produce the highest viscosity values at a given temperature. These fillers have large specific area (low voids content) and are designated as “strong” fillers since they have greater potential to adsorb bitumen. Conversely, fillers with larger particles are less incorporated into the bitumen due to their lower specific area (relatively high voids content) and are designated as “weak” fillers.

Figure 2.29 shows schematically the effect of filler geometry and dispersion during the mixing process on the stiffening potential of the binder/mastic and thus resistance to stripping.



ϕ_m = max. amount of filler that can be added to bitumen without introducing air voids.

K_E (Generalised Einstein Coefficient) = stiffening rate of the mastic as a function of filler addition.

Figure 2.29: Schematic diagram illustrating the factors affecting the stiffening potential (Shashidhar et al. 1999).

Filler/Bitumen (f/b) ratio / concentration

According to the bitumen-filler concept, originally proposed by Rigden, the binder in the mastic is assumed to be either “free” or “bound/fixed”. Figure 2.30 shows the fractional voids in a bitumen-filler system. The “bound” binder is the amount of binder that fills the space (voids) between the filler particles without changing its bulk volume (maximum packing configuration). Free binder is the amount of binder in addition to that used to fill the voids between the particles at the filler’s densest dry packing configuration. Thus, the “free” binder is free to lubricate the mastic and to allow the mastic to flow under applied stress (Shashindhar et al. 1999).

The voids content in fines compacted to maximum density, i.e. the Rigden voids, have been used by researchers to characterize fines. Void content is regulated by four basic properties of the fines, which are the particle shape, particle size, particle size distribution, and particle surface structure. The voids content in fillers, i.e. Rigden voids, that takes into consideration the filler geometry, is given by Equation 2.21.

$$V, \text{ percent} = 100 \left[1 - \frac{G_{fB}}{G_{fS}} \right] \quad (2.21)$$

Where:

G_{fB} = bulk specific gravity.

G_{fS} = apparent specific gravity (AASHTO T133).

V = void content [%].

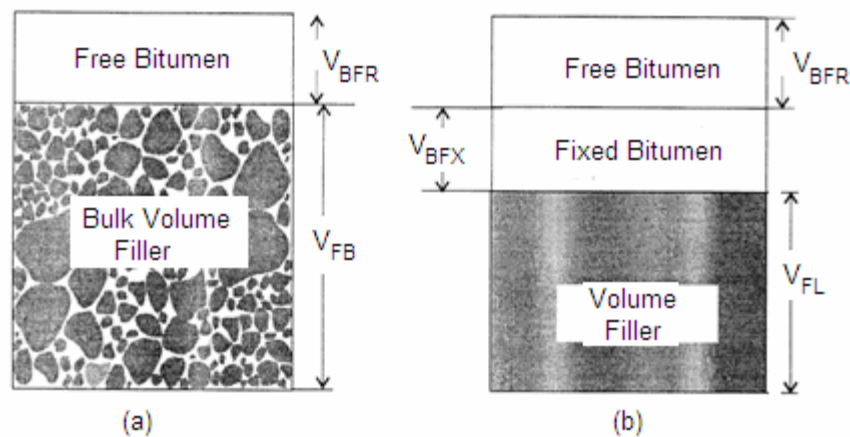


Figure 2.30: A schematic of fractional voids in bitumen-filler system. The subscripts are A_{FR} = free asphalt, F_L = filler, and A_{FX} = fixed asphalt (Source: Shashindhar et al. 1999)

However, there is a critic that the Rigden voids do not take into account agglomeration, degree of dispersion, and binder-filler interface contributions (Shashindhar et al. 1999). It is understood that the effectiveness of fillers in modifying binders depends among other factors such as the uniformity of dispersion of the filler in the binder. Agglomeration (poor dispersion of the filler) occurs mainly due to mixing problems and has a negative effect on the performance and durability of asphalt mixtures.

Several investigations of bitumen-filler systems indicate that fillers with different nature blended with different types of binders to form mastic behave differently (Gubler et al. 1999; Kavusi and Hicks 1997; Shashidhar et al. 1999). However, an increase in filler content generally will result in an increase in stiffness of an asphalt mixture till optimum filler concentration is reached, after which the stiffness decreases again. At this peak, the material requires the greatest amount of energy to reach failure. The study by Kavusi and Hicks (1997) on four types of fillers showed that the maximum fracture energy (toughness) corresponds to a filler/bitumen (f/b) ratio of 0.25 – 0.75 by weight depending on the voids of the filler while the practical ratio seems to be in the range of 0.5 – 1.5 by weight. This implies that the practical range for optimum performance need to be adjusted. The lowest f/b ratio is related to fillers with high voids content and the highest f/b ratio corresponds to lower filler voids content. The increased stiffness of an asphalt mixture due to the addition of filler is particularly critical at low temperatures where bituminous mixtures become brittle. Under these conditions, the combined effect of low temperatures and heavy traffic loading will result in susceptibility to cracking of the mixture.

The Belgian Road and Research Centre (BRRC) have included in its asphalt mixture design software – PRADO (Program for Road Asphalt Design and Optimization developed to promote practical use of a mix design method in Belgium) the criteria for the softening point of the mastic which strongly

depends on the amount and voids content of the fines. Accordingly, the viscosity of the mastic is strongly influenced by the amount and type of bitumen. Figure 2.31 shows the optimum range of f/b ratio depending on the effect of the voids content of the filler and the difference in the softening point of the mastic and pure bitumen $\Delta(T_{RB(mastic)} - T_{RB(bitumen)})$. The composition of the mastic should fall within the recommended range of the difference in softening point, i.e. between 12°C to 16°C, as indicated by the white area in Figure 2.31.

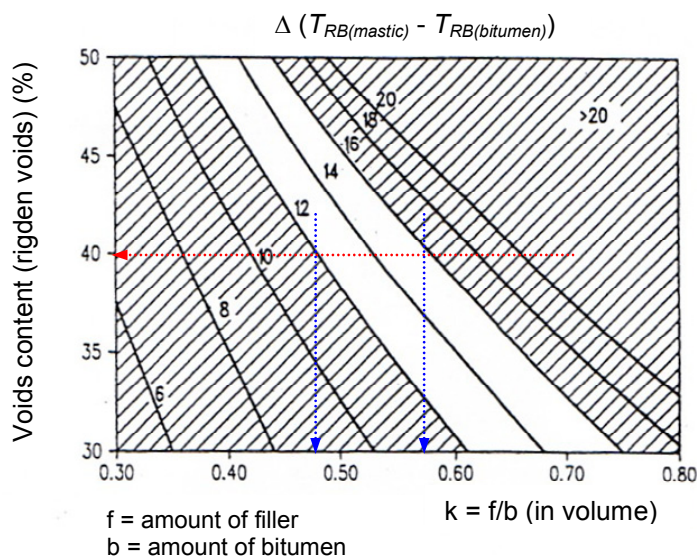


Figure 2.31: The effect of the amount of filler and its voids content on the softening point (Source: asphalt mixture design PRADO).

NB: In Figure 2.31, the $\Delta(T_{RB})$ lines are dependant on the filler and bitumen type and may show a shift depending on the mastic property.

2.5.3 Effect of Fibres on Aging

The use of fibres to reinforce binders has long been in practice. The effect of fibres in improving binder performance has also been the subject of research. Essentially, the main objective of using fibres is to improve the aging behaviour of the bitumen by achieving thicker binder film and preventing drain-off of the mastic in such a way that it may significantly improve the resistance to ravelling of PA. The application of fibres has the advantage to reduce the occurrence of cracking in the mastic as a result of thermal or traffic stresses at low temperatures. It has been shown for example that fibres improve the mechanical properties of dense asphalt mixtures by providing a continuous network (grid) that contributes to the stability and structural strength. The fibre's network plays the function of distributing stress and also linking the grains of the mixture (Passeto 2000). The contribution of fibres to mixture performance of open graded asphalt, however, requires further research. Because of different types and nature of fibres, binder performance varies with the types and concentration of fibre.

In general, fibres seem to reinforce binders and contribute to improved mechanical properties (cohesive properties) of asphalt mixtures. Fibres also

permit higher binder content in an asphalt mixture than it is possible without. This helps to prevent drain-off problems. This is especially important for open-graded friction courses, stone matrix asphalt and PA to improve their durability. A higher bitumen content results in a thicker binder film that increases the durability of paving mixtures. Hence, the use of fibres in relation to the aging effect of the binder lays in achieving thicker binder films that improve (delay) the age hardening of the bitumen. Typically, related to the bitumen content, 0.15 to 0.4 percent fibres by total weight of mixture are added in HMA depending on the application (Roberts et al. 1996).

Below, some of the qualities that fibres need to acquire are mentioned (Passeto 2000):

- Fibres should be stiff and adequately long in a way to form a widespread net inside the mixture (if too short, they simply become a “filler” and do not perform the function of arresting cracks; and if too long, they could cause mixing problems).
- The fibres should be ductile and tough, with the purpose to assure an adequate resistance to cyclic stresses.
- Fibres should be compatible with the binder (good dispersion) and result in workable mixtures.
- It is important to ascertain the physio-chemical and mechanical compatibility of the fibre with the binder and the ability to retain enhanced properties under repeated loading and climatic actions.
- The geometry or width/length ratio of fibres is an important factor to consider. Lateral surface area of fibres is a significant parameter in differentiating fibres modifying potential; experiments showed that circular cross sections are the worst and rectangular cross sections appear to be better in this respect. An irregular cross section helps for good binder/fibre adhesion, but requires a higher bitumen content.

Table 2.4: Some Major Fibre Materials [Source: Franken L, 1998]

Natural Fibres	Synthetic (mineral) Fibres	
	Organic Type	Inorganic Type
Cellulose Wool Asbestos (silicate)	Polyacrilonitrile (PAN) Polypropylene (PP) Polyester Polyurethane Aromatic polyamides	Carbon Glass Steel

A number of fibre types are available with varying modification effect on binder rheology and enhancement of asphalt mixture performance. In more general terms fibres can be classified as cellulose fibres, steel fibres, glass fibres, and synthetic fibres. The main fibre materials are given in Table 2.4 classified according to their type. The Polyacrilonitrile (PAN) synthetic high modulus fibres are believed to contribute to the durability of porous asphalt mixtures.

2.5.4 Summary

- Aging of the binder in PA causes changes in the binder property resulting in hardening of the material. Stiffening of the binder might be desirable but at some critical stage the binder starts to behave in a brittle mode and subjects the asphalt mixture to wear due to its sensitivity to traffic loading and other influences such as water damage.
- Achieving a thicker binder film in porous asphalt concrete is important for PA durability since longer time is required for oxygen to diffuse into the binder, thus reducing the rate of age hardening. In addition, a thicker binder film is believed to be more resistant to water damage since greater energy is required for water to displace thicker binder film.
- Polymer Modified Binders (PMB) allow to increase the binder film thickness around aggregates because of increase in viscosity of the base bitumen. Better resistance to aging is, therefore, expected to be attained that contributes to improvement in the resistance to ravelling of the porous asphalt.
- Aging results in degradation (molecular breakdown) of the SBS polymer in elastomer modified binders; but improves its aging behaviour. The PMB can perform better than conventional (unmodified) binder in resisting stripping/ravelling that improves the performance of PA.
- In the filler-bitumen systems, the type (limestone, quartzite, etc), nature (acidic or basic nature), and geometry (particle size, shape, gradation, interface, etc as expressed as Rigden voids) of the filler are important factors to consider. The concentration of fillers greatly depends on these factors and the binder type for a particular type of filler and its effect on the performance of the mastic. Agglomeration of the filler decreases the performance of mastics because of its influence on the maximum packing potential of the filler.
- The D10 – particle size corresponding to 10% pass in the gradation distribution of the filler – or percentage of filler passing 10 μm grain size appear to be defining criteria for the ability of fillers to provide increased resistance to stripping, in which lower value for D10 and higher percentage passing at 10 μm indicate positive effects. However, the filler/binder ratio for optimum performance also depends on the nature of the filler and the type of the binder.
- Fibres allow higher binder content in asphalt mixtures to be used than with plain bitumen. Fibres also play an important role in preventing drain-off of the mastic especially in open graded mixtures and provide the possibility to attain thicker binder film thickness, which is significant to improve the aging behaviour of the binder and, hence, the durability of porous asphalt.
- Fibres are useful to enhance the mechanical performance of mastics depending on the nature and type of the filler. Fibres provide a continuous network (grid) that contributes to the stability and structural strength of asphalt mixtures and reduce the cracking potential of the binder under high stress. The fibre network plays the function of distributing stress and also linking the grains (aggregates) of the mixture.

2.6 The Dutch Experience on Porous Asphalt

In this section, the research work done at the Road and Hydraulic Engineering Institute (Dienst Weg- en Waterbouwkunde, RWS, DWW) of the Ministry of Transport Public Works and Water Management with regards to porous asphalt durability and the effect of binder aging is discussed. It will be called “the Dutch experience”. Most of the reports on PA research in the Netherlands are written in the Dutch language. This makes it difficult for non-Dutch speaking person to retrieve as much information as possible. Hence, the reader should understand that the Dutch experience on PA is much more extensive than what is presented in this section.

An extensive literature study and research work on porous asphalt has been performed for the last 10-15 years by DWW and other research centres. The researches aim to reduce traffic noise and improve performance of PA. A considerable number of reports and publications are available that address durability related problems of porous asphalt such as binder properties and performances, binder-aggregate interaction, and the effect of aggregate type and mineralogical characteristics.

The most relevant DWW reports in relation to the durability of porous asphalt are discussed below.

Causes of early ravelling in porous asphalt (Voskuilen 2001):

1. Poor control of asphalt temperature during production. Production at too low temperature leads to a need of high compaction effort and possibly crushing of aggregates. At high mixing temperatures, drainage / segregation of the bituminous mortar is likely to occur.
2. Variation in mixture composition and presence of lower quality aggregates in the asphalt mixture (Crushing tests do not discriminate weaker stones within aggregates of good quality).
3. Insufficient filler fraction in the mixture, low lime content, and high volume of traffic contributes to early ravelling.

Suggested recommendations include:

- a. Improved temperature control during hot-mix asphalt production.
- b. Avoid segregation during laying, especially the upper part of the PA layer.
- c. Develop test methods to discriminate weaker materials in coarse aggregates through better quality control.
- d. Consider maximum compaction level in order to avoid excessive compaction that leads to aggregate crushing.
- e. Use own filler from crushed material.

Experience with porous asphalt in the Netherlands (Swart 1997)

It is necessary that porous asphalt be considered with its positive and negative aspects during its application, including all the costs involved. The following are the positive and negative features associated with the application of porous asphalt:

Positive features:

1. Reduced splash and spray because of open voids that allow water to drain.
2. The voids reduce traffic noise.
3. Porous asphalt is a good rutting resistant material.
4. Lower polluting effect to the environment.

Negative features:

1. Winter maintenance requires planning and attention.
2. Skid resistance is critical during early periods of newly laid porous asphalt because of bitumen film (skin) cover of the surface aggregates.
3. Clogging has a detrimental effect on the noise reducing potential of porous asphalt.

Two layered porous asphalt (DWW report 1997)

Optimising the reduction of traffic noise by porous asphalt layers has led to the development of fine graded porous asphalt mixture on top of coarse graded porous asphalt – normally called Two Layer Porous Asphalt (TLPA). At that moment in time the advantages of this new generation porous asphalt were considered to be:

- Additional noise reduction (6 dBA) compared to single layer porous asphalt (4 dBA).
- Reduction of noise at high and low vehicle speeds (essential for applicability in urban areas) that can be maintained over longer time periods.
- Reduced clogging of the voids.
- Mechanical resistance towards traffic forces are higher.

Durability of porous asphalt (CROW 1996)

Definition: Durability is the resistance to influences (temperature, moisture, and loads) and processes (oxidation, stripping, and cracking) caused by weather and traffic, which affects the structural cohesion of the surface layers of porous asphalt and finally causes failure.

The findings of the durability study on porous asphalt include:

- Among the different test methods employed to investigate the durability of porous asphalt, the dynamic direct tensile test (DTT) was selected for its applicability and ease of interpretation. The candidate tests include, the Cantabro test, the indirect tensile test (splitting test), the wheel track test with laterally changing tracks, and the dynamic direct tensile test.

- The type of damage restricting the durability of porous asphalt is the deterioration of the surface integrity because of loss of stones from the surface or ravelling.
- The influence of traffic could not be accounted for in the study.
- The mechanical tests employed were perhaps not directly related to the performance of porous asphalt in relation to aging.

Life period of porous asphalt (Klomp 1996)

The report summarizes activities of the project group ZOAB/LEV/T on the 1994 project on the study of PA durability. According to the research findings, ravelling is the dominant damage in PA resulting in durability problems. The following were discussed in the report:

- ravelling mechanisms and test methods to get insight about the occurrence of ravelling in PA;
- possibilities to improve durability;
- rheological properties are considered important for the assessment of the effect of aging on the binders adhesion properties;
- a method for visual inspection of PA;
- research on field sections using selected test methods was proposed.

Investigation of fillers for PA application (Voskuilen and Verburg 1994)

This is a research into the use of fly ash filler with hydroxide in porous asphalt. Fly ash filler was compared with two types of limestone fillers with hydroxide. Porous asphalt specimens with these fillers were tested using the direct tensile test (monotonic) and the wheel tracking test. Mastics (filler + bitumen) from these fillers were tested for softening point (ring and ball temperature) and force ductility. Data shows that at lower temperatures PA with fly ash has a higher susceptibility to water compared to the limestone fillers. The effect of higher temperatures was not measured in the wheel tracking test. In order to reduce the water susceptibility of PA at lower temperatures the study recommended the use of filler with lower specific gravity.

Learning from the road (TU Aachen report, Gharabaghy and Csink 2006)

A draft report on a research project "Learning from the road" conducted by TU Aachen draws important conclusions. The study was carried out on field PA specimens obtained from different road sections in the Netherlands. The main findings of the study are as follows:

- Identification of road sections with the same bitumen source/origin based on the vanadium content of the binder.
- The mastic in PA undergoes internal degradation with time that contributes to the ravelling of the surface aggregates. The process of degradation leads to the formation of "micro-ZOAB" in the mortar. The diffusion of water in the mastic and the pumping effect of traffic facilitate the degradation of the mastic.
- Aging is a major factor resulting in embrittlement of the mastic. The mastic becomes brittle and at the same time permeable. This causes the weakening

of the transfer of stresses in the asphalt matrix leading to ravelling by the abrasive action of traffic.

Micro-structural assessment of PA (DRI report, Nielsen 2007)

As part of the IPG research (IPG = Innovatie Programma Geluid = Noise Innovation Program) a study has been carried out by DRI (Danish Road Institute) on the ravelling of PA. The DRI study focuses on the clogging and ravelling problems of PA. With regard to ravelling, the study adopted two methods to look into the micro-structure of PA, a CT scan and thin-sections analysis of asphalt specimens cored from the road. The aim of the study was to understand the ravelling process from a micro level investigation of the bituminous mortar. The asphalt specimens were from the same road sections as those considered in this study. The main conclusions of the DRI study indicated that the deterioration of PA is related to both cohesive and adhesive failures, i.e. failure in the bituminous mortar and the interface between the mortar and the aggregate respectively. In general, cohesive failure seems not related to the pavement age. Adhesion failure is well related to clogging of the voids in PA because of the deterioration of the mortar with time, which is consistent with the findings of the research by TU Aachen (Gharabaghy and Csink 2006). The deterioration of the mastic with time was mainly observed with poor performing pavements.

2.7 Summary of the Literature Review

The summary of the literature survey is presented below.

- Conventional or standard laboratory bitumen aging methods do not combine the main factors that play a role in the aging process of the binder in the field. In this respect, a weatherometer tests that can combine the effects of temperature, UV light, and humidity/moisture during aging seems more realistic aging protocol to simulate field aging conditions.
- During asphalt production (short term aging) major mass loss of the binder is encountered due to the loss of volatiles which alters the original binder properties. The sensitivity of different binders to aging can be distinguished by the loss of oily components during the short term aging, which is crucial to the subsequent performance of the binder.
- Oxidation is an irreversible chemical process that changes the molecular composition of binders increasing the binder hardness or stiffness. Compositional change due to oxidative aging results in the transformation of components from non-polar to more polar fractions. The formation of polar products alters the state of dispersion of the binder's chemical components which also change the chemical reactivity because of change in the mobility of the molecules.
- Ketones also known as carbonyl ($C = O$) and sulfoxides ($S = O$) are the two major functional groups formed during oxidative aging; they are characteristic peaks at 1700 cm^{-1} and 1030 cm^{-1} wave number in the IR spectrum respectively. The formation of ketones and sulfoxides shows an

increase as a function of aging time and the sum of the area under the characteristic IR peaks can be used as an indicator for rating the degree of sensitivity of binders to oxidative aging.

- The presence of hetero-atoms in bitumen contributes to the difference in physical properties and their aging behaviour. Binders from different sources have different amounts of hetero-atoms. The presence of vanadium in higher quantity is considered to be an indication of high amount of hetero-atoms in the binder composition. Vanadium content provides an indication of the source/origin of the binder and its susceptibility to oxidation (aging).
- The colloidal structure (chemical composition) of the binder indicates the balance of the binder compositional components which can be used as an indication of the stability of the binder. The Gaestel Index (*IC*), a ratio of the sum of the amounts of asphaltenes and saturates to the sum of the amounts of polar aromatics (resins) and naphthene aromatics (aromatics), is a measure used as colloidal stability indicator.
- The GPC and IR tests are useful chemical test methods that indicate chemical changes caused by oxidative aging of binders. They provide qualitative and quantitative information in determining the extent of age hardening.
- Aggregates, depending on their mineral composition, may have a dual role in binder oxidation: 1) as a catalyst promoting the formation of the oxidation products (ketones and sulfoxides) in the low polar generic fractions, 2) they may absorb the highly polar fractions making them less oxidable. The adhesion of bitumen to the aggregate surface is dependent on the types of functionalities at the interface and their ability to bond strongly to the surface.
- In the filler-bitumen systems, the type (limestone, quartzite, etc), nature (acidic or basic nature), and geometry (particle size, shape, gradation, interface, etc as expressed as Rigden voids) of the filler are important factors to consider. These factors together with the type of binder determine the performance of the mastic. When agglomeration of the filler occurs, the performance of the mastic decreases because of the influence on the maximum packing potential of the agglomerated filler.
- Achieving thicker binder film in porous asphalt is important for PA durability since longer time is required for oxygen to diffuse into the binder, thus reducing the rate of age hardening (change in the cohesive properties of the binder). In addition, a thicker binder film is believed to be more resistant to water damage since greater energy is required for water to displace thicker binder films which also implies that the adhesive bond is improved.
- Polymer Modified Binders (PMB) allow thicker binder films around aggregates because they increase the viscosity of the base bitumen. Better resistance to aging is, therefore, expected to be attained that contributes to the improvement of porous asphalt resistance to ravelling. The degradation (molecular breakdown) of the polymer upon aging of elastomer modified

binders could improve the aging behaviour of the binder. Hence, the use of PMB can improve the overall performance of PA.

2.8 References

- Airey, G. D. (2003). "State of the Art Report on Aging Test Methods for Bituminous Pavement Materials." *International Journal of Pavement Engineering*, 4(3), pp. 165-176.
- Airey, G. D., Choi, Y. K., Collop, A. C., and Elliot, R. C. (2003). "Development of an Accelerated Durability Assessment for High Modulus Base (HMB) Materials." *6th RILEM symposium PTEMB'03*. pp160-166.
- Anderson, D. A., Christensen, D. W., Bahia, H. U., Dongre, R., Sharma, M. G., and Antle, C. E. (1994). "Binder characterization and evaluation: Volume 3 Physical characterization." *Rep. No. SHRP-A-369*, National Research Council, Washington DC.
- Bahia, H. U., Hanson, D. I., Zeng, M., Zhai, H., Khatri, M. A., and Anderson, R. M. (2001). "Characterisation of Modified Asphalt Binders in Superpave Mix Design." *National Cooperative Highway Research Program (NCHRP), Rep. No. 459*, National Academy Press, Washington DC.
- Bahia, H. U., Hislop, W. P., and Zhai, H. (1998). "Classification of Asphalt Binders into Simple and Complex Binders." *Association of Asphalt Paving Technologists (AAPT)*, Vol. 63.
- Bell, C. A., AbWahab, Y., and Cristi, M. E. (1994). "Selection of laboratory aging procedures for asphalt-aggregate mixtures." *SHRP report, Rep. No. SHRP-A-383*, National Research Council, Washington DC.
- Bell, C. A., and Sosnovske, D. (1994). "Aging: Binder Validation." *SHRP report, Rep. No. SHRP-A-384*, National Research Council, Washington DC.
- BitVal report (2006). "BitVal - Analysis of available data for validation of bitumen tests." *Forum of European National Highway Research Laboratories (FEHRL)*.
- COST 333 (1999). "Bituminous Materials and Hydraulically Bound Materials." *Development of New Bituminous Pavement Design Method*, European commission, Brussels, pp. 115-172.
- CROW (1996). "ZOAB Rest Levenduur." *Rep. No. publikatie 103*. Netherlands.
- Curtis, C. W., Ensley, E. K., and Epps, J. (1993). "Fundamental properties of asphalt-aggregate interactions including adhesion and adsorption." *Rep. No. SHRP-A-341*, National Research Council, Washington, DC.
- Domke, C. H., Davison, R. R., and Glover, C. J. (1999). "Effect of Oxidation Pressure on Asphalt Hardening Susceptibility." *Transportation Research Record* (issue no. 1661), pp. 114-121.
- Domke, C. H., Liu, M., Davison, R. R., Bullin, J. A., and Glover, C. J. (1997). "Study of Strategic Highway Research Program pressure aging vessel

procedure using low-temperature aging experiments and asphalt kinetics." *Transportation Research Record*, (no. 1586), pp. 10-15.

DWW (1997). "De "European Conference on Asphalt"." *Rep. No. W-DWW-97-058*, Ministrie van Verkeer en Waterstaat, Rijkswaterstaat, Dienst Weg- en Waterbouwkunde (RWS, DWW), Delft, The Netherlands.

ETG (2000). "Minutes of TRB Superpave Asphalt Binder." *Minutes of TRB Superpave Asphalt Binder (Meeting on long range plan - Superpave 2005)*. November 13 & 14, 2000 Tampa, Florida.

Francken, L., Vanelstraete, A., and Verhasselt, A. (1997). "Long term aging of pure and modified bitumen: Influence on the rheological properties and relation with the mechanical performance of asphalt mixtures." pp. 1259-1278.

Gharabaghy, C., and Csink C. (2006). "Learning from the road - service life of ZOAB." TU Aachen (Instituut voor Straatwezen Aken), Aachen, Belgium.

Gubler, R., Lui, Y., Anderson, D. A., and Partl, M. N. (1999). "Investigation of the system filler and asphalt binders by rheological means." *Association of Asphalt Paving Technologists (AAPT)*, Vol. 68.

Heslop, M. W., and Catt, C. A. (1997). "Specifying durability for bituminous surfacing - The importance of binder rheology." *2nd European Symposium on performance and durability of bituminous materials*. pp. 19-37. Aedificato, Zurich.

Isaccson, U., and Lu, X. (1999). "Laboratory investigation of polymer modified bitumen." *Association of Asphalt Paving Technologists (AAPT)*, Vol. 68, pp. 35-63.

Ishai, I. (1996). "The Effects of Asphalt Composition on its Physical and durability Characteristics." *Transportation Research Record*, (Transport Research Board 75th annual meeting).

Ishai, I., Brule, B., Vaniscote, J. C., and Ramond, G. (1988). "Some rheological and physio-chemical aspects of long term asphalt durability." *Association of Asphalt Paving Technologists (AAPT)*, Vol. 57, Viking Press Inc.

Kandhal, P. S., and Chakraborty, S. (1996). "Effect of Asphalt Film Thickness on Short and Long-Term Aging of Asphalt Paving Mixtures." *Transportation Research Record*, (TRR No. 1535, pp. 83).

Kandhal, P. S., Lynn, C. Y., and Parker, F. (1998). "Characterization tests for mineral fillers related to performance of asphalt paving mixtures." *Transport Research Record*, (TRR no. 1638).

Kavusi, A., and Hicks, R. G. (1997). "Properties of Bitumen Mixtures Containing Different Fillers." *Association of Asphalt Paving Technologists (AAPT)*, Vol. 66.

Khalid, H., and Walsh, C. M. (1997). "Design for long-term performance of porous asphalt." *2nd European Symposium on performance and durability of bituminous materials*. pp. 211-226. Aedificato, Zurich.

Khalid, H., Walsh, C. M., and Miro Recasens, J. R. (1998). "Rheological and Mechanical Characterization of Aged and Unaged Porous Asphalt Binders."

Institution of Civil Engineers. Transport (Proc. Inst. Civ. Eng. , Transp.), 129, pp. 240-246.

Klomp, A. J. G. (1996). "Materiaaltechnisch Levensduur van ZOAB (in Dutch)." *Rep. No. W-DWW-96-047 rapport*, Ministrie van Verkeer en Waterstaat, Rijkswaterstaat, Dienst Weg- en Waterbouwkunde (RWS, DWW), Delft.

Konitpong, K., and Bahia, H. U. (2003). "Role of Adhesion and Thin Film Tackiness of Asphalt Binders on Moisture Damage of HMA." *Association of Asphalt Paving Technologists (AAPT)*.

Kumar, A., and Goetz, W. H. (1997). "Asphalt Hardening as Affected by Film thickness, Voids, and Permeability in Asphaltic Mixtures." *Association of Asphalt Paving Technologists (AAPT)*, Vol. 46 pp.571-605.

Lytton, R. L. (2004). "Adhesive fracture in asphalt concrete mixtures." J. Youtcheff, ed. (submitted for publication).

Mes, B. (2003). "Ontrafeling van Verouderingseigenschappen van Bitumen in ZOAB (in Dutch)." *MSc thesis*, Rijkswaterstaat, Road and Hydraulic Engineering Institute (DWW).

Mouillet, V., Durrieu, J. L. F., Kister, J., and Martin, D. (2003). "Development of a New Methodology for Characterization of Polymer Modified Bitumens Aging by Infrared Microspectrometry Imaging." *The 6th International RILEM Symposium, PTEBM2003. Zurich*.

Nielsen, C. B. (2007). "Ravelling of Porous Asphalt Pavements - Assessment of test sections." *Rep. No. M5 (Technical note 48)* , Danish Road Directorate (DRI), Denmark.

Oliver, J. W. H., and Tredrea, P. F. (1997). "The change in properties of polymer modified binders with simulated field exposure." *Association of Asphalt Paving Technologists (AAPT)*, Vol. 66.

Parmeggiani, G. (2000). "Nitrogen Rolling Thin Film Oven Test Laboratory Testing Proposals." *Euroasphalt and Eurobitume Congress*, Barcelona.

Passeto, M. (2000). "Porous asphalt concretes with added Micro-fibres." *Euroasphalt and Eurobitume Congress*, Barcelona.

Peterson, J. C. (2000). "Chemical composition of asphalt as related to asphalt durability." Included in series *Asphaltenes and Asphalts, 2. Developments in Petroleum Science*, 40B. ELSEVIER, USA.

Peterson, J. C., and Harnsberger, P. M. (1998). "Asphalt Aging: Dual Oxidation Mechanism and its Relationship with Asphalt Composition and Oxidative Age Hardening." *Transportation Research Record, (TRR No. 1638)*. National Academy Press.

Plancher, H., Green, E. L., and Peterson, J. C. (1976). "Reduction of oxidative hardening of asphalts by treatment with hydrated lime - a mechanistic study." *Association of asphalt paving technologists* , 45, pp. 1-24.

- Ramaiah, S., D'Angelo, J., and Dongre, R. (2004). "Evaluation of modified german rotating flask." *Transportation Research Record*, (1875), 80-88.
- Read, J., and Whiteoak, D. (2003). "The Shell bitumen handbook." Shell Bitumen, Surrey, UK.
- Roberts, F. L., Kandhal, P. S., Ray Brown, E., Lee, D.-Y., and Kennedy, T. W. (1996). "Hot mix asphalt materials, mixture design, and construction." *NAPA Research and Education Foundation*, Lanham, Maryland.
- Shashidhar, N., Needham, S. P., Collar, B. A., and Romero, P. (1999). "Prediction of the performance of mineral fillers in stone matrix asphalt." *Association of Asphalt Paving Technologists (AAPT)*, Vol. 68.
- Su, Z. (1996). "Mineral aggregates: their classification and properties." *Rep. No. RT010-96-02*, ESHA, Groningen, the Netherlands.
- Swart, J. H. (1997). "Experience with porous asphalt in the Netherlands." *European conference on porous asphalt*. Madrid.
- Verhasselt, A. F. (2000). "A Kinetic Approach to the Aging of Bitumens." *Asphaltenes and Asphalts, 2. Developments in Petroleum Science, 40B*, Elsevier Science BV.
- Verhasselt, A. F. (2002). "Long Term Aging - Simulation by RCAT aging Test." *International Conference on Asphalt Pavements (ICAP)*. Copenhagen, Denmark.
- Verhasselt, A. F., and Choquet, F. S. (1997). "Field Aging of Bituminous Binders: Simulation and kinetic approach." *5th RILEM Symposium on Mechanical Test Methods for Bituminous Materials*. Lyon, France.
- Voskuilen, J. L. M. (2001). "Oorzaak van Vroegtijdige Rafeling in ZOAB (in Dutch)." *Rep. No. DWW 2001-069*, Ministrie van Verkeer en Waterstaat, Rijkswaterstaat, Dienst Weg- en Waterbouwkunde (RWS, DWW), Delft, the Netherlands.
- Voskuilen, J. L. M., and Verburg, H. A. (1994). "Onderzoek naar Vliegashoudende Middelsoort Vulstof met Hydroxide voor Toepassing in ZOAB (in Dutch)." *Rep. No. Rapportnr P-DWW-94-502*, Ministrie van Verkeer en Waterstaat, Rijkswaterstaat, Dienst Weg- en Waterbouwkunde (RWS, DWW), Delft, the Netherlands.
- Wegan, V., and Brule, B. (1999). "The structure of Polymer Modified Binders and Corresponding Asphalt Mixtures." *Association of Asphalt Paving Technologists (AAPT)*, Vol. 68. pp. 64-84.
- Zupanick, M., and Baselice, V. (1997). "Characterizing Asphalt Volatility." *Transportation Research Board, TRR no. 1586*. pp. 1-9. Washington, DC.

3 The Research Methodology

3.1 Introduction

It is understood that ravelling of PA occurs due to failure in the bituminous mortar (cohesion) and/or failure in the binder-aggregate interface (adhesion). Thus, if one aims to model the system in PA, two aspects are important concerning material characteristics: the role of the bituminous mortar (cohesive strength) and the binder-aggregate interface characteristics (adhesive properties) considering that the likelihood of aggregate failure is low. The factors involved in the ravelling process of PA are schematically described in Figure 3.1.

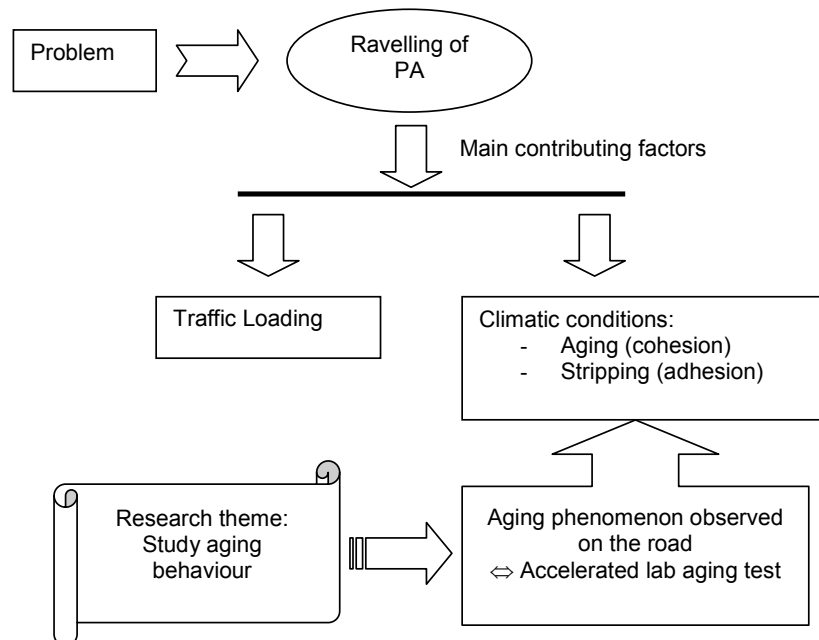


Figure 3.1: Major factors contributing to PA ravelling

The cohesive properties of the bituminous mortar are influenced by the effects of weathering (age hardening and the effect of water) resulting in ravelling. Resistance to ravelling determines the effective service life of PA. Binder aging is considered as a dominant factor for cohesive failure leading to ravelling of PA pavement layers. This assumption appears to be the basis to focus on the study of the performance of the cohesive characteristics of the bituminous mortar with time.

3.2 Lessons from Literature Review

From the literature review conducted on the effect of binder aging, the following points are regarded important for consideration in the research methodology to be adopted.

- The RTFOT and RCAT laboratory aging procedures are recommended to conduct the short and long term aging of bitumen respectively.
- In addition to the conventional aging method, the aging of PA in a weathering apparatus (weatherometer) that combines the effects of temperature, UV light, and moisture/humidity is considered necessary to simulate the aging process in the real life. For this reason, field specimens would also be important to consider in the research.
- The change in rheological and chemical properties of the binder is used to characterise the effects of aging on the binder properties. In this regard, the change in the viscoelastic properties expressed by the modulus and phase angle (relaxation and retardation spectrum) of the binder, the tensile strength, and fatigue properties are used to assess the aging effect of the binder with respect to rheology. With regard to chemical changes, changes in the molecular weight distribution and functional groups that are associated with the oxidation process (ketons and sulfoxides) will be used to determine the degree of age hardening.
- It is the mastic/mortar that covers the aggregates and acts as a binding material in PA. Thus, it is essential to examine the effect of aging on the properties of the mastic in addition to studying the changes in the binder property.

From the point of view of the research goal, i.e. the effect of aging on binder properties of porous asphalt concrete, it is recognized that the research deals with the effect of age hardening on the cohesive properties of the binding material (mortar). Performance of PA mixes is mainly dependent on the performance of the bituminous mortar, which implies that the binder stiffness, the amount of filler, and the binder film thickness play an important role. In this regard, the characterization of binders and bituminous mastic/mortar in relation to aging becomes the core aim in addressing the research goals. It is considered crucial that an accelerated laboratory aging test of bituminous materials should simulate (or agree with) real life weathering (Figure 3.1) in order to understand the process of age hardening in relation to the ravelling of

PA. In this regard, the effect of temperature, UV light, and moisture are considered the main weathering factors resulting in aging of the binder. Other related factors that may occur in real life situations such as rainwater (electrolytes) simulation, effect of contaminations (oil or fuel leakage), de-icing problems etc, will not be taken into account in order to keep the tests as simple as possible.

The effect of binder aging is regarded critical at lower temperatures in relation to PA pavement deterioration, which also seems in agreement with ravelling observations in the field. In practice, ravelling of PA is experienced during and/or immediately after the winter period. This implies that the need for characterizing binders for low temperature performance is crucial. In this respect, the change in the physical (rheological and failure properties) and chemical properties of the binder, can be used as fundamental tools to study the performance of the bituminous materials.

3.3 The Research Approach

From practical observations and the literature survey on PA aging, two research topics related to factors influencing cohesion were proposed. Based on the research topics, a methodology has been planned bound to restrictions with regards to practical considerations of experimenting and sampling. The research aims to characterize and understand the influence of aging through simulation of binder aging in the laboratory (artificial aging of binder and asphalt mixture) and recovery of binders from asphalt concrete specimens cored from the road. This scheme provides insight into the laboratory aging behaviour of bituminous materials in relation to field aging and the influence of age hardening on the viscoelastic and failure properties of the binder. The characterization of the effect of aging on the binder properties would allow better understanding of the cohesive characteristics of a PA mixture. In addition, the results of the study will be used to model the viscoelastic properties of the binding material to provide essential input data to the finite element modelling of PA mixtures.

The research is based on the hypothesis that...

“binder aging is a dominant factor in the cohesive failure of the binding material (mortar) contributing to the occurrence of ravelling in PA pavement layers”

3.3.1 The Research Topics

Based on extensive literature review and practical experiences on PA, two research topics are considered (Hagos 2003), which focus on:

1. the effect of aging on cohesive strength and failure properties of bitumen, and
2. the effect of bitumen/mortar aging on the ravelling of PA layer.

Research topic I: Effect of aging on cohesive properties

Aging influences the cohesive characteristics of the bituminous mortar particularly its low temperature performance. It is recognized that the cohesive strength of PA depends on the type/stiffness of the binder, the type and amount of filler and the film thickness (Tolman and van Gorkum 1997, Lytton 1998).

The effect of binder hardening on the cohesive properties of the bituminous mortar was studied by simulating the aging of the binder and asphalt mixture. Since the conventional accelerated aging method (artificial aging) does not accurately simulate the complex field aging of PA, this initiated the need for a new aging procedure. The cyclic effect of weathering, i.e. effects of temperature, UV light, and moisture combined, is believed to have an influence on aging of the bituminous mortar. This assertion implies that realistic simulation of weathering actions is essential to understand and characterize the performance of the binder in relation to field aging. Binder hardening is occurring as a result of aging contributions during high temperature periods (summer) playing a critical role to PA performance at low temperatures. The assessment of the physical (rheological and mechanical properties) and chemical properties of the binder is the main tool to investigate the effect of aging on the properties of the binding material. The cohesive and adhesion characteristics of the bitumen are related to the changes in chemical composition of the material.

Research topic II: Effect of aging on ravelling occurrence

The aging of the binder or bituminous mortar is not expected to be the same throughout the thickness of the PA layer for the following reasons:

- The effect of UV light is mainly anticipated at the top part of the PA layer due to inaccessibility of the bottom part of the layers to light (i.e., the top zone in PA layer is mainly subject to the influences of air and UV light in addition to abrasive action of traffic),
- The wearing out of the bitumen cover at the surface due to abrasion by traffic creates weak spots for possible entry of water in the bitumen-aggregate interface of the surfacing layer (Detail A, Figure 3.2b),
- Drainage of the bituminous mortar, if any, results in the decrease in the binder film thickness at the upper zone of the pavement layer. It also prevents the infiltration of surface water into the bottom zone and reduces the efficiency of the layer to drain water sideways. This will promote the damaging effect of water (stripping effect) and the subsequent loss of stones from the upper zone. A thin bitumen film as a result of binder (mortar) drainage will also result in a higher rate of age hardening of the binder on the upper zone. (NB: Drainage is expected to happen mainly during the construction phase if the mix is not laid at the right temperature (low binder viscosity), if the bitumen content is excessive, or due to segregation during paving operations). Studies indicate that the bottom half of PA samples obtained from the road have higher bitumen content than

the upper half which underscore the assumption that mastic/mortar drainage may occur in PA (Figure 3.2a).

- Water stays for a longer period at the bottom layer (Zone 2 in Figure 3.2a) especially when the side drainage becomes inefficient due to clogging of the air voids by dirt or dust. Moreover, the pumping effect imposed by traffic loading on the PA pavement increases the chance of stripping of the binding material (mortar) in PA. This may cause ravelling through initiation of damage at the bottom layer that propagates to the top layer (Zone 1) where traffic could easily result in the loss of aggregates. Another assumption is that any instability in the bottom zone (due to adhesive and/or cohesive cracking or the crushing of the aggregates) could be directly reflected at the top zone of the PA layer through initiation of ravelling.

For the reasons stated above, it is believed that the aging behaviour of the bituminous mortar for top, intermediate and bottom zones in the PA layer needs to be investigated to understand the performance of the aging process in the PA layer in relation to ravelling failure. However, for practical reasons it was not possible to study the three zones. Hence, the investigation has been performed on the top half and bottom half zones of the PA layer (Figure 3.2a).

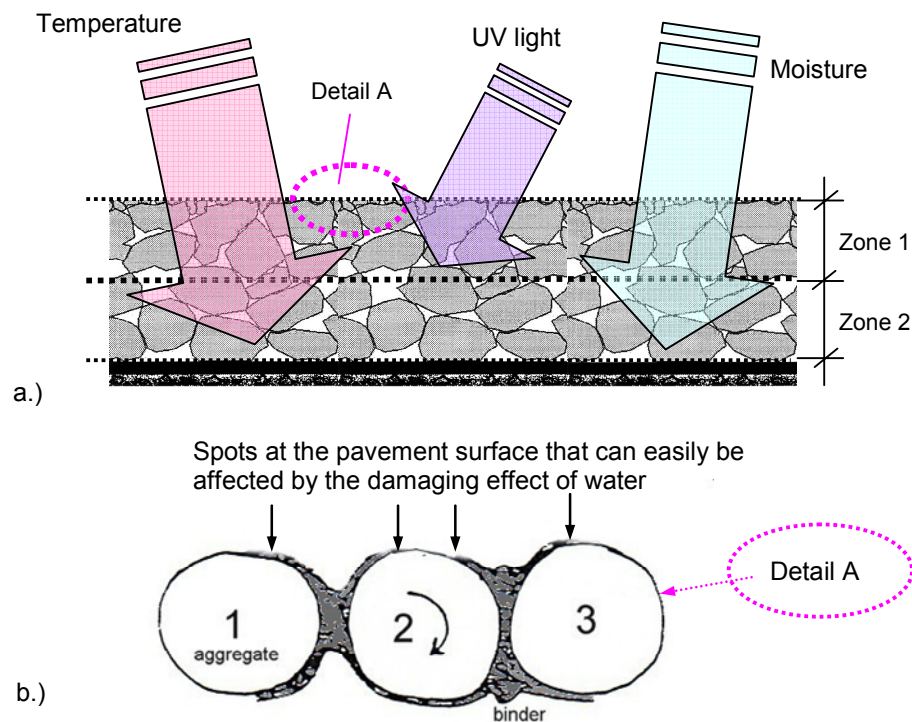


Figure 3.2: Meso-level (zone) investigation into porous asphalt layer b.) Micro-level investigation of binder film performance

The research methodology

Weathering actions change the properties of the bitumen or bituminous mortar in PA pavement layers with time. Aging of the bituminous mortar occurs predominantly during high temperature periods while ravelling is mainly a low temperature phenomenon. This implies that high temperature contributes to the age hardening process and low temperature contributes to damage development in PA pavement. Both warm and cold periods, therefore, have adverse effects on the performance of PA.

To understand the effect of aging on the rheology and chemical properties of bitumen, accelerated aging tests were conducted to simulate field conditions. It is important to recognize that there is a difference between the field (natural aging) and simulated laboratory aging approaches as illustrated in the schematic diagram, Figure 3.4. The following differences are apparent when comparing field aging with accelerated laboratory aging:

1. The effect of traffic loading is not simulated in the accelerated laboratory aging procedures.
2. The laboratory aging of bitumen to simulate long term field aging is performed at higher temperatures than the anticipated temperature on the pavement to accelerate the aging process.
3. The aging of PA in the field is a complex process involving the combined effects of temperature, UV exposure, moisture, and other factors, whereas artificial aging in the laboratory is comparatively less complex involving constant factors.

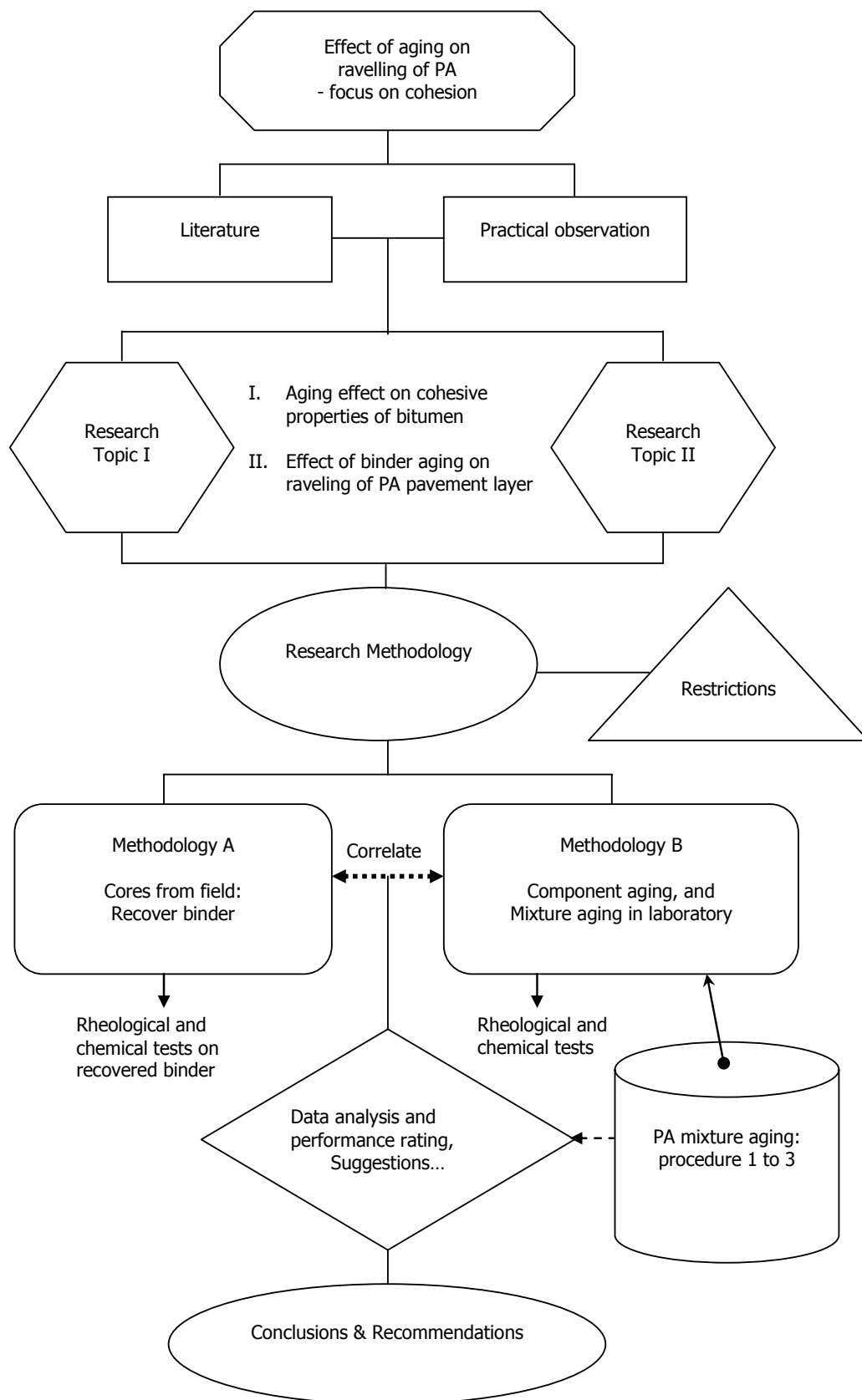


Figure 3.3: A general overview of the research approach

Despite differences in aging, the experimental approach is designed to correlate test results of laboratory accelerated aging and field aging conditions. To better understand the aging process, laboratory aging of PA mixtures under a combined influence of temperature, UV light, and moisture seems crucial to consider. The aim is to understand the influence of the “*mechanisms of aging*” on the aging process and the physical and chemical properties of the binder. It is understood that there is a huge scatter in the mixture composition and material properties in the field resulting in possible variations in aging behaviour of the binder in PA mixtures. Moreover, possible contaminations of the pavement due to fuel/oil leakage from vehicles, winter- maintenance activities, and so forth might have adverse effects on the pavement performance which is not taken into account in the laboratory experimental design. Nevertheless, the major factors were considered during accelerated laboratory aging of asphalt mixture to understand the effects of the “*aging mechanisms*” in the field (natural weathering).

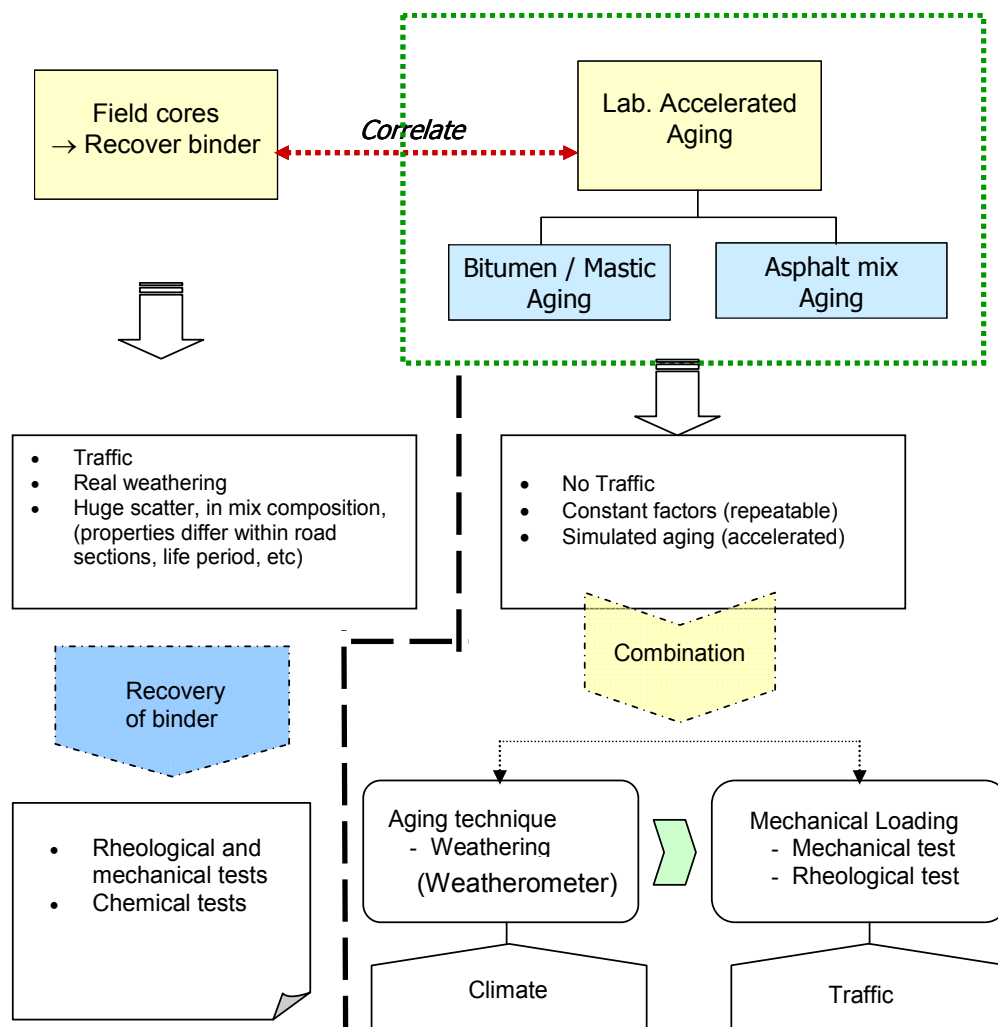


Figure 3.4: Schematic diagram showing differences and relationships between field and laboratory aging techniques

To understand the mechanisms of aging on the rheological, mechanical, and chemical properties of the bitumen and make correlations with the actual field aging behaviour of the binder, the laboratory and field materials are compared. The laboratory aging procedure involves artificial aging of bitumen using conventional short and long term aging methods and PA mixture aging to predict field aging. The binder aging was performed using RTFOT (Rotating Thin Film Oven Test) procedure (EN 12607-1) for short term aging and the recommended RCAT (Rotating Cylinder Aging Test) procedure for long term aging (Draft NEN-EN 15323). The short term aging STA (RTFOT) and long term aging LTA (RTFOT + RCAT) were performed to simulate binder aging during the construction phase and the service period of asphalt concrete respectively.

The aging of PA mixture in the laboratory was conducted using a weatherometer and three aging procedures, which are:

- *Procedure 1:* Temperature aging (oxidation),
- *Procedure 2:* Temperature + UV light aging (the effect of UV on the aging susceptibility or degradation),
- *Procedure 3:* Temperature + UV light + moisture/humidity aging (combined influences of weathering actions)

The effects of traffic loading, road condition, and service period (age) were considered in investigating cores of asphalt specimens from the field (pavement). For a broad understanding of the aging behaviour of PA with time, the field specimens are taken from new construction/rehabilitation section and sections with a 1, 3, 7, and 12 years service period. Samples are taken from the Emergency Lane / Shoulder SH (without traffic) and the heavily loaded lane (Slow Lane, SL) to take into account the effect of traffic on the performance and aging of PA. The flow chart in Figure 3.5 shows the aging approach adopted in the research. The recovery of bitumen from the upper and lower part of the field specimens and the laboratory aged PA mixture are conducted independently. The aging methods are discussed in detail in Chapter 4.

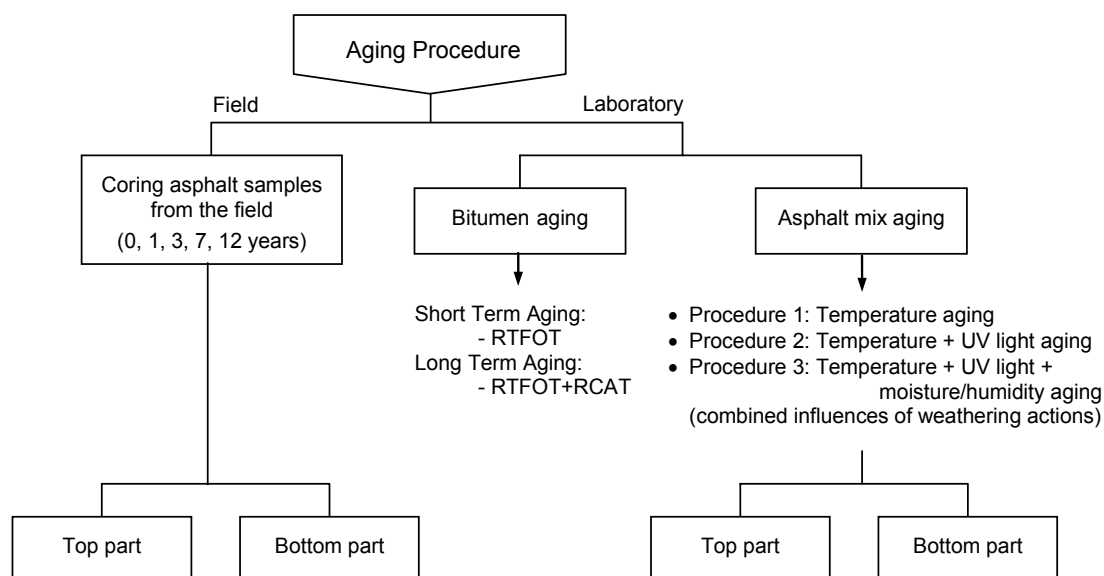


Figure 3.5: Flow chart describing the procedure for aging of samples

Age hardening changes the cohesive characteristics of the bitumen or bituminous mortar. Effects of aging on the cohesive strength increases the susceptibility of the material to damage or crack development (reduces fatigue performance of the binding material) leading to ravelling occurrence. The development of damage is expected to be critical at low temperatures where the potential of the binding material to relieve stress through viscous flow is very low. Thus, failure/fracture properties and fatigue performance are thought to be significant factors to characterize the contribution of the binder (or bituminous mortar) to cohesive strength of the PA mixture. The term “mastic” (bitumen + filler) will be used hereafter instead of “mortar” for two reasons: 1.) in PA mixture, only a portion of the sand, i.e. less than 0.5mm grain sizes, is considered to be part of the binding material or mortar (Muraya 2006), and 2.) the dynamic shear rheometer used to conduct rheological characterization of samples allows the testing of bitumen and mastic samples only. Mechanical and rheological tests on bitumen or mastic provide useful information on the responses of bituminous materials to loading which is related to traffic and/or climatic loadings in practice. The change in rheological and mechanical (strength) properties of bitumen stems from the irreversible chemical change in the composition of the binder as a result of aging. The research methodology therefore has two blocks of testing program; i.e. 1.) chemical characterization of bituminous samples, and 2.) rheological and mechanical investigation. The research methodology is designed to understand the effects of the different aging protocols through assessment of the binder properties. Important conclusions could be drawn based on the correlations made between laboratory and field aging material properties.

In Table 3.1, the relation between the two research topics and the proposed research methodology is outlined. Mechanical tests on the field specimens and the characterisation of recovered bitumen from the field specimens provides

the effect of “*natural aging*” on the mixture performance and binder properties in time, which is related to research topic I and II. The natural aging of PA is also a reference for the laboratory aging protocol in simulating field aging conditions.

Table 3.1: Relationship between research topics and research methodology

	Bitumen recovery Field cores	Laboratory simulation (aging)	
		Bitumen/mastic	Asphalt mix
Research Topic I	x	x	x
Research Topic II	x	indirectly	indirectly

Practical Restrictions:

- Recovery of binder from core samples of a PA layer will be limited to the upper and lower half zones of PA layer in order to obtain sufficient amount of binder for testing. This will lower the number of core asphalt samples from the road, which also overcomes the difficulties to get cores from the road.
- Because of the limitations on testing capabilities of some laboratory equipment, only bitumen+filler (mastics) are considered in the testing program.
- The accelerated aging of PA mixture in a weathering chamber will be carried out at a maximum temperature of 60°C to prevent possible drainage of the bituminous mortar that could also influence the results of the test. The implication of this is possibly long aging times are needed to achieve comparable degree of binder aging as a field material with 10 – 12 year of service.

3.3.2 The Research Method

Bituminous Materials

Laboratory Aging Tests: Accelerated aging of bitumen and PA mixtures.

1. Binder aging: Artificial aging of bitumen using conventional aging methods (RTFOT and RCAT) to simulate short and long term aging of bitumen during hot mix asphalt production, placing, and compaction and in service.
2. Asphalt mixture aging: The aging of PA mixture combines the factors involved in the aging process of field materials (natural aging). The recovery of bitumen from laboratory asphalt mixtures is conducted in the same way as the recovery of binder from field specimens to perform further tests on the properties of the recovered bitumen. The aging method takes into account the effect of filler and aggregate type in the aging process of the binder. The simulation of aging in the laboratory is conducted under the influences of temperature, UV light, and humidity to understand the sensitivity of the binder (binding material / mastic) to the influences of the “mechanisms of aging” on the upper and lower part of the asphalt.

Summary of the laboratory aging tests is given in Table 3.2.

Table 3.2: Summary of the experimental design for accelerated laboratory aging.

Binder aging	Asphalt mixture aging (Weathering)		
Set A	Set B	Set C	Set D
a. RTFOT aging: Short term aging (evaporation of volatile components during production of bitumen)	Effect of temperature on PA mixture aging	Effect of temperature + UV light on PA mixture aging	Combined effects of temperature + UV light + humidity on PA mixture aging
b. RCAT aging: Long term aging (oxidation in service)	<i>Procedure 1</i>	<i>Procedure 2</i>	<i>Procedure 3</i>
<i>NB: Aging of asphalt mixture (slab) is conducted in a weathering chamber or oven that combines the effects of temperature, UV light, and moisture.</i>			
<i>NB: Dutch standard Porous Asphalt was used for mixture aging in a weathering chamber.</i>			

Field Specimens

To study the aging behaviour of the binder on the top and bottom zones of PA during its service period, cores were taken from a newly laid section and sections with 1, 3, 7, and 12 years of service. Factors considered to influence the binder aging behaviour were taken into account in the selection of road sections for sampling asphalt cores from the road; these factors include:

- the age of the road,
 - the road condition,
 - the effect of traffic loading on the aging and performance of PA, and
 - the weather condition.
1. *Service period:* Samples were taken from sections immediately after construction and with a service life of 1, 3, 7, and 12 years. The rate of hardening of the bituminous material in PA layer is assumed to be high during the first few years of service period and decreases gradually with time.
 2. *Road condition:* Experience on the performance of PA (trafficked lane, SL) in the Netherlands shows that the initiation of ravelling begins on average 4 to 5 years after construction. But, the variability of performance is such that there is a fair chance that a road can be in a good condition or badly deteriorated after 5 years of service. Moreover, it is assumed that variation in the production and laying process are reflected in the performance of the PA during its service period, which indicates the need for considering road sections with different performance. For this reason, it is deemed important to consider coring of PA samples from sections with good and poor surface condition having a service life of 7 and 12 years.

3. *Traffic loading*: Volume of traffic and the percentage of heavy vehicles vary from one road section to another. The loading condition also varies from lane to lane within a road section. To take into account the effect of traffic loading, samples were cored from the heavily loaded lane (Slow Lane, SL), and the emergency lane (EL). The emergency lane is also sometimes called "Shoulder" (SH).

The variability in the asphalt mixture across the road cross-section is assumed to have been taken into account through the sampling of cores along the right and left traffic wheel paths as shown in Figure 3.6. Samples were taken within a 100 m long section.

4. *Weather*: Considering the size of the Netherlands, the climatic condition throughout the country is assumed to be uniform or with minimum variations. Thus, the impact of small differences in weather conditions in different regions of the country is not considered significant on the aging characteristics of PA.

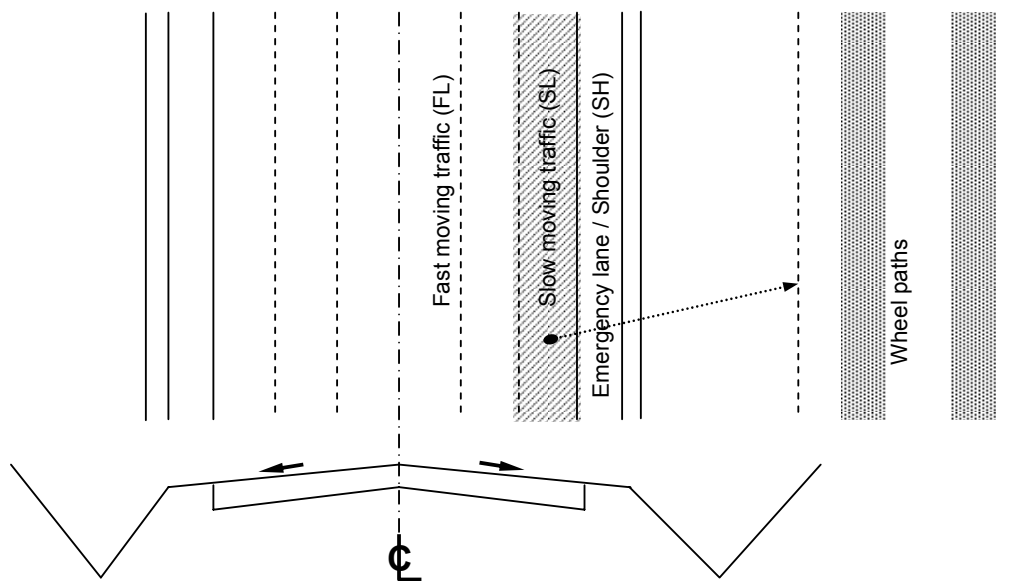


Figure 3.6: Typical road plan and cross- sectional view

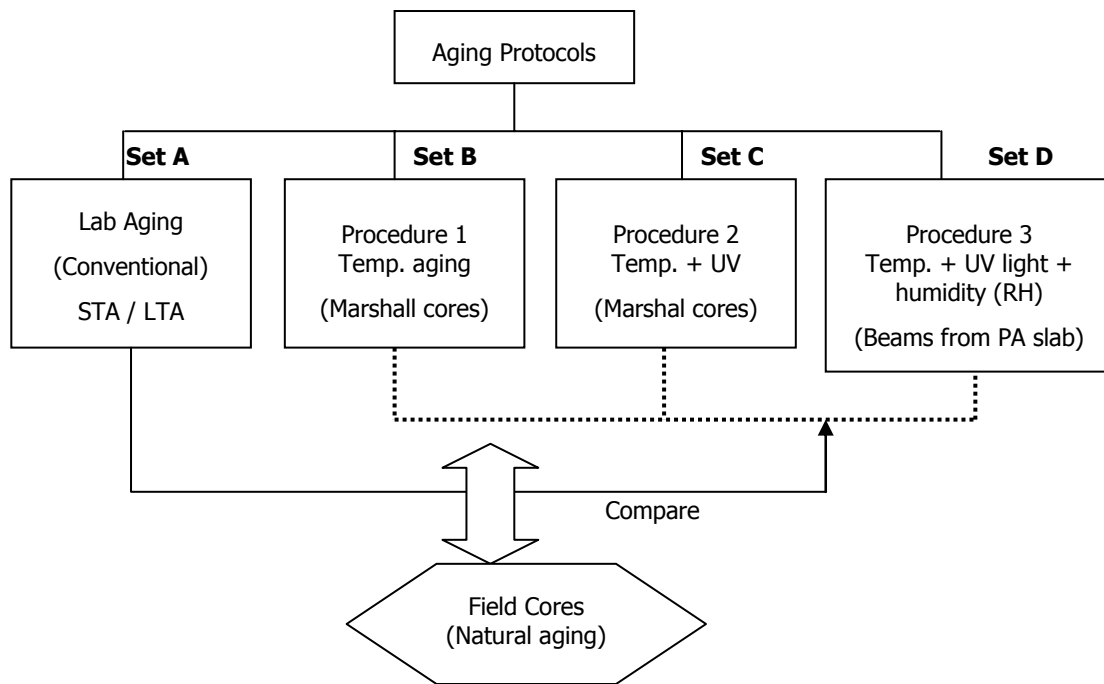


Figure 3.7: Schematic illustration of the aging procedures (based on Table 3.2)

Table 3.3: The coring program

Service period (yrs)	0	1	3	7	12
Est. remaining life, yr (refer to figure 7b)	12 - 14	10 - 12	8 - 10	6 - 8	2 - 4
Road condition: (based on extent of ravelling)	Good	Good	Good	Good Poor	Good Poor
Traffic levels: (ESA)	↓	↙ 2 ↘	↙ 2 ↘	↙ 2 ↘	↙ 2 ↘
	-	EL SL	EL SL	EL SL	EL SL
Road Sections = 7	1	1	1	2	2
No. of combinations = 17	1	2	2	4	4

Remark: It is recognized that there can be a significant variability of the mixture composition along the road cross section, longitudinal, and possibly vertical alignment (along the pavement thickness) due to segregation of the binder (bituminous mortar) during the paving operations (Molenaar et al. 2006).

Experimental Design

The main aim of the research is to study the effect of bitumen aging on the cohesive characteristics of the bitumen (durability), which is related to the changes in the physical and chemical properties. For this reason, the following evaluation mechanisms were adopted to characterize the bitumen and mixture properties before and after aging (Figure 3.7):

1. Bitumen/Mastic

- Changes in the rheological and mechanical characteristics of bitumen/mastic are determined by the following tests.
 - i. Dynamic Shear Rheometer (DSR): Determination of viscoelastic properties - modulus as a function of frequency and fatigue behaviour.
 - ii. Bending Beam Rheometer (BBR): Low temperature creep properties.
 - iii. Direct Tensile Test (DTT): Low temperature tensile strength properties.
- Changes in the chemical properties of bitumen are determined in the following way.
 - i. Gel Permeation Chromatography (GPC) or Size Exclusion Chromatography (SEC): to determine the effect of aging on the molecular size distribution of the binder.
 - ii. Attenuated Total Reflectance - Infrared Spectroscopy (ATR-FTIR): Identification of change in functional groups associated with oxidation.
 - iii. Vanadium Content: Determination of the origin of bitumen samples.

2. Mixture

- In order to relate mixture performance with properties of the recovered bitumen the repeated load Indirect Tensile Test (ITT) was carried out.
 - Determination of resilient modulus and temperature susceptibility of the mixtures.

A summary of the testing plan is provided in Table 3.4. The detailed experimental procedures are discussed in chapter 4 and 5 for the rheological and chemical tests respectively.

Table 3.4: Summary of binder investigation recovered from core asphalt samples

Planned Tests	Test description	Apparatus/Test
1. Bitumen (recovered) Rheological/Mechanical properties: <ul style="list-style-type: none"> i. Viscoelastic properties and fatigue characteristics of bitumen/mastic ii. Creep and Failure properties: Failure stress, Failure strain, Energy at failure Chemical characterization: <ul style="list-style-type: none"> i. Molecular distribution ii. Determination of oxidation products. iii. Vanadium Content 	<ul style="list-style-type: none"> - Dynamic Shear Rheometer (DSR): Frequency sweep: Temp. -10, 10, 30, and 50°C Time-sweep: fatigue test - Direct Tensile Test - Bending Beam Rheometer - Molecular size distribution, - Identification of oxidation products - Source of bitumen indication 	DSR DTT BBR GPC ATR/FTIR
2. Asphalt mix Mechanical Performance: Strength and Resistance to fracture (cracking)	<ul style="list-style-type: none"> - Indirect Tensile Test (ITT) $\phi = 100 \text{ mm}$, $h = 50 \text{ mm}$ 	ITT
<i>NB: Tests on asphalt mixture were performed on core asphalt samples before recovering of the binder.</i>		
<u>Remark:</u> Tests on recovered bitumen from the top and bottom zones of PA layer both for laboratory aging and field specimens.		

3.4 References

- Fonsceca, O. A., and Witczak, M. W. (1996). "A Prediction Methodology for the Dynamic Modulus of In-Place Aged Asphalt Mixtures." *Association of Asphalt Paving Technologists (AAPT)*, Vol. 65.
- Francken, L., Vanelstraete, A., and Verhasselt, A. (1997). "Long term aging of pure and modified bitumen: Influence on the rheological properties and relation with the mechanical performance of asphalt mixtures." *8th International Conference on Asphalt Pavements (ICAP)*. Vol. II, pp. 1259-1278. Seattle, Washington.
- Hagos, E. T. (2003). "The Effect of Aging of the Bituminous Mortar on the Ravelling of Porous Asphalt Pavement Layers, A Literature Review." *Rep. No. 7-04-132-1*, Road and Railway Engineering, TU Delft, The Netherlands.
- Lytton, R. L., Chen, C. W., and Little (1998). "A Micromechanics Fracture and Healing Model for Asphalt Concrete" in Fundamental properties of asphalts and modified asphalts, Task K: Microdamage and Healing in Asphalt and Asphalt Concrete." *Rep. No. Final Report, Vol. 37*, The Federal Highway Administration (FHWA).
- Molenaar, A. A. A., Meeker, A. J. J., Miradi, A., and van der Steen, T. (2006). "Performance of Porous Asphalt." *Association of Asphalt Paving Technologists (AAPT)*, Vol. 75 (CD).
- Molenaar, J. L. M., and Molenaar, A. A. A. (2002). "An Investigation into the Contribution of Bituminous Binder to the Resistance to Ravelling of Porous Asphalt." *Euroasphalt and Eurobitume Congress*. Barcelona.
- Muraya, P. (2006). "Permanent Deformation Characteristics of Aggregate Skeleton in Asphalt Mixes." *10th International conference on asphalt pavements (ICAP)*. Aug. 12-16. Quebec, Canada.
- Tolman, F., and van Gorkum, F. (1997). "A model for the mechanical durability of porous asphalt." *European conference on porous Asphalt*. Madrid.
- Verra, N., Bol, M. v. d., and Gaarkeuken, B. (2003). "De levensduur van ZOAB." *Rep. No. DWW-2003-066*, Road and Hydraulic Engineering Institute (DWW). Netherlands.

4 Materials and Methods

The materials used in this research as well as the preparation of specimens and the aging methods are presented in this chapter. Furthermore, the rheological tests conducted to characterize the properties of the bituminous materials along with the testing conditions are described. The results of a repeated load ITT test performed on field cores to determine the resilient modulus of the mixtures is also presented.

4.1 Laboratory Binder Aging Test

The selection of materials was made to match the type of materials commonly used in porous asphalt pavement layers. Accordingly, bitumen pen grade 70/100 was used for short and long term aging of the bulk bitumen and as a binder in porous asphalt mixture aging. The properties of the virgin (unaged) 70/100 pen bitumen are given below.

Bitumen: 70/100 pen (Source: Q8 / Kuwait Petroleum B.V.)
Properties: Penetration = 93 dmm
Softening point T_{RB} = 45.0°C (as determined by Q8)
(measured: Pen = 90.7 dmm and T_{RB} = 45.4°C)
Density = 1030 kg/m³

4.1.1 Short Term Aging (STA)

As mentioned before, conventional aging methods were adopted for short term aging of bitumen in this research.

- RTFOT (EN 12607-1): Rotating Thin Film Oven Test
- RCAT163 (draft NEN-EN 15323): Rotating Cylinder Aging Test

Test conditions:

	RTFOT	RCAT163
Temperature (°C)	163	163
Duration (min)	75	235
Amount of bitumen (g)	8 bottles x 35g	500g

4.1.2 Long Term Aging (LTA)

Long term aging refers to the aging of bitumen during the service period of an asphalt pavement. The laboratory accelerated aging method used to simulate long term aging of bitumen was the RCAT90 (Rotating Cylinder Aging Test). This test was performed based on the standard test for RCAT90 test (draft NEN-EN 15323) after the binder has been exposed to short term aging.

Test conditions:

	RCAT90
Temperature (°C)	90
Duration (hr)	185*
Amount of bitumen (g)	500g

NB: *The long term aging time of bitumen in the standard is specified as 140 hours. An aging time of 185 hours was used to account for the high amount of aging of PA mixtures. This testing condition was also used to compare the results with those obtained in previously performed studies at DWW.

4.2 Preparation of Porous Asphalt Specimens

According to the Dutch specification (RAW 2005), PA mixtures are required to have a minimum voids content of 20%. Use of a middle sort filler with 25% hydrated lime (bitumen number BN54/60, NEN-EN 13043 / NEVUL 2006) and a 70/100 pen grade bitumen is also specified regardless of the origin/source of the bitumen.

Porous asphalt mixture aging was conducted in a weathering chamber to combine effects of temperature, UV light, and humidity, in the aging process. The reason for combining these effects in the accelerated aging of asphalt mixture is to simulate the aging conditions of PA in the field. Three aging protocols were considered for the aging of porous asphalt. They are discussed in detail in Section 4.3 Table 4.3. The first two protocols were conducted using Marshall Tablet specimens. The third protocol was performed with asphalt beams cut from a PA slabs. This was done to effectively use the aging space in the weathering chamber and minimize the effect of aging on the side of the specimens.

4.2.1 Specimens for Aging Protocol 1 and 2

The materials used in the preparation of PA specimens for aging are presented in Table 4.1.

Table 4.1: Material properties used in the aging of bulk bitumen and asphalt mix

Type of material	Grade / Size	Density (kg/m ³)
Bitumen	70/100 pen	1030
Aggregate (Quarry material)	2 mm – 16 mm	2770 (average)
Sand (crushed sand)	0.063 mm – 2 mm	2781
Filler (Wigro 60K)	< 0.063 mm	2620

The Marshall method was used to compact the asphalt specimens according to the procedure in the Dutch standard specifications (RAW 2005, Table 4.2). The specimens were compacted using 50 blows on each side of the tablet. The specimen dimensions are 100 mm in diameter and of varying thickness. The thickness of the samples was within the range of 40 – 43 mm. With the CT scan method and the conventional void content determination procedure, it was verified that the mixes had uniform voids throughout the thickness but most samples had lower voids content than the anticipated target voids content above 20% (see also section 4.3.3).

Core size (Marshall Tablets):

Thickness h = variable (40 – 43 mm),

Void content (average) = 15.9%, Diam. ϕ = 100 mm.

Table 4.2: Composition of PA mixture based on the Dutch standard (RAW 2005)

Sieve / Aggregate size (mm)	Density (kg/m ³)	RAW Spec. % retained	% ret. by weight.	Cumm. % ret.	Weight (gm)
C 22.4 – 16.0	2778	0 – 5	1.7	1.7	12.3
C 16.0 – 11.2	2774	15 – 30	21.0	22.7	151.6
C 11.2 – 8.0	2762	50 – 65	33.5	56.2	241.9
C 8.0 – 5.6	2765	70 – 85	21.7	77.9	156.7
C 5.6 – 2.0	2677	85	7.1	85.0	51.3
2.0 – 0.063	2781	95	10.9	95.9	78.7
< 0.063	2720	100	4.1	100.0	29.6
(Filler: Wigro 60K)					722.0
Bitumen 70/100	1030	4.5% by wt.			34.7
Total wt.					756.7

Aggregate: Quarry material (Bestone, Bremanger Quarry, Norway),
Type: Sand stone, supplied by Graniet Import BV
Average density = 2770 kg/m³ (see Table 4.2)

Sand: Crushed sand (size: 0.063 mm – 2 mm)

Sieve size (mm)	% retained	Cumm. % ret.
2.0	8.2	8.2
0.5	49.0	57.2
0.18	28.4	85.7
0.063	12.6	98.2
< 0.063	1.8	100.0

Filler: Wigro 60K (size: < 0.063 mm)
limestone filler with 25% hydrated lime (KA25)
Bitumen: 70/100 pen bitumen,
supplied by Q8 / Kuwait Petroleum B.V.
(Pen = 90.7 dmm, Softening point $T_{R\&B}$ = 45.4°C)

4.2.2 Specimens for Aging Protocol 3

The specimens for aging protocol 3 are PA mixture beams cut out from a PA slab. The dimensions of the mould used to prepare the PA slab are provided in Table 4.3.

Table 4.3: Input data for PA slab preparation

Mould / slab dimension ¹	700 × 700 × 50 mm
Volume of slab	0.0245 m ³
Density of PA (assumed)	1950 kg/m ³
Slab weight	47.8 kg

¹SHRP specifies slab size: 762 mm x 762 mm x 101.6 mm

Material Composition: The material quantities used to prepare the PA mixture slabs are presented in Table 4.4 and Figure 4.1.

Table 4.4: Material quantities of PA slab according to Dutch PA mixture standard

	Fractions	Spec. (% ret.)	Frac. by wt.	volume (m ³)	unit wt. (kg/m ³)	Tot. wt. (kg)
Aggregate	11/16	15 - 30	0.25	0.0042	2770	11.43
	8/11	50 - 65	0.35	0.0059	2770	16.00
	4/8	70 - 85	0.25	0.0042	2770	11.43
Sand	0.063 - 2mm	85	0.105	0.0017	2781	4.80
Filler	Wigro 60K	95.5	0.045	0.0008	2620	2.05
Bitumen	70/100 pen	4.5%	0.045	0.0020	1030	2.06
		Sum	1.045	0.0189*		47.78

*Expected Voids content: $(0.0245 - 0.0189)/0.0245 \times 100 = 22.9\%$

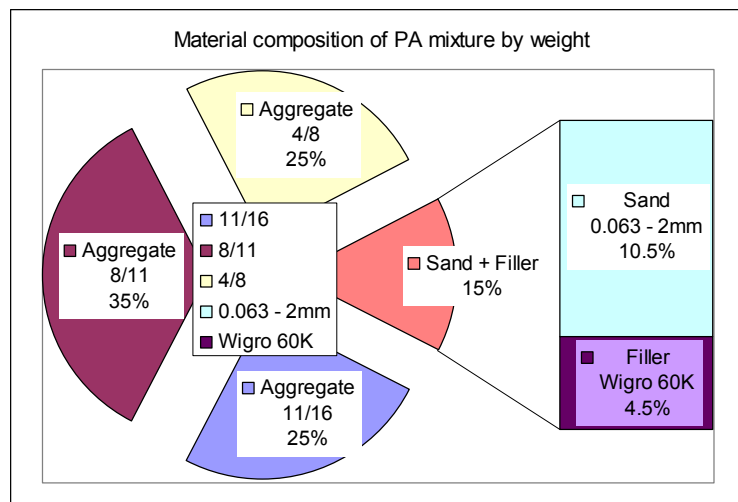


Figure 4.1: Aggregate composition of a standard PA mixture based on weight fractions

The preparation of the porous asphalt slab was performed according to the SHRP bituminous mixture preparation procedure (SHRP Designation: M-008 based on SHRP product 1015). First, all the materials needed for the asphalt slab preparation were placed in an oven at a temperature of 160°C (EVT) for about 3 hours before the start of the mixing. In addition to the materials, the apparatus necessary for the preparation (i.e. the mixing bowl, compacting plates and other equipment) were also kept in the oven at the same temperature and for the same duration. Bitumen was heated for 1.0 – 1.5 hours in the oven before the mixing of the materials took place. Each material was weighed in two portions in order to carry out the mixing in two runs. Before the start of the mixing, bitumen was poured into the bowl and the other materials were placed in the mixing bowl according to their sizes, i.e. courser aggregates were placed first followed by sand and filler. The mixing was conducted for a duration of 3 min using a Hobert H600 mixer (capacity 60 Quart \approx 56.8 lt). This mixing time was considered necessary to ensure thorough mixing of the bulky amount of asphalt.

After mixing, the asphalt mixture was poured into the mould and the spreading and leveling of the loose mixture in the mould was performed manually before rolling the mixture. The compaction was first performed using a vibratory plate (Kango hammer) followed by rolling with a smooth steel/wheel roller (hand roller weights 164.4 kg width = 60 cm and ϕ = 50 cm, Figure 4.2). The compaction was performed before the temperature of the asphalt drops below 100°C. To avoid the bitumen from sticking to the roller during the compaction process, water was applied to wet the surface. To ensure compaction along the edges, the rolling was performed outside the slab dimensions. This was made possible because of extra spacing of about 40 cm along all sides of the mould (see Figure 4.2). The compaction was carried out in all directions in order to apply uniform compaction effort.



Figure 4.2: Mixing and pouring of porous asphalt mixture during slab preparation

The preparation of beams for aging in a weathering chamber (weatherometer) was carried-out according to the schematic plan shown in Figure 4.3. About 50 mm from all edges of the slab was trimmed-off to avoid inadequately compacted parts of the slab. As shown in Figure 4.3, the slab was divided into four each having 300 × 300 × 50 mm size. Beams with dimensions 100 × 300 × 50 mm were cut from the slabs for aging in the weatherometer. Four cylindrical specimens with 100 mm diameter were also cored from the slab for the

determination of density (both bulk and maximum densities), voids content and bitumen content.

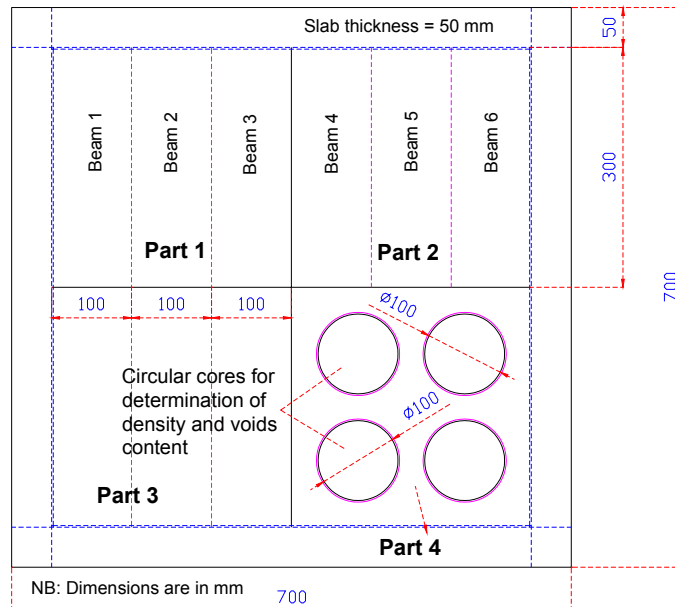


Figure 4.3: Layout showing beam segments and cores made from the fabricated slab

4.3 Weatherometer Aging of Porous Asphalt

4.3.1 Accelerated Weathering Test

Available equipment

The available laboratory equipment for accelerated weathering test is SUNTETST XXL+ from Atlas Materials (Figure 4.4). The testing instrument simulates the environmental parameters of sunlight, temperature, and moisture/humidity. It uses an artificial light source (Xenon arc lights) that closely simulates the UV and visible part of the solar radiation (Figure 4.5). This equipment is recommended to accelerate the aging of materials exposed to natural sunlight during service. The instrument is suitable to age PA mixture slabs or cores since it allows horizontal positioning of the specimen.



Features:

- 1 The XXL+ with its rain and humidity functions is ideal for weathering testing.
- 2 Measurement and control of Chamber Air Temperature (CHT, max. 70° C during light phase)
- 3 3 air-cooled xenon lamps with adjustable power range between 1.7 and 2.1 kW
- 4 Static, flat sample array, maximum exposure area 3081 cm²
- 5 Specimen tray with 5° slope (as recommended in many standards) for optimum spray water drain
- 6 Measurement and control of irradiance, broad band in the UV range (300-400 nm) in W/m², or narrow band at 340 nm or at 420 nm in W/(m²nm); switch between control points without having to change hardware
- 7 Measurement and control of Black Standard Temperature (BST, max. 100° C during light phase) or Black Panel Temperature (BPT) at sample level
- 8 Selectable temperature control: CHT or dual control of CHT and BST/BPT
- 9 Measurement and control of relative humidity
- 10 Ultrasonic humidification and specimen spray system

Figure 4.4: The SUNTEST XXL+ weathering instrument used for aging asphalt specimens

Past experiences

Aging protocols to simulate outdoor aging conditions were developed by DWW for porous asphalt concrete. The aging protocols used to simulate the Dutch climate are given in Table 4.5 (CROW 1996).

Table 4.5: Artificial Aging procedures

Procedure 1a			Procedure 1b			Procedure 2		
Duration [hrs]	Condition	Temp. [°C]	Duration [hrs]	Condition	Temp. [°C]	Duration [hrs]	Condition	Temp. [°C]
4	Rain	20	4	Rain	20	16.25	Open	50
4	UV	60	7	UV	50	4.0	NaCl	40
3	Rain	40	4	UV	50	1.0	Rain	20
4	UV	60	3	Rain	40	2.75	Frost	-20
3	Rain	20	6	Frost	-20			
6	Frost	-20						

Porous asphalt specimens were aged in a climate chamber build-up to conduct the artificial aging under the aging protocols stated in Table 4.5. Specimens were aged for 1, 2, 3, 4, 6, 8, 10, and 12 weeks and it was expected that 1 week aging will correspond to 1 year aging in the field. This assumption did not work with procedure 1a and this led to procedure 1b. This procedure was chosen by DWW to prevent the observed deformation and segregation (drainage of mortar) of the PA specimens by reducing the aging temperature to 50°C. Finally, DWW adopted procedure 2 with the introduction of salt water. According to the results of the test, no change in the Indirect Tensile Strength was observed in relation to aging time under both aging procedures. The penetration dropped by 28% after 10 weeks of aging time. This means that the aging method did not simulate the field aging conditions of PA accurately according to the results of tests performed on field binders (refer to chapter 5).

The difference between the aging protocol of DWW and this study is that the aging conditions in this research are uniform throughout the aging process. The

aging protocols combine the effects of environmental factors (i.e. temperature, UV light, and humidity) (refer to Table 4.13). Moreover, the aging process did not take into account the conditioning of the specimen at low temperature (frost) because the aging of bitumen occurs at higher temperatures due to oxidation.

4.3.2 Background on Weathering Factors

Any material is subject to the influence of environmental factors during its life time. These factors include (but are not limited to) temperature, UV exposure, rainfall, and humidity. Absorption of UV radiation results in degradation of materials that changes the chemical composition of the material. Change in the chemical characteristics of a material is also reflected in a change in the physical property of the material such as its strength and deformation abilities. The effect of UV radiation is, therefore, an important factor to consider during the aging process of bituminous materials. In setting out an accelerated weathering procedure, not only temperature but all the factors of weathering in real life need to be taken into account to simulate “natural aging”. In order to accelerate the aging process, the weathering test should be conducted at elevated temperature. Nevertheless, care should be taken to conduct the test at realistic temperature to avoid deviation from chemical reactions that take place in practice. To determine the realistic conditions of weathering, it is imperative to analyse the prevailing weather conditions.

Exposure to UV light

The light from the sun basically consists of three components: UV, VIS, and IR representing ultra-violent, visible, and infra-red lights respectively (Table 4.6). The shorter wave lengths have a greater influence on the degradation of a material since higher energies are absorbed by the material that may exceed bond energies.

Table 4.6: Relative Spectral irradiance

Range Name	Wavelength range	% of Total solar
UV	295 – 400 nm	6.8%
VIS	400 – 800 nm	55.4%
IR	800 – 2450 nm	37.8%

(Source: CIE pub. 85, table 4)

The irradiance data in Table 4.6 corresponds with CIE no. 85, table 4. Xenon arc lights, when appropriately filtered, produce radiation with a spectral power distribution that simulates the average daylight throughout the UV and visible region (Atlas materials 2001). Figure 4.5 shows the spectral energy distribution of sun light and Xenon lights in the UV and VIS region (wavelength 295 – 800 nm). It can be seen from Figure 4.5 that the Xenochrome 300 reasonably simulates the natural (sunlight) spectrum in the UV region (i.e. 295 – 400 nm).

A number of factors can be mentioned for the poor degree of correlation between accelerated laboratory tests using light sources and exterior or outdoor exposures (ISO 4892-1, ISO 4892-2):

- difference in the spectral distribution of the laboratory light source and daylight;
- light intensities higher than those experienced in actual-use conditions;
- exposure cycles that use continuous exposure to light from a laboratory light source without any dark periods;
- specimen temperatures higher than those in actual conditions;
- exposure conditions that produce an unrealistic temperature differences between light- and dark-coloured specimens;
- exposure conditions that produce very frequent cycling between high and low specimen temperatures, or that produce unrealistic thermal shock;
- unrealistically high or low levels of moisture;
- the absence of biological agents or pollutants;
- the absence of traffic loading; etc.

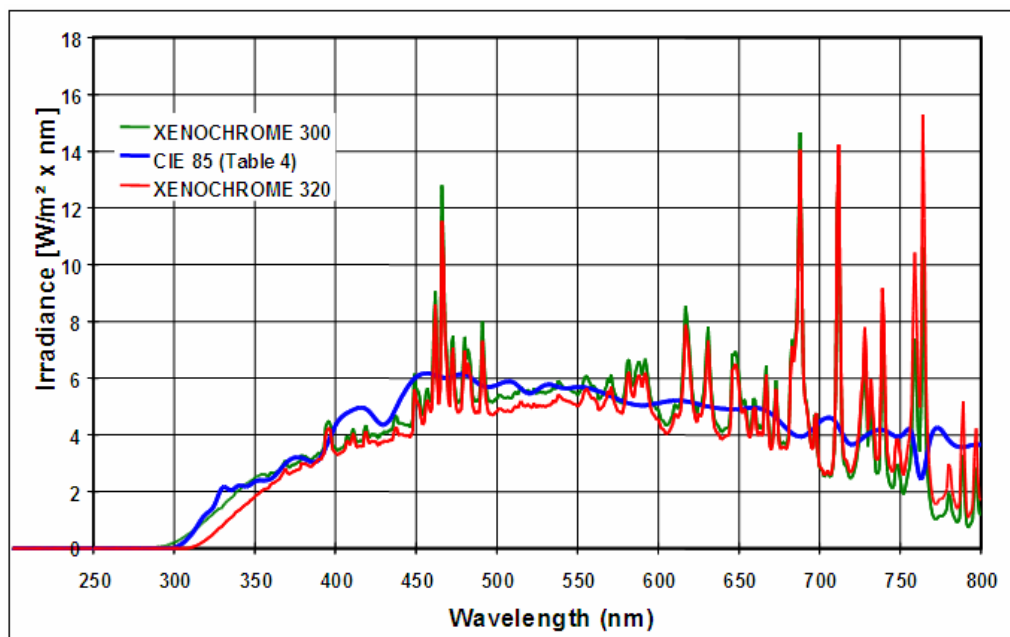


Figure 4.5: Filter combination for Xenotest instrument (Source: ATLAS Materials)

In simulating real life weathering conditions, one has to consider the site specific conditions. These are related to aspects such as latitude/longitude, elevation (altitude), temperature, rainfall, etc. as well as the effects of seasonal changes. Some relevant climatic data are given in Table 4.7.

Table 4.7 gives weather information for Lochem and Hoek van Holland, which are locations in the Netherlands, and for central Europe.

Table 4.7: Climatological data for Lochem (the Netherlands, NL), Hoek van Holland (NL), and Central Europe

Climatological Data	Lochem (Netherlands, NL)	Hoek van Holland (NL)	Central Europe
Latitude	52°30'N	51°57'N	
Longitude	6°30'E	4°10'E	
Elevation above MSL (m)	35	6	35
Average Amb. Temp. (°C)	9	10	10
Relative Humidity RH annual mean (%)	83	87	82
Annual mean rainfall (mm)	715	800	800
Annual mean radiant exposure (MJ/m ²)			
Total (295 - 3000 nm)	3700	3800	3550
UV (295 - 385 nm)			215
UV+VIS (295 - 800 nm)			2050
UV at 340 nm			1.90
Xenon light	550 W/m ² (300 - 800 nm) → (UV + VIS) 60 W/m ² (300 - 400 nm) → (UV) 0.55 W/m ² (340 nm) → (UV, at one wavelength)		

(Source: ATLAS Materials 2001, Weather Testing Guidebook)

The weathering instrument uses Xenon lamps which simulate the characteristic exposure irradiance given in Table 4.6. These values can be used to convert the exposure of a material in the natural weathering to accelerated equivalent number of hours in the weatherometer. The time required to expose a sample material in the weatherometer to equivalent number of hours in the field can be calculated using Equation 4.1.

$$t(hr) = \frac{\text{Radiant Exposure } H (Ws / m^2)}{\text{Irradiance } E (W / m^2) * 3600 (s / hr)} \quad (4.1)$$

The exposure time needed for simulating one year Central Europe based on 300 - 800 nm exposure in the field can be calculated as follows:

$$t(hr) = \frac{H (Ws / m^2)}{E (W / m^2) * 3600 (s / hr)} = \frac{2050 * 10^6}{550 * 3600} = 1035 hr \quad (1 \text{ MJ/m}^2 = 10^6 \text{ Ws/m}^2)$$

Similarly, if we consider irradiance exposed in the UV range (300 - 400 nm) for one year, the equivalent hours to simulate field conditions will be:

$$t(hr) = \frac{H (Ws / m^2)}{E (W / m^2) * 3600 (s / hr)} = \frac{215 * 10^6}{60 * 3600} = 995 hr$$

From the above calculations, 1000 hours of UV exposure in a weathering chamber seems realistic to simulate the effect of 1 year UV radiation. Since

laboratory aging is conducted at elevated temperatures, the rate of reaction is also accelerated. Therefore, combining the effect of high aging temperature with UV exposure (simulation of sunlight irradiation) will accelerate the overall aging process. The other factors involved in weathering, such as temperature and humidity, are determined by analysing data of prevailing weather conditions. The provision of rest periods (light and dark periods) in the aging process may be important to allow healing of the material. And, in simulating real weathering situations, some chemical reactions that might take place during dark periods may have the chance to occur. On the other hand, it is desired to achieve the end results of the aging effect in a shorter aging period. For that reason, no rest periods were applied in the weathering process.

Analysis of meteorological data

Meteorological data of five locations in the Netherlands were considered for analysis. The objective behind the weather data analysis is to develop an aging protocol for a porous asphalt mixture based on outdoor weather conditions. The climatic data was obtained from the Koninklijk (Royal) Netherlands Meteorological Institute (KNMI) database. The six major meteorological stations are De Bilt, Den Helder, Groningen (Eelde), Maastricht (Beek), Twente, and Vlissingen which are situated in the central, north-west, north-east, south, east, and south-west regions of the country respectively. Data on temperature, rainfall, humidity, sunshine hours, rainfall duration collected over 25 years, i.e. from 1981 – 2005, have been analysed.

The year 2003 registered the highest temperatures during the summer period. For this reason, the 2003 data is presented in comparison to the average for the period 1981 – 2005 to come up with extreme but practical weather conditions which can be used for the aging protocol in the available weathering equipment.

Temperature data: The daily average temperature data and standard deviations for the 12 months of the year are presented in Table 4.8. The data is the averages of the six meteorological stations. The temperature data is categorized in two seasons: the hottest months or “summer” period (May - October) and the coldest months or “winter” period (November - April) instead of combining the whole year data. The minimum, maximum, and mean daily average temperatures on monthly basis are presented in Figure 4.6.

Table 4.8a: Monthly mean temperature data for the year 2003

	Min temp		Max temp		Mean	
	Avg. (°C)	Stdev.	Avg. (°C)	Stdev.	Avg. (°C)	Stdev.
January	-0.4	5.5	4.9	4.4	2.5	4.6
February	-1.9	3.3	5.5	4.2	1.6	3.2
March	2.5	3.0	12.0	3.3	7.2	2.3
April	4.3	4.5	14.8	5.6	9.7	4.7
May	8.7	2.8	17.6	3.5	13.2	2.7
June	12.2	2.2	23.1	2.8	17.9	1.8
July	13.7	2.1	23.7	3.8	18.8	2.6
August	14.0	2.8	24.8	4.7	19.5	3.4
September	9.4	2.6	20.2	3.6	14.8	2.7
October	3.7	4.3	11.8	3.2	7.8	3.5
November	5.3	2.9	10.6	2.5	8.0	2.4
December	1.5	3.7	7.0	2.8	4.3	3.1
Summer ⁴	10.3	2.8	20.2	3.6	15.4	2.8
Winter ⁵	1.9	3.8	9.1	3.8	5.5	3.4
Average	6.1		14.7		10.4	

Table 4.8b: Monthly mean temperature data for the year 1981 - 2005

	Min temp		Max temp		Mean	
	Avg. (°C)	Stdev.	Avg. (°C)	Stdev.	Avg. (°C)	Stdev.
January	0.5	4.8	5.3	4.3	3.0	4.4
February	0.2	4.6	5.9	4.2	3.1	4.2
March	2.5	3.4	9.3	3.6	5.9	3.1
April	4.3	3.3	12.8	4.1	8.6	3.3
May	8.1	3.1	17.2	4.5	12.7	3.4
June	10.7	2.7	19.5	4.1	15.2	3.0
July	13.0	2.5	21.9	3.9	17.4	2.8
August	13.0	2.7	22.2	3.8	17.6	2.8
September	10.5	2.8	18.5	3.1	14.4	2.4
October	7.3	3.6	14.1	3.3	10.7	3.1
November	3.8	3.8	9.2	3.5	6.6	3.5
December	1.4	4.2	6.1	3.9	3.9	4.0
Summer	10.4	2.9	18.9	3.8	14.7	2.9
Winter	2.1	4.0	8.1	3.9	5.2	3.7
Average	6.3		13.5		9.9	

⁴ "Summer" in this context refers to the months May - October⁵ "Winter" refers to the months November - April

The average maximum temperature during the summer period for 2003 is 20.2°C while that of the 1981-2005 is 18.9°C. And the average minimum temperature during the winter period is 1.9°C and 2.1°C for the year 2003 and 1981-2005 respectively. The highest average temperature recorded was 24.8°C (Standard deviation, STD = 4.7°C) registered in the month of August in 2003. The average minimum and maximum temperatures presented in Table 4.8 are shown graphically in Figure 4.6.

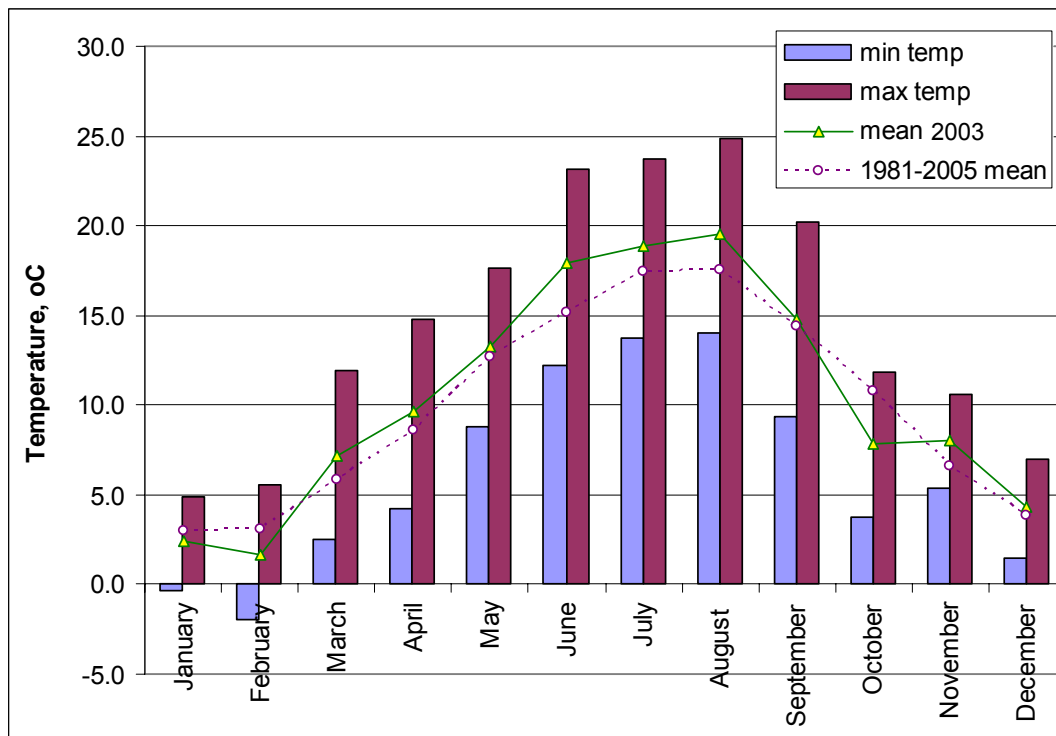


Figure 4.6: Monthly mean minimum, maximum, and average temperatures for 2003

Sunshine hours and Humidity: Table 4.9 shows the monthly distribution of average sunshine duration in hours (average of the six meteorological stations), which is also presented graphically in Figure 4.7. This figure also shows relative humidity data. According to the meteorological data in Table 4.9, about 65% of the total sunshine duration prevails during the summer period and the remaining 35% during the winter period.

Table 4.9: Monthly mean sunshine duration and relative humidity data

2003

	Sunshine duration, hr	Humidity RH, %
January	70.7	86.9
February	153.5	80.9
March	192.0	78.1
April	230.9	68.1
May	211.0	78.5
June	254.4	74.8
July	237.7	75.4
August	241.4	73.4
September	210.8	77.9
October	151.4	83.1
November	75.1	89.5
December	64.5	87.7
Summer	1306.7	75.9
Winter	786.6	81.8
Total/ Avg.	2093.3	79.5

Sunshine duration (hrs/yr.):

Total duration	23.9 %
Summer	14.9 %
Winter	9.0 %

1981 - 2005

	Sunshine duration, hr	Humidity RH, %
January	58.0	88.1
February	86.1	84.9
March	116.3	82.9
April	164.8	77.3
May	205.4	77.0
June	186.0	78.3
July	203.7	78.5
August	193.6	78.8
September	136.6	83.3
October	108.5	85.6
November	63.1	88.8
December	45.3	89.4
Summer	1033.8	79.8
Winter	533.6	85.2
Total/ Avg.	1567.4	82.7

Sunshine duration (hrs/yr.):

Total duration	17.9 %
Summer	11.8 %
Winter	6.1 %

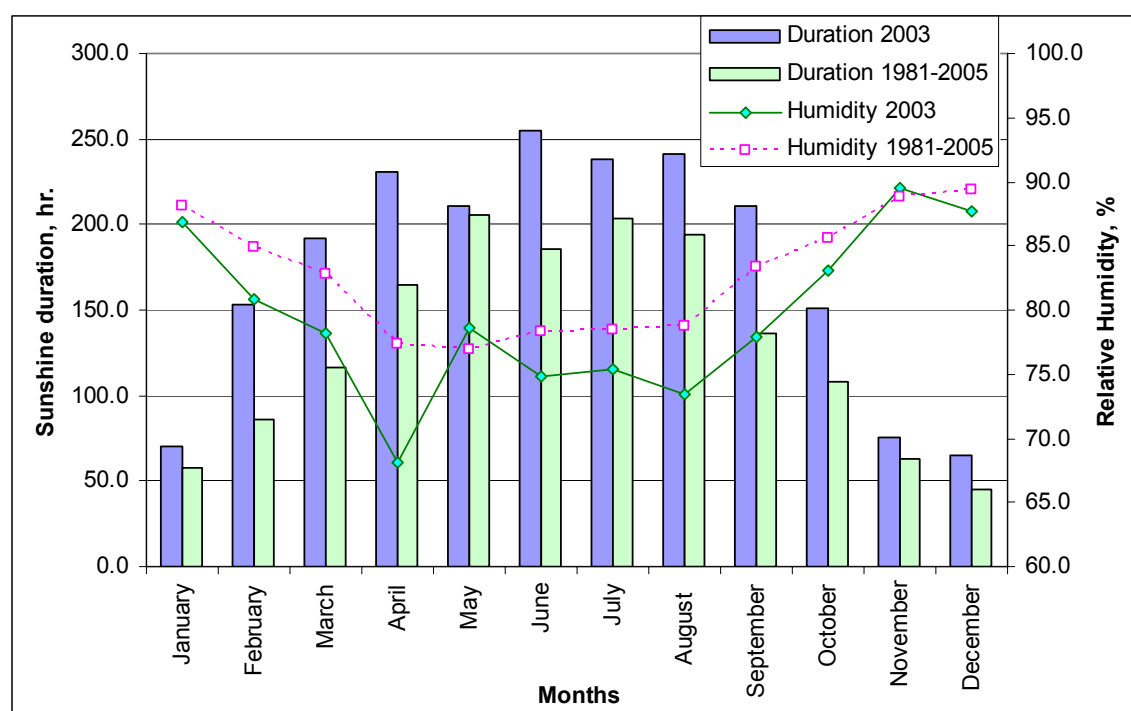
NB: Total duration/yr = $365 \times 24 = 8760$ hrs

Figure 4.7: Monthly mean sunshine hours and humidity for the year 2003 and 1980 – 2005

The relative humidity for the Netherlands is on average 82.7% and varies between 77.0% and 89.4% throughout the year. The lowest relative humidity is observed during the summer periods as shown in Figure 4.7. It can be observed from the 2003 data that the relative humidity drops with increase in temperature.

Rainfall duration and amount: Meteorological data of rainfall for the period 1981 – 2005 shows that on average the duration of rainfall covers 7.5% of the total time in a year and amounts to 783 mm. It should be noted, however, that the period during which the pavement is wet or moist is longer than the rainfall duration. The precipitation amount during summer and winter periods is respectively 52.8% and 47.2% of the total average. The monthly average amount of precipitation and duration for the year 1981-2005 and 2003 is shown in Figure 4.8.

Table 4.10: Monthly mean precipitation data for the year 2003 and 1981 – 2005

2003			1981 - 2005		
Precipitation	Amount	Duration	Precipitation	Amount	Duration
	(mm)	(hr)		(mm)	(hr)
January	70.6	76.3	January	69.4	74.8
February	23.1	23.3	February	49.9	55.3
March	25.0	28.0	March	59.4	64.5
April	42.3	28.7	April	44.1	45.4
May	83.7	63.6	May	55.9	42.4
June	38.1	14.3	June	69.4	46.0
July	45.7	27.8	July	66.2	35.8
August	24.9	19.2	August	64.4	34.1
September	53.8	33.0	September	78.4	53.4
October	73.4	52.9	October	79.4	61.1
November	44.3	62.7	November	72.1	70.7
December	84.8	76.1	December	74.5	76.8
Summer	319.6	210.8	Summer	457.8	272.7
Winter	290.2	295.0	Winter	369.2	387.5
Total	609.8	505.8	average	783.0	660.2
Duration		5.8%	Duration		7.5%

NB: Data is average of the six meteorological stations

From the analysis of the data for the six stations, it was observed that the temperature and sunshine duration shows a decline away from the coastline, i.e. from west towards east of the country. On the other hand, precipitation duration and amount seems to increase further from the coastline.

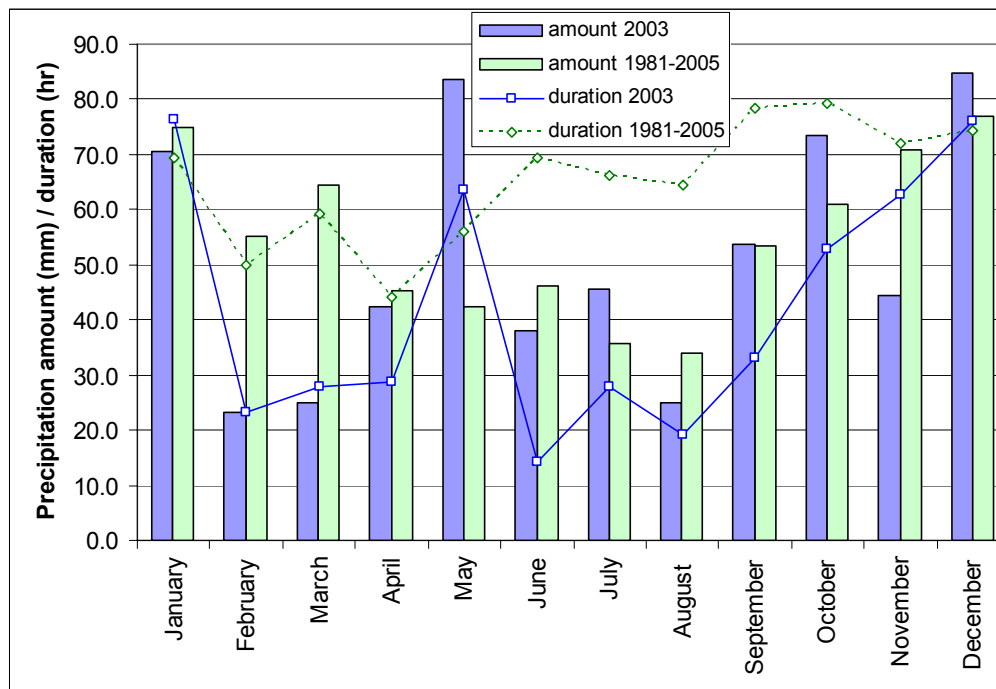


Figure 4.8: Monthly mean precipitation amount and duration for 2003 and 1981 – 2005

Pavement temperature prediction

Different methods exist to predict pavement temperatures in relation to atmospheric temperature and other meteorological parameters. Existing methods include the Finite Element program WEGTEM, BELLS3 model (CROW - The national information and technology platform for infrastructure, traffic, transport and public space in the Netherlands), and Solaimanian and Kennedy (1993) method. Equation 4.2 by Solaimanian and Kennedy (1993) was employed to estimate the pavement surface temperature from maximum air temperatures. The equation is based on energy balance at the pavement surface.

Table 4.11: Predicted pavement temperatures from atmospheric temperature data

2003 max temp data			(95% confd.)	Pavement temperature
	max. air temp.	Stdev.	Air temp.	
June	23.1	2.8	28.7	
July	23.7	3.8	31.3	
Aug.	24.8	4.7	34.2	51.2
Sep.	20.2	3.6	27.4	
Average			30.4	47.8

$$422\alpha\tau_{\alpha}^{1/\cos z} \cos z + 0.7\sigma T_a^4 - h_c(T_s - T_a) - 90k - \varepsilon\sigma T_s^4 = 0 \quad (4.2)$$

Where:

- z = zenith angle (approx. z = latitude - 20 for May through August),
- τ_{α} = sunshine factor (0.81 for perfectly sunny conditions)
- α = solar absorptivity (default 0.9)
- σ = Stefan Boltzman constant (0.1714E-08 Btu/(hr.ft².R⁴))

h_c	=	surface coefficient of heat transfer (default 3.5 Btu/(hr.ft ² .F))
k	=	thermal conductivity (default 0.8 Btu/(hr.ft ² .F)/ft)
ε	=	surface emissivity (default 0.9)
T_a	=	max air temperature (Rankine)
T_s	=	max pavement surface temperature (Rankine)

Using the 2003 temperature data for the months that have registered average max air temperature greater than 20°C, the max pavement temperature has been calculated. Accordingly, the expected maximum pavement surface temperature for the month of August that registered an average max air temperature of 34.2 (95% confidence level) is determined to be 51.2°C. This is close to the recorded max pavement temperature of 52.7°C reported by Voskuilen 2001. Similarly, the average monthly pavement surface temperature based on the June to September data is estimated to be 47.8°C.

The pavement temperature at any depth can be calculated using the empirical formula given in Equation 4.3 (Solaimanian and Kennedy 1993).

$$T_d = T_s (1 - 0.063d + 0.007d^2 - 0.0004d^3) \quad (4.3)$$

Where:

T_d = the maximum pavement temperature at depth d (°F),

T_s = the maximum pavement temperature at the surface (°F),

d = the depth in inches (in).

Using Equation 4.3, the pavement temperature at the bottom of a PA layer is calculated as 43.2°C (Table 4.12). However, this model was developed for dense asphalt. The variation in temperature within the asphalt thickness is expected to be insignificant for PA because of its high porosity.

Table 4.12: Pavement temperature along pavement thickness

Depth	Depth		Temp @ depth d (°C)	
	(mm)	(in)	$T(d)$	Percentage
Depth	0	0	47.8	100.0
	-50	1.27	43.2	90.5
	-100	2.54	39.8	83.3
	-150	3.81	37.2	78.0
	-200	5.08	35.2	73.7
	-250	6.35	33.3	69.8
	-300	7.62	31.3	65.6

The sunshine duration of the hottest summer in 2003 and the average for the period 1981-2005 are 1307 and 1034 hours respectively. Hence, the exposure of samples for 1000 hours of sunlight simulation in a weathering chamber seems to be in agreement with 1 year PA aging in the field since most of the aging takes place during summer. Nevertheless, since the weathering test is

conducted at elevated temperature in the laboratory, the process of aging (oxidation and UV absorption) is in effect accelerated. The extent of accelerated aging will be checked with a kinetic approach based on the changes in the property of the bitumen with time (refer to Chapter 6).

Proposed PA weathering test

According to a study (Voskuilen et al. 2001) pavement temperature measurements conducted on 6 road sections in the Netherlands in the period 1995 to 2000 registered a maximum of 52.7°C. The selection of the aging temperature in the laboratory was made to reconcile with the maximum temperature expected in the field. Although higher temperatures are preferred to accelerate the aging process, care need to be taken not to alter the chemical reactions that take place in the reality. Another point of concern is the draining-off of the bituminous mortar and/or disintegration of the porous asphalt concrete during the weathering process. The standard norm for weathering plastics (NEN-EN-ISO 4892-2) suggests a temperature of 65°C as an aging/weathering temperature. Nevertheless, a lower temperature of 60°C BST (Black Surface Temperature) and 40°C air temperature was selected on the basis of the points of argument mentioned, which are:

- the temperature of 60°C is assumed as the highest temperature to maximize the rate of aging (minimize the aging time) while maintaining the integrity of the asphalt mixture during aging;
- conducting the aging at elevated temperature accelerates the aging process of PA; even if the effects of one year real life weathering in the field is applied in the process;
- the aging temperature is not too far from the highest practical pavement temperature, thus the chemical process is expected to be similar to field aging;
- results of the test can be compared with the results of other researches conducted at the same aging temperature.

Method of comparing accelerated aging with field aging

In order to correlate the rate of aging in the weatherometer with field aging, the beams are aged for 200, 500, 800, and 1000 hours and after that the binder was recovered for rheological and chemical characterization. The recovery of bitumen is conducted in the same manner as the recovery of bitumen from field materials. So, the correlation of the binder properties will be based on the same grounds which avoid any bias with respect to the effects of recovery on the binder property.

Assessment of the effect of accelerated laboratory aging on the properties of bitumen has been carried out in relation to the aging rate of field materials (natural aging) as shown in Figure 4.9. The method of correlation is based on a kinetic approach. The change in chemical property of binders aged in the

laboratory is compared with the aging rate observed in the field. The aging rate of bitumen recovered from field specimens, i.e. from a newly laid PA layer and from sections with a service life of 1, 3, 7, and 12 years, is used as a reference for correlating the aging effect of accelerated weathering in the laboratory. As illustrated in Figure 4.9, aging properties of laboratory binders are identified along the line describing the aging property of field materials. These points will provide the equivalent number of years of PA aging in the field for the aging achieved using the laboratory procedures.

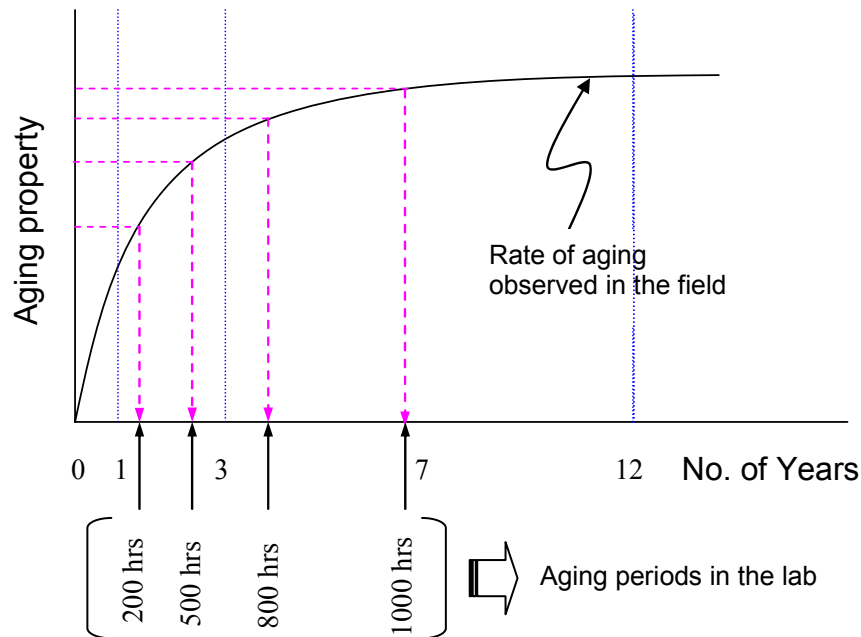


Figure 4.9: Illustration of correlation between field and laboratory aging protocols

4.3.3 The Aging of Asphalt Mixtures Produced in the Laboratory

Different aging protocols were proposed for accelerated aging of PA:

- Aging protocol 1: Temperature aging,
- Aging protocol 2: Temperature and UV light exposure,
- Aging protocol 3: Temperature + UV light + humidity,

The details of the aging protocols are given in Table 4.13. A fourth protocol that takes into account the effect of cyclic dry and wet aging has been excluded from the testing program due to time shortage.

Table 4.13: Proposed aging protocols

Aging Protocol	Protocol 1	Protocol 2	Protocol 3
	<u>Marshall specimens</u>		<u>Beams from slab</u>
Air temp. [°C]	40	40	40
*BST Temp. [°C]	60	60	60
UV light (300 - 400 nm) [W/m ²]	-	60	60
Rain/Water application [-]	-	-	-
Humidity [%]	-	-	70
Time [hr]	1000	1000	1000

*NB: BST = Black Surface Temperature → temperature at the surface of the specimen

Although the mean average relative humidity for the entire year is between 77.0% and 89.4% based on climate data, a lower value of 70% was used in aging protocol 3 because of the limitations of the weathering equipment.

PA Mixture Aging: Protocol 1 and 2

The aging of laboratory produced mixtures following protocol 1 and 2 was done on Marshall specimens (see Table 4.14). The aging tests were conducted at Atlas materials laboratory using a weathering instrument named SUNTEST XLS+. This equipment has similar functions as the one used for aging protocol 3 (Figure 4.10).

- Protocol 1: aging under the influence of temperature, and
- Protocol 2: aging under the combined effects of temperature and UV light.

Table 4.14 shows the test conditions for the two aging protocols. The binder recovery was performed separately for the upper and lower zones of the asphalt cores to investigate the difference in the aging process in the two zones, which is also believed to reflect the conditions of aging in the field.

Table 4.14: Test conditions for aging protocol 1 (temperature) and 2 (temp. + UV)

Marshall Specimens	Reference Samples	Temperature aging (Aging protocol 1)	Temperature + UV (Aging protocol 2)
No. of core samples $\phi = 100$ mm, h = variable	8	8	8
Avg. Voids Content (%)	18.2	16.2	17.8
Test Conditions:			
Aging Temperature	Unaged	60°C	60°C
Time of aging	-	1000 Hrs	1000 Hrs
UV exposure (300-400 nm)	-	-	60 W/m ²

PA Mixture Aging: Protocol 3

Five PA beams were used for aging in the weatherometer (Table 4.15, Figure 4.10). Following protocol 3, the beams were taken from the climate chamber after 200, 500, 800, and 1000 hours of aging time for chemical and rheological characterization. Also the binder of a reference sample from an unaged PA beam was recovered for characterization. During the aging process, the beam positions were shifted every 7 days (every week) to ensure uniform exposure to UV radiation. The test was conducted during the summer period, June 13 to September 23, 2006.

Table 4.15: Test conditions for aging protocol 3 (temp. + UV + RH)

Beams from PA slab		Temperature + UV light + humidity (<i>Aging protocol 3</i>)	
No. of beams (300×100 mm)		5	
Avg. Voids Content (%)		23.1	
<i>Test Conditions:</i>			
Aging Temperature	60°C	UV exposure (300-400 nm)	60 W/m ²
Time of aging	1000 Hrs	Humidity (RH)	70 %

The aging of the PA mixture beams in the weatherometer has been repeatedly interrupted due to technical failures of the weathering equipment. The main causes for the interruption were the malfunctioning of the UV lights due to circuit related problems and a defect encountered in the temperature sensors. Moreover, the humidity in the weatherometer was not maintained constant during testing for some unknown reason. The probable causes are believed to be defective humidity sensors and/or high outside (room) temperature. Outside (summer) temperature during the time of testing was reaching above 30°C and could have resulted in the fluctuation of the level of humidity in the weatherometer. The actual humidity has not been either recorded properly or maintained at the target humidity of 70% as per the aging procedure. This has to be taken into account in the interpretation of the results. The laboratory report on the downtime of the weathering equipment is given in Table 4.16.

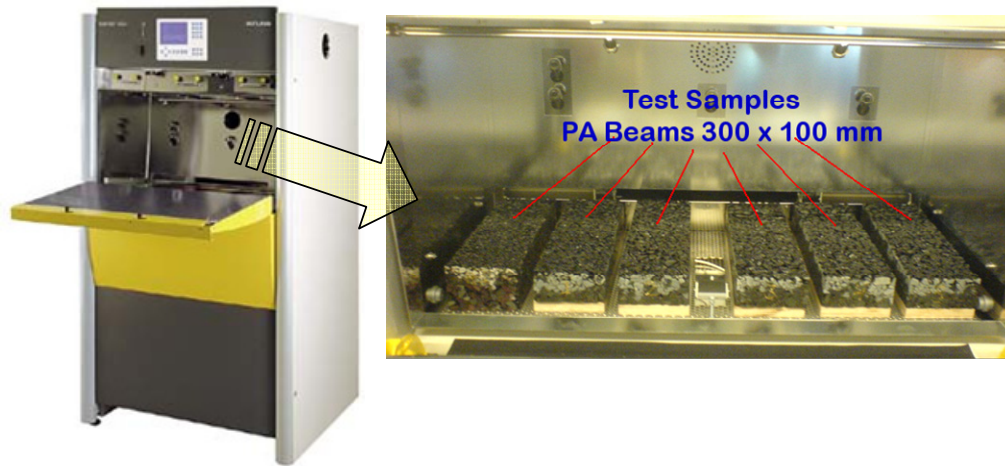


Figure 4.10: Weatherometer (environmental chamber) used for aging PA specimens

Table 4.16: Laboratory report on weatherometer aging of PA mixture

Specimen	Aging time	Humidity*, avg (%)	Remark
1	192	65	192 hr × 65%
2	528	50	200 hr × 65% + 328 hr × 40%
3	768	47	200 hr × 65% + 568 hr × 40%
4	1000	44	200 hr × 65% + 656 hr × 40%
5	1000	44	+ 114 × 35%
			200 hr × 65% + 656 hr × 40%
			+ 114 × 35%
Test started:		13/06/06	
Test finished:		23/09/06	
<u>Aging Test</u>		<u>Downtime</u>	<u>Repair</u>
13/06/06 – 22/07/06		22/06/06 – 07/07/06	07/07/06
07/07/06 – 18/07/06		18/06/06 – 25/07/06	25/07/06
25/07/06 – 07/08/06		07/08/06 – 31/08/06	16/08/06 and 24/08/06
07/09/06 – 15/09/06			15/09/06
*NB: Planned humidity was 70%			

In Table 4.17, the actual and planned aging times are given. The difference arises from the downtime of the weathering equipment due to the encountered technical problems during the process of aging. Some samples had to be taken from the weatherometer before or after weekends because of the caused inconveniences to follow the schedule.

Table 4.17: Planned and actual aging time of PA slabs in the weatherometer.

Specimen #	Desirable aging duration (hr)	Planned aging duration		Actual aging duration (hr)
		(Days)	(hr)	
Ref.	0	0	0	0
1	200	9	216	232
2	500	21	504	472
3	800	33	792	808
4	1000	42	1008	1008
5	1000	42	1008	1008

NB: the duration of actual aging time is higher or lower than the planned time since samples were taken out of the weatherometer before or after the week-end (Friday or Monday) if the actual day falls on Saturday or Sunday.

4.4 Field Asphalt Core Specimens

In order to determine the amount of aging in the field, cores were taken from a PA pavement taking into account the following:

1. Age or service period of the pavement: 0 (new construction), 1, 3, 7, 12 years.
2. Performance: Good and poor ravelling performance.
3. Traffic level: Slow Lane, SL (heavily loaded lane) and Emergency Lane, EL (lane with no traffic loading).

A number of factors can be cited that affect the sampling of representative PA specimens from the road. The variability in the performance of the pavement is associated with those factors, they include:

- traffic level (especially the number of heavy traffic intensity);
- difference in the structural design of the pavements;
- materials used in the PA mixture (bitumen type, filler type, aggregate type, etc.) and mixture composition (binder content, filler/binder ratio, etc.);
- weather conditions;
- quality of construction (asphalt mixture production, laying, & compaction, and weather condition during the construction phase);
- maintenance activities (maintenance frequency and techniques), etc.

4.4.1 Field Specimens

The coring of PA samples was conducted according to the plan outlined in Table 4.18. The three major factors that were taken into account are the age, condition of the road and the level of traffic. In total, PA specimens from 12 road sections were cored.

Table 4.18: Asphalt mixture specimens from the field

Service period, yr	Section	Road condition	Lane	Remaining ** Serv. life, yr	Location	Traffic, vpd (veh./day)
0	G	Good	EL	11.1	A13, 7.5 – 7.7	TT* HT*
1	A	Good	EL SL	10.1	A15, 38.8 – 39.0	TT HT
3	B	Good	EL SL	8.1	A15, 45.6 – 45.8	TT 111,439 HT 20,616
7	C	Good/Fair	EL SL	4.7	A15, 52.8 – 53.0	TT 11,978 HT 20,716
	D	Poor	EL SL	4.3	A15, 52.1 – 52.3	TT HT
12	E	Good/Fair	EL SL	4.9	A15, 71.7 – 71.9	TT 134,250 HT 18,795
	F	Poor	EL SL	3.1	A15, 71.3 – 71.8	TT HT

NB: * TT = Total Traffic, HT = Heavy Traffic

** Predicted using ravelling model (CROW 2002)

In order to get as representative samples as possible, the following were undertaken.

- The cores were taken from one major road in order to ensure that they were all exposed to a similar traffic loading. The A15 motorway that extends from the western to eastern part of the country was chosen for the sampling of the specimens (Figure 4.11) with the exception of cores from newly laid PA. These cores were taken from A13 motorway right after the construction of the surfacing layer.
- In all the 12 road sections, the coring of specimens was planned to be carried out along the cross-sectional and longitudinal profiles, i.e. along the right and left wheel paths of the trafficked lane and at 10 metres distance in the longitudinal direction. Nevertheless, all the samples have been extracted only along one wheel path as shown in Figure 4.12, with the exception of section E.
- The pavement condition in terms of ravelling was measured using a vehicle mounted with a laser device. This device provides information about the condition of the pavement which is related to the loss of stones from the surface of the PA layer. The extent of ravelling is classified as light, moderate, or severe based on the measurement data. In Table 4.19,

the criterion for maintenance intervention adopted by DWW (DWW 2003) is provided in addition to the criterion used for the selection of road sections with good and poor performance.

Table 4.19: DWW's PA pavement condition survey criteria and requirements employed in field materials selection

		Ravelling			
		L	M	E	M+E
Maintenance criteria:	Area % (m²/m²)	11.41	7.32	4.01	11.33
	Length (m)	50	33.53	16.47	50
	Length % (m/m)	25	16.77	8.33	25
Equivalent damage		$M_{eq} = 0.25L + 1.0M + 5.0E$			
NB: L = light, M = moderate, E = severe					
Selection criteria:					
	Road condition*	(length, m)			
	poor	> 30	> 20	> 10	> 30
	good	< 15	< 10	< 5	< 15

*NB: Table 4.19

- Maintenance is necessary when one of the maintenance criteria is met.
- One of the conditions in the selection criteria should be met to describe the performance of the PA pavement as good or poor. The selection criterion was adopted in the selection process of road sections for the coring of field specimens.



Figure 4.11: The A15 motorway selected for the coring of field samples (Source: DWW, Rijkswaterstaat)

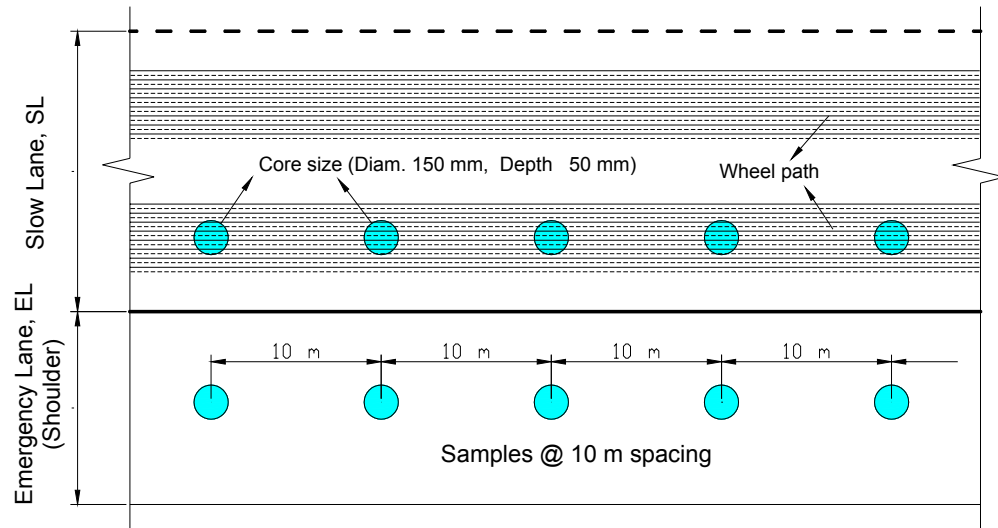


Figure 4.12: The coring of field specimens from motorway A15

Mechanical tests were performed on the field specimens before recovering the bitumen. The results of these tests and their interpretation are presented in Chapter 5. In addition, 3 specimens from each of the road sections were sent to DRI (Danish Road Institute) for the analysis of thin layer and CT-scan data.

The binder of the field core specimens has been recovered for physical and chemical characterization. The recovery process was conducted separately for the upper and lower part of the specimens. As indicated in Figure 4.13, each of the field specimens was cut into upper and lower parts (UZ and LZ) and the upper zone specimens from the same road section were combined during the extraction process.

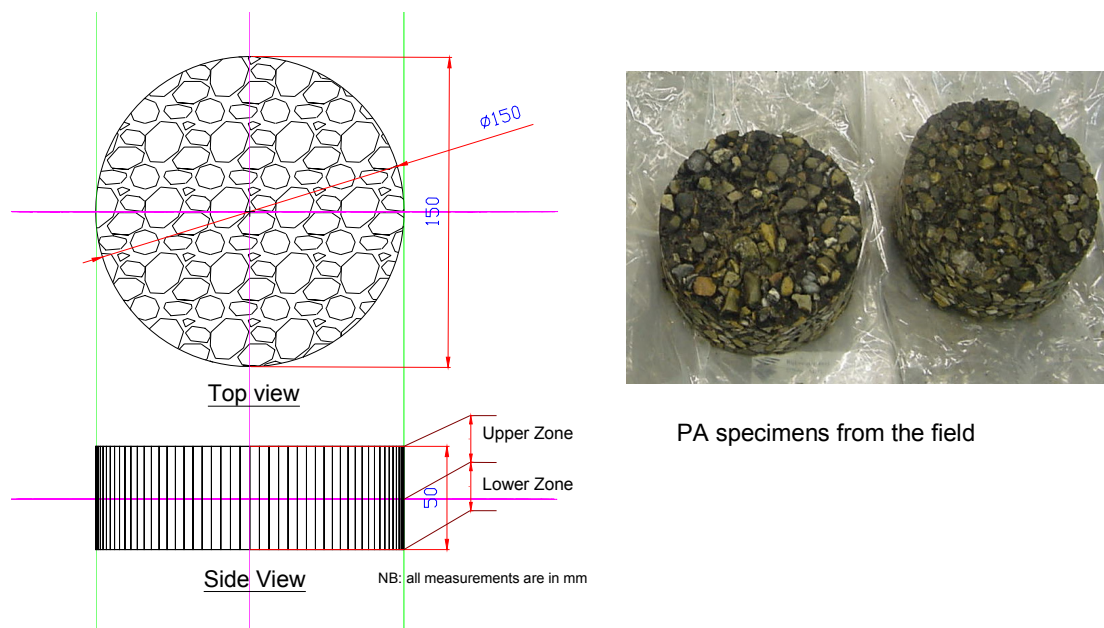


Figure 4.13: The upper and lower zones of field core specimens

Reasons for conducting a separate extraction process for the upper and lower zones are as follows:

- Weathering factors influence the top and bottom part of PA differently. For example, the upper part is more exposed to UV radiation than the lower part. It is important to know the aging behaviour of the binder in the upper part because ravelling takes place on the surface.
- A possible segregation or drainage of the mastic/mortar will reduce the binder film thickness of the upper zone, which influences the aging rate of the binder.

4.4.2 Bitumen Recovery

Bitumen extraction is a process necessary to regain the binder from PA mixture aging (laboratory) and field specimens. The regained binders are used for rheological and chemical tests. In addition, mixture composition of the specimens is determined by the use of the extraction method.

In preparation for the recovery of bitumen from asphalt mixture specimens, both for laboratory aged mixtures and field specimens, the following activities were performed.

- Sawing of the specimens into the upper and lower zones. According the research methodology, the characterization of the recovered bitumen will be conducted independently for the top and bottom part of the mixture.
- Specimens belonging to the same family (aging protocol) were put together in a pan and placed in an oven at 110°C for about 1 hour. The specimens were fragmented and blended together for recovery.
- An amount less than 3.5 kg was placed in a sieve drum for soaking by a solvent.

The recovery of the binder from the bituminous mixture was performed according to the European standard EN 12697-3 and NEN3971, which entails the following.

1. Extraction of the binder from the mixture: separation of the aggregates, sand, and filler from the binder using Dichloromethane (Methylene Chloride, CH_2Cl_2) solvent.
 - a. Binder extraction by dissolving the asphalt mix in cold solvent (Dichloromethane, CH_2Cl_2).
 - b. Separation of mineral matter from the binder solution (centrifuge extraction method).
2. Recovery of the binder from the solution (EN 12697-3): recovery of the bitumen from the solvent using the rotary evaporation method.

Extraction of the binder from the mixture

Due to the limitation to handle more than 3.5 kg of material by the extraction equipment, the extraction of bitumen from specimens cored from the same road

sections were conducted in two steps. The asphalt mixture in the sieve drum was first soaked in a Dichloromethane solvent (Methylene Chloride, CH_2Cl_2) and left overnight to dissolve the bitumen from the mix. The main use of this process was to be able to separate the bitumen from the mixture, i.e. aggregates, sand, and filler, and reduce the workload of the recovery process since less solvent quantity can be used. The extraction was conducted using the fast extraction apparatus InfraTest (Figure 4.14). The extraction process is performed automatically by the “InfraTest” machine once the asphalt material is put in place after specifying the necessary washing and drying steps.

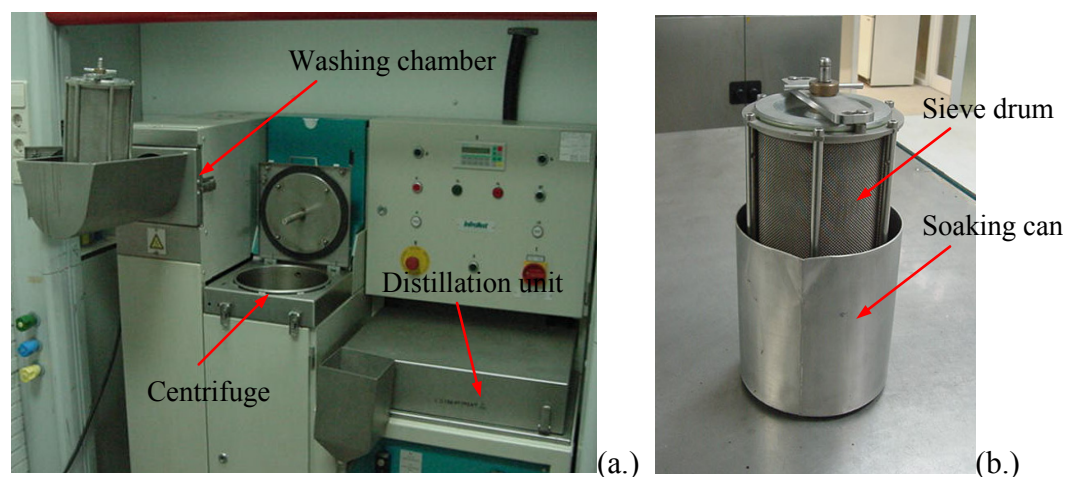


Figure 4.14: a.) “InfraTest” Fast automatic extraction apparatus, b.) Soaking of the bituminous sample in a sieve drum

The extraction process was performed in the following way. The asphalt specimen in the sieve drum and the bitumen solution from the soaking of the specimen (i.e. bitumen + dichloromethane solvent) were placed in the washing chamber for automatic extraction. When the washing process starts, the bitumen solution goes directly to the centrifuge that continuously separates the insoluble material (filler) from the solution. The complete extraction of the bitumen from the asphalt mixture was performed using three washing and two drying cycles. Only the solutions from the first two washing cycles and the solution used for pre-soaking the sample were collected for the recovery process. The third cycle was merely for washing the remaining materials in the system to make it clean and ready for the next use. The extraction process for one run took 35 to 45 min and the complete soaking, extraction and recovery process was performed in less than 24 hours in accordance to the norm EN 12697-3. After completion of the recovery, the mineral aggregates were left in the sieve drum whereas the binder solution and filler were washed-out into the continuous centrifuge unit. Filler was retained in the centrifuge while the binder and solvent was collected from the connected distillation unit for the second stage recovery process of the bitumen using the rotary evaporation method.

Recovery of the binder from the solution (EN 12697-3)

The second step for the recovery of the bitumen from the Dichloromethane solvent was performed using the rotary evaporation method (Büchi Rotavapor R-200). The recovery process was performed according to the standard procedure NEN-EN 12697-3. The bitumen solutions from two separate extractions of asphalt materials from the same road section were combined for the recovery process. Figure 4.15 shows the rotary evaporator apparatus used for recovering bitumen from bitumen solutions. The recovery process involves the separation of the solvent from the bitumen by heating-up the bitumen solution and collecting the evaporated solvent by condensation. The process is conducted under a suction pressure to accelerate the condensation. In the process, the oil bath was maintained at a temperature of 150°C; nevertheless, the temperature of the bitumen in the rotating flask is much lower due to constant introduction of the cold bitumen solution. In order to facilitate the condensation of the evaporating solvent, cold water was continuously supplied from a cooling unit that maintained the water temperature at 7°C. After all the bitumen solution was collected at the rotating flask, the system was kept running to make sure that the solvent was completely removed from the bitumen. The condensation process continued for about 20 minutes after the pressure in the system reached below 10 bars. Samples were taken from the recovered binders for the determination of the binder's ash content. Preparation of samples for penetration and softening point tests was also done as soon as the recovery process was complete.

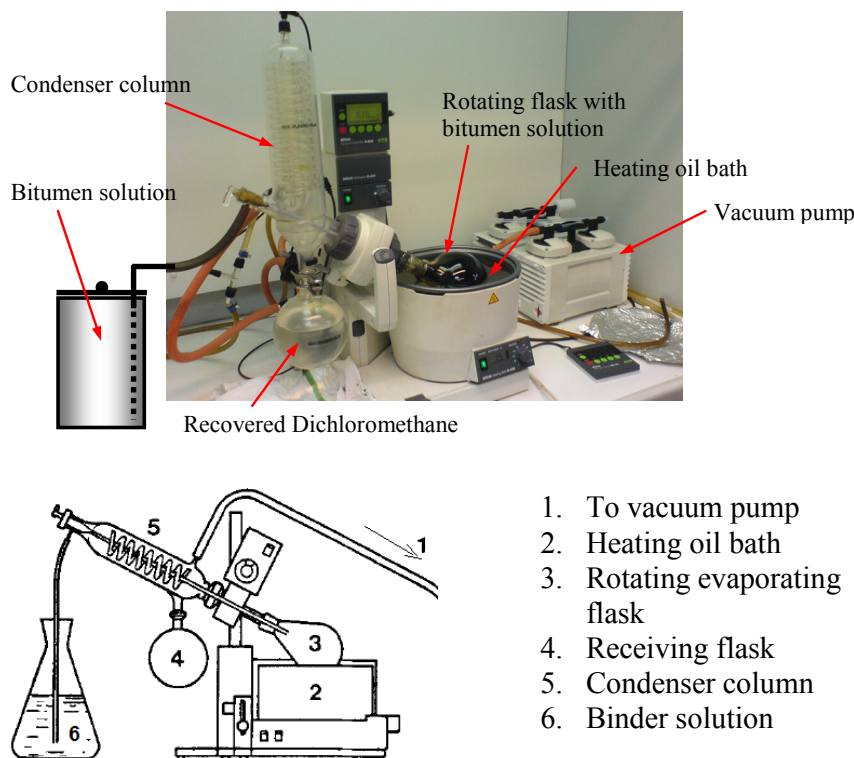


Figure 4.15: A rotary evaporator used in the recovery of bitumen (Büchi Rotavapor R-200)

The above bitumen recovery process was adopted to regain bitumen for further rheological and chemical testing. This was done mainly because of the necessity to separately recover the binder from the upper and lower zones. For the determination of asphalt composition of laboratory and field materials, i.e. voids content, bitumen content, and aggregate gradation determination, the separation of the bitumen from the mixture was performed using the soxhlet extraction method (experiment 65.1, RAW 2005) shown in Figure 4.16.



Figure 4.16: Multi-column soxhlet extraction apparatus

Effect of Bitumen Recovery

In several studies, it is reported that the binder recovery process can have a significant influence on the properties of the recovered bitumen (Burr et al. 1990, Burr et al. 1991). These studies claim that hardening is occurring due to the heating of the sample in the process of solvent removal. To verify this effect on the 70/100 pen bitumen used in this research, 150 ml of virgin bitumen was diluted in 2 litres of Dichloromethane. The solution was left overnight and recovered the next day using the same recovery procedure (EN 12697-3) used to recover specimens. Test results before and after recovery on the property of the virgin bitumen shows:

- decrease in penetration by 10% (from 76.5 to 68.1 dmm),
- increase in softening point by 2.5% (from 46.8 to 47.9°C).

However, chemical analysis using the infrared spectrometer to determine whether there was an increase of the C=O and S=O peaks (these peaks indicate hardening due to oxidative aging) showed no notable change. It can, therefore, be said that the hardening of the bitumen is probably as a result of the effect of the reaction between the solvent and the material. The hardening effect of the solvent is supposed to have only minor influence on the recovery of aged materials.

4.5 Porous Asphalt Mixture Assessment

4.5.1 Composition of Asphalt Mixtures

Laboratory materials

As it was described in section 4.2, Marshall tablets and beams from a PA slab were prepared. Four specimens were randomly selected from the Marshall tablet specimens and other four specimens with a diameter of 100 mm were cored from the fabricated asphalt slab (refer to Figure 4.3) for the determination of asphalt mixture composition. The asphalt composition of both the Marshall specimens and cores from the slab are presented in Table 4.20.

Table 4.20: Composition of asphalt specimens (Marshall tablets)

Sample #	Dimensions (average)		Weight (g)	Volume (cm ³)	Bulk Density (kg/m ³)	Max. Density (kg/m ³)	Voids content (%)
	H, mm	D, mm					
1. Marshal specimens							
009	40.77	101.58	719	330.3	2176.5	2568.6	15.4
012	42.80	101.70	772	347.6	2220.7	2577.2	18.2
014	42.22	101.75	725	343.2	2112.2	2579.0	18.1
015	41.85	101.75	719	340.3	2113.1	2517.6	11.9
2. Cores from Slab							
S1	50.00	101.14	791.1	401.66	1969.4	2513.4	22.3
S2	48.83	101.36	775.5	393.97	1968.5	2517.7	22.4
S3	48.07	101.35	725.0	387.76	1869.6	2515.0	26.0
S4	47.97	101.44	766.7	387.64	1977.9	2517.6	21.8
NB:	1.) Specimens from aging protocol 1 and 2, and 2.) Specimens from aging protocol 3.						

The determination of maximum density and voids content of the mixture was performed according to RAW 2005 experiment no. 68 (pycnometer method). This procedure was followed by soxhlet extraction to determine the bitumen content of the specimens according to experiment no. 65.1 (RAW 2005).

Field asphalt mixtures

Asphalt mixture specimens were extracted from roads with a service life of 0 (new construction), 1, 3, 7, and 12 years. The specimens were taken from sections of the road with traffic and without traffic; i.e. the Slow Lane SL (trafficked by heavy vehicles) and the Emergency Lane, EL or Shoulder SH (without traffic). The composition of the field cores given in Table 4.21 was determined using conventional laboratory test methods. The following procedures were employed:

- Measurement of the specimen dimensions for volume calculation. This was done by taking the average of the specimen diameter and thickness measurements. Four measurements at different sides of the specimen were taken using a calliper with a precision of 0.1 mm.
- Weighing of the specimens.
- Determination of bulk density.
- Determination of max density and voids content using pycnometer method (RAW experiment no. 68).

- Determination of bitumen content using soxhlet extraction method (RAW experiment no. 65.1).
- Determination of aggregate, sand, and filler proportions in the asphalt mixture using sieve analysis method (RAW experiment no. 6).

Except for section G, information on the type of aggregate, source of bitumen, etc of the field materials was not available. The standard specifies that a certain bitumen type and grade be used in PA pavements, i.e. unmodified 70/100 pen bitumen. Chemical investigation performed on the field materials suggests that the bitumen appear to be from the same origin/source for all the specimens including the bitumen from section G, which has got some difference in hetro-atom composition from the other binders (refer to Chapter 6 section 6.1 for chemical characterization of the binders).

Table 4.21: Composition of field specimens

	Sect.A, 1 yr		Sect.B, 3 yr		Sect.C, 7 yr		Sect.D, 7 yr	
	EL	SL	EL	SL	EL	SL	EL	SL
Bulk density: Asph. mix (kg/m³)	1985	1994	1955	2169	1791	1840		2030
max. density: Asph. mix (kg/m³)	2488	2503	2565	2523	2496	2502		2531
Voids content (Vol.) (%)	20.4	20.5	23.9	14.2	28.4	26.6		21.0
Bitumen content (by wt.) (%)	4.3	4.4	4.3	4.3	3.9	3.9		4.2
- on 100% mineral aggregates								
Aggregate fractions (Vol.)								
Coarse agg. > 2mm (%)	81.9	79.7	78.1	75.6	84.3	83.8		80.3
Sand 0.063 – 2mm (%)	10.6	9.8	11.3	13.2	10.2	9.7		13.0
Filler < 0.063mm (%)	7.5	10.5	10.7	11.1	5.5	6.5		6.7
f/b ratio (by wt.)	1.63	2.21	2.25	2.35	1.30	1.54		1.44
(by vol.)	0.65	0.88	0.90	0.94	0.52	0.62		0.58
	Sect.E, 12 yr		Sect.F, 12 yr		Sect.G, 0 yr		Laboratory PA mixtures	
	EL	SL	EL	SL	EL	Mat.*	Cores	Slab
Bulk density: Asph. mix (kg/m³)	1822	1997	1875	1949	1941	2007	2210	1946
max. density: Asph. mix (kg/m³)	2505	2519	2515	2505	2525	2544	2560	2516
Voids content (Vol.) (%)	27.4	20.9	25.6	22.3	22.9	21.1	15.9	23.1
Bitumen content (by wt.) (%)	4.1	3.6	3.8	4.1	4.4	4.4	4.3	4.3
- on 100% mineral aggregates								
Aggregate fractions (Vol.)								
Course agg. (%)	81.6	82.9	82.2	80.3	83.5	85.1	85.0	85.0
Sand (%)	13.1	12.4	12.1	13.7	10.9	10.5	10.5	10.5
Filler (%)	5.3	4.7	5.7	6.0	5.6	4.1	4.5	4.5
f/b ratio (by wt.)	1.18	1.21	1.39	1.36	1.17	0.85	0.93	0.97
(by vol.)	0.47	0.48	0.56	0.54	0.47	0.34	0.37	0.38
NB:					*Filler (Sect.G)			
Density of sand and coarse aggregates			Sand		Aggregate		Wigro 60K	
(average of tests conducted on 25 samples).			2700		2650		2575	
							Unit	
							kg/m³	
Remark:			NB: * Material information from the field for sect. G.					
Sect. = Section			- The results shown for each of the road subsections is the average of test results from three cores.					
EL = Emergency Lane (Shoulder, SH)			- Sect.D and Sect.E are sections with poor performance.					
SL = Slow lane								

According to the Dutch specification (RAW 2005), the requirements for PA mixture are shown in Table 4.22.

Table 4.22: Single layer PA mixture gradation according to Dutch standard (Source: RAW 2005, *Tolman et al, 1996 and 1997, **NEVUL 2006)

	Dutch Standard PA Mixes	
Sieve size	0/16	0/11*
C 16	0.0 – 7.0	
C 11.2	15.0 – 30.0	– 5.0
C 8	50.0 – 65.0	60.0 – 85.0
C 5.6	70.0 – 85.0	80.0 – 85.0
2 mm	85.0	85.0
63 mm	95.5	95.5
Layer thickness	50 mm	30 mm
Bitumen	4.5% by weight	4.5%
Fibre	-	-
<u>Requirements:</u>		
Bitumen: 70/100 pen	4.5% by wt. of total agg. (≈ 8% by vol.)	
Aggregates:	95.7% by wt. of total mix	
Aggregate: Retained on 2mm sieve	85.0% by wt.	
Sand: Pass 2mm and retained 63 mm	10.5% by wt.	
Filler: Pass 63 mm	4.5% by wt.	
** middle sort filler with 25% hydrated lime (KA25, bitumen number BN54/60)		
Voids:	≥ 20%	

The material data for section G satisfies the requirements of a standard PA. The information that was available on section G during construction was the following:

- bitumen content = 4.4%. It agrees with the determined quantity in Table 4.21.
- f/b ratio = 0.85 by wt. (0.34 by vol.) based on material data from the field. Prediction of the f/b ratio for section G based on laboratory data is rather on the higher side.
- bitumen penetration (pen) = 85 dmm. The bitumen grade used in this research is 90.7 dmm.
- mixture voids content = 21.1%. This shows slight variation with the laboratory determined value of 22.9%.

In general, the determination of the composition of field materials in the laboratory seems quite acceptable from the comparisons of predicted and provided material information on section G. In terms of voids content, all sections satisfy the minimum requirement with the exception of Sect. B (SL). Section A and B showed a higher filler content (higher f/b ratio) than the quantity specified in the specification. The reason for the higher filler content is not clear since section A and B are relatively new sections where clogging is not yet expected. One possible reason could be the segregation of the mix during

the construction of the pavement. The bitumen-filler ratio (f/b ratio) of the field materials in Table 4.21 can be compared with the standard f/b ratio of PA mix, which is 1.0 by weight (approx. 0.40 by volume using the material properties of the laboratory PA mixture). In this regard, the laboratory prepared PA mixes seem to have reasonable filler-bitumen proportions. Note that the unit weight of Wigro 60K filler of section G was used in determining the f/b ratio of all the field materials as no information is available on the filler properties of the other sections. The aggregate and sand properties of the field materials were determined in the laboratory for representative materials.

In Figure 4.17, the difference in softening point of the bitumen and the mastic for the laboratory prepared PA mixture is shown. The mark (+) falls well within the desired range of 12 – 16. NB: the $\Delta(T_{RB})$ may shift position depending on the filler and binder type, thus it was not possible to show all the points corresponding to the field mastic in the same figure.

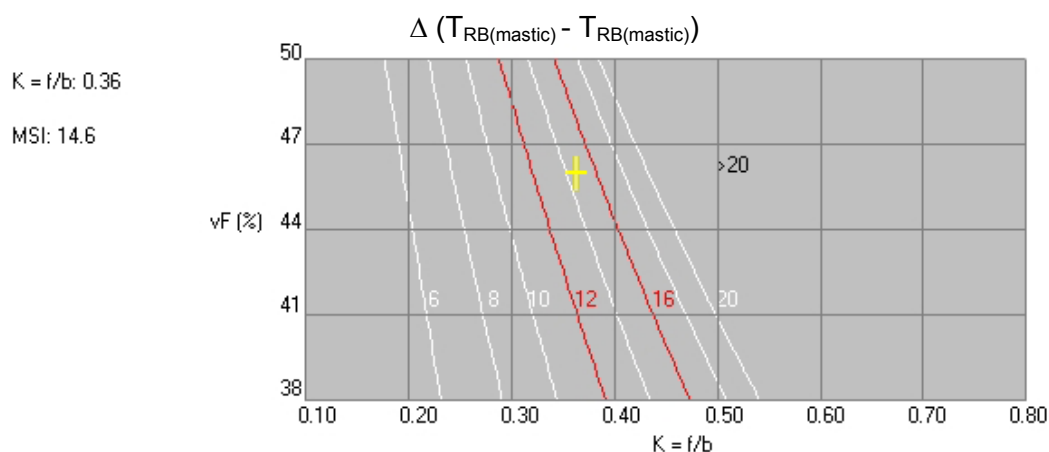


Figure 4.17: Difference in softening point of the mastic in the laboratory prepared PA mix

4.5.2 CT-scan and Thin-film Analysis

CT-scan analysis of field materials

The CT-scan image analysis method, also known as X-ray tomography, was used to study the field specimens. The aim of the CT-scanning of the field materials was to determine:

- the distribution of the voids of the asphalt cores,
- the volume of the different asphalt components, and
- the bitumen content in the upper and lower zones of the asphalt core specimens.

The principle of the CT-scanner is based on the emission of x-rays. The extinction depends mainly on the atomic number and the density of the material. The amount of emission is expressed in Hounsfield Units (HU). The output of the CT-scanner consists of a series of 2D 512 × 512 pixel images. Each

pixel is assigned a 12 bits grayscale value, which represents a certain HU (Remijn 2005). The images are taken at a specific interval. By combining a series of 2D images, a 3D image can be constructed as shown in Figure 4.18. The maximum resolution of the scanner (SOMATOM Plus4) used for scanning PA core specimens was 0.3×0.3 mm at 1 mm spacing. Using this level of resolution, the distinction of three groups in the asphalt mixes was possible: the aggregates (sizes > 2 mm.), the mortar (bitumen + filler + sand fraction), and the voids. With a higher resolution scanner (nano-scanner), the following tasks would have been possible to perform:

- determination of the binder/mortar film thickness around aggregates, and
- micro level investigation of the mortar at aggregate-to-aggregate contact points.

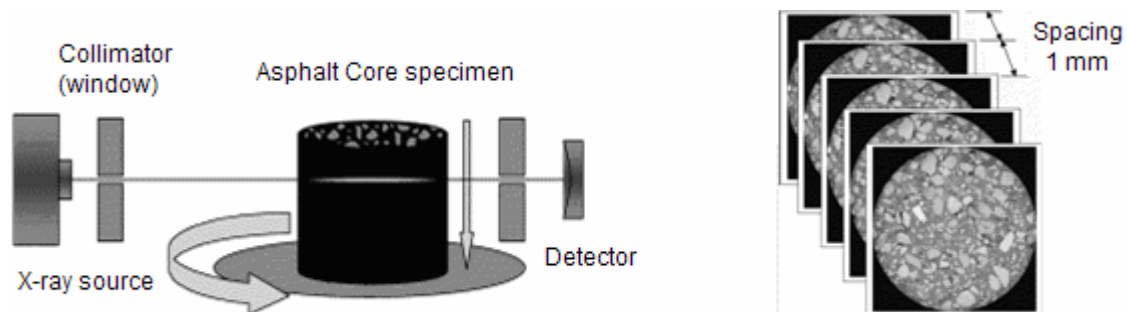


Figure 4.18: The CT-scan (X-ray tomography) technique

After acquiring the images using the SOMATOM Plus4 scanner, the Amira 3.0 software package was used for analyzing the asphalt cores. A software package known as Osiris 4.18 was first used to save the scan/image data of the individual cores for processing using Amira. The distinction between the different materials was made by assigning a range of grayscale values to one of the three groups (mortar, aggregate and void space). The boundary between the three groups is not fixed; it varies depending on the composition of the material (material type, proportions, and size). The determination of the boundaries was performed by matching the segment analysis of the 2D grayscale (intensity) images with the material composition as determined in the laboratory and given in Table 4.21.

Figure 4.19 shows a histogram of a CT-scan image with the boundaries or range of grayscales (colour) for the three groups. The boundaries are made to match with the actual proportions of the materials. From the histogram in Figure 4.19 it can be noticed that the voids-mastic boundary is not sensitive compared to the mastic-aggregate boundary in terms of their effects on the determination of the material compositions.

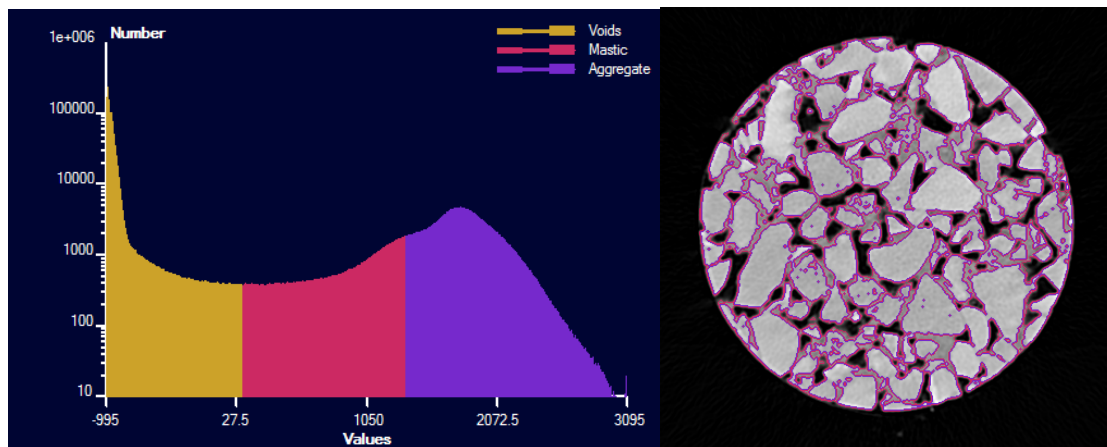


Figure 4.19: Histogram of the grayscale (colour) with boundaries for Voids–Mortar–Aggregate

The detailed procedure of CT-scan image analysis provided by Remijn 2005 was adopted in conducting the analysis. The procedure is briefly discussed below:

- Load the series of images of the field specimen.
- Use the function “*OrthoSlice*” in the Amira software package to make different orientation views, i.e. x-sectional view along the specimen thickness (axial) and across the specimen thickness (Coronal and Sagittal). The grayscale should be adjusted to the range -1000 to 3000 HU.
- Determine the first and last images that should be included in the analysis through visual evaluation. This is done to exclude the blank images during the start and end of scanning. Besides, some specimen images at the start and end of the scanning are only partly scanned due to slight tilt or imperfect sawing of the specimens.
- An important part of the image analysis is identifying the three groups/segments, i.e. the voids, mastic/mortar, and aggregates, in the asphalt mixture. The “*Label Voxel*” function was used to classify the regions of the three segments in the CT-scan images. A boundary is set for the identification of each region in the slide/image as shown in the histogram in Figure 4.19. Volume calculation of the segments per slice/image was performed using the “*Tissue Statistics*” function of the software. The output volume-per-slice is given in a tabulation form for each of the slices and segments. The volume-per-slice data is exported to a text document and finally imported to excel for processing.
- In order to determine the grayscale boundaries, the volume of each segment is compared with the asphalt composition of the corresponding specimen as determined in the laboratory. The volume of the segments is adjusted to match with the laboratory results by changing the boundary of the regions in the grayscale. This is done by trial and error till the errors are minimised.
- The final output consists of:
 - a. the visualization of the distribution of the three groups, i.e. voids-mastic-aggregate, along the thickness of the specimen, and

- b. estimation of asphalt content in the upper and lower parts of the PA specimens based on the bitumen-filler ratio (b/f) determined from laboratory results of asphalt composition.

A 3D view of the asphalt specimens can be made using the “*Voltex*” function of the Amira software with a colour map selection. By combining the “*Voltex*” function with “*Ortho Slice*”, cross-sectional views of the specimen can also be constructed as shown in Figure 4.20. Using the method of image analysis outlined above, it was not possible to differentiate the interconnected voids from the localized voids. It may be possible to do so if the resolution of the images is improved, which depends on the quality of the image (max. number of pixels) that the CT scanner can produce.

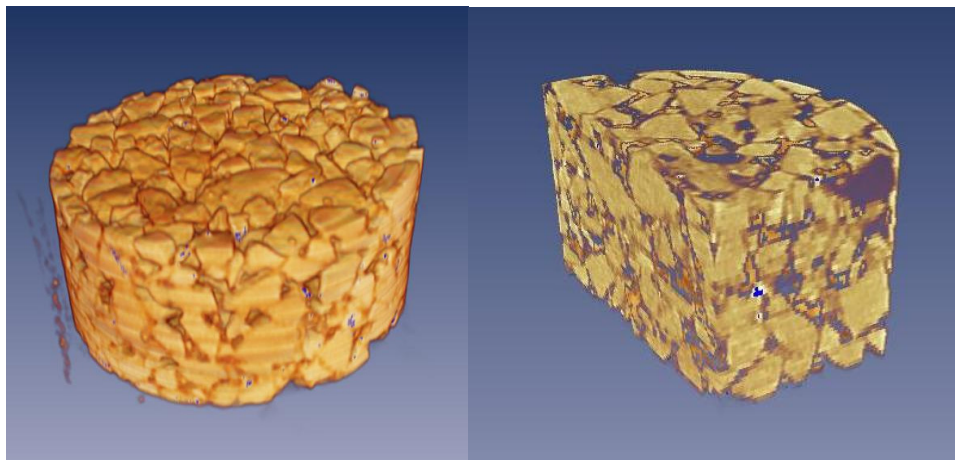


Figure 4.20: 3D view of asphalt specimen constructed using Amira

The results of CT-scan image analysis of the field specimens are given in Table 4.23. Also the average bitumen content and grayscale boundaries of the voids-mortar-aggregate determined for three specimens from each road section are given in Table 4.23. The bitumen content for the upper zone is determined for the top 25 mm. From the results, it can be seen that the boundary for voids-mortar and mortar-aggregate is not constant. A number of factors have a direct influence on the boundary values, such as the uniformity of the mixture composition during laying, segregation/drainage of the mortar, clogging of the voids, and so forth. The bitumen content calculation is based on the proportion of bitumen in the mortar as determined from the laboratory specimens. In general, the bitumen content of the field specimens at the lower zone seems to be higher than that at the upper zone. From the scans it appeared that a higher amount of mastic is present in the bottom part of the specimen. What is not known is whether this implies a higher amount of bitumen or whether it means clogging. The real reason is not known because only the mastic can be detected and not the bitumen and fines separately.

In Figure 4.22 and Figure 4.23, the distribution of voids, mortar, and aggregate of the field specimens is shown for the materials from the emergency lane and the slow lane respectively. The voids and mortar distribution seems slightly non-uniform through the sample thickness for most of the specimens (as

indicated by the broken line). The varying amount of mastic with the sample height indicates lower bitumen content of the specimens at the top part. However, another plausible reason for the lower binder content could be the wearing out of the bitumen coat from the surface aggregates because of traffic abrasion. This implies that the non-uniformity of the distribution of the asphalt components as a result of clogging is likely.

Table 4.23: Results of CT-scan analysis of field specimens

1. Bitumen content %				CT-scan			Laboratory (recovered) bitumen data
Section		Service Year	Sample code	Upper Zone (UZ)	Lower Zone (LZ)	Overall*	
G	EL	0	05041.IPG	3.9	4.4	4.1	4.4
A	EL	1	05033.IPG	3.9	4.5	4.1	4.3
	SL			3.9	4.3	4.1	4.4
B	EL	3	05034.IPG	3.9	4.0	3.9	4.3
	SL			4.2	4.9	4.4	4.3
C	EL	7	05036.IPG	3.5	3.5	3.5	3.9
	SL			3.5	3.7	3.6	3.9
E	EL	12	05039.IPG	3.6	4.1	3.7	4.1
	SL			3.4	4.3	3.6	3.6
Average				3.8	4.2	3.9	4.2
*NB: The CT-scan bitumen content was determined based on the proportion of the bitumen in the mastic according to laboratory asphalt composition of the specimens.							
2. Grayscale boundary							
Section		Year	Sample code	Voids – Mortar		Mortar – Aggregate	
G	EL	0	05041.IPG	525		1558	
A	EL	1	05033.IPG	742		1478	
	SL			642		1523	
B	EL	3	05034.IPG	808		1645	
	SL			758		1608	
C	EL	7	05036.IPG	737		1407	
	SL			808		1395	
E	EL	12	05039.IPG	967		1527	
	SL			808		1480	
Average				695		1563	

The quantities of mastic at the UZ (top 25 mm part) and LZ were determined from the CT scan analysis. Accordingly, the CT-scan bitumen content was determined based on the proportion of the bitumen in the mastic from laboratory asphalt composition of the specimens. This approach seems to result in a lower bitumen content compared to the quantities determined in the laboratory. This may have to do with the appropriate identification of the asphalt components in the CT-scan analysis due to lower resolution of the scanning. Hence, the bitumen content determined in the laboratory should be taken as a dependable data and the CT-scan information as indication of the proportion of bitumen in the UZ and LZ.

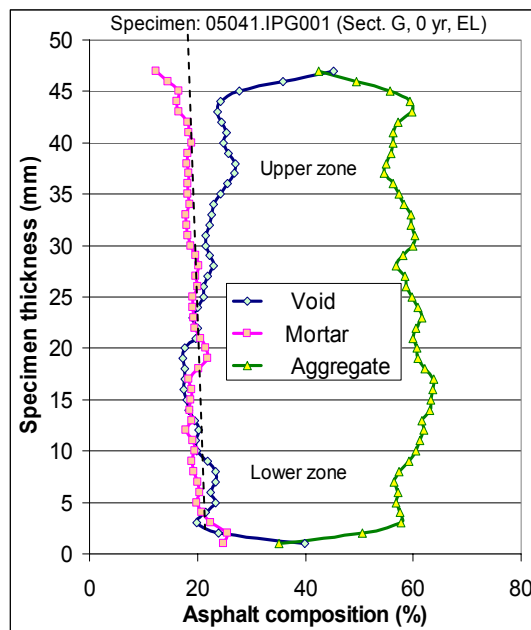


Figure 4.21: Distribution of asphalt components for a new PA pavement (EL)

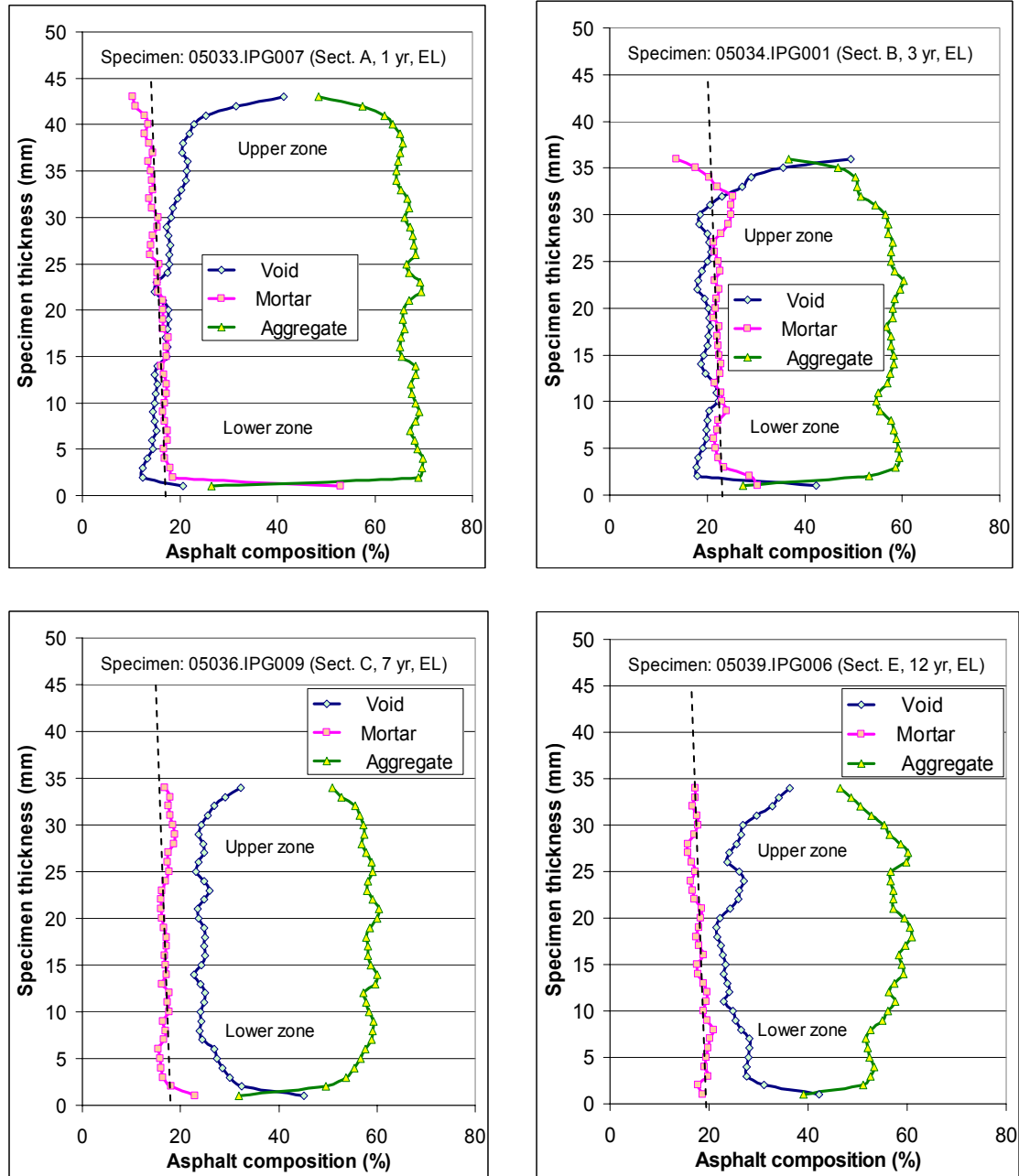


Figure 4.22: Distribution of asphalt components of field specimens from the Emergency Lane EL (Shoulder, SH) with 1, 3, 7, and 12 year service period

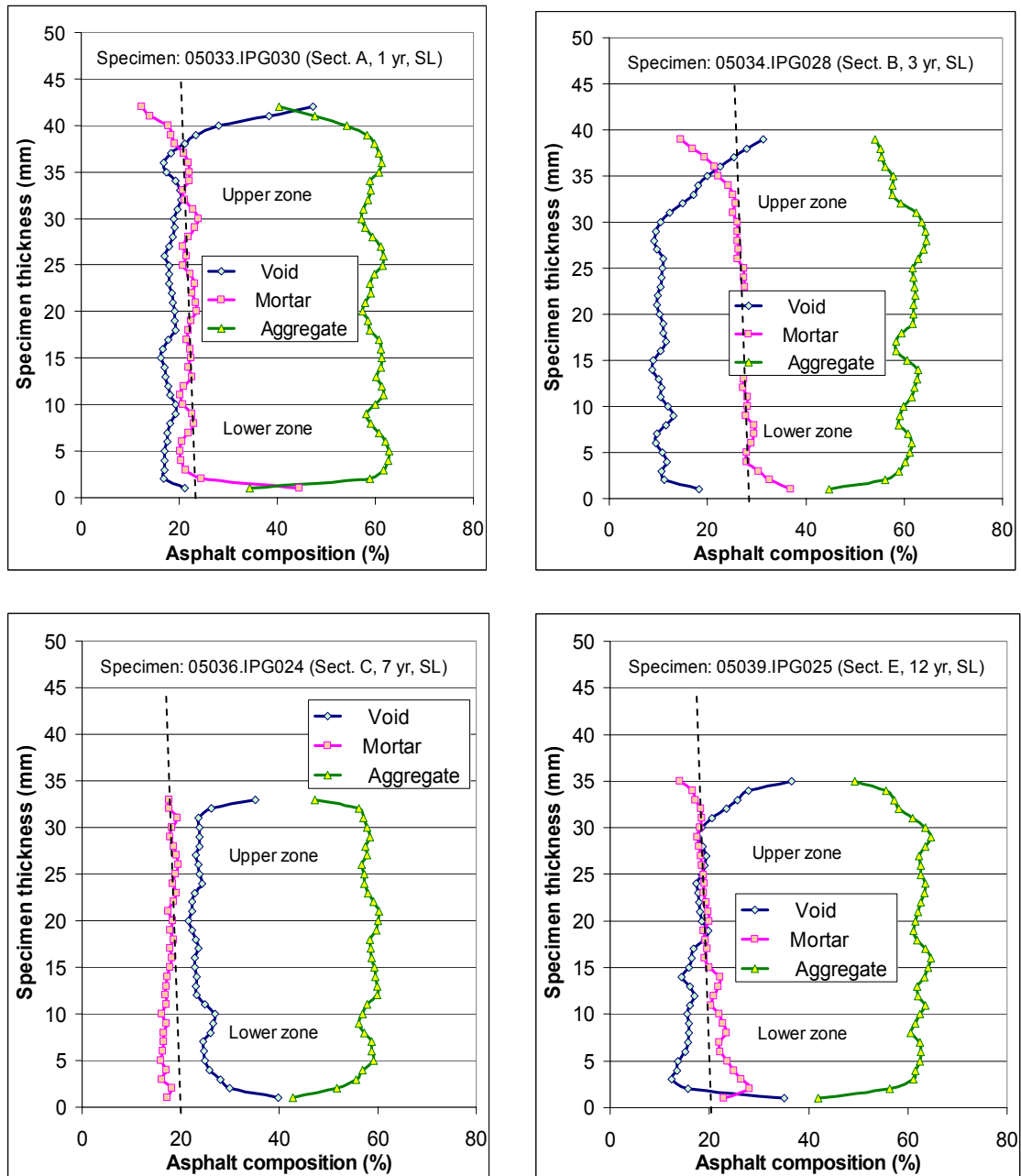


Figure 4.23: Distribution of asphalt components of field specimens from or Slow Lane SL (trafficked lane) with 1, 3, 7, and 12 year service period

4.5.3 Thin-Film Sections of Field Materials

The investigation of the micro-structure of the same field specimens was performed by DRI (Danish Road Institute). Thin sections were used to investigate the materials (Nielsen 2007). The DRI test results are discussed in chapter 5 in combination with the results of this research. A thin section of 1 year and 12 year old field materials is shown in Figure 4.24.

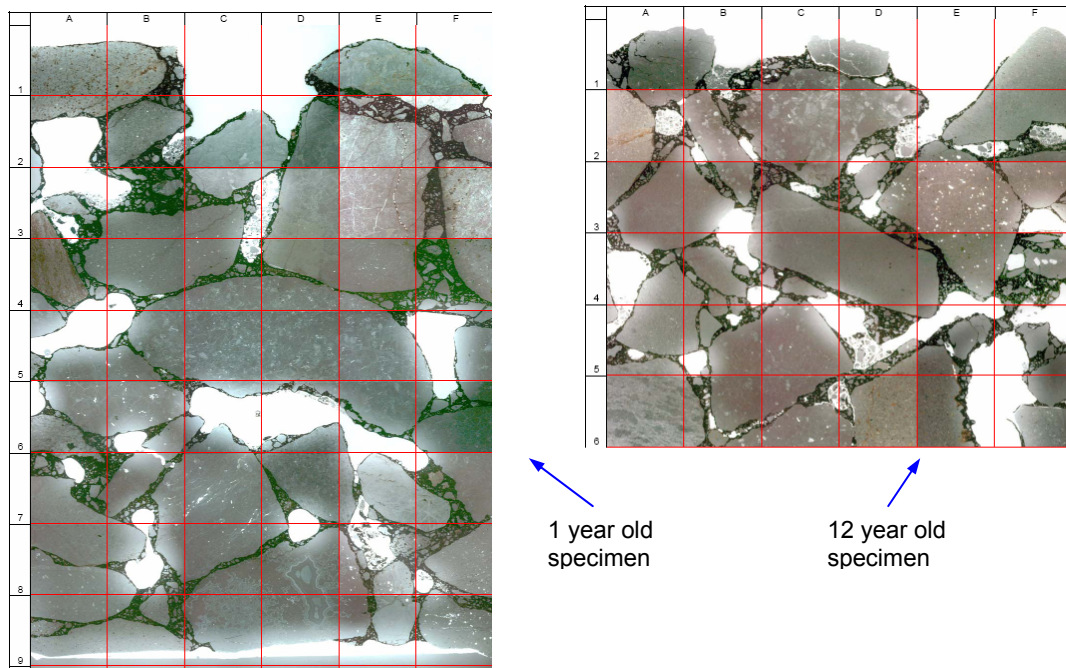


Figure 4.24: Thin section images for 1 and 12 year old field specimens (Nielsen 2007)

4.6 Asphalt Mixture Test Results

4.6.1 Repeated Load Indirect Tensile Test (RLITT)

Asphalt cores from road sections with an age of 0 (after construction), 1, 3, 7, and 12 years were tested using the Repeated Load Indirect Tensile Test (RLITT). The RLITT was performed to study the resilient (elastic) characteristics of the asphalt specimens. The test was conducted at low stress levels not exceeding 10% of the failure stress to ensure linear response of the materials.

Testing conditions:

- Temperature: 5, 15, 25, and 35°C
- Frequency: 1, 2, 4, 8, and 16 Hz
- Pulse count: 5
- Pulse width: 1 Hz = 1000 ms, 2 Hz = 500 ms, 4 Hz = 250 ms,
8 Hz = 125 ms, and 16 Hz = 62.5 ms
- Pulse period: 3000 ms

The RLITT was performed according to the standard procedure in ASTM 4123. The resilient modulus computation was performed using Equation 4.4. The RLITT specimens are the same specimens as used in the CT scanning with a diameter of 100 mm. Three specimens were tested from each group or road section at all the temperatures and frequencies. The test results given in Table 4.24 are the average of five independent measurements performed at each combination of the test conditions for every specimen. The RLITT was performed using a Universal Testing Machine (UTM V2.21). The equipment has

a temperature controlled compartment convenient for testing at the desired temperature. The specimens were conditioned at the testing temperature for minimum 3 - 4 hours before conducting the test. The RLITT test set up is shown in Figure 4.25.

$$M_r = \frac{F}{HT}(0.27 + \nu) \quad (4.4)$$

Where:

- M_r = resilient modulus (MPa),
- F = applied load (N),
- ν = Poisson's ratio (assumed $\nu = 0.35$),
- H = horizontal deformation (mm), $H = \varepsilon_r \cdot D$
- D = specimen diameter (mm)
- ε_r = recoverable horizontal strain ($\mu\text{m}/\text{m}$)
- T = specimen thickness (mm)

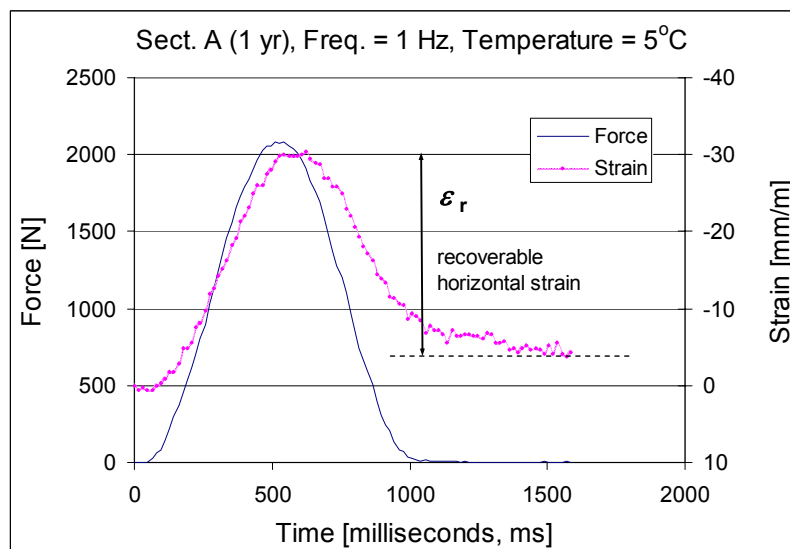
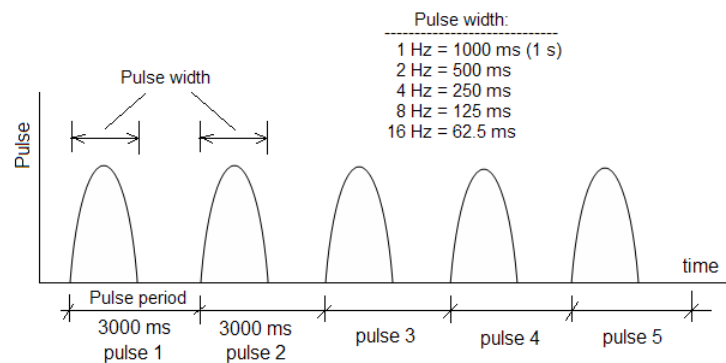
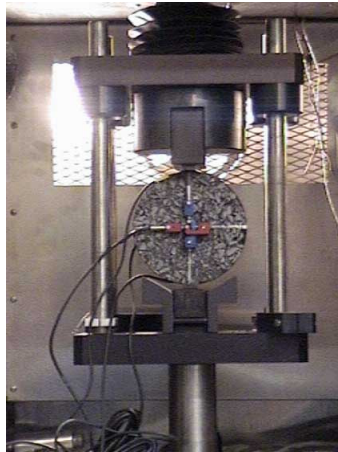


Figure 4.25: Repeated Load Indirect Tensile Test set up, test condition and an example of RLITT result

Table 4.24: Result of RLITT test for materials from Section A (1 yr old in the field)

Summary table Section A 1 yr Shoulder, SH (Emergency Lane, EL)						Section A 1 yr Slow Lane, SL					
Temp	Target Force	Actual force	Target pulse width	Actual pulse width	Resilient modulus	Temp	Target Force	Actual force	Target pulse width	Actual pulse width	Resilient modulus
[°C]	[N]	[N]	[ms]	[ms]	[MPa]	[°C]	[N]	[N]	[ms]	[ms]	[MPa]
5	2100	2084.6	999	912.8	9433	5	2100	2085.8	999	901.6	8875
5	2100	2093.4	500	467.6	10404	5	2100	2094	500	463.6	9930
5	2100	2091.1	250	244	11605	5	2100	2094	250	234.2	11369
5	2100	2096.4	125	115	12896	5	2100	2093.4	125	111.4	12422
5	2100	2103.4	63	56	12668	5	2100	2084.6	999	909.6	11332
5	2100	2097.5	63	53.8	13848	5	2100	2092.8	500	470.8	12771
5	2100	2085.8	999	910.4	9259	5	2100	2095.2	250	241.6	13541
5	2100	2092.3	500	466	9958	5	2100	2095.8	125	113.6	15420
5	2100	2094	250	238.6	11016	5	2100	2085.8	999	915.2	7555
5	2100	2095.8	125	115.8	12324	5	2100	2094	500	458.8	8452
5	2100	2087.6	999	903.2	6777	5	2100	2090.5	250	240.6	9531
5	2100	2093.4	500	466	7658	5	2100	2094.6	125	110.8	10524
5	2100	2096.4	250	236.4	8605						
5	2100	2094	125	113.6	9502						
15	700	695.09	999	932.8	4240	15	700	695.67	999	930.4	3812
15	700	696.26	500	450.4	5089	15	700	698.02	500	456	4470
15	700	699.78	250	227.8	6153	15	700	699.19	250	226.6	5162
15	700	701.53	125	119	7533	15	700	697.43	125	119.4	5863
15	700	695.09	63	55.8	8229	15	700	690.98	63	54.4	5728
15	700	695.67	63	55.4	8669	15	700	701.53	63	56.2	7142
15	700	697.43	999	936.8	3545	15	700	696.26	999	930.4	3884
15	700	698.02	500	456.4	4151	15	700	700.36	500	454.4	4553
15	700	696.84	250	228	4949	15	700	696.84	250	227.4	5407
15	700	699.78	125	118.8	5830	15	700	699.19	125	115.4	6344
15	700	692.74	63	55.8	6583	15	700	696.84	63	54.6	6588
15	700	702.12	63	55.2	6841	15	700	698.02	63	55.4	7322
15	700	694.5	999	933.6	2894	15	700	698.02	999	932.8	3632
15	700	699.19	500	465.2	3495	15	700	698.6	500	459.6	4296
15	700	698.6	250	228	4223	15	700	700.36	250	225	4926
15	700	699.78	125	122.6	5082	15	700	699.19	125	113.4	5964
15	700	690.98	63	55.8	5674	15	700	700.95	63	55.8	6608
15	700	704.46	63	56.2	5706	15	700	698.6	63	56.6	6762
25	350	348.13	999	952.8	1538	25	350	348.13	999	954.4	1523
25	350	348.71	500	473.2	1923	25	350	347.54	500	483.6	1927
25	350	350.47	250	235.4	2603	25	350	350.47	250	247.4	2429
25	350	348.71	125	121.8	2720	25	350	348.71	125	116.8	3049
25	350	351.06	63	56.4	757.7	25	350	349.3	63	56	3513
25	350	348.13	63	56.2	868.9	25	350	348.71	63	56.2	3139
25	350	347.54	999	942.4	1502	25	350	347.54	999	940	1349
25	350	349.3	500	482	1853	25	350	346.95	500	481.2	1676
25	350	347.54	250	249.8	2431	25	350	351.06	250	250.8	2105
25	350	351.64	125	119.2	3123	25	350	349.89	125	114.4	2714
25	350	347.54	63	56.4	3580	25	350	339.34	63	55	2827
25	350	347.54	63	56	3162	25	350	346.95	63	57	3081
25	350	348.71	999	957.6	1138	25	350	348.13	999	960.8	1197
25	350	348.71	500	484.4	1442	25	350	350.47	500	480.8	1557
25	350	349.89	250	231	2016	25	350	349.3	250	251.4	2074
25	350	347.54	125	119.6	2719	25	350	351.06	125	117.4	2849
25	350	346.95	63	55.2	1792	25	350	342.85	63	55.2	2188
25	350	348.13	63	57	1842	25	350	349.89	63	56.6	2817
35	150	147.69	999	948	536.4	35	150	151.79	999	985.6	728.7
35	150	151.2	500	507.2	676.5	35	150	148.86	500	484.4	1116
35	150	149.45	250	265.6	892.6	35	150	151.2	250	279.4	1639
35	150	148.27	125	156.8	1275	35	150	150.03	125	167.6	2482
35	150	152.38	63	118.4	2556	35	150	151.79	63	96.6	2773
35	150	148.86	63	97.4	1310	35	150	149.45	63	127.8	1533
35	150	147.1	999	950.4	608.8	35	150	148.27	999	959.2	566
35	150	150.03	500	507.6	819.1	35	150	151.79	500	500.8	770.3
35	150	150.62	250	280.6	1022	35	150	150.62	250	266.4	979.2
35	150	151.2	125	196.2	1551	35	150	150.03	125	174.6	1386
35	150	149.45	63	130.2	2360	35	150	150.03	63	103.2	2403
35	150	149.45	63	109.6	1332	35	150	148.86	63	89.6	1389
35	150	150.03	999	1007	396.9	35	150	151.2	999	982.4	480
35	150	150.62	500	523.6	509.3	35	150	151.79	500	527.6	593.7
35	150	150.03	250	275.4	729.8	35	150	148.86	250	289.2	781.3
35	150	150.03	125	172.6	1173	35	150	151.2	125	157.4	1110
35	150	149.45	63	130.2	2955	35	150	150.62	63	89	2254
35	150	152.96	63	129.4	925.5	35	150	148.27	63	128.2	1119

NB: Refer to Appendix A for the results table of the remaining field materials.

Time-Temperature Dependency Model

The unified model developed by Medani (2006) was adopted to quantify the time-temperature dependency of the field materials. The model describes a wide range of asphalt properties with respect to their time and temperature dependency. The unified model is given in Equation 4.5 through 4.7.

$$P = P_{high} + (P_{low} - P_{high})S \quad (4.5)$$

$$S = \exp\left(-[u_r \cdot \beta_T]^\gamma\right) \quad (4.6)$$

$$u_r = \frac{u}{u_0} \quad \text{and} \quad \beta_T = \exp[-T_s (T - T_0)] \quad (4.7)$$

Where:

P	=	a mixture property (resilient modulus)
P_{high}	=	a value of the property as the time derivative $u \rightarrow \infty$
P_{low}	=	a value of the property as the time derivative $u \rightarrow 0$
u	=	a time derivative variable ($u = 1/t$, t = loading time)
u_0	=	a reference value of the time derivative variable
γ	=	model parameter
β_T	=	a temperature susceptibility function
T_s	=	temperature susceptibility factor
T_0	=	a reference temperature
T	=	temperature

The parameters of the unified model to fit the RMITT (Resilient Modulus Indirect Tensile Test) data of field materials are given in Table 4.25. The model parameters in Table 4.25 that describe the curve of the shifted rheological data are determined by minimizing the sum of deviations between the data and the model.

Table 4.25: Unified model parameters for the resilient modulus of field specimens

Section	Service year	location	Model Parameters				Resilient modulus [MPa]	
			γ	T_s	T_0	u_0	P high	P low
G	0	EL	0.26	0.30	278.00	54.80	17998.55	0.00
A	1	EL	0.24	0.41	278.00	8.46	18000.00	20.19
		SL	0.28	0.33	278.00	8.73	17999.96	20.21
B	3	EL	0.27	0.31	278.00	3.07	17998.95	0.00
		SL	0.22	0.41	278.00	2.72	17999.97	20.29
C	7	EL	0.24	0.32	278.00	13.35	17998.91	0.00
		SL	0.21	0.36	278.00	6.57	17999.93	14.23
D	7	EL						
		SL	0.22	0.35	278.00	6.42	17999.93	14.24
E	12	EL	0.20	0.35	278.00	13.00	17998.91	0.00
		SL	0.26	0.33	278.00	6.70	17999.91	13.94
F	12	EL	0.09	0.77	278.00	1.65	17999.65	0.00
		SL	0.12	0.66	278.00	1.32	17999.99	12.98

An example of the fitted data is shown in Figure 4.26 for an asphalt specimen from section A with a service life of 1 year.

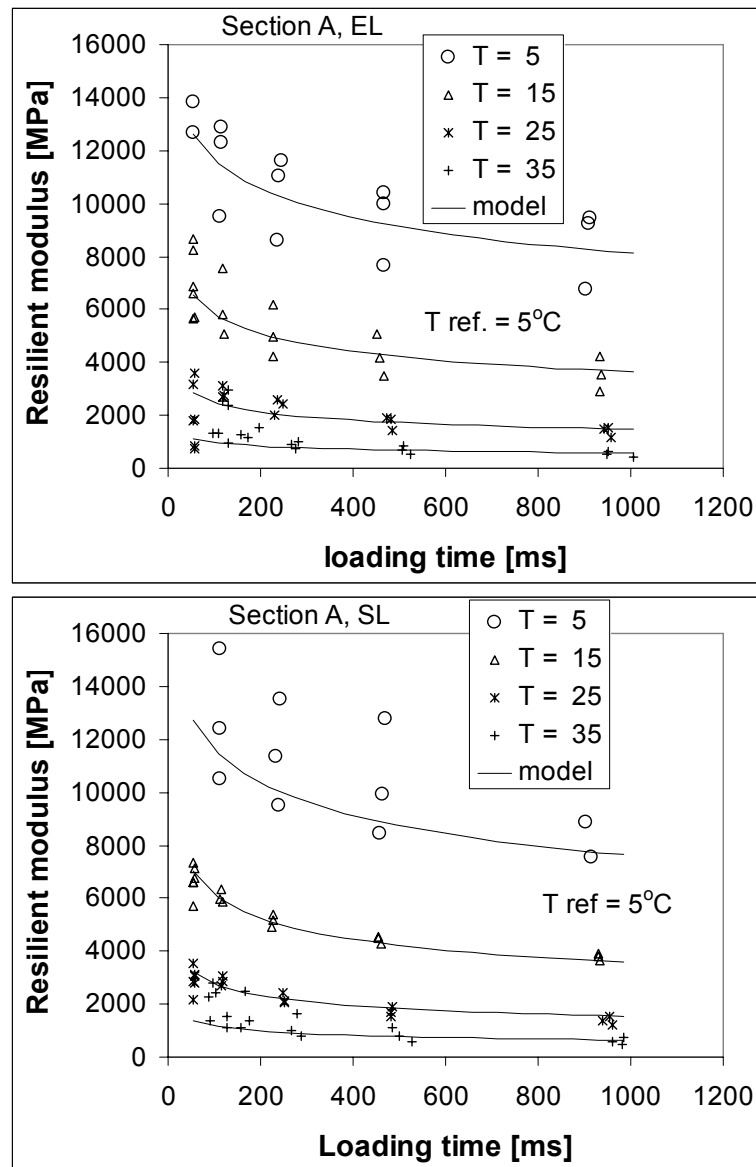


Figure 4.26: Model fit for RMITT of field material from section A

Assessment of the Resilient Modulus of field materials

The master curve of the resilient modulus for the field specimens is shown in Figure 4.27 at a reference temperature of 5°C.

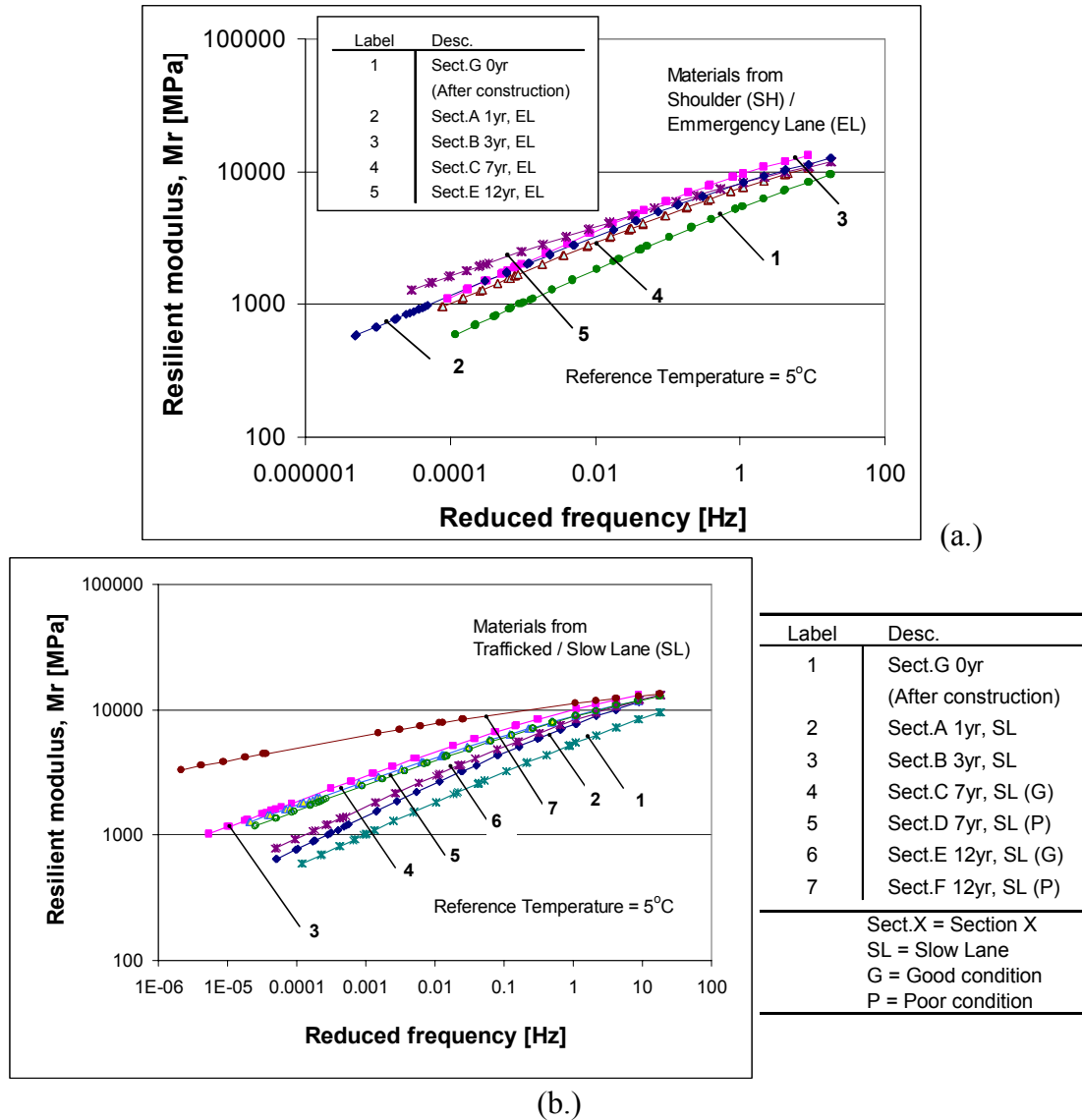


Figure 4.27: Master curve of the RMITT results of field specimens from (a.) Slow (trafficked) Lane and (b.) Shoulder (Emergency Lane) at reference temperature of 5°C.

Figure 4.27 shows that the resilient modulus of the field specimens increases with aging. Nevertheless, the increase in resilient modulus starts to decline for aged materials with 7 and 12 years of age. Similar results were obtained by Voskuilen et al. (1992) with monotonic Indirect Tensile Test of field PA materials. The maximum stiffness modulus of the specimens was found to be around 3 to 4 years service period. The most likely explanation for such a behaviour could be attributed to the aging of the binder coupled with the cohesive damage (micro cracks) of the mortar and/or adhesive damage at the stone-mastic interface. Aging considerably increases the stiffness of binding material during the initial periods of the pavement life.

In Figure 4.28, the data shown in Figure 4.27 is presented in a different format. The resilient modulus at different frequencies is plotted against the pavement service life. The Figure clearly shows that the resilient modulus of the field materials gets to a maximum value at the service period of 3 – 4 years. The mixture resilient modulus in Figure 4.28 decreases with time after 4 years service period. Whereas, the binder complex shear modulus shown in Figure 4.29 (DSR test data) seems to attain a maximum value between the 3rd and 4th years and stays constant. This explains the decrease of the mixtures resilient modulus since damage continues to weaken the bond strength of the mixture. Further explanation is provided below.

The effect of aging on the mixture strength is most likely higher than the damage development in the mortar due to traffic during the first few years of the pavement life. It is assumed that the stresses and strains imposed by traffic loading may cause initiation of micro cracks in the material; however, the aging effect is dominant which increases the overall strength of the mixture. Besides, during the initial periods of the pavement life, traffic loadings are sustained because the bituminous mortar has both sufficient stiffness and stress relaxation potential (flexibility) until the critical aging of the bitumen is reached, which accelerates damage development in the binding material. The increase in stiffness of the mixture due to the aging of the bitumen/mortar reduces the stress relaxation potential of the mixture. Damage occurs mainly through development of cracking in the material which is critical at low temperatures (high frequency or short loading time). This is consistent with the observation of the occurrence of ravelling in the field that occurs during or immediately after the winter period. It seems that the decrease in stiffness modulus of the asphalt mix is associated with the second phase of damage development, i.e. damage propagation, which overcomes the effect of binder age hardening on the mixture stiffness. At this stage, the aggregates at the pavement surface with insufficient support in the mixture are more susceptible to ravelling.

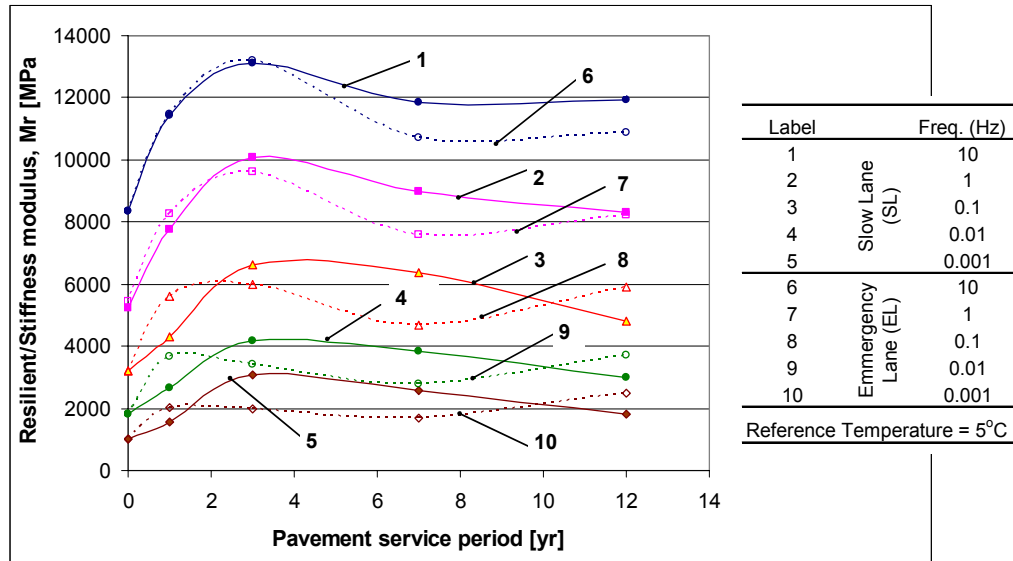


Figure 4.28: The combined effect of age hardening and damage development on the resilient modulus of field PA mixtures.

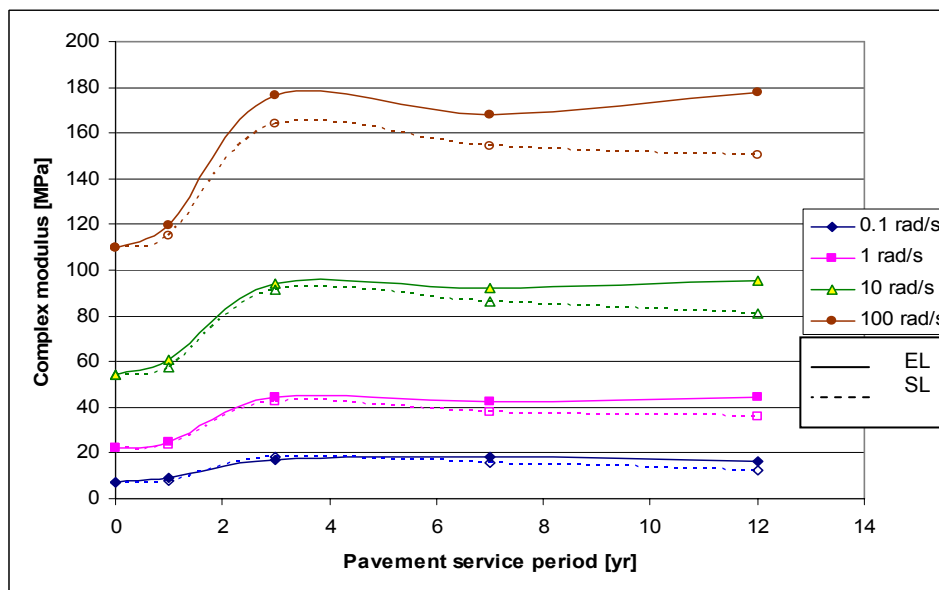


Figure 4.29: The complex shear modulus (G^*) of recovered field binders (Slow Lane, SL and Shoulder or Emergency Lane, EL).

4.7 Bitumen Rheology Tests

The aim of this research is to determine the effect of aging on the rheological and mechanical properties of the bitumen and mortar. To this end, the test conditions of the rheological and mechanical tests performed on binders aged in the laboratory and recovered from laboratory/field mixture aging are presented below.

4.7.1 Penetration and Softening point

Penetration and softening point (ring and ball temperature) are empirical test methods used to describe the viscosity characteristics of bitumen. These bitumen characterization methods, in combination with other properties, have been effectively used as measurement of bitumen quality in contract specifications. In this study, both the penetration and softening point tests have been carried out. The standard procedure NEN-EN 1427 was adopted to determine the softening point of binders. The penetration test was performed in a modified sample holder due to insufficient recovered material from the asphalt mixtures. In executing the penetration test with the modified cup, the standard procedure NEN-EN 1426 was employed. As shown in Figure 4.30, a ring with inside diameter of about 35.8 mm was inserted in the penetration cups to reduce the quantity of material needed to perform the test. The penetration test using three needles was performed as per the requirement in the standard procedure. This procedure was repeated on the same specimen after conditioning the sample at 25°C in a water bath for another 1 hour. Records show that the determination of penetration using the modified method and the standard procedure provide similar results.

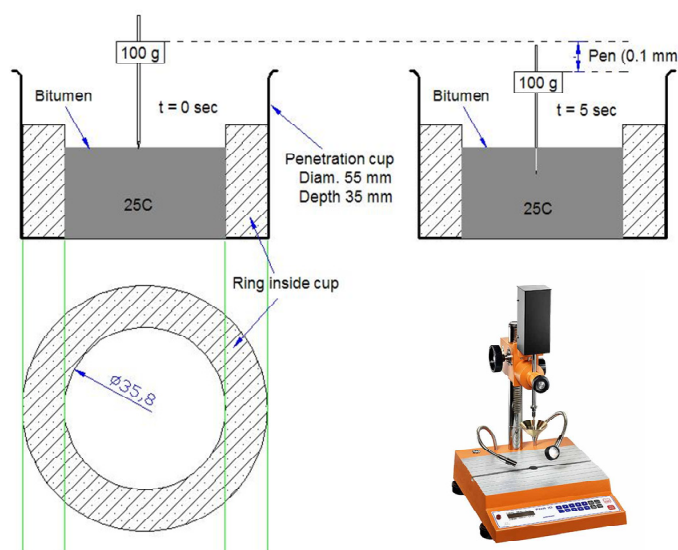


Figure 4.30: The penetration test

4.7.2 The Bending Beam Rheometer (BBR)

The BBR test was conducted according to ASTM D6648-01 standard (draft prEN 14771) at low temperatures to determine the stiffness (flexural) modulus of the bitumen and mastic materials. In Table 4.26 the materials tested with the Applied Testing Systems (ATS) BBR equipment are presented. The testing was conducted at temperatures ranging from -12 to -21°C for the bitumens and -8 to -15°C for the mastic materials. The beam specimens of bitumen and mastic had dimensions of 125 x 12.7 x 6.35 mm (Length x Depth x Width). The dimensions

of the mould and the bituminous sample are shown in Figure 4.31. The span length of the bending beam between the two supports is 102 mm.

Table 4.26: Materials used in the BBR test

Materials					
Bitumen			Mastic (bitumen+filler)		
Unaged	STA	LTA	Unaged	Aged (LTA)	Unaged
70/100 pen	RTFOT	RTFOT + RCAT	f/b = 1.0		f/b = 1.3
Testing temperature: -12 to -21°C			Testing temperature: -8 to -15°C		
<i>Remark:</i> *STA = Short Term Aging *LTA = Long Term Aging			*f/b = filler bitumen ratio by weight		

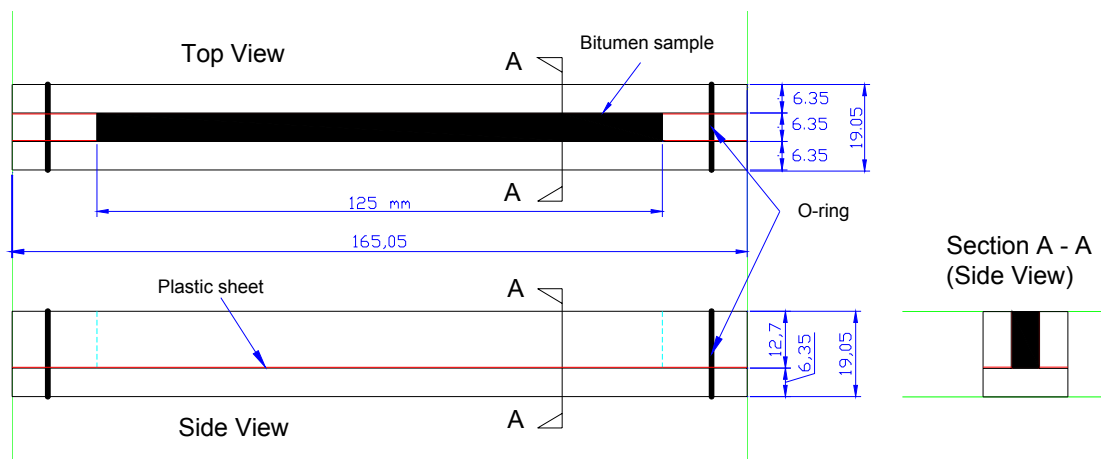


Figure 4.31: Dimensions of a BBR specimen and mould

The pattern of the central point beam deflection with time due to the applied constant load is shown in Figure 4.32. From this deflection, the creep stiffness is calculated using Equation 4.8.

$$S(t) = \frac{PL^3}{4bh^3\delta(t)} = \frac{1}{D(t)} \quad (4.8)$$

Where:

- $S(t)$ = time dependant flexural creep stiffness [MPa],
- P = applied constant load [N],
- L = span length (distance between beam supports) [mm],
- b = width of beam [mm],
- h = depth of beam [mm],
- $\delta(t)$ = deflection of beam at time t [mm], and
- $D(t)$ = creep compliance

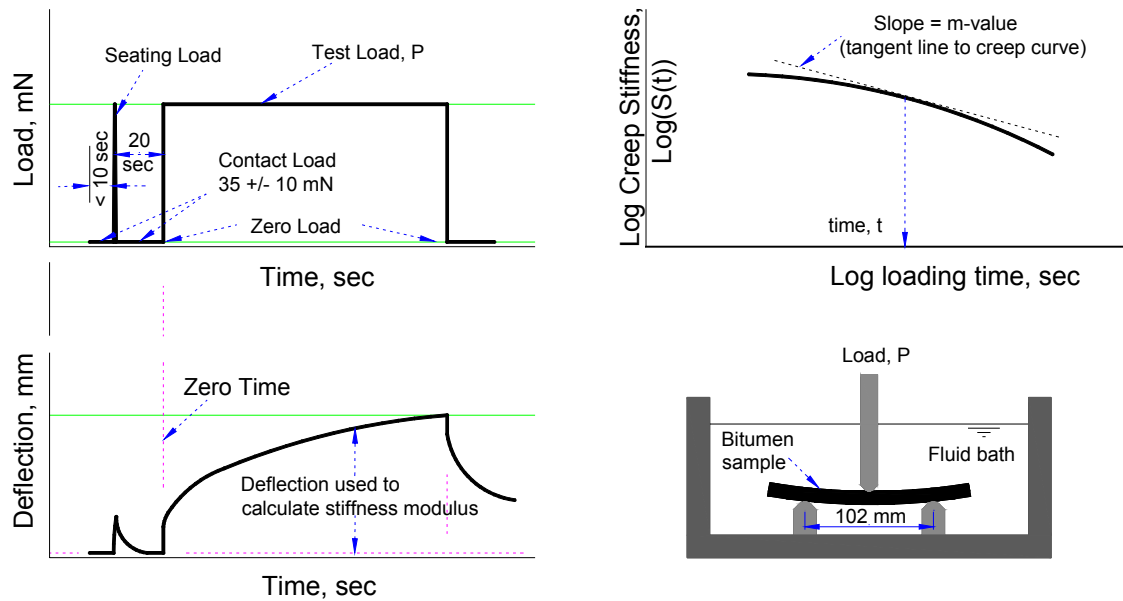


Figure 4.32: Deflection, load pattern and test setup of a BBR test

4.7.3 The Direct Tensile Test (DTT)

The Direct Tensile Test (DTT) of bitumen and mastic materials has been performed according to the SHRP standard procedure TP3.

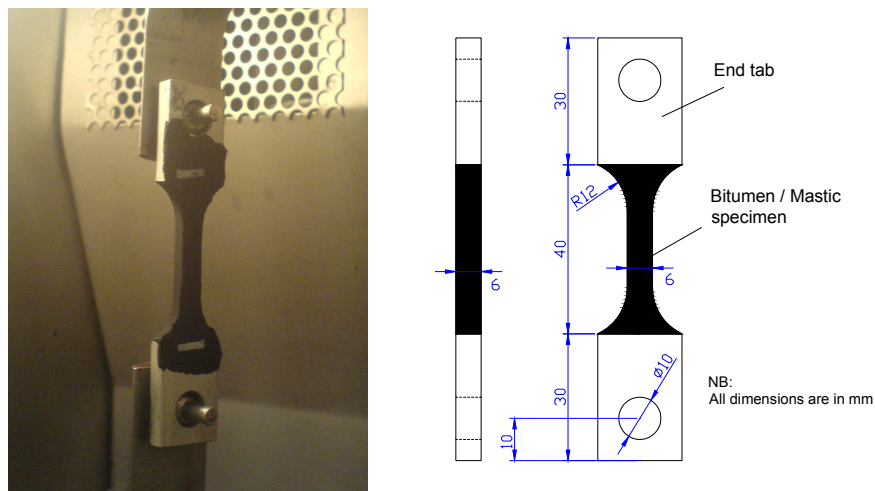


Figure 4.33: DTT test specimen set-up and geometry

The DTT samples, with an effective length of 33.8 mm and a sample cross-section of $36 \times 10^{-6} \text{ m}^2$, were prepared according to the standard Superpave procedure TP3 (Figure 4.33). The tests were carried out at temperatures of -10, -5, and 0°C and elongation/loading speeds of 1, 10, 20, 50, and 100 mm/min depending on the testing temperature as outlined in Table 4.27. Lower loading rates were used at low temperatures and higher rates at higher testing temperature to capture a broader picture of the effect of temperature and strain rates on the binders tensile properties.

Table 4.27. Testing conditions for the bitumen and mastic DTT test.

Bitumen	Loading rate (mm/min)					
	1	10	20	50	100	200
Temp. (°C)						
-10	x	x	x			
-5		x	x	x		
0			x	x	x	
5						
Mastic	Loading rate (mm/min)					
	1	10	20	50	100	200
-10						
-5	x	x	x			
0		x	x	x	x	
5				x	x	x

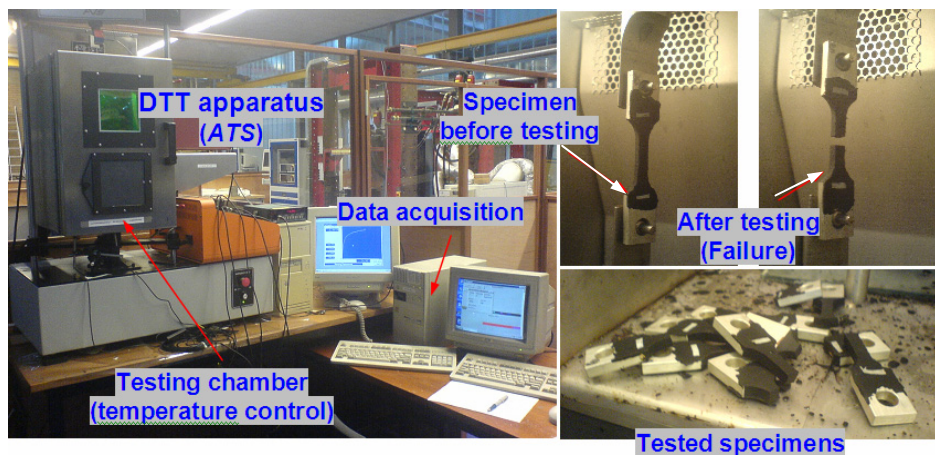


Figure 4.34: DTT specimen before and after failure

The ATS equipment used to perform the DTT test of bitumen and mastic materials is shown in Figure 4.34.

4.7.4 Dynamic Shear Rheometer (DSR)

Dynamic Shear Test

Dynamic shear tests were conducted using a Rheometrics RAA asphalt analyzer – Dynamic Shear Rheometer (DSR). The DSR test was basically conducted to determine the viscoelastic properties, i.e. the response or dependence of the materials on temperature and loading time. In this regard, the complex modulus and phase angle at different temperatures and loading frequencies were determined. In addition, the fatigue performance of the materials at intermediate temperature of 20°C was performed using the DSR instrument. The tests were conducted for bitumen (laboratory aged and recovered from field specimens) and mastic prepared from the laboratory aged bitumen.

DSR Test Setup

Figure 4.35 shows the DSR equipment. The specimen is placed between two circular parallel plates. The upper plate is fixed; while the lower part oscillates applying the shear strain during testing. The test is carried out in a temperature controlled mini-oven (chamber). The temperature is controlled with air for temperatures above 20°C and nitrogen gas is used for temperatures below 20°C. The temperature control has an accuracy of $\pm 0.1^\circ\text{C}$ when adequate time (usually 10 min) is provided to stabilize the temperature. The controlling mechanism and data acquisition is performed by a computer connected to the DSR equipment.

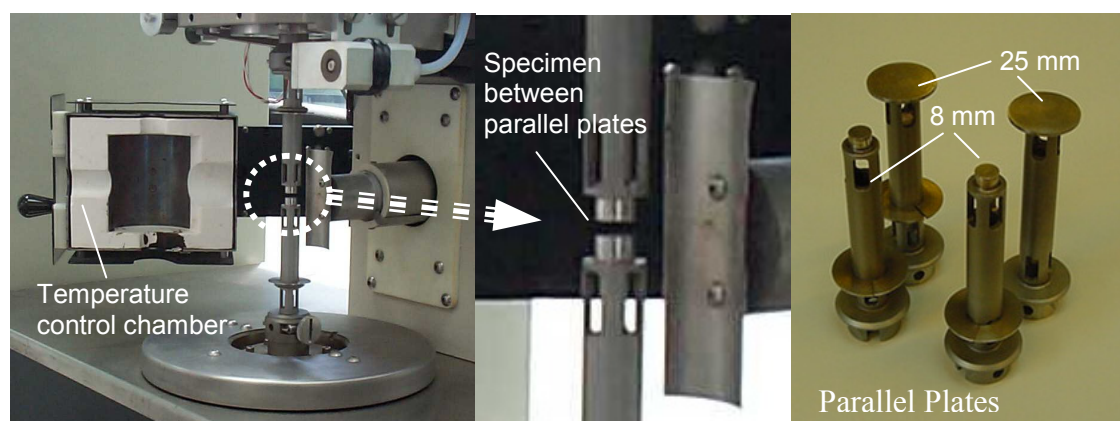


Figure 4.35: The DSR test setup

DSR Test Conditions

In the DSR test, the bituminous materials were subjected to a sinusoidal loading of constant strain at different loading frequencies (frequency sweep). The frequency sweep test was conducted at four temperatures ranging between -10°C and 50°C . Every test was carried out at frequencies ranging between 0.01 – 400 rad/s. Two parallel plate geometries with a diameter of 8 mm and 25 mm were used for testing at lower ($< 20^\circ\text{C}$) and intermediate-to-high ($30 - 50^\circ\text{C}$) temperatures respectively. Table 4.28 provides the testing conditions of bitumen and mastic materials in the DSR.

Table 4.28: DSR test conditions

Sample	Bitumen and mastic		Remark
Temperatures	-10 and 10°C	30 and 50°C	$\pm 0.1^\circ\text{C}$
Parallel plates	8 mm	25 mm	
Sample thickness	2 mm	1 mm	target thickness
Zero gap setting temp.	20°C	40°C	zero gap of plates
Frequency	0.1 – 400 rad/s		

The gap between the two parallel plates was set to zero at the start of the DSR test in order to adjust the thickness of the bitumen sample between the two plates to the target thicknesses. The zero gap setting of the 8 mm diameter parallel plates was done at 20°C for the tests performed at 20°C and lower

temperatures. A minimum of 10 minutes was provided to allow the temperature to stabilize before the zero gap setting. This temperature was selected because at this temperature the sample could be deformed to the target binder thickness without difficulty. Once the trimming and thickness adjustment of the binder is achieved, the sample is left for a minimum conditioning time of 10 min at 20°C. The temperature is then reduced gradually by 10°C followed by the minimum conditioning time. In the process of reducing the temperature, the thickness is automatically adjusted to allow the shrinkage of the sample due to temperature change. During testing at higher temperatures, the auto-adjustment of the sample thickness had little influence on the sample thickness.

Frequency sweep tests were performed at testing temperatures of -10, 10, 30, and 50°C. Before conducting the frequency sweep tests (constant strain, varying frequency), a strain sweep test (constant frequency, varying strain) was performed to determine the strain level at which the material response remains in the linear region. The strain level is calculated using Equation 4.9 (SHRP-A-370, Peterson et al. 1994) using the complex modulus obtained from the strain sweep test.

$$\gamma = \frac{12}{(G^*)^{0.29}} \quad (4.9)$$

Where:

γ = shear strain [%],

G^* = complex modulus from a strain sweep test [kPa].

4.7.5 Fatigue Test

The objective of conducting this test was to explore the effect of aging on the fatigue performance of the materials. The fatigue test is a cyclic load application test which is either strain or stress controlled. Due to repeated traffic loading, the binder/mortar in the PA pavement is assumed to be subjected to fatigue (Bahia 2001). In order to simulate this effect, a repeated loading of constant strain was applied to simulate the fatigue performance of the materials. The fatigue test, also known as time sweep test, was conducted using a DSR instrument.

In this research, a strain controlled fatigue test was performed at intermediate temperature of 20°C (assumed as average pavement temperature in the Netherlands) using 8 mm parallel plate geometry. The complex modulus of the specimen was predicted at specific time intervals or number of loading cycles from the material response to the applied strain and the geometry of the sample (i.e. the diameter and thickness of the binder). The complex modulus of the

binder decreases with time because of initiation and progression of damage in the material due to the repeated load application.

Materials aged under aging protocol 1 and 2 (AP1 and AP2) were only tested at 10% strain level. The other materials, which are selected from different aging processes, were tested at three strain levels as shown in Table 4.29. The test was run for a minimum of 3600 sec and a maximum of 10800 sec to allow adequate time for the development of damage in the materials. The time needed depends on the strain level used in conducting the fatigue testing and the degree of aging of the binder. Accordingly, less time was required to perform the test at higher strain levels and more time was needed to conduct the test at lower strain levels.

The test conditions and the materials tested are shown in Table 4.29.

Table 4.29: Test conditions used to conduct the binder / mastic fatigue tests

	Test conditions		
Strain level*	3% or 4%	6% or 7%	10%
Frequency	10 rad/s	10 rad/s	10 rad/s (1.6 Hz)
Temperature	20°C	20°C	20°C
Duration	1 – 3 hours	1 – 3 hours	1 – 3 hours
Parallel plate	8 mm	8 mm	8 mm
Film thickness (Gap)	2.0 mm	2.0 mm	2.0 mm
Materials:			
Weatherometer aging: (AP = aging protocol) AP0 = Unaged PA mixture AP1 = Temp aging AP2 = Temp+UV aging			AP0: Reference (recovered) AP1: Temp aging (UZ) AP1: Temp aging (LZ) AP2: Temp+UV aging (UZ) AP2: Temp+UV aging (LZ)
Assorted materials: - LTA laboratory aging - Weatherometer aging - Field materials	Virgin (Unaged) LTA: RTFOT+RCAT AP3: Temp+UV+RH (UZ) Field aging: 7 yr old Field aging: 12 yr old		
*NB: Changes to the strain levels were made when necessary			
Legend:			
AP3UZ1.0 = aging protocol 3 (upper zone), f/b ratio = 1.0			
FA7UZ1.0 = field aging 7 yr old specimen (upper zone), f/b ratio = 1.0			

4.8 References

ATLAS materials (2001). Weathering testing guidebook. *ATLAS materials testing solutions*.

Bahia, H. U., Hanson, D. I., Zeng, M., Zhai, H., Khatri, M. A., and Anderson, R. M. (2001). "Characterisation of Modified Asphalt Binders in Superpave Mix Design." *Transport Research Board: National Cooperative Highway Research Program (NCHRP) Rep. No. 459*, National Academy Press, Washington DC.

Burr, B. L., Davison, R. R., Glover, C. J., and Bullin, J. A. (1990). "Solvent removal from asphalt." *Transportation Research Board, Rep. No. 1269*, pp. 1-8. Washington DC.

Burr, B. L., Davison, R. R., Jemison, H. B., Glover, C. J., and Bullin, J. A. (1991). "Asphalt hardening in extraction solvents." *Transportation Research Record, Rep. No. 1323*, pp.70-76. Washington DC.

CROW (2002). "Modellen voor Wegbeheer (In Dutch)." CROW (*The national information and technology platform for infrastructure, traffic, transport and public space*) Rep. No. 169. Netherlands.

CROW (1996). "ZOAB Rest Levenduur (in Dutch)." Rep. No. publikatie 103. CROW (*The national information and technology platform for infrastructure, traffic, transport and public space*) Rep. No. 169. Netherlands.

DWW (2003). "Kalibratie ARAN-lasermetingen (in Dutch)." Rep. No. DWW-2003-133. Rijkswaterstaat, Road and Hydraulic Engineering Institute (DWW). The Netherlands.

ISO 4892-1 (1999). "Plastics - Method of exposure to laboratory light sources - Part 1: General guidance." International Organization for Standardization (ISO).

ISO 4892-2 (2006). "Plastics - Methods of exposure to laboratory light sources - Part 2: Xenon-arc lamps." International Organization for Standardization (ISO).

Medani, T. O. (2006). "Design principles of surfacings on orthotropic steel bridge decks.", *PhD thesis*, Technical University of Delft, The Netherlands.

NEVUL (2006). "Lijst erkende vulstofmerken (in Dutch)." (NEVUL – Nederlandse Vereniging van Fabrikanten en Importeurs van Vulstof voor Bitumineuze Werken).

Nielsen, C. B. (2007). "Raveling of Porous Asphalt Pavements - Assessment of test sections." Rep. No. M5 (*Technical note 48*), Danish Road Directorate (DRI), Denmark.

Peterson, J. C., Anderson, D. A., Bahia, H. U., and et al. (1994). "Binder characterization and evaluation, Volume 4: Test methods." Rep. No. SHRP-A-370, National Research Council, Washington, DC.

RAW (2005). *Standaard RAW Bepalingen (Standard)*. CROW (*The national information and technology platform for infrastructure, traffic, transport and public space*), The Netherlands.

Remijn M. (2005). "A methodology for the analysis of computerized tomography scans of asphalt cores using Amira software." *Rep. No. ISSN: 1386-5072*, Technical University of Delft (TU Delft), section of Engineering Geology. Delft, The Netherlands.

Solaimanian, M., and Kennedy, T. W. (1993). "Predicting maximum pavement surface temperature using maximum air temperature and hourly solar radiation." *Transportation Research Record (Rep. No. 1417)*, pp. 1-11. Washington DC.

Voskuilen, J. L. M., Bol, M. v. d., and Jautze, R. (2001). "Grip op Spoorvorming: Spoorvorming en Rafeling nader Onderzocht (in Dutch)." *Rep. No. W-DWW 2001-016*, Ministrie van Verkeer en Waterstaat, Rijkswaterstaat, Dienst Weg- en Waterbouwkunde (DWW), The Netherlands.

Voskuilen, J. L. M., and Kooij, J. v. d. (1992). "Splitproeven op Zeer Open Asfaltbeton uit Nederland Wegvakken (in Dutch)." *Rep. No. Rapportnr W-DWW-92-MA501*, Ministrie van Verkeer en Waterstaat, Rijkswaterstaat, Dienst Weg- en Waterbouwkunde (RWS, DWW). Delft, The Netherlands.

5 Effect of aging on Rheological and Mechanical Characteristics

In this chapter, the results of rheological and mechanical tests performed on bituminous materials are presented. Based on the analysis of the results, the effects of aging on the properties of bitumen are discussed.

5.1 Penetration and Softening Point

The temperature susceptibility of bitumen can be determined from penetration and softening point tests. The slope of the line connecting the Penetration at 25°C and the softening point (equivalent temperature at pen 800 dmm) in the Heukelom Bitumen Test Data Chart (BTDC) characterizes the temperature susceptibility of the binder (Heukelom 1973). The temperature dependency of bitumen is described by the Penetration Index (PI) shown in Equation 5.1 (Reed and Whiteoak 2006). For unmodified penetration grade bitumen, the Fraass point, penetration, softening point and viscosities at 60°C and 135°C fall along a straight line in the BTDC.

$$PI = \frac{1952 - 500 \cdot \log pen - 20T_{RB}}{50 \cdot \log pen - T_{RB} - 120} \quad (5.1)$$

Where:

PI = penetration index [-],
 T_{RB} = softening point [°C], and
 pen = penetration at 25°C [dmm],

The materials presented in this section include bitumen aged in the laboratory using standard aging methods and bitumen recovered from field specimens. Bitumen samples recovered from a laboratory mixture aging test are not included because of inadequate quantity of regained material. The penetration and softening point results for all the materials including predicted Fraass breaking point and PI values are given in Table 5.1. The Fraass breaking point

test determines the temperature at which bitumen reaches a critical stiffness (≈ 2.1 GPa); at this equi-stiffness or equi-viscous temperature the binder sample shows cracking (Reed and Whiteoak 2006).

The penetration and softening point (ring and ball temperature) test results for unaged and aged 70/100 pen bitumen are shown in Figure 5.1a. The laboratory aging of bitumen for short term (RTFOT EN 12607-1) and long term (RCAT90 draft NEN-EN 15323) simulates the aging of the bitumen during production, transportation, laying and compaction and during the service period of the bitumen respectively. The penetration test results for materials recovered from field specimens are shown in Figure 5.1b and Figure 5.1c. Similarly, the softening point of the field materials is shown in Figure 5.2a and Figure 5.2b. It can be concluded that LTA is by far not severe enough to simulate field aging. The bitumen properties after short term aging (STA) of the laboratory aged and field aged materials satisfies the requirements of the European specification for paving grade bitumen which stipulates a retained penetration of $\geq 46\%$ and an increase in softening point of ≤ 9 or ≤ 11 in severe cases (prEN-12591: 2005). The only sample that seems not to satisfy the requirement with reference to the virgin bitumen is the softening point of the field binder from the lower zone of the EL.

The ash content in the recovered binders was determined and found to be less than the maximum allowed quantity of 2% (NEN 3971). The determined quantities have a mean value of 0.587% and standard deviation 0.214%.

Table 5.1: Test results of penetration and softening point

Section	Year		Penetration	Softening point	Fraass point	Penetration Index
			Pen [dmm]	T _{RB} [°C]	[°C]	PI [-]
1. Laboratory Aging						
Virgin	70/100 pen		90.7	45.4	-15.1	-0.97
RTFOT	STA		46.0	51.8	-8.8	-0.95
RTFOT + RCAT	LTA		29.0	57.8	-6.1	-0.62
2. Field Materials			Emergency Lane, EL			
Section	Year	Ash content				
a. Upper Zone, UZ		[%]	Pen [dmm]	T _{RB} [°C]	Fraass [°C]	PI [-]
G	0	0.327	45.1	51.2	-7.6	-1.15
A	1	0.443	25.0	57.7	-3.2	-0.93
B	3	0.532	15.8	61.6	1.4	-1.00
C	7	0.508	12.7	65.3	2.4	-0.72
E	12	0.999	8.4	72.8	5.1	-0.24
b. Lower Zone, LZ						
G	0	0.323	42.7	51.1	-6.4	-1.28
A	1	0.448	26.8	57.0	-3.9	-0.93
B	3	0.578	14.8	62.7	1.6	-0.91
C	7	0.598	11.7	65.3	3.7	-0.85
E	12	1.060	7.3	73.7	6.7	-0.31
			Slow Lane, SL (Trafficked lane)			
Section	Year	Ash content				
a. Upper Zone, UZ		[%]	Pen [dmm]	T _{RB} [°C]	Fraass [°C]	PI [-]
G	0	0.327	45.1	51.2	-7.7	-1.15
A	1	0.392	26.1	56.8	-3.2	-1.02
B	3	0.616	17.2	61.8	-0.1	-0.83
C	7	0.741	11.1	66.7	3.7	-0.71
E	12	0.511	20.0	59.6	-1.0	-0.97
b. Lower Zone, LZ						
G	0	0.323	42.7	51.1	-6.5	-1.28
A	1	0.367	26.4	57.1	-3.9	-0.94
B	3	0.852	18.8	61.3	-1.2	-0.76
C	7	0.704	11.2	66.8	3.5	-0.68
E	12	0.572	17.5	60.6	0.4	-1.00

NB: The reduction in the penetration and softening point of the 70/100 pen bitumen after aging (STA: RTFOT) satisfies the requirements set by the European norm EN 12591.

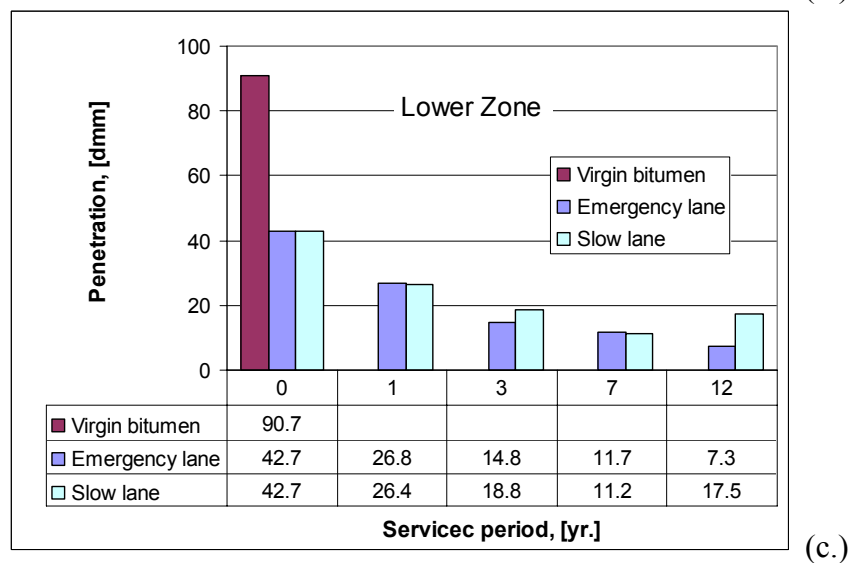
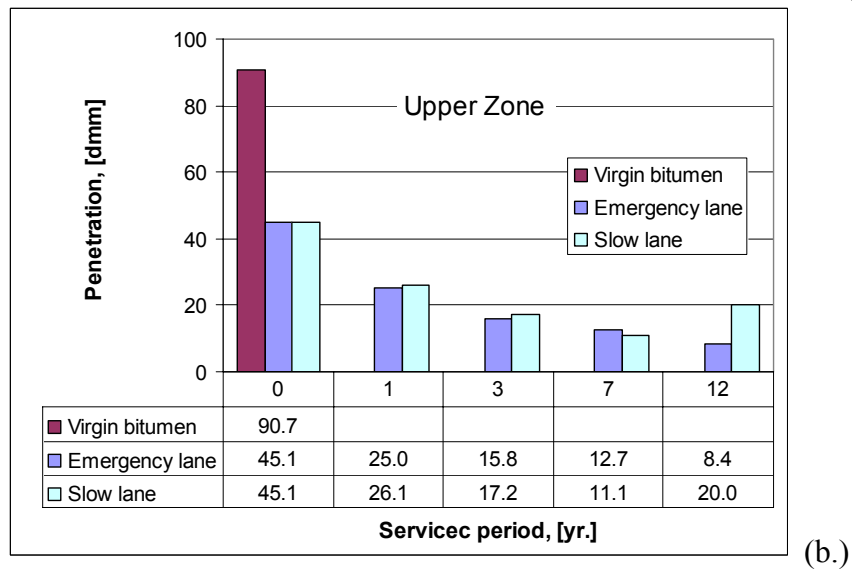
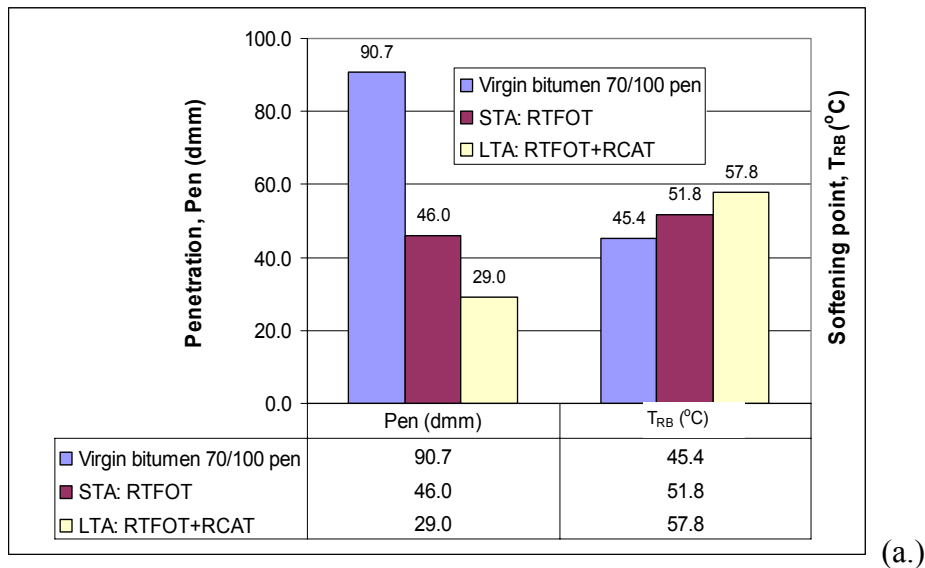


Figure 5.1: (a.) Penetration and softening point of unaged, short term (STA), and long term aged (LTA) 70/100 bitumen (b. and c.) Penetration of bitumen recovered from field specimens

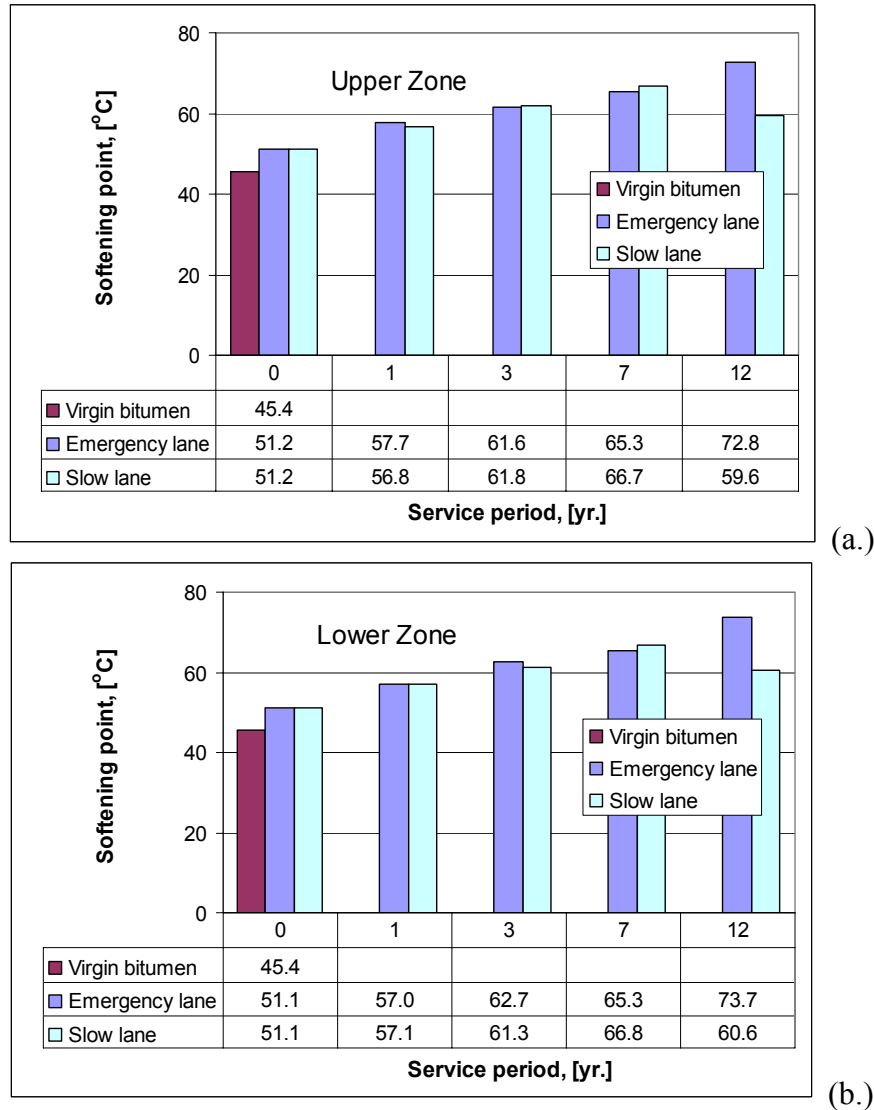


Figure 5.2: Softening point of bitumen recovered from field specimens

The pen and softening point (ring and ball temperature) test results of laboratory and field materials reveal that the standard simulation of bitumen aging is not the same as the aging of PA layers in the field. The penetration has reduced by 68.0% and softening point increased by 27.3% relative to the virgin bitumen for the long term aged material in the laboratory. These results are comparable to the 1 year aged material in the field. In comparison, the 12 year aged field material has dropped in penetration by about 90.7% and shows an increase in softening point by 60.4%. For dense mixtures it is assumed that the long term laboratory aging test simulates the aging of bitumen in the pavement after service period of about 10 years. The reason for such big discrepancy is that the conventional long term laboratory aging method is calibrated to simulate binder aging in dense mixes with voids contents between 3 and 5%. Aging has little effect on dense asphalt mixes in which the prime influence is on the top few millimetres while the bulk bitumen is hardly subjected to aging (Verhasselt 2000).

Some factors are considered to have contributed to lower penetration and higher softening point values in the case of the field specimens. These are:

- The bitumen recovery/extraction process with the use of solvents to extract the bitumen might have some effect on the bitumen structure and hardening (Burr et al. 1991, Burr et al. 1994, refer also to section 4.4.2).
- The fact that a small quantity of ash is present in the extracted binders.

Nevertheless, these factors are not believed to result in significant differences in the aging indicators.

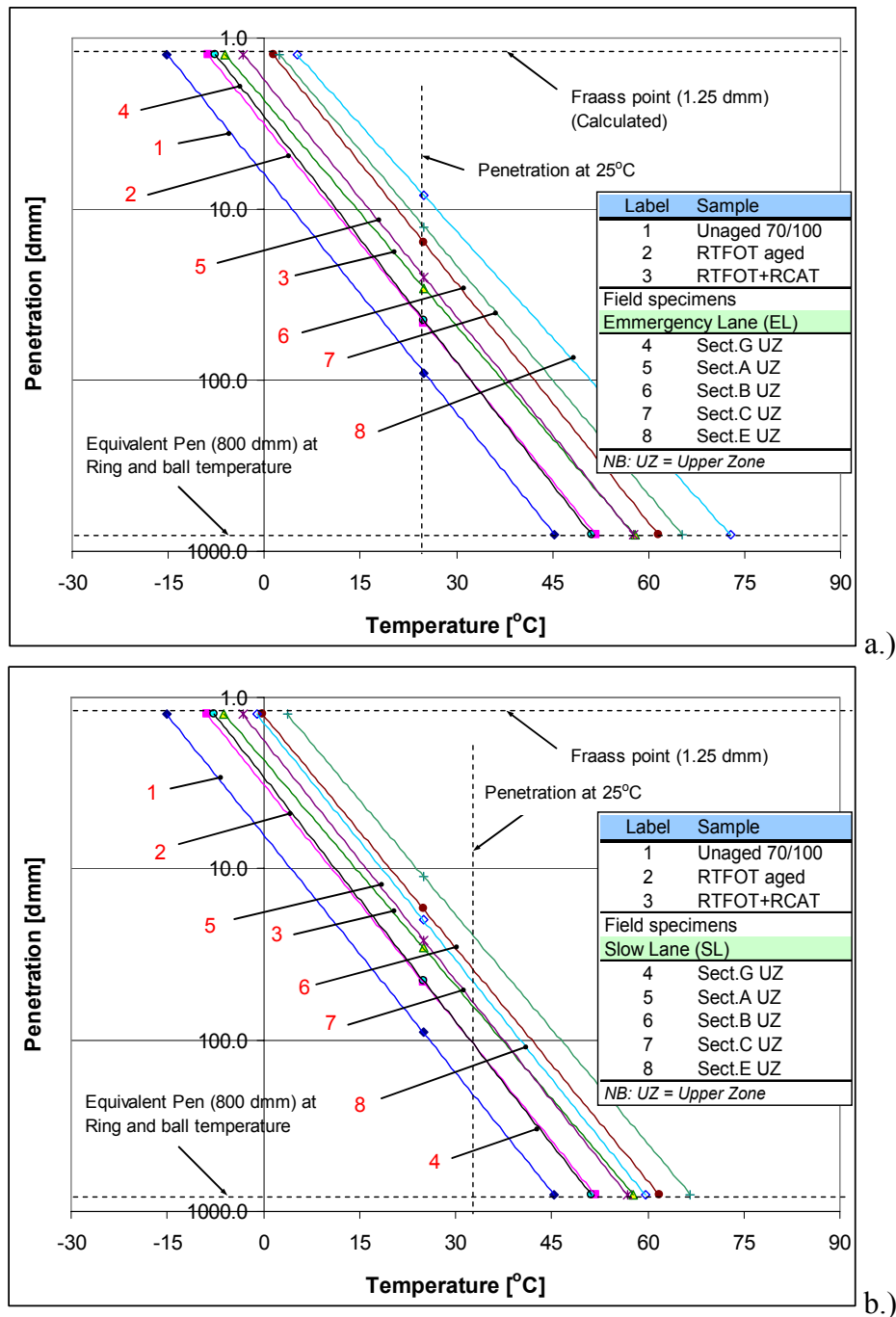


Figure 5.3: Log penetration versus temperature plot of bitumen samples

The effect of aging on the temperature dependency of the laboratory aged and field materials are shown in Figure 5.3. The Fraass breaking point (at 1.25 dmm) was determined based on the property of bitumen (i.e. slope PI) on the Heuklom's Bitumen Test Data Chart (BTDC). A horizontal shift in the temperature dependency can be observed, which implies a higher temperature at which the binder is likely to behave brittle. The projected cracking temperature (Fraass breaking point) of unaged and laboratory aged materials remains below 0°C while the critical temperature of the field materials with service periods greater than 3 years extends above 0°C. The critical temperature of the most aged material from a good performing 12 year old pavement is determined to be about 5°C, which is about the same temperature as the mean temperature during winter periods (refer to section 4.3.2 table 4.8b). This supports the hypothesis that ravelling occurs during and immediately after the winter period. It also implies that the effect of traffic on the performance of PA pavements after 3 years of service life is critical.

5.2 The Bending Beam Rheometer (BBR)

5.2.1 BBR Data Fitting

The BBR⁶ tests can provide more insight into the materials performance at low temperatures close to the critical temperature. According to the SHRP requirement (TP1), a critical temperature of a binder is the temperature at which the material becomes very stiff and brittle: a maximum stiffness of 300 MPa and/or a minimum m -value of 0.3 after 60 sec are set as requirements. The parameter m -value is the slope of the log-log plot of the Creep stiffness versus time.

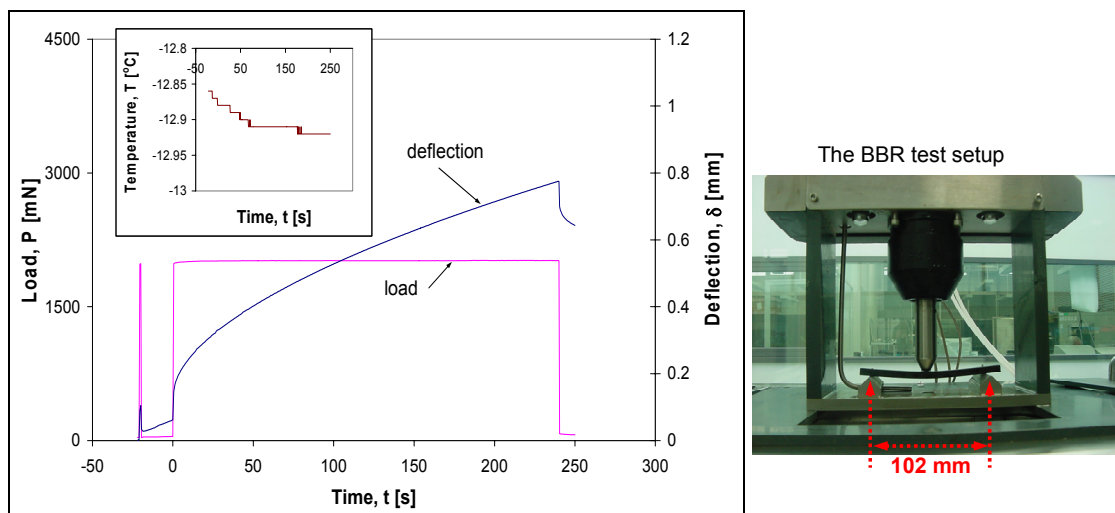


Figure 5.4: Deflection and load pattern of a BBR test

⁶ The BBR test, $S(t=60s)$, is meant to simulate asphalt binder stiffness after two hours of loading at the minimum HMA pavement design temperature (SHRP).

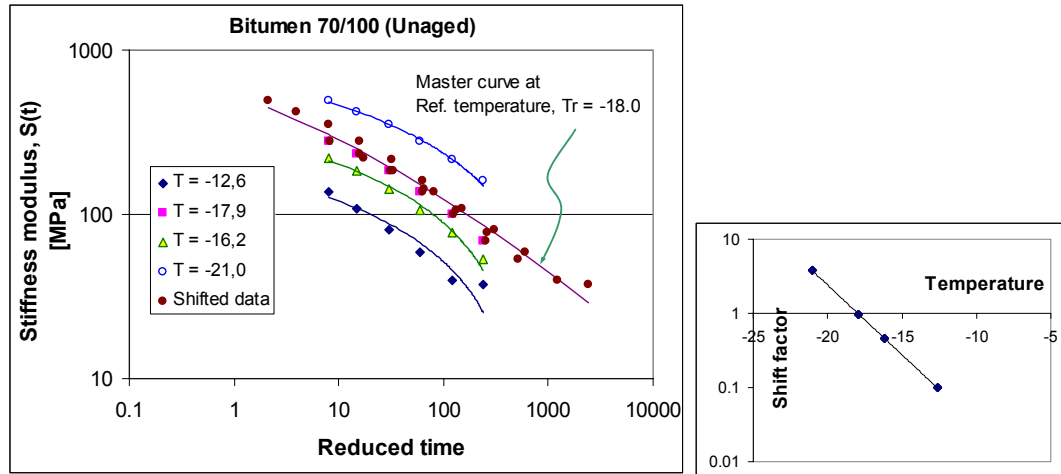


Figure 5.5: BBR data before and after shifting to a reference temperature of -18.0°C

An example of BBR data conducted at four different temperatures is shown in Figure 5.5. The stiffness master curves shown in Figure 5.5 are generated by fitting the Christensen-Anderson-Marasteanu (CAM) model given in Equation 5.2 to the BBR stiffness data measured at different temperatures. The time-temperature dependency of the data was modelled with the shift factor based on the Arrhenius equation (Equation 5.4). An arbitrary reference temperature of -18.0°C was selected for shifting the data.

$$S(T_{ref}, \xi) = S_{glassy} \left[1 + \left(\xi / \lambda \right)^{\beta} \right]^{-k/\beta} \quad (5.2)$$

$$\xi = \frac{t}{a_T} \quad (5.3)$$

$$\ln(a_T) = \frac{-E_a}{2.303R} \left(\frac{1}{T} - \frac{1}{T_{ref}} \right) \quad (5.4)$$

where:

$S(\xi)$	=	creep stiffness at a reduced time ξ [MPa],
S_{glassy}	=	glassy modulus (assumed constant ≈ 3 GPa),
$\lambda, \beta, \text{ and } k$	=	parameters in the model
ξ	=	reduced time [s],
t	=	time of loading [s],
a_T	=	shift factor [-] (Arrhenius equation)
E_a	=	the activation energy [J/mol]
R	=	the universal gas constant (8.314) [J/mol/K],
T	=	temperature in degree kelvin [$^{\circ}\text{K}$], and
T_{ref}	=	a reference temperature [$^{\circ}\text{K}$],

5.2.2 Test Results and Analysis

The bending stiffness modulus master curve and m -values of the materials tested are shown in Figure 5.6. The CAM model parameters for fitting the data are presented in Table 5.2.

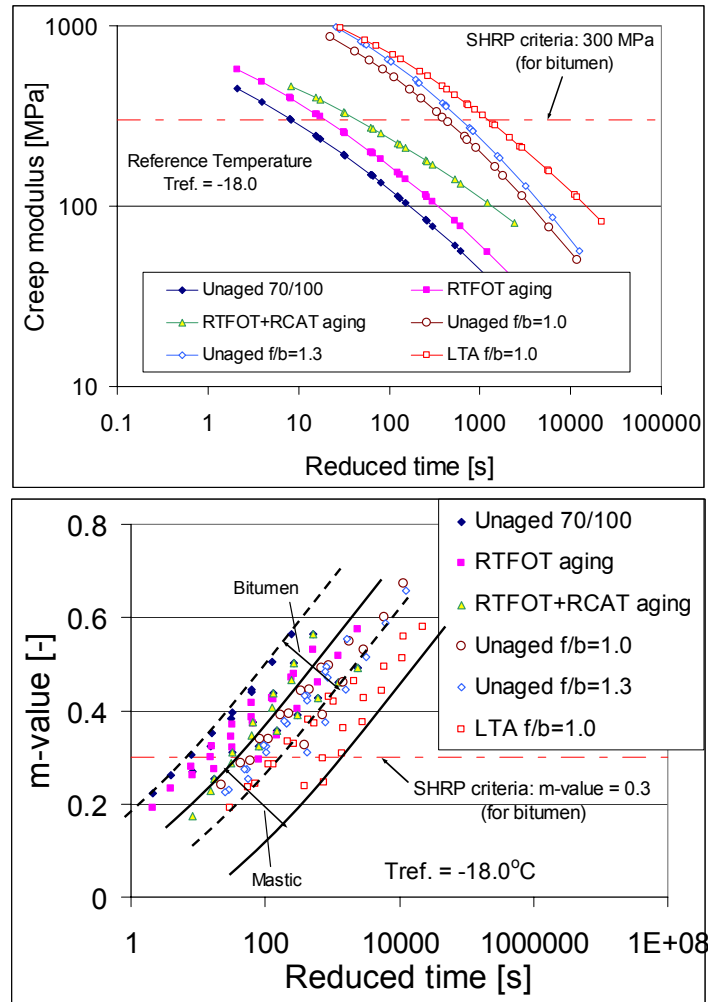


Figure 5.6: Stiffness master curve of bitumen and mastic specimens at reference temperature of -18°C

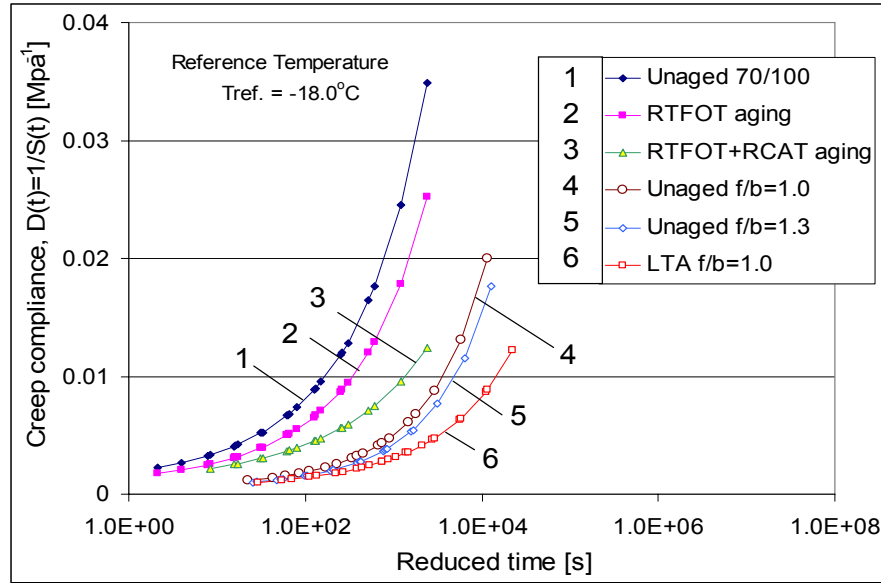


Figure 5.7: Effect of aging on creep compliance of the binder and mastic

Table 5.2: CAM Model parameters

	Bitumen			Mastic		
Parameter	Vergin Bitumen	STA RTFOT	LTA RTFOT+RCAT	STA f/b=1.0	STA f/b=1.3	LTA f/b=1.0
S_{glassy} [MPa]	3000.0	3000.0	3000.0	3000.0	3000.0	3000.0
E_a [KJ/mol]	0.545	0.545	0.545	0.545	0.545	0.545
k [-]	0.869	0.852	0.645	0.835	0.824	0.652
β [-]	0.169	0.181	0.159	0.280	0.302	0.262
λ [-]	248.22	248.22	248.22	248.22	248.22	248.22

The BBR test results for the bitumen and mastic materials are presented in Table 5.3.

Figure 5.6 shows that the stiffness of the bitumen and mastic materials decreases as the loading time increases. The effect of aging shifts the stiffness master curve towards the high temperature (high loading time), which increases the critical temperature of the material. It is understood that this change in behaviour is accompanied by a decrease in the m -value, a parameter related to stress relaxation potential of the materials. The m -value provides an indication of the viscoelastic property of the material relating the elastic and viscous components of the stiffness. A decrease of m is associated with a decrease of the viscous component. Furthermore, an increase in the susceptibility of the material to cracking is strongly associated with the decrease in m -value (refer to Equation 5.8 through Equation 5.12). As shown in Equation 5.12, the parameter m -value is inversely proportional to the parameter n in the Paris law of crack susceptibility (Lundstrom & Isacsson 2003, Molenaar 1983, Molenaar and Molenaar 2000, Shapery 1975).

The following observations are made from Figure 5.6, Figure 5.7, and Figure 5.10.

- Aging increases the stiffness and relaxation modulus of the bitumen and mastic materials. Both the stiffness and relaxation modulus of the aged materials showed a horizontal shift in the reduced time scale and a decrease in slope relative to the unaged (reference) bitumen.
- The stiffness and relaxation modulus of the aged bitumen/mastic shows an increment with loading time (temperature) relative to the unaged materials, which indicates lower sensitivity of the aged materials to creep.
- The effect of filler alters the creep behaviour of the bitumen material.
- Short term binder/mastic aging affects the relaxation and creep properties of the binder; long term aging has greater effect.
- The creep behaviour of the mastic and the bitumen materials is different. The time needed to achieve the same deformation by the aged mastic material relative to the unaged mastic is much greater compared to the corresponding time required by the aged bitumen relative to the unaged.

The stiffness and m -value (at 60 s loading time) for unaged and aged bitumen and mastic materials in relation to temperature are shown in Figure 5.8. The critical temperatures are indicated based on Superpave (SHRP) TP1 requirements. The following observations can be made from the figure.

- The stiffness of the aged materials showed a horizontal shift in the temperature domain relative to the unaged material both for the bitumen and mastic.
- The mastics (filler + bitumen with f/b ratio by mass 1.0 and 1.3) have higher critical temperatures compared to the bitumen. (NB: The SHRP criteria are valid for bitumen and not for mastic. Nevertheless, a higher critical temperature is expected for the mastics).
- The unaged mastic with f/b ratio of 1.3 has a lower critical temperature than the mastic of the aged bitumen with f/b ratio of 1.0. This implies that a higher degree of hardening (stiffness) is achieved by the binder aging rather than increasing the filler content from 1.0 to 1.3.
- The slope/gradient of the m -value of the mastic materials is steeper than the bitumen materials indicating sensitivity to brittle behaviour as the temperature decreases.

Table 5.3: BBR test data for bitumen and mastic materials

Reference / Virgin 70/100					
Temp[°C]	time [s]	Red. Time @ Tref = -18.0	Stiffness [MPa]	CAM model	m-value [-]
-12.6	8	80.88	135.72	135.15	0.323
-12.6	15	151.65	108.56	104.78	0.357
-12.6	30	303.30	81.24	77.81	0.392
-12.6	60	606.61	58.30	56.78	0.426
-12.6	120	1213.21	39.70	40.71	0.461
-12.6	240	2426.42	37.72	28.69	0.492
-17.9	8	8.36	277.76	301.12	0.269
-17.9	15	15.67	233.12	245.62	0.324
-17.9	30	31.34	184.13	193.10	0.384
-17.9	60	62.68	138.28	149.24	0.444
-17.9	120	125.36	99.80	113.35	0.504
-17.9	240	250.73	69.30	84.59	0.565
-16.2	8	17.49	219.56	236.72	0.254
-16.2	15	32.79	182.43	189.99	0.311
-16.2	30	65.57	142.70	146.67	0.375
-16.2	60	131.15	107.12	111.27	0.438
-16.2	120	262.30	76.91	82.94	0.501
-16.2	240	524.60	53.26	60.74	0.564
-21.0	8	2.12	492.82	448.65	0.221
-21.0	15	3.97	422.14	376.59	0.262
-21.0	30	7.95	349.26	305.88	0.306
-21.0	60	15.90	275.64	244.44	0.351
-21.0	120	31.80	213.82	192.10	0.396
-21.0	240	63.59	159.92	148.41	0.440

Mastic: Virgin f/b=1.0					
Temp[°C]	time [s]	Red. Time @ Tref = -18.0	Stiffness [MPa]	CAM model	m-value [-]
-8.8	8	389.29	275.11	311.62	0.327
-8.8	15	729.92	221.00	233.09	0.391
-8.8	30	1459.84	164.70	164.87	0.461
-8.8	60	2919.68	116.14	113.58	0.532
-8.8	120	5839.36	78.10	76.32	0.602
-8.8	240	11678.72	50.67	50.11	0.672
-13.3	8	60.25	592.29	644.61	0.293
-13.3	15	112.97	493.56	516.07	0.340
-13.3	30	225.94	386.62	393.31	0.392
-13.3	60	451.87	281.67	291.49	0.444
-13.3	120	903.75	201.42	210.10	0.496
-13.3	240	1807.50	144.70	147.39	0.548
-15.6	8	22.64	895.73	872.33	0.241
-15.6	15	42.45	764.46	722.63	0.288
-15.6	30	84.90	617.76	572.55	0.339
-15.6	60	169.79	475.83	441.40	0.390
-15.6	120	339.58	352.33	330.92	0.442
-15.6	240	679.16	259.99	241.26	0.493

Mastic: Virgin f/b=1.3					
Temp[°C]	time [s]	Red. Time @ Tref = -18.0	Stiffness [MPa]	CAM model	m-value [-]
-8.6	8	422.33	299.42	359.58	0.310
-8.6	15	791.86	242.45	268.54	0.374
-8.6	30	1583.72	182.65	189.34	0.445
-8.6	60	3167.45	130.39	129.86	0.516
-8.6	120	6334.89	88.84	86.79	0.587
-8.6	240	12669.79	58.05	56.65	0.657
-13.5	8	55.37	683.50	781.89	0.255
-13.5	15	103.82	574.04	631.73	0.310
-13.5	30	207.64	453.06	485.57	0.372
-13.5	60	415.29	342.38	362.28	0.433
-13.5	120	830.58	247.31	262.39	0.494
-13.5	240	1661.16	173.01	184.64	0.555
-15.1	8	28.05	853.10	959.30	0.231
-15.1	15	52.59	733.33	794.84	0.275
-15.1	30	105.18	594.98	628.79	0.324
-15.1	60	210.36	466.57	483.04	0.373
-15.1	120	420.73	350.15	360.19	0.421
-15.1	240	841.46	260.95	260.74	0.470
-15.3	8	25.75	1115.43	982.48	0.225
-15.3	15	48.28	956.35	816.56	0.273
-15.3	30	96.55	777.78	648.27	0.326
-15.3	60	193.10	607.02	499.84	0.379
-15.3	120	386.21	457.25	374.09	0.432
-15.3	240	772.42	334.55	271.78	0.485

Mastic: LTA f/b=1.0					
Temp[°C]	time [s]	Red. Time @ Tref = -18.0	Stiffness [MPa]	CAM model	m-value [-]
-7.2	8	744.35	319.77	364.28	0.246
-7.2	15	1395.65	268.87	285.81	0.308
-7.2	30	2791.30	213.38	214.70	0.376
-7.2	60	5582.60	159.61	158.31	0.444
-7.2	120	11165.19	114.07	114.71	0.512
-7.2	240	22330.39	78.82	81.79	0.580
-8.8	8	389.29	451.70	459.78	0.239
-8.8	15	729.92	378.26	366.94	0.298
-8.8	30	1459.84	301.67	280.72	0.363
-8.8	60	2919.68	231.48	210.62	0.428
-8.8	120	5839.36	166.66	155.12	0.494
-8.8	240	11678.72	115.87	112.28	0.559
-12.9	8	71.30	726.88	777.16	0.243
-12.9	15	133.70	621.31	649.07	0.284
-12.9	30	267.39	504.01	521.90	0.329
-12.9	60	534.79	391.24	411.13	0.374
-12.9	120	1069.57	294.87	317.35	0.419
-12.9	240	2139.15	220.94	240.17	0.464
-15.0	8	29.27	1009.92	975.28	0.193
-15.0	15	54.89	883.77	833.60	0.236
-15.0	30	109.78	739.06	688.01	0.285
-15.0	60	219.55	595.08	556.45	0.333
-15.0	120	439.11	463.40	440.91	0.381
-15.0	240	878.22	351.71	342.30	0.429

STA: RTFOT Aging					
Temp[°C]	time [s]	Red. Time @ Tref = -18.0	Stiffness [MPa]	CAM model	m-value [-]
-12.6	8	80.88	177.40	181.67	0.294
-12.6	15	151.65	145.97	141.75	0.346
-12.6	30	303.30	112.84	105.94	0.403
-12.6	60	606.61	83.17	77.72	0.460
-12.6	120	1213.21	58.79	55.98	0.517
-12.6	240	2426.42	40.86	39.60	0.574
-16.2	8	17.49	274.87	312.32	0.273
-16.2	15	32.79	229.13	252.71	0.321
-16.2	30	65.57	180.47	196.69	0.373
-16.2	60	131.15	135.94	150.32	0.426
-16.2	120	262.30	99.20	112.78	0.478
-16.2	240	524.60	70.44	83.06	0.531
-17.9	8	8.36	416.52	393.23	0.262
-17.9	15	15.67	354.34	323.59	0.301
-17.9	30	31.34	284.20	256.70	0.343
-17.9	60	62.68	217.55	200.03	0.386
-17.9	120	125.36	162.13	153.06	0.428
-17.9	240	250.73	121.81	114.97	0.471
-21.0	8	2.12	557.21	573.80	0.190
-21.0	15	3.97	487.76	486.38	0.232
-21.0	30	7.95	408.81	399.15	0.278
-21.0	60	15.90	331.71	322.09	0.325
-21.0	120	31.80	260.43	255.42	0.371
-21.0	240	63.59	198.36	198.96	0.417

LTA: RTFOT + RCAT Aging					
Temp[°C]	time [s]	Red. Time @ Tref = -18.0	Stiffness [MPa]	CAM model	m-value [-]
-12.6	8	80.88	278.52	254.13	0.323
-12.6	15	151.65	236.70	210.23	0.357
-12.6	30	303.30	191.34	168.58	0.392
-12.6	60	606.61	147.95	133.53	0.426
-12.6	120	1213.21	111.90	104.49	0.461
-12.6	240	2426.42	81.83	80.77	0.492
-16.2	8	17.49	373.21	386.87	0.254
-16.2	15	32.79	320.06	327.90	0.311
-16.2	30	65.57	262.66	270.12	0.375
-16.2	60	131.15	208.07	219.84	0.438
-16.2	120	262.30	158.99	176.74	0.501
-16.2	240	524.60	115.86	140.36	0.564
-17.9	8	8.36	467.96	464.07	0.174
-17.9	15	15.67	411.10	397.80	0.228
-17.9	30	31.34	348.03	331.92	0.288
-17.9	60	62.68	278.85	273.65	0.347
-17.9	120	125.36	209.09	222.89	0.407
-17.9	240	250.73	158.86	179.34	0.466

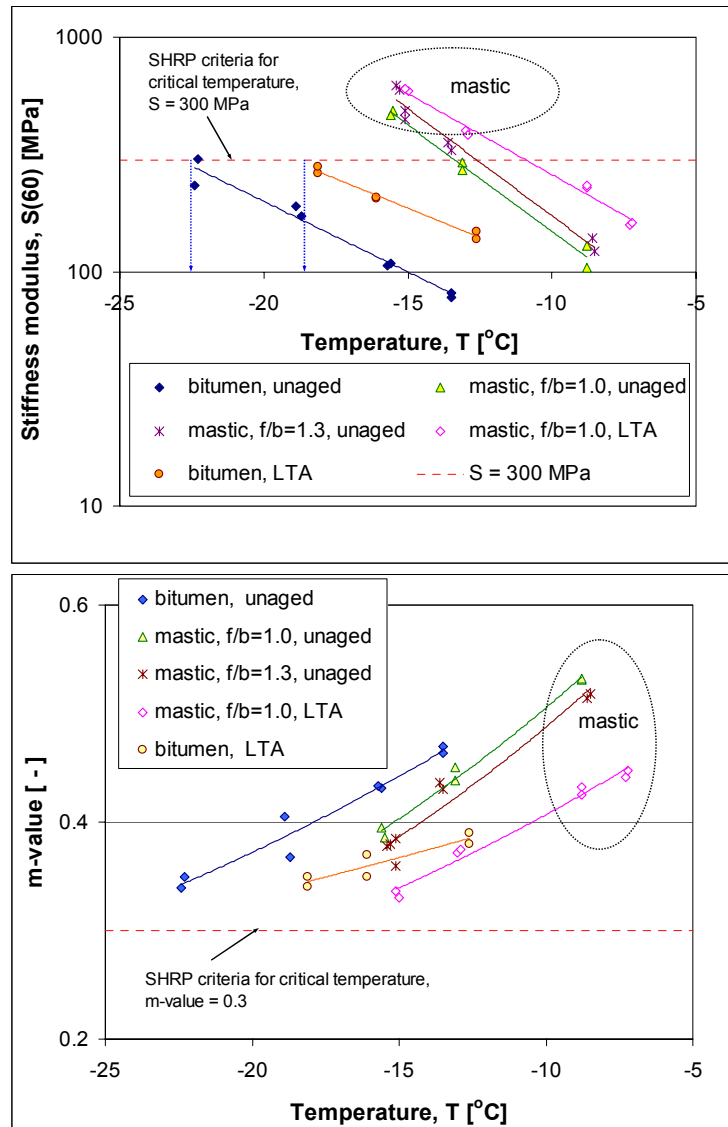


Figure 5.8: Stiffness and m -value results of BBR test on bitumen and mastics of un-aged and aged materials at loading time of 60 sec.

5.2.3 Prediction of Relaxation Modulus

The relaxation modulus can be obtained from the creep compliance through an inter-conversion. The need for inter-conversion arises when it is difficult to run a constant strain relaxation test on stiff materials (usually at low temperatures) while a constant stress creep test is easier to carry out (BBR test).

The creep compliance of the bitumen can be calculated from the stiffness master curve (fitted to the CAM model, Equation 5.2) by taking its inverse. Algorithms are developed to convert the creep data derived from the BBR test into a relaxation modulus. The standard practice for determining the low temperature performance of bitumen (ASTM D 6816-02) recommends the use of Hopkins and Hamming (1957) numerical method for converting the creep compliance to relaxation modulus. The interrelationship between relaxation modulus and creep response in the time domain is given by Equation 5.5.

$$\int_0^t E(t-\xi) \cdot D(\xi) d\xi = \int_0^t E(\xi) \cdot D(t-\xi) d\xi = t \quad (5.5)$$

Where:

- $E(\xi)$ = relaxation modulus at reduced time ξ
- $D(\xi)$ = creep compliance at reduced time t , $D(\xi) = 1/S(\xi)$
- $S(\xi)$ = stiffness modulus at reduced time t
- t = time

A MATLAB program developed by Jansen (2006) was used to solve the convolution integral through an iterative way using the algorithm (Tschoegl 1989) in Equation 5.6.

$$E(t_n) = -E(t_{n-1}) + \frac{4t_n - term}{[D(0) + D(t_n - t_{i-n})](t_n - t_{n-1})} \quad (5.6)$$

$$term = \sum_{i=1}^{n-1} [E(t_{i-1}) + E(t_i)] \cdot [D(t_n - t_i) + D(t_n - t_{i-1})](t_i - t_{i-1}) \quad (5.7)$$

Where:

- $D(0)$ = instantaneous (glassy) compliance, $D(0) = 1/S_{glassy}$
- n = interval of integration

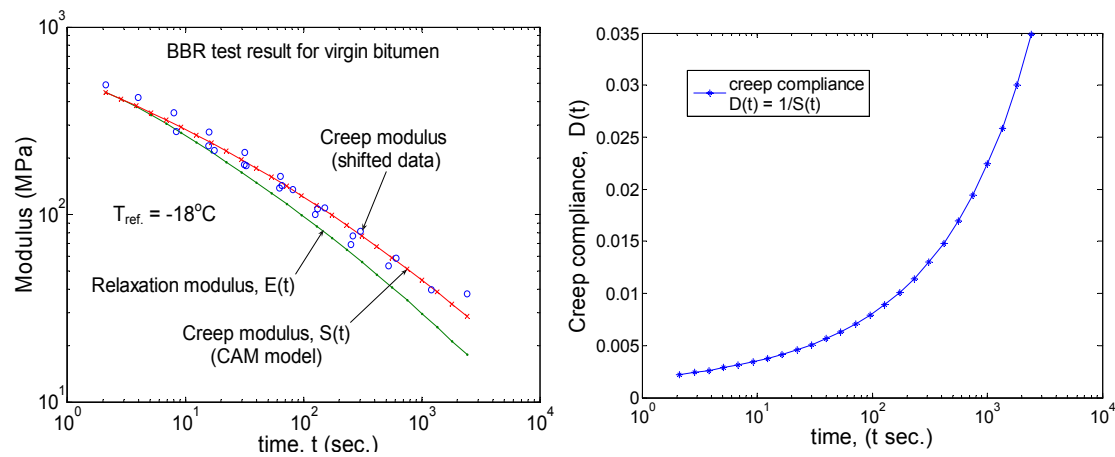


Figure 5.9: Relaxation modulus and creep compliance of a virgin (unaged) bitumen determined from a BBR stiffness modulus data

The predicted relaxation modulus from the BBR stiffness data (at a reference temperature of -18°C) based on Equation 5.6 and 5.7 is shown in Figure 5.10. The assessment of the relaxation behaviour of the bitumen and mastic is basically similar to the assessment based on the stiffness modulus of the materials. It has been shown that the effect of aging increases the stiffness but decreases the m -value (viscous component) of the binder / mastic (section 5.2.2).

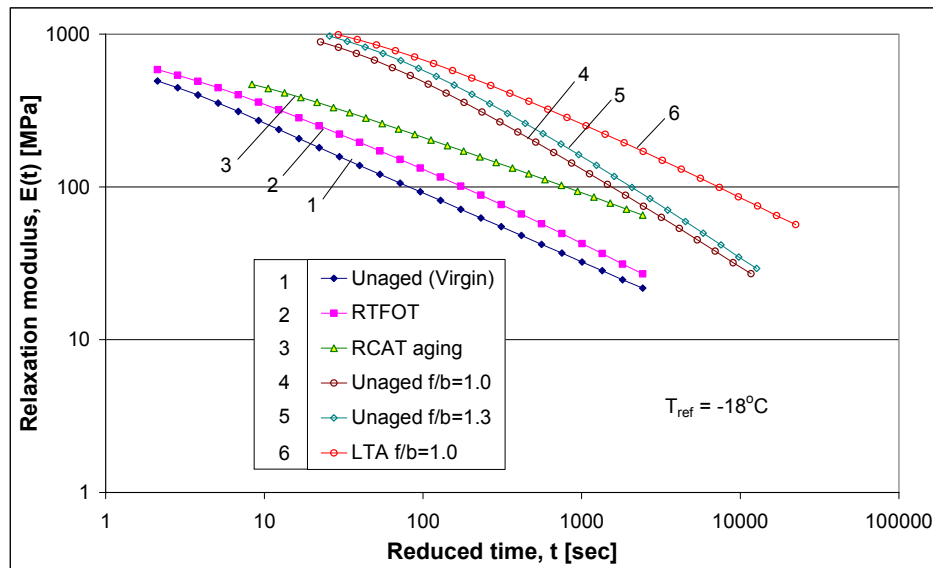


Figure 5.10: Effect of aging on the relaxation modulus ($E(t)$) of bitumen and mastic materials

5.2.4 The Effect of Aging on Damage Susceptibility

From literature, it is known that the slope of the creep compliance $D(t)$ is strongly related to the slope of the crack growth relation described by means of Paris law. The governing equations are given in Equation 5.8 through 5.13.

$$D(t) = D_0 + D_1 \cdot t^m \quad (5.8)$$

$$m = \frac{d \log D(t)}{d \log t} \quad (5.9)$$

Where:

- $D(t)$ = creep compliance [MPa^{-1}]
- D_0 = instantaneous creep compliance [MPa^{-1}]
- D_1 = creep compliance after 1 sec. [MPa^{-1}]
- t = loading time [sec]
- m = linear viscoelastic creep susceptibility [-]
(slope of the creep compliance master curve).

The parameters of the model fitting the compliance are shown in Table 5.4.

Table 5.4: Parameters of creep compliance model

Specimen		D0	D1	m	factor, m_i/m_{virgin}
Bitumen	Virgin	1.588E-03	5.937E-04	0.5158	1.00
	RTFOT	1.272E-03	4.382E-04	0.5128	0.99
	RCAT	9.749E-04	5.160E-04	0.3966	0.77
Mastic	Virgin 1.0	8.617E-04	5.621E-05	0.6218	1.00
	Virgin 1.3	7.476E-04	4.479E-05	0.6275	1.01
	LTA 1.0	6.955E-04	6.959E-05	0.5098	0.82

The crack propagation according to Paris law:

$$\frac{dc}{dN} = AK^n \quad \Rightarrow \quad \log\left(\frac{dc}{dN}\right) = \log A + n \cdot \log K \quad (5.10)$$

$$K = Y\sigma\sqrt{\pi a} \quad (5.11)$$

$$n = f(m) \rightarrow \begin{cases} n = 2\left(1 + \frac{1}{m}\right) & \text{for stress controlled test} \\ n = \frac{2}{m} & \text{for strain controlled test} \end{cases} \quad (5.12)$$

Where:

$\frac{dc}{dN}$	=	rate of crack propagation (increase of crack length per loading cycle N)
K	=	stress intensity factor at the tip of a crack (fracture toughness)
A, n	=	material constants $n = f(m)$ [-]
Y	=	constant related to sample geometry
σ	=	stress applied to the material
a	=	crack length (surface crack), one half crack length (internal crack)

Shapery (1978) developed an equation that relates the constant A of Paris law to the fundamental properties of a material. This equation is given below (Equation 5.13).

$$A = \frac{\pi}{6\sigma_m^2 I_1^2} \left[\frac{(1-\nu^2)D_1}{2\Gamma} \right]^{\frac{1}{m}} \left[\int_0^{\Delta t} w(t)^n dt \right] \quad (5.13)$$

Where:

σ_m	=	maximum stress a material can withstand before cracking
I_1	=	result of the integration of stresses near the crack tip (fracture process zone)
ν	=	Poisson's ratio of the material
Γ	=	fracture energy defined as work done on a material to increase the fractured surface with unit area
$w(t)$	=	waveform of normalized stress intensity factor
Δt	=	period of the loading to complete one cycle of loading

From the Paris law equation, it is clear that the higher the value of the material constants A and n , the higher the sensitivity of the material to cracking or damage. How are these parameters affected by the effect of aging?

- Aging decreases the parameter m (slope of the creep compliance) which in turn increases the parameter n in the Paris law equation according to the

relationship in Equation 5.12. This increases the rate of crack propagation according to the relationship in Equation 5.10.

- The parameter A in Equation 5.13 increases as a result of a decreasing m -value with aging. Accordingly, the rate of crack growth given by Equation 5.10 increases.
- The maximum stress the aged materials can withstand before failure increases with aging until a critical aging is reached (refer to section 5.3 for tensile strengths of aged and unaged materials). The fracture energy of the aged bitumen is also expected to increase due to aging until the critical point. As a result, the parameter A according to the Shapery's relationship in Equation 5.13 initially decreases, which reduces the crack susceptibility factor.
- Once a critical aging of bitumen is reached, the sensitivity of the aged material to cracking exceeds that of the unaged bitumen. This implies that the value of A will increase. This eventually leads to a higher susceptibility of the binder/mortar to cracking.

5.3 The Direct Tensile Test (DTT)

5.3.1 DTT Test Output

Direct Tensile Tests (DTT) on bitumen and mastic were performed at constant elongation rates. The test conditions are presented in section 4.7.3. Figure 5.11 shows a typical result of a DTT test. The stress and strain in the bituminous specimen is calculated using Equation 5.14 and 5.15, respectively. The maximum stress is considered as the failure stress and the corresponding strain is the failure strain.

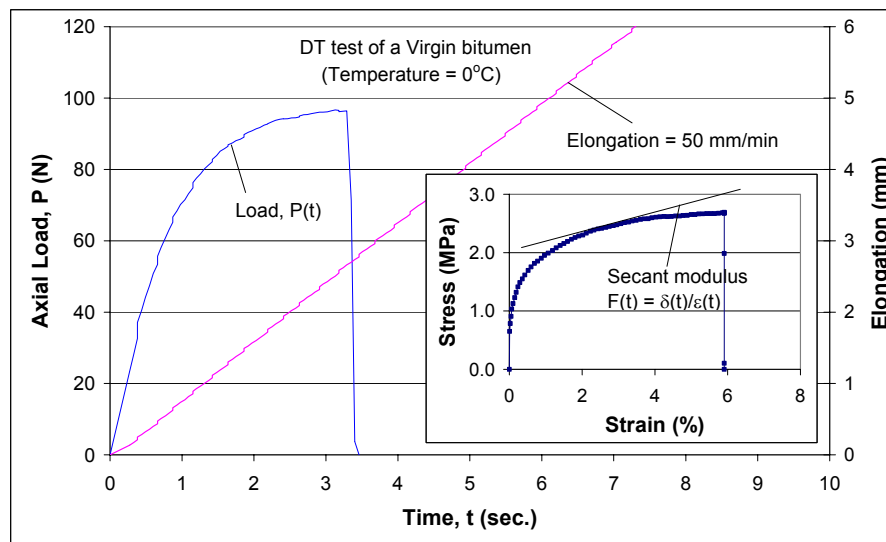


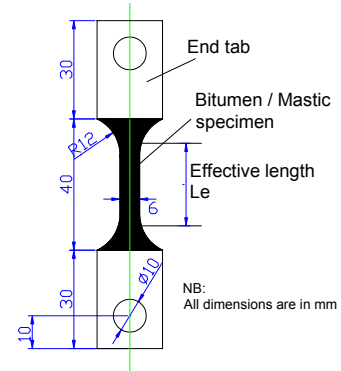
Figure 5.11: Typical test result of a DTT test

$$\sigma(t) = \frac{P(t)}{A} = \frac{P(t)}{(b \cdot h)} \quad (5.14)$$

$$\varepsilon = \left(\frac{\Delta l}{L_e} \right) \times 100\% \quad (5.15)$$

Where:

$\sigma(t)$	=	time dependant stress [MPa]
ε	=	strain [%]
$P(t)$	=	applied axial force [N]
A	=	cross-sectional area of specimen ($\approx 36 \text{ mm}^2$)
b	=	average width of the specimen [mm]
h	=	average thickness of the specimen [mm]
Δl	=	change in length or elongation [mm]
L_e	=	effective length = 33.8 mm



5.3.2 Analysis of DTT Test Results

Bitumen

Results of the DTT test for virgin, short term and long-term aged bitumen specimens are shown in Figure 5.12, Figure 5.13, Figure 5.14 and Table 5.5. The failure stress of the aged and unaged specimens remains below 4 MPa under the specified test conditions.

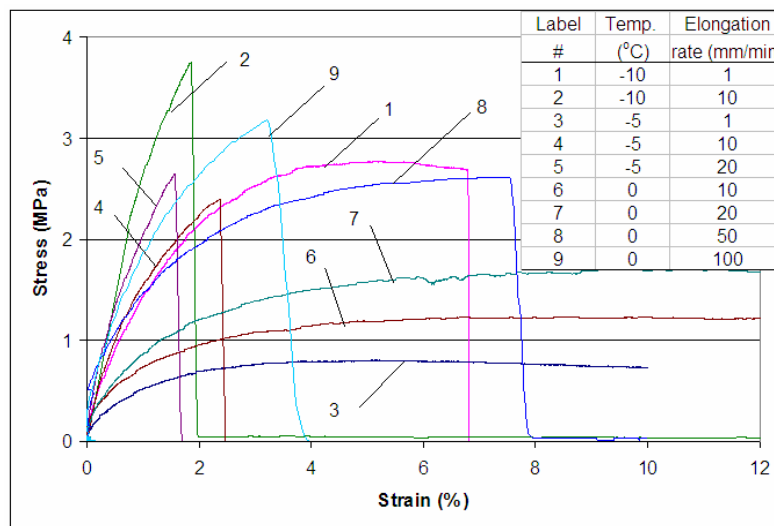


Figure 5.12: Stress versus strain plot of a virgin (unaged) bitumen at different testing conditions

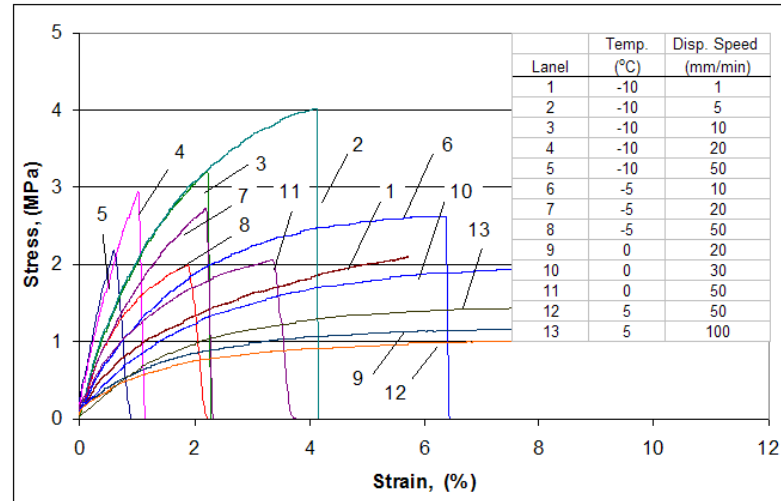


Figure 5.13: Stress versus strain plot of a STA bitumen at different DTT testing conditions

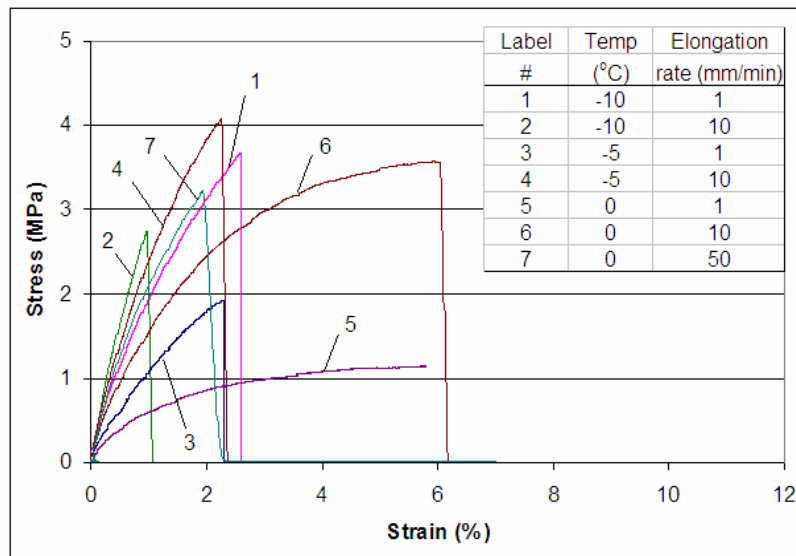


Figure 5.14: Stress versus strain plot of a long-term aged bitumen at different DTT testing conditions

The failure stress and failure strain as determined on the bitumen before and after aging are also shown in Figure 5.15 and Figure 5.16. As it is expected, the data set shows some scatter and contains outliers. The outliers at low loading speeds may be a result of testing errors or factors associated with the brittle behaviour of the material. A general trend line can describe the behaviour observed at the different testing temperatures. The figures clearly show that age hardening of bitumen decreases the failure strain and increases the failure stress of the material. The effect of aging on the failure property of bitumen is indicated by an arrow in Figure 5.16.

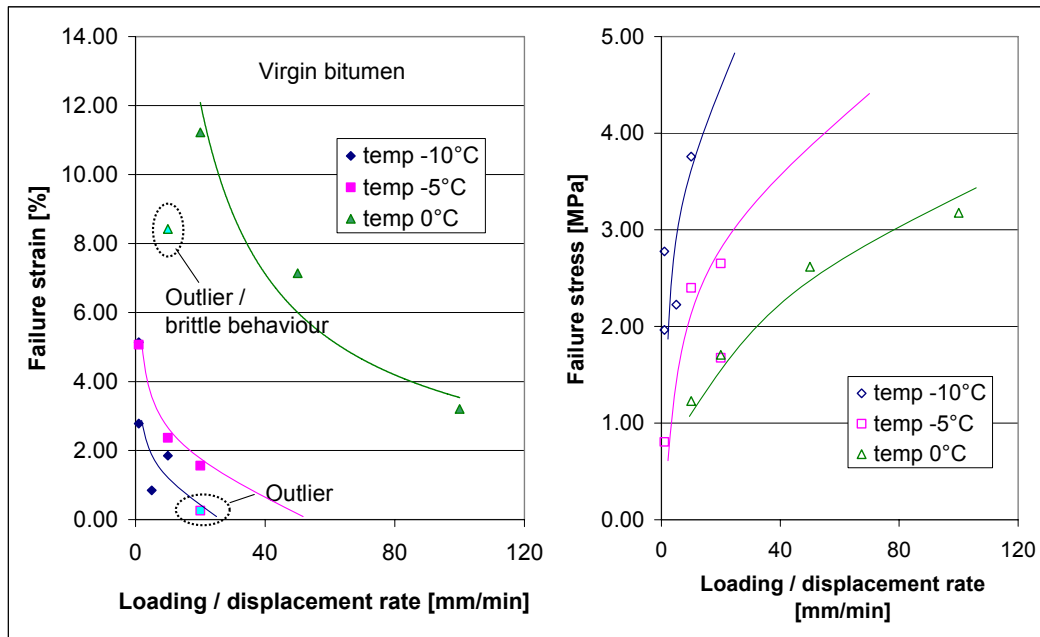


Figure 5.15: Failure stress and strain vs loading speed of virgin bitumen

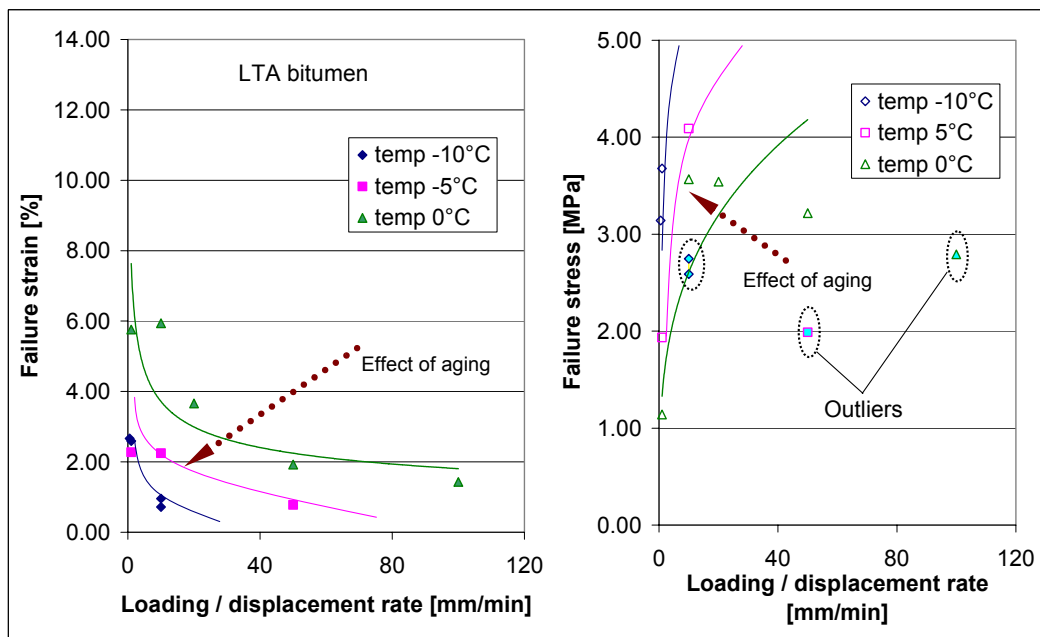


Figure 5.16: Failure stress and strain vs loading speed of LTA bitumen

Table 5.5: DTT test results for unaged and aged bitumen materials

Binder Type	Sample no.	Label #	Temp [oC]	Loading rate $\dot{\epsilon}$ [mm/s]	failure Strain ϵ_f [%]	failure Stress σ_{max} [MPa]	time @ failure stress [sec]
Virgin bitumen 70/100 pen	# 001		-10	1	2.79	1.96	60.0
	# 012	1	-10	1	5.14	2.78	107.6
	# 002	2	-10	10	1.85	3.76	2.3
	# 011		-10	5	0.85	2.22	6.5
	# 006	3	-5	1	5.07	0.80	106.3
	# 007	4	-5	10	2.37	2.40	8.3
	# 008	5	-5	20	1.56	2.65	4.4
	# 009		-5	20	0.26	1.68	3.3
	# 004	6	0	10	8.42	1.23	21.3
	# 013	7	0	20	11.22	1.71	14.3
	# 014	8	0	50	7.14	2.62	5.8
	# 005	9	0	100	3.21	3.18	3.0
STA bitumen (RTFOT Aging)	# 042	1	-10	50	2.18	0.59	3.4
	# 043	2	-10	20	2.96	1.02	3.3
	# 044	3	-10	10	3.23	2.23	7.3
	# 106	4	-10	1	2.11	5.71	119.8
	# 107	5	-10	5	4.02	4.13	19.9
	# 049	6	-5	50	1.99	1.89	3.1
	# 051	7	-5	10	2.63	6.35	15.2
	# 110	8	-5	20	2.72	2.20	4.6
	# 112	9	0	20	1.19	11.56	14.1
	# 113	10	0	50	2.07	3.37	3.8
	# 115	11	0	30	2.02	11.80	10.4
	# 103	12	5	50	1.02	13.34	8.0
	# 105	13	5	100	1.45	9.74	4.5
LTA bitumen (RCAT, 140 hr)	# 025		-10	0.5	2.66	3.14	108.0
	# 022	1	-10	1	2.59	3.68	57.6
	# 024 (2)	2	-10	10	0.96	2.75	4.7
	# 026		-10	10	0.71	2.59	3.6
	# 021	3	-5	1	2.27	1.93	49.7
	# 020	4	-5	10	2.24	4.09	7.0
	# 019		-5	50	0.78	1.99	2.5
	# 029	5	0	1	5.76	1.14	119.3
	# 017	6	0	10	5.94	3.57	18.5
	# 015		0	20	3.66	3.54	5.9
	# 016	7	0	50	1.92	3.22	3.0
	# 018		0	100	1.43	2.79	2.9

Mastic

As an example, the DTT results obtained on the mastic materials at a temperature of 5°C and loading speed of 100 mm/min are shown in Figure 5.17. Similar to the bitumen, the effect of bitumen aging increases the failure stress and decreases the failure strain of the mastic. The mastics with unaged (Virgin) and short term aged (STA) bitumen are characterized by a ductile type of failure at the given testing conditions. On the other hand, the long term aged materials (LTA mastics) exhibit properties between a ductile and brittle failure. The effects of aging and displacement speed on the failure strain and stress of the mastics at a temperature of 5°C are shown in Figure 5.18.

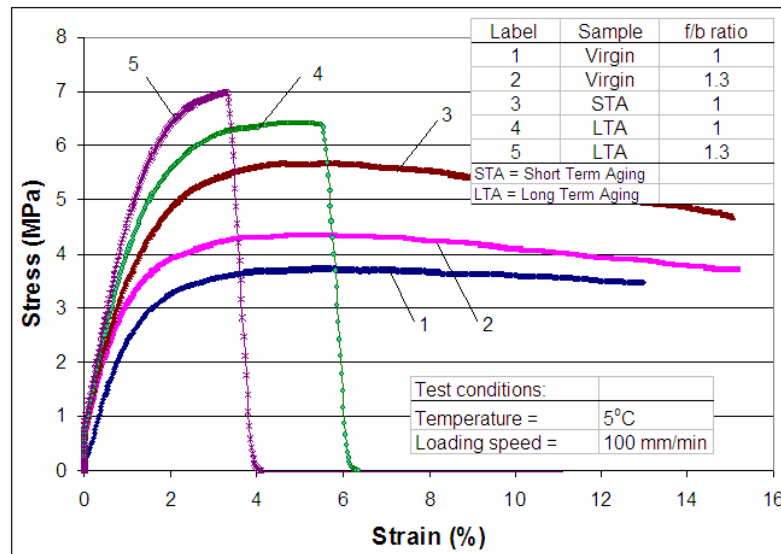


Figure 5.17: DTT test result of mastic materials at 5°C and elongation rate of 100 mm/min

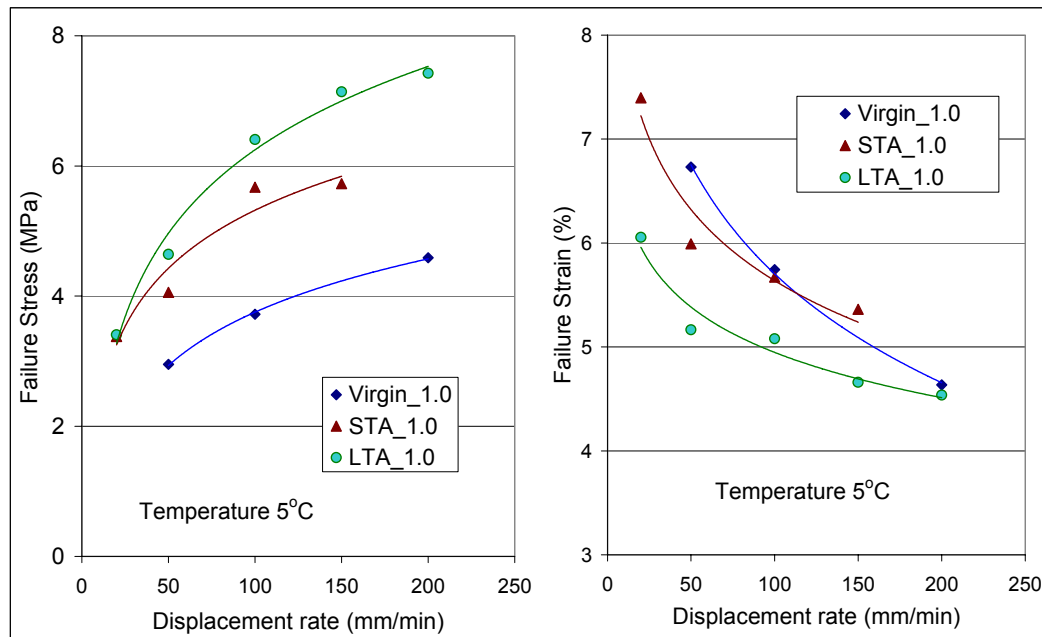


Figure 5.18: DTT test result for mastic (bitumen + filler) materials with f/b ratio = 1.0 (Virgin / unaged bitumen 70/100, STA Short Term Aged bitumen, and LTA Long Term Aged bitumen)

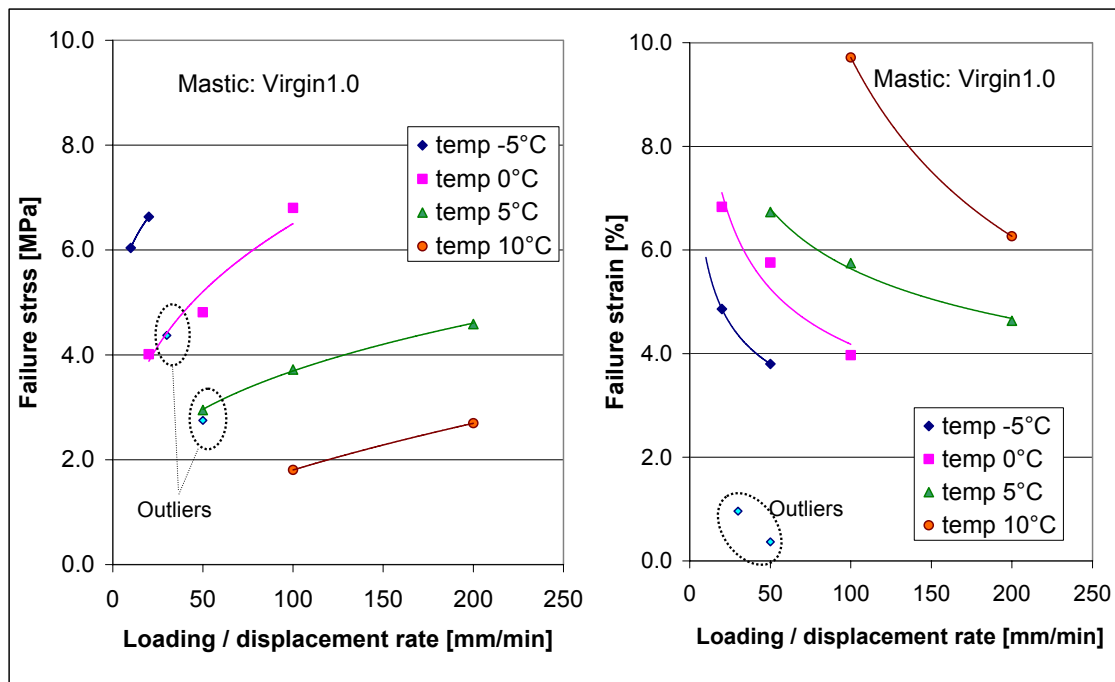
The failure stress and strain of mastic materials determined from all DTT tests are shown in Table 5.6 and Table 5.7 for materials with $f/b = 1.0$ and $f/b = 1.3$ respectively. The failure stress and strains were determined from Equation 5.14. The data in Table 5.6 is shown graphically in Figure 5.19 for the unaged mastic and Figure 5.20 for the LTA aged mastic.

Table 5.6: DTT test results of mastic materials with $f/b=1.0$

Mastic Type	Sample no.	Temp [°C]	Loading rate $\dot{\epsilon}$ [mm/s]	failure Stress ϵ_f [%]	failure Strain σ_{max} [MPa]	time @ max stress/strain [sec]
Virgin $f/b=1.0$	# 056	-5	50	2.75	0.37	2.1
	# 057	-5	20	6.63	3.80	6.1
	# 058	-5	10	6.04	4.86	12.1
	# 059	-5	30	4.37	0.96	2.9
	# 062	0	100	6.80	3.97	3.2
	# 063	0	50	4.81	5.76	4.7
	# 064	0	20	4.01	6.83	9.1
	# 053	5	50	2.95	6.73	4.9
	# 054	5	100	3.72	5.74	3.8
	# 055	5	200	4.59	4.64	3.2
	# 065	10	100	1.80	9.71	4.1
	# 066	10	200	2.70	6.26	2.9
	# 060	15	100	0.86	10.21	4.2
	# 061	15	200	1.16	10.70	3.2
STA $f/b=1.0$	# 093	-5	1	3.86	5.73	120.0
	# 094	-5	5	6.52	2.56	15.8
	# 095	-5	20	7.62	3.79	6.2
	# 096	-5	5	5.89	4.46	21.0
	# 097	-5	10	6.83	3.48	9.3
	# 087	0	10	4.35	4.82	12.4
	# 088	0	20	5.35	5.36	7.8
	# 089	0	50	7.31	5.10	4.3
	# 090	0	1	0.92	1.11	26.1
	# 091	0	5	3.71	6.17	27.6
	# 092	0	100	7.07	1.43	2.5
	# 098	5	50	4.06	5.99	5.2
	# 099	5	100	5.67	5.67	3.6
	# 100	5	200	2.08	0.64	2.4
LTA $f/b=1.0$	# 101	5	150	5.73	5.36	3.2
	# 102	5	20	3.38	7.40	13.6
	# 077	-5	1	4.30	3.71	78.0
	# 078	-5	10	8.64	3.55	10.0
	# 079	-5	20	3.96	0.66	3.3 *
	# 080	-5	0.5	3.62	7.28	296.7
	# 081	-5	15	7.73	1.70	4.6
	# 067	0	50	8.00	4.19	4.0
	# 068	0	20	5.50	4.92	7.4
	# 069	0	10	4.80	4.25	10.8
	# 070	0	100	7.08	1.26	3.2
	# 071	0	50	7.57	3.61	3.8
	# 072	5	20	3.40	6.06	8.4
	# 073	5	50	4.64	5.17	4.6
	# 074	5	100	6.40	5.08	3.2
	# 075	5	150	7.14	4.66	3.2
	# 076	5	200	7.43	4.54	3.1
	# 082	10	100	3.55	7.35	3.8
	# 083	10	200	4.21	6.36	3.4
	# 084	10	300	5.33	6.58	3.2
	# 085	10	50	2.61	7.08	5.2
	# 086	10	350	5.03	2.85	1.4

Table 5.7: DTT test results of mastic materials with $f/b=1.3$

Mastic Type	Sample no.	Temp [°C]	Loading rate $\dot{\epsilon}$ [mm/s]	failure Stress ϵ_f [%]	failure Strain σ_{max} [MPa]	time @ failure stress/strain [sec]
Virgin $f/b=1.3$	# 116	-5	1	2.60	7.15	149.9
	# 117	-5	10	5.72	3.52	9.7
	# 118	-5	20	4.23	0.69	3.5
	# 119	-5	15	7.29	3.59	7.3
	# 120	0	10	3.17	6.38	15.4
	# 121	0	20	5.45	4.77	7.4
	# 122	0	50	6.21	3.86	4.0
	# 123	0	100	5.86	4.46	3.3
	# 124	0	100	0.00	15.36	5.5
	# 133	5	50	3.70	6.32	4.7
	# 134	5	100	4.35	5.50	3.4
	# 135	5	200	4.79	6.99	3.5
LTA $f/b=1.3$	# 125	-5	1	5.29	5.61	115.6
	# 126	-5	10	6.77	0.99	4.4
	# 127	-5	5	7.25	4.20	20.1
	# 128	-5	15	4.21	0.53	3.2
	# 129	0	10	6.12	3.83	9.9
	# 130	0	20	7.46	4.28	7.1
	# 131	0	50	7.31	1.74	3.2
	# 132	0	1	3.18	9.46	194.3
	# 136	5	50	4.43	5.03	4.7
	# 137	5	100	6.99	3.28	3.0
	# 138	5	200	7.46	2.17	2.7

Figure 5.19: Effect of aging on failure property of unaged (virgin) mastic $f/b=1.0$

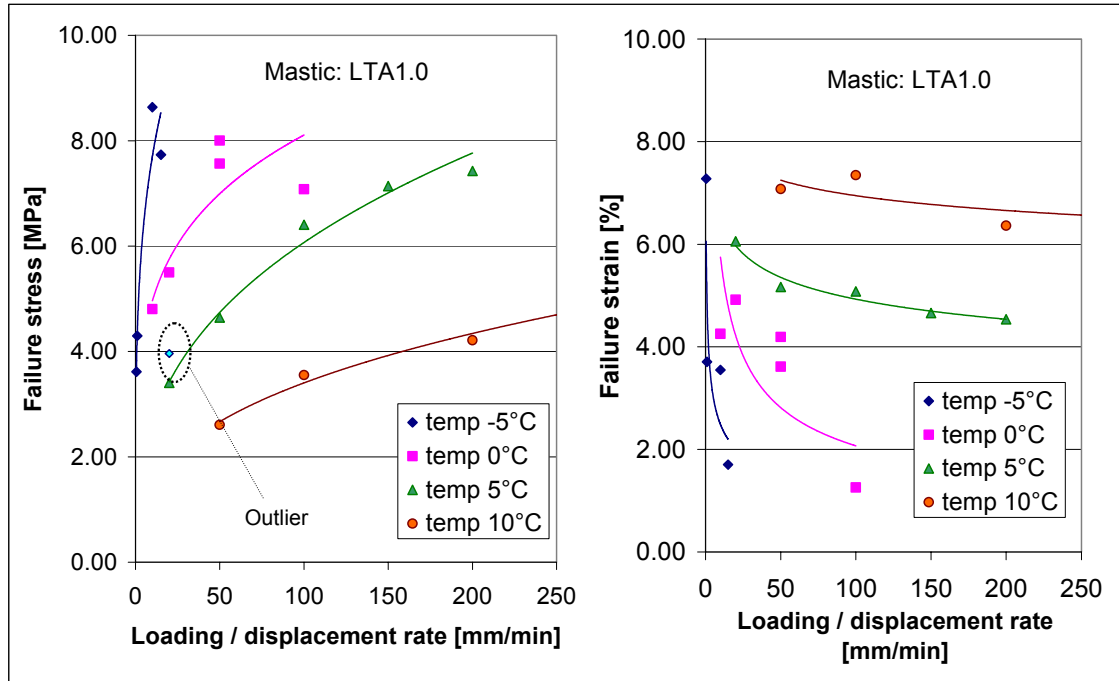


Figure 5.20: Effect of aging on failure property of LTA aged mastic $f/b=1.0$

In general, the observations made in relation to the effect of aging on the failure properties of the bitumen are applicable to the mastic as well. The failure stress of the mastic is higher compared to that of the bitumen. The failure stress of the mastic ranges between 2 – 9 MPa while that of the bitumen range between 1 – 4 MPa. In terms of failure strain, the mastics fail between 4 – 10% strain which drops to 1 – 8% after LTA aging. In the case of the bitumen, the failure strain ranges between 1 – 12% which drops considerably to 1 – 7% after LTA aging. These numbers should be related to the testing conditions employed in the research. However, the results are expected to reflect the general failure properties of bituminous material in view of brittle type of failure of these materials at lower temperatures or higher loading speeds.

5.3.3 Effect of aging on Binder Low Temperature Performance

In Figure 5.21, results of DTT tests performed on a virgin (unaged) and long term aged bitumen are shown after shifting the data to a reference temperature of -5°C. The unified model in Equation 4.5 to 4.7 was used to shift the data to the reference temperature. From the figure, it can be observed that the strength of the materials increases with increasing rate of loading till a maximum is reached after which the failure stress starts to drop. This property is typical for low temperature performance of bitumen due to the change in the material property to a brittle behaviour. A similar behaviour is also shown in Figure 5.22 which was developed by researchers at Shell (Shell 1973). This illustrates the sensitivity of bitumen to the development of damage at low temperatures.

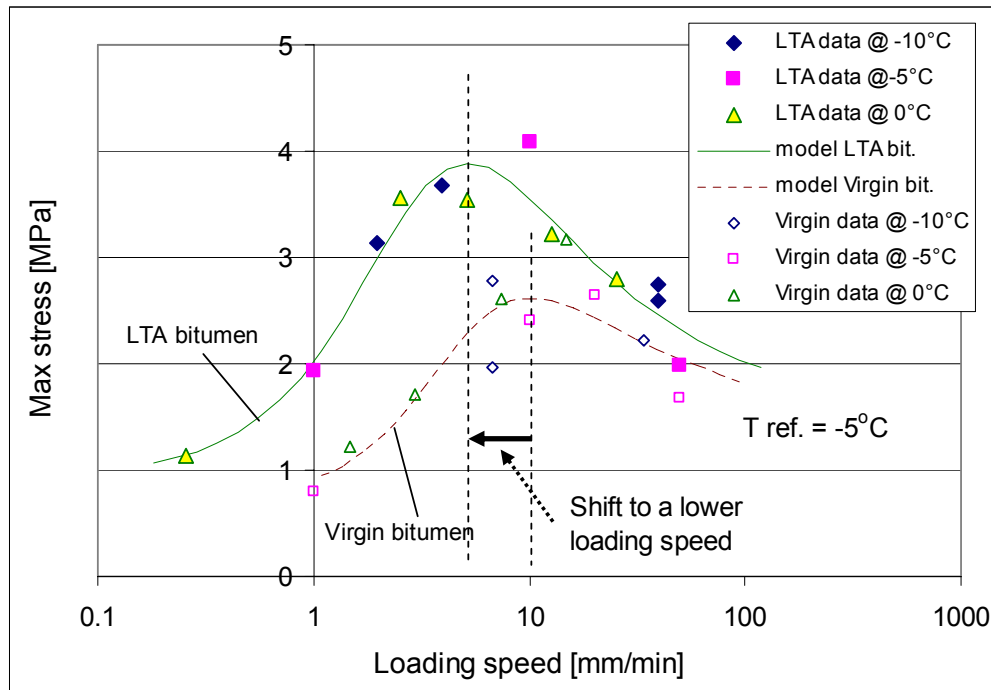


Figure 5.21. Virgin and aged bitumen failure mastercurve from DTT shifted to reference temperature of -5°C .

In Figure 5.21, the following observations can be made:

- The failure stress master curve of the LTA bitumen reaches its maximum failure value at lower loading speed compared to unaged bitumen. This shift is an indication of the hardening of the binder and it can be described as the transition to brittle behaviour.
- Stresses that develop because of a temperature drop (thermal stress) are higher in the aged bitumen than the unaged. This may result in a formation of micro-cracks (damage) in the binder/mortar that eventually reduce the fatigue life of the LTA bitumen. In other words, load associated damage increases the chance of failure in aged bitumen.
- It is necessary to look at the failure mastercurve to investigate the effect of aging on the low temperature performance of binders.

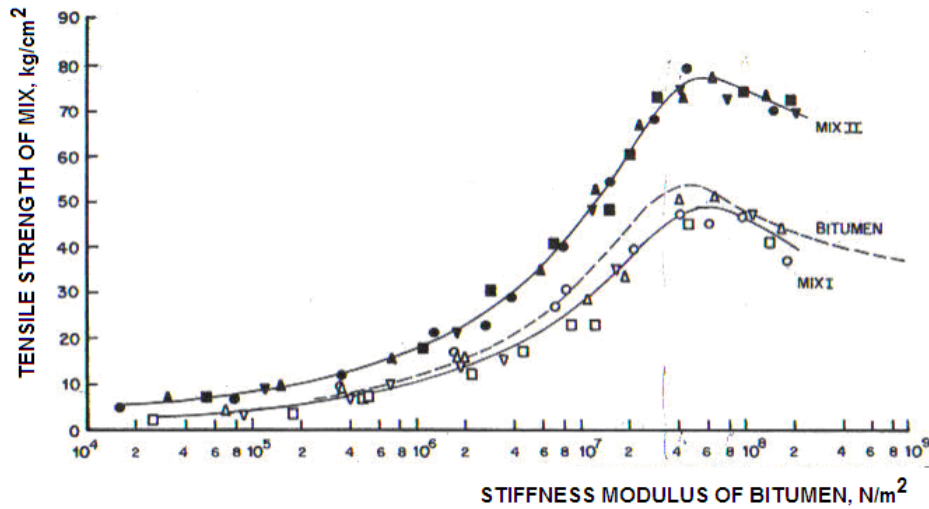


Figure 5.22. Tensile strength of bitumen and mixtures as a function of bitumen stiffness modulus (Shell 1973)

5.3.4 Prediction of Time Dependant Modulus from DTT test

As is the case with the BBR test results, the DTT results can be used to predict the stiffness modulus of bitumen/mastic. In a DTT, the time dependant stress in the bituminous specimen due to an applied constant rate of uni-axial elongation is represented by Equation 5.16:

$$\sigma(t) = E(t) \cdot \varepsilon = \int_0^t E(t-u) \cdot \frac{d\varepsilon}{du} du = \bar{\varepsilon} \cdot \int_0^t E(t-u) du \quad (5.16)$$

Where:

- $\sigma(t)$ = time-dependant stress [MPa],
- $E(t)$ = time dependant stiffness modulus [MPa],
- t = time [s],
- u = time related to strain history [s],
- ε = applied strain [-] $\left(\varepsilon = \frac{\Delta l}{L_e} \right)$
- $\bar{\varepsilon}$ = constant rate of strain $\left(\bar{\varepsilon} = \frac{\varepsilon(t)}{t} \right)$

Chen and Tsai (1998) derived the expression for the time dependant modulus (Equation 5.18) by substituting Equation 5.16 in the definition of the secant modulus $F(t)$ as shown in Equation 5.17:

$$F(t) = \frac{\sigma(t)}{\varepsilon(t)} = \frac{1}{t} \int_0^t E(t-u) du \quad (5.17)$$

Re-arranging Equation 5.17, the expression for the relaxation modulus can be derived:

$$E(t) = F(t) \cdot \left[1 + \frac{d \log F(t)}{d \log t} \right] \quad (5.18)$$

A simple and direct method of predicting the relaxation modulus $E(t)$ from DTT is by differentiating the stress-strain curve. A model fitting the stress strain curve can be represented by Equation 5.19. This relationship is a modified version of the statistical Weibull distribution adopted to fit the DTT data in this research. Substituting Equation 5.19 in the definition of $E(t)$, Equation 5.20, the relaxation modulus with time can be derived.

$$\sigma(t) = \kappa \cdot \left(\frac{\varepsilon(t)}{\beta} \right)^\lambda \cdot \exp \left(- \left(\frac{\varepsilon(t)}{\beta} \right)^\lambda \right) \quad (5.19)$$

$$\begin{aligned} E(t) &= \frac{d\sigma(t)}{d\varepsilon(t)} = \frac{d}{d\varepsilon(t)} \left[\kappa \cdot \left(\frac{\varepsilon(t)}{\beta} \right)^\lambda \cdot \exp \left(- \left(\frac{\varepsilon(t)}{\beta} \right)^\lambda \right) \right] \\ \Rightarrow E(t) &= \left(\frac{\lambda}{\varepsilon(t)} \right) \cdot \left[1 - \left(\frac{\varepsilon(t)}{\beta} \right)^\lambda \right] \left[\kappa \cdot \left(\frac{\varepsilon(t)}{\beta} \right)^\lambda \cdot \exp \left(- \left(\frac{\varepsilon(t)}{\beta} \right)^\lambda \right) \right] \end{aligned} \quad (5.20)$$

Where:

- $\sigma(t)$ = stress developed in the material as a function of time [MPa]
- $\varepsilon(t)$ = applied strain as a function of time [-] $\left(\varepsilon(t) = \frac{\Delta l(t)}{L_e} \right)$
- $E(t)$ = relaxation modulus as a function of time
- κ, β, λ = model parameters

The model parameters have physical meaning in fitting the stress-strain curve. Parameter κ has control over the vertical scale, β has control over the horizontal scale, and λ has control over the shape of the stress-strain curve. In the case of brittle failure, the model is fitted to the stress-strain curve till failure. Fitting the data with the model and the differentiation of the model to predict the relaxation modulus has been performed using Matlab. As an example, the model fitted to stress-strain data of unaged mastic and the predicted $E(t)$ are shown in Figure 5.24 and Figure 5.23 respectively.

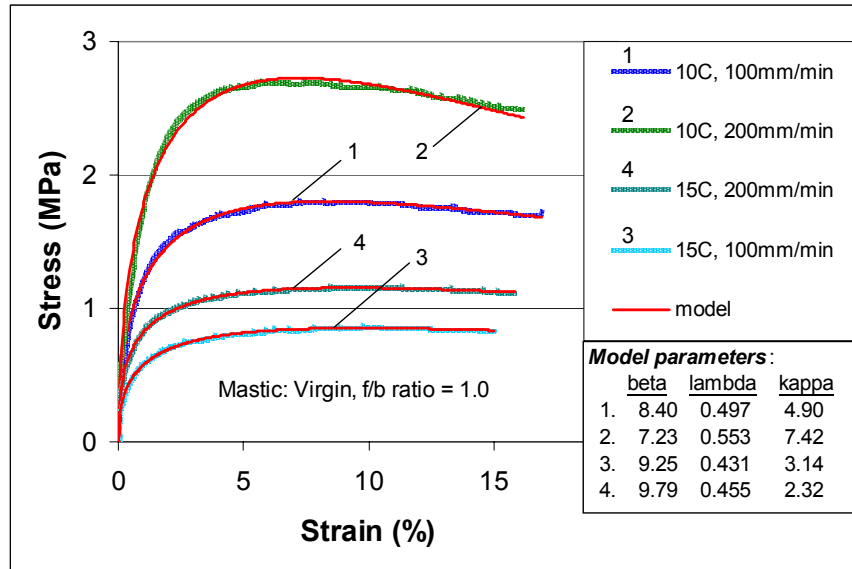


Figure 5.23: Model fitted to DTT stress-strain data of unaged mastic

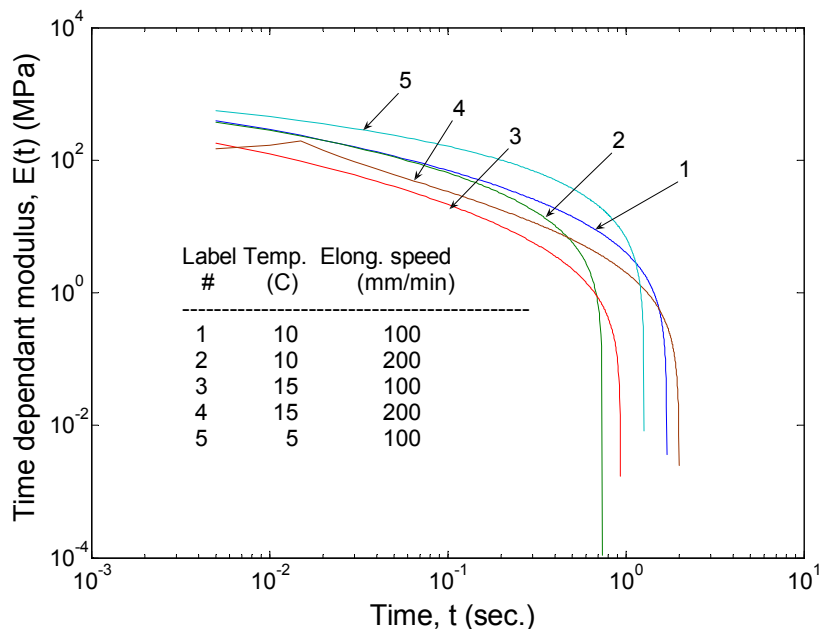


Figure 5.24: Prediction of relaxation modulus from stress-strain curve

From Figure 5.24, it can be observed that the materials release the stress at certain point. This point is a point where the ultimate tensile strength or the breaking point of the material is reached. The figure also illustrates that the ultimate tensile strength at higher elongation speed does not necessarily result in longer time to release the stress.

5.4 Dynamic Shear Rheometer (DSR)

5.4.1 DSR Test Principles

Figure 5.25 shows the sinusoidal loading of a specimen with applied constant shear strain at frequency f . For a viscoelastic material like bitumen, the stress response will be out of phase by a phase angle δ , as shown in Figure 5.25. The deformation angle of the specimen at given testing conditions is determined from the shear strain in the linear response and the geometry of the specimen. The governing relationships for the shear strain and shear stress are given in Equation 5.21. The dynamic modulus or complex shear modulus is the ratio of the amplitudes of shear stress and the shear strain as given by Equation 5.22.

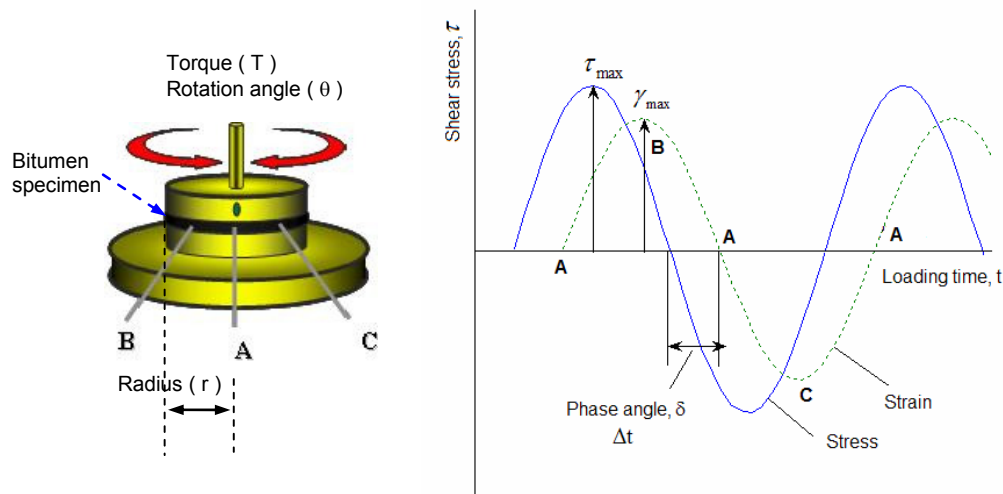


Figure 5.25: Applied dynamic strain and dynamic stress response

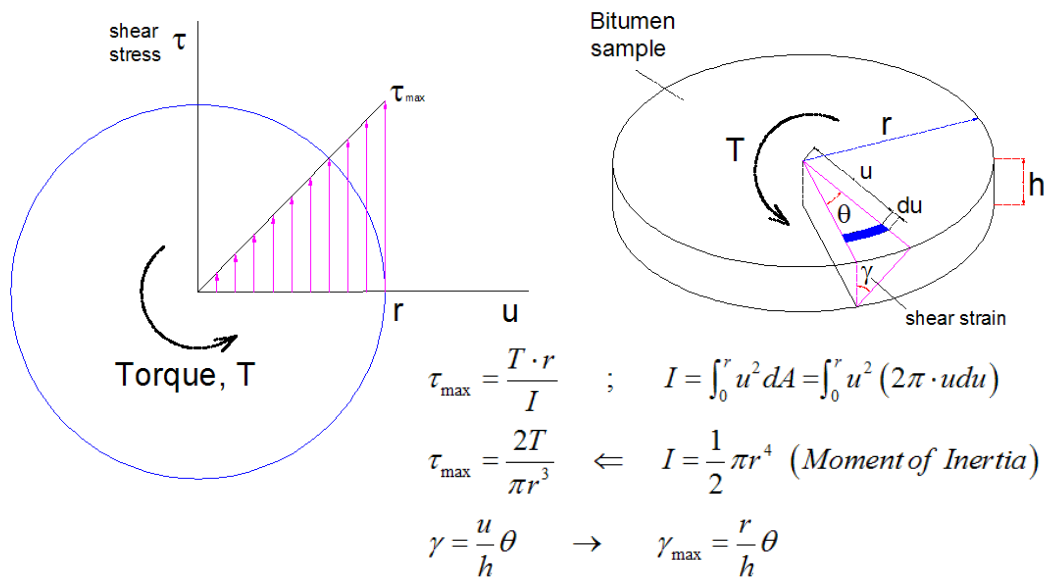


Figure 5.26: Shear stress and strain situation in the bitumen sample in the DSR test

$$\gamma_{\max} = \frac{\theta r}{h} \quad \text{and} \quad \tau_{\max} = \frac{2T}{\pi r^3} \quad (5.21)$$

$$G^* = \frac{(\tau_{\max} - \tau_{\min})}{(\gamma_{\max} - \gamma_{\min})} \quad (5.22)$$

$$\delta = 2\pi f \cdot \Delta t = \omega \cdot \Delta t \quad (5.23)$$

Where:

τ	=	shear stress [10^5 Pa],
T	=	torque [g-cm],
γ	=	shear strain [%],
r	=	radius of specimen [mm],
h	=	specimen thickness [mm],
θ	=	deflection angle [rad],
δ	=	phase angle [$^\circ$],
f	=	frequency [Hz],
ω	=	radial frequency ($\omega = 1/t = 2\pi f$) [rad/s],
Δt	=	time lag [s], ($t = \text{time [s]}$),
G^*	=	complex modulus [Pa].

The sinusoidal signals can be represented by a complex notation. The corresponding equations for the applied shear strain and the stress response are represented by Equation 5.24 and 5.26 respectively.

$$\gamma^* = \gamma_d e^{i\omega t} = \gamma_d (\cos \omega t + i \sin \omega t) \quad (5.24)$$

$$\tau^* = \tau_d e^{i(\omega t + \delta)} = \tau_d (\cos[\omega t + \delta] + i \sin[\omega t + \delta]) \quad (5.25)$$

Accordingly, the complex modulus and creep compliance are given by Equation 5.26 and Equation 5.28, respectively. The in-phase and out-of-phase components of the complex shear modulus are shown in Figure 5.27.

$$G^*(\omega) = \frac{\tau^*}{\gamma^*} = \frac{\tau_d}{\gamma_d} e^{i\delta} = \frac{\tau_d}{\gamma_d} (\cos \delta + i \sin \delta) = G' + iG'' \quad (5.26)$$

$$\tan \delta = \frac{G''}{G'} \quad (5.27)$$

$$J^*(\omega) = \frac{\gamma^*}{\tau^*} = \frac{1}{G^*} = J' - iJ'' \quad (5.28)$$

Where:

γ^*	=	complex shear strain ($\gamma^* = 2\varepsilon_{12}$),
------------	---	--

γ_d	=	shear strain amplitude,
τ^*	=	complex stress (Also designated as σ^*),
σ_d	=	stress amplitude,
G^*	=	complex modulus, $ G^* = \frac{\sigma_d}{\gamma_d} = \sqrt{(G')^2 + (G'')^2}$
G'	=	storage modulus (elastic component), $G' = G^* \cos \delta$
G''	=	loss modulus (viscous component), $G'' = G^* \sin \delta$
J^*	=	creep compliance,
J'	=	storage compliance, $J' = J^* \cos \delta$
J''	=	loss compliance, $J'' = J^* \sin \delta$
δ	=	phase angle

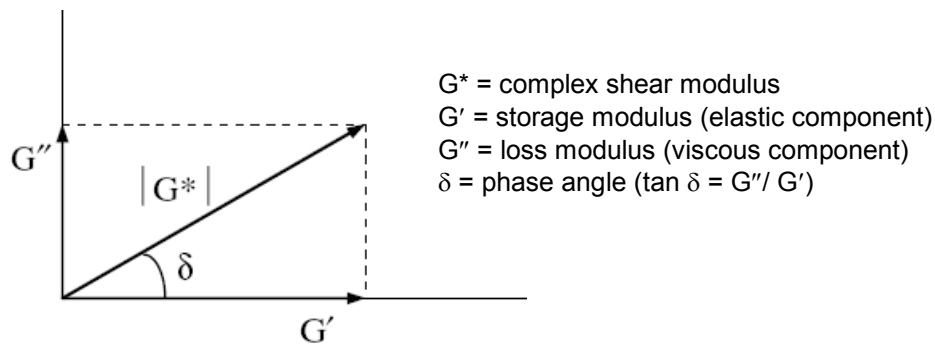


Figure 5.27: Relationship between the complex shear modulus (G^*), the in-phase component (G') and out-of-phase component (G''), and the phase angle (δ)

The total resistance to deformation under load is represented by G^* (complex shear modulus). The phase angle δ represents the relative contribution to the total response of an in-phase component and an out-of-phase component. The relative distribution of these components is a function of the composition of the material, loading time, and temperature (Stroup-Gardiner and Newcomb 1995). The effect of aging influences the parameters that describe the viscoelastic behaviour of the bitumen as illustrated in section 5.4.3.

Some common characteristics of the rheological behaviour of bitumen are the following (Stroup-Gardiner and Newcomb 1995):

- At low temperatures or high frequencies bitumen tends to approach a limiting value of G^* of approximately 1.0 GPa and a limiting value of δ of zero degrees. The 1.0 GPa reflects the rigidity of the carbon-hydrogen bond as the bitumen reaches its minimum thermodynamic equilibrium volume. The zero value of δ represents the completely elastic nature of the bitumen at these temperatures.
- At high temperatures the phase angle δ approaches 90°C, which reflects a tendency to a complete viscous behaviour or complete dissipation of energy in viscous flow. The complex modulus G^* varies significantly

reflecting the difference in consistency (viscosity property) of the bitumen.

5.4.2 Modeling Bitumen Viscoelasticity

A better understanding and analysis of rheological properties of viscoelastic materials can be made with the use of master curves. Master curves allow the estimation of properties at a wider range of temperatures and frequencies. A mathematical model developed by Bahia et al. (2001) was used for constructing the master curve. The complex modulus master curve was constructed using the model in Equation 5.29 and for the phase angle master curve Equation 5.30 was used. The determination of the model parameters (S-curve) was performed independently but simultaneously by minimising the sum of errors of the shifted data points with the respective models.

$$G^* = G_{\min}^* + (G_{\max}^* - G_{\min}^*) * S \quad (5.29)$$

$$\delta = \delta_{\max} - (\delta_{\max} - \delta_{\min}) * S \quad (5.30)$$

$$S = \left[1 + \left(\frac{\omega_c}{\omega'} \right)^k \right]^{-m_e/k} \quad (5.31)$$

$$\omega' = a_T \cdot \omega \quad (5.32)$$

Where:

G^*	=	complex modulus [MPa],
G_{\min}^*	=	complex modulus as $\omega \rightarrow 0$ [MPa],
G_{\max}^*	=	complex modulus as $\omega \rightarrow \infty$ [MPa],
δ	=	phase angle [°],
δ_{\min}	=	phase angle as $\omega \rightarrow \infty$ [°],
δ_{\max}	=	phase angle as $\omega \rightarrow 0$ [°],
ω	=	frequency [rad/s]',
ω_c	=	location parameter [rad/s],
ω'	=	reduced frequency [rad/s],
k, m_e	=	shape parameters [-],
a_T	=	shift factor [-].

The Time-Temperature Superposition (TTS) principle was used to generate master curves of the complex modulus and phase angle at a reference temperature of 20°C. The Williams-Landel-Ferry (WLF) model (Equation 5.33) was used to accomplish the shifting of the rheological data to the reference temperature. For rheological data of polymers above the glass transition temperature (T_g), the shift factor curve is best approximated by the WLF equation while below the T_g the Arrhenius shift factor (Equation 5.34) is preferred (Jansen 2006). The superposition of viscoelastic curves for

Thermorheological Simple Materials (TSM) like bitumen is a continuous overlap to form a master curve (Jansen 2006, Medani and Huurman 2005, Cheung 1995, Groenedijk 1998).

$$\log a_T(T) = \frac{C_1(T - T_R)}{C_2 + T - T_R} \quad (5.33)$$

Where:

- a_T = shift factor (horizontal) at temperature T [-],
- T_R = reference temperature [°C],
- C_1 = constant [-],
- C_2 = temperature constant [-],

$$\log a_T(T) = \frac{\Delta H}{2.303R} \left(\frac{1}{T} - \frac{1}{T_R} \right) \quad (5.34)$$

Where:

- ΔH = activation energy (typical 250 KJ/mol) [J/mol],
- R = gas constant (8.314 [J/mol/K])
- T_R = reference temperature [°K],

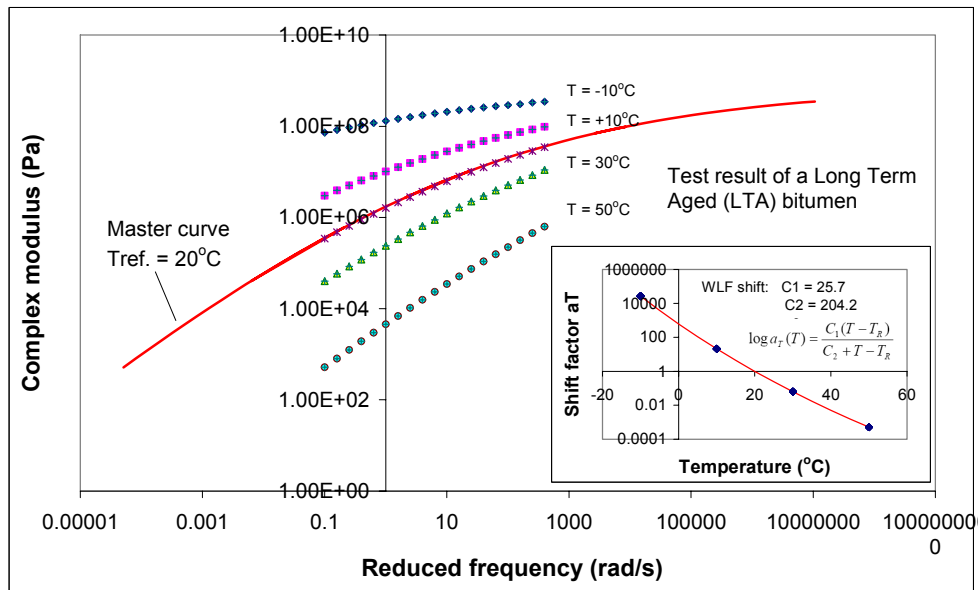


Figure 5.28: Frequency sweep test results at different temperatures and a master curve at a reference temperature of 20°C for a LTA bitumen

5.4.3 Characterization of Bitumen Materials

Bitumen Materials Aged Under Standard Procedures

In Table 5.8 the strain level, plate geometry, and binder thickness (plate gap) used in the DSR testing at all the testing temperatures is shown. An example of DSR frequency sweep test at different temperatures (Isotherms) for a long term aged (LTA) bitumen is shown in Figure 5.28. A master curve with the WLF shifting of the curves has been constructed at a reference temperature of 20°C. The same procedure has been adopted for all the bituminous materials in constructing the master curves. In Figure 5.29, the master curves of short and long term laboratory aged specimens are shown. It is clear from the figure that the effect of aging is significant on the rheological behaviour of the materials. The increase in complex modulus due to aging is accompanied by a decrease in the phase angle.

Table 5.8: Strain level and specimen thickness (gap) used in testing laboratory aged bitumen materials

Plate size (mm)	Temp. (°C)	Virgin bitumen (Unaged)		Partial aging (STA: RTFOT)		Full aging (LTA: RTFOT+RCAT)	
		Strain (%)	Gap (mm)	Strain (%)	Gap (mm)	Strain (%)	Gap (mm)
8	-10	0.40	1.987	0.40	1.976	0.30	1.994
8	10	0.90	2.010	0.90	2.000	0.60	1.996
8	30	2.90	2.020	2.20	2.000	1.50	2.000
25	30	2.60	1.000	2.30	1.000	1.50	--
25	50	6.80	1.000	5.90	1.000	4.20	1.000

NB: The 8 mm parallel plate was also used for testing at 30°C for verifying the DSR data performed using the 25 mm plate.

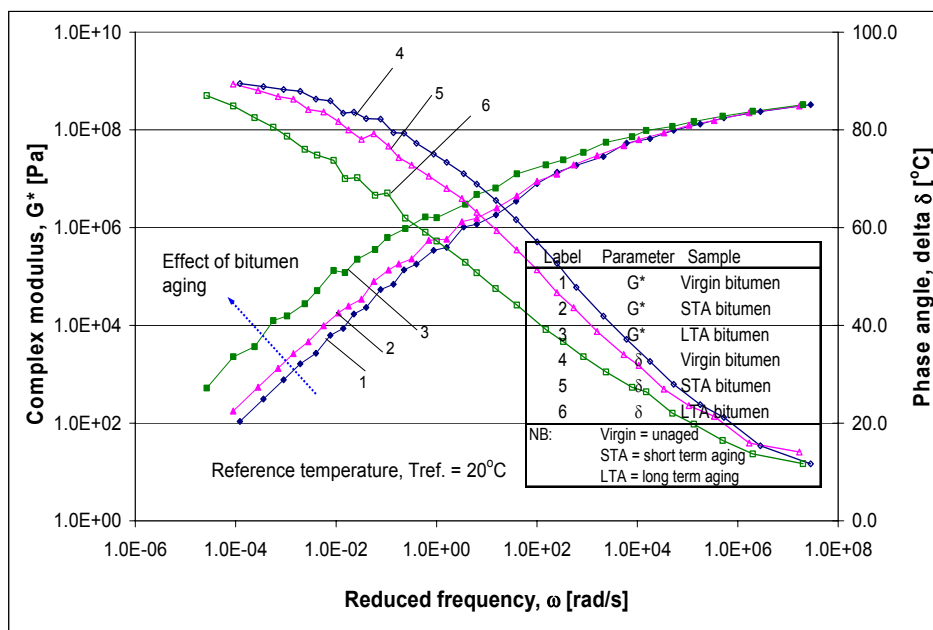


Figure 5.29: Master curves of laboratory aged materials at a reference temperature of 20°C

The model parameters for the laboratory aged bitumen are shown in Table 5.9. A significant change in the model parameter ω_c is noted in fitting the master curve representing the data obtained on aged bitumen.

Table 5.9: Model parameters for complex modulus and phase angle master curve

	Parameter	Virgin/unaged	STA bitumen	LTA bitumen
Shift factor, a_T	C1	12.28	12.56	25.66
	C2	104.99	106.83	203.37
Complex modulus, G^*	ω_c	179.44	45.69	5.75
	k	0.193	0.166	0.157
	m_e	0.033	0.023	0.022
	G^*_{max}	581.65	718.23	704.63
	G^*_{min}	0.00	0.00	0.00
Phase angle, δ	ω_c	8.40	1.94	0.31
	k	0.209	0.186	0.179
	m_e	0.107	0.093	0.107
	δ_{max}	90.00	90.00	90.00
	δ_{min}	4.81	4.94	4.94

NB: The shift factors (a_T) are used to shift both the G^* and δ .

Binders Recovered from Mixture Aging

The master curves of asphalt materials recovered from mixture aging under aging protocols 1 (temperature aging), 2 (temperature + UV light aging), and 3 (temperature + UV light + humidity (RH) aging) are shown in Figure 5.30. Laboratory aged materials using conventional aging methods for short term (STA) and long term (LTA) are also included in Figure 5.30. The complex modulus and phase angle master curve in Figure 5.30 are models fitted to the DSR test data. The shifting was performed to a reference temperature (T_r) of 20°C. Table 5.10 shows the input data used to conduct the frequency sweep test of the materials at the testing temperatures. The model parameters and the shifting factors are shown in Table 5.11.

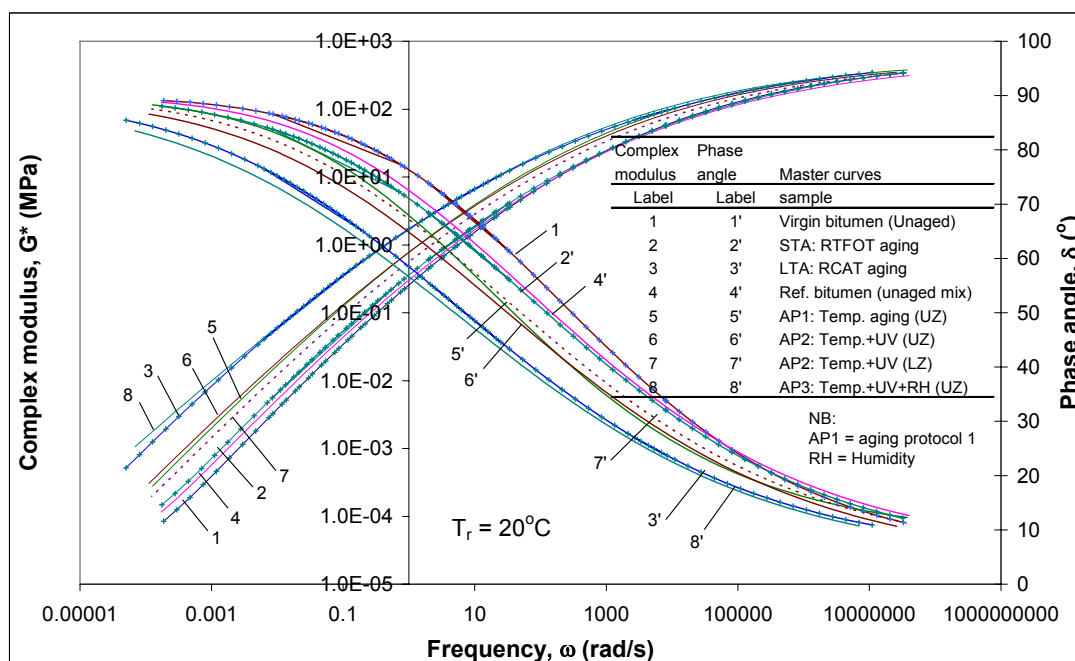


Figure 5.30: Master curve of laboratory aged bitumen materials using the conventional bitumen aging method and mixture aging protocols

Table 5.10: Strain level and specimen thickness (gap) used in testing bitumen materials recovered from mixture aging

		Recovered Bitumen: mixture aging							
Plate size (mm)	Temp. (°C)	Virgin bitumen (Unaged)		Unaged mixture (Reference bitumen)		Aging protocol 1: Temp. aging			
		Strain (%)	Gap (mm)	Strain (%)	Gap (mm)	Upper Zone (UZ)		Lower Zone (LZ)	
						Strain (%)	Gap (mm)	Strain (%)	Gap (mm)
8	-10	0.40	1.987	0.40	2.016	0.30	2.003	0.30	1.993
8	10	0.90	2.010	0.80	2.007	0.60	1.998	0.70	2.007
8	30	2.90	2.020	--	--	1.70	2.001	2.00	2.001
25	30	2.60	1.000	2.50	1.001	1.90	1.000	2.20	1.001
25	50	6.80	1.000	6.30	1.001	4.90	1.000	5.50	1.001
Plate size (mm)	Temp. (°C)	Aging protocol 2: Temp.+UV aging				Aging protocol 3: Temp.+UV+RH aging			
		Upper Zone (UZ)		Lower Zone (LZ)		Upper Zone (UZ)		Lower Zone (LZ)	
		Strain (%)	Gap (mm)	Strain (%)	Gap (mm)	Strain (%)	Gap (mm)	Strain (%)	Gap (mm)
8	-10	0.30	2.002	0.34	1.999	0.35	2.271		
8	10	0.70	2.011	0.70	2.001	0.63	2.169		
8	30	1.70	2.001	1.90	2.001	1.50	2.006		
25	30	1.90	0.999	2.10	1.001	--	--		
25	50	4.90	0.999	5.40	1.002	4.00	0.981		

NB: The data obtained using the 8 mm or 25 mm plate at 30°C can be used alternatively. The data with errors are not included in the above table.

From Figure 5.30, the following observations can be made:

- A general observation is that the phase angle of the binders converges both at high and low frequency regions.
- The partially aged binder (STA: RTFOT) and the recovered bitumen from unaged mixture (after fabrication of the mix) have comparable complex modulus, whereas their phase angles show slight differences.
- Aging protocol 1 and 2 (AP1 and AP2) seem to result in a comparable complex modulus values except for some differences at the low frequency

region. The phase angles are comparable only at higher frequency region. At the lower frequency region, the phase angle of the AP1 binder is also comparable with the STA binder and the binder from unaged mixture.

- The binder recovered from the upper zone (UZ) of the mixture aged under protocol 2 (AP2) has a higher complex modulus and lower phase angle compared to the lower zone (LZ).
- Only aging protocol 3 (AP3) seems to predict the long term aging of the binder in the laboratory. The long term aged (LTA) binder and the binder recovered from aging protocol 3 (AP3) have comparable complex modulus that show only some difference in the low frequency region.

Table 5.11: Complex modulus and phase angle master curve model parameters for binders recovered from mixture aging

Parameters		Reference (unaged mix)	AP1: Temp. aging (UZ) (LZ)		AP2: Temp.+UV (UZ) (LZ)		AP3: Temp.+UV+RH (UZ)
shift factors							
aT	C1	12.34	13.86	15.25	15.25	14.14	24.88
	C2	104.04	113.60	125.05	125.05	115.45	205.96
complex modulus							
G*	ω_c	132.67	131.87	130.93	130.93	131.74	124.19
	k	0.186	0.207	0.198	0.198	0.194	0.199
	m_e	0.031	0.042	0.039	0.039	0.036	0.044
	G^*_{max}	541.24	540.87	539.92	539.92	540.59	535.06
	G^*_{min}	0.00	0.00	0.00	0.00	0.00	0.00
phase angle							
d	ω_c	0.297	1.017	0.652	0.652	0.391	0.782
	k	0.182	0.214	0.176	0.176	0.178	0.178
	m_e	0.068	0.114	0.094	0.094	0.082	0.126
	δ_{max}	90.00	90.00	90.00	90.00	90.00	90.00
	δ_{min}	5.63	8.75	3.67	3.67	4.63	4.16

NB: AP = aging protocol

Field (Road) binders

In Table 5.12, the strain levels used in the frequency sweep tests performed on the field materials are shown. The strain levels were determined to be in the linear region of the response of the materials. The input parameters, i.e. thickness of the specimen (gap of the parallel plates) and the corresponding plate geometry, are also shown in Table 5.12 for each testing temperature. The complex modulus master curve of the upper half (upper zone) and lower half (lower zone) of the field specimens is shown in Figure 5.31 and Figure 5.32 respectively. For comparison purposes, the master curve of laboratory aged materials that simulate short and long term aging in the field are also shown in the figures. A reference temperature of 20°C was selected for constructing the master curves.

The following observations are made from the rheological behaviour of field materials shown in Figure 5.31 and Figure 5.32

- The complex modulus of the field materials increases with increasing service life due to the effect of aging.

- The response of the materials recovered from a new (0 year) and 1 year old PA pavement are comparable with the long term laboratory aged bitumen. This suggests that the laboratory aging method is not as severe as the field aging of PA. This also happens to be true for the materials recovered from mixture aging under aging protocol 1, 2, and 3 in the laboratory.
- There is a small difference in response of the materials recovered from the emergency lane and slow lane (trafficked lane) of the field specimens. In most cases, the bitumen from the emergency lane has a higher modulus compared to the slow lane materials. The 12 year old binder from both lanes shows an exceptionally large difference in G^* while the 7 year old binders show reasonably similar characteristics (especially the binders from the lower zone).
- It seems that there is not much difference in the response of the upper and lower zones of the PA specimens tested. Since ravelling of PA is a surface phenomenon, the materials from the upper zone will be considered further in the analysis of the aging process.

Table 5.12: Strain level and specimen thickness (gap) used in testing bitumen materials recovered from field specimens

		Upper Zone (UZ)				Lower Zone (LZ)			
		Year 0				Year 0			
Plate size	Temp. (oC)	New construction				New construction			
		Strain (%)	Gap (mm)			Strain (%)	Gap (mm)		
8 mm	-10	0.33	2.225			0.33	2.325		
8 mm	10	0.60	2.183			0.58	2.228		
8 mm	30	1.50	1.957			1.50	2.032		
25 mm	50	4.50	0.981			4.10	0.981		
		Year 1				Year 1			
Plate size	Temp. (oC)	Emergency Lane, EL		Slow Lane, SL		Emergency Lane, EL		Slow Lane, SL	
		Strain (%)	Gap (mm)	Strain (%)	Gap (mm)	Strain (%)	Gap (mm)	Strain (%)	Gap (mm)
8 mm	-10	0.33	2.332	0.35	2.343	0.33	2.340	0.33	2.333
8 mm	10	0.57	2.240	0.58	2.147	0.58	2.228	0.58	2.197
8 mm	30	1.41	1.966	1.50	1.960	1.50	1.948	1.50	1.963
25 mm	50	4.10	0.981	4.20	0.981	4.40	0.981	4.20	0.981
		Year 3				Year 3			
Plate size	Temp. (oC)	Emergency Lane, EL		Slow Lane, SL		Emergency Lane, EL		Slow Lane, SL	
		Strain (%)	Gap (mm)	Strain (%)	Gap (mm)	Strain (%)	Gap (mm)	Strain (%)	Gap (mm)
8 mm	-10	0.31	2.348	0.30	2.334	0.30	2.341	0.30	2.324
8 mm	10	0.50	2.281	0.50	2.218	0.47	2.221	0.50	2.128
8 mm	30	1.20	1.975	1.20	1.958	1.10	2.024	1.20	1.970
25 mm	50	3.30	0.981	3.50	0.981	3.20	0.981	3.60	0.981
		Year 7				Year 7			
Plate size	Temp. (oC)	Emergency Lane, EL		Slow Lane, SL		Emergency Lane, EL		Slow Lane, SL	
		Strain (%)	Gap (mm)	Strain (%)	Gap (mm)	Strain (%)	Gap (mm)	Strain (%)	Gap (mm)
8 mm	-10	0.30	2.303	0.29	2.308	0.29	2.344	0.29	2.309
8 mm	10	0.47	2.191	0.45	2.204	0.45	2.206	0.43	2.162
8 mm	30	1.00	1.968	0.98	1.965	0.98	1.970	0.97	2.062
25 mm	50	3.00	0.981	2.65	0.981	2.70	0.981	2.50	0.981
		Year 12				Year 12			
Plate size	Temp. (oC)	Emergency Lane, EL		Slow Lane, SL		Emergency Lane, EL		Slow Lane, SL	
		Strain (%)	Gap (mm)	Strain (%)	Gap (mm)	Strain (%)	Gap (mm)	Strain (%)	Gap (mm)
8 mm	-10	0.30	2.291	0.31	2.313	0.20	2.337	0.30	2.350
8 mm	10	0.45	2.134	0.52	2.152	0.40	2.232	0.54	2.223
8 mm	30	0.90	1.990	1.50	1.993	0.83	2.141	1.30	1.966
25 mm	50	2.12	0.981	3.50	0.981	2.00	0.981	3.80	0.981

NB: The field materials were tested using the 8 mm parallel plate at the temperature of 30°C.

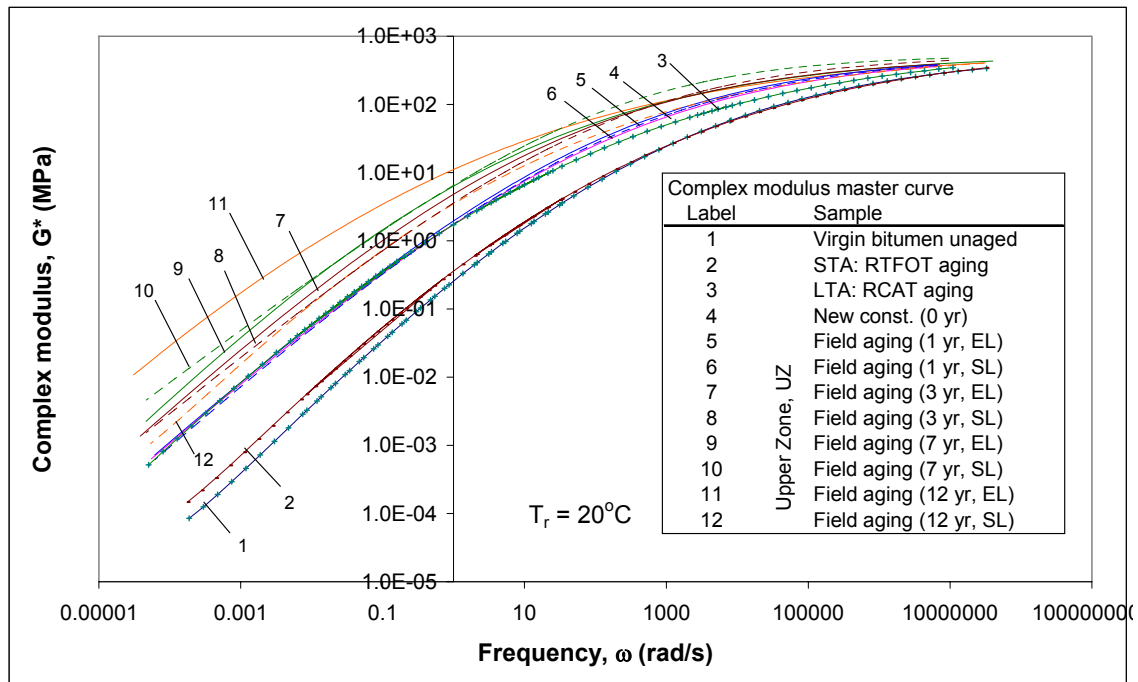


Figure 5.31: Complex modulus master curve of field materials (Upper Zone, UZ) extracted from the emergency lane (EL) and slow lane (SL)

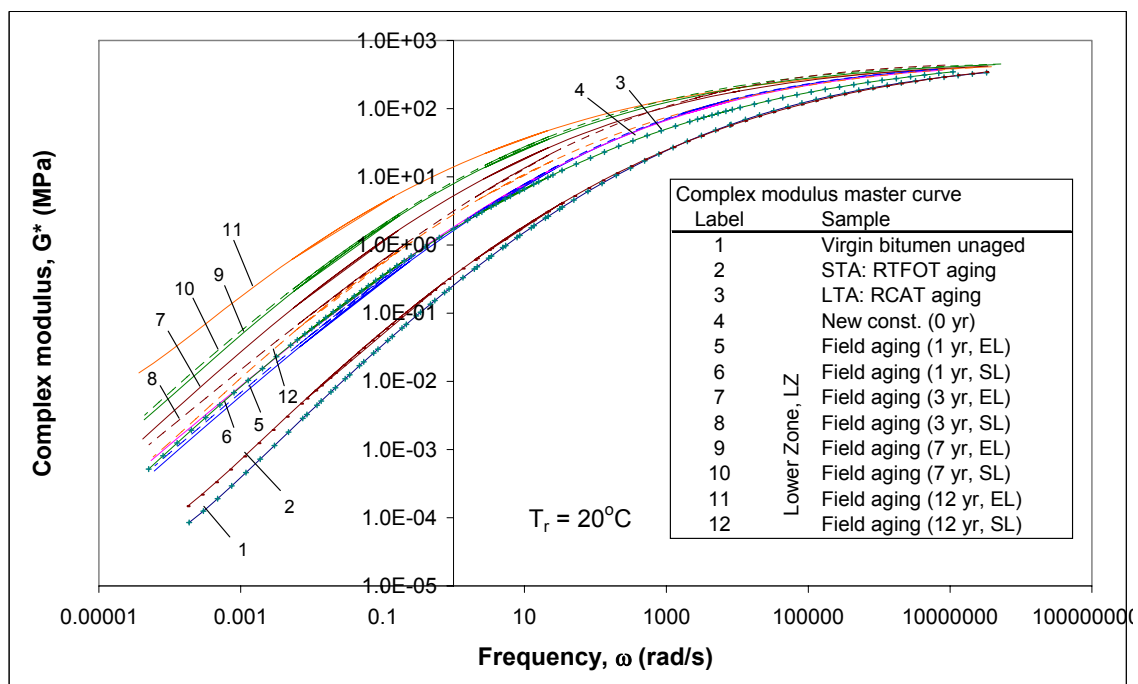


Figure 5.32: Complex modulus master curve of field materials (Lower Zone, LZ) extracted from the emergency lane (EL) and slow lane (SL)

The complex modulus and phase angle model parameters of the field specimens are shown in Table 5.13.

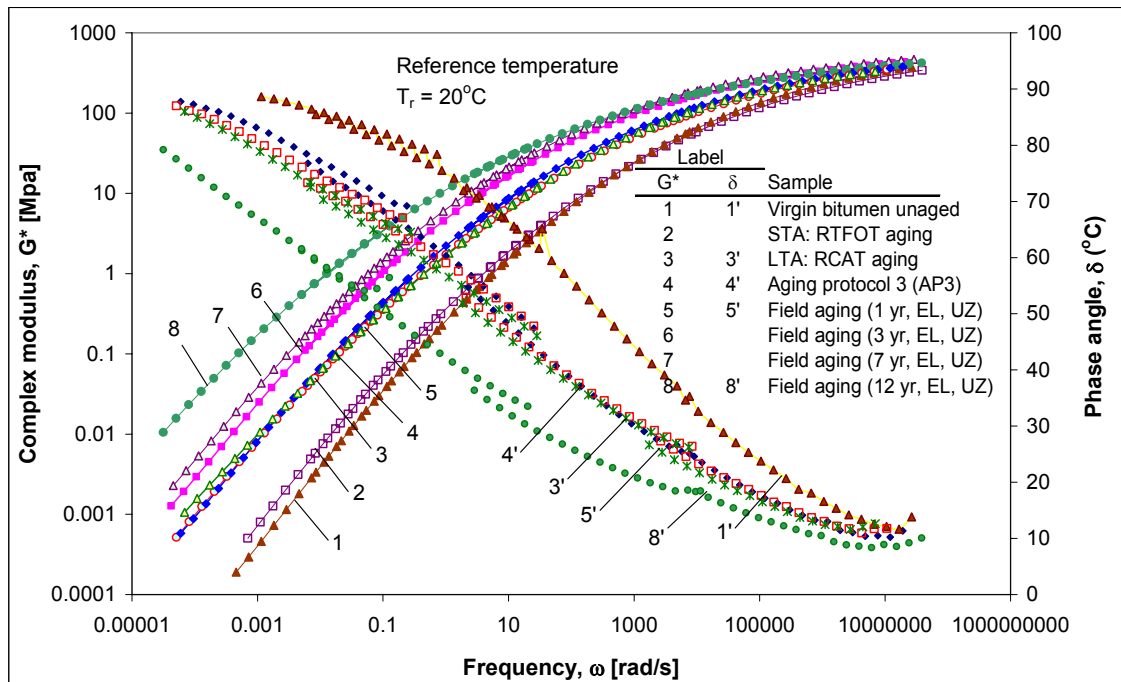


Figure 5.33: Complex modulus master curve of laboratory aged and field materials (Upper zone)

As mentioned before, some researchers believe that the recovery process has some influence on the physical property of the field materials (Burr et al. 1991, Burr et al. 1994). In order to ensure that the recovery process had no influence on the interpretation of the results, the binders recovered from laboratory-aged mixtures of PA (aging protocol 1, 2, and 3) have gone through the same recovery process as the binders recovered from the field cores.

The binders recovered from aging protocol 3 have shown similar characteristics as the 1 year old field material (Figure 5.33) in terms of the complex modulus and the phase angle master curves. The materials with service periods of 3, 7, and 12 year have a much higher complex modulus (lower phase angle) compared to the laboratory aged materials. The laboratory aging methods are simply not severe enough to simulate PA aging occurring in the field.

Table 5.13: Complex modulus and phase angle master curve model parameters for binders recovered from field specimens

Materials:										
Field materials: recovered		Upper Zone, UZ								
Parameters		New Const. 0 yr	Year 1		Year 3		Year 7		Year 12	
			EL	SL	EL	SL	EL	SL	EL	SL
shift factors										
aT	C1	27.34	26.98	26.97	23.40	27.82	20.04	19.77	24.75	20.52
	C2	221.52	221.76	221.57	177.83	221.60	149.97	145.47	181.67	158.21
complex modulus										
G*	ω_C	122.38	122.32	122.40	3.27	122.20	1.96	1.41	0.16	2.26
	k	0.216	0.227	0.222	0.187	0.255	0.185	0.187	0.153	0.172
	m_e	0.051	0.056	0.053	0.032	0.075	0.031	0.032	0.022	0.026
	G^*_{\max}	533.37	533.33	533.31	546.87	533.38	560.80	560.71	591.93	608.37
	G^*_{\min}	0.00	0.00	0.00	0.00	0.00	0.00	0.00	0.00	0.00
phase angle										
δ	ω_C	0.662	1.376	0.756	0.388	0.936	0.821	0.970	0.026	0.462
	k	0.191	0.204	0.203	0.218	0.220	0.223	0.217	0.165	0.191
	m_e	0.120	0.140	0.124	0.143	0.160	0.180	0.187	0.124	0.123
	δ_{\max}	90.00	90.00	90.00	90.00	90.00	90.00	90.00	90.00	90.00
	δ_{\min}	4.03	4.31	3.83	5.79	4.18	5.82	4.41	4.55	4.09
Parameters		Lower Zone, LZ								
		Year 1		Year 3		Year 7		Year 12		
		EL	SL	EL	SL	EL	SL	EL	SL	
shift factors										
aT	C1		21.67	26.87	20.90	27.63	20.41	19.56	22.19	19.87
	C2		175.86	221.03	155.44	221.65	152.12	144.63	163.70	154.54
complex modulus										
G*	ω_C		101.32	122.39	2.98	122.06	0.89	2.29	0.04	2.67
	k		0.220	0.225	0.190	0.254	0.184	0.197	0.160	0.173
	m_e		0.050	0.054	0.033	0.073	0.030	0.037	0.021	0.025
	G^*_{\max}		524.27	533.42	539.13	533.34	561.22	546.78	546.05	607.58
	G^*_{\min}		0.00	0.00	0.00	0.00	0.00	0.00	0.00	0.00
phase angle										
δ	ω_C		0.331	0.886	0.069	1.471	0.534	1.089	0.200	1.301
	k		0.182	0.204	0.189	0.224	0.208	0.213	0.200	0.215
	m_e		0.094	0.123	0.099	0.163	0.158	0.183	0.200	0.150
	δ_{\max}		90.00	90.00	90.00	90.00	90.00	90.00	90.00	90.00
	δ_{\min}		0.96	3.25	3.29	3.68	3.56	3.37	5.76	5.76

Mastic

The input parameters used for the frequency sweep tests of mastic materials are shown in Table 5.14. These include the geometry of the parallel plate, the mastic thickness (gap), and strain levels corresponding to the linear response of the materials at the testing temperatures. The fitted model to the complex modulus and phase angle master curves at a reference temperature of 20°C is shown in Figure 5.34 and the model parameters are given in Table 5.15.

Table 5.14: Strain level and specimen thickness (gap) used in testing mastic materials

		Mastic materials					
Plate size (mm)	Temp. (°C)			Unaged f/b=1.0		Unaged f/b=1.3	
				Strain (%)	Gap (mm)	Strain (%)	Gap (mm)
8	-10			0.27	2.429	0.26	2.443
8	10			0.55	2.228	0.47	2.259
8	30			2.00	2.002	1.40	2.201
25	50			5.00	1.000	4.50	1.001
Plate size (mm)	Temp. (°C)	STA f/b=1.0		LTA f/b=1.0		LTA f/b=1.3	
		Strain (%)	Gap (mm)	Strain (%)	Gap (mm)	Strain (%)	Gap (mm)
8	-10	0.27	2.401	0.26	2.400	0.25	2.427
8	10	0.47	2.316	0.40	2.264	0.38	2.330
8	30	1.20	2.113	1.20	2.213	0.96	2.184
25	50	3.30	0.999	3.10	1.000	2.80	1.003

NB: The field materials were tested using the 8 mm parallel plate at the temperature of 30°C.

Table 5.15: Complex modulus and phase angle master curve model parameters for mastic

Mastic materials		Unaged bitumen		Short term aging	Long term aging	
Parameters		Virgin 1.0	Virgin 1.3	STA 1.0	LTA 1.0	LTA 1.3
shift factors						
aT	C1	12.93	19.15	19.33	24.48	24.98
	C2	110.21	158.46	158.71	194.97	194.90
complex modulus						
G*	ω_C	316.28	312.97	312.78	292.33	292.10
	k	0.253	0.297	0.275	0.303	0.349
	m_e	0.062	0.092	0.087	0.110	0.153
	G^*_{max}	822.63	820.59	820.56	815.24	815.33
	G^*_{min}	0.00	0.00	0.00	0.00	0.00
phase angle						
d	ω_C	147.872	147.946	147.954	148.245	148.254
	k	0.284	0.341	0.304	0.330	0.327
	m_e	0.243	0.368	0.432	0.549	0.555
	δ_{max}	90.00	90.00	90.00	90.00	90.00
	δ_{min}	5.62	7.54	6.40	7.35	6.35

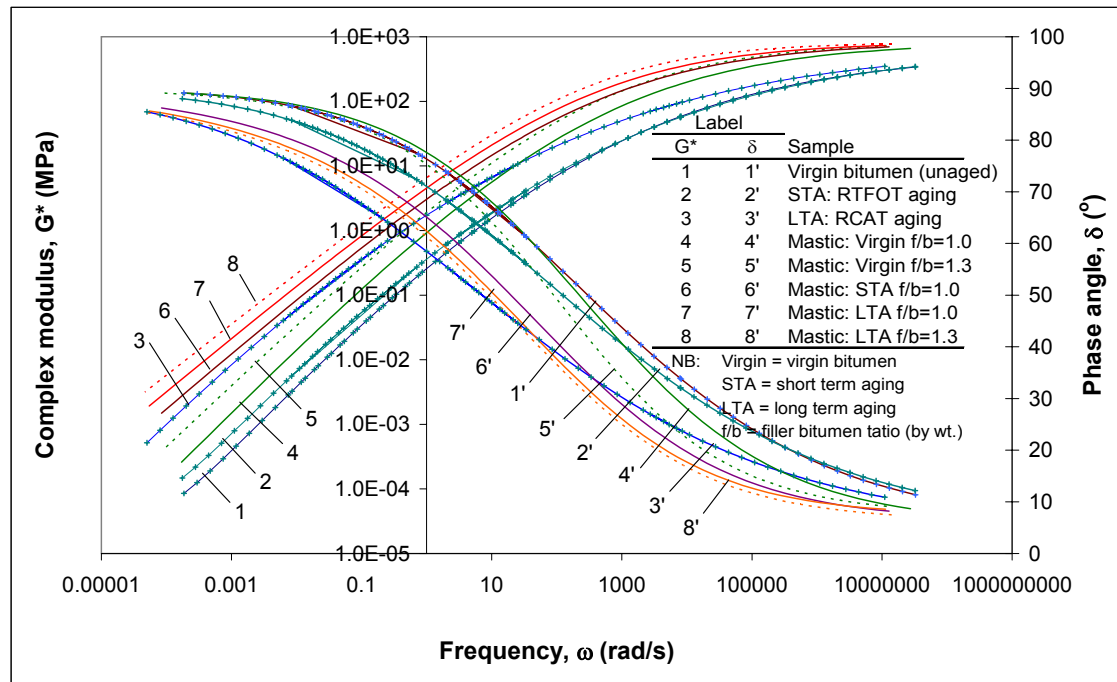


Figure 5.34: Complex modulus and phase angle master curve of mastic and laboratory aged bitumen at a reference temperature of 20°C

The following observations can be made from Figure 5.34:

- As anticipated, the mastics have a higher modulus than the corresponding bitumens from which the mastics were prepared. The increase in stiffness is relatively larger in the high frequency region. At low frequencies, the increase in complex modulus of the STA1.0 mastic (short term aged material with filler bitumen ratio $f/b = 1.0$) shows a much higher increment compared to the LTA1.0 mastic relative to their respective binder stiffness. This shift can also be noticed with respect to the phase angle master curves of the materials. The aged mastics show comparable phase angles and the reason for such behaviour could be that the filler contribution to the modulus of the mastic becomes lower as the binder ages. This implies that the effect of the binder aging becomes more dominant on the rheological behaviour of the mastic at higher temperatures.
- At high frequencies, the mastics have higher modulus and lower phase angle values due to the addition of filler to the bitumen. As the temperature increases (frequency decreases) the susceptibility of the materials to temperature increases, implying that the property of the materials start to be governed by the property of the binder. Hence, the stiffness drops sharply with temperature (low frequency) towards the value obtained for the plain binder. The resistance to flow of the materials is related to their phase angles, which shows higher rate of increment in the case of the mastics with increasing temperature (decrease in frequency).
- The shape of the master curves remains the same at any reference temperature; the change in reference temperature results in a horizontal shift of the master curves along the frequency scale. Hence, the above remarks hold true for any reference temperature.

5.4.4 Binder Fatigue

In order to determine the effect of aging on the fatigue performance of binders, fatigue tests were performed on laboratory and field aged binders. The test results are partly presented in conference proceedings (Hagos et al. 2005 and Hagos et al. 2006).

Effect of Aging on Binder fatigue

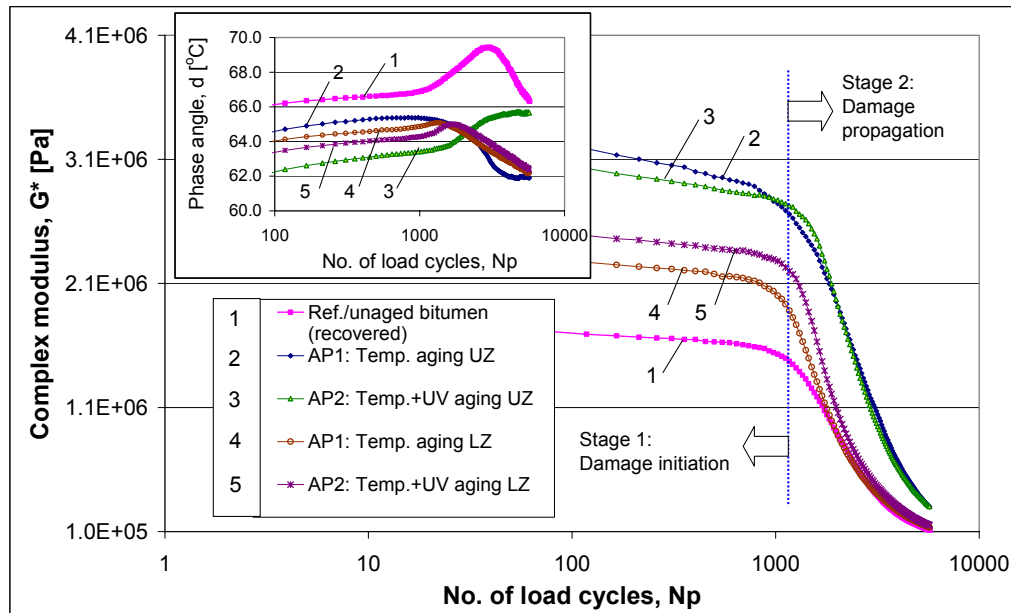
Two stages of damage can be defined in a binder fatigue test, being:

- Stage 1: damage initiation and
- Stage 2: damage propagation.

In stage 1, the energy per cycle of loading is dissipated in viscoelastic damping with negligible damage. The transition phase from stage 1 to 2 is a stage where the damage initiation consumes an additional amount of energy beyond the viscoelastic damping, which is attributed to a slight increment in the phase angle. Stage 2 is the critical stage during which a noticeable increase in dissipated energy per cycle is observed. In this stage irrecoverable fatigue damage takes place (Bahia et al. 2001). Damage development in the two stages of fatigue is as a result of crack initiation and propagation.

A typical fatigue test result of binders is shown in Figure 5.35 for materials aged under protocols AP1 and AP2 at a shear strain of 10%. All fatigue tests were performed as strain controlled test using shear strains⁷ of 3%, 6%, and 10% (refer to the testing program in Chapter 4, Table 4.29 for details on materials and strain levels used). Figure 5.35 also shows the two phases of damage developed in the materials.

⁷ Shear strains of 3% or 4% and 6% or 7% were used during the binder fatigue test.



Nomenclature:

- Reference refers to bitumen recovered from unaged asphalt mix
- Temp refers to bitumen recovered from asphalt mix aged under aging protocol 1
- Temp+UV refers to bitumen recovered from asphalt mix aged under aging protocol 2
- UZ and LZ are Upper Zone and Lower Zone of a mixture sample respectively

Figure 5.35: Fatigue test on recovered binders at 20°C, 10 rad/sec, and 10% strain

From Figure 5.35, the following observations can be made:

- The aged materials have a higher complex modulus in the damage initiation stage (stage 1).
- The aging of PA specimens in a weatherometer seems to have greater effect on the upper zone compared to the lower zone.
- The decrease in the complex modulus of the binders is much greater in the damage propagation stage (stage 2) than the initiation stage (stage 1).
- All the materials seem to have changed their fatigue performance, i.e. damage progression from stage 1 to stage 2, after nearly the same number of loading cycles.

A plot of the complex modulus as a function of loading cycles (N) is also shown in Figure 5.36 for laboratory aged and field binders to show the effect of different aging protocols. The figure illustrates that the fatigue performance of laboratory aged binders greatly differs from that of the field aged materials. The RCAT and AP3 aged binders have similar fatigue performance. Similarly, the binders from AP1 and AP2 seem to have comparable fatigue behaviour. However, the 7 and 12 year old binder samples from the field have shown completely different fatigue behaviour compared to fatigue performance of the materials aged under laboratory aging protocols. The transition from stage 1 to stage 2 fatigue of the field materials is occurring at lower number of loading cycles while the initial stiffness is much higher.

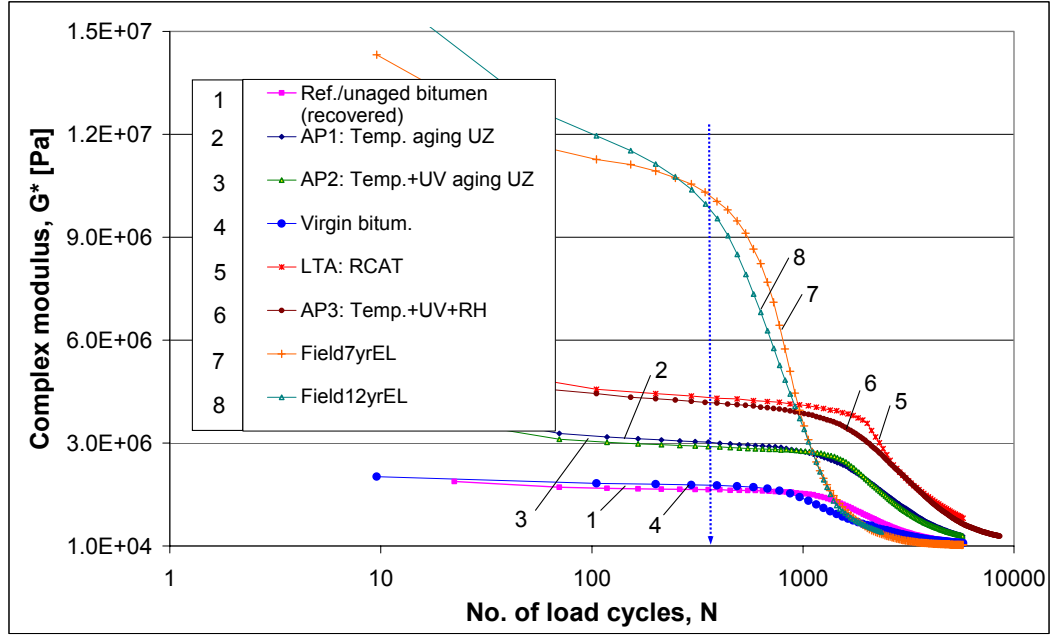


Figure 5.36: Fatigue test results of binders at 10 rad/s, 10% strain, and 20°C temperature

Fatigue Parameter N_p

The energy dissipated per cycle, the accumulated dissipated energy after N cycles of loading/strain applications, and the Dissipated Energy Ratio (DER) can be calculated using Equation 5.35 to 5.37:

$$W_i = \pi \sigma_i \varepsilon_i \sin \delta_i \quad (5.35)$$

$$W_c = \sum_{i=1}^n W_i \quad (5.36)$$

$$DER = \frac{\sum_{i=1}^n W_i}{W_n} = \frac{W_c}{W_n} \quad (5.37)$$

where:

- W_i = dissipated energy per cycle per unit volume,
- W_c = accumulated dissipated energy after n cycles,
- W_n = dissipated energy at the n th cycle,
- σ_i = the stress amplitude at cycle i ,
- ε_i = the strain amplitude at cycle i ,
- δ_i = the phase angle between the stress and strain signals,
- n or N = number of cycles $N = \omega \cdot t / (2\pi)$,
- ω = radial frequency [rad/s],
- t = time [s], and
- DER = Dissipated Energy Ratio (fatigue parameter) [-].

The fatigue criteria DER proposed by Pronk and Hopman (1990) and Pronk (1995) and the change in the rate of the dissipated energy suggested by

Carpenter and Jansen (1997) are effective tools to evaluate the fatigue performance of materials. Bahia et al. 2001 recommends the fatigue life to crack propagation (N_p) to be used as a fatigue resistance indication parameter to mark the transition from the crack initiation to crack growth. The parameter N_p can be determined from the intersection point of the slopes (tangent lines) of the damage initiation (stage 1) and irrecoverable fatigue (stage 2) in a DER vs N plot. The fatigue tests performed at different strain levels are shown in Figure 5.37 and Figure 5.38 for the virgin and field (12yr, EL) binders respectively.

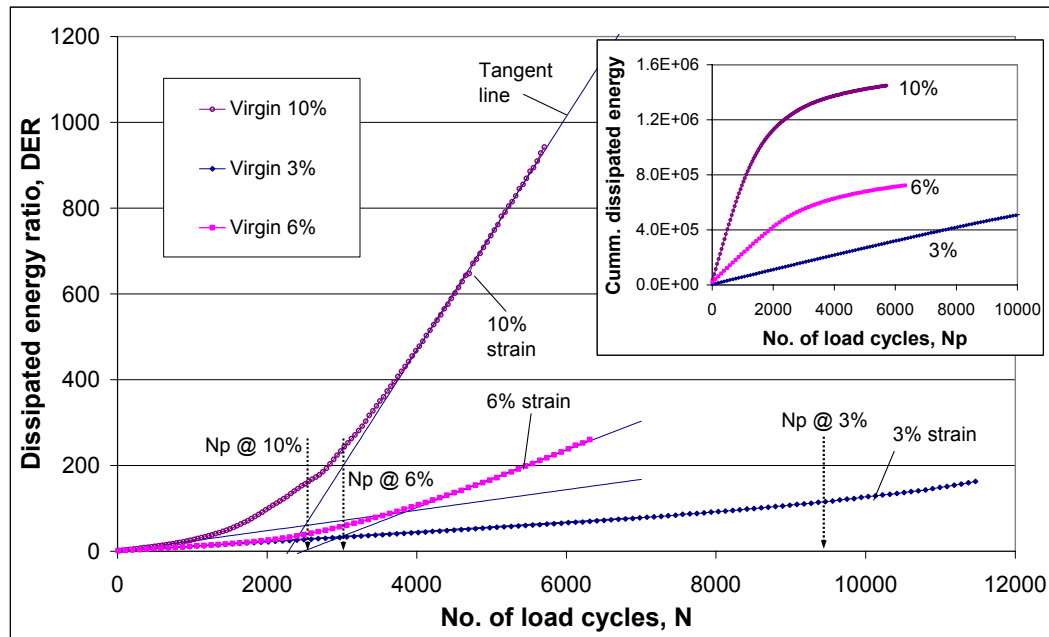


Figure 5.37: A plot of dissipated energy ratio (DER) of a virgin bitumen at 3, 6, and 10% strain

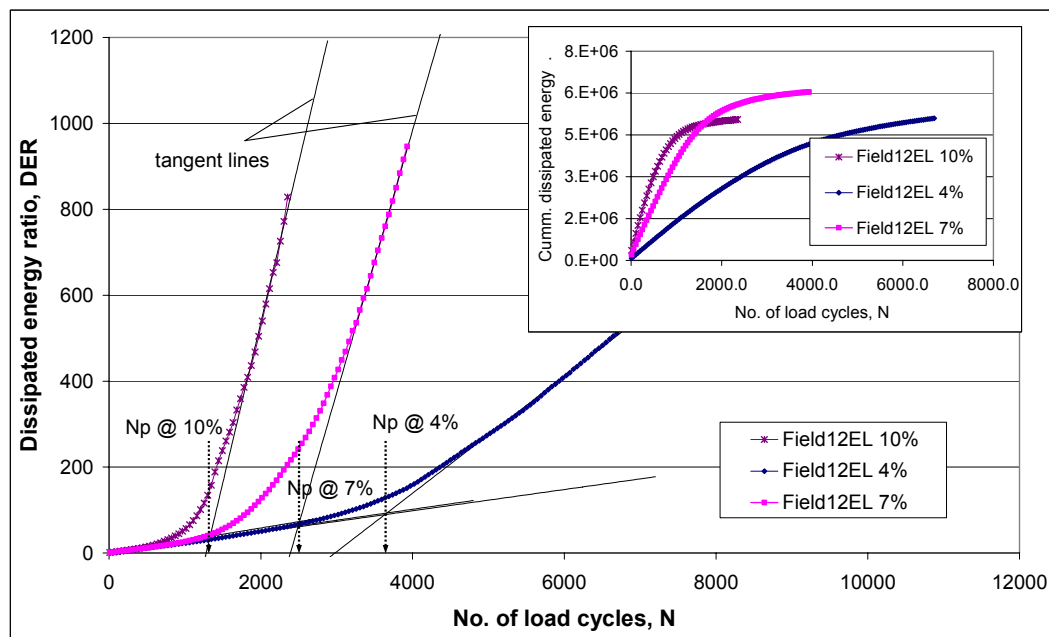


Figure 5.38: A plot of dissipated energy ratio (DER) of 12 yr old field bitumen (EL) at 4, 7, and 10% strain

The tangent lines to the data points in the 1st and 2nd damage phases were determined by fitting lines to the data points independently. Fatigue tests performed at lower strain levels require long time to reach at the number of cycles to fatigue and generate the data points in the damage propagation stage, which makes the test uneconomical to be carried out. For this reason, the determination of the tangent line for the 2nd phase fatigue line at 3% strains are merely subjective (mainly for the virgin bitumen) because only few data points were used to determine the tangent line in the damage propagation stage.

Fatigue Test Results Analysis

Analysis of the fatigue performance of binders was done based on the DER approach. The cumulative dissipated energy versus number of load cycles at 10% strain is shown in Figure 5.39. The corresponding plot of the DER as a function of loading cycles is shown in Figure 5.40. From the two figures, it can be seen that the aging method has a significant effect on the fatigue performance of the binders based on both the rate of energy dissipation and fatigue parameter N_p . The following remarks can be made:

- The fatigue parameter N_p depends on the rate of energy dissipation in stage 1 (damage initiation), stage 2 (damage propagation) and the transition from stage 1 to stage 2. This creates difficulties in making consistent interpretations of the fatigue performance based on the rate of energy dissipation in stage 1 and the fatigue parameter N_p .
- Figure 5.40 shows that the fatigue parameters of the field binders are lower than the virgin (unaged) bitumen; whereas the N_p of the laboratory aged binders is greater than that of the virgin bitumen (refer also to Figure 5.41). The reason for such behaviour in fatigue performance has to do with the fatigue indicator N_p . In view of this, the rate of energy dissipation might be a preferable option for evaluating the fatigue performance of binders.
- The rate of aging of the field materials is much higher compared to the laboratory aged materials. This indicates that the binder in the field is very sensitive to fatigue relative to the long term aged materials in the laboratory, which are supposed to simulate the material behaviour in the field.
- From the difference in fatigue performance of the laboratory aged materials, UV light seems to have considerable effect on the rate of damage (cumulative dissipated energy) of the binder. Aging protocol 3 or AP3 bitumen is the material recovered from a mixture aged under the combined effect of temperature, UV light, and humidity (RH) for 1000 hours. The LTA bitumen is the bitumen aged under the standard protocol for short and long term aging (RTFOT+RCAT).

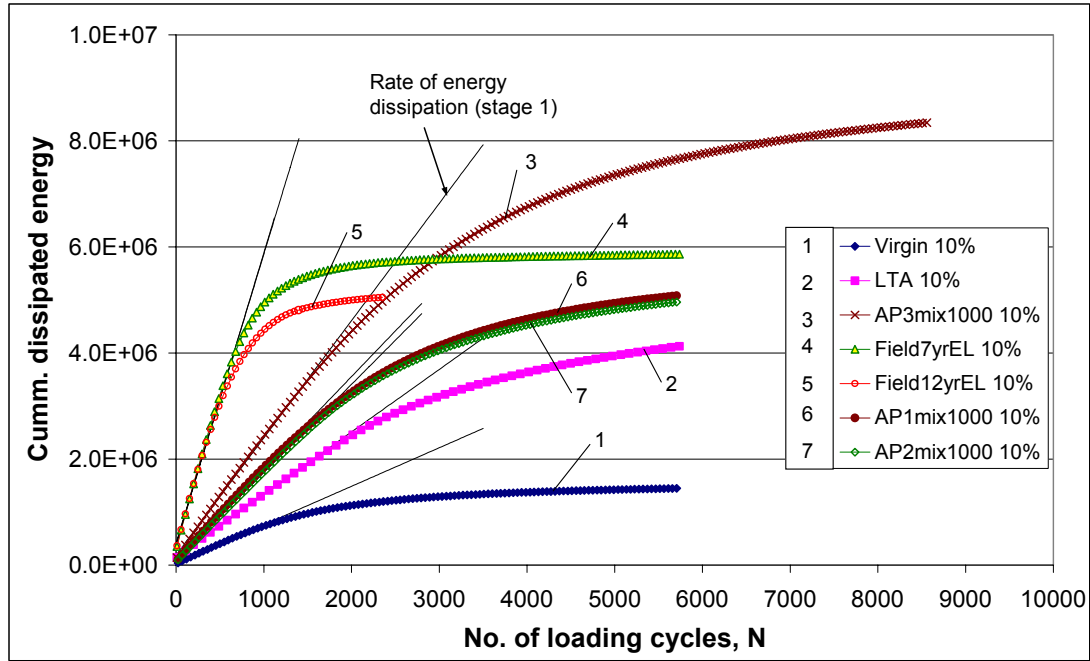


Figure 5.39: Cumulative dissipated energy (DE) of materials at 10% strain and 20°C temperature fatigue test

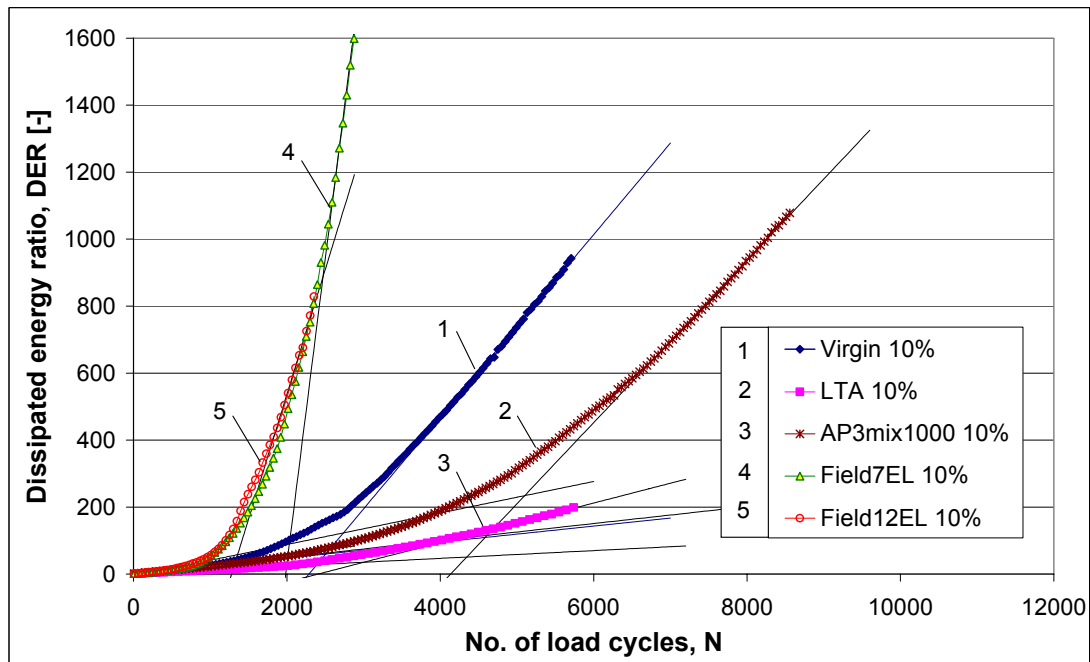


Figure 5.40: Dissipated energy ratio (DER) plot of materials fatigue test

In Figure 5.41, the fatigue parameter N_p determined from fatigue test of materials performed at different strain levels is shown. The power-law model used to fit the N_p data is given in Equation 5.38. The N_p values for the laboratory aged and field materials are presented in Table 5.16. The parameters of the fitted curve using Equation 5.38 are also shown in Table 5.16.

$$N_p = a \cdot \varepsilon^b \quad (5.38)$$

Where:

N_p = fatigue parameter,
 a, b = constants [-],
 ε = strain [%].

Table 5.16: Fatigue parameter N_p of tested binders

Item	Material	Strain levels					Fit parameters	
		3%	4%	6%	7%	10%	a	b
1	Virgin bitumen	9481	7386	2996		2505	27860	-1.0413
2	LTA bitumen		13012	8324	4662	3005	135286	-1.6569
3	AP3 mixaging bitumen		11123		5221	4612	41813	-0.9955
4	Field 7yr SH		4321		2797	2032	13542	-0.8192
5	Field 12yr SH		3632		2494	1331	16726	-1.0579
6	Ref./unaged bitumen					3236		
7	AP1: Temp. aging UZ					3455		
8	AP1: Temp. aging LZ					2831		
9	AP2: Temp.+UV aging UZ					3139		
10	AP2: Temp.+UV aging LZ					3031		
Fatigue life to 0.5G*								
		4%	6 or 7%	10%	NA = not applicable			
Virgin bitumen		NA	NA	2294.9	NB: The field bitumens showed poor fatigue performance interms of their fatigue to half life (i.e.the reduction of the complex modulus by 50% or 0.5G*).			
LTA: RCAT		NA	8699.4	3256.3				
Mix aging 1000 Hr		NA	5357.2	2303.0				
Field 7 yr SH		3210.2	1107.7	725.7				
Field 12 yr SH		3017.6	1251.0	536.4				

The criteria for fatigue life of asphaltic materials is usually assumed to occur when the original stress level is reduced by half in strain controlled tests and when the strain level is doubled in stress controlled tests. In the sinusoidal strain controlled binder tests performed in this study, the dissipated energy per cycle has shown a decrease because of changes in the stress level and phase angle during testing. The total amount of energy dissipated during the test is given by Equation 5.39.

$$W_{FAT} = A_F \cdot N_{FAT}^Z \quad (5.39)$$

Where:

W_{FAT} = total amount of dissipated energy
 N_{FAT} = number of load repetitions to fatigue
 A_F, Z = material constants

The cumulative dissipated energy in Equation 5.39 is independent of the test type. In order to account for the change in dissipated energy during fatigue tests, a factor Ψ has been introduced (van Dijk 1975, van Dijk and Visser 1977, Molenaar 2007). This factor is 1 during the start of the fatigue test and approaches a limiting value of 1.5 and 0.5 for strain controlled and stress controlled tests respectively. It is independent of the test type and testing conditions. The modified equation is shown in Equation 5.40 based on the initial dissipated energy.

$$W_{FAT} = N_{FAT} \cdot W_{IN} / \Psi \quad (5.40)$$

Where:

W_{IN} = initial dissipated energy ($W_{IN} = \pi \cdot \tau_0 \cdot \gamma_0 \cdot \sin \phi_0$)

Ψ = factor that takes into account the variation in dissipated energy per cycle during the test

Using the above approach, the factor Ψ has been determined for the binder fatigue tests performed in this study. The number of cycles to fatigue life N_p was taken as a fatigue life parameter. Other parameters such as the initial dissipated energy, the energy at N_p expressed as a percentage of the initial energy, the initial binder complex shear modulus G^* , and the complex shear modulus at the fatigue life expressed as a percentage of the initial G^* for the different binders are shown in Table 5.17.

The factor Ψ at failure (fatigue life N_p) increases with the increase in strain level at which the fatigue test was conducted. Similarly, the energy and the binder stiffness ratios (i.e. the value at failure relative to the initial) increases with strain level. Moreover, the aged materials showed higher Ψ factor compared to the virgin bitumen due to a higher dissipated energy per cycle. However, this does not imply that the aged binders are incurring more damage than the unaged because their stiffnesses are different. The fatigue life of the binders depends on the binder's ability to absorb energy without incurring damage (micro-cracking).

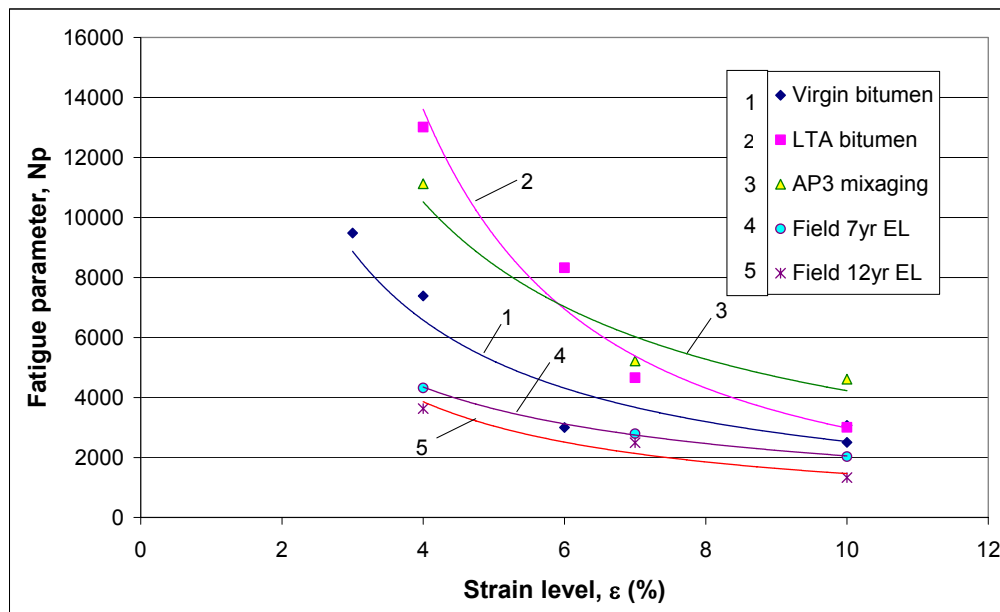
Table 5.17: Fatigue parameters and factor Ψ at fatigue life N_p

Binder type	Strain level	Fatigue model parameters		Factor	No. of cycles to fatigue life	Initial dissipated energy	Dissp. Energy at N_p	Initial binder stiffness	Stiffness at failure
		A	Z			W_o	% W_o	G^*_o	% G^*_o
Virgin	4%	7237.4	1.0000	1.006	7386	7.28E+03	17.4	1.58E+06	N/A
	6%	22455	0.9819	1.103	2996	2.14E+04	54.9	2.09E+06	55.4
	10%	44244	0.9681	1.158	2505	4.00E+04	80.0	1.36E+06	79.9
LTA	4%	25709	0.9913	1.087	13012	2.58E+04	11.5	6.73E+06	15.0
	6%	60917	0.9749	1.207	8324	5.86E+04	43.7	6.68E+06	47.2
	10%	164446	0.9555	1.316	3005	1.52E+05	43.3	5.95E+06	46.8
AP3	4%	23503	0.9897	1.085	11123	2.33E+04	7.9	6.08E+06	11.1
	6%	74312	0.9697	1.231	5221	7.06E+04	45.8	5.85E+06	48.8
	10%	151294	0.9549	1.350	4612	1.40E+05	80.1	5.50E+06	81.3
Field 7yr	4%	76608	0.9704	1.143	4321	6.84E+04	69.6	1.90E+07	70.5
	6%	247323	0.9414	1.361	2797	2.11E+05	91.5	1.82E+07	91.8
	10%	426104	0.9287	1.430	2032	3.54E+05	96.8	1.43E+07	96.3
Field 12yr	4%	82905	0.96	1.190	3632	7.11E+04	55.3	2.30E+07	59.4
	6%	233560	0.9516	1.293	2494	2.07E+05	88.7	2.04E+07	88.5
	10%	448950	0.9171	1.474	1331	3.65E+05	90.3	1.63E+07	89.5

Table 5.18: Fatigue parameters and factor Ψ at fatigue life $N_p = 50\% G^*$

Bitumen type	Strain	Model parameters $W_f = AN^Z$		No. of cycles $N_p @ 0.5G^*$	Dissp. Energy at $N_p = 0.5G^*$ %Wo	Factor Ψ at $N_p = 0.5G^*$
		A	Z			
Virgin	4%	7237.4	1.0000	2295	76.8	1.155
	6%	22455	0.9819			
	10%	44244	0.9681			
LTA	4%	25709	0.9913	8699	46.0	1.208
	6%	60917	0.9749			
	10%	164446	0.9555			
AP3	4%	23503	0.9897	5357	47.5	1.232
	6%	74312	0.9697			
	10%	151294	0.9549			
Field 7yr	4%	76608	0.9704	3210	48.5	1.133
	6%	247323	0.9414			
	10%	426104	0.9287			
Field 12yr	4%	82905	0.9600	3018	44.5	1.181
	6%	233560	0.9516			
	10%	448950	0.9171			

The binder's fatigue performance (strain controlled) can be observed in Figure 5.41 in which the laboratory aged materials have shown improved performance while the field materials are poor in their fatigue life compared to the virgin bitumen.

Figure 5.41: The effect of aging and strain level on the fatigue parameter N_p (Temp. 20°C)

As in the fatigue ranking at 10% strain, Figure 5.41 reveals that the fatigue lines of the laboratory aged materials and field materials relative to the virgin bitumen performance are completely different. The field binders showed poor performance while the laboratory aged binders have shown improved fatigue

life relative to the virgin bitumen. The following observations are made with regard to the fatigue performance of the materials shown in Figure 5.41:

- The fatigue performance of the laboratory aged binders is better compared to the virgin (unaged) bitumen based on the parameter N_p . On the other hand, the field binders fatigue performance is lower than the virgin bitumen. This is an important result.
- The difference in fatigue life of the aged and unaged materials is higher at lower strain levels. The laboratory aged binders seems to have high susceptibility to fatigue failure with increasing fatigue strain.
- At high strain levels, the fatigue performance of the binders decreases. This may be explained by the fact that the binders are dissipating more energy to overcome the accumulation of damage which reaches the failure point at lower number of cycles. It may also be as a result of “brittle” behaviour of the binder after aging.
- The rating of fatigue performance according to half life or reduction of the complex modulus by 50% is shown in Table 5.16. This analysis was done to verify if the same conclusions can be reached based on different approaches of estimating fatigue life. Accordingly, the field materials appear to have poor performance.

5.5 Modelling of Bituminous Materials

In this section, the viscoelastic properties of unaged and aged binders as well as mastic materials have been modelled based on the principles of the Generalised Maxwell Model. The relaxation modulus of viscoelastic materials can be represented by the Generalized Maxwell Model using Prony series. The approximation of the relaxation modulus for modelling the material was also used to analyse the stress situation in PA pavement using FE modelling of a PA by simulating real loading on the PA structure. This is regarded important because interpretations can be made on the performance of PA and the effect of aging on the rheological properties of the binder/mortar.

5.5.1 Bitumen Viscoelastic Properties

Prony series representation

Viscoelastic materials such as bitumen have both elastic and viscous components. Perfectly elastic and viscous properties of a viscoelastic material are represented by a spring and dashpot elements respectively. The stiffness of the spring is designated by G and the viscosity of the dashpot is represented by η . A combination of a spring and a dashpot in series and in parallel represents a Maxwell model and a Kelvin-Voigt model respectively. The combination of Maxwell and Kelvin-Voigt elements in series is known as a Burger’s model (Figure 5.42). These models describe the rheological behaviour of very simple systems.

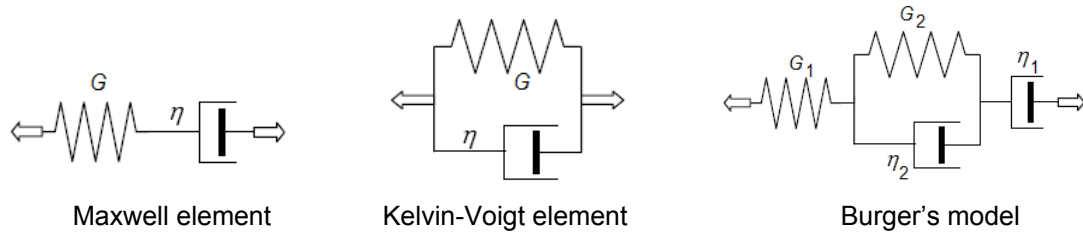


Figure 5.42: Maxwell, Kelvin-Voigt, and Burger's models

$$\begin{aligned} \sigma(t) &= G \cdot \varepsilon(t) && \text{Elastic (spring)} \\ \sigma(t) &= \eta \frac{\partial \varepsilon}{\partial t} && \text{Viscous (dashpot)} \end{aligned} \quad (5.41)$$

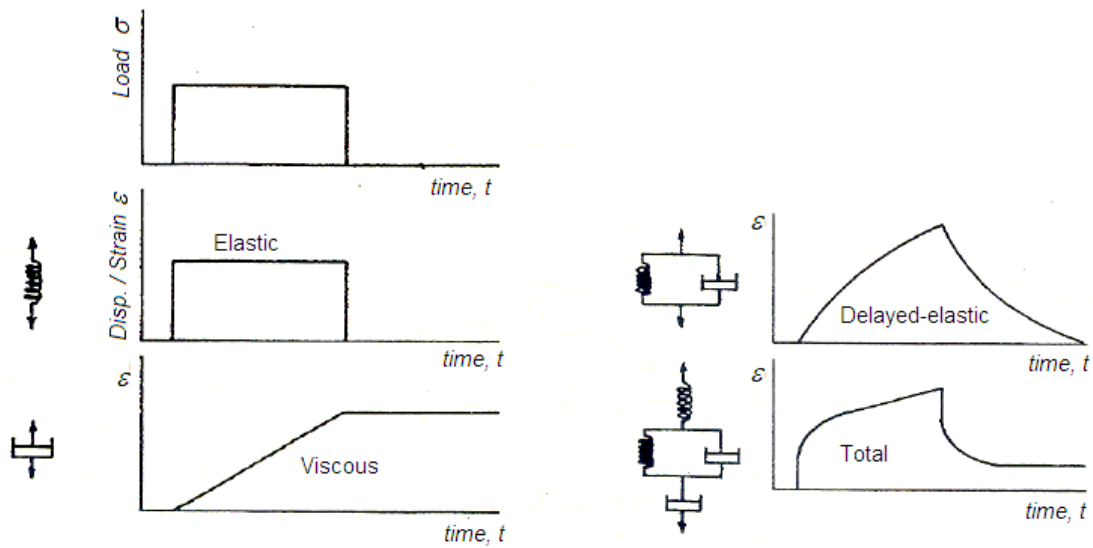
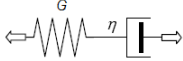
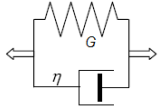
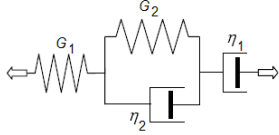
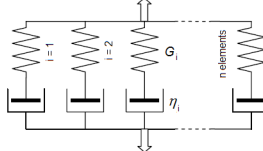
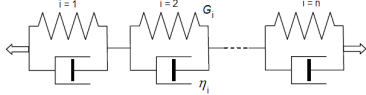


Figure 5.43: Response of model elements to an applied load

The governing equations for the models in Figure 5.43 and Generalized Maxwell and Kelvin-Voigt models are given in Table 5.19.

Table 5.19: Models and their corresponding constitutive equations

Models	Representation	Constitutive equations
Maxwell model - Elastic + viscous		Compliance: $J(t) = 1/G + t/\eta$ Relaxation: $G(t) = G \cdot \exp(-t/\tau)$, $\tau = G/\eta$
Kelvin-Voigt model - Delayed elastic		Compliance: $J(t) = 1/G \left[1 - \exp\left(-\frac{t}{\tau}\right) \right]$
Burgers model - Viscoelastic		Compliance: $J(t) = 1/G_1 + 1/\eta_1 + 1/G_2 \left[1 - \exp\left(-\frac{t}{\tau_2}\right) \right]$
Generalized Maxwell Model (GMM) - Relaxation		Relaxation: $G(t) = G_e + \sum_{i=1}^n G_i \exp[-t/\tau_i]$
Generalized Kelvin-Voigt Model (GVM) - Retardation		Compliance: $J(t) = J_g + \sum_{i=1}^n J_n \left(1 - \exp[-t/\tau_n] \right) + \frac{t}{\eta_0}$

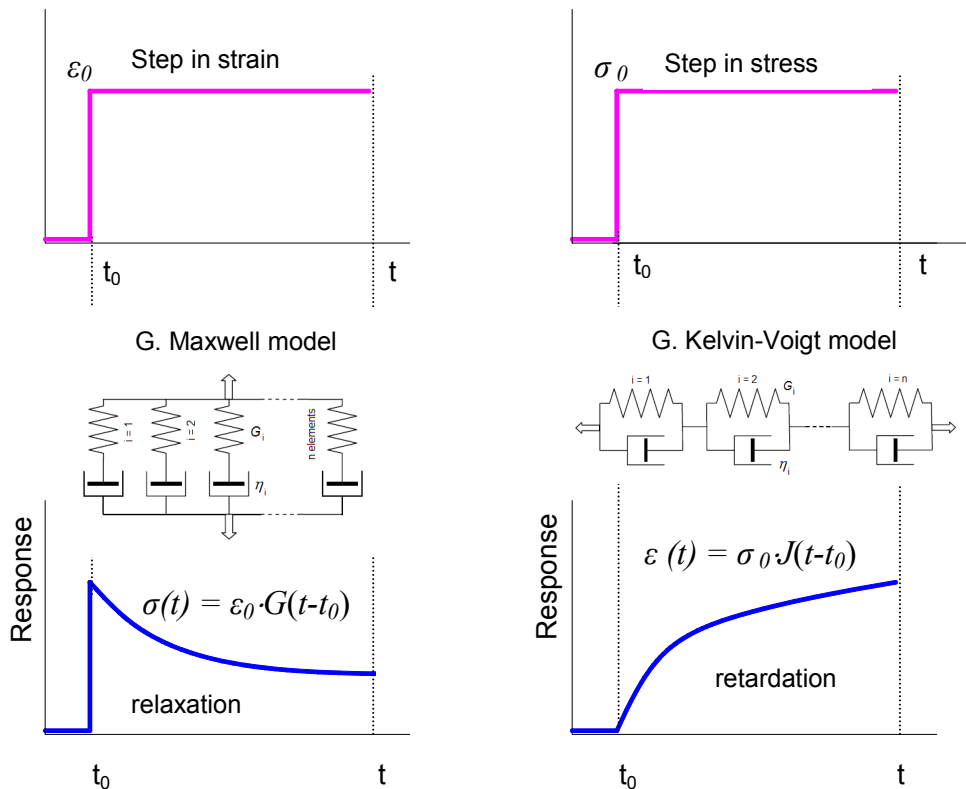


Figure 5.44: The behaviour of Generalized Kelvin-Voigt and Maxwell models during creep (constant stress) and relaxation (constant strain) loading

The stress in the spring (elastic component) and the dashpot (viscous component) are given in Equation 5.41. In the Maxwell model, the stress developed by an applied load in the spring and the dashpot are equal and the total strain is the sum of the strains in the spring and the dashpot. In the Kelvin-Voigt model, an applied load results in the same strain level in the spring and the dashpot while the total stresses are additive. These principles are used to derive the constitutive equations of complex models such as generalized models which more closely represent the actual behaviour of materials shown in Figure 5.44. A number of Maxwell elements in parallel form a *Generalized Maxwell Model* (GMM), which is useful to predict stress relaxation of viscoelastic materials. The approximation of relaxation functions using GMM is also referred as *Prony Series*. Similarly, Kelvin-Voigt models in series form a *Generalized Kelvin-Voigt Model* (GVM), which is also useful in modelling the retardation (creep) behaviour of viscoelastic materials.

Relaxation spectrum

A Prony Series which is essentially a Generalized Maxwell Model provides a good fitting to the relaxation function of viscoelastic materials (Figure 5.45). The governing equations associated with the model are given in Equation 5.42 to Equation 5.45.

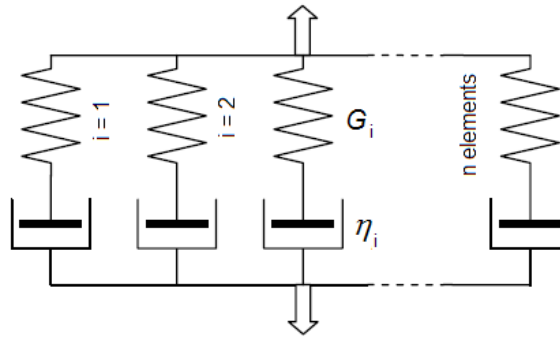


Figure 5.45: Generalized Maxwell Models (Relaxation)

$$G(t) = G_e + \sum_{i=1}^n G_i \exp[-t / \tau_i] \quad (\text{Generalized Maxwell modulus}) \quad (5.42)$$

$$G^*(\omega) = \sum_{i=1}^n \frac{G_i i \omega \tau_i}{1 + i \omega \tau_i} \quad (\text{Complex relaxation modulus}) \quad (5.43)$$

$$G'(\omega) = \sum_{i=1}^n \frac{G_i \omega^2 \tau_i^2}{1 + \omega^2 \tau_i^2} \quad (\text{Storage modulus}) \quad (5.44)$$

$$G''(\omega) = \sum_{i=1}^n \frac{G_i \omega \tau_i}{1 + \omega^2 \tau_i^2} \quad (\text{Loss modulus}) \quad (5.45)$$

Where:

$G(t)$	=	transient relaxation modulus [Pa]
G_e	=	rubbery (min.) modulus [Pa]
$G^*(\omega)$	=	complex (dynamic) relaxation modulus [Pa]
G'	=	storage modulus [Pa]
G''	=	loss modulus [Pa]
ω	=	angular frequency [rad/s]
t	=	time [s]
τ_i	=	relaxation time, $\tau_i = G_i / \eta_i$ [s]
G_i	=	discrete spectral stiffness [Pa]

If the number of discrete relaxation elements $[\tau_i, G_i]$ increases indefinitely, then the result is a continuous spectrum with $G(\tau)$ as the continuous relaxation function. Replacing $d\tau$ with $\tau d \ln \tau$ and defining $H(\tau) = \tau G(\tau)$, Equation 5.46 can be derived.

$$G(t) = G_r + \int_0^{\infty} G(\tau) \cdot e^{-t/\tau} d\tau = G_r + \int_{-\infty}^{\infty} H(\tau) \cdot e^{-t/\tau} d \ln \tau \quad (5.46)$$

(Continuous relaxation spectrum)

Retardation spectrum

The conversion from relaxation to retardation functions is not direct. Hence, the use of the GVM is employed to describe the retardation behaviour with “Prony series” representation given by Equations 5.47 to 5.50.

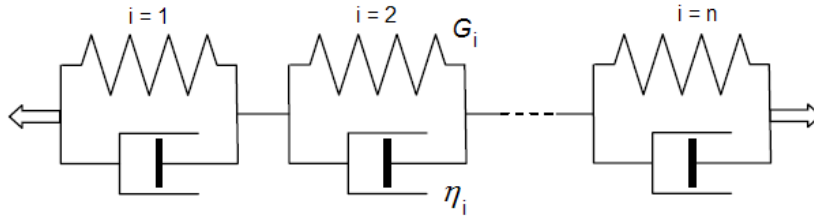


Figure 5.46: Generalized Kelvin-Voigt model (Creep/Retardation)

$$J(t) = J_g + \sum_{i=1}^n J_n \left(1 - \exp[-t / \tau_n]\right) + \frac{t}{\eta_0} \quad (\text{Generalized Voigt compliance}) \quad (5.47)$$

$$J^*(\omega) = \sum_{i=1}^n \frac{J_i}{1 + i\omega\tau_i} \quad (\text{Complex creep compliance}) \quad (5.48)$$

$$J'(\omega) = \sum_{i=1}^n \frac{J_i}{1 + \omega^2\tau_i^2} \quad (\text{Storage compliance}) \quad (5.49)$$

$$J''(\omega) = \sum_{i=1}^n \frac{J_i\omega\tau_i}{1 + \omega^2\tau_i^2} \quad (\text{Loss Compliance}) \quad (5.50)$$

Where:

$J(t)$	=	transient shear compliance [Pa]
J_g	=	instantaneous shear compliance, $J_g = 1/G_g$ [Pa]
$J^*(\omega)$	=	complex (dynamic) shear compliance [Pa]
J'	=	creep storage compliance [Pa]
J''	=	creep loss compliance [Pa]
ω	=	angular frequency [rad/s]
t	=	transient time [s]
τ_i	=	discrete retardation time, $\tau_i = G_i / \eta_i$ [s]
J_i	=	discrete spectral compliance, $J_i = 1/G_i$ [Pa]

As in the case of the relaxation spectrum, the retardation can alternatively be described as a continuous spectrum given by Equation 5.51.

$$J(t) = J_g + \int_{-\infty}^{\infty} L(\tau) (1 - e^{-t/\tau}) d \ln \tau + \frac{t}{\eta_0} \quad (\text{Continuous retardation spectrum}) \quad (5.51)$$

The spectra $H(\tau)$ and $L(\tau)$ are regarded as a “fingerprint” of the behaviour of a material and the terms $(e^{-t/\tau})$ and $(1 - e^{-t/\tau})$ as “intensity” functions (Jansen 2006, Riande et al. 2000).

5.5.2 Modelling of Test Data

Dynamic shear tests of unaged and aged binders have been performed with constant strain levels within the linear viscoelastic response range. This implies that the test is basically a stress relaxation test which can be modelled using the GMM. A Matlab program developed by Jansen 2006 was used to fit the experimental data to the Prony representation or the GMM model. It is recognized that Prony representations are required as input for FE simulation softwares like ABAQUS.

In fitting the Prony functions (τ_i, G_i) to the laboratory test data (i.e. the storage and loss complex shear modulus master curves at a reference temperatures of 0°C and 20°C), first 2 points of relaxation times (τ_i) were chosen per decade of time and the prediction of the corresponding spectral stiffness (G_i) was performed using a non-negative least squares fitting method in the Matlab program. Equation 5.44 and 5.45 were used in fitting the model to the storage and loss shear modulus data respectively. The transient shear modulus was then determined using Equation 5.42.

In Figure 5.47 and Figure 5.48, the relaxation shear modulus of laboratory aged binders, a 12 year old bitumen from the road and mastics (virgin and LTA bitumen with f/b ratio of 1.0) are shown at a reference temperature of 20°C and 0°C respectively. The corresponding plot of Prony functions (τ_i, G_i) from which the relaxation modulus was predicted is shown in Figure 5.49 and Figure 5.50.

The characteristic material function ($H(\tau)$) versus the relaxation time is also shown in Figure 5.51 and Figure 5.52. The predicted values of the Prony functions are presented in Table 5.20 for a reference temperature of 20°C and in Table 5.21 for a reference temperature of 0°C.

NB: The term binder and bitumen are alternatively used to denote pure bitumen.

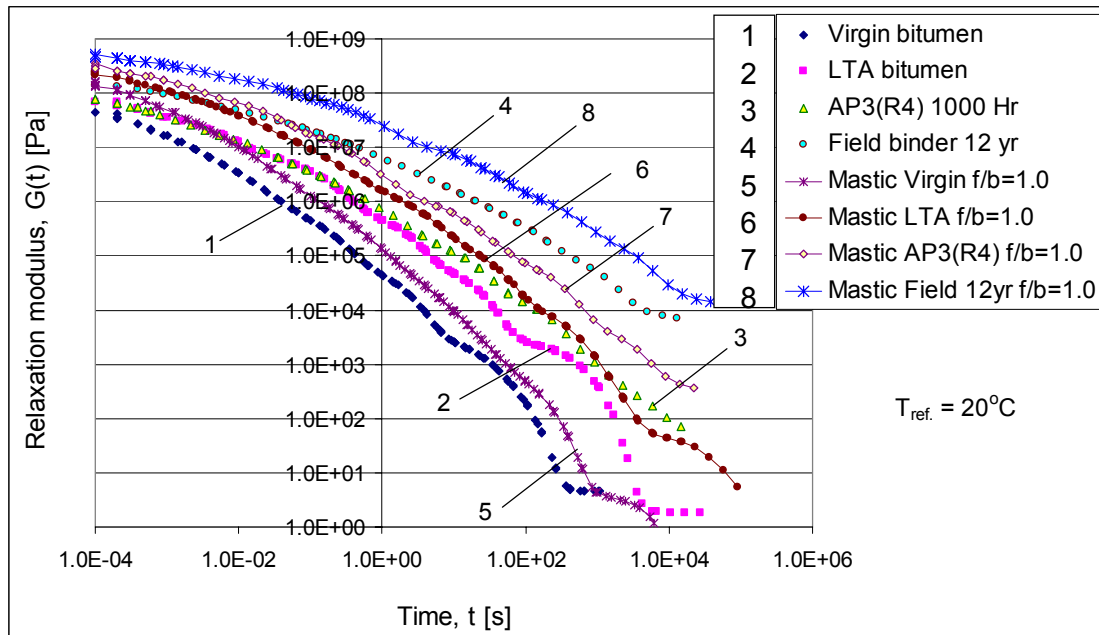


Figure 5.47: Relaxation modulus $G(t)$ of laboratory and field binders and mastics ($T_{ref} = 20^\circ\text{C}$)

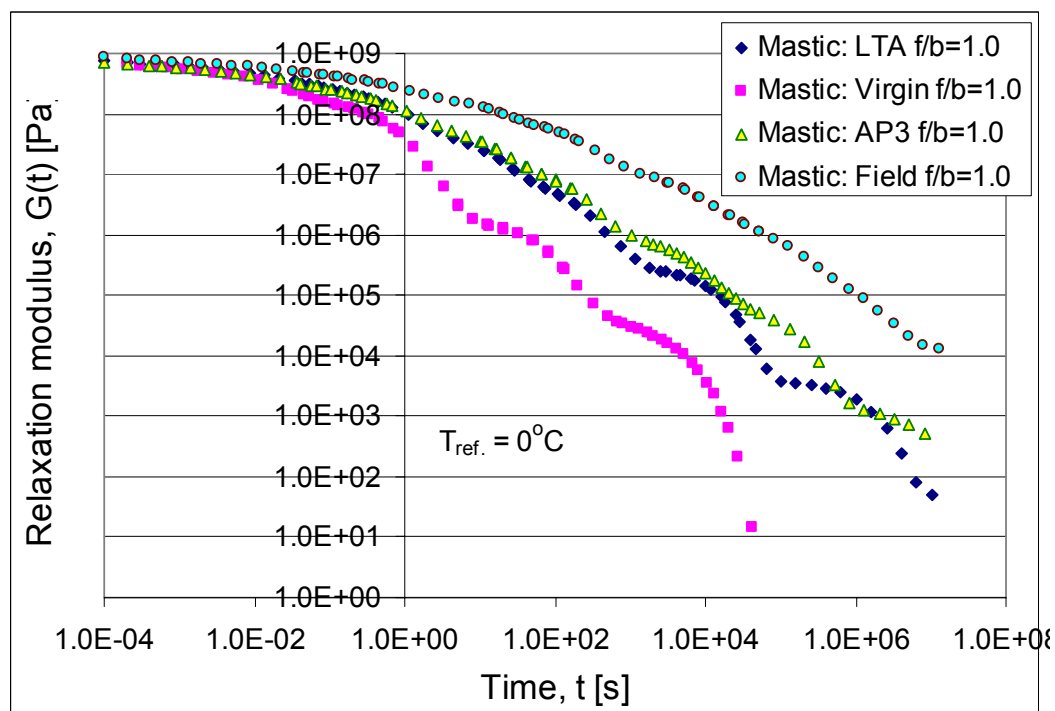


Figure 5.48: Relaxation modulus $G(t)$ of laboratory and field binders and mastics ($T_{ref} = 0^\circ\text{C}$)

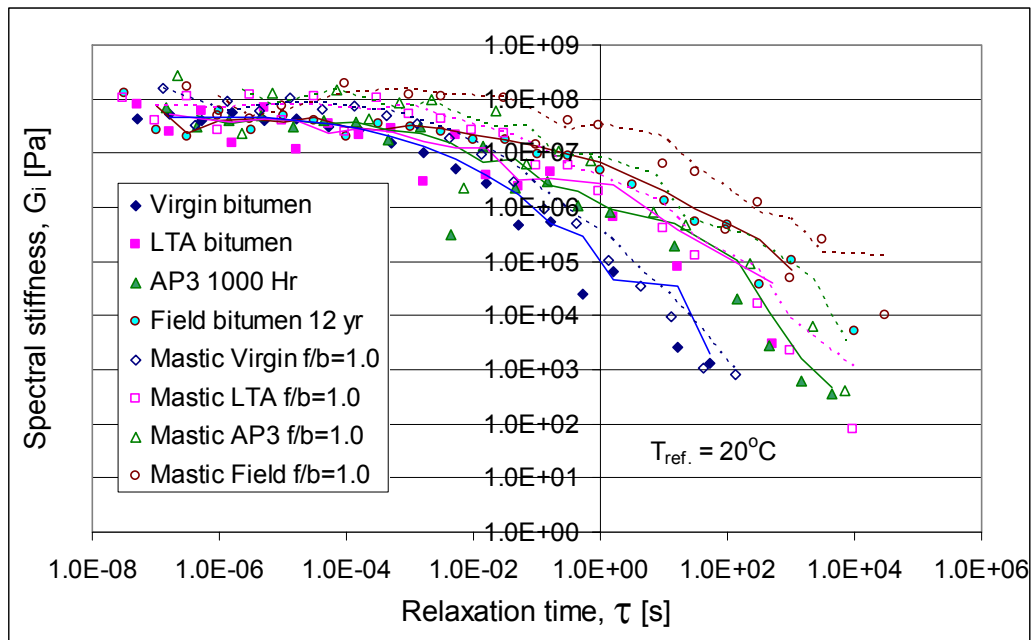


Figure 5.49: Plot of the spectral stiffness G_i versus relaxation time τ ($T_{ref.} = 20^\circ\text{C}$)

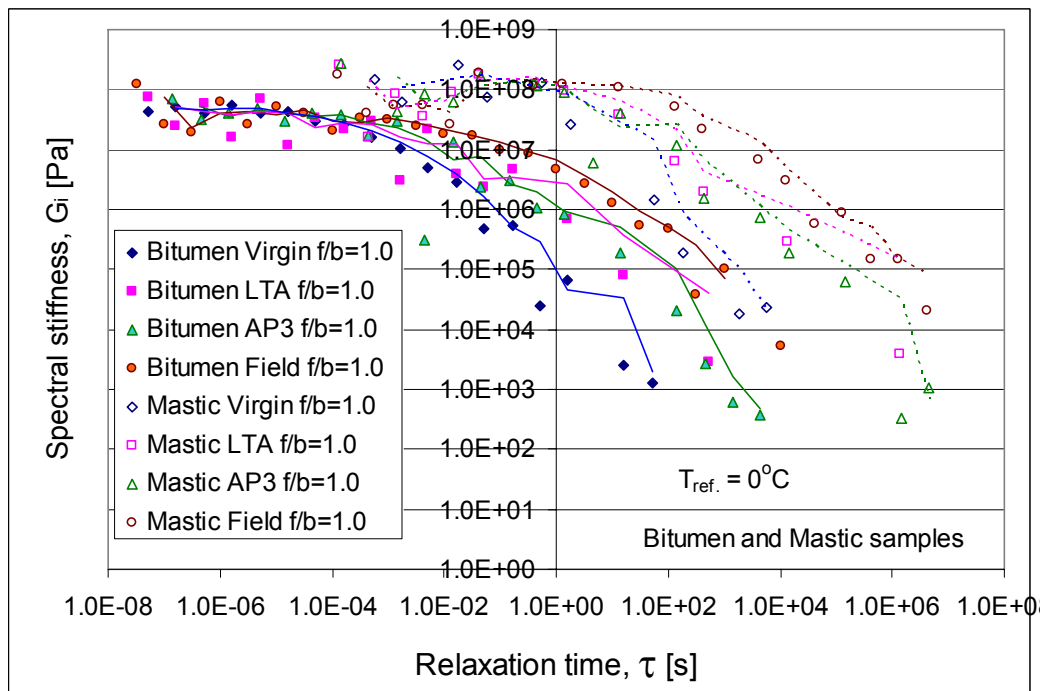


Figure 5.50: Plot of the spectral stiffness G_i versus relaxation time τ ($T_{ref.} = 0^\circ\text{C}$)

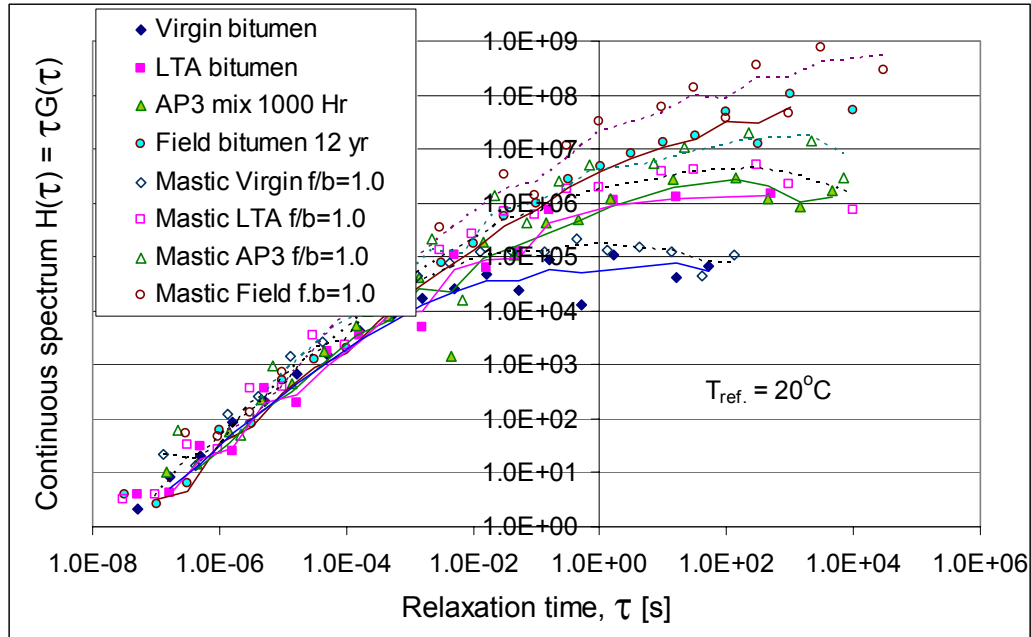


Figure 5.51: Plot of the continuous spectrum $H(\tau)(T_{ref.} = 20^{\circ}C)$

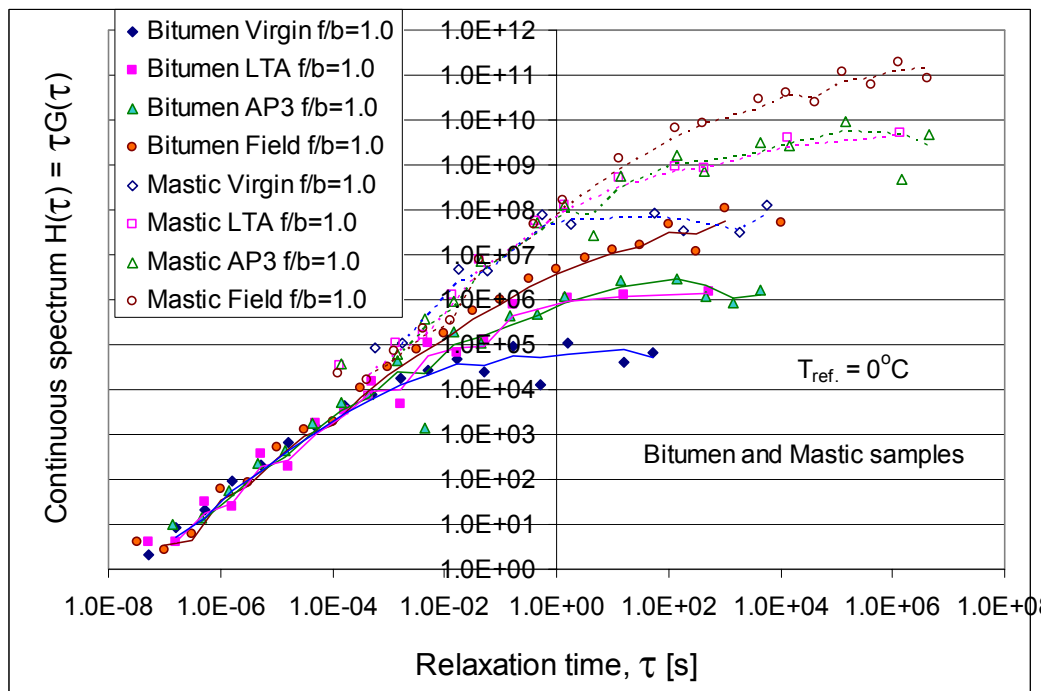


Figure 5.52: Plot of the continuous spectrum $H(\tau)(T_{ref.} = 0^{\circ}C)$

From Figure 5.47 and Figure 5.48, the following can be observed:

- The aged materials show a higher relaxation modulus than the unaged.
- The relaxation modulus of the field material is higher compared to laboratory aged specimens (both with respect to bitumen and mixture aging).

- The 12 year old field binder has greater relaxation modulus than the LTA $f/b=1.0$ and AP3(1000 hr) $f/b=1.0$ mastics.
- The difference in relaxation modulus of the binders is mainly notable at higher loading times. This implies that the aged binders require longer time to relax stress, which has an effect on the response of the binder during repeated loading (fatigue). This may be related to the results of binder fatigue discussed in section 5.4.4. Because of the delayed stress relaxation, the healing of the aged materials may also require more time than the unaged binder.
- The response of the materials indicates that the characteristic of the field binder is different compared to the laboratory aged binders revealing differences in the aging process.

The plots of the Prony functions in Figure 5.49 and Figure 5.50 and the continuous spectrum $H(\tau)$ in Figure 5.51 and Figure 5.52 show the fact that aging has an influence on the higher relaxation times where the function $H(\tau)$ reaches its limiting value. In other words, the limiting value of the aged binders is higher than the unaged binders or it increases with the aging time. In the case of the Prony functions shown in Figure 5.49 and Figure 5.50, the relaxation time increases with the aging of the binder. As expected, the effect of temperature has increased the stiffness of the binders/mastics and the difference between the spectral stiffness of the binders and mastics is more noticeable at low temperature. Similarly, the relaxation time of field binders with different service periods shows an increase with time as shown in Figure 5.54. The limiting value of the continuous spectrum function $H(\tau)$ also increases with time as shown in Figure 5.55.

Table 5.20: Predicted values of Prony functions by fitting the viscoelastic data of laboratory and field binders (T_{ref} , 20°C)

Virgin bitumen			LTA bitumen			AP3: 1000 hrs			Field binder, 12 yrs		
τ	G_n	$G(\tau)$	τ	G_n	$G(\tau)$	τ	G_n	$G(\tau)$	τ	G_n	$G(\tau)$
5.15E-08	42389779	2.1817	5.15E-08	77134846	3.97	4.43E-07	70614265	10.1073	3.18E-08	125181060.9	3.9759
1.63E-07	52496739	8.5441	1.63E-07	25179404	4.0981	4.53E-07	31459686	14.2396	1E-07	26251414.87	2.6366
5.15E-07	39611375	20.3871	5.15E-07	59431313	30.588	1.43E-06	40051397	57.3271	3.18E-07	19909811.5	6.3236
1.63E-06	54920035	89.3855	1.63E-06	15817366	25.7437	4.53E-06	48949651	221.5605	1E-06	62497145.29	62.7704
5.15E-06	40084012	206.3038	5.15E-06	69948370	360.0093	1.43E-05	30559077	437.4041	3.18E-06	26043717.3	82.7176
1.63E-05	41924256	682.3411	1.63E-05	11965809	194.7503	4.53E-05	39856322	1804.014	1E-05	51010387.23	512.3344
5.15E-05	30433603	1566.353	5.15E-05	34077294	1753.886	0.000143	37148030	5317.144	3.18E-05	40507960.27	1286.575
0.000163	25943709	4222.486	0.000163	21959959	3574.108	0.000453	17382856	7867.99	0.0001	19975075.29	2006.242
0.000515	15732794	8097.333	0.000515	29036598	14944.52	0.001431	30076828	43050.15	0.000318	34679273.69	11014.5
0.001628	10525895	17131.49	0.001628	3018569	4912.892	0.004526	312181.5	1413.025	0.001004	31252678.14	31389.33
0.005147	5112131	26311.05	0.005147	21573813	111035.8	0.014313	13338973	190926	0.003176	25116961.76	79774.11
0.016276	2872390	46749.78	0.016276	3979332	64765.89	0.045263	2347182	106240.3	0.010044	17801813.43	178796.5
0.051468	476725.3	24536.03	0.051468	2387489	122879	0.143134	2947722	421919.1	0.031761	17366494.44	551578.1
0.162756	547325.9	89800.4	0.162756	4634745	754331.1	0.452629	1068607	483682.8	0.100437	9754465.069	979711.8
0.514679	24446.25	12581.96	1.627557	680292.5	1107215	1.431339	822452.2	1177208	0.317611	8821926.774	2801937
1.627557	66624.41	108435	16.27557	78765.25	1281949	14.31339	187421.2	2682634	1.004373	4711698.9	4732301
16.27557	2577.315	41947.26	514.6786	2907.93	1496650	143.1339	20456.25	2927983	3.176105	2667693.078	8472874
51.46786	1272.98	65517.55				452.6293	2699.226	1221748	10.04373	1314134.362	13198806
						1431.339	609.5986	872542.5	31.76105	531209.2686	16871765
						4526.293	361.9389	1638242	100.4373	481693.4812	48379974
									317.6105	38621.4625	12266582
									1004.373	104339.1561	1.05E+08

Mastic: Virgin f/b=1.0			Mastic: LTA f/b=1.0			Mastic: AP3(1000hr) f/b=1.0			Mastic: Field12yr f/b=1.0		
τ	G_n	$G(\tau)$	τ	G_n	$G(\tau)$	τ	G_n	$G(\tau)$	τ	G_n	$G(\tau)$
1.33E-07	1.6E+08	21.2183	3.06E-08	1.07E+08	3.2677	2.2E-07	2.76E+08	60.8703	3.03E-07	173129366.9	52.4634
4.2E-07	31670144	13.3068	9.67E-08	40808032	3.9464	2.2E-06	23209445	51.1636	9.58E-07	49535492.09	47.4682
1.33E-06	91631478	121.7497	3.06E-07	1.09E+08	33.2417	6.97E-06	1.33E+08	925.8247	3.03E-06	44217693.17	133.993
4.2E-06	61589848	258.7809	9.67E-07	27161327	26.2666	6.97E-05	1.52E+08	10624.64	9.58E-06	74526807.61	714.165
1.33E-05	1.07E+08	1415.692	3.06E-06	1.2E+08	368.1497	0.00022	43559613	9602.416	9.58E-05	190612998.5	18265.79
4.2E-05	63299076	2659.625	9.67E-06	41201158	398.4388	0.000697	82955771	57828.66	0.000958	118654597.7	113702.7
0.000133	75436739	10023.19	3.06E-05	1.16E+08	3538.788	0.002204	95038842	209506.6	0.00303	115761384.8	350792.1
0.00042	50696736	21301.15	9.67E-05	24470611	2366.449	0.006971	2242266	15630.89	0.030303	107635138.4	3261671
0.001329	34591408	45961.19	0.000306	1.06E+08	32400.91	0.022044	60670001	1337428	0.095827	14340951.36	1374245
0.004202	18744498	78758.39	0.000967	54478278	52683.62	0.06971	6264655	436710.5	0.30303	38917166	11793081
0.013287	9510277	126361.9	0.003058	44375201	135704	0.220443	11225937	2474680	0.958266	33224749.9	31838147
0.042017	3025116	127105.7	0.009671	26847119	259627.1	0.697102	7430441	5179778	9.58266	6256924.432	59957977
0.132869	953986	126755	0.030581	23321972	713210.2	6.971023	792878.4	5527173	30.30303	4571826.803	1.39E+08
0.420168	501215.5	210594.8	0.096706	6114143	591272.7	22.04431	486477.9	10724070	95.8266	380320.4967	36444818
1.328688	102036.9	135575.2	0.30581	5964246	1823928	220.4431	92737.29	20443296	303.0303	1217367.968	3.69E+08
4.201681	35704.86	150020.4	0.967057	1977224	1912089	2204.431	6247.529	13772246	958.266	48496.2677	46472322
13.28688	9489.619	126087.4	9.670574	398742.4	3856068	6971.023	407.6248	2841562	3030.303	246150.6441	7.46E+08
42.01681	1041.129	43744.89	30.58104	132538.3	4033158				30303.03	9892.1388	3E+08
132.8688	806.9047	107212.5	305.8104	16057.45	4910534						
			967.0574	2281.599	2206437						
			9670.571	77.8855	753197.3						

Table 5.21: Predicted values of Prony functions by fitting the viscoelastic data of laboratory and field binders (T_{ref} , 0°C)

Virgin1.0			LTA1.0			AP3(1000hr)1.0			Field1.0		
τ	G_n	$G(\tau)$	τ	G_n	$G(\tau)$	τ	G_n	$G(\tau)$	τ	G_n	$G(\tau)$
0.000569	1.52E+08	86423.4188	0.000135	2.59E+08	351110.38	0.000142	2.68E+08	38049.12	0.000129	1.82E+08	23456.07
0.0018	60727235	109322.8289	0.000428	16338509	6998.963	0.001417	42932919	60856.6	0.000408	39823274	16243.26
0.018002	2.59E+08	4666119.14	0.001355	83371202	112937.3	0.004482	84241505	377609.9	0.00129	56652504	73072.74
0.056928	74338994	4231984.209	0.004284	36734197	157359.1	0.014175	64267639	910981.7	0.004079	54919973	224009.6
0.569282	1.33E+08	75624315.96	0.013546	92249132	1249636	0.044825	1.67E+08	7468363	0.012898	26689267	344249.2
1.800227	26270335	47292575.16	0.042837	1.8E+08	7721992	0.448247	1.15E+08	51517033	0.040788	1.84E+08	7517861
56.92819	1489428	84790462.19	0.428372	1.27E+08	54207982	1.417481	88245400	1.25E+08	0.407884	1.17E+08	47549163
180.0227	188010.9	33846231.52	1.354632	95743745	1.3E+08	4.482469	6150993	27571636	1.289841	1.23E+08	1.59E+08
1800.227	17986.23	32379296	13.54632	38283162	5.19E+08	14.17481	41209671	5.84E+08	12.89841	1.09E+08	1.41E+09
5692.819	22582.76	128559572.8	135.4632	6529541	8.85E+08	141.7481	11774999	1.67E+09	128.9841	50655306	6.53E+09
			428.3722	1930059	8.27E+08	448.2469	1565531	7.02E+08	407.8836	21376769	8.72E+09
			13546.32	290409	3.93E+09	4482.469	724199.6	3.25E+09	4078.836	6868193	2.8E+10
			1354632	3825.117	5.18E+09	14174.81	187289.2	2.65E+09	12898.41	3127667	4.03E+10
						141748.1	63776.66	9.04E+09	40788.36	588724.1	2.4E+11
						1417481	334.0691	4.74E+08	128984.1	891758.2	1.15E+11
						4482469	1072.993	4.81E+09	407883.6	145128.4	5.92E+10
									1289841	146871.5	1.89E+11
									4078836	20860.87	8.51E+10

The results of relaxation modulus of field binders recovered from road sections with different service life are shown in Figure 5.53. The figure also includes the virgin and the AP3 bitumen (bitumen recovered from aging protocol 3). The relaxation modulus of the AP3 bitumen is comparable with the relaxation modulus of the 1 year field aged binder. Similar results were also obtained on the complex shear modulus of the binders. Therefore, the same conclusions can be drawn with respect to the aging of the laboratory and field binders – the laboratory aging protocols, both the standard aging and the proposed mixture aging, did not simulate the complex nature of field aging accurately.

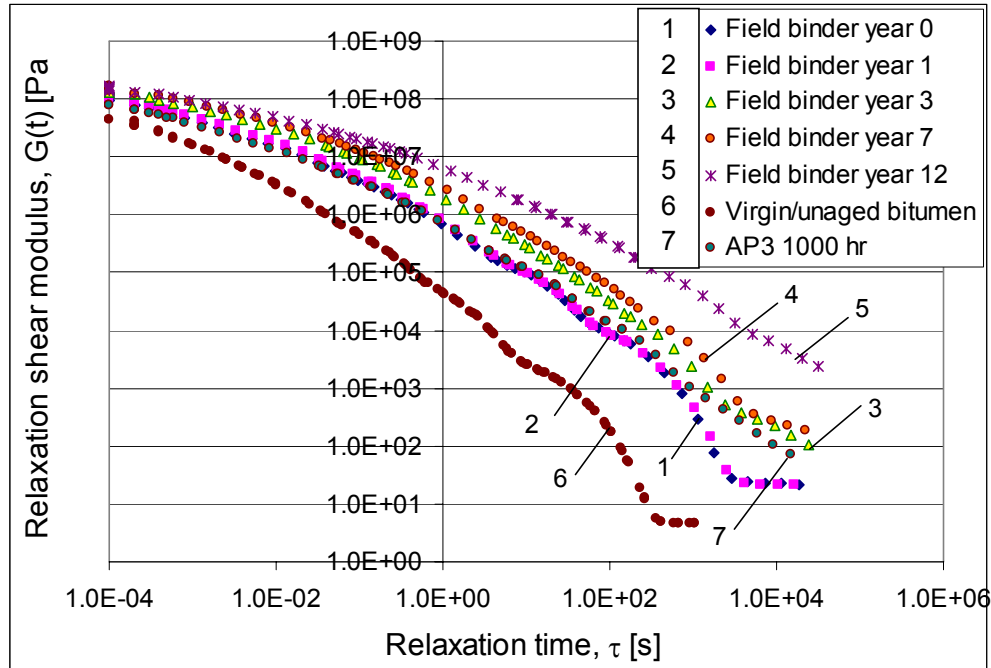


Figure 5.53: Relaxation modulus $G(t)$ of field with service life 0, 1, 3, 7, and 12 year and laboratory aged binders ($T_{ref} = 20^{\circ}\text{C}$)

In Figure 5.54 and Figure 5.55, the plots of the Prony functions (τ_i, G_i) and the continuous spectral function $H(\tau)$ are shown respectively. The Prony functions are also presented in Table 5.23. Similar trends of the change of the relaxation modulus are predicted for the field binders as for the laboratory aged binders.

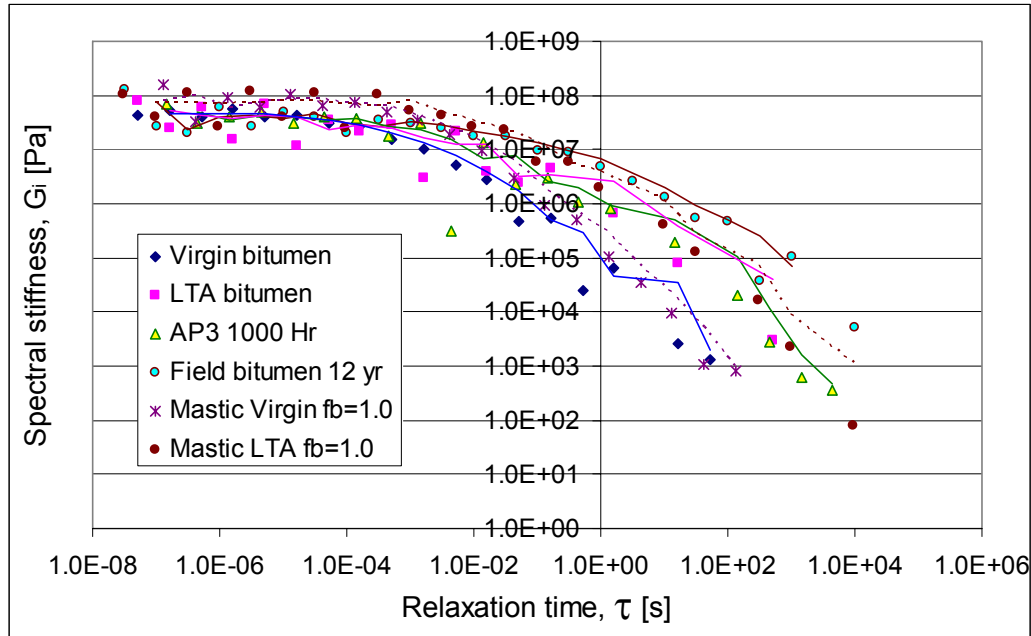


Figure 5.54: Spectral stiffness G_i versus relaxation time τ plot of field binders ($T_{ref.} = 20^\circ\text{C}$)

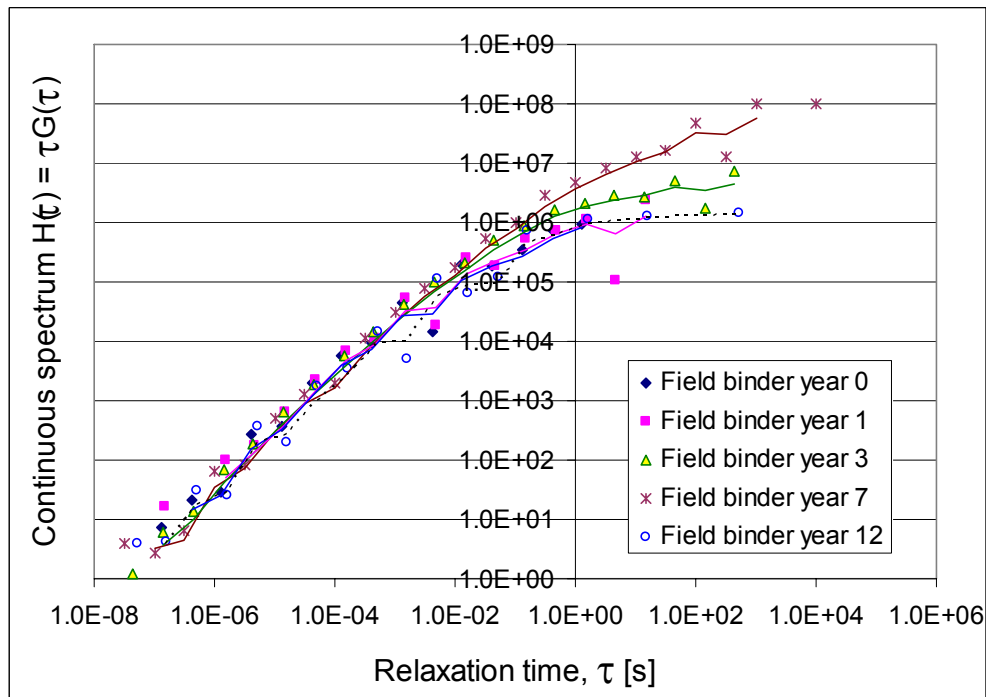


Figure 5.55: The continuous spectrum $H(\tau)$ plot of field binders ($T_{ref.} = 20^\circ\text{C}$)

Table 5.22: Prediction of the Prony functions in fitting the viscoelastic data of field binders with zero (after construction), 1, and 3 year of service life

Year 0			Year 1			Year 3		
τ	G_n	η	τ	G_n	η	τ	G_n	η
1.31E-07	57844945	7.5526	1.51E-07	1.06E+08	16.0279	4.46E-08	26322537	1.1731
4.13E-07	50828603	20.9864	1.51E-06	66441603	100.0393	1.41E-07	44486662	6.2694
1.31E-06	22277280	29.0866	4.76E-06	37697647	179.4918	4.46E-07	31449723	14.0156
4.13E-06	67105453	277.0693	1.51E-05	41790718	629.2311	1.41E-06	48479408	68.3208
1.31E-05	28282888	369.2788	4.76E-05	48648056	2316.306	4.46E-06	42384866	188.8888
4.13E-05	49384123	2039.004	0.000151	45830432	6900.56	1.41E-05	45094267	635.5018
0.000131	43370164	5662.676	0.000476	23190824	11041.97	4.46E-05	42479468	1893.104
0.000413	22205059	9168.168	0.001506	36675958	55221.96	0.000141	39775453	5605.451
0.001306	33685122	43981.37	0.004761	3872934	18440.41	0.000446	32170637	14336.9
0.004129	3429959	14161.83	0.015057	16676928	251099.8	0.001409	29222089	41181.93
0.013057	14923819	194854.6	0.047614	3944161	187795.4	0.004457	22179508	98843.33
0.041289	4473230	184693.6	0.150567	3477981	523669.8	0.014093	14988732	211232.3
0.130566	2636556	344244.9	0.476135	1569846	747459	0.044565	11015422	490904
0.412886	1785151	737064.5	1.505672	770796.5	1160567	0.140927	6143764	865824.7
1.305662	710246.8	927342	4.761353	22032.99	104906.9	0.445652	3790441	1689216
13.05662	175256	2288250	15.05672	160354.9	2414418	1.409274	1474153	2077485
130.5662	11379.54	1485783	150.5672	10112.29	1522579	4.456516	638454.4	2845282
412.8864	4387.186	1811410	476.1353	3695.78	1759691	14.09274	198048.5	2791046
13056.72	3.9204	51187.55				44.56516	114249.4	5091544
						140.9274	12084.22	1702997
						445.6516	16055.85	7155316
						4456.516	288.1559	1284172
						14092.74	243.6856	3434197

Table 5.23: Prediction of the Prony functions in fitting the viscoelastic data of field binders with 7 and 12 years of service life

Year 7			Year 12		
τ	G_n	η	τ	G_n	η
2.44E-08	83526762	2.0399	3.18E-08	1.25E+08	3.9759
7.72E-08	11055975	0.8539	1E-07	26251415	2.6366
2.44E-07	49908154	12.1889	3.18E-07	19909812	6.3236
7.72E-07	35608205	27.5006	1E-06	62497145	62.7704
2.44E-06	49171424	120.0895	3.18E-06	26043718	82.7176
7.72E-06	43301752	334.4243	1E-05	51010387	512.3344
2.44E-05	46613854	1138.433	3.18E-05	40507961	1286.575
7.72E-05	44212061	3414.547	0.0001	19975074	2006.242
0.000244	34462291	8416.595	0.000318	34679276	11014.5
0.000772	34543430	26678.28	0.001004	31252674	31389.33
0.002442	28030172	68457.03	0.003176	25116970	79774.14
0.007723	21424261	165462	0.010044	17801800	178796.4
0.024423	14847606	362617.5	0.031761	17366517	551578.8
0.077231	10861388	838837.1	0.100437	9754428	979708
0.244226	5781234	1411929	0.317611	8821994	2801958
0.772311	3820816	2950859	1.004373	4711570	4732172
2.442262	1202582	2937020	3.176105	2667924	8473608
7.723111	653065	5043694	10.04373	1313761	13195053
24.42262	187028.9	4567735	31.76105	531821	16891192
77.23111	124652.1	9627021	100.4373	480618.8	48272033
244.2262	6384.058	1559154	317.6105	40518.03	12868951
772.3111	17254.88	13326138	1004.373	102018.4	1.02E+08
7723.111	350.107	2703915	10043.73	9993.957	1E+08

5.5.3 Finite Element Modelling

A few Finite Element runs were performed in order to analyse the stress situation of the binding material in PA under real traffic loading. The prony series representation of materials was used as input for the binder/mastic viscoelastic behaviour. Four materials at temperatures of 0°C and 20°C were analysed using the FEM software ABAQUS following the principles developed by Huurman et al. (2008). The simulation plan using the unaged and aged binders/mortar is shown in Table 5.24.

Table 5.24: Bituminous materials analysed using FEM

Mastic (f/b = 1.0)	Virgin bitumen	LTA bitumen	AP3 (1000 hr)	Field (12 yr)
- 0°C	x	x	x	x
- 20°C	x			x

The 2D PA structure used to perform the FEM is shown in Figure 5.56. As shown in Figure 5.57 and Figure 5.58, two points were considered for analysing the stress conditions in the binding material. These points were considered because earlier research (Woldekidan 2006, Huurman et al. 2008) has shown that the largest stresses and strains occur in these points when the aggregate skeleton is loaded by a moving wheel load. It should be noted that Huurman et al. (2008) also provided finite element meshes for real aggregate skeletons. In order not to complicate the comparison of the binders by introducing effects of the aggregate skeleton, the idealized aggregate structure shown in Figure 5.56 was used instead of a realistic skeleton.

Two trucks travelling at a speed of 80 Km/h were simulated for the prediction of the stress, strain, and dissipated energy in the binding material. Each truck has two axles with 80 KN load per axle; the rear axle is motor driven while the front one is rolling. The FEM of the materials in ABAQUS was performed in accordance to the procedures developed in the Lifetime Optimization Tool (LOT) project by Huurman et al. (2008).

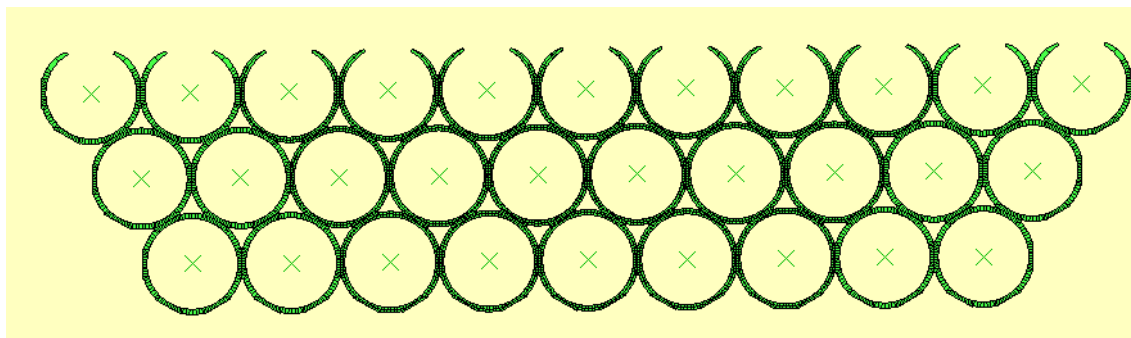


Figure 5.56: PA structure used to perform FE analysis of stresses of binders and mortars using ABAQUS

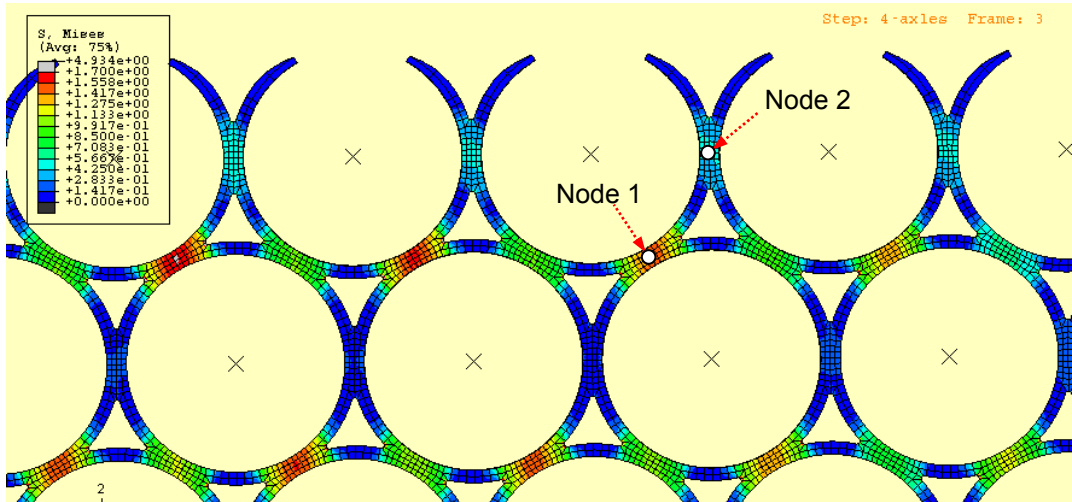


Figure 5.57: PA geometry used for modeling using FEM

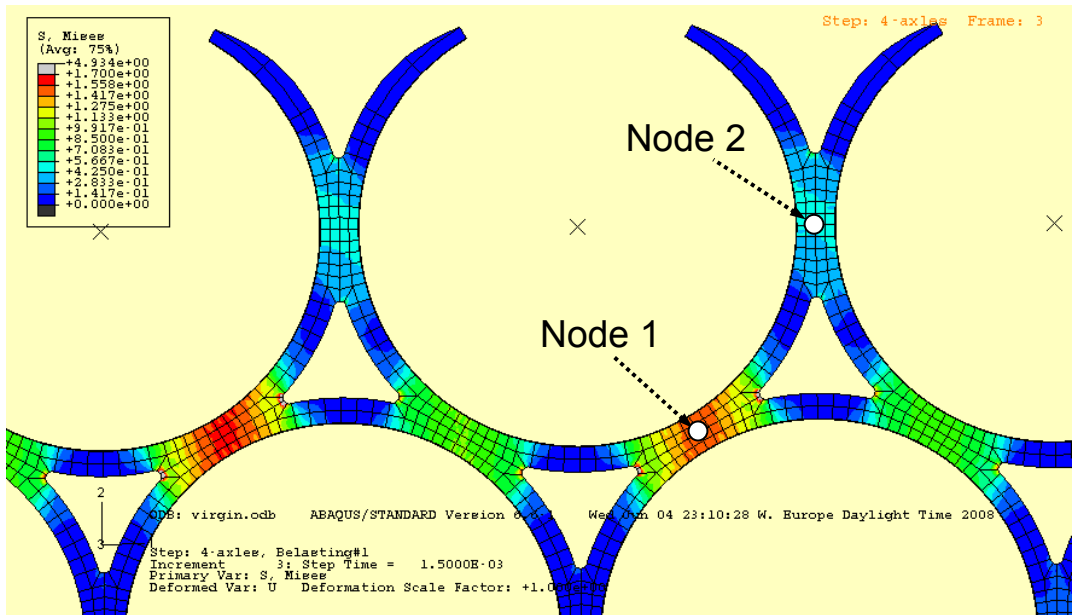


Figure 5.58: The stress conditions in the binding material / mastic

Input data and simulation results

The ABAQUS program requires the viscoelastic property (α_i^E, τ) of the binder/mastic as an input data based on Equation 5.52. Hence, the factor α_i^E was recalculated from the prony series (G_i, τ) predicted in section 5.5.2. A poisson's ratio of 0.45 was considered for all the materials.

$$E(t) = E_0 \left(1 - \sum_{i=1}^n \alpha_i^E (1 - \exp(-t / \tau)) \right) \quad (5.52)$$

$$\alpha_i^E = (E_i - E_{i-1}) / E_0 \quad ; \quad E_i = G_i \cdot 2(1 + \nu)$$

Where:

- $E(t)$ = stiffness as a function of time [MPa]
 E_0 = instantaneous stiffness [Pa]
 n = number of terms in the prony series [-]
 i = term indicator
 α_i^E = relative reduction of stiffness due to i^{th} term
 t = time [s]
 τ = relaxation time [s]
 G_i = Shear modulus of the i^{th} term
 E_i = Elastic modulus of the i^{th} term
 ν = Poissons ratio (0.45) [-]

To get an insight into the performance of the binding materials, a dissipated energy analysis was considered at the selected nodes in the mastic. Details of the stress conditions in the mastic are shown in Figure 5.58. The results of the FEM simulation, i.e. the strain, stress, and dissipated energy as a function of loading time, for the unaged mastic (Virgin $f/b=1.0$) at a temperature of 0°C is shown in Figure 5.59, Figure 5.60, and Figure 5.61 respectively.

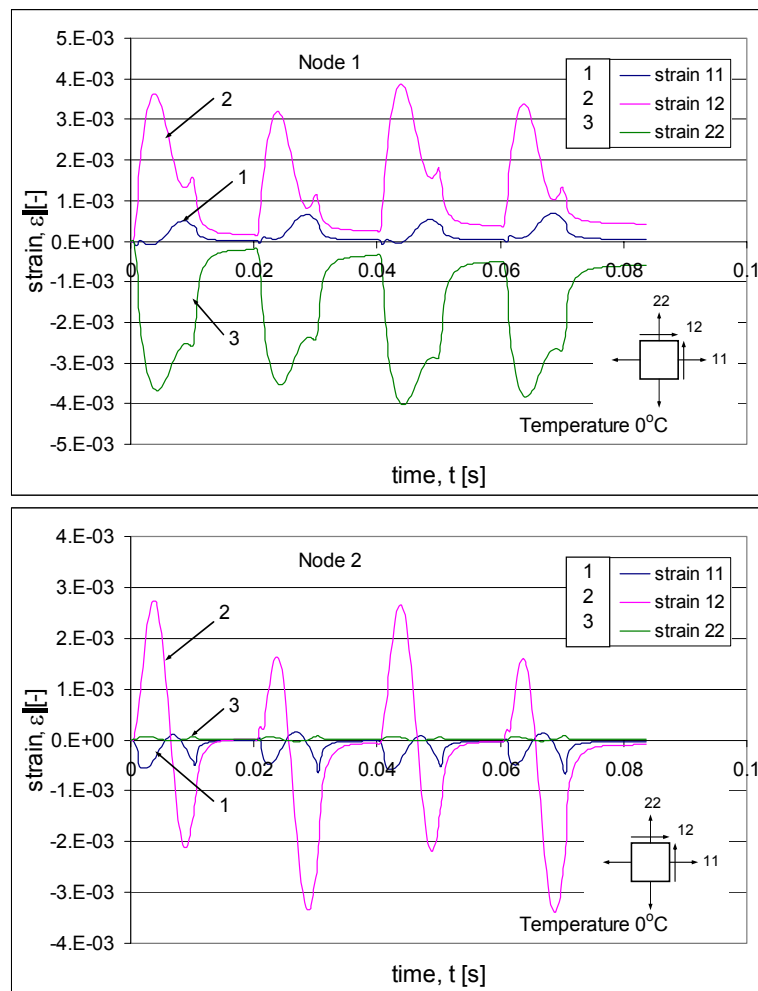


Figure 5.59: Strain in the principal directions at node 1 and 2 (mastic virgin $f/b=1.0$, 0°C)

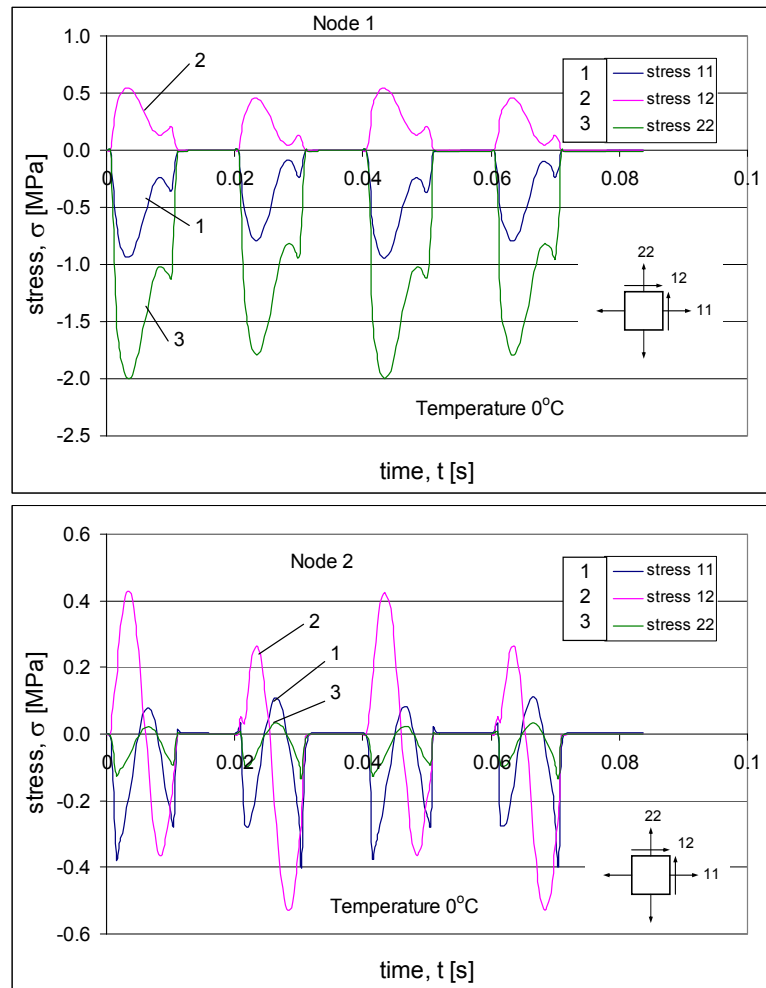


Figure 5.60: Stress in the principal directions at node 1 and 2 (mastic virgin $f/b=1.0$, 0°C)

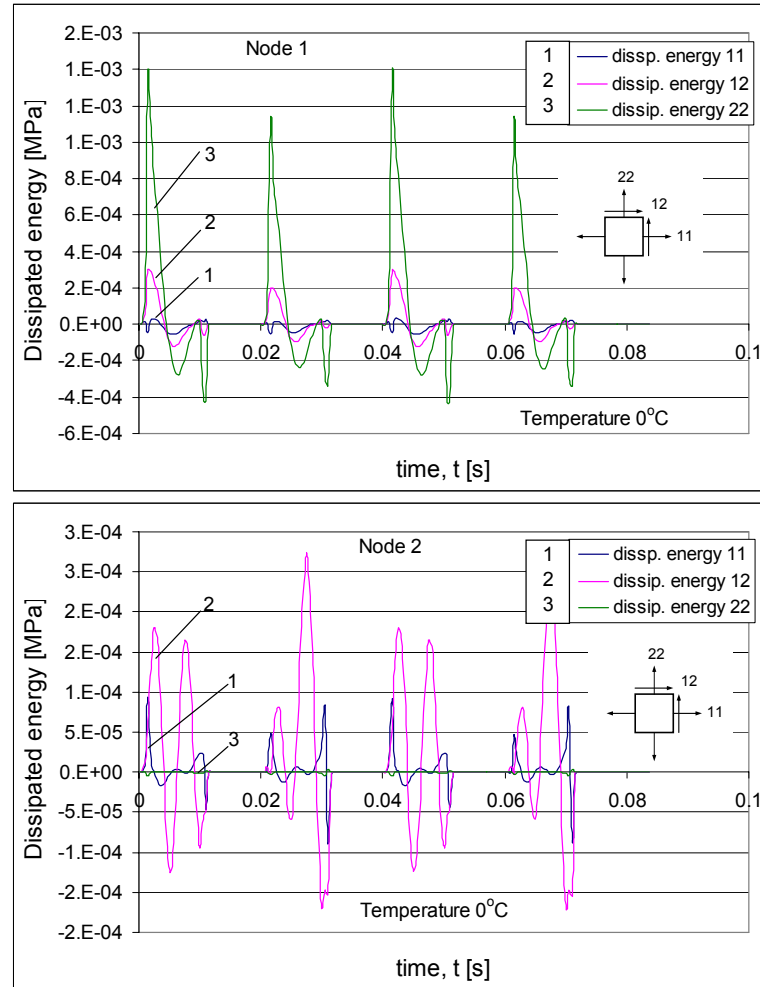


Figure 5.61: Dissipated energy in the principal directions at node 1 and 2 (mastic virgin $f/b=1.0$)

The dissipated energy has been determined by calculating the area under the stress-strain curve. The dissipated energy in the principal directions 11, 12, and 22, the total dissipated energy (which is the summation of dissipated energies in the principal directions)⁸, and the maximum Von Mises stress (VMS) at node 1 and 2 are shown in Table 5.25. It is recalled that the Von Mises stress is defined as (Equation 5.53):

$$\sigma_v = \sqrt{\frac{(\sigma_1 - \sigma_2)^2 + (\sigma_2 - \sigma_3)^2 + (\sigma_3 - \sigma_1)^2}{2}} \quad (5.53)$$

Where:

σ_v = Von Mises equivalent stress [MPa]
 $\sigma_1, \sigma_2, \sigma_3$ = stresses in the principal coordinates [MPa]

⁸ In principle, dissipated energy can not be negative. The negative sign in Table 5.25 indicates that the work done is counter to the dissipated energy due to the traffic loading because of the confinement from the sides. Hence, the total dissipated energy is the net dissipated energy in the principal directions.

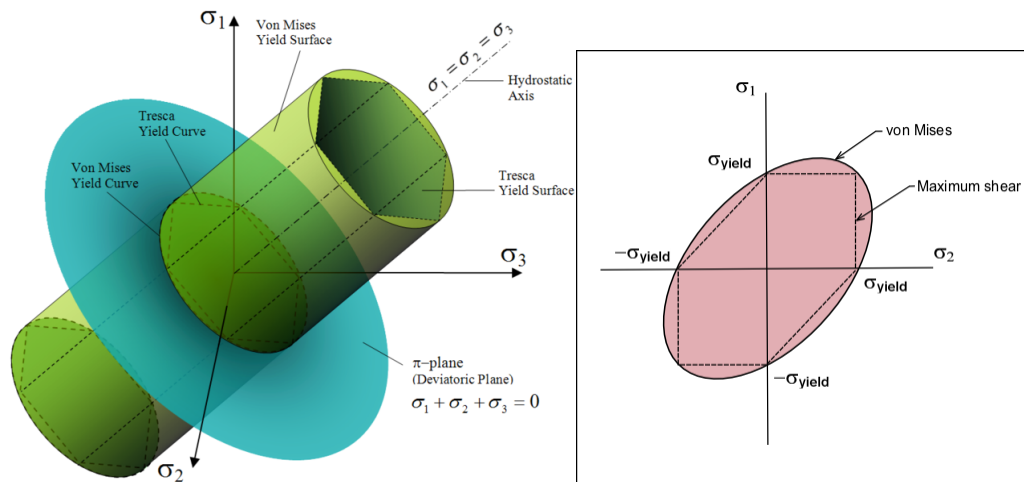


Figure 5.62: Von Mises yield surface in principal stress coordinates (Wikipedia 2008)

From Table 5.25, one can observe that the dissipated energy in the different directions seems to be similar for the virgin and field mastics at 0°C, but the field material dissipates less energy at a temperature of 20°C. The mastics made from laboratory aged binders (LTA and AP3 mastics) show higher dissipated energy than the virgin and field mastics. Since the stiffness of the field material is greater than the stiffness of laboratory aged binders and the response in the FEM is in the linear region, it is expected that the field mastic should be able to absorb most of the input energy and dissipate less energy than the laboratory binders. Because of its sensitivity to damage (cracking) of aged binders at low temperatures, it is considered crucial to look at the strain levels to further evaluate the performance of the binders. Accordingly, the hysteresis diagrams of the virgin and field mastics are shown in Figure 5.63 and Figure 5.64 for node 1 and 2 respectively.

Table 5.25: Dissipated energy and Von Mises stress (VMS) at node 1 and 2

Node	Temp. (°C)	Mastic	Dissipated energy * [MPa]				max. VMS
			axis 11	axis 12	axis 22	Total	[MPa]
1	0	Virgin f/b=1.0	-8.22E-04	1.65E-03	7.90E-03	8.73E-03	1.9720
		LTA f/b=1.0	-5.53E-04	3.16E-04	2.00E-03	1.76E-03	1.9333
		AP3(R4) f/b=1.0	-5.14E-04	3.71E-04	2.24E-03	2.09E-03	1.9276
		Field12yr f/b=1.0	-9.82E-04	1.63E-03	8.04E-03	8.68E-03	1.9801
	20	Virgin f/b=1.0	-3.39E-03	1.65E-02	8.18E-02	9.49E-02	2.0328
		Field12yr f/b=1.0	-1.95E-03	5.43E-03	2.59E-02	2.94E-02	2.0186
2	0	Virgin f/b=1.0	3.77E-04	2.66E-03	-1.51E-05	3.03E-03	0.9152
		LTA f/b=1.0	6.37E-05	4.34E-04	-2.76E-06	4.95E-04	0.9011
		AP3(R4) f/b=1.0	5.57E-05	4.84E-04	-2.44E-06	5.38E-04	0.8982
		Field12yr f/b=1.0	3.17E-04	2.60E-03	-1.27E-05	2.90E-03	0.9188
	20	Virgin f/b=1.0	2.22E-03	2.06E-02	-9.08E-05	2.27E-02	0.9321
		Field12yr f/b=1.0	9.84E-04	8.46E-03	-3.95E-05	9.40E-03	0.9317

NB: Principal axis 11 represents the principal axis along the longitudinal (traffic) direction.
Principal axis 22 represents the axis along the depth of the PA.
Principal axis 33 represents the axis along the x-section. (In 2D modelling the axis 33 is constrained).

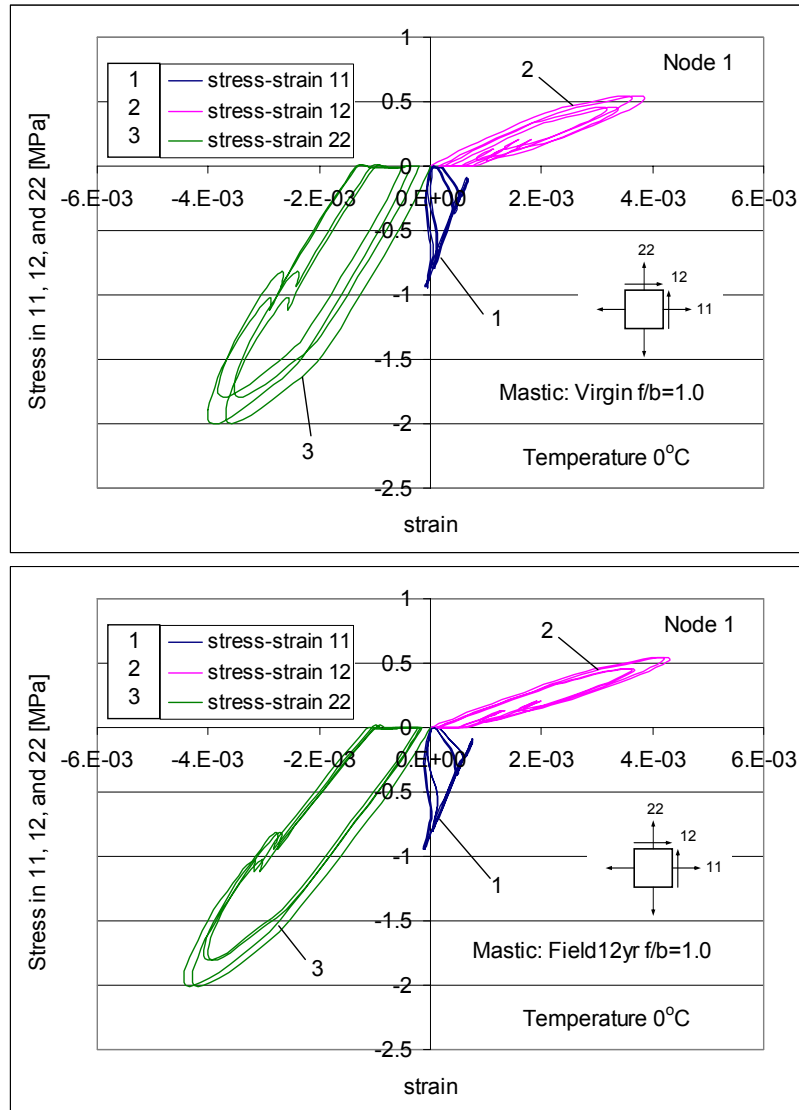


Figure 5.63: Stress-strain hysteresis diagram for virgin and field materials at node 1

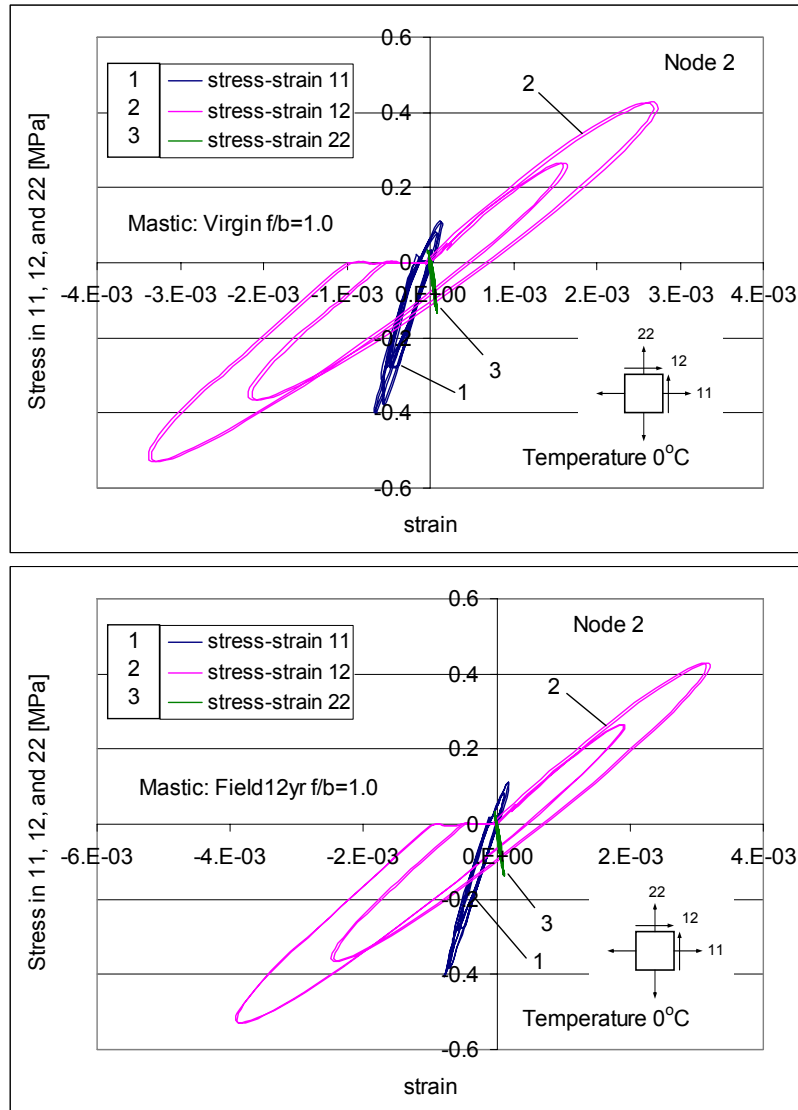


Figure 5.64: Stress-strain hysteresis diagram for virgin and field materials at node 2

From Figure 5.63 and Figure 5.64, it can be observed that the stress levels are the same in the unaged and field aged binding materials. It can also be observed that the strain level in the field mastic is equivalent to the unaged mastic. This signifies that the likelihood of the field material to damage accumulation is greater because of its poor fatigue performance when subjected to same strain (refer to section 5.4.4).

Note that the virgin and 12 years old field mastics have comparable dissipated energy loops. The FEM simulation, however, is performed in the linear response of the materials. Hence, combining the performance of the binder fatigue with the dissipated energy can provide the basis for proper interpretation of the binding materials performance.

Discussion

The expectation from the FEM simulation was that higher stresses would develop in the aged mastics than in the unaged one. In reality, however, the results show that there is no significant difference in the stress conditions for unaged and aged mastics. From Table 5.25, one can observe that the difference in Von Misses stress of the mastics is almost nil at the simulated temperatures. The influence of the stress condition on the performance of the binding materials can be interpreted as follows.

The aged mastics are likely to sustain more damage as a result of the stresses developed in the binding material because of reduced relaxation behaviour of the mastics (longer time required to relax stress) at low temperatures. It could mean that the aged mastics will sustain the stresses with damage incurred (micro-cracking) while the unaged mastic will relax (deform) to decay the stress. In other words, the fatigue life of the binder/mastic becomes important to distinguish the performance of the materials to failure. The binder fatigue test results (strain controlled) presented in section 5.4.4 show that the laboratory aged binders perform better, but the 12 year old field binder has lower fatigue life compared to the unaged bitumen. This results in a simple but important conclusion that one has to be careful to use fatigue results of laboratory aged binders and mastics for pavement life predictions.

As aging reduces the binder fatigue life and increases the temperature at which the binder's critical temperature occurs (transition to brittle behaviour), the aged materials will perform poorly at low temperatures. Low temperature is regarded critical for PA performance as damage accumulation is accelerated facilitating the occurrence of ravelling.

5.6 Findings and Summary

The main findings of the rheological investigation are summarized below.

5.6.1 In relation to Low Temperature Properties

- Aging reduces the penetration value of bitumen and increases the softening point (ring and ball temperature), which signifies an increase in the critical temperature of the binder (The critical temperature depends on the type of test and is defined as a temperature at which the binder reaches the transition to a brittle behaviour). The Fraass temperature of the aged binders has shown a shift towards higher temperature with reference to the virgin bitumen. A rise in Fraass temperature from -15°C corresponding to the virgin bitumen to $> 0^{\circ}\text{C}$ for field binders with service life of 3 years and older was noticed when estimating the Fraass breaking point by means of the Bitumen Test Data Chart (BTDC) using the penetration and softening points

of the binders as input. The long term aged binder using standard laboratory aging method has shown lower Fraass temperature than the 1 year old field binder which has a Fraass temperature below 0°C. An increase in the Fraass temperature is an indication of the sensitivity to damage of the aged binders at relatively higher temperatures than the virgin/unaged bitumen.

- The critical temperature predictions based on the conventional binder properties, i.e. penetration and softening point, implies that the effect of traffic has negative implications on the performance of PA after 3 years of its service life. This is because of low temperatures reaching 0°C during the winter periods. The results substantiate the occurrence of ravelling on PA roads during and immediately after the winter periods.
- Bending Beam Rheometer (BBR) test results indicate that the aged binders/mastic show an increase in the stiffness modulus but at the same time a decrease in the m -value (slope of the creep curve). The m -value is an important factor associated with the viscous component, in which a decrease in the m -value implies a reduction in the relaxation⁹ property of the binder. An increase in the susceptibility of the binder to cracking is strongly associated with a decrease in the m -value as the parameter m is inversely proportional to the parameter n in the Paris law of crack susceptibility. The conversion of the BBR stiffness modulus to relaxation modulus reveals that the latter, which is an important property that indicates the binder's ability to relaxing stress, is also affected by the effect of aging. Similar behaviour can also be observed with the transient modulus of the binder/mastic determined using the Prony series in section 5.5.2.
- The slope/gradient or the m -value of the mastic materials is steeper than the bitumen materials indicating higher sensitivity to brittle behaviour of the mastic with decreasing temperature. When a critical aging of the bitumen is reached, the sensitivity of the aged binder to cracking (damage) exceeds that of the unaged bitumen. This eventually leads to the susceptibility of the binder/mortar to cracking.
- As the results of penetration and softening point indicated, the brittle behaviour of bitumen has also been demonstrated using the Direct Tension Test (DTT) at lower temperatures and higher loading speeds. An increase in the failure stress and a decrease in the failure strain are in general associated with a decrease in the testing temperature or an increase in the loading speed. However, the failure stress of both bitumen and mastic showed a reduction in failure stress beyond a "critical" point (in terms of temperature or loading speed) because of failure associated with brittle behaviour of the materials. The effect of aging basically increases the "critical" temperature or

⁹ Relaxation and brittleness are binder properties with literally opposite meaning. Relaxation refers to the ability of a material to relax stress after a load has been applied. Brittle materials fail or sustain damage (cracking) at lower strains when subject to load. A reduction in relaxation property indicates an increment of the temperature at which the material fails in a brittle mode.

decreases the “critical” loading speed at which failure occurs, which implies that aging increases the sensitivity to cohesive failure of the binder/mastic.

- According to the DTT results, the failure stress of the mastic ranges between 2 – 9 MPa while that of the bitumen ranges between 1 – 4 MPa. In terms of failure strain, the mastics fail between 4 – 10% which drops to 1 – 8% after LTA aging. The bitumen is characterized by a broader range of failure strain of 1 – 12%, which considerably dropped to 1 – 7% after LTA aging.
- The failure stress curve of the aged bitumen reaches a maximum value at lower loading speed compared to unaged bitumen. This shift is an indication of the hardening of the binder and explains the transition towards a brittle behaviour. Because of this shift, stress developed in the binding material as a result of traffic loading and/or thermal contraction may result in a greater damage in the aged binder.
- As stated earlier, aging reduces the stress relaxation ability of the binding material, which is a crucial binder property strongly related to PA durability.

5.6.2 In relation to Laboratory/Field Binder Aging Properties

- The aging of bitumen in the laboratory using the standard aging procedure (RTFOT+RCAT) and mixture aging (new aging method in a weatherometer – aging protocol 3 (AP3) that exposes the sample to combined effects of temperature, UV light, and humidity) have resulted in comparable binder rheological properties. Nevertheless, some minor differences were apparent with their complex shear modulus master curves at the lower frequency region.
- It seems that there is not much difference in the rheological characteristics of the binders from the upper and lower zones (UZ and LZ) of the field PA specimens. Whereas, the UZ and LZ of the laboratory aged mixture specimens showed minor differences in aging.
- It appears that the difference in aging behaviour of the field binders from the emergency and slow lanes (EL and SL) is negligible. In general, the binders from the EL have comparatively higher shear modulus than the SL binders. The 12 year old materials from EL and SL showed exceptionally large difference in their aging property. It is difficult to explain the reason, but these 12 year old EL and SL binders have different vanadium content which is indirectly indicative of the binder source. In comparison, the 7 year field materials, especially the binders from the lower zone, exhibited reasonably similar characteristics.
- The laboratory aging methods are not as severe as the long term field aging of PA, i.e. laboratory aging could not simulate the complex nature of field aging. The long term laboratory aging of bitumen using the standard aging procedure and the new mixture aging protocol (AP3) seem to predict only the aging characteristics of the field binder after construction and after 1 year service, respectively. The binders recovered from the mixture aging under aging protocol 1 and 2 in the laboratory have resulted in even less severe aging compared to the standard binder aging method and AP3.

- The effect of binder aging on the rheological behaviour of the mastic seems more significant at higher temperatures. At low frequencies (high temperature), the increase in complex modulus of STA1.0 mastic (short term aged binder with filler bitumen ratio $f/b = 1.0$) shows a much higher increment compared to the LTA1.0 mastic relative to their respective binder stiffnesses. The same tendency was also observed with respect to the phase angle master curves of the mastics and the corresponding aged binders. At high frequencies (low temperature), the aged mastics have a higher modulus and lower phase angle compared to the plain bitumens. As the temperature increases (frequency decreases) the mastic stiffness drops sharply.
- The long term laboratory aged bitumen samples have shown improved fatigue performance compared to the virgin/unaged bitumen. Whereas, the 7 and 12 year field binders have shown lower performance relative to the virgin bitumen. This significant difference in fatigue performance is believed to be as a result of differences in the degree of aging that resulted in brittle nature of the field binders.

5.6.3 General Discussion

The analysis of the test results has shown clear differences in the rheological properties of the laboratory aged and field materials. The materials recovered from mixture aging under aging protocol 1, 2, and 3 were intended to simulate the aging of PA in the field. In addition, the mixture aging tests were performed with the intention to avoid the influence of the binder recovery process on the material properties in order to make a comparison with field materials reliable. Nevertheless, the outcome did not match the long term aging of bitumen in the field (road) despite the aging process adopted to simulate the field conditions by combining the influences of temperature, UV light, and humidity (Aging protocol 3). Thus, it can be said that the laboratory aging methods adopted are not capable of simulating 7 – 12 years of PA aging in the field. The following points might have an influence on the aging properties of the laboratory and field binders, although not to the extent that they alter the main conclusions.

- The extraction and recovery process does not fully recover the bitumen from the field specimens (Peterson et al. 1999), which might leave some components of the bitumen to be retained by the aggregates. Moreover, some fractions of bitumen are adsorbed by the aggregates resulting in significant change in property of the bitumen (Stroup-Gardner and Nelson 2000). Depending on the type of the aggregate, i.e. surface mineralogical characteristics and adsorption properties, the fractions of bitumen retained in the aggregates may have an effect for the rheological differences.
- Some bitumen components might be washed away or eroded by the action of water during the real life of the pavement in the field. The pumping action of vehicle tyres can be mentioned as a possible mechanism in the wearing process of the bitumen/mortar. This is not happening during the aging of either plain bitumen or asphalt mixture in the laboratory.

The aging of bitumen in a PA surface layer is complex to simulate. The above mentioned factors involved in the process of aging are difficult to incorporate in the simulation of field binder aging. The other important point in relation to aging is the aging time. It is not recommended to accelerate aging at higher temperature since it will result in a different aging mechanism and, in the contrary, lower temperatures would lengthen the aging time, which is also undesirable. Hence, it seems reasonable to consider improvement to the aging protocol. The weatherometer aging can be improved by reducing the humidity during aging from 70% to 50% and the aging temperature can be increased step-by-step during the aging process. The aging of the mastic/mortar instead of the mixture at aging temperature not exceeding 90°C could also be seen as an alternative method. As in PAV aging, a 3.2 mm layer thickness of mortar (i.e. bitumen + filler + sand fraction less than 0.5 mm in size) can be aged under the aging protocol AP3 used in this study. This procedure would also prevent possible drain-off of the binding material in mixture aging.

The rheological tests performed at low temperatures have shown that the effect of aging has a negative role in the binder performance. The aged binders have failed at low strain levels at low temperatures, which is a characteristic of brittle materials. The fact that aging is occurring at higher temperatures makes both high and low temperatures critical for PA performance. Aging of the binder takes place during summer periods (at high pavement temperatures) and has detrimental implications to the pavement performance due to the damaging action of traffic during winter periods. The results of PA modelling using the rheological properties of the mastics as input has shown that the same stress levels are developed in the field aged and unaged binding materials and the dissipated energies are similar. However, the fatigue resistance of field aged binders is much lower than that of virgin binders. This implies that aging is incurring damage. The laboratory aged binders have shown better performance with regard to accumulation of damage (fatigue) compared to the unaged binder. On the other hand, the 7 and 12 year binders from the field have shown poor fatigue performance and different rheological properties compared with the laboratory aged binders. This implies that conclusions derived from the study of laboratory aged materials alone in relation to the reality could be misleading. The performance of the field materials in terms of their rheological and fatigue behaviour has provided the verification that aging is a critical factor for ravelling occurrence in PA.

In addition to the effect of aging, water contributes to the deterioration or ravelling of PA, but it is not believed to be the main factor. Because of the porosity of the mixture, water can easily drain to the bottom layer and sideways. Nevertheless, the higher the rate of damage development in the binder/mortar, the higher the acceleration of damage due to additional factors such as moisture damage or freeze and thaw actions leading to stripping of the stones. Besides, the reduced self healing potential of the bitumen at low

temperatures due to age hardening (Bahia et al 2001a, Bonnetti et al 2002, Phillips 1999) will contribute to damage.

5.7 References

- Bahia, H. U., Hanson, D. I., Zeng, M., Zhai, H., Khatri, M. A., and Anderson, R. M. (2001). "Characterisation of Modified Asphalt Binders in Superpave Mix Design." *Rep. No. 459*, National Academy Press, Washington DC.
- Bonnetti, K. S., Nam, K., and Bahia, H. U. (2002). "Measuring and Defining Fatigue Behaviour of Asphalt Binders." *Transport Research Board (TRB), Bituminous Binders*(No. 1810). Washington DC.
- Burr, B. L., Davison, R. R., Glover, C. J., and Bullin, J. A. (1994). "Softening of asphalts in dilute solutions at primary distillation conditions." *Transportation Research Record*,(1436). Washington DC.
- Burr, B. L., Davison, R. R., Jemison, H. B., Glover, C. J., and Bullin, J. A. (1991). "Asphalt hardening in extraction solvents." *Transportation Research Record*,(1323), pp. 70-76. Washington DC.
- Carpenter, S. H., and Jansen, M. (1997). "Fatigue Behavior under New Aircraft Loading Conditions." *American Society of Civil Engineers*, pp. 259-277.
- Chen, J.-S., and Tsai, C.-J. (1998). "Relating tensile, bending, and shear test data of asphalt binders to pavement performance." *Journal of Materials Engineering and Performance*, 7(6), 805-811.
- Cheung, C. Y. (1995). "Mechanical behaviour of bitumens and bituminous mixes.", *PhD dissertation*. University of Cambridge, Engineering department. Cambridge UK.
- Des Cloizeaux, J. (1990). "Relaxation and viscosity anomaly of melts made of long entangled polymers. Time dependent reptation." *Journal of Macromolecules*, 23, 4678-4687.
- Doi, M., and Edwards, S. F. (1986). "The Theory of Polymer Dynamics." *Chapter in a Book* pp.156. Clarendon Press, Oxford, UK,
- Groenendijk, J. (1998). "Accelerated testing and surface cracking of asphaltic concrete pavements". *PhD dissertation*. Delft University of Technology, Road and Railway Engineering. Delft, The Netherlands.
- Hagos, E.T., 2007. Investigation into the effect of bitumen aging. *6th International PhD Symposium in Civil Engineering*. Zurich, Switzerland.
- Hagos, E.T., Molenaar, A.A.A., Ven, M.F.C. van de, 2005. The Effect of Aging on the Rheology and Fatigue Response of Bitumen in Relation to Raveling in Porous Asphalt. *7th Int. Conference on the Bearing Capacity of Roads, Railways and Airfields*, NTNU Trondheim, Norway.

Hagos, E.T., Molenaar, A.A.A., Ven, M.F.C. van de, Voskuilen, J.L.M., 2007. Durability related investigation into Porous Asphalt. *Proceedings of Advanced Characterisation of Pavement and Soil Engineering Materials*. Athens, Greece.

Heukelom, W. (1973). "An improved method of characterising asphaltic bitumens with the aid of their mechanical properties." *Association of Asphalt Paving Technologists*, 62-98.

Hopkins, I. L., and Hamming, R. W. (1957). "On creep and relaxation." *Journal of Applied Physics*, 28(8), 906-909.

Huurman, M. (2008). "Lifetime optimization tool, LOT, Main report." *Rep. No. 7-07-170-1*, Delft University of Technology, Road and Railway Engineering, Delft, The Netherlands.

Jansen, K. M. B. (2006). "Thermomechanical modeling and characterization of polymers." *Rep. No. WB 1433-04*, Delft University of Technology (TU Delft), 3ME. Delft, The Netherlands.

Lundstrom, R., and Isacsson, U. (2003). "Characterization of Asphalt Concrete Mixtures using Monotonic and Cyclic Tests." *International Journal of Pavement Engineering*, 4(3), 143-153.

Maier, D., Eckstein, A., Friedrich, C., and Honerkamp, J. (1998). "Evaluation of models combining rheological data with the molecular weight distribution." *Journal of rheological*, 42(5), 1153-1173.

Medani, T. O., and Huurman, M. (2005). "Superposition principle to determine properties of bituminous mixtures in the time-temperature domain." *Bearing Capacity of Roads, Railways, and Airfields (BCRA)*. Trondheim, Norway

Mo, L. T., Huurman, M., Wu, S. P., and Molenaar, A. A. A. (2007). "Investigation into stress states in porous asphalt concrete on the basis of FE-modelling." *Finite Elem. Anal. Des.*, 43(4), 333-343.

Mo, L., Huurman, M., Shaopeng, W., and Molenaar, A. A. A. (2008). "Ravelling investigation of porous asphalt concrete based on fatigue characteristics of bitumen-stone adhesion and mortar." *Journal Materials and Design*, Article in press.

Molenaar, A. A. A. (1983). "Structural performance and design of flexible road constructions and asphalt concrete overlays." *PhD Dissertation*, Technical University of Delft (TU Delft).

Molenaar, A. A. A. (2007). "Road materials: Part III Asphaltic materials." *Lecture note CT 4850*. Delft University of Technology (TU Delft). Delft, The Netherlands.

Molenaar, J. M. M., and Molenaar, A. A. A. (2000). "Fracture toughness of asphalt in the semi-circular bend set." *Euroasphalt and Eurobitume congress*, Barcelona.

- Peterson, R. L., Soleymani, H. R., Anderson, R. M., and McDaniel, R. S. (1999). "Recovery and testing of rap binders from recycled asphalt pavement." *Rep. No. Research paper*, The Asphalt Institute.
- Phillips, M. C. (1999). "Multi-Step Models for Fatigue and Healing and Binder Properties Involved in Healing." *Eurobitumen Workshop*.
- Pronk, A. C. (1995). "Evaluation of the Dissipated Energy Concept for the Interpretation of Fatigue Measurements in the Crack Initiation Phase." Road and Hydraulic Engineering Division, the Netherlands.
- Pronk, A. C., and Hopman, P. C. (1990). "Energy Dissipation: The Leading Factor of Fatigue." *Conference – Strategic Highway Research Program (SHRP): Sharing the Benefits*. London, UK.
- Reed, J., and Whiteoak, D. (2006). "The shell bitumen handboook." Thomas Telford.
- Riande, E., Diaz-Calleja, R., Prolongo, M. G., Masegosa, R. M., and Salom, C. (2000). "Polymer viscoelasticity: stress and strain in practice." Marcel Dekker, Inc..
- Shapery, R. A. (1975). "A theory of crack initiation and growth in viscoelastic media, Part I: Theoretical development. Part II: Appropriate methods of analysis. Part III: Analysis of continuous growth." *International Journal of Fracture*, Vol. 11.
- Shapery, R. A. (1978). "A method for predicting crack growth in nonhomogeneous viscoelastic media." *International Journal of Fracture*, 14(3), 293-309.
- SHELL (1973). "Bitumen testing." Koninklijke/Shell - Laboratorium, Amsterdam.
- Stroup-Gardiner, M., and Newcomb, D. (1995). "Evaluation of rheological measurements for unmodified and modified asphalt cements." *Transportation Research Record*, (1488).
- Stroup-Gardiner, M., and Newcomb, D. (2000). "Use of normal propyl bromide solvents for extraction and recovery of asphalt cements." *Rep. No. 00-06*, National Center for Asphalt Technology (NCAT).
- TA Instrumnets. (2000). Calculation of polymer molecular weight distribution. *Notes on rheology advantage data analysis*, TA Instruments.
- Tschoegl, N. W. (1989). "The phenomenological theory of linear viscoelastic behaviour: An introduction." Springer verlag, Berlin.
- van Dijk, W. (1975). "Practical fatigue characterization of bituminous mixes." *Association of Asphalt Paving Technologists (AAPT)*, Vol. 44, pp. 38.
- van Dijk, W., and Visser, W. (1977). "The energy approach to fatigue for pavement design." *Association of Asphalt Paving Technologists (AAPT)*, Vol. 46, pp. 1.

Wikipedia (2008). Von Mises yield criterion. Wikipedia - the free encyclopaedia. Internet weblink http://en.wikipedia.org/wiki/Von_Mises_stress . Last accessed on September 15, 2008.

Woldekidan, M. F. (2006). "Performance study of C-Fix in Porous Asphalt Concrete using a 2D Finite Element Model." *MSc thesis*, Delft University of Technology (TU Delft).

6 Chemical Characterization

In this chapter, the results and interpretation of the chemical changes in the properties of bitumen in relation to aging are addressed. The use of analytical methods, i.e. spectroscopic and chromatographic methods, was adopted to assess the effect of bitumen aging on the composition (functional groups) and structure (Molecular Weight Distribution, MWD) of the bitumen materials. In addition to the analytical methods, the vanadium content of the bitumen samples was determined in order to obtain information related to the origin of the binders.

6.1 Vanadium Content

Bitumen samples consist of hydro-carbons (about 95%) and the so called hetro-atoms (nitrogen, sulphur (from < 1% – 5%) and oxygen) with trace amounts of metals – vanadium and nickel. The compositions of bitumen samples, especially the hetro-atoms and the metals, vary widely depending on the origin/source of the bitumen. These variations result in the difference in the chemical and physical properties among bitumens of difference sources (Peterson 2000). The aging behaviour of bitumen also is greatly influenced by the proportion of the hetro-atoms present in the binder. The origin of bitumen can be related to the trace amounts of metal (eg. vanadium content) of the bitumen. Vanadium and nickel concentrations in bitumens extracted from a variety of organic sedimentary rocks of different geological ages and geographical areas are found in quantities ranging between 7 – 1590 ppm for vanadium and 10 – 139 ppm for nickel (Reed and Whiteoak 2006). Crudes from Venezuela and Mexico generally have the highest vanadium levels. Table 6.1 shows the elemental analysis of representative binders from different sources. The effect of aging during the service period of the pavement is believed to have no influence on the vanadium content of bitumen. Sensitivity to aging of the binder, however, is indirectly related to the quantity of vanadium content present since, as will be explained later in this chapter, the amount of sulphur

in the hetro-atoms that influences aging due to formation of sulfoxide is usually present in quantities proportional to the vanadium content.

Table 6.1: Elemental analysis of representative binders (Peterson 2000, Roberts et al. 1996)

Element	Mexican B-2959	Ark. Lousiana B-3036	Boscan (Venez.) B-3051	Californian B-3602
Carbon (%)	83.77	85.78	82.90	86.77
Hydrogen (%)	9.91	10.19	10.45	10.94
Nitrogen (%)	0.28	0.26	0.78	1.10
Sulphur (%)	5.25	3.41	5.43	0.99
Oxygen (%)	0.77	0.36	0.29	0.20
Vanadium (ppm)	180	7	1380	4
Nickel (ppm)	22	0.4	109	6

The vanadium content of the bitumen used in this research (70/100 pen bitumen from Kuwait) is 120 ppm. There is no information with regards to the origin of the bitumen used in the road sections from which the field specimens were cored. Hence, the reason behind the determination of the vanadium content of the field specimens is to determine if the samples belong to the same family or source.

Table 6.2 shows the vanadium content of bitumen samples used for aging in the laboratory and recovered from field specimens. The determination of the vanadium content was conducted using the x-ray spectrometry method according to the standard procedure DIN 51790-7. The test was conducted by Kuwait petroleum (Q8) laboratory in the Netherlands.

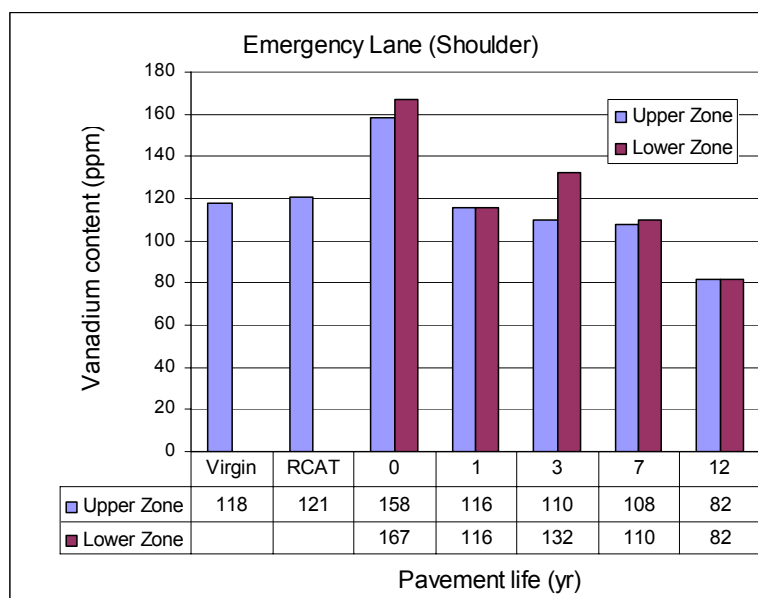


Figure 6.1: Vanadium content of field and laboratory materials (Emergency Lane)

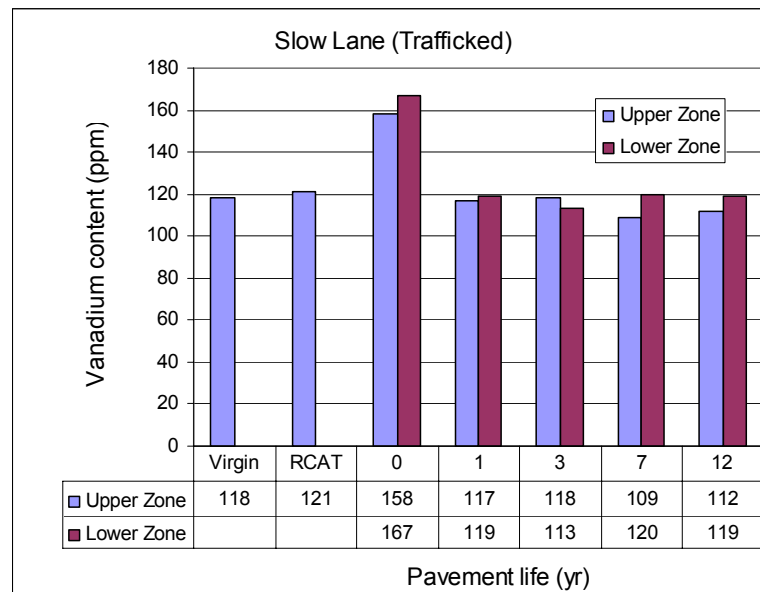


Figure 6.2: Vanadium content of field and laboratory materials (Slow Lane)

Table 6.2: Vanadium content of field and laboratory aged materials

Section	Serv. Year	Zone	No Traffic	Sample Vanadium		Traffic	Sample Vanadium	
			Emergency Lane (EL)	Nr.	(ppm)	Slow Lane, SL	Nr.	(ppm)
G	0	Upper	06020.IPG001	1	158			
A	1		06020.IPG011	11	116	06020.IPG013	13	117
B	3		06020.IPG007	7	110	06020.IPG009	9	118
C	7		06020.IPG015	15	108	06020.IPG017	17	109
E	12		06020.IPG003	3	82	06020.IPG005	5	112
G	0	Lower	06020.IPG002	2	167			
A	1		06020.IPG012	12	116	06020.IPG014	14	119
B	3		06020.IPG008	8	132	06020.IPG010	10	113
C	7		06020.IPG016	16	110	06020.IPG018	18	120
E	12		06020.IPG004	4	82	06020.IPG006	6	119
Virgin bitumen 70/100 pen				19	118			
LTA: RTFOT + RCAT aging				20	121			

Based on the results shown in Figure 6.2, the range of vanadium content is between 80 – 170 ppm with the lowest corresponding to the 12 year old field specimen and highest corresponding to the bitumen recovered from section G (after construction). It seems that the difference in the vanadium content is small considering the expected range in the amount of vanadium content among different sources. This indicates that the source of the bitumen samples considered in this study is the same or it comes from the same geological stratum. The slight differences in the vanadium content of the samples recovered from the top and bottom part of the pavement layer is regarded negligible. The field sample from section G seems to have particularly high vanadium content compared to the other bitumen samples.

6.2 Infrared Spectroscopy

The Attenuated Total Refraction Fourier Transform Infrared (ATR/FTIR) spectroscopy is a technique used to identify functional groups in organic compounds, which is an effective method to investigate the chemical composition of materials. It is a valuable tool to identify the chemical composition of materials at molecular level. ATR/FTIR spectroscopy makes use of the Infrared part of the electromagnetic spectrum. Commonly, the spectrum of light is classified into Ultraviolet (295 – 400 nm), Visible (400 – 800 nm), and Infrared (800 – 2450 nm) depending on the wavelength of the light according to CIE Pub. 85, table 4 (Atlas 2001, CIE 1989) (see Figure 6.3).

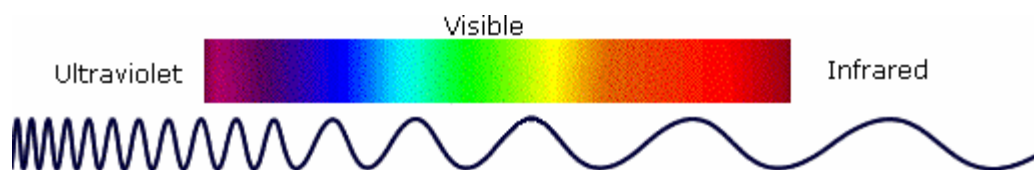


Figure 6.3: the IR region of the electromagnetic spectrum (MSU 2007)

Infrared spectroscopy deals with the interaction of infrared light with matter. The energy of an infrared photon is calculated using the Planck's energy relation given in Equation 6.1. The energy of light spectrums is inversely proportional to the wavelength, hence an increase in wavenumber (a decrease in wavelength) corresponds to an increase in energy. It implies that the Infrared spectrum has lower energy compared to Ultraviolet (UV) and Visible spectrums. The amount of energy transmitted in the form of electromagnetic radiation per unit time is given by Equation 6.2.

$$E = h\nu = \frac{hc}{\lambda} = hc\tilde{\nu} \quad (6.1)$$

$$P = E\phi \quad (6.2)$$

Where:

- E = photon energy [Joule],
- h = Plank's constant (approx. 6.62610×10^{-34} Joule-seconds),
- ν = frequency [cycles/s], $\nu = \frac{c}{\lambda} = c\tilde{\nu}$,
- $\tilde{\nu}$ = wavenumber [cm^{-1}], $\tilde{\nu} = \frac{1}{\lambda}$,
- c = velocity of light (3×10^{10} cm/s),
- λ = wavelength of the light,
- P = the radiant power, also referred as Intensity (I) [Joules/s, Watt],
- ϕ = the photon flux, the number of photons per unit time [s^{-1}].

The Infrared (IR) part of the light spectrum is divided into Near- (approx. $4000 - 12800 \text{ cm}^{-1}$), Middle- (approx. $200 - 4000 \text{ cm}^{-1}$) and Far- (approx. $10 - 200 \text{ cm}^{-1}$)

infrared regions, which are named with respect to their relation to the Visible (VIS) spectrum (Table 6.3). The mid- infrared region is used to study the fundamental vibrations and associated rotational/vibrational structure of molecules, whilst the higher energy region (near-IR) can excite overtone or harmonic vibrations (Wikipedia 2007). The most frequently used region, i.e. the middle infrared region, has been adopted to identify the components of bitumen materials. In this research, the "finger-print" region¹⁰ (600 – 1800 cm⁻¹) was the most useful region to study the development of oxidation products (ketones and sulfoxides) as a result of aging.

Table 6.3: Infrared spectral regions (source: Skoog and Leary 1992)

Region	Energy (KJ/mol)	Wavenumber ($\tilde{\nu}$) Range (cm ⁻¹)	Wave length (λ) Range (μm)
Near IR	150 – 50	12800 – 4000	0.78 – 2.5
Middle IR	50 – 2.5	4000 – 200	2.5 – 50
Far IR	2.5 – 0.1	200 – 10	50 – 1000
Most used		4000 – 670	2.5 – 15

A plot of an IR spectrum is expressed as wavenumber (x-axis) vs percent absorbance (y-axis). The wavelength can be used instead of wavenumber and transmittance instead of percent absorbance. The relationship between absorbance (A) and transmittance (T) is given by Equation 6.3. The baseline method for the determination of absorbance is shown in Figure 6.4.

$$\begin{aligned}
 A &= \log_{10}(1/T) = -\log_{10} T = -\log_{10}(I/I_0) = \log_{10}(I_0/I) \\
 &= -\left[\log_{10}(\%T \cdot 10^{-2})\right] = -\left[\log_{10}(\%T) + \log_{10} 10^{-2}\right] = 2 - \log_{10}(\%T)
 \end{aligned}
 \tag{6.3}$$

Where:

- A = absorbance [AU],
- T = transmittance, $T = I/I_0$ [%],
- I = radiant power transmitted by the sample,
- I_0 = radiant power incident in the sample.

¹⁰ The mid-infrared region is divided into "group-frequency" region (1300-4000 cm⁻¹) and the "finger-print" region (650-1300 cm⁻¹).

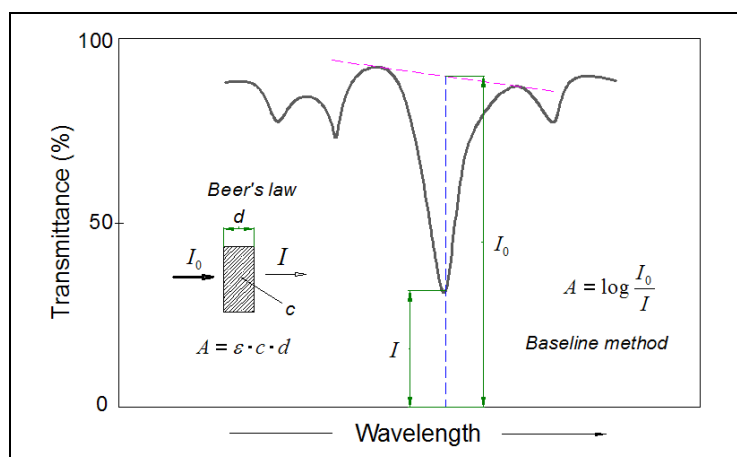


Figure 6.4: Baseline method for determination of absorbance (Reference: Plus 2000, Skoog and Leary 1992)

Beer's Law stipulates the quantitative analysis of infrared spectrum. Absorbance is proportional to the concentration of the absorbing species and the path travelled. Following Beer's Law, the absorption A is given by the Equation 6.4.

$$A = \log \frac{I_0}{I} = \varepsilon \times c \times d \quad (6.4)$$

Where:

- ε = the molar absorptivity coefficient,
- c = the concentration of the absorbing species,
- d = the path length.

6.2.1 Principles of Infrared (IR) Spectroscopy

The chemical composition of a material determines the bond energy between the components of the material. The bonds are instigated to a higher state of vibration when infrared radiation passes through the material; the amount of energy needed to do this varies from bond to bond. Each different bond will absorb a different frequency (and hence energy) of infra-red radiation corresponding to the energies involved in bond vibrations of the material. The multiplicity of vibrations occurring simultaneously produces a highly complex absorption spectrum that is uniquely characteristic of the functional groups that make up the molecule and the overall configuration of the molecule (Willard 1998).

For a molecule to absorb IR, the vibrations or rotations within a molecule must cause a net change in the dipole moment of the molecule. If the frequency of the radiation matches the vibrational frequency of the molecule then radiation will be absorbed, causing a change in the amplitude of molecular vibration. Every molecule will have its own characteristic spectrum that depends on the structure of the molecule.

Molecular rotations

The use of rotational transitions in the spectroscopic study of materials is limited.

Molecular vibrations

Molecular vibrations are very significant in identifying the type of functional groups in a material. The position of atoms in molecules are not fixed; they are subject to a number of different vibrations. Vibrations fall into the two main categories: stretching and bending.

Stretching: Change in inter-atomic distance along the bond axis.

Bending: Change in angle between two bonds.

Four types of bending are recognized: Rocking, Wagging, Scissoring, and Twisting.

- Rocking or In-plane bending: the structural unit swings back and forth in the symmetry plane of the molecule.
- Scissoring (Deformation): the two atoms connected to a central atom move toward and away from each other with deformation of the valence angle.
- Wagging or Out-of-plane bending: the structural unit swings back and forth in the plane perpendicular to the molecule's symmetry plane.
- Twisting: the structural unit rotates back and forth around the bond that points it to the rest of the molecule.

Figure 6.5 shows the types of molecular vibrations instigated by the electromagnetic radiation. The vibration modes are also shown for some of the functional groups in the middle IR region in Figure 6.7. An example of functional groups and the corresponding wave numbers in the infrared region is given in Figure 6.7 and Table 6.4.

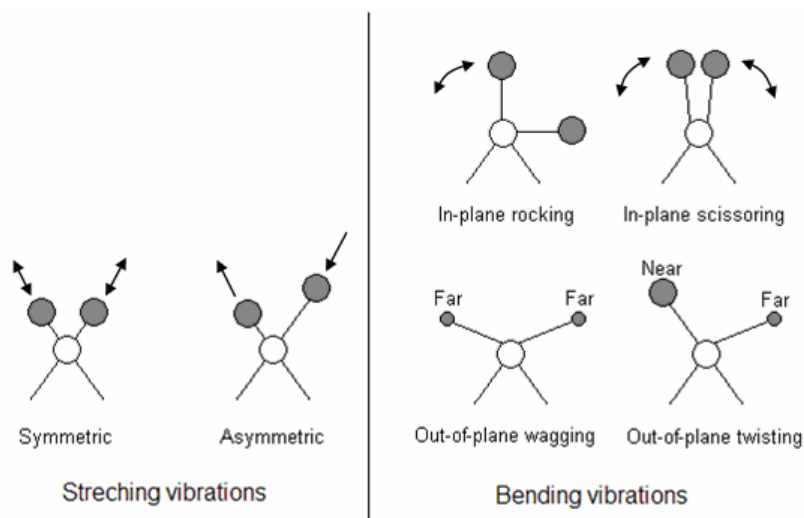


Figure 6.5: Types of molecular vibrations during exposure to electromagnetic IR radiation (UColorado 2002, Skoog and Leary 1992)

The stretching frequencies of any two atoms connected by a chemical bond may be roughly calculated by assuming that the bond energies arise from the vibration of a diatomic harmonic oscillator, and obey Hook's law. In this approximation, two atoms and the connecting bond are treated as a simple harmonic oscillator composed of two masses (atoms) joined by a spring. The frequency of the vibration of the spring is related to the mass and the force constant of the spring and is given in Equation 6.5.

$$\nu = \frac{1}{2\pi} \sqrt{\frac{k}{\mu}} \quad , \quad \mu = \frac{m_1 m_2}{m_1 + m_2} \quad (6.5)$$

$$\tilde{\nu} = \frac{\nu}{c} = \frac{1}{2\pi c} \sqrt{\frac{k(m_1 + m_2)}{m_1 m_2}} \quad (6.6)$$

Where:

- ν = the vibrational frequency [Hz or cycles/sec],
- $\tilde{\nu}$ = the vibrational frequency [cm^{-1}], $\tilde{\nu} = 1/\lambda$,
- k = the force constant of bond,
- μ = the reduced mass of the two atoms,
- m_1, m_2 = the mass of atoms 1 and 2 respectively [g],
- c = the velocity of light [cm/sec].

From Equation 6.6, it can be noticed that the vibrational frequency (wavenumber) increases as the force constant (k) increases and it decreases as the mass of atoms (μ) increases.

A simplified version of the energy levels of diatomic molecules is derived from the principles of quantum mechanics and is given by Equation 6.7 (Burns 2001, UColorado 2002).

$$E_n = \left(n + \frac{1}{2}\right) h\nu = \left(n + \frac{1}{2}\right) \frac{h}{2\pi} \sqrt{\frac{k}{\mu}} \quad (n = 1, 2, 3, \dots) \quad (6.7)$$

Where:

- E_n = vibrational energy level in diatomic molecules,
- h = Planck's constant ($\approx 6.62610 \times 10^{-34}$ Joule-seconds),
- n = the quantum number,

In the harmonic oscillator mode, the lowest energy is $E_0 = 1/2 h\nu$ and according to the selection rule molecules are allowed to absorb the next energy level, which is an amount of $h\nu$. However, transitions of $2h\nu$, $3h\nu$, or higher are observed that correspond to bonds called overtone (integral multiples of the fundamental absorption frequencies) in an IR spectrum. In reality, a bond between molecules is an *anharmonic* oscillator, as the inter-atomic distance increases the energy reaches the maximum limit as shown in Figure 6.6. The

energy levels become more closely spaced with increasing inter-atomic distance and the allowed transitions ($h\nu$) become smaller in energy.

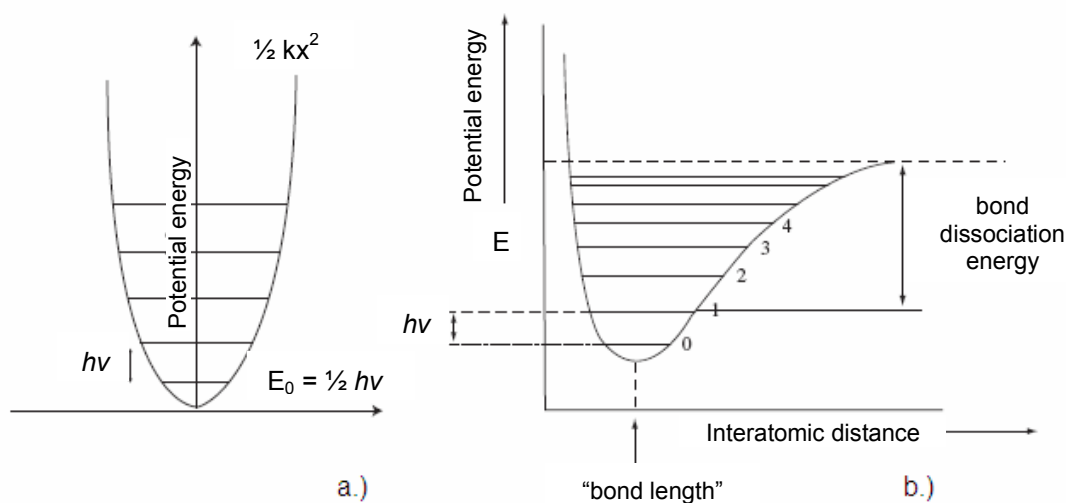


Figure 6.6: a.) Energy curve for harmonic oscillator and b.) Energy curve for an anharmonic oscillator showing the vibrational levels in a vibrating mode (UColorado 2002, Skoog and Leary 1992)

The regions on the IR spectrum where stretching vibrations are located depend primarily on the type of the bonds, i.e. whether the bonds are single, double, or triple. The force constants, k , of the bonds are 5×10^5 , 10×10^5 , and 15×10^5 dyne/cm for single, double, triple bonds respectively. Table 6.4 shows the regions corresponding to the different types of bonds in the IR spectrum, which is also shown in Figure 6.7 (UColorado 2002).

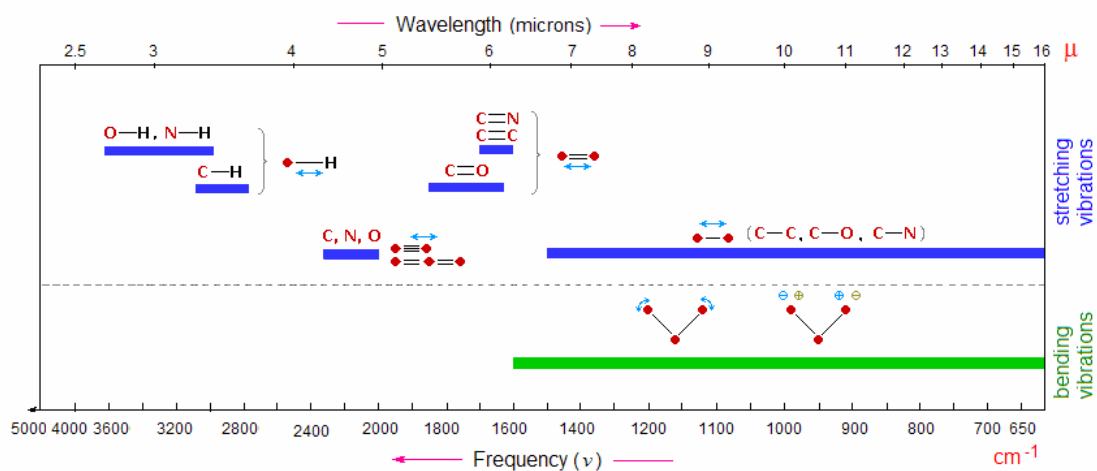


Figure 6.7: Molecules and their vibrational modes in the middle infrared region (UColorado 2002)

Table 6.4: IR absorption by single, double, and triple bonds (UColorado 2002)

Bond	Absorption region (cm^{-1})	Force constant, k
C - C, C - O, C - N	800 - 1300	5×10^5
C = C, C = O, C = N, N = O	1500 - 1900	10×10^5
C \equiv C, C \equiv N	2000 - 2300	15×10^5
C - H, N - H, O - H	2700 - 3800	5×10^5

Vibrational coupling

In addition to the vibrations mentioned above, interaction between vibrations (coupling) can occur if the vibrating bonds are joined to a single central atom.

Vibrational coupling is influenced by a number of factors (SHU 2007);

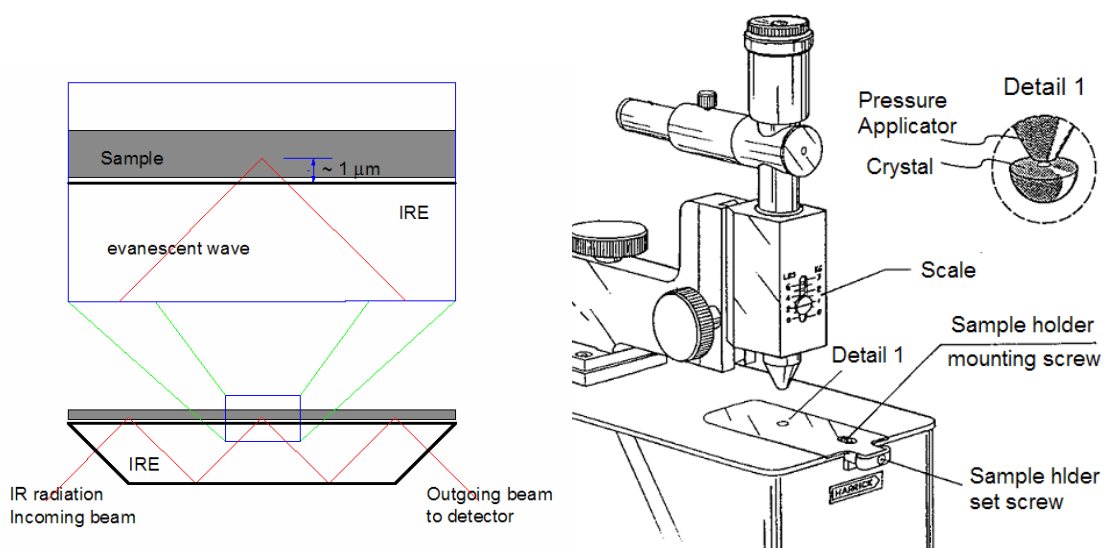
- strong coupling of stretching vibrations occurs when there is a common atom between the two vibrating bonds;
- coupling of bending vibrations occurs when there is a common bond between vibrating groups;
- coupling between a stretching vibration and a bending vibration occurs if the stretching bond is one side of an angle varied by bending vibration;
- coupling is greatest when the coupled groups have approximately equal energies;
- no coupling is seen between groups separated by two or more bonds.

The combination and blending of all the factors create a unique IR spectrum for each compound. The response (absorbance or transmittance of IR radiation) of binder samples in the range 1800 to 600 cm^{-1} wavenumber, i.e. the “finger-print” region, provides essential information to quantify functional groups in a bitumen. The method of IR spectroscopy has been used to characterize the chemical composition of bitumen, studying effects of binder aging and polymer modification, and identification of impurities. For example, the peaks in the finger-print region that indicate formation of oxidation products (aging) are to be expected at wavenumber 1700 cm^{-1} and 1030 cm^{-1} for ketones (bond C = O) and sulfoxides (bond S = O) respectively.

6.2.2 The ATR/FTIR Spectrometry

Attenuated Total Reflectance/Fourier Transform Infrared (ATR/FTIR) spectrometry is a sampling technique used in conjunction with infrared spectroscopy which enables samples to be examined directly in the solid or liquid state without the need for sample preparation (Perkin Elmer 2005).

ATR uses a property of total internal reflection called the evanescent wave. A beam of infrared light is passed through the ATR crystal in such a way that it reflects at least once off the internal surface in contact with the sample. This reflection forms the evanescent wave which extends into the sample, typically by a few microns ($\approx 1 \mu\text{m}$). The beam is then collected by a detector as it exits the crystal. The principle of ATR/FTIR spectroscopy is schematically illustrated in Figure 6.7.



a.) The Internal Reflection Element (IRE) and the path of the evanescent wave

b.) The IR spectroscopy apparatus (the sample covers the crystal as shown in Detail 1)

Figure 6.8: The ATR/FTIR spectroscopy method (Perkin Elmer 2005, DWW 2004)

Mid-infrared spectra are obtained by pressing small pieces of material against an internal reflection element (IRE). Light enters the IRE and reflects down the length of the crystal. At each internal reflection, the evanescent wave penetrates into the material from the surface of the IRE. This evanescent effect works best if the crystal is made of an optical material with a higher refractive index than the sample being studied. Typical materials for ATR crystals include germanium (Ge), KRS-5 and zinc selenide (ZnSe), while silicon is ideal for use in the Far-IR region of the electromagnetic spectrum. The excellent mechanical properties of diamond make it an ideal material for ATR, particularly when studying very hard solids.

6.2.3 Materials and Testing Method

Materials

The materials used in the IR spectroscopic investigation are materials from the laboratory aging protocols and field aged materials.

- Laboratory aging protocols
 - Conventional aging method: short (RTFOT/RCAT) and long (RCAT) term aging.
 - Porous Asphalt (PA) mixture aging: weatherometer aging of PA slabs under the combined influence of temperature, UV light, and humidity.
- Field materials - Core specimens taken from the road with service periods 0, 1, 3, 7, and 12 years.

Testing method

All bitumen materials were put in a desiccator to minimize absorption of moisture by the material that could influence the results of the IR spectrum. In addition, a device was connected to the IR apparatus to introduce nitrogen into the system that helps decrease the presence of moisture inside the ATR/FTIR apparatus and improve the clarity of the IR scan. This apparatus was made to function half an hour before the actual scanning begins.

The apparatus used to conduct the IR test was a Galaxy Series FTIR 3000. A background scan was run at the beginning and every 30 min during the scanning of the sample. The purpose of running a background scan was to take into account changes in moisture level or other occurrences that might have an influence on the testing results. The background and sample scans were performed with 128 or 256 scans with a resolution of 4 cm^{-1} . The scanning was performed in the Middle Infrared Region (MIR, $400 - 4000\text{ cm}^{-1}$). Depending on the scan frequency and resolution required, the test takes 5 – 10 min to record the interferogram. A computer software “WinFirst” was used to process the ATR interferogram into an absorption diagram (spectrum) through Fourier Transformation function, thus the name ATR/FTIR. A thin layer of binder sample (about 50 to 200 mg), that is enough to cover the tip of the crystal or ATR prism, is placed for scanning. For every sample, a second repetition scan was conducted and the agreement between the two scans was checked to be good. The tip of the crystal was cleaned by means of asphalt remover and acetone after every test to make it ready for the next scan. The IR test was conducted at room temperature.

6.2.4 IR Spectrum Quantitative Analysis

Data processing

The quantitative analysis of the IR spectrum of binder samples was carried out based on relative comparison of the absorption peaks characterizing the formation of aging products, especially ketones and sulfoxides. The aging indicators at 1700 (ketones $\text{C}=\text{O}$) and 1030 cm^{-1} (Sulfoxides $\text{S}=\text{O}$) are the two characteristic bands at which the peak height and the area under the peak were used for the assessment of the effect of aging of the binder samples. In addition, the absorption at 1600 cm^{-1} (i.e., $\text{C}-\text{C}$ stretch) was incorporated in the data interpretation since changes were observed at this peak as a result of aging. One of the two spectrums was used to represent the IR spectrum of every bitumen sample because the matching between the two scans was in good harmony.

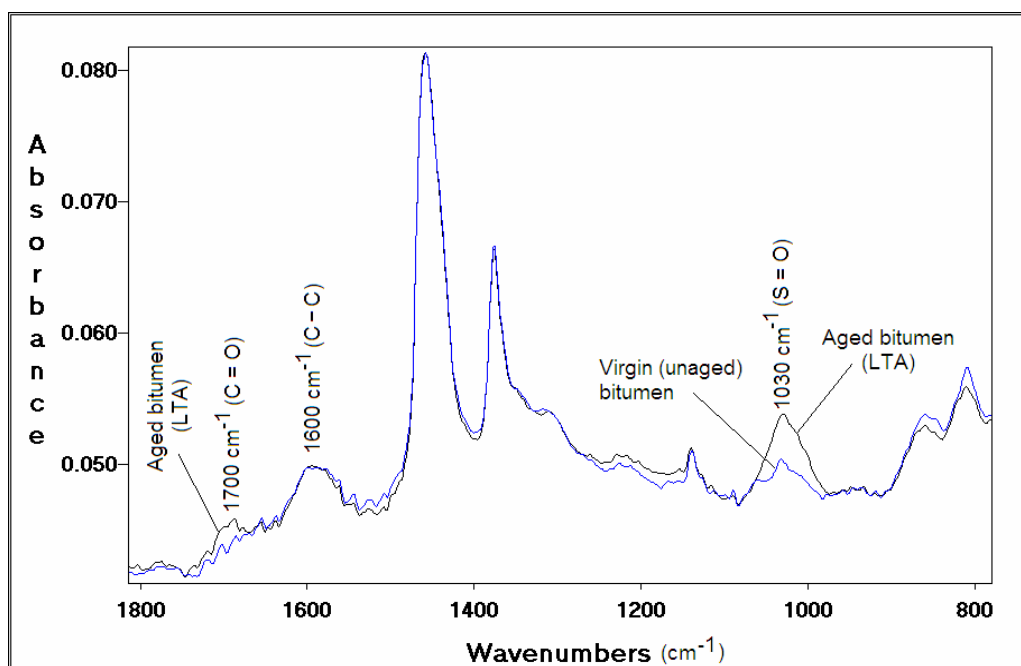


Figure 6.9: Typical IR spectra of aged (LTA) and unaged bitumen at the "fingerprint" region

Figure 6.10 shows the determination of peak area and the peak height used to analyse the development of the functional groups, C=O (carbonyls/ketones) and S=O (sulfoxides), after aging. The ratio of the peak areas (PA) and peak height (PH) of unaged (virgin) bitumen was used as a parameter to indicate changes in the laboratory and field aged binders. The area under the peaks is bound by a baseline that connects the lowest points of the curve. The baseline boundary was determined for the virgin bitumen and used in the determination of the peak area and the peak height of the other samples. In other words, the PA and PH calculation of all the bitumen samples was based on the same boundary points as the virgin bitumen. The peak height determination was carried out from the tip of the curve to the base line. In addition to the peak height under the curve (P3), the peak height relative to the baseline of the virgin bitumen (P3') was determined for the S=O (sulfoxide) peak as shown in Figure 6.10. The boundaries used to establish the baseline for the integration of the peak area and the determination of peak height are given in Table 6.5.

Table 6.5: Boundaries used for peak area and peak height calculations

Peak designation	Functional group	Boundary, Wavenumber (cm ⁻¹)
Peak 1 - P1	C = O (Ketones / Carbonyls)	1650.77 - 1747.20
Peak 2 - P2	C - C ring stretch	1535.06 - 1633.42
Peak 3 - P3 / P3'	S = O (Sulfoxides)	952.66 - 1102.59
Peak ratios (relative to virgin bitumen)		
Ratio 1 - R1 = ratio at P1	R3' = ratio relative to P3'	
Ratio 2 - R2 = ratio at P2	R4 = ratio P3/P1 (Sulfoxide/ketones)	
Ratio 3 - R3 = ratio at P3	R4' = ratio P3'/P1	

NB: The C-C stretch is not an oxidation product, but it is included to indicate changes in the peak after aging due to other associated factors.

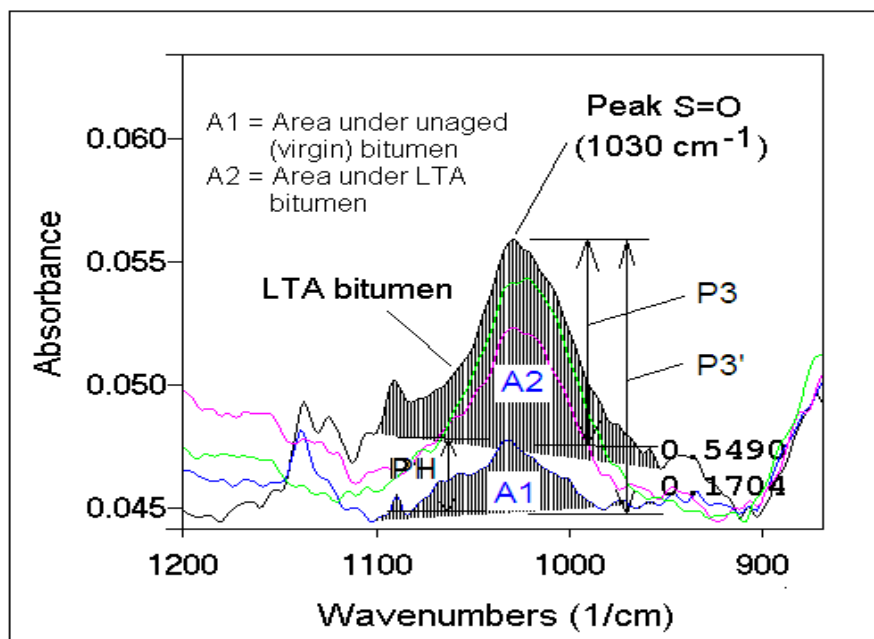


Figure 6.10: Method adopted to determine the peak area (PA) and peak height (PH) at the functional groups designated as aging indicators

Laboratory STA and LTA Bitumen Samples

The IR spectrum of bitumen samples aged in the laboratory under the standard aging protocol STA (short term aging) and LTA (long term aging) are shown in Figure 6.11. Figure 6.11 also includes the spectrums of bitumen samples taken during the LTA process at 65, 140, and 185 hours of aging in the RCAT equipment designated as RCAT65, RCAT140, and RCAT185 respectively. The unaged (virgin) bitumen showed small change in the carbonyl/ketone peak ($C=O$), the first characteristic peak for aging, and significant developments are observed at the second characteristic peak, i.e. the sulfoxide ($S=O$) peak. An increment both in the height and area of the $S=O$ peak is apparent. The RCAT140 material seems to show exceptional behaviour at the sulfoxide ($S=O$) peak compared to the RCAT185 bitumen. It is difficult to explain why the peak area has not increased as aging is an irreversible process. The aging of the bitumen also shows some changes at the $C-C$ bond.

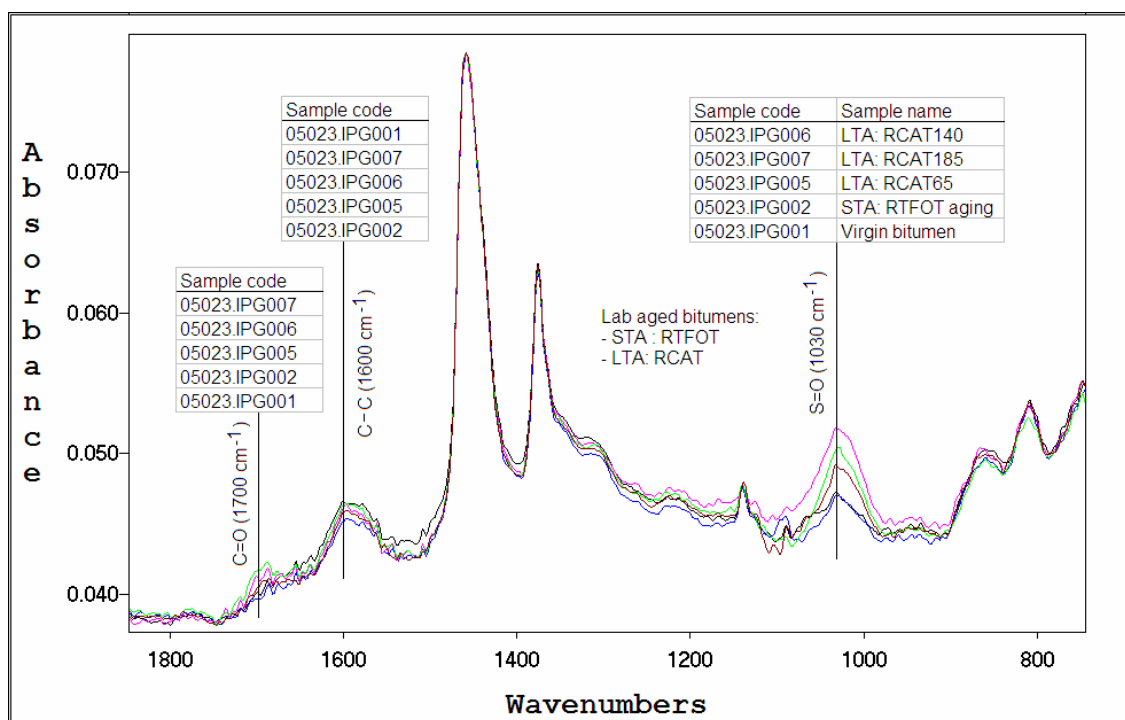


Figure 6.11: IR spectrum of laboratory-aged bitumens at the region "Finger print"

The peak areas and peak heights of the laboratory-aged bitumen samples at the functional groups 1030 cm^{-1} (S=O), 1600 cm^{-1} (C-C), and 1700 cm^{-1} (C=O) are shown in Figure 6.12 and Figure 6.13 respectively.

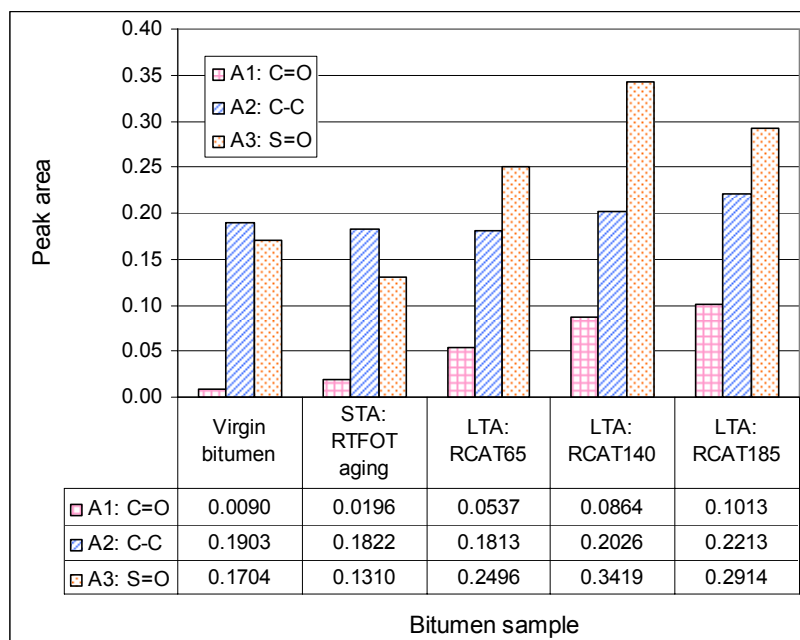


Figure 6.12: Peak areas of laboratory-aged bitumen at the functional groups of oxidation

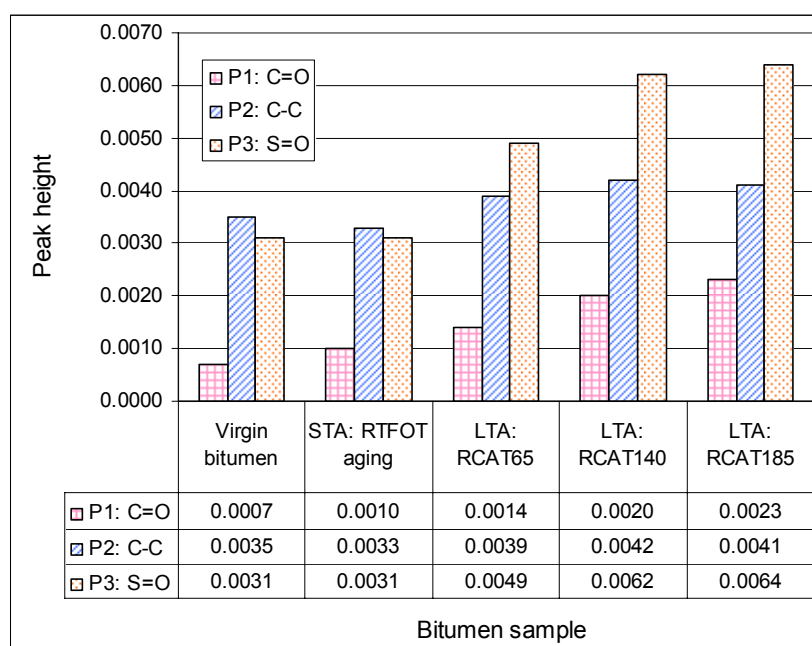


Figure 6.13: Peak heights of laboratory-aged bitumen at the functional groups of oxidation

Recovered Bitumen from Mixture Aging

Bitumen materials recovered from PA mixture aging under aging protocol AP1 (temp. aging), AP2 (temp.+UV aging), and AP3 (temp.+UV+RH) are shown in Figure 6.14. The spectrum includes the upper zone (UZ) and lower zone (LZ) of the specimens aged under AP1 and AP2 protocols and the UZ of AP3 protocol. According to the IR spectrum results at the finger print region shown in Figure 6.14, the peak heights at the S=O bond are decreasing in the order of AP1, AP2, and AP3 for the UZ samples. The AP3 (UZ) and AP2 (UZ) binders have shown considerable increment at the C–C peak, whereas only the AP3 seems to result in a significant increment at the C=O peak. In other words, AP3 the combined effect of temperature, UV light, and humidity in the aging process is contributing in the formation of both sulfoxides and ketones resulting in the increment of the oxidation peaks at the S=O and C=O. The effect of only temperature aging (AP1), however, is resulting predominantly in the formation of sulfoxide characterized by the peak at the S=O bond. To put it more clearly, the increase in peak height at the two oxidation products (C=O and S=O) seems balanced in the case of aging using the AP3 protocol, while AP1 protocol has predominantly increased the sulfoxide peak. These differences in aging behaviour unquestionably have implications in the simulation of bitumen aging in relation to field aging of PA.

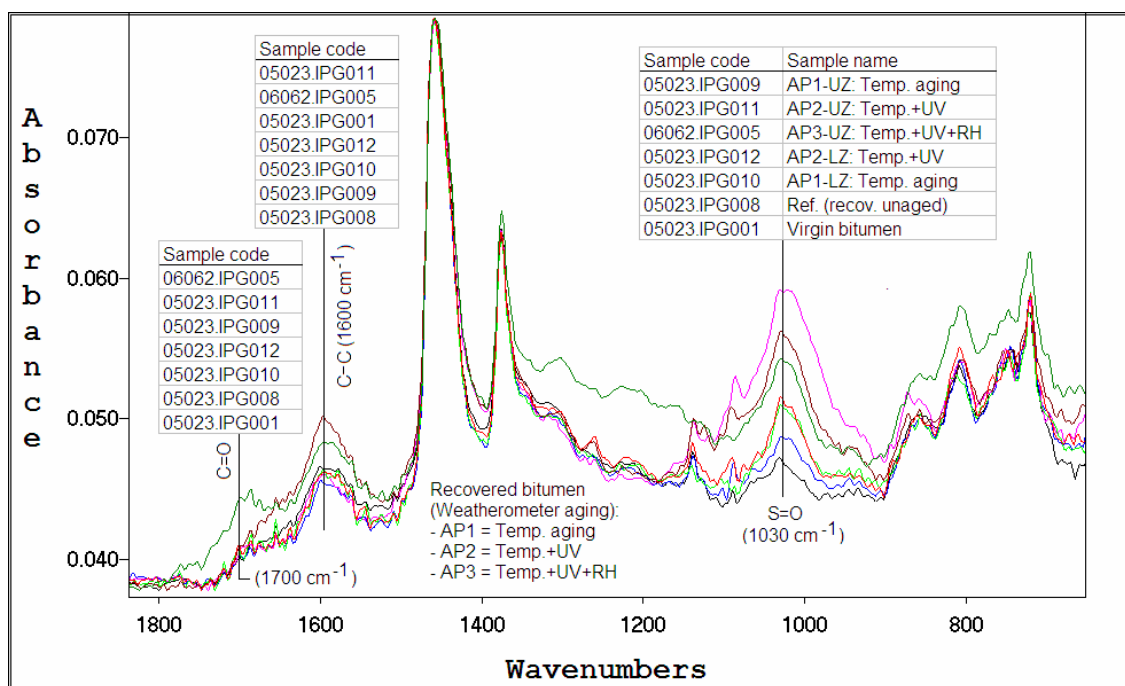


Figure 6.14: IR spectrum of recovered bitumen from PA mixture aged under AP1, AP2, and AP3 aging protocols

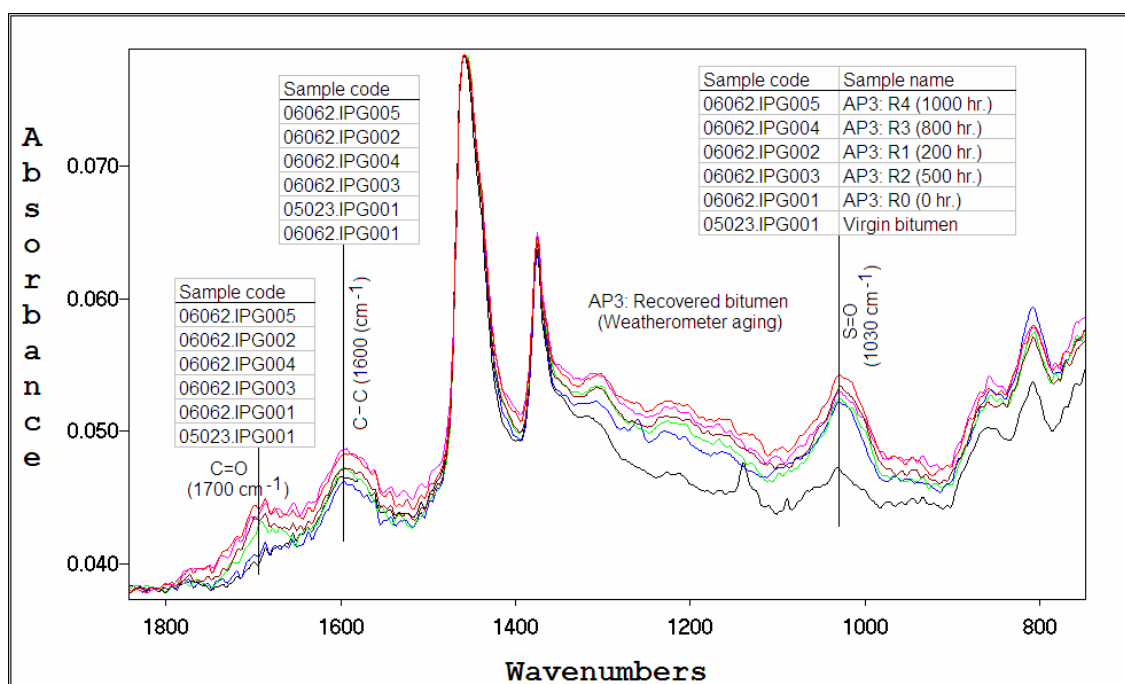


Figure 6.15: IR spectrum of bitumen recovered during AP3 mixture aging process

The AP3 protocol, as illustrated further in this section, correlates well with the aging process in the field in terms of oxidation peaks of the bitumen at the ketone (carbonyl) and sulfoxide functional groups. In order to correlate the rate of aging of the bitumen with field aging, samples were taken during the progress of AP3 weatherometer aging. The results of the IR spectrum of AP3 aging after 0, 200, 500, 800, and 1000 hours of aging are shown in Figure 6.15. In general, the peaks at the sulfoxide and ketones have shown increment with

aging time. Nevertheless, the R2 material aged for 200 hrs has shown unpredicted behaviour in the IR analysis of binders aged under the AP3 protocol. A unique behaviour about the aging protocol AP3 is a general rise in the response/spectrum throughout the frequency range in addition to the developments at the specific oxidation related peaks. The peak area and peak height of the functional groups are shown in Figure 6.16 and Figure 6.17.

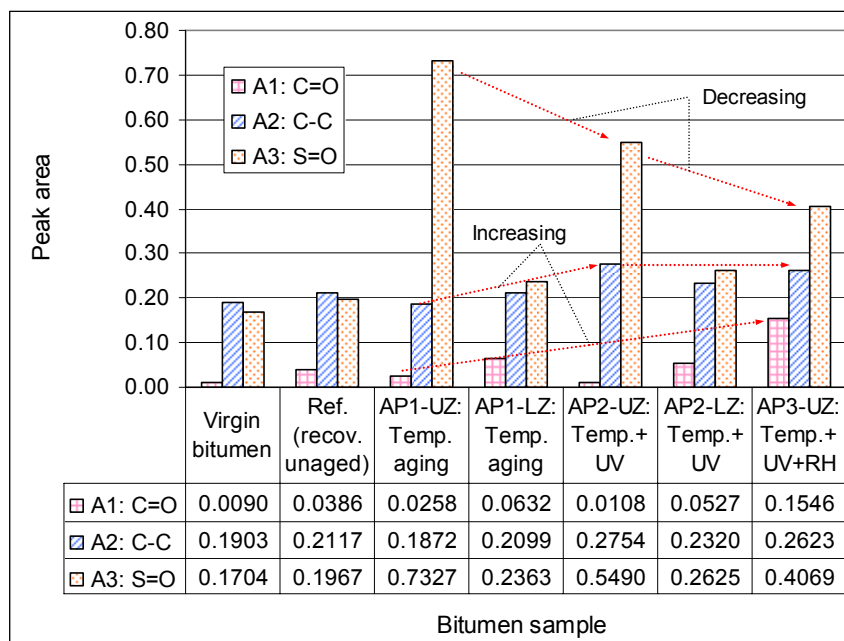


Figure 6.16: Peak areas of the oxidation products of bitumen recovered from mixture aging

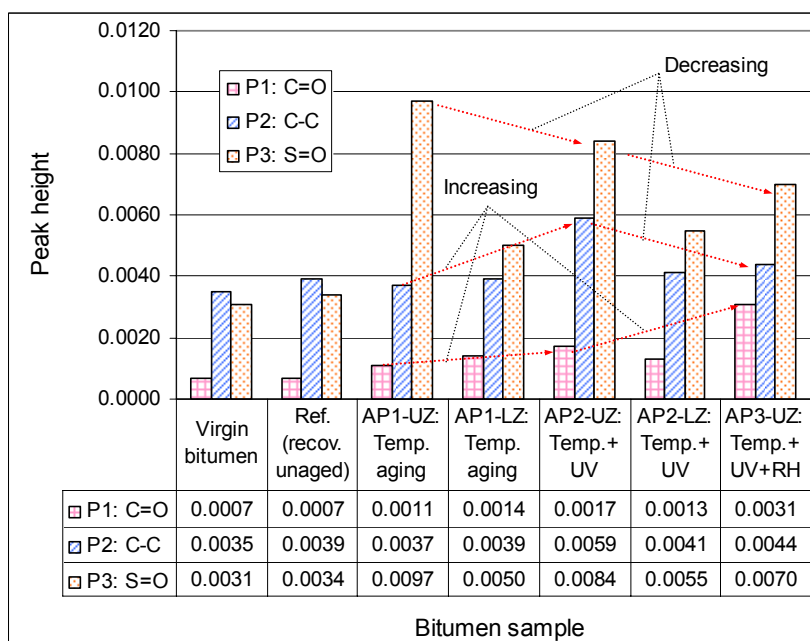


Figure 6.17: Peak heights of the oxidation products of bitumen recovered from mixture aging

Bitumen Recovered from Field specimens

Upper Zone (UZ)

The IR spectrum of the bitumen samples from field specimens with service periods of 0 (new construction), 1, 3, 7, and 12 year were analysed. Accordingly, the results of the upper zone (UZ) are shown in Figure 6.18 and Figure 6.19 for the emergency lane (EL) and slow lane (SL) respectively.

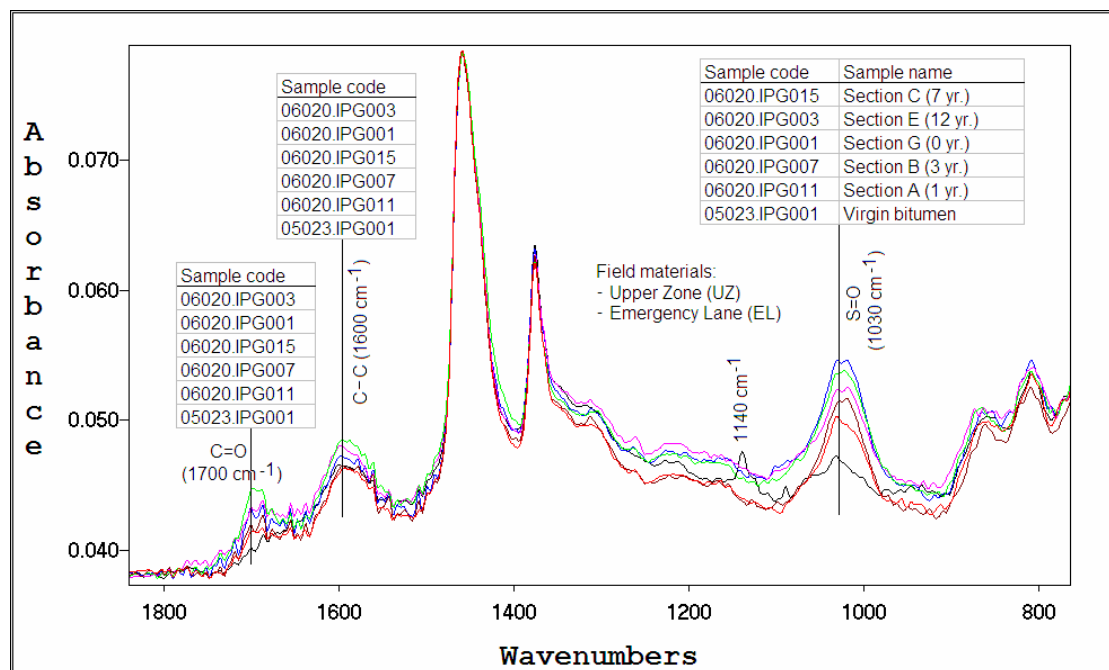


Figure 6.18: IR spectrum of bitumen recovered field specimens (UZ, EL)

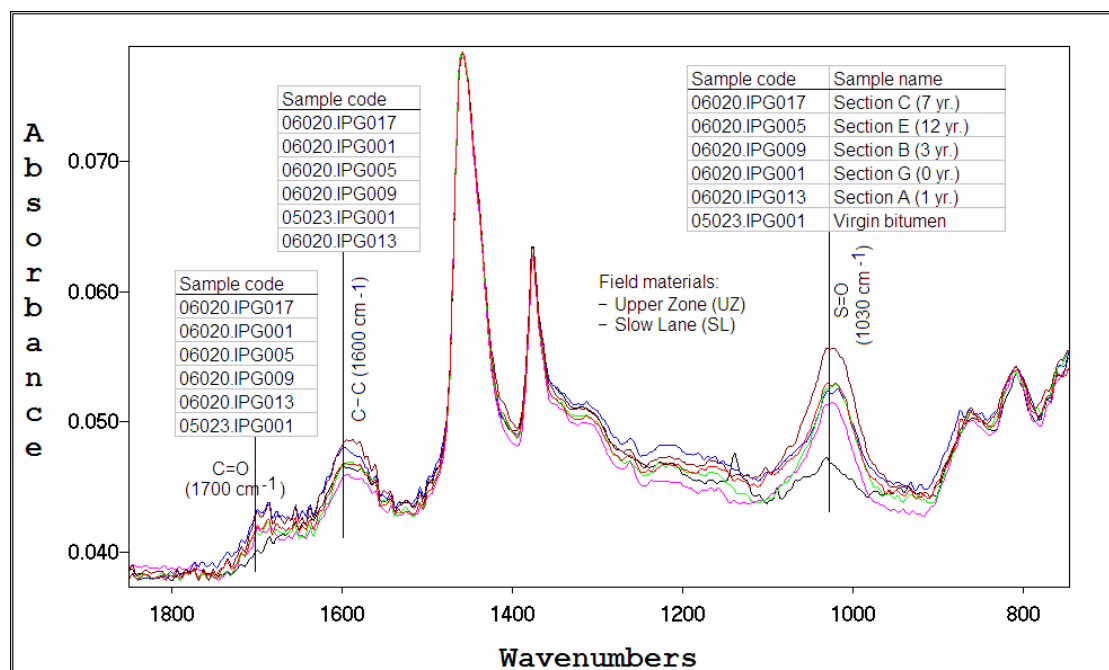


Figure 6.19: spectrum of bitumen recovered field specimens (UZ, SL)

In Figure 6.18 and Figure 6.19, the aging of the bitumen during the service period of the PA layer has generally resulted in an increase in the peak of the functional groups related to oxidation. An exception was observed in the general increasing trend of the specimen's characteristic peaks, which may be related to the percentage of hetro-atoms (indirectly to the vanadium content) of the bitumens. It is recognized that the bitumen from the new construction and the emergency lane 12 year old bitumen have shown higher and lower quantities of vanadium content respectively compared to the other binders. Although the binders are considered to belong to the same source/origin, the difference in vanadium content seems to be having an influence on the aging behaviour of the binders.

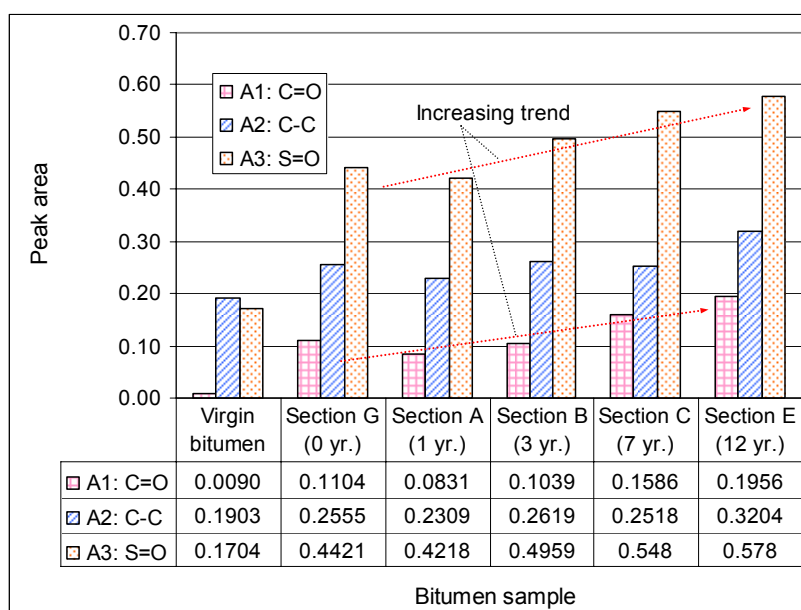


Figure 6.20: Peak area of the oxidation products of field specimens (UZ, EL - No traffic)

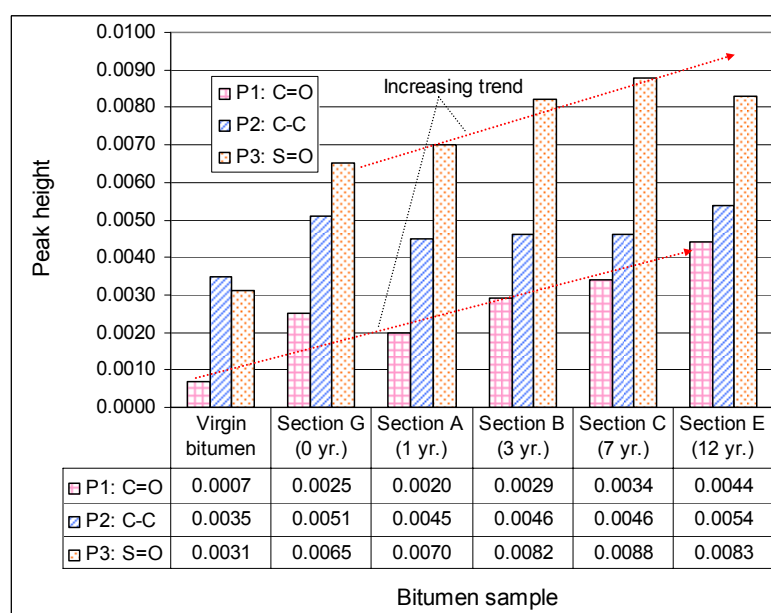


Figure 6.21: Peak height of the oxidation products of field specimens (UZ, EL – No traffic)

Observation of peak areas and peak heights of the UZ EL binders in Figure 6.20 and Figure 6.21 confirms the exceptional behaviour of the field binder from the new construction. The peak area and height of the UZ SL in Figure 6.22 and Figure 6.23 in turn shows the exceptional behaviour of the 12 year old field binder. Nevertheless, what we can observe from the peak areas and peak heights of the EL and SL specimens is the fact that the aging behaviour is influenced by the effect of traffic (refer also to Figure 6.24). For comparison purposes, the IR spectra of field specimens from the emergency and the slow lanes are shown in Figure 6.24.

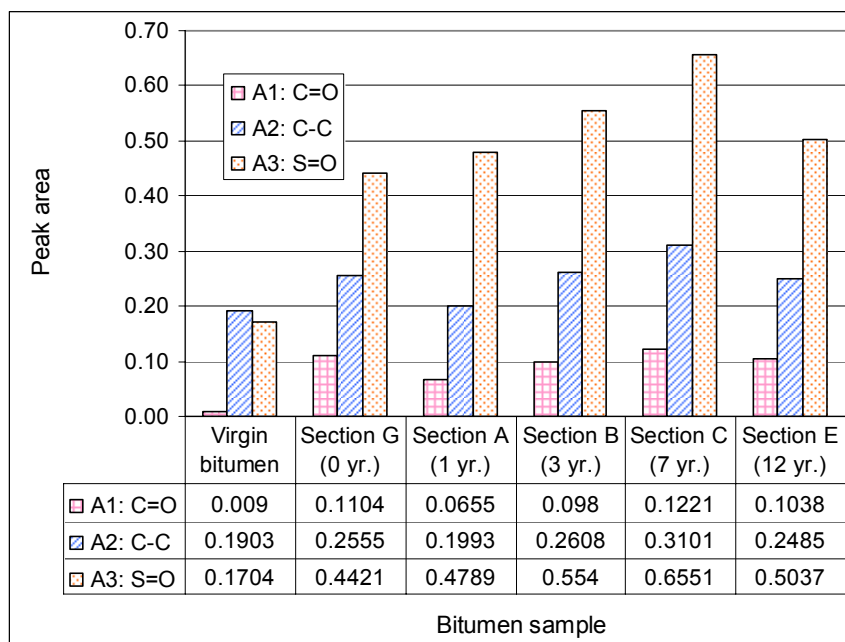


Figure 6.22: Peak area of the oxidation products of field specimens (UZ, SL - trafficked)

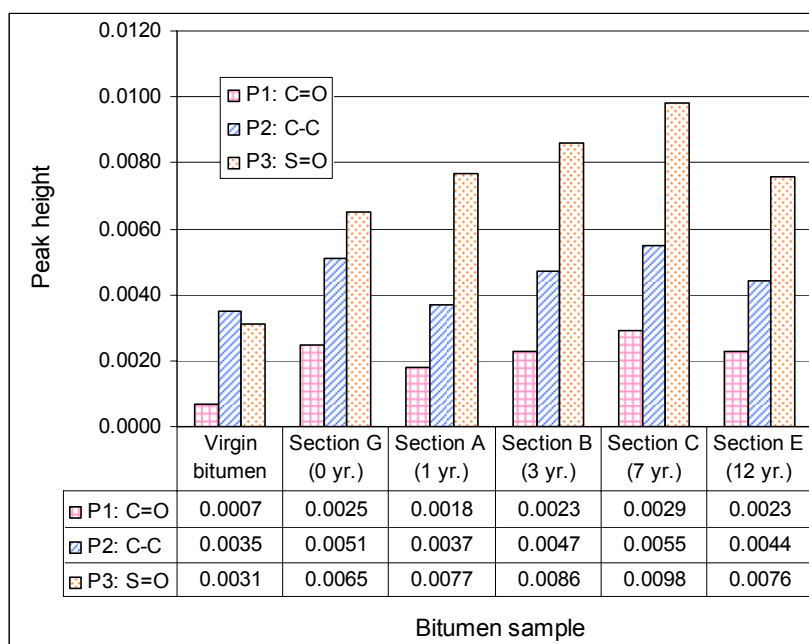


Figure 6.23: Peak area of the oxidation products of field specimens (UZ, SL - trafficked)

The field aging resulted in the increment of the oxidation products, i.e. ketones (1700 cm^{-1}) and sulfoxides (1030 cm^{-1}). The effect of traffic loading in the aging behaviour of bitumen can be indirectly addressed from the difference in IR spectrums of the EL and SL field specimens. From Figure 6.24, no consistent trends of aging rate of the EL and SL binders can be distinguished based on the peak heights. It should be noticed that a possible effect of traffic on aging could not be detected. However, the kinetic approach using peak areas clearly showed a difference in aging rate (Figure 6.30).

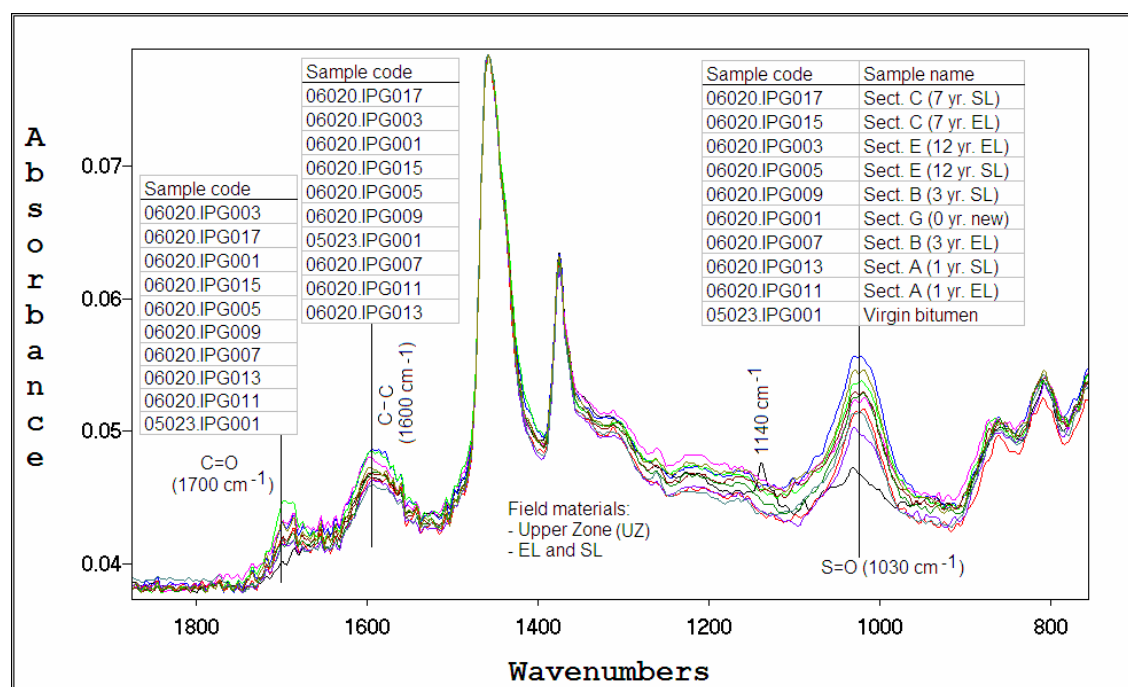


Figure 6.24: IR spectrum of the UZ field binders (EL and, SL)

The presence of a higher quantity of vanadium content in binders is an indication of the presence of higher quantities of hetero-atoms. This implies also that the aging of bitumen with higher hetero-atom concentrations will be influenced because of the formation of sulfoxide (one of the main oxidation products). This could be the reason for the unanticipated S=O peak of the binder from section G exceeding the aging condition of the binders from road sections with 1 and 3 years of service life.

One observation worth mentioning is the peak at 1140 cm^{-1} which is noticed with the unaged (virgin) bitumen but the binders from the road do not possess. This peak exists with the binders aged in the laboratory both using the standard aging procedure and the mixture aging protocols. It perhaps shows that the aging mechanism in the field is entirely different (complex) from laboratory aging involving interaction with the fines (filler + hydrated lime) and aggregate materials apart from the oxidation products occurring at the specified frequencies (wavenumbers).

Lower Zone (LZ)

Since the ravelling of bitumen is occurring at the surface of the PA pavement, the aging of bitumen at the UZ is considered important in relation to the durability of PA. However, the possibility of failure propagation from the bottom upwards could also be the reason for durability problems. Hence, the LZ is also important for complete understanding of binder aging in the UZ and LZ of PA. The IR spectrum can explain the influence of the different factors in the aging process of the LZ binder in PA.

The results of IR spectrum of the binders from the lower zone (LZ) of field specimens were analysed. The spectrums of the EL and SL binders are shown in Figure 6.25 and Figure 6.26 respectively. The corresponding peak area and peak height for the LZ binders is shown in Table 6.6. The ratios of the peak area and the peak height relative to the virgin bitumen are shown in Table 6.7.

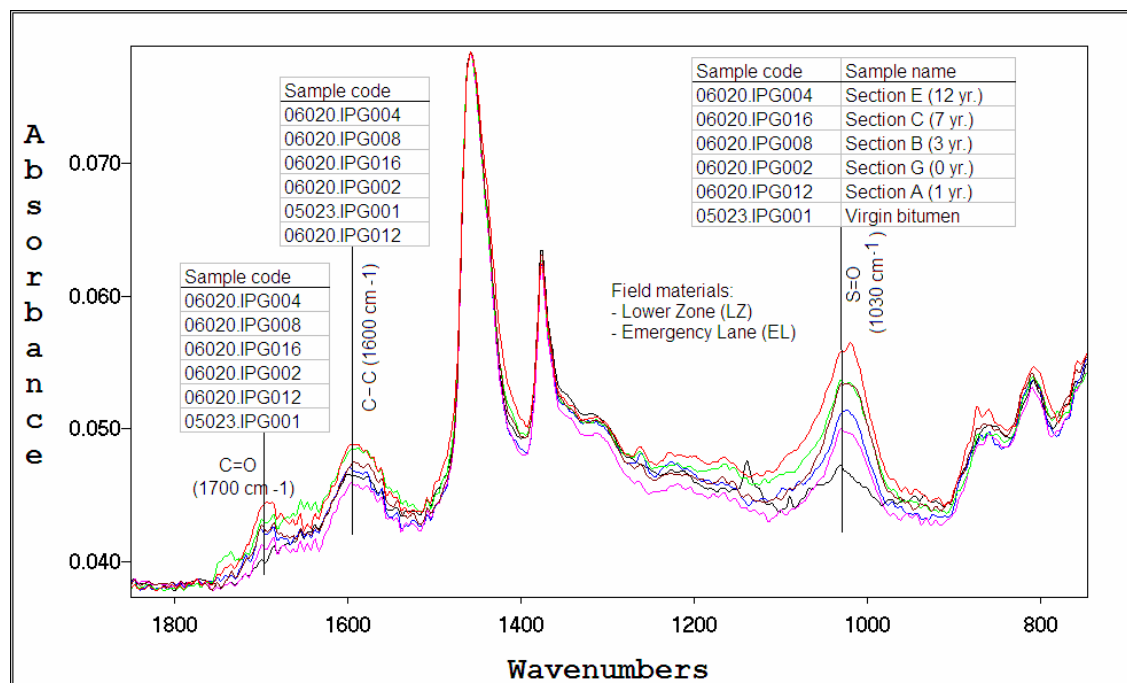


Figure 6.25: IR spectrum of bitumen recovered field specimens (LZ, EL)

In general, the LZ binders have shown an increase of the oxidation products C=O (ketones) and S=O (sulfoxides). Similarities can be observed in the effect of aging of the binder in the emergency lane (no traffic lane, Figure 6.25) and the slow lane (trafficked lane, Figure 6.26). The only exception noticeable is the aging behaviour of the binder from section E SL (12 year old) pavement. It was expected that the EL binder but not the SL binder will show a unique aging behaviour given the lower vanadium content of the material. The unexpected aging behaviour may be attributed to other factors that influence the aging process of the binder such as the type of aggregate used or contaminations from traffic.

For comparison purposes, the IR spectra of the EL and SL are shown in Figure 6.27.

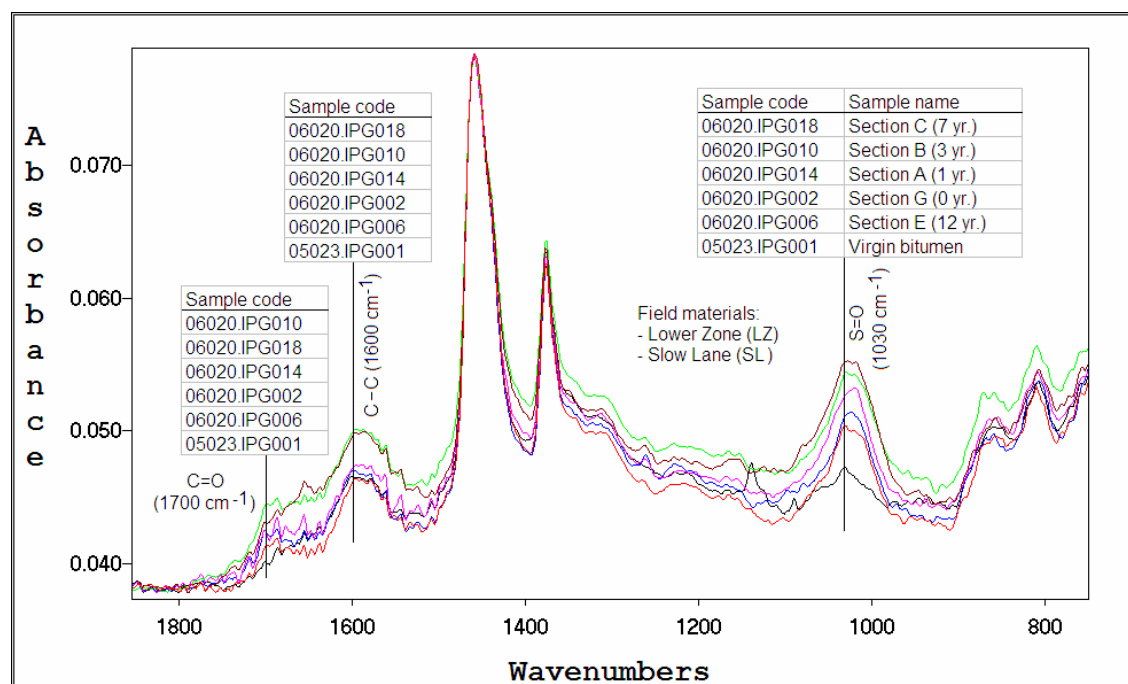


Figure 6.26: IR spectrum of bitumen recovered field specimens (LZ, SL)

Table 6.6: Peak area (PA) and peak height (PH) of LZ binders at functional groups related to oxidation products (C=O, C–C, and S=O)

				(1700 cm-1)	(1600 cm-1)	(1030 cm-1)	
		Sample code	Sample name	A1: C=O	A2: C-C	A3: S=O	A1+A3
Peak Area (PA)	Emergency Lane (EL)	05023.IPG001	Virgin bitumen	0.0090	0.1903	0.1704	0.1794
		06020.IPG002	Section G (0 yr.)	0.0718	0.2497	0.4093	0.4811
		06020.IPG012	Section A (1 yr.)	0.0650	0.2319	0.3511	0.4161
		06020.IPG008	Section B (3 yr.)	0.0103	0.2292	0.4755	0.4858
		06020.IPG016	Section C (7 yr.)	0.0937	0.2624	0.5586	0.6523
		06020.IPG004	Section E (12 yr.)	0.1637	0.2977	0.7067	0.8704
	Slow Lane (SL)	05023.IPG001	Virgin bitumen	0.0090	0.1903	0.1704	0.1794
		06020.IPG002	Section G (0 yr.)	0.0718	0.2497	0.4093	0.4811
		06020.IPG014	Section A (1 yr.)	0.0939	0.2626	0.5163	0.6102
		06020.IPG010	Section B (3 yr.)	0.1018	0.2985	0.5327	0.6345
		06020.IPG018	Section C (7 yr.)	0.0068	0.2487	0.6323	0.6391
		06020.IPG006	Section E (12 yr.)	0.0926	0.2420	0.4113	0.5039
						Relative Peak	
	Sample code	Sample name	P1: C=O	P2: C-C	P3: S=O	P3' @ S=O	
Peak Height (PH)	Emergency Lane (EL)	05023.IPG001	Virgin bitumen	0.0007	0.0035	0.0031	0.0031
		06020.IPG002	Section G (0 yr.)	0.0022	0.0046	0.0070	0.0074
		06020.IPG012	Section A (1 yr.)	0.0018	0.0042	0.0063	0.0059
		06020.IPG008	Section B (3 yr.)	0.0013	0.0043	0.0079	0.0095
		06020.IPG016	Section C (7 yr.)	0.0025	0.0045	0.0086	0.0093
		06020.IPG004	Section E (12 yr.)	0.0034	0.0052	0.0103	0.0125
	Slow Lane (SL)	05023.IPG001	Virgin bitumen	0.0007	0.0035	0.0031	0.0031
		06020.IPG002	Section G (0 yr.)	0.0022	0.0046	0.0070	0.0074
		06020.IPG014	Section A (1 yr.)	0.0022	0.0044	0.0082	0.0091
		06020.IPG010	Section B (3 yr.)	0.0025	0.0047	0.0075	0.0103
		06020.IPG018	Section C (7 yr.)	0.0008	0.0042	0.0089	0.0112
		06020.IPG006	Section E (12 yr.)	0.0023	0.0043	0.0069	0.0063

Table 6.7: Ratios of the peak area (PA) and peak height (PH) of LZ binders at functional groups related to oxidation products (C=O, C–C, and S=O)

PA Ratio (relative to virgin bitumen)							
	Sample code	Sample name	A1	A2	A3	A4	
Emergency Lane (EL)	05023.IPG001	Virgin bitumen	1.000	1.000	1.000	18.933	
	06020.IPG002	Section G (0 yr.)	7.978	1.312	2.402	5.701	
	06020.IPG012	Section A (1 yr.)	7.222	1.219	2.060	5.402	
	06020.IPG008	Section B (3 yr.)	1.144	1.204	2.790	46.165	
	06020.IPG016	Section C (7 yr.)	10.411	1.379	3.278	5.962	
	06020.IPG004	Section E (12 yr.)	18.189	1.564	4.147	4.317	
Slow Lane (SL)	05023.IPG001	Virgin bitumen	1.000	1.000	1.000	18.933	
	06020.IPG002	Section G (0 yr.)	7.978	1.312	2.402	5.701	
	06020.IPG014	Section A (1 yr.)	10.433	1.380	3.030	5.498	
	06020.IPG010	Section B (3 yr.)	11.311	1.569	3.126	5.233	
	06020.IPG018	Section C (7 yr.)	0.756	1.307	3.711	92.985	
	06020.IPG006	Section E (12 yr.)	10.289	1.272	2.414	4.442	
PH Ratio (relative to virgin bitumen)							
	Sample code	R1	R2	R3	R3'	R4	R4'
Emergency Lane (EL)	05023.IPG001	1.000	1.000	1.000	1.000	4.429	4.429
	06020.IPG002	3.143	1.314	2.258	2.387	3.182	3.364
	06020.IPG012	2.571	1.200	2.032	1.903	3.500	3.278
	06020.IPG008	1.857	1.229	2.548	3.065	6.077	7.308
	06020.IPG016	3.571	1.286	2.774	3.000	3.440	3.720
	06020.IPG004	4.857	1.486	3.323	4.032	3.029	3.676
Slow Lane (SL)	05023.IPG001	1.000	1.000	1.000	1.000	4.429	4.429
	06020.IPG002	3.143	1.314	2.258	2.387	3.182	3.364
	06020.IPG014	3.143	1.257	2.645	2.935	3.727	4.136
	06020.IPG010	3.571	1.343	2.419	3.323	3.000	4.120
	06020.IPG018	1.143	1.200	2.871	3.613	11.125	14.000
	06020.IPG006	3.286	1.229	2.226	2.032	3.000	2.739

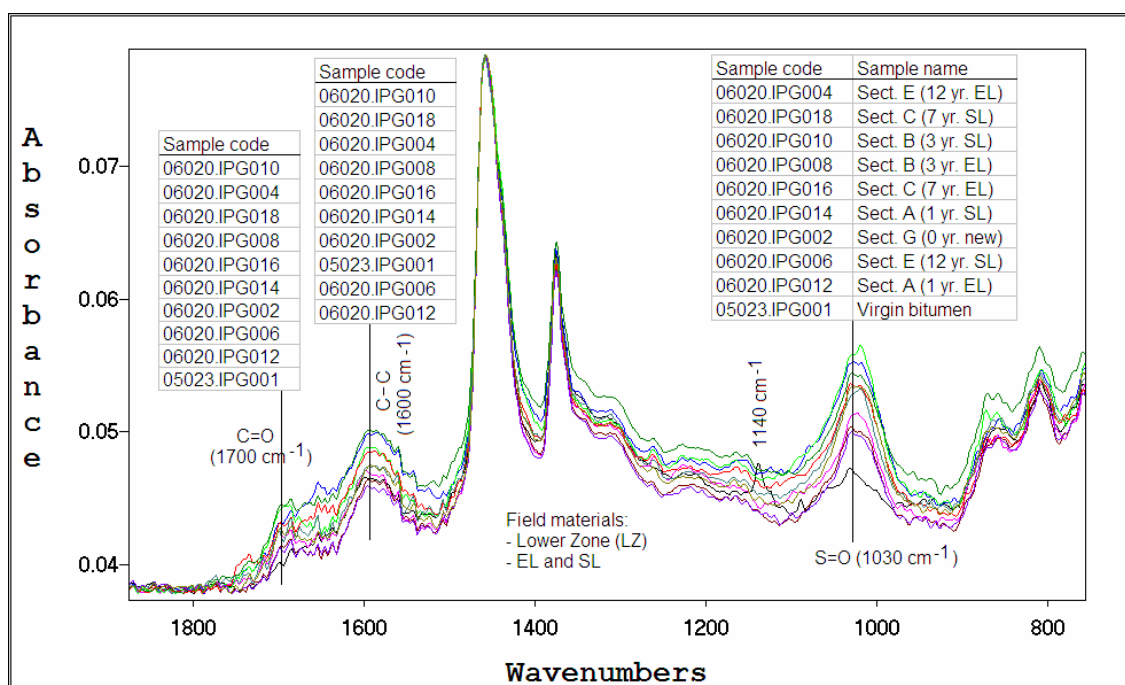


Figure 6.27: IR spectrum of the LZ field binders (EL and SL)

Field and laboratory bitumen aging behaviour

The aging of the binder in PA is a complex process involving many factors. Nevertheless, the combined results of the field binders and the laboratory aged binders are discussed in this section to highlight the effects of different aging mechanisms (major factors) in relation to real aging of PA in the road.

Figure 6.28 shows the IR spectrum in the finger print region of laboratory aged bitumens (RCAT185), 12 year old field specimen (UZ), and binders recovered from weatherometer aging (AP3). As it can be observed in Figure 6.28, the materials from the 12 yr old pavement and the 1000 hr weatherometer aging have comparable peaks at the S=O band and seem to have relatively higher peaks at the C=O band. The LTA binder (conventional long term aging using RCAT) does not seem to have significant effect on the C=O band at 1700 cm^{-1} and has the lowest peak in the S=O band at 1030 cm^{-1} next to the virgin bitumen. The recovered bitumen from the laboratory mixture aging test (AP2: temp.+UV aging) has the highest peak at the sulfoxide peak (S=O) while showing a small increment at the ketones peak (C=O). This indicates that the effect of temperature and UV light on the aging process seem to be reflected in the development of the sulfoxide peak. The combined effect of the UV light and temperature has greater effect on binder aging than the protocol with only the effect of temperature in the weatherometer. The effect of the UV light on the aging process can also be seen at the C–C band (1600 cm^{-1}). The combination of the three aging effects, i.e. temperature, UV light, and humidity (RH), is resulting in the development of the two major oxidation products (C=O and S=O), which is consistent with the characteristic of the field aged binders. To recap, the combined effect of temperature, UV exposure and humidity/moisture seems to result in the formation of both the ketones and sulfoxides similar to the field aging whereas the conventional aging results in S=O formation with minimum effect on C=O development. This supports the assertion that the conventional binder aging method does not simulate field aging.

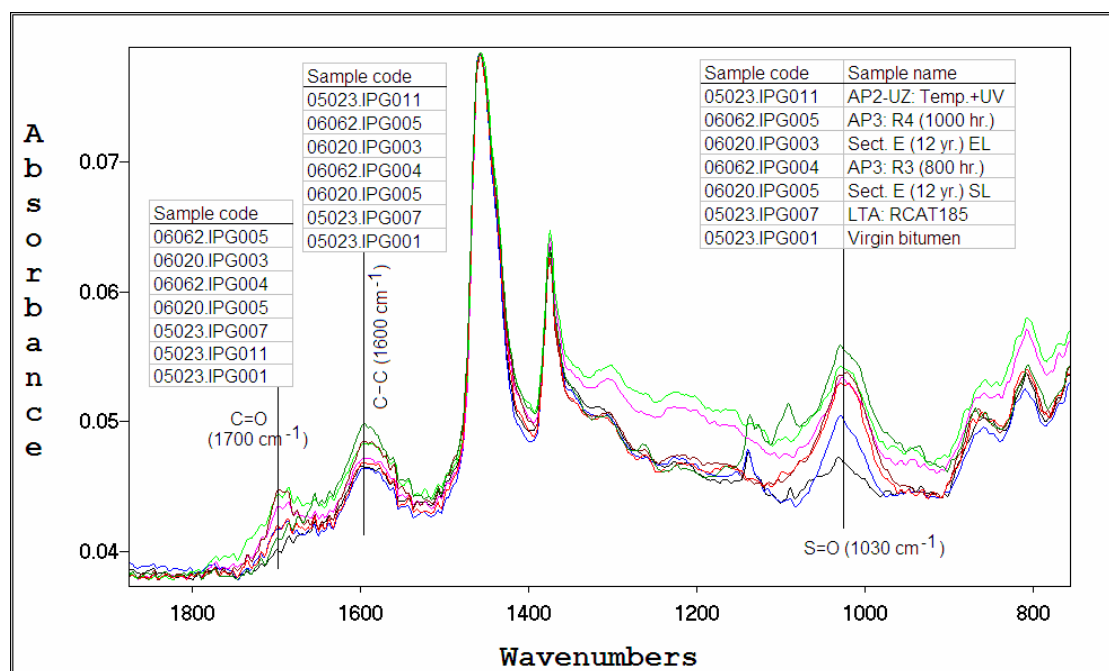


Figure 6.28: IR spectrum of laboratory-aged and UZ field binders

From Figure 6.28 and Figure 6.29, the aging of bitumen in the field seems to be reasonably in compliance with the laboratory aging procedure AP3 with regard to the development of the aging products at the sulfoxide and ketone peaks. In Figure 6.29, the aging method employed for the aging of mixes in the weatherometer seems good enough to predict field aging conditions both in the emergency and slow lanes of the UZ. However, one should keep in mind that not only the peak values are of importance; also the areas have to be taken into account.

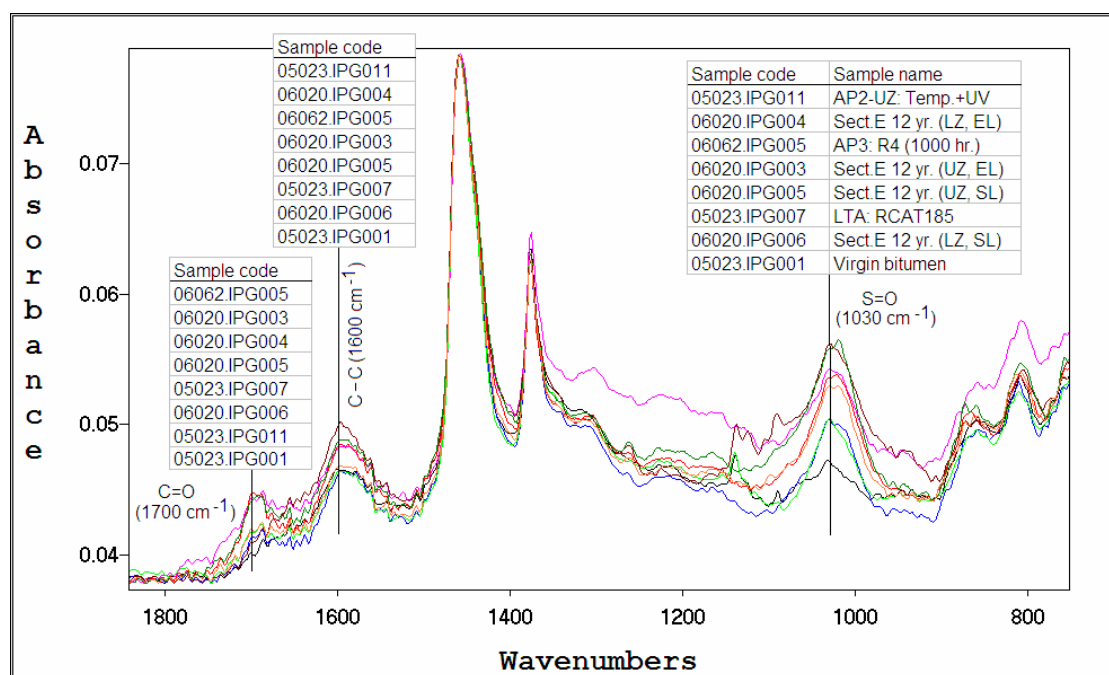


Figure 6.29: IR spectrum of binders from laboratory aging and recovered from field specimens

The kinetic approach (Equation 2.17) was used to fit the development of the oxidation products (C=O and S=O) of the EL and SL field binders in Figure 6.30. This approach was used by Verhasselt 2000 to predict the aging rate of field and laboratory binders based on the development of the asphaltene content with aging time. In Figure 6.30, the aging curve was determined based on the sum of the characteristic peak areas for oxidation at C=O and S=O. Accordingly, the most aged binders in the laboratory using the standard and weatherometer aging have less area than the 1 year old pavement binders. The LTA bitumen using RCAT predicted 0.43 year and the binder aged for 1000 hrs in the weatherometer predicted 2.1 years of field aging using the EL model. Hence, it was practically not possible to correlate the laboratory and field aging of binders. The kinetic model based on the peak height (PH) data at the C=O and S=O bonds also shows that the prediction of the laboratory aged binders to the aging in the field is not consistent (Table 6.8). The aging of asphalt mixtures for 1000 hr (weatherometer AP3) prediction seems to provide the intended aging life in the field according to the evaluation of peaks at P3'. Nevertheless, it can be concluded that both the existing and proposed laboratory aging methods as used seem to predict field aging of PA that occurs over a limited period of time.

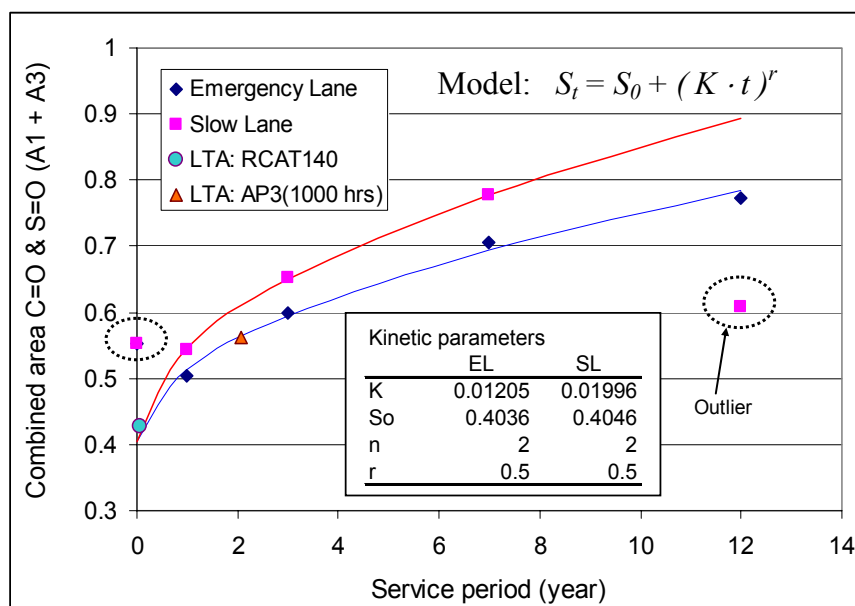


Figure 6.30: Development of oxidation products of field materials (UZ)

Table 6.8: Parameters of kinetic models based on peak heights at C=O and S=O and the predicted aging time (in years) of laboratory aged binders

		kinetic model:		$S_t = S_o + (K^*t)^r$	
		parameter	P1: C=O	P3: S=O	P3': S=O (relative peak)
Emergency lane, EL	K	0.008511	0.00852	0.02914	
	So	0.1136	0.6384	0.4552	
	r	0.5	0.5	0.5	
Slow lane, SL	K	0.004461	0.01551	0.008207	
	So	0.1136	0.6476	0.7072	
	r	0.5	0.5	0.5	
Predicted year		P1: C=O	P3: S=O	P3': S=O (relative peak)	
EL	RCAT140	0.87	0	3.17	
	AP3: 1000 hrs	3.67	0	10.94	
SL	RCAT140	1.68	0	0.35	
	AP3: 1000 hrs	6.97	0	11.9	

NB: The kinetic model parameters provided above predict $100 \times PH$ (Peak Height).

In Figure 6.30, the aging rate of the emergency and slow lanes can be observed. The aging rate of the trafficked lane (SL) binder is higher than the lane with no traffic (EL). The logical explanation for this could be as follows: The damaging effect of traffic loading especially at lower temperatures results in micro-cracks. Micro-cracks create new surfaces to be exposed to the influence of the environmental factors promoting aging to take place. Another factor could be related to the maintenance operations. The EL, for example, is not cleaned as often as possible and hence will have an effect on the aging of the binder film compared to the SL that is cleaned more often.

In summary, the following observations are made:

- Similar aging pattern as in the field is seen with the AP3 weatherometer aging. But the laboratory mixture aging is not as severe as the field aging. Accordingly, similarities in aging do not result in the same physical properties.
- In comparing the binder aging at the UZ and LZ of PA, the influence of the dominant environmental factors at the upper and bottom layer of PA, i.e. UV light at the UZ and the effect of moisture at the LZ, do not seem to have resulted in significant differences in the aging behaviour of the binder.
- The aging of the binder in the EL (no traffic) and SL (trafficked lane) show that the effect of traffic may contribute to the reduced aging rate of the binder on the emergency lane (Figure 6.30).
- Unexpected aging behaviour of the binders from the road can be partly due to the difference in the compositions of the binders.
- Binder aging in the field is a complex process.

6.3 Gel-Permeation Chromatography (GPC)

Gel-Permeation Chromatography (GPC), also known as Size Exclusion Chromatography (SEC), is a chromatographic method in which particles are separated based on their molecular size, or in more technical terms, their hydrodynamic volume. GPC or SEC is a technique used to analyze the Molecular Weight Distribution of materials soluble in organic solvent. Commonly used solvents for GPC¹¹ are Tetrahydrofuran (THF) and Toluene. The technique is widely used to determine the molecular distribution of bituminous materials (Branthaver et al. 1993, SHRP-A-368). It is a powerful method to study the effects of bitumen modification and age hardening in bitumen related researches (Molenaar et al. 2004).

6.3.1 The Principles of GPC

The principle of Size Exclusion Chromatography (SEC) is based on the separation of a solution of particles according to their sizes. The process involves a solution of molecules with different sizes eluting (filtering) through a porous medium (cross-linked polystyrene beads) that prompt the molecules to move at different speeds resulting in the separation of the particles based on their size. This process occurs in the column, which consists of a hollow tube tightly packed with extremely small porous medium (stationary phase) with pores of different sizes. As the solution travels through the column, the larger particles move faster with minimum obstruction by the pores and take less time to travel the length of the column (Skoog and Leary 1992, Wikipedia 2007). The smaller size particles enter into the pores, thus, taking longer time to come out of the column. The sample emerges from the column in the opposite order of molecular size; that is, the largest molecules emerge first followed by progressively smaller molecules (Figure 6.31). In order to determine the concentration and molecular weight of the emerging sample, detectors are located at the end of the column. The volume of solvent flow is also monitored to provide a means of characterizing the molecular size of the eluting species. The two common spectroscopic detection techniques employed were Refractive Index (RI) and Photodiode Array (PDA). In this research, the PDA light scanning method was used to process the information of the GPC test (refer to section 6.3.3).

¹¹ In Gel Permeation Chromatography test an organic solvent is used as a mobile phase to transport the sample through the columns (If an aqueous solution is used, the technique is known as gel filtration chromatography).

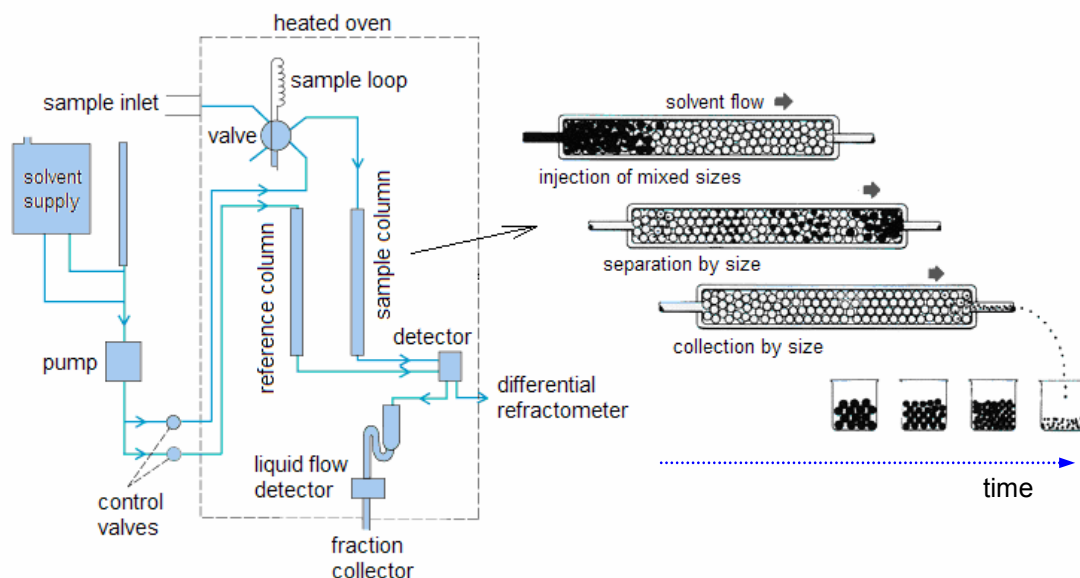


Figure 6.31: Gel-Permeation Chromatography technique (Answers 2003, Waters 2008)

6.3.2 Molecular Weight Distribution (MWD)

GPC results in measurement of the entire Molecular Weight Distribution (MWD) (see Figure 6.32) from which the molecular weight averages or *moments* of molecular weight can be determined. Statistical measures such as the number-average and weight-average molecular weights, respectively M_n and M_w , are convenient expressions to describe the distribution. The most common parameters are given in Equation 6.9 through Equation 6.13.

$$M_\varphi = \frac{\sum(n_i \cdot M_i^\varphi)}{\sum(n_i \cdot M_i^{(\varphi-1)})} \quad (\varphi = 1, 2, 3, 4) \quad (6.8)$$

$$M_n = \frac{\sum m}{\sum n} = \frac{\sum(n_i \cdot M_i)}{\sum n_i} \quad (\varphi = 1) \quad (6.9)$$

$$M_w = \frac{\sum(n_i \cdot M_i^2)}{\sum(n_i \cdot M_i)} = \frac{\sum(c_i \cdot M_i)}{\sum c_i} \quad (\varphi = 2) \quad (6.10)$$

$$M_z = \frac{\sum(n_i \cdot M_i^3)}{\sum(n_i \cdot M_i^2)} = \frac{\sum(c_i \cdot M_i^2)}{\sum(c_i \cdot M_i)} \quad (\varphi = 3) \quad (6.11)$$

$$M_{z+1} = \frac{\sum(c_i \cdot M_i^3)}{\sum(c_i \cdot M_i^2)} \quad (\varphi = 4) \quad (6.12)$$

$$PDI = \frac{M_w}{M_n} \quad (6.13)$$

Where:

- M_n = number-average molecular weight [g/mol, daltons],
 M_w = weight-average molecular weight [g/mol],
 M_z = z-average molecular weight [g/mol],
 M_{z+1} = (z+1)-average molecular weight [g/mol],
 M_p = peak molecular weight [g/mol],
 M_i = molecular weights [g/mol],
 m = mass of molecules of molecular weight M_i [g/mol],
 n_i = number of molecules of molecular weight M_i [-],
 c_i = concentration, $c_i = n_i \cdot M_i$ [g/mol],
 PDI = Polydispersity Index – relative spread in molecular weights [-].

Each measure of molecular mass provides a different information. M_n (the 1st moment) emphasizes the smaller molecules present whereas M_w (the 2nd moment divided by 1st moment) and M_z (the 3rd moment divided by 2nd moment) emphasize the larger molecules. The molecular weights are of the order $M_z > M_w > M_n$ as shown in Figure 6.32. Given M_w and M_n the standard deviation σ of the distribution can be determined using Equation 6.14:

$$\sigma = M_n \left(\frac{M_w}{M_n} - 1 \right)^{1/2} = M_n (PDI - 1)^{1/2} \quad (6.14)$$

Where:

- σ = standard deviation [-].

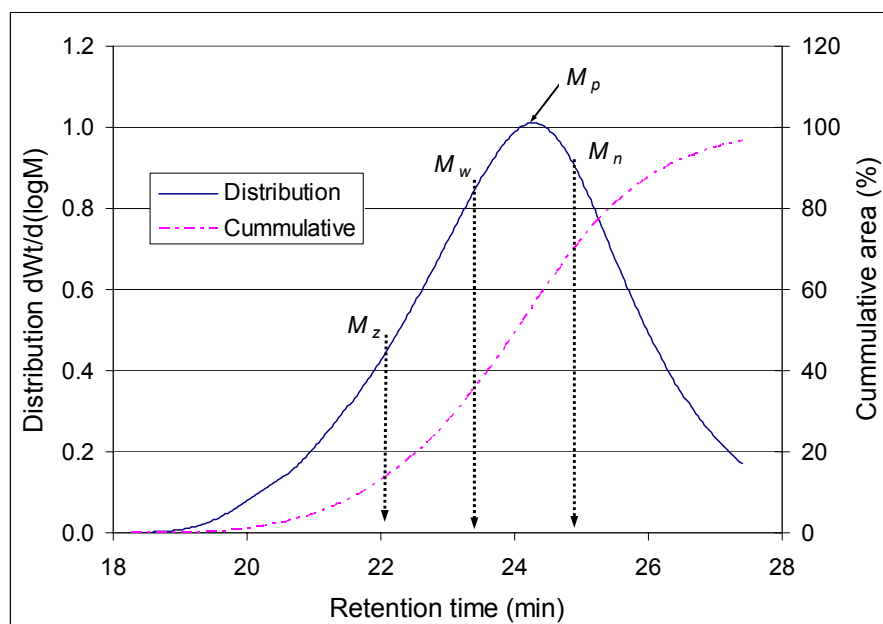


Figure 6.32: Molecular weight distribution (MWD) plot of a virgin (unaged) bitumen

A viscosity-average molecular mass M_v , which lies between M_n and M_w , is defined by Equation 6.15. A measure of the contribution of the solute to the

viscosity η of the solution (THF) is described by the intrinsic viscosity given in Equation 6.16.

$$M_v = \left[\frac{\sum n_i \cdot M_i^{1+a}}{\sum n_i \cdot M_i} \right]^{1/a} = \left[\sum n_i \cdot M_i^a \right]^{1/a} \quad (6.15)$$

$$[\eta] = KM_i^a \quad (\text{Mark-Houwink equation}) \quad \Rightarrow \quad \log[\eta] = \log K + a \log M_i \quad (6.16)$$

Where:

M_v	=	viscosity-average molecular mass [g/mol, daltons],
a	=	a constant in the equation (range 0.6 – 0.8),
$[\eta]$	=	intrinsic viscosity of the binder in the solution [ml/g],
K	=	characteristic constant of the solution (range 0.5 – 5×10^{-4}).

6.3.3 Sample Preparation and Testing

Waters GPC apparatus consisting of an auto-sampler, two detector systems, a column-box (oven/heater), pump, and other units was used for testing (Figure 6.34). The auto-sampler unit (*Waters 717plus*) takes a representative sample from a solution of the samples for testing. Two detector systems are connected to the system to provide information regarding the concentration and molecular weight of the sample. These are: 1) *Waters 2414* Reflective Index (RI) and 2) *Waters 996* Photodiode Array (PDA). The column box consists of columns with pore sizes 5×10^3 , 2×10^4 , 7×10^4 , and 4×10^6 Å¹². The whole system works according to the principle explained in section 6.3.1. The sample solution preparation and testing procedure was conducted according to DWW standard WV 017 (DWW 2004).

The first step in performing the GPC test is the preparation of the bitumen solution. An amount of 30 ± 3 mg of binder sample was dissolved in 25 ml of strong organic solvent Tetra Hydro Furan (THF: Chemical formula C₄H₈O). The same THF fluid was also used during the test as an eluent (mobile phase in the columns) with 50 mg/l of Ionol added for the purpose of stabilization. The sample preparation process involved a gentle shaking of the solution (bitumen sample and THF) to facilitate the dissolving of the binder in the organic solvent. Before taking representative samples, light swirling of the samples was performed to enhance dissolution (uniform mixing). Representative samples were taken in a 20 ml clear glass vials by the use of a syringe. A filter membrane was inserted in the syringe during extraction in order to prevent probable blockage of the columns while running the test. Finally, the amount of sample needed to conduct the test (i.e. ≈ 4 ml) was extracted from the 20 ml vials.

¹² Angstrom: 1 Å = 0.1 nm = 1×10^{-10} m

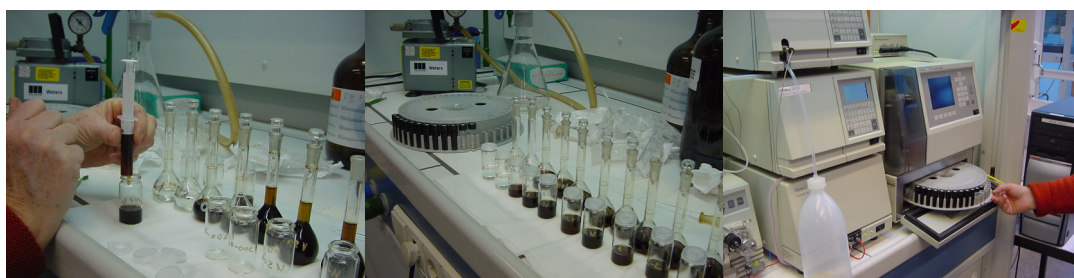


Figure 6.33: Sample preparation in a GPC test

The bitumen samples in 4 ml vials were put in a numbered rack for sampling by the auto-sampler. The sampling was performed automatically by the auto-sampler, which avoids possible human error that may occur in injecting the exact amount of sample and possible spilling during injecting. It also saves considerable time, limiting the task of the laboratory technician to sample preparation and data analysis. The computer can be programmed to perform the test according to the programmed numbering sequence that corresponds with the sample-rack. The testing order is important to match the test results with the corresponding samples. As a standard procedure, GPC is usually calibrated using monodisperse standards called polystyrene to ensure the reliability of GPC test results by comparing with their respective specifications. Two standard fluids were used for calibration to produce a linear relationship between the log molecular weight ($\log(M_w)$) and retention time (t_r) of the molecules. The two standard samples have four and three distinctive peaks respectively, which are characteristic peaks of molecular distribution having different peak heights and elution time to distinguish their respective unique characteristics (Table 6.9). All the bitumen samples and the standard fluids were put in the numbered rack with the standard fluids first in the row. The auto-sampler takes twice an amount of 50 μlt (micro-liters) or 0.05 ml out of the sample to run two separate MWD tests for each sample.

Table 6.9: Summary of the testing conditions

Mobile phase	THF ($\text{C}_4\text{H}_8\text{O}$)
Solvent	THF ($\text{C}_4\text{H}_8\text{O}$)
Sample concentration	30 mg / 25 ml
Injection volume	50 μlt
Flow rate	1.5 ml/min
Test temperature	35°C
Detector	Photo Diode Array (PDA)
Column pore sizes	4×10^6 , 7×10^4 , 2×10^4 , and 5×10^3 Å
Calibration standards	Polystyrene
	Group 1: $M_p = 162, 1370, 9130, 34300$
	Group 2: $M_p = 582, 3250, 1960$

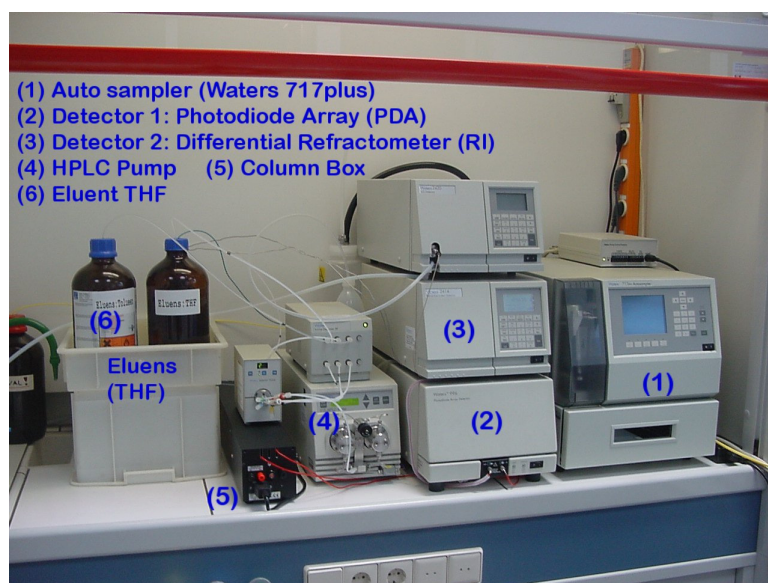


Figure 6.34: The GPC apparatus

During testing, the flow rate of the mobile fluid (THF) was 1.5 ml/min and a total time of 40 minutes was allocated for running the test of one sample. Hence, 60 ml of THF was used to perform the test for every sample. The columns-box in which the size separation process is conducted was maintained at a temperature of 35°C during the entire experimentation process. The GPC equipment was connected to two detector systems for recording the molecular size of the sample passing through the columns during testing. The PDA detector was used to produce the MWD data in the range 190 – 450 nm wavelength. The data at 254 nm wavelength is typically used to characterise most specimens. The photodetector measures transmitted light I , and converts this signal to absorption (A) (according to logarithmic relationship in Equation 6.4) to determine the concentration.

6.3.4 Test Data and Interpretation

Researchers classify the MWD of bitumen into three categories of equal retention time as shown in Figure 6.35. The molecules come out of the GPC column according to their molecular size with the larger molecules first in the row. Accordingly the first 1/3 of the retention time contains the Large Molecular Size (LMS), the second 1/3 contains the Medium Molecular Size (MMS), and the last 1/3 contains the Small Molecular Size (SMS) fractions (Al-AbdulWahhab et al. 1999). The distribution is produced based on the calibration data of the standard fluids.

Figure 6.36 and Figure 6.37 show the response of the GPC molecular weight distribution (MWD) at different wavelengths. The figures form part of the 3D data produced by the PDA detector. Figure 6.36 is the MWD of unaged (virgin) 70/100 bitumen and Figure 6.37 corresponds to the binder recovered from a 12 year old PA specimen. From the figures, it can be observed that the effect of

aging results in a decrease in the peak molecular weight (M_p) and an increase in the large molecules (M_{z+1}) at all wavelengths.

For further analysis of GPC data, the response at 254 nm wavelength is considered.

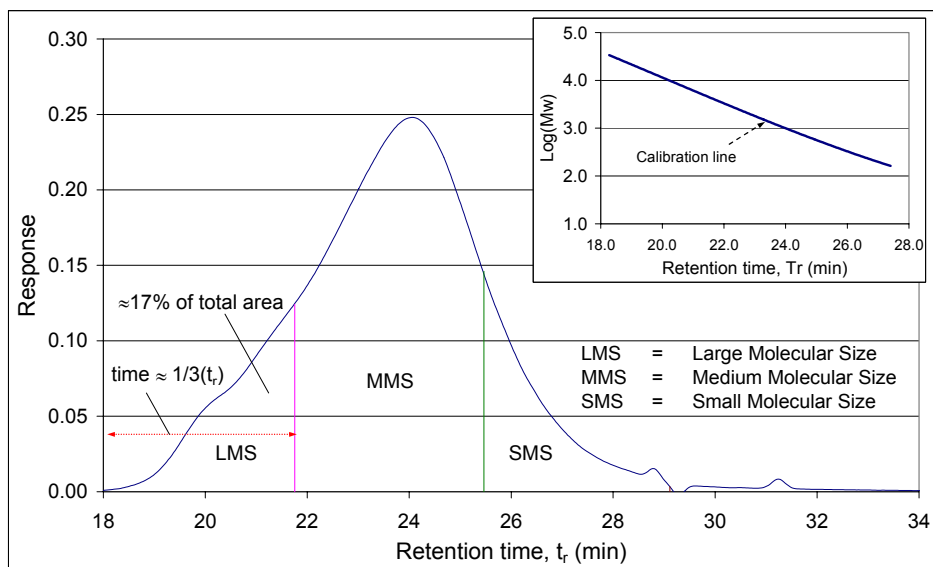


Figure 6.35: Typical GPC chromatogram showing three groups of molecular sizes: LMS, MMS, and SMS

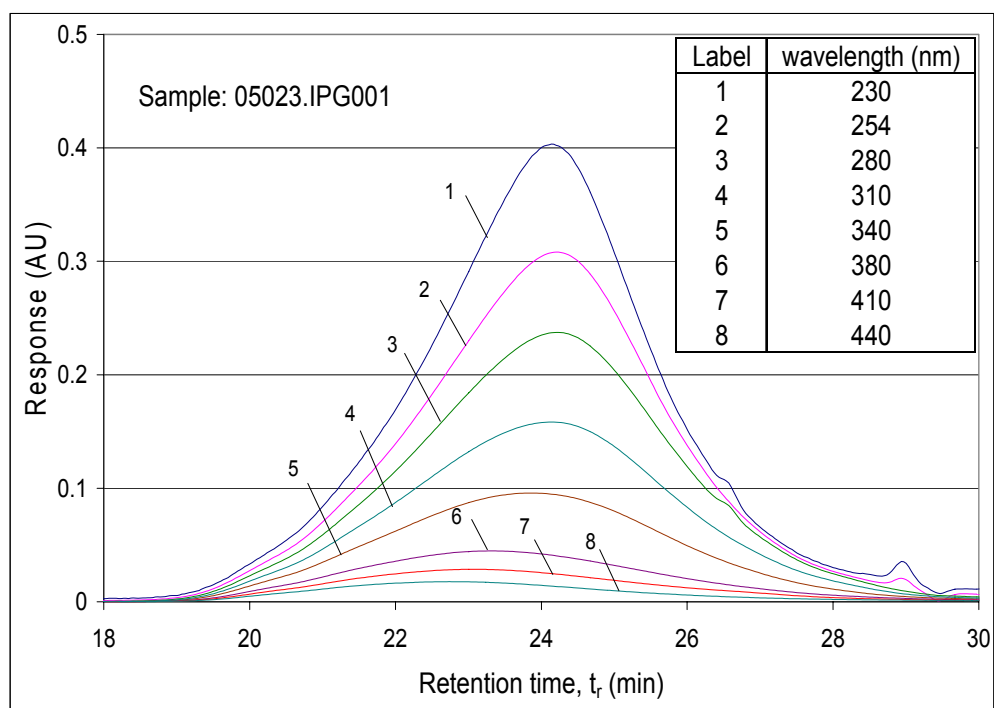


Figure 6.36: MWD of bitumen sample before aging (Virgin bitumen)

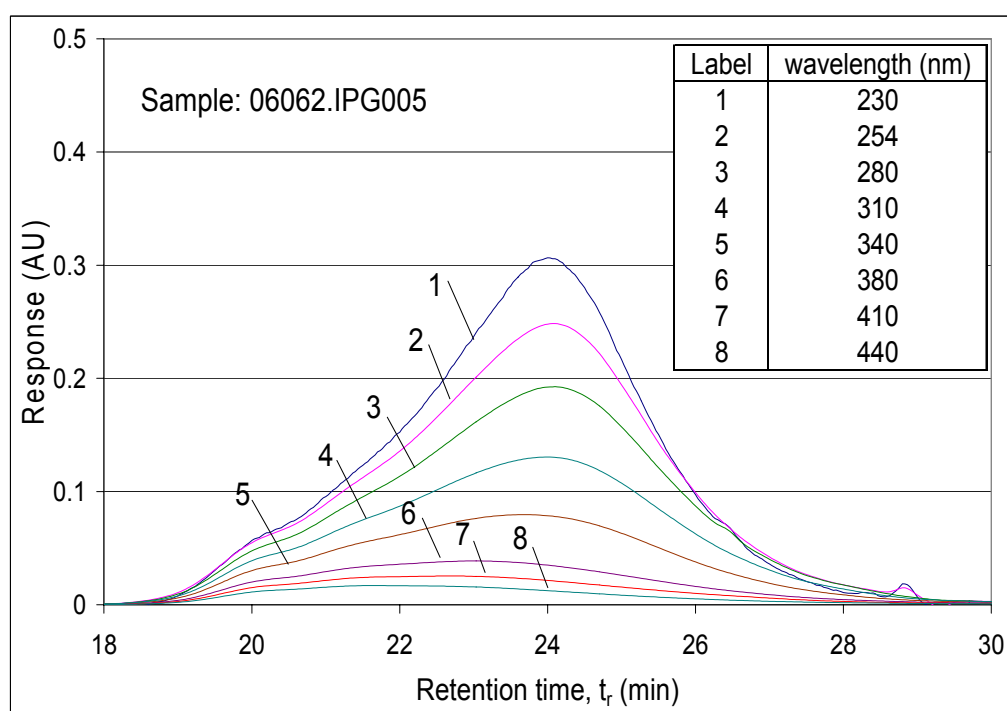


Figure 6.37: MWD of bitumen after 12 years of aging in the road

Test results

Bitumen aging

Table 6.10 shows the indicators of the molecular distribution (MWD) for virgin bitumen and samples aged using standard aging procedures. RTFOT aging was employed for short term aging (STA) and RCAT for long term aging (LTA) of the bitumen samples. In addition to STA and LTA samples, samples obtained during the process of long term aging, i.e. at zero (after STA), 65, 140, and 185 hours of aging time were also considered. The average molecular weight of the MWD is shown in Figure 6.39 for each sample. The chromatograms of the bitumen samples are shown in Figure 6.38 and Figure 6.40.

Table 6.10: Laboratory-aged bitumen samples

Sample name	Sample code	Injec- -tion	M_n	M_w	M_p	M_z	M_{z+1}	PDI
1. Virgin bitumen (70/100 pen.)	05023.IPG001	1	741	1765	881	4601	8960	2.382562
		2	744	1775	885	4626	9008	2.38688
2. RTFOT aged bitumen (STA)	05023.IPG002	1	762	1929	886	5184	9733	2.530093
		2	766	1940	891	5206	9742	2.533357
3. RTFOT+RCAT aging (LTA)	05023.IPG003	1	792	2199	894	6175	11077	2.777947
		2	794	2215	897	6235	11179	2.789374
4. RCAT aging (STA/LTA, t=0)	05023.IPG004	1	787	2087	904	5723	10489	2.652215
		2	787	2090	905	5735	10509	2.654462
5. RCAT aging (LTA, t=65 hr)	05023.IPG005	1	803	2234	904	6256	11191	2.782196
		2	804	2241	908	6279	11223	2.786489
6. RCAT aging (LTA, t=140 hr)	05023.IPG006	1	812	2321	905	6577	11630	2.858705
		2	812	2324	909	6588	11639	2.862139
7. RCAT aging (LTA, t=185 hr)	05023.IPG007	1	825	2425	911	6925	12068	2.940232
		2	826	2432	914	6952	12111	2.946232

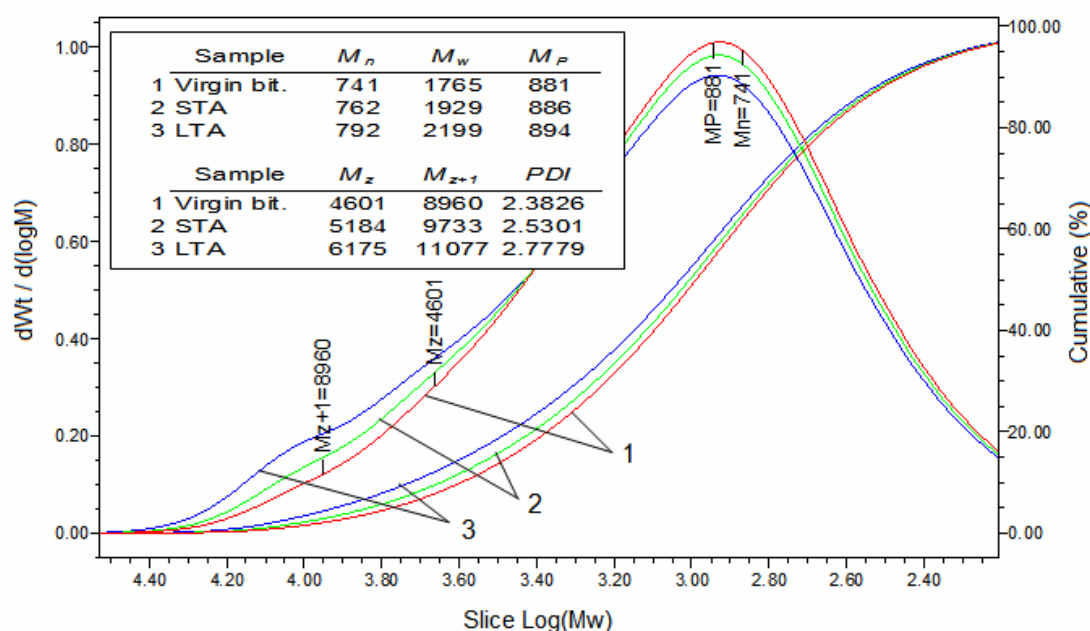


Figure 6.38: MWD of virgin (unaged) and aged bitumen samples

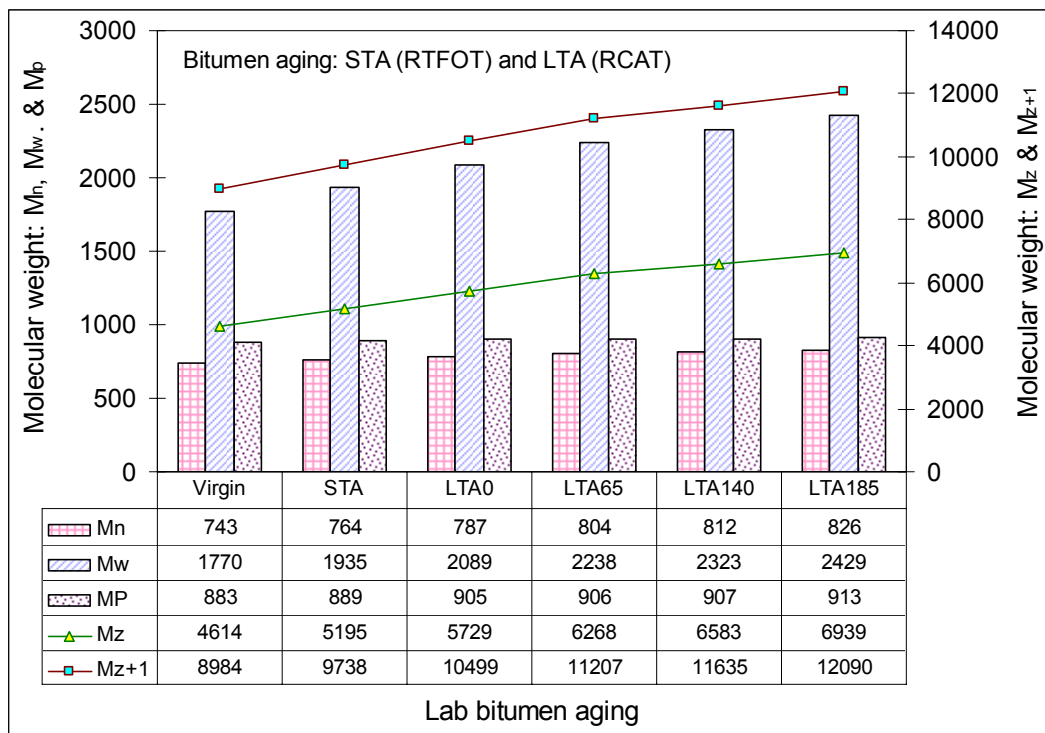


Figure 6.39: MWD indicators for unaged, STA (RTFOT), and LTA (RTFOT/RCAT) bitumen samples

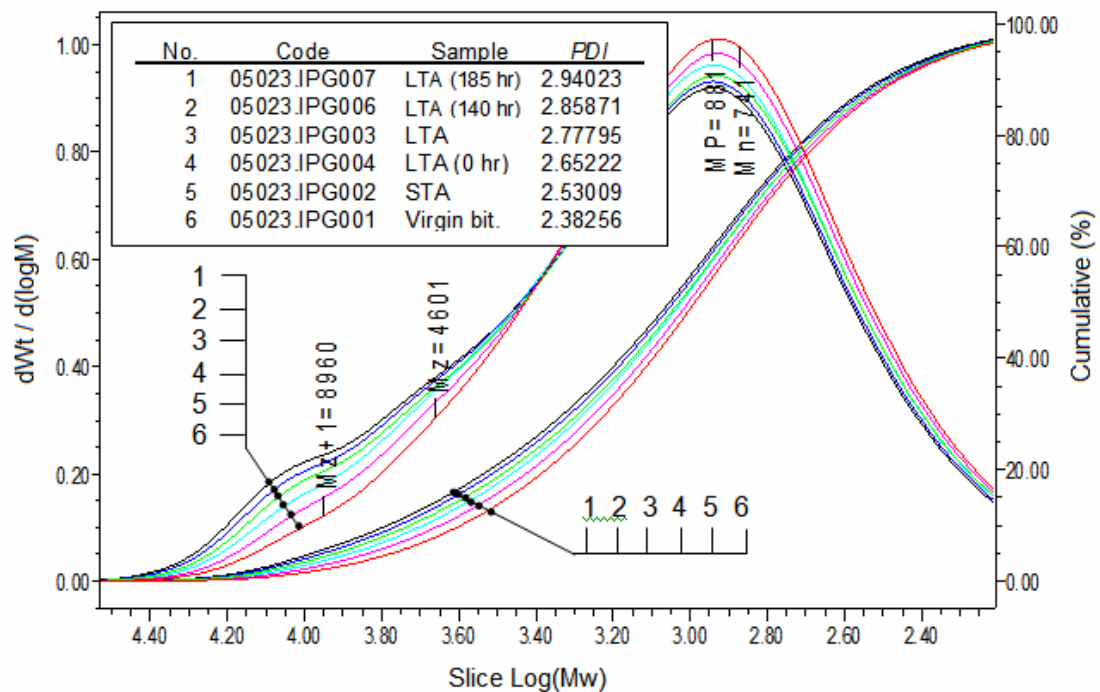


Figure 6.40: MWD distribution of bitumen samples including samples from LTA process

From Figure 6.38 and Figure 6.40, the following observations can be made:

- The effect of aging increases the Large Molecular Size (LMS) in the molecular distribution.
- The peak molecular weight decreases because of the aging effect, i.e. LMS increases at the expense of the MMS molecules. A shift in retention time shows an increase in LMS.
- The PDI parameter increases with aging indicating that the spread of the distribution has changed.

The increase in LMS molecules because of the effect of aging seems indicative of the formation of highly polar functional groups (asphaltenes) during aging.

Weatherometer Aging

The molecular weight of bitumen samples recovered from asphalt mixtures aged under aging protocol 1, 2, and 3 (respectively, AP1, AP2, and AP3) were determined using the GPC test. In Table 6.11, the parameters describing the MWD of the samples are shown. In addition, the results of the AP3 aging test results at different aging times are included. The change in molecular weight during the process of aging can provide useful information how aging influences the MWD.

Table 6.11: Recovered bitumen samples from laboratory mixture aging (weatherometer aging)

Sample name	Sample code	Inject-ion	M_n	M_w	M_p	M_z	M_{z+1}	PDI
1. Reference (Unaged mix)	05023.IPG008	1	780	2028	906	5620	10542	2.599246
		2	779	2023	908	5589	10451	2.595867
2. AP1: Temp aging (Upper Zone, UZ)	05023.IPG009	1	781	2037	912	5645	10623	2.607673
		2	781	2036	909	5632	10566	2.607814
3. AP1: Temp aging (Lower Zone, LZ)	05023.IPG010	1	784	2033	912	5584	10435	2.593419
		2	783	2033	910	5597	10493	2.59603
4. AP2: Temp+UV aging (UZ)	05023.IPG011	1	792	2082	906	5737	10680	2.627882
		2	785	2074	913	5766	10807	2.642449
5. AP2: Temp+UV aging (LZ)	05023.IPG012	1	776	1998	898	5455	10218	2.575811
		2	774	1993	899	5436	10173	2.574346
AP3: Temp.+UV+RH aging (UZ)								
6. RO: 0 hrs	06062IPG001	1	762	1954	881	5362	10128	2.565153
		2	762	1959	884	5376	10164	2.571283
7. R1: 200 hrs	06062IPG002	1	781	2096	891	5877	10928	2.682966
		2	784	2100	894	5870	10875	2.680216
8. R2: 500 hrs	06062IPG003	1	798	2230	901	6348	11553	2.795336
		2	800	2240	898	6396	11667	2.798785
9. R3: 800 hrs	06062IPG004	1	801	2255	900	6468	11800	2.816178
		2	802	2256	899	6462	11773	2.813191
10. R4: 1000 hrs	06062IPG005	1	797	2297	887	6660	12023	2.881359
		2	791	2278	874	6633	12024	2.878985

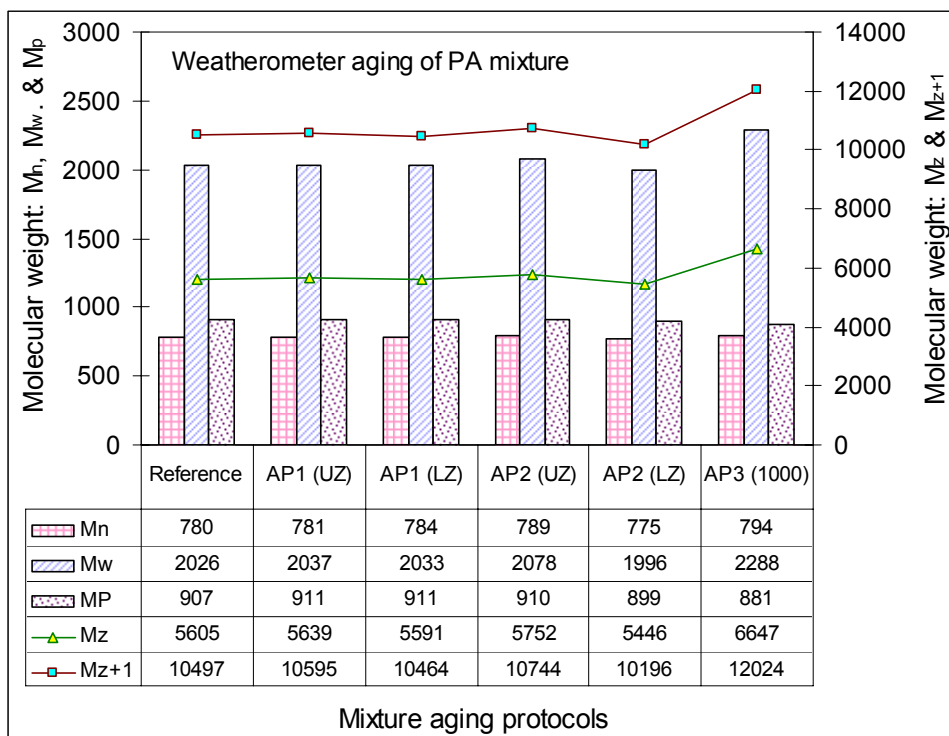


Figure 6.41: MWD indicators for bitumen samples recovered from weatherometer aging (AP1, AP2, and AP3) of PA mixture

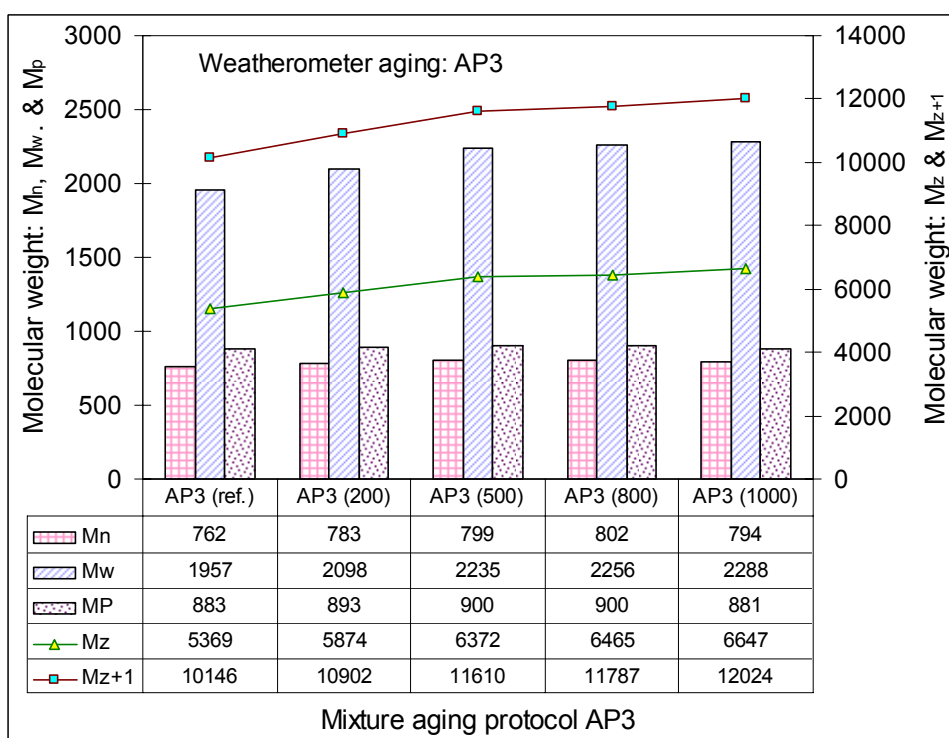


Figure 6.42: MWD indicators for bitumen samples recovered from AP3 weatherometer aging

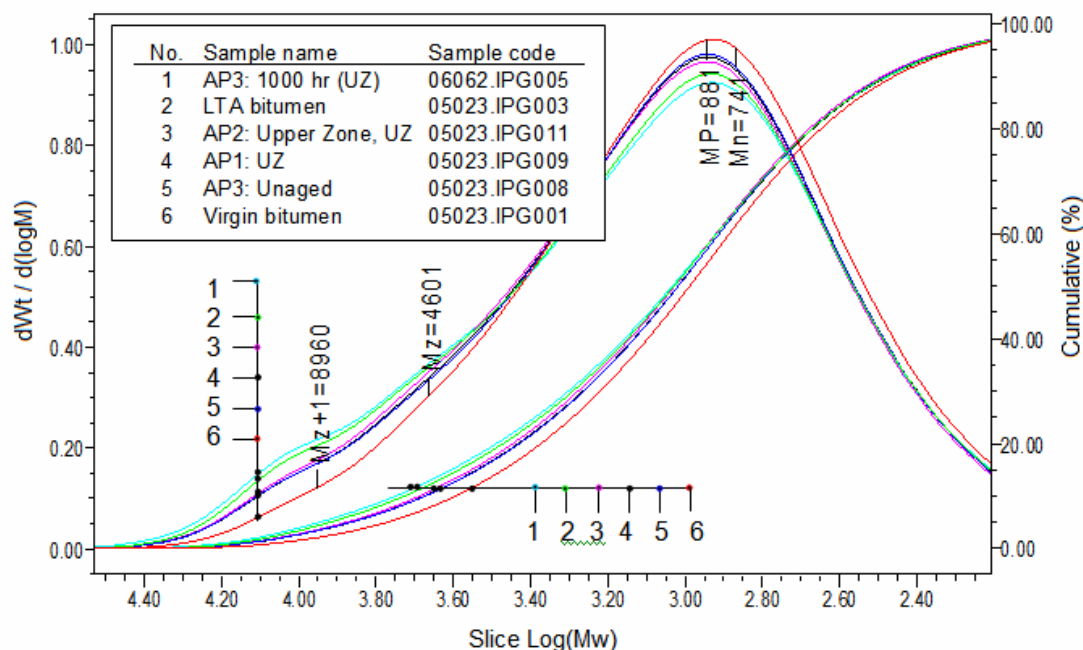


Figure 6.43: MWD of bitumen samples aged under standard protocol and recovered from mixture aging in the weatherometer

Figure 6.43 shows that the samples recovered from the upper zones of AP1 (temperature aging) and AP2 (Temperature + UV aging) have similar molecular weight distributions. The AP3 aging, which is an aging protocol that combines the effects of temperature, UV light, and humidity (RH), and the laboratory LTA aging seem to have resulted in severe aging compared to the AP1 and AP2 aging as shown by the increment of the LMS of the distribution. The AP3 binder seems to have comparable LMS fractions with the LTA bitumen. This can be further validated by the M_z and M_{z+1} parameters of the respective sample given in Table 6.10 and Table 6.11.

Field Specimens

The MWD indicators for the recovered bitumen samples from field specimens are shown in Table 6.12 and Table 6.13 for the upper zone (UZ) and lower zone (LZ) binders respectively.

Table 6.12: GPC test results for field binder samples - Upper Zone (UZ)

Section	Year	Sample code	Inject-ion	M_n	M_w	M_P	M_z	M_{z+1}	PDI
Emergency Lane (EL) - Shoulder									
G	0	06020.IPG001	1	807	2238	894	6455	11685	2.773
			2	808	2255	899	6519	11807	2.790
A	1	06020.IPG011	1	778	2186	877	6321	11457	2.810
			2	782	2199	880	6365	11549	2.812
B	3	06020.IPG007	1	815	2272	937	6493	11894	2.786
			2	814	2272	936	6489	11879	2.791
C	7	06020.IPG015	1	792	2293	901	6639	11890	2.895
			2	794	2299	898	6659	11916	2.894
E	12	06020.IPG003	1	758	2356	866	7241	12837	3.110
			2	759	2370	869	7291	12916	3.124
Slow Lane (SL) – Trafficked lane									
A	1	06020.IPG013	1	791	2243	892	6484	11670	2.836
			2	793	2250	891	6516	11732	2.838
B	3	06020.IPG009	1	799	2217	924	6353	11741	2.775
			2	794	2200	919	6288	11592	2.772
C	7	06020.IPG017	1	794	2308	907	6694	11992	2.909
			2	797	2313	911	6701	11991	2.903
E	12	06020.IPG005	1	803	2297	921	6651	12056	2.862
			2	803	2285	925	6558	11813	2.847

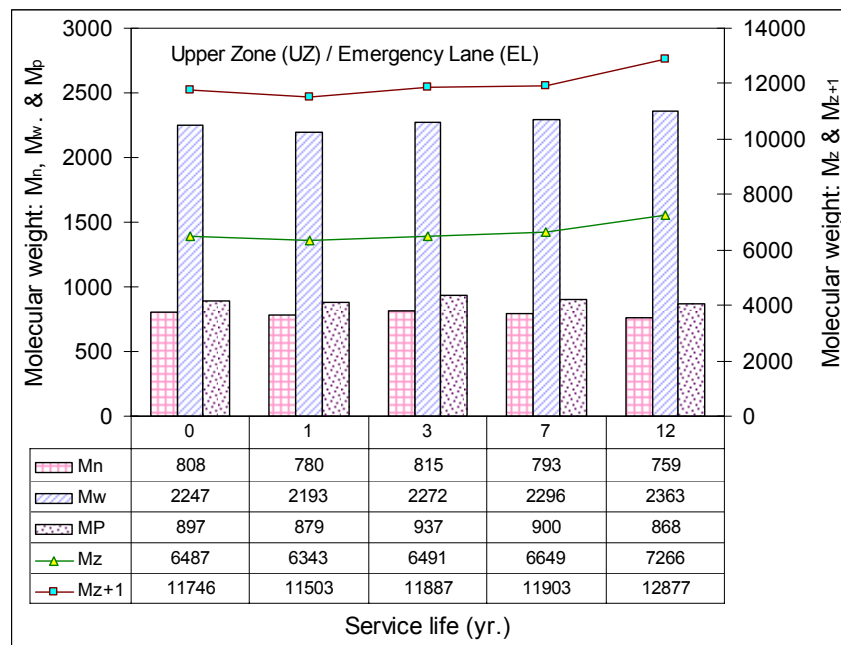


Figure 6.44: MWD of field specimens from Upper Zone (UZ) / Emergency Lane (EL)

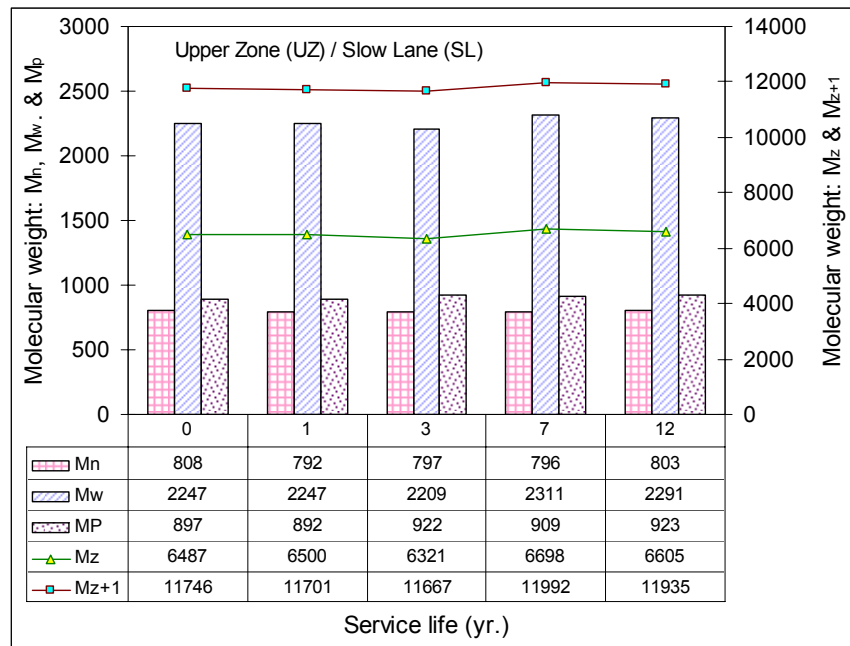


Figure 6.45: MWD of field specimens from Upper Zone (UZ) / Slow Lane (SL)

The average of the MWD parameters for the set of tests in Table 6.12 is shown in Figure 6.44 and Figure 6.45 for the emergency lane (EL) and the slow lane (SL) respectively. Similarly, the WMD information in Figure 6.46 (Table 6.13) for field materials is shown in Figure 6.47 (EL) and Figure 6.48 (SL).

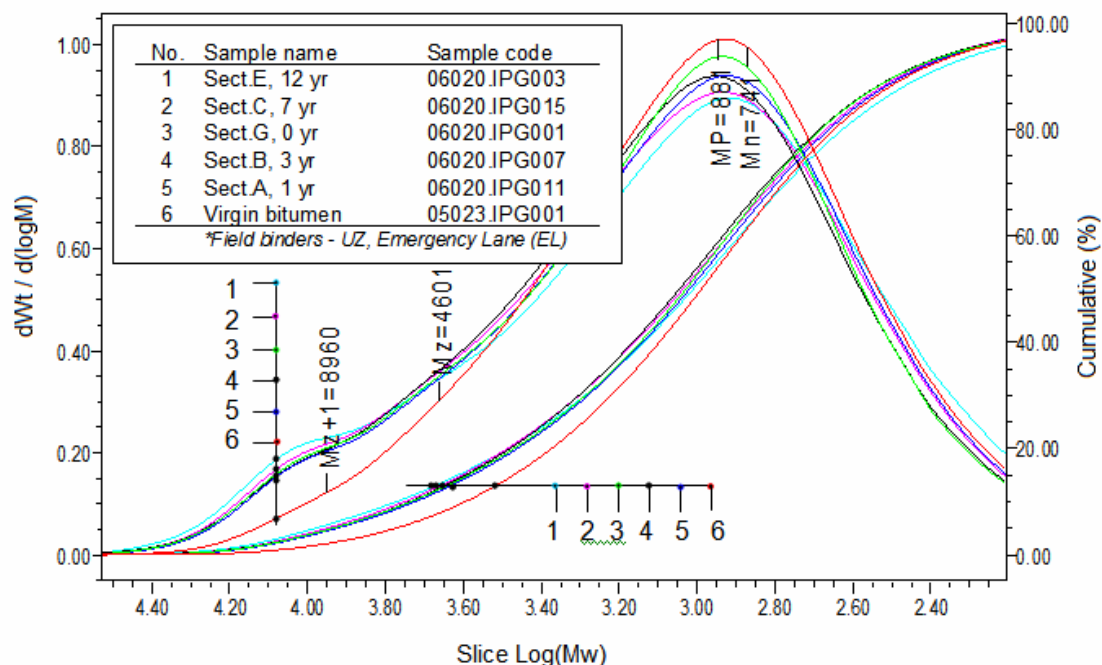


Figure 6.46: WMD of binders from field specimens - Upper Zone (UZ), Emergency Lane (EL)

Figure 6.46 shows the graphical representation of the MWD of field binders from the upper zone (UZ) of the emergency lane (EL). The molecular distribution of the bitumen sample from section G (new construction) shows

exceptional behaviour at the LMS with similar response as the 3 year old specimen. This is probably attributed to the fact that the variation in hetro-atoms could contribute in the aging process. It is noted that the vanadium content of the section G bitumen is different from the other binders as discussed in section 6.1.

Table 6.13: GPC test results for field binder samples - Lower Zone (LZ)

Section	Year	Sample code	Inject-ion	M_n	M_w	M_P	M_z	M_{z+1}	PDI
Emergency Lane (EL) - Shoulder									
G	0	06020.IPG002	1	805	2287	894	6674	12020	2.840512
			2	806	2297	899	6717	12120	2.85072
A	1	06020.IPG012	1	778	2153	881	6185	11285	2.766208
			2	781	2160	882	6194	11289	2.764158
B	3	06020.IPG008	1	800	2253	930	6480	11871	2.815862
			2	796	2249	925	6481	11881	2.824351
C	7	06020.IPG016	1	798	2274	916	6556	11856	2.849215
			2	798	2270	918	6513	11740	2.843757
E	12	06020.IPG004	1	763	2394	870	7337	12939	3.135026
			2	761	2391	872	7328	12922	3.140944
Slow Lane (SL) – Trafficked lane									
A	1	06020.IPG014	1	790	2231	891	6435	11584	2.822838
			2	793	2235	894	6439	11591	2.818051
B	3	06020.IPG010	1	784	2155	892	6172	11366	2.746862
			2	781	2151	886	6170	11351	2.75307
C	7	06020.IPG018	1	795	2347	910	6846	12179	2.953166
			2	795	2351	908	6864	12208	2.958345
E	12	06020.IPG006	1	787	2243	903	6434	11568	2.850915
			2	789	2248	902	6435	11545	2.847274

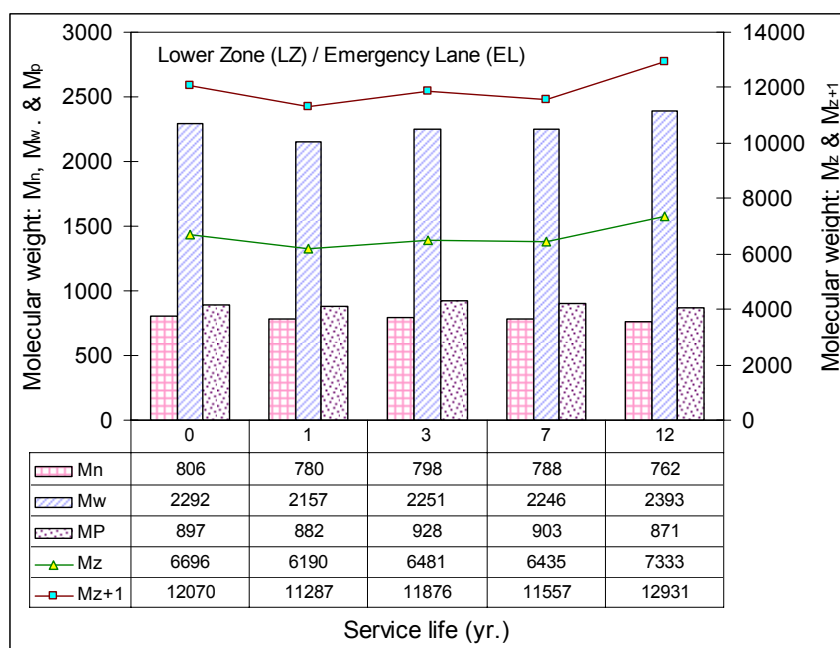


Figure 6.47: MWD of field specimens from Lower Zone (LZ) / Emergency Lane (EL)

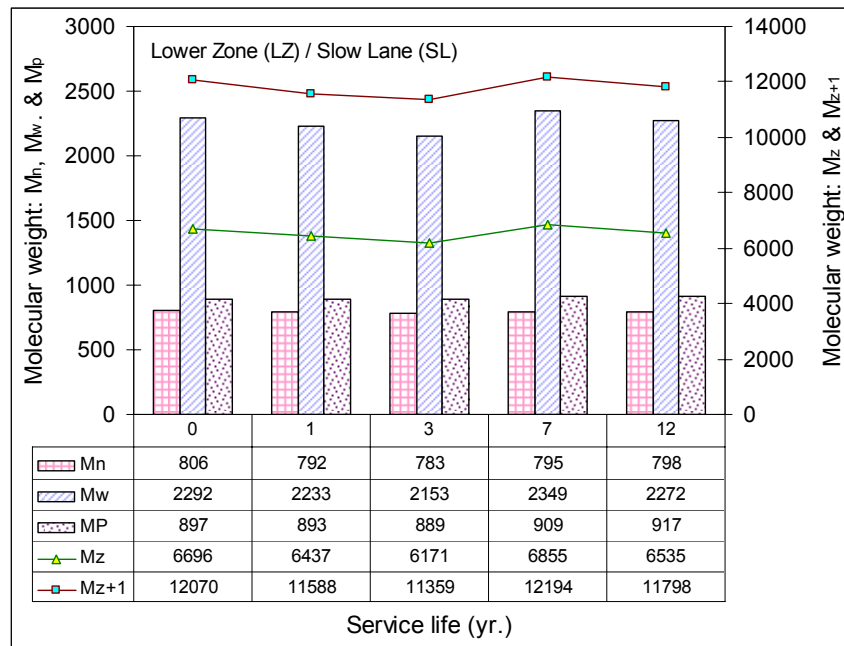


Figure 6.48: MWD of field specimens from Lower Zone (LZ) / Slow Lane (SL)

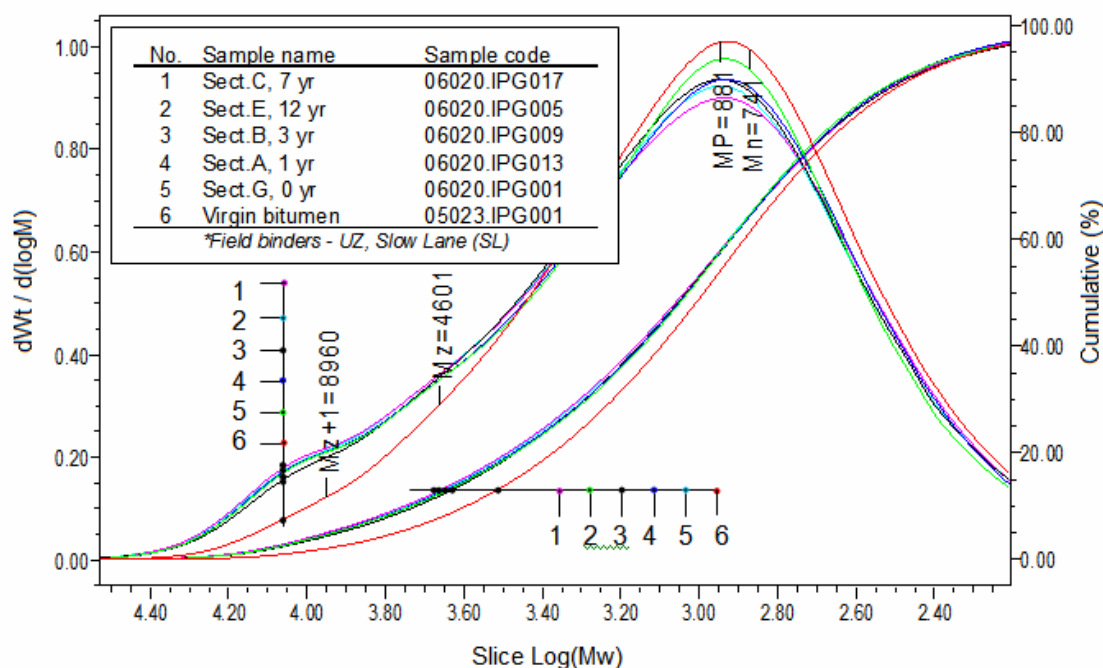


Figure 6.49: WMD of binders from field specimens - Upper Zone (UZ), Slow Lane (SL)

The comprehensive information on the MWD of the upper zone binders in Figure 6.44 and Figure 6.45 reveals that the molecular weight and the service life relationship of the bitumen from the trafficked lane or slow lane (SL) is very similar to the values obtained for bitumen from the shoulder or emergency lane (EL). In both cases a slight increment of the LMS in time can be observed as illustrated by means of the M_z and M_{z+1} parameters. For the lower zone (LZ) samples, it does not show consistent increase or decrease in the MWD

indicators as shown in Figure 6.47 and Figure 6.48. Hence, it is difficult to make a solid assessment of the change in MWD based on the data.

Analysis of GPC test Results

Research studies have shown an attempt to establish relationships between the GPC parameters that describe the MWD (M_n , M_w , M_z , M_{z+1} and PDI) and the binder physical (rheological) properties. Accordingly, the M_n has been related to the flow properties, M_w has been related to strength properties, and M_z has been related to elongation and flexibility properties of the binder (Levin 2007). Studies have also shown that the large molecular size (LMS) has good correlation with physical binder properties (Kim and Burrati 1993, Al-AbdulWahhab et al. 1999, Lee et al. 2006). This is because greater relative amounts of LMS are related to increased asphaltenes content which plays a significant role with regard to sensitivity to brittle behaviour (cracking) of the material and as a result contributes to poor low performance of the pavement (Al-AbdulWahhab 1999, Glover et al. 1988). In trying to establish reliable relationships between physical properties and MWD of the bitumen, a partitioning approach of the distribution into equal retention times or areas was adopted by many researchers. Garrick and Wood 1986 used 8 equal retention times, Kim and Burrati 1993 used 3, 6, and 10 equal parts, and Kim et al. 1995 used 30 equal parts. The most significant correlations were found in the LMS portion, which is about 17% of the total area of the distribution curve and approximately 1/3 of the total retention time (Figure 6.35). Based on this, it was intended to investigate the effect of aging on the LMS of the molecular distribution by dividing the area under the curve into six equal regions in which each part is approximately 17% of the area. In addition, three markers corresponding to M_z , M_w , and M_n of the virgin bitumen were used to show the effect of aging on the area bound by molecules larger than the molecular sizes of the markers.

The cumulative area, retention time, and molecular weight of the laboratory aged binders and recovered binders from mixture aging in the weatherometer are presented in Table 6.14. Similarly, the same information for the upper zone (UZ) of the emergency and slow lane (EL and SL) field binders is presented in Table 6.15. The information shown in both tables is at the 6 equal area markings. As an example, the molecular weights of laboratory aged bitumen and binders recovered from laboratory PA mixture aging are shown in Figure 6.50 and Figure 6.51 respectively. The molecular weight for the field binders is also shown in Figure 6.52 and Figure 6.53 for the EL and SL respectively. From the figures, it can be observed that the molecular weight of the LMS increases with aging for all the aging protocols. Nevertheless, the rate of aging of the laboratory binders can not be compared with the aging rate of the field materials. The field binders show higher aging behaviour at the early stage of the pavement service life, which is comparable to LTA bitumen aging in the laboratory, followed by a slower rate of aging. The aging rate of the field materials can be described by a general trend line.

The following general points can be mentioned with regard to the information in Table 6.14 and Table 6.15.

- The laboratory binders seem to have different rates of aging compared to the field materials. The field binders show higher aging behaviour at the early stage of the pavement service life followed by a gradual aging rate.
- The laboratory aging method shows slight decrease in retention time of the LMS portion with aging which does not seem apparent with the field binders. The difference in retention time disappears after the 50% area mark for all the specimens.
- The cumulative area shows an increase with aging at all the markings for the laboratory bitumen and binders recovered from mixture aging. The AP3 binder aged for 1000 hours (06062.IPG005) seems exceptional. The field materials seem to have irregular trend in their cumulative areas.
- The molecular weight of the LMS increases with aging for all the aging protocols.

Table 6.14: Cumulative area, retention time, and molecular weight of laboratory aged bitumen and mixture binders at the partition markings for 6 equal areas

1. Laboratory bitumen aging (standard aging)						
% Area	16.7 %	33.3 %	50%	66.7 %	83.3 %	100 %
Cumulative area, A						
05023.IPG001	12585737	25171474	37757211	50342948	62928685	75514422
05023.IPG004	10529041	21058082	31587123	42116164	52645205	63174246
05023.IPG005	11068634	22137268	33205902	44274536	55343170	66411804
05023.IPG006	11244447	22488895	33733342	44977789	56222236	67466684
05023.IPG007	12828145	25656289	38484434	51312578	64140722	76968867
Retention time, Tr						
05023.IPG001	22.34	23.31	24.04	24.74	25.67	29.41
05023.IPG004	22.01	23.11	23.91	24.64	25.58	29.31
05023.IPG005	21.88	23.04	23.88	24.61	25.54	29.38
05023.IPG006	21.81	23.01	23.84	24.57	25.51	29.34
05023.IPG007	21.74	22.94	23.81	24.54	25.48	29.38
Molecular weight, M _w						
05023.IPG001	2686	1498	973	652	390	
05023.IPG004	3288	1685	1049	688	411	
05023.IPG005	3570	1754	1070	702	418	
05023.IPG006	3727	1793	1093	716	427	
05023.IPG007	3876	1862	1113	729	434	
2. Laboratory mixture aging (weatherometer aging)						
% Area	16.7 %	33.3 %	50%	66.7 %	83.3 %	100 %
Cumulative area, A						
06062.IPG001	11285428	22570856	33856284	45141711	56427139	67712567
06062.IPG002	11476056	22952113	34428169	45904225	57380281	68856338
06062.IPG003	11727900	23455801	35183701	46911601	58639501	70367402
06062.IPG004	11835899	23671797	35507696	47343594	59179492	71015391
06062.IPG005	11069995	22139990	33209985	44279979	55349974	66419969
Retention time, Tr						
06062.IPG001	22.03	23.10	23.87	24.57	25.50	29.23
06062.IPG002	21.88	23.01	23.78	24.51	25.44	29.21
06062.IPG003	21.78	22.91	23.75	24.48	25.41	29.21
06062.IPG004	21.74	22.91	23.74	24.48	25.41	29.21
06062.IPG005	21.71	22.91	23.75	24.48	25.41	29.25
Molecular weight, M _w						
06062.IPG001	2992	1562	991	662	395	
06062.IPG002	3297	1649	1045	684	407	
06062.IPG003	3500	1748	1063	695	414	
06062.IPG004	3581	1751	1066	697	414	
06062.IPG005	3652	1750	1064	696	414	

NB: Reference can be made to Table 6.10 and Table 6.11 for the sample code indications.

Table 6.15: Cumulative area, retention time, and molecular weight of field binders at the partition markings for 6 equal areas

1. Field Aging (Emergency Lane, EL)						
% area	16.7 %	33.3 %	50%	66.7 %	83.3 %	100 %
Cumulative Area, A						
06020.IPG001	11062381	22124761	33187142	44249523	55311903	66374284
06020.IPG011	11230496	22460991	33691487	44921983	56152478	67382974
06020.IPG007	13817914	27635828	41453743	55271657	69089570	82907485
06020.IPG015	12183036	24366072	36549108	48732143	60915179	73098215
06020.IPG003	11204979	22409957	33614936	44819915	56024893	67229872
Retention time, Tr						
06020.IPG001	21.85	23.02	23.82	24.55	25.45	29.32
06020.IPG011	21.92	23.08	23.88	24.62	25.58	29.32
06020.IPG007	21.82	22.95	23.75	24.48	25.45	29.25
06020.IPG015	21.80	23.00	23.83	24.60	25.53	29.27
06020.IPG003	21.78	23.02	23.88	24.68	25.72	29.28
Molecular weight, M _w						
06020.IPG001	3478	1707	1062	695	422	
06020.IPG011	3396	1668	1038	681	399	
06020.IPG007	3551	1777	1104	722	422	
06020.IPG015	3645	1752	1068	686	409	
06020.IPG003	3625	1707	1021	645	365	
2. Field Aging (Slow Lane, SL)						
% area	16.7 %	33.3 %	50%	66.7 %	83.3 %	100 %
Cumulative area, A						
06020.IPG001	11062381	22124761	33187142	44249523	55311903	66374284
06020.IPG013	12172311	24344622	36516933	48689243	60861554	73033865
06020.IPG009	11247769	22495538	33743308	44991077	56238845	67486615
06020.IPG017	10979904	21959808	32939712	43919616	54899520	65879424
06020.IPG005	12071720	24143439	36215159	48286879	60358598	72430318
Retention time, Tr						
06020.IPG001	21.85	23.02	23.82	24.55	25.45	29.32
06020.IPG013	21.87	23.03	23.83	24.60	25.50	29.27
06020.IPG009	21.88	22.98	23.82	24.55	25.52	29.28
06020.IPG017	21.80	22.97	23.80	24.57	25.53	29.27
06020.IPG005	21.78	22.95	23.78	24.55	25.52	29.25
Molecular weight, M _w						
06020.IPG001	3478	1707	1062	695	422	
06020.IPG013	3498	1717	1068	686	417	
06020.IPG009	3407	1742	1062	695	407	
06020.IPG017	3645	1788	1089	700	409	
06020.IPG005	3625	1777	1083	695	407	

NB: Reference can be made to Table 6.12 for the sample code indications.

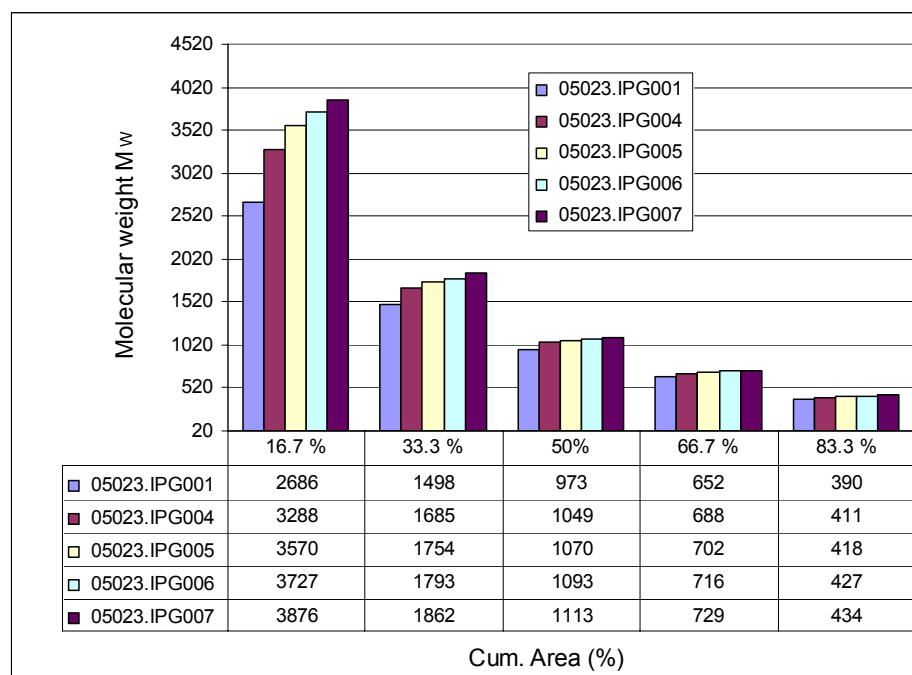


Figure 6.50: Molecular weight of laboratory aged bitumen at 6 equal area markings

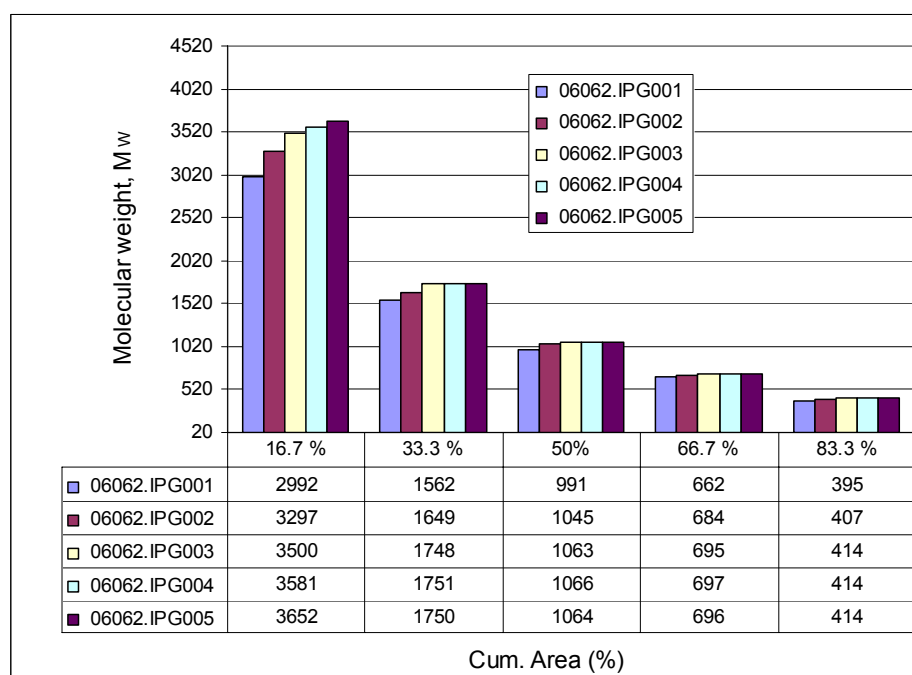


Figure 6.51: Molecular weight of laboratory PA mixture aging binders at the 6 equal area markings

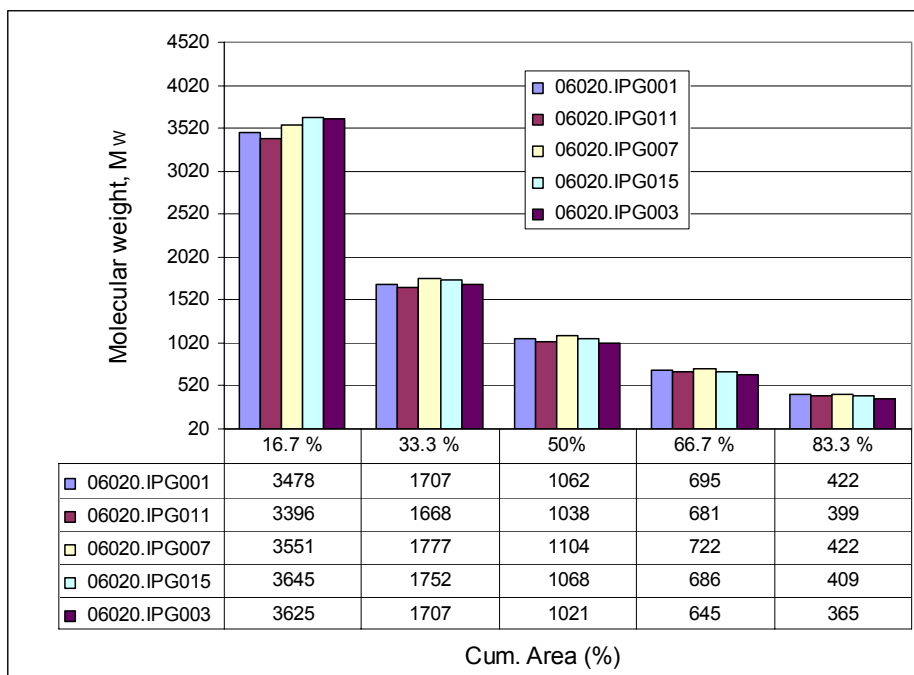


Figure 6.52: Molecular weight of field binders (Emergency Lane) at the 6 equal area markings

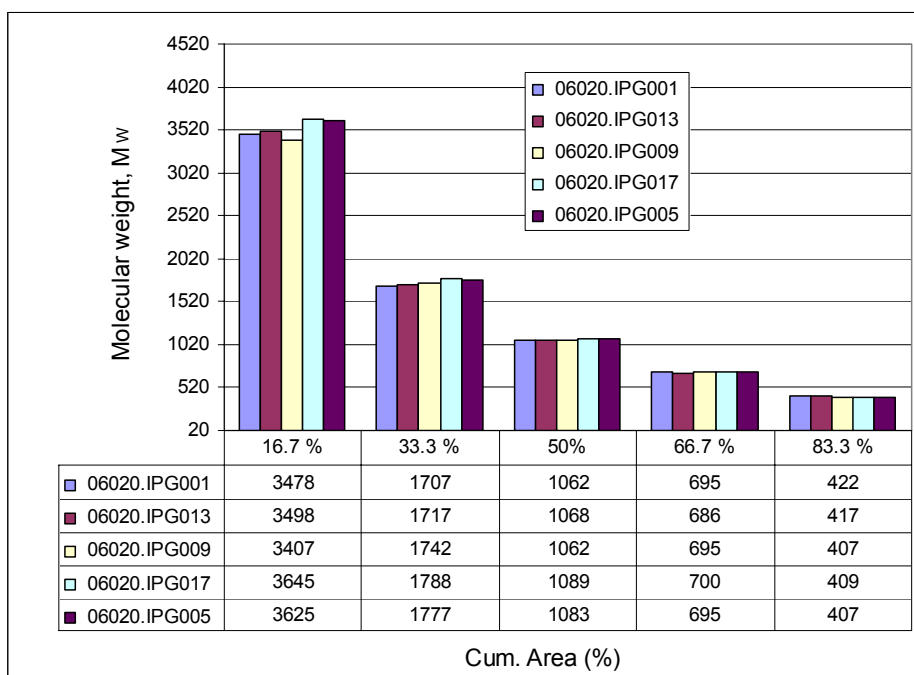


Figure 6.53: Molecular weight of field binders (Slow Lane) at the 6 equal area markings

Table 6.16: Cumulative areas at specific retention times for laboratory and field binders

Cumulative area %	Retention time, Tr (min)						
Lab. bitumen aging	18	20	22	24	26	28	30
05023.IPG001	0	0.97	12.59	48.44	87.29	98.13	100
05023.IPG004	0	1.87	16.36	51.82	88.27	98.20	100
05023.IPG005	0	2.40	17.87	52.93	88.62	98.30	100
05023.IPG006	0	2.72	18.67	53.43	88.78	98.36	100
05023.IPG007	0	3.16	19.70	54.38	89.22	98.53	100
Mixture aging AP3							
06062.IPG001	0	1.98	16.58	53.85	89.33	98.44	100
06062.IPG002	0	2.40	17.92	54.71	89.59	98.50	100
06062.IPG003	0	2.95	19.36	55.90	89.93	98.57	100
06062.IPG004	0	3.06	19.53	56.01	89.98	98.60	100
06062.IPG005	0	3.28	19.91	55.78	89.64	98.44	100
Field binders, EL (Upper Zone, UZ)							
06020.IPG001	0	2.86	18.36	54.11	89.57	98.09	100
06020.IPG011	0	2.60	17.66	52.50	88.46	98.28	100
06020.IPG007	0	2.89	18.82	55.48	89.65	98.34	100
06020.IPG015	0	3.05	19.01	54.29	89.01	98.49	100
06020.IPG003	0	3.59	19.14	52.13	86.68	97.75	100
Field binders, SL (Upper Zone, UZ)							
06020.IPG001	0	2.86	18.36	54.11	89.57	98.09	100
06020.IPG013	0	2.89	18.47	53.89	89.29	98.54	100
06020.IPG009	0	2.69	18.21	54.41	88.85	98.03	100
06020.IPG017	0	3.10	19.13	54.44	88.89	98.40	100
06020.IPG005	0	3.05	19.01	54.76	88.89	98.12	100

NB: Reference can be made to Table 6.10, Table 6.11, and Table 6.12 for the sample code indications.

In Table 6.16, the cumulative area under the MWD curve is given for some laboratory and field materials. The cumulative area curve has been modelled with an S-curve (similar to Equation 5.31) in which the model and the model parameters are shown in Table 6.17. The m and k parameters of the model are related to the slope of the S-curve. But the k parameter is controlled by the upper side of the S-curve while the m parameter is controlled by the lower side of the S-curve. Hence, the k and m parameters have different effects to the change in the slope of the S-curve. The f parameter changes the horizontal position of the S-curve.

According to the information given in Table 6.16 and Table 6.17, the following remarks can be made.

- The remarks made with regards to cumulative area for equal area partitioning also apply for the cumulative area at the specified retention times shown in Table 6.16.
- The determined model parameters for the laboratory aged binders are similar except for the m parameter that shows a decrease with aging. This is related to the increase in the cumulative area.
- The field materials have relatively constant m parameters, but a decreasing k parameter with aging. The f parameter shows a decreasing tendency for the emergency lane binders. This implies that the cumulative area of the EL

binders have shifted to the lower side of the retention time with aging while showing a decrease in the slope of the S-curve. The overall effect is an increase in the cumulative area.

- The SL field binder seems to have a decreasing trend in cumulative area with aging at the specified retention times (because of constant f parameter), which is not as per the expectation.

Table 6.17: Model parameters for cumulative area of laboratory and field binders

Model:	$A = 100 \times \left(1 + \left(\frac{f}{T_r} \right)^k \right)^{(-m/k)}$				Model parameters		LMS (17% area)
Lab. bitumen aging	Sample	f	k	m	Tr	Cum.area	
	05023.IPG001	24.37	25.82	19.86	22.38	12837225	
	05023.IPG004	24.41	25.52	17.35	22.11	10739116	
	05023.IPG005	24.45	25.61	16.33	21.99	11290007	
	05023.IPG006	24.48	25.68	15.80	21.93	11469958	
	05023.IPG007	24.49	25.88	15.26	21.85	13084707	
Mixture aging AP3							
	06062.IPG001	24.31	25.70	18.00	22.10	11510495	
	06062.IPG002	24.32	25.68	17.06	21.98	11705577	
	06062.IPG003	24.33	25.62	16.28	21.88	11962458	
	06062.IPG004	24.34	25.67	16.14	21.86	12072616	
	06062.IPG005	24.36	25.33	15.80	21.83	11291394	
Field binders, EL	(Upper Zone, UZ)						
	06020.IPG001	24.46	26.33	16.09	21.96	11283689	
	06020.IPG011	24.52	25.94	16.04	22.01	11455127	
	06020.IPG007	24.32	25.36	16.55	21.91	14094443	
	06020.IPG015	24.48	25.59	15.70	21.92	12426815	
	06020.IPG003	24.60	24.31	14.85	21.88	11429214	
Field binders, SL	(Upper Zone, UZ)						
	06020.IPG001	24.46	26.33	16.09	21.96	11283689	
	06020.IPG013	24.52	26.38	15.79	21.96	12415756	
	06020.IPG009	24.31	24.72	16.86	21.95	11472725	
	06020.IPG017	24.45	25.25	15.76	21.90	11199889	
	06020.IPG005	24.35	24.77	16.21	21.89	12312992	

NB: Reference can be made to Table 6.10, Table 6.11, and Table 6.12 for the sample code indications.

The areas under the MWD of the laboratory and the field binders and the cumulative areas at the MWD parameters of the virgin bitumen were analysed. The results of the analysis can be summarised as follows:

- The binders aged in the laboratory using the standard aging method and those recovered from mixture aging showed an increase in their total area with aging. The AP3 binder aged for 1000 hour in the weatherometer (06062.IPG005) showed a peculiar behaviour.
- The field binders showed an exceptional behaviour with regard to the total area in relation to aging time. Both the emergency and the slow lane binders have shown an increase followed by a decrease in the total area with aging. The binders have the highest total area at a pavement service life of 3 and 1

year corresponding to the emergency and the slow lanes respectively. The total area of the emergency lane is higher than the slow lane binder.

- The cumulative area shows an increase of the parameters M_z , M_w , and M_n that describe the MWD of the virgin bitumen.

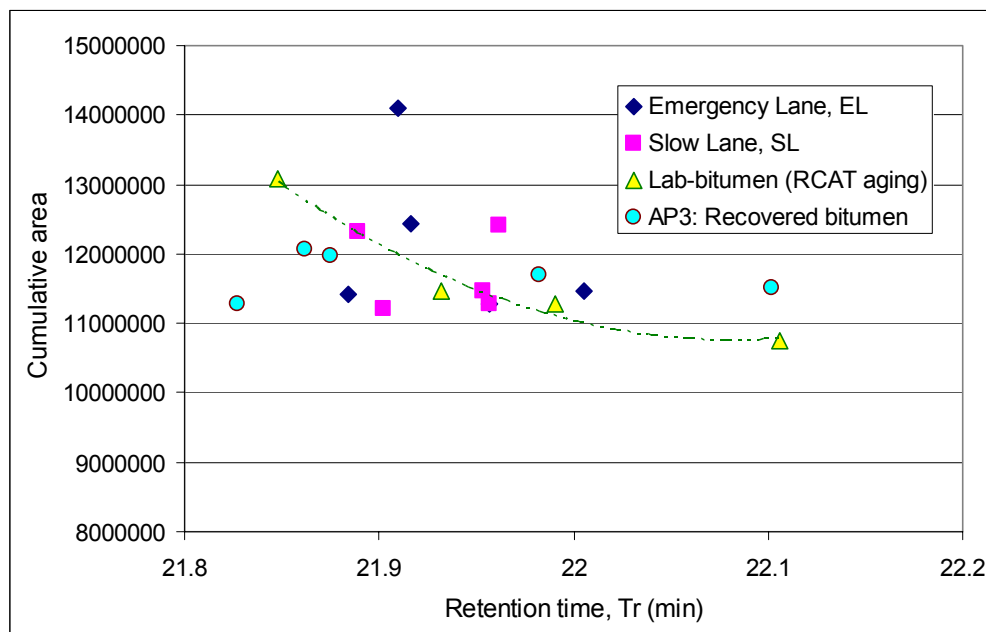


Figure 6.54: Cumulative areas of laboratory and field aged binders at 17% of the total area

Given the variability of the data and mismatch between the laboratory and field specimens, it is difficult to find a meaningful correlation between laboratory and field aging methods. The intention was to make use of the kinetic approach to describe the effect of aging with time. Figure 6.54 shows the cumulative area at 17% of the total area which provides information on the LMS portion of the molecular distribution. There is no clear trend of an increase or decrease in area except for the binders aged using standard aging method. The variability of the results of the GPC test for the laboratory and field aged binders (Figure 6.54) reveals the complex nature of field aging under the influence of the combination of different aging factors.

6.4 Relationship between Rheology and Molecular Structure

The rheological properties of bitumen are strongly related with the molecular structure or the chemical composition of the binder. In polymer science, a relationship between the molecular weight distribution (MWD) and the relaxation modulus has been developed, which is widely known as the “*mixing rule*” (Equation 7.12). The value of the parameter β is either 1 (linear mixing rule, Doi and Edwards (1986)) or 2 (quadratic mixing rule, des Cloizeaux (1990) and Tsenoglou (1987)) or any other value if determined based on the best fit to

the test data (Maier et al. 1998). A scaling relationship between the molecular weight and the relaxation modulus is given in Equation 6.18.

The Rouse and Reptation modes contribute to the relaxation spectrum $H(t)$. The part of the spectrum due to reptation modes $H_{rept}(t)$, which is strongly related to the molecular weight, is used to predict the MWD or $w(M)$ (TA Instruments 2000).

$$G(t) = G_N \left(\int_{M_e}^{\infty} F(t, M)^{1/\beta} \frac{w(M)}{M} dM \right)^{\beta} = \int_{-\infty}^{\infty} H_{rept}(\tau) \exp(-t/\tau) d \ln \tau \quad (6.17)$$

$$\tau = k_{\tau} M^{\alpha}, \quad \eta_0 = k_{\eta} M^{\alpha}, \quad k_{\tau} = k_{\eta} / G_N \quad (6.18)$$

Where:

$F(t, M)$	=	Prony (kernel) function describing the relaxation behaviour of the molecular weight fraction with a molecular weight M .
β	=	parameter that characterizes the mixing behaviour.
$w(M)$	=	molecular weight distribution (MWD).
M_e	=	entanglement molecular weight.
M	=	molecular weight.
G_N	=	the plateau modulus.
τ	=	the relaxation time.
k_{τ}, k_{η}	=	characteristic constants.
η_0	=	zero shear viscosity.
α	=	a constant in the equation.
t	=	the experimental time.
$H_{rept}(\tau)$	=	reputation dynamic contribution to the relaxation spectrum.

The “mixing rule” in Equation 6.17 shows the possibility of conversions between the rheological properties and the molecular structure. Much experience exists in the use of the “mixing rule” in materials other than bitumen. The rheological behaviour of polymer modified binders and pure bitumen for example is completely different that it makes it complex to adopt the rule for bitumen. It can be understood, however, that the changes both in the rheological and chemical properties due to the effect of binder aging stems from the strong relationship between the two.

6.5 Summary and Findings

6.5.1 In relation to Infrared Spectrometer Test Results

The functional groups responsible for bitumen aging are sulfoxide (S=O) and ketone/carbonyl (C=O) groups. The peak areas and peak heights of the infrared spectrum at wavelengths 1030 cm^{-1} (sulfoxide) and 1700 cm^{-1} (ketones) were used to characterize chemical changes due to aging. A summary of the findings is given below.

- The aging of bitumen has resulted in the increment of the peak height (PH) and the peak area (PA) of the characteristic indicators for ketones and sulfoxides in the infrared spectrum. The standard laboratory aging of bitumen, i.e. long term RTFOT+RCAT aging, and the weatherometer aging protocol 3 (AP3) have resulted in an equal increment of the characteristic peaks. The other two weatherometer aging protocols (AP1 and AP2) resulted predominantly in the increment of the S=O peak.
- Bitumen materials recovered from the upper zone of PA mixture aging in the laboratory, i.e. aging protocols AP1 (temperature aging), AP2 (temp.+UV aging), and AP3 (temp.+UV+RH), have S=O peak in decreasing order AP1, AP2, and AP3. The combined effect of temperature, UV light, and humidity (AP3) has resulted in the formation of both sulfoxides and ketones similar to the field aging of bitumen.
- Vanadium content provides an important indication of the source of bitumen as it is not influenced by the process of aging. Vanadium content is related to the amount of hetro-atoms in the bitumen, which can range between less than 1% and 5%. Binders with high quantity of vanadium also tend to have higher quantities of sulfur that increase the susceptibility of the binder to aging because of the formation of sulfoxide.
- Similar aging patterns as in the field have been realized with the AP3 weatherometer aging procedure. However, the laboratory mixture aging is not as severe as the field aging, which has also been revealed in the rheological properties of the binders.
- Field bitumens have shown increment in the peak height and peak area of the characteristic functional groups. Some irregular trends in the peaks may be attributed, among other possible factors, to the difference in vanadium content of the binders. Binders with higher or lower vanadium content have shown such irregular trends.
- The influence of the dominant environmental factors at the upper and bottom layer of PA, i.e. UV light at the UZ and the effect of moisture at the LZ, do not seem to have resulted in significant differences in the aging behaviour of the binder.
- The upper zones of the emergency and slow lane (EL and SL) field binders have shown differences in their aging behaviour. Analysis using the kinetic approach based on the sum of the peak areas at the C=O bond (ketone) and S=O bond (suloxide) have shown that the aging rate of the EL (lane without traffic) is lower than the SL (trafficked lane). The damaging effect of traffic on the cohesive property of the bitumen/mortar, i.e. cohesive (micro)

cracking that exposes new surfaces of the bitumen to aging and differences in clogging, are cited as probable reasons for the higher rate of aging of the trafficked lane.

- The standard long term laboratory bitumen aging procedure has achieved less than 1 year of equivalent aging in field according to analysis based on kinetic approach. Similarly, the new mixture aging procedure (AP3) has predicted only 2.1 years of field aging. This indicates that the aging of PA in the field has not been simulated accurately because of the complex nature of the aging process. Nevertheless, the new weatherometer aging protocol (AP3) appears to be a promising aging method since it results in a similar chemical characteristics as field aging.

6.5.2 In relation to Molecular Weight Distribution

The Gel Permeation Chromatography (GPC) method has revealed some important aspects of the effect of aging on the Molecular Weight Distribution (MWD) of the binder. A summary of the findings is presented below.

- The effect of aging increases the Large Molecular Size (LMS) portion of the MWD (LMS: molecules retained in the first 1/3 portion of the retention time which is equivalent to about 17% in terms of the area of the molecular distribution). The increase in LMS is attained at the expense of the Medium Molecular Size (MMS) molecules with a decrease in the peak molecular weight (M_p). As a result, a shift in retention time of the LMS molecules was observed after aging.
- The effect of aging has an influence on the values of the parameters that describe the MWD of bitumen. The increase in the Polydispersity Index (PDI) parameter with aging indicates a change in the spread of the distribution. The parameters that have significantly increased as a result of aging are the z-average molecular weights (M_z and M_{z+1}). The change in the z-average parameters, which are associated with the increase in LMS molecules, indicates the formation of highly polar functional groups (asphaltenes) as the binder ages.
- Based on the MWD parameters, the long term laboratory mixture aging protocol (AP3) seem to have resulted in severe aging compared to the AP1 and AP2 aging procedures according to the changes to the LMS portion of the distribution. However, the AP3 protocol seems to have comparable LMS fractions with the standard long term aging of bitumen (LTA) and the upper zone of field binders with 3 and 7 years of service life.
- Based on the LMS area analysis of the MWD distributions, the long term laboratory aging protocols seem to have comparable changes in area with the 12 year old binders from the Emergency Lane (EL) and the Slow Lane (SL). This indicates that the MWD analysis alone is not adequate to predict field aging since the results of the infra-red have shown differences in chemical products. The physical properties of the binders have also revealed differences in the performance of the binders.

6.6 Reference

Al-AbdulWahhab, H. I., si, I. M., and Al-Dubabi, I. A. (1999). "Prediction of Asphalt Rheological Properties Using HP-GPC." *Journal of Materials in Civil Engineering*, 11(1), 6-14.

Answers.com (2003) "Gel permeation chromatography." <http://www.answers.com/topic/gel-permeation-chromatography?cat=technology> Webpage accessed in 2007.

ATLAS materials (2001). Weathering testing guidebook. Rep. no. 2062/098/200/AA/03/01, ATLAS materials testing solutions.

Branthaver, J. F., Peterson, J. C., Robertson, R. E., Duvall, J. J., and Kim, S. S. (1993). "Binder characterization and evaluation: Volume 2 Chemistry." Rep. No. SHRP-A-368, SHRP - Strategic Highway Research Program (National Research Council), Washington DC.

Burns, D. A., and Ciurczak, E. W. (2001). "Handbook of Near-Infrared analysis." Marcel Dekker, Inc, New York, USA.

CIE (1989). "Solar Spectral Irradiance." Rep. No. CIE 85, CIE International Commission on Illumination.

DWW (2004). Moleculaire Gewichtsverdeling van bitumen (GPC). Rep. no. WV 017 Version 6.3. DWW (Dienst Weg and Waterstaat). The Netherlands.

Glover, C. J. e. al. (1988). "Chemical characterization of asphalt cement and performance-related properties." *Transport Research Record*, (No. 1171), pp. 71-81.

Kim, K. W., and Burati Jr, J. L. (1993). "Use of GPC Chromatograms to Characterize Aged Asphalt Cements." *Journal of Materials in Civil Engineering*, 5(1), 41-52.

Kim, K. W., Burati Jr, J. L., and Park, J. S. (1995). "Methodology for Defining LMS Portion in Asphalt Chromatogram." *Journal of Materials in Civil Engineering*, 7(1), pp. 31-40.

Lee, S. J., Amirkhanian, S. N., and Shatanawi, K. (2006). "Effects of Reaction Time on Physical and Chemical Properties of Rubber-modified Binders". *International Rubber conference*, Lyon (France).

Levin, S. (2007). "GPC course handout". Source: <http://www.forumsci.co.il/HPLC/program.html>. Webpage accessed in 2007.

Molenaar, J. M. M., Hagos, E. T., Ven, M. F. C. v. d., and Hofman, R. (2004). "An investigation into the analysis of polymer modified bitumen (PMB)." *3rd Eurasphalt & Eurobitume Congress*. Vienna, Austria.

MSU (Michigan State University). (2007). "Infrared spectroscopy." <http://www.cem.msu.edu/~reusch/VirtualText/Spectrpy/InfraRed/infrared.htm>. Webpage accessed in 2007.

Perkin Elmer. (2005) "FTIR Spectroscopy -- Attenuated Total Reflectance (ATR)." http://en.wikipedia.org/wiki/Attenuated_total_reflectance. Webpage accessed in 2007.

Peterson, J. C. (2000). "Chemical composition of asphalt as related to asphalt durability." In *Asphaltenes and Asphalts, 2. Developments in Petroleum Science, 40B*. 1st edition, Elsevier Science BV.

Plus, C., Harders, O., Kreide, M., and Teugels, W. (2000). "The qualitative und quantitative Bestimmung von Polymeren in Polymermodifizierten Bitumen / Asphalten mittels Infrarot-Spektroskopie (In German)." *BITUMEN*, 62(4), 130-133.

Reed, J., and Whiteoak, D. (2006). "The shell bitumen handbook." Thomas Telford.

Roberts, F. L., Kandhal, P. S., Ray Brown, E., Lee, D.-Y., and Kennedy, T. W. (1996). "Hot mix asphalt materials, mixture design, and construction." *NAPA Research and Education Foundation*, Lanham, Maryland.

SHU (Sheffield Hallam University) (2007) "Infra-red absorption spectroscopy - theoretical principles." Source <http://teaching.shu.ac.uk/hwb/chemistry/tutorials/molspec/irspec1.htm>.

Skoog, D. A., and Leary, J. J. (1992). "Principles of instrumental analysis." Saunders collage publishing.

UColorado (University of Colorado). (2002). "Handbook for Organic Chemistry Lab: Infrared spectroscopy - theory." *Online edition for students of chemistry*. Source <http://orgchem.colorado.edu/hndbksupport/irtutor/IRtheory.pdf> Webpage accessed in 2007.

Verhasselt, A. F. (2000). "A Kinetic Approach to the Aging of Bitumens." *Asphaltenes and Asphalts, 2. Developments in Petroleum Science, 40B*, Elsevier Science BV.

Waters (2008). "Polymer analysis - Introduction." Source <http://www.waters.com/WatersDivision/ContentD.asp?watersit=JDRS-5LTGJR>. Webpage accessed in 2008.

Wikipedia (2007). "Infrared Spectroscopy". Source http://en.wikipedia.org/wiki/Infrared_spectroscopy Webpage accessed in 2007.

Willard, H. H., Merritt, J. L. J., Dean, J. A., and Settle, F. A. J. (1998). "Instrumental methods of analysis." Wadsworth Publishing, Belmont, California (USA).

7 Conclusions and Recommendations

The aim of this research was to understand the effects of aging on the rheological and chemical characteristics of the binder in porous asphalt pavement layers. To realise this objective, two approaches were employed to study the aging of the binder, which are investigations on laboratory aged binder samples and field specimens. The characterization of the effects of aging on the bituminous materials is discussed in the previous chapters. In this chapter, the major conclusions of the rheological and chemical characterization are presented along with implications to the ravelling of porous asphalt. Finally, recommendations related to the study are provided.

7.1 Main conclusions

A summary of the rheological and chemical investigations are given at the end of the respective chapters. The main conclusions of the research are presented below.

- Laboratory aging methods do not simulate field aging of PA. Both rheological and chemical results indicated that the laboratory aging protocol is not capable of simulating more than 3 years of field aging. In terms of chemical changes, the weatherometer aging procedure (AP3: temperature + UV light + humidity) has resulted in more years of aging than the standard aging method in relation to field aging.
- The AP1 and AP2 laboratory mixture aging protocols have shown differences in the aging property of the binder in the upper zone (UZ) and the lower zone (LZ). The binders recovered from the field cores have not shown such significant difference in their rheological properties as the laboratory binders.
- The rate of aging in the SL is higher than the EL for the field samples studied in this research. The main reason could be associated with the damaging effect of traffic loading, exposing new surface in the cohesive

zone (the binding material) to aging and other secondary effects such as water related damage.

- Low temperature test results of aged and unaged bitumen/mastic indicate that aging reduces the relaxation potential of the binder, which is an indication of brittle behaviour (increase in the critical temperature) and sensitivity to damage of the binding material at low temperatures.
- Fatigue tests on laboratory aged binders conducted in the DSR at intermediate temperature (20°C) gave better results compared to unaged bitumen. The 7 and 12 year field binders, however, have shown a lower fatigue life compared to the reference (unaged) bitumen. The accumulation of damage of the aged binders is believed to be higher at low temperatures due to sensitivity to failure of the materials at lower strain levels. This has a negative effect on the resistance to ravelling of PA.
- Finite Element Modelling (FEM) of real traffic loading on PA using the rheological properties of unaged and aged materials indicates that the binding materials experience the same stress situation at low temperatures. This implies that the materials sensitive to damage accumulation are likely to fail first. In this regard, the field materials which showed low fatigue performance at intermediate temperatures will certainly have a shorter life.
- Both high and low temperatures are important factors in relation to PA performance. At high temperatures the aging of the binder takes place which increases the sensitivity of the binding material to cracking at low temperatures.
- Aging is believed to be the main reason for ravelling failure in PA surface layers because of its effects on the cohesive characteristics of the binding material. Such effects include the reduction of the relaxation properties of the binder and a shift to a higher temperature of the critical temperature. The effect of moisture is believed to be a secondary factor that contributes to the accelerated failure or ravelling of PA.
- Ravelling is a surface failure phenomenon in PA. The presence of water at the upper zone for a longer time is not likely because of the porous nature of the mixture. This makes the role of water damage less efficient in the ravelling process. When there is damage (cracking) either in the cohesive or the adhesive bonds, the implications will be accelerating the deterioration rate of the failure. Hence, the effect of water/moisture is thought as a secondary effect to the damage development, which is primarily caused by load related damage. As argued before, aging increases the chance of damage development because of applied traffic loading (including thermal stresses) and reduces the fatigue life.
- The aging of bitumen as a result of environmental effects is regarded a major factor contributing to cohesive failure and lower service life of PA. Damage to the cohesive properties of the binding material or mortar is induced when certain stress/strain levels of the mortar are exceeded. Tensile, compression, shear or a combination of these factors is imposed by the actions of the environment and/or traffic loading. The resistance to ravelling (durability) of PA in terms of cohesive failure depends on the

ability of the binding material to resist the accumulation of damage due to such stresses (fatigue) and its ability to heal.

- Adhesive failure is largely attributed to a combination of load related damage at the binder aggregate interface (cracking) and the damaging effect of water that accelerates the deterioration of the bond strength. It is recognized that the binder film thickness plays a role. Cohesive failure is mainly caused when certain stress levels in the binder/mortar are exceeded. The hardening of the binder increases the brittle behaviour of the material resulting in a decrease in cohesive strength. Diffusion of water into the binder also increases the chance of cohesive failure.
- In relation to aging, the quality control of porous asphalt during the entire construction phase, i.e. production, transportation, and laying, is critically important to improve PA performance. The short term bitumen aging during the construction has vast implications on the subsequent PA pavement performance. Both short term aging and the quality of the laid asphalt have interconnected implications on the long term aging and performance of the PA.

7.2 Recommendations

- Field aging of bitumen is a complex process. The standard aging protocol can not simulate the field aging of Porous Asphalt (PA). In addition, the new aging protocol could not predict the long term field aging of PA accurately. Nevertheless, the weatherometer AP3 aging combines the major factors that play a role in the real aging process and has resulted in similar aging behaviour with field aging in terms of chemical changes. Hence, it is suggested to improve the aging protocol in order to make a reasonable prediction of the long term (10-12 year) field aging of PA. It is proposed to first age the mixture for extended short term aging (e.g. following the SHRP mixture aging procedure) before preparing the mixture for LTA (long term aging) under the proposed aging protocol. Secondly, it is recommended to reduce the humidity from 70% to 50% to accelerate the aging. This can be done in combination with increasing the temperature in steps during the aging process. A second alternative is to expose a thin layer of the mastic (eg. 3.2 mm as in PAV aging) to the same aging protocol AP3 in the weatherometer. This option provides the means to increase the temperature up to 90°C and decrease the aging time.
- To determine the aging rate and evaluate the simulation of laboratory binder aging with the binder aging in the field, a kinetic approach was adopted with the use of the infra-red spectrum characteristic peaks area as input data. In addition to this method, however, it is highly recommended to perform elemental analysis (SARA classification) of bitumen samples for a comprehensive qualitative and quantitative chemical investigation.
- In order to improve the aging characteristics of bitumen, the selection of binders from a source with lower content of hetro-atoms is recommended.

This is believed to improve the aging behaviour of the binder that would contribute to resistance of PA to ravelling.

- The filler and aggregate have effects on the aging characteristics of the bitumen. Given the complexity of aging in the field, these aspects need to be addressed further in studies related to bitumen aging.
- The outcome of this research points out that care should be taken in using information from standard laboratory bitumen aging methods for the prediction of field performance of PA. It is recommended to use the rheological properties of recovered binders from the pavement (field aging). In this regard, the results of this research will be helpful to studies planned to be carried out to improve the bitumen/mortar characteristics and resistance to ravelling of PA through modelling and use of Finite Element Models (FEM).
- Future research needs to focus on improving low temperature performance of PA through the use of binders with improved aging, fatigue and relaxation characteristics. In this regard, the use of Polymer Modified Bitumen (PMB) could be an option provided that it improves the cohesive characteristics of the bitumen/mortar at low temperatures after aging. Hence, the cohesive properties of the bitumen/mortar in relation to damage development (cracking) at low temperatures need to be exhaustively studied to improve the resistance to ravelling of PA.

Appendix

Appendix A:

Results of RLITT for Asphalt Specimens from the Field

Summary table Section G 0 yr (New Construction)
Shoulder, SH (Emergency Lane, EL)

Temp	Target Force	Actual force	Target pulse width	Actual pulse width	Resilient modulus
[°C]	[N]	[N]	[ms]	[ms]	[MPa]
5	2100	2085.8	999	920	5796
5	2100	2091.7	500	466.8	6603
5	2100	2093.4	250	236.8	7467
5	2100	2094	125	113.8	8403
5	2100	2096.9	63	55.8	8720
5	2100	2095.8	63	53.8	9188
5	2100	2084.6	999	909.6	5536
5	2100	2093.4	500	465.6	6375
5	2100	2095.8	250	239.2	7436
5	2100	2096.9	125	111.2	8360
5	2100	2094	63	56.6	8449
5	2100	2095.2	63	54	8940
5	2100	2084.6	999	920	7254
5	2100	2093.4	500	468	8037
5	2100	2095.8	250	241.6	8943
5	2100	2097.5	125	114.6	9478
5	2100	2095.2	63	56.2	9153
5	2100	2093.4	63	55.2	9034
15	700	695.09	999	935.2	2841
15	700	699.19	500	458.8	3378
15	700	699.19	250	226.4	4111
15	700	699.19	125	119.8	4946
15	700	693.91	63	55.8	4719
15	700	695.67	63	56	5627
15	700	695.67	999	928.8	1870
15	700	700.95	500	459.6	2258
15	700	697.43	250	226.2	2816
15	700	697.43	125	120	3284
15	700	693.91	63	56.4	3480
15	700	700.95	63	56.2	3949
15	700	698.6	999	936.8	2714
15	700	698.6	500	456.4	3240
15	700	698.02	250	233.6	3870
15	700	699.19	125	119.6	4716
15	700	690.98	63	55.2	5160
15	700	699.78	63	56.6	5494

Temp	Target Force	Actual force	Target pulse width	Actual pulse width	Resilient modulus
[°C]	[N]	[N]	[ms]	[ms]	[MPa]
25	350	347.54	999	951.2	1210
25	350	347.54	500	480	1528
25	350	348.71	250	230.4	1833
25	350	349.89	125	132.4	2500
25	350	349.3	63	56	2720
25	350	350.47	63	56.6	2593
25	350	348.13	999	952	847
25	350	351.06	500	492.8	1278
25	350	349.89	250	229.2	1698
25	350	349.3	125	110	2462
25	350	342.85	63	55.8	3101
25	350	348.71	63	59	1944
25	350	349.89	999	944.8	986.4
25	350	349.89	500	482.4	1190
25	350	351.06	250	229.6	1618
25	350	349.3	125	115.6	2207
25	350	351.06	63	55.4	2248
25	350	352.82	63	57.6	2386
35	150	149.45	999	988	671.4
35	150	151.79	500	537.6	821.1
35	150	150.03	250	286.4	1132
35	150	150.62	125	182.8	1980
35	150	148.27	63	92	1354
35	150	151.2	63	117.2	1566
35	150	149.45	999	994.4	478
35	150	150.62	500	514.4	589
35	150	151.2	250	274.6	849.9
35	150	150.03	125	171	1222
35	150	152.38	63	112.6	768.6
35	150	148.86	63	128.8	1191
35	150	149.45	999	976.8	522.6
35	150	150.03	500	524.4	702.1
35	150	151.2	250	289.4	1098
35	150	150.62	125	166.4	2687
35	150	151.2	63	85.6	2170
35	150	150.03	63	120.4	1224

Summary table Section A 1 yr
Shoulder, SH (Emergency Lane, EL)

Section A 1 yr
Slow Lane, SL

Temp	Target Force	Actual force	Target pulse width	Actual pulse width	Resilient modulus	Temp	Target Force	Actual force	Target pulse width	Actual pulse width	Resilient modulus
[°C]	[N]	[N]	[ms]	[ms]	[MPa]	[°C]	[N]	[N]	[ms]	[ms]	[MPa]
5	2100	2084.6	999	912.8	9433	5	2100	2085.8	999	901.6	8875
5	2100	2093.4	500	467.6	10404	5	2100	2094	500	463.6	9930
5	2100	2091.1	250	244	11605	5	2100	2094	250	234.2	11369
5	2100	2096.4	125	115	12896	5	2100	2093.4	125	111.4	12422
5	2100	2103.4	63	56	12668	5	2100	2084.6	999	909.6	11332
5	2100	2097.5	63	53.8	13848	5	2100	2092.8	500	470.8	12771
5	2100	2085.8	999	910.4	9259	5	2100	2095.2	250	241.6	13541
5	2100	2092.3	500	466	9958	5	2100	2095.8	125	113.6	15420
5	2100	2094	250	238.6	11016	5	2100	2085.8	999	915.2	7555
5	2100	2095.8	125	115.8	12324	5	2100	2094	500	458.8	8452
5	2100	2087.6	999	903.2	6777	5	2100	2090.5	250	240.6	9531
5	2100	2093.4	500	466	7658	5	2100	2094.6	125	110.8	10524
5	2100	2096.4	250	236.4	8605						
5	2100	2094	125	113.6	9502						
15	700	695.09	999	932.8	4240	15	700	695.67	999	930.4	3812
15	700	696.26	500	450.4	5089	15	700	698.02	500	456	4470
15	700	699.78	250	227.8	6153	15	700	699.19	250	226.6	5162
15	700	701.53	125	119	7533	15	700	697.43	125	119.4	5863
15	700	695.09	63	55.8	8229	15	700	690.98	63	54.4	5728
15	700	695.67	63	55.4	8669	15	700	701.53	63	56.2	7142
15	700	697.43	999	936.8	3545	15	700	696.26	999	930.4	3884
15	700	698.02	500	456.4	4151	15	700	700.36	500	454.4	4553
15	700	696.84	250	228	4949	15	700	696.84	250	227.4	5407
15	700	699.78	125	118.8	5830	15	700	699.19	125	115.4	6344
15	700	692.74	63	55.8	6583	15	700	696.84	63	54.6	6588
15	700	702.12	63	55.2	6841	15	700	698.02	63	55.4	7322
15	700	694.5	999	933.6	2894	15	700	698.02	999	932.8	3632
15	700	699.19	500	465.2	3495	15	700	698.6	500	459.6	4296
15	700	698.6	250	228	4223	15	700	700.36	250	225	4926
15	700	699.78	125	122.6	5082	15	700	699.19	125	113.4	5964
15	700	690.98	63	55.8	5674	15	700	700.95	63	55.8	6608
15	700	704.46	63	56.2	5706	15	700	698.6	63	56.6	6762
25	350	348.13	999	952.8	1538	25	350	348.13	999	954.4	1523
25	350	348.71	500	473.2	1923	25	350	347.54	500	483.6	1927
25	350	350.47	250	235.4	2603	25	350	350.47	250	247.4	2429
25	350	348.71	125	121.8	2720	25	350	348.71	125	116.8	3049
25	350	351.06	63	56.4	757.7	25	350	349.3	63	56	3513
25	350	348.13	63	56.2	868.9	25	350	348.71	63	56.2	3139
25	350	347.54	999	942.4	1502	25	350	347.54	999	940	1349
25	350	349.3	500	482	1853	25	350	346.95	500	481.2	1676
25	350	347.54	250	249.8	2431	25	350	351.06	250	250.8	2105
25	350	351.64	125	119.2	3123	25	350	349.89	125	114.4	2714
25	350	347.54	63	56.4	3580	25	350	339.34	63	55	2827
25	350	347.54	63	56	3162	25	350	346.95	63	57	3081
25	350	348.71	999	957.6	1138	25	350	348.13	999	960.8	1197
25	350	348.71	500	484.4	1442	25	350	350.47	500	480.8	1557
25	350	349.89	250	231	2016	25	350	349.3	250	251.4	2074
25	350	347.54	125	119.6	2719	25	350	351.06	125	117.4	2849
25	350	346.95	63	55.2	1792	25	350	342.85	63	55.2	2188
25	350	348.13	63	57	1842	25	350	349.89	63	56.6	2817
35	150	147.69	999	948	536.4	35	150	151.79	999	985.6	728.7
35	150	151.2	500	507.2	676.5	35	150	148.86	500	484.4	1116
35	150	149.45	250	265.6	892.6	35	150	151.2	250	279.4	1639
35	150	148.27	125	156.8	1275	35	150	150.03	125	167.6	2482
35	150	152.38	63	118.4	2556	35	150	151.79	63	96.6	2773
35	150	148.86	63	97.4	1310	35	150	149.45	63	127.8	1533
35	150	147.1	999	950.4	608.8	35	150	148.27	999	959.2	566
35	150	150.03	500	507.6	819.1	35	150	151.79	500	500.8	770.3
35	150	150.62	250	280.6	1022	35	150	150.62	250	266.4	979.2
35	150	151.2	125	196.2	1551	35	150	150.03	125	174.6	1386
35	150	149.45	63	130.2	2360	35	150	150.03	63	103.2	2403
35	150	149.45	63	109.6	1332	35	150	148.86	63	89.6	1389
35	150	150.03	999	1007	396.9	35	150	151.2	999	982.4	480
35	150	150.62	500	523.6	509.3	35	150	151.79	500	527.6	593.7
35	150	150.03	250	275.4	729.8	35	150	148.86	250	289.2	781.3
35	150	150.03	125	172.6	1173	35	150	151.2	125	157.4	1110
35	150	149.45	63	130.2	2955	35	150	150.62	63	89	2254
35	150	152.96	63	129.4	925.5	35	150	148.27	63	128.2	1119

Summary table Section B 3 yr
Shoulder, SH (Emergency Lane, EL)

Section B 3 yr
Slow Lane, SL

Temp	Target Force	Actual force	Target pulse width	Actual pulse width	Resilient modulus	Temp	Target Force	Actual force	Target pulse width	Actual pulse width	Resilient modulus
[°C]	[N]	[N]	[ms]	[ms]	[MPa]	[°C]	[N]	[N]	[ms]	[ms]	[MPa]
5	2100	33.06	999	909.6	9986	5	2100	2085.8	999	904.8	10094
5	2100	2094	500	466.4	10761	5	2100	2096.4	500	468	11050
5	2100	2094.6	250	237.8	11758	5	2100	2094.6	250	244.6	11778
5	2100	2098.1	125	113.6	12416	5	2100	2094.6	125	113.8	12334
5	2100	2087	999	900	10280	5	2100	2085.2	999	907.2	10116
5	2100	2094	500	460	10598	5	2100	2093.4	500	462.8	11281
5	2100	2090.5	250	231.2	10980	5	2100	2094	250	230.4	12222
5	2100	2097.5	125	115.6	13631	5	2100	2095.2	125	110.4	12797
5	2100	2085.8	999	909.6	10261	5	2100	2084.6	999	904	11268
5	2100	2092.3	500	460.8	10940	5	2100	2094.6	500	461.6	12305
5	2100	2094	250	236	12074	5	2100	2095.2	250	230.6	13448
5	2100	2094	125	114	12972	5	2100	2096.4	125	111.2	14991
15	700	697.43	999	928.8	4804	15	700	698.02	999	930.4	5460
15	700	698.02	500	456	5663	15	700	700.36	500	462	6512
15	700	697.43	250	227	6511	15	700	698.02	250	226.6	7263
15	700	699.19	125	118.8	7739	15	700	694.5	125	117.6	8185
15	700	699.78	63	55	7460	15	700	697.43	63	55.4	8181
15	700	698.6	63	56	7862	15	700	698.02	63	56.8	8817
15	700	697.43	999	932.8	5342	15	700	696.26	999	930.4	4623
15	700	696.84	500	446.8	6265	15	700	698.02	500	454.4	5304
15	700	696.26	250	226.4	6991	15	700	696.84	250	228	6198
15	700	696.26	125	120.8	7822	15	700	698.6	125	119.2	7283
15	700	696.26	63	56.2	8091	15	700	696.84	63	55.6	8318
15	700	696.26	63	56.2	8004	15	700	698.02	63	56.2	7924
15	700	698.02	999	940.8	5922	15	700	697.43	999	935.2	5108
15	700	696.84	500	466	6629	15	700	699.19	500	467.2	5877
15	700	698.6	250	228.8	7500	15	700	698.6	250	232.4	6680
15	700	699.78	125	114.4	8450	15	700	699.19	125	113.4	7751
15	700	692.16	63	56	8688	15	700	693.33	63	55.4	8370
15	700	697.43	63	55.4	9366	15	700	698.6	63	55.8	8782
25	350	346.37	999	931.2	2014	25	350	347.54	999	944	2274
25	350	349.3	500	488.4	2461	25	350	348.71	500	486.8	2832
25	350	349.3	250	232	3062	25	350	348.71	250	233.4	3519
25	350	349.89	125	122.6	3741	25	350	346.95	125	124.2	4578
25	350	344.61	63	56	3430	25	350	349.3	63	56.2	5435
25	350	346.95	63	59	3681	25	350	348.71	63	59.8	4853
25	350	347.54	999	944.8	2910	25	350	348.71	999	956	1911
25	350	349.3	500	478.4	3530	25	350	349.3	500	482.4	2323
25	350	349.89	250	231.6	4518	25	350	348.13	250	239.6	2968
25	350	350.47	125	112.4	5772	25	350	350.47	125	122	3727
25	350	347.54	63	57	6293	25	350	345.78	63	56	613.2
25	350	350.47	63	61.6	6163	25	350	349.89	63	57.8	838.6
25	350	348.13	999	958.4	2794	25	350	349.3	999	952	2291
25	350	350.47	500	474.4	3293	25	350	349.89	500	490.8	2894
25	350	351.64	250	240	3919	25	350	349.89	250	230.4	3542
25	350	348.71	125	121	4509	25	350	350.47	125	125	4552
25	350	348.13	63	54.2	4919	25	350	353.4	63	56.8	5407
25	350	347.54	63	55.2	4170	25	350	346.37	63	58.8	4087
35	150	149.45	999	956	977.5	35	150	148.86	999	986.4	1022
35	150	150.03	500	505.6	1251	35	150	150.62	500	511.2	1285
35	150	151.79	250	300.2	1549	35	150	149.45	250	270.2	1628
35	150	151.2	125	165.8	2154	35	150	151.79	125	142.6	2227
35	150	149.45	63	92.8	2570	35	150	151.79	63	61.2	1802
35	150	148.86	63	119.2	1912	35	150	150.62	63	124.2	2096
35	150	150.03	999	965.6	740.4	35	150	148.27	999	960	804.8
35	150	150.62	500	512	908.7	35	150	150.62	500	522	1045
35	150	151.2	250	291.8	1270	35	150	151.79	250	295.6	1340
35	150	150.03	125	171	1780	35	150	152.38	125	168.8	1676
35	150	147.69	63	114.8	2742	35	150	152.96	63	103.6	2157
35	150	149.45	63	142.6	1796	35	150	147.1	63	121.4	1844
35	150	151.2	999	980.8	996.2	35	150	148.27	999	961.6	787.7
35	150	150.62	500	531.2	1155	35	150	150.03	500	482.4	983.8
35	150	150.62	250	276.6	1555	35	150	151.79	250	263.2	1309
35	150	151.2	125	179.4	1944	35	150	149.45	125	155.8	1806
35	150	151.2	63	111.2	2562	35	150	153.55	63	86.8	2406
35	150	152.96	63	105.8	2136	35	150	147.69	63	106.4	1811

APPENDIX

Summary table Section C 7 yr Good condition)						Section C 7 yr Good condition)					
Shoulder, SH (Emergency Lane, EL)						Slow Lane, SL					
Temp	Target Force	Actual force	Target pulse width	Actual pulse width	Resilient modulus	Temp	Target Force	Actual force	Target pulse width	Actual pulse width	Resilient modulus
[°C]	[N]	[N]	[ms]	[ms]	[MPa]	[°C]	[N]	[N]	[ms]	[ms]	[MPa]
5	2100	2085.8	999	897.6	8493	5	2100	2084.6	999	915.2	8249
5	2100	2092.3	500	458.8	9168	5	2100	2094	500	465.2	8893
5	2100	2090.5	250	237.6	10008	5	2100	2094	250	239.6	9598
5	2100	2095.2	125	115	9573	5	2100	2094.6	125	115.2	10110
5	2100	2087	999	911.2	8385	5	2100	2085.2	999	916	8982
5	2100	2091.1	500	465.6	9058	5	2100	2093.4	500	468.8	9803
5	2100	2092.3	250	241.6	9658	5	2100	2096.4	250	240.2	10618
5	2100	2094	125	114.6	9316	5	2100	2095.8	125	113.6	11385
5	2100	2086.4	999	917.6	6061	5	2100	2087	999	913.6	8764
5	2100	2092.3	500	467.2	6760	5	2100	2092.8	500	463.2	9628
5	2100	2091.7	250	220	7786	5	2100	2097.5	250	228.8	10332
5	2100	2096.4	125	115	4440	5	2100	2096.4	125	111.2	9509
15	700	697.43	999	931.2	5727	15	700	696.84	999	929.6	5904
15	700	699.19	500	456.4	6182	15	700	699.19	500	455.2	6437
15	700	699.78	250	235.6	6854	15	700	698.6	250	226.6	7172
15	700	698.02	125	110	6438	15	700	698.02	125	119.8	7777
15	700	702.12	63	56.2	6998	15	700	695.67	63	55.8	7620
15	700	696.26	63	56.4	7588	15	700	695.09	63	55.4	8590
15	700	698.6	999	929.6	3923	15	700	699.19	999	936.8	6330
15	700	699.19	500	450.4	4266	15	700	695.67	500	457.2	6991
15	700	699.19	250	228.6	5029	15	700	700.36	250	224.2	7159
15	700	698.6	125	117	5487	15	700	696.26	125	113	5595
15	700	698.6	63	55.4	5943	15	700	699.19	63	57.6	3678
15	700	701.53	63	57.2	6699	15	700	700.95	63	55.2	2834
15	700	695.67	999	929.6	4043	15	700	696.84	999	938.4	5674
15	700	699.78	500	462	4794	15	700	698.02	500	452	6273
15	700	697.43	250	228	5644	15	700	697.43	250	228.6	7030
15	700	695.67	125	119.2	6493	15	700	697.43	125	118	7985
15	700	692.74	63	55.4	7254	15	700	697.43	63	55	8409
15	700	702.12	63	56.4	7073	15	700	699.19	63	56.4	8405
25	350	346.95	999	947.2	2180	25	350	346.95	999	924.8	2948
25	350	349.3	500	482.4	2516	25	350	351.06	500	492.4	3507
25	350	348.71	250	227.6	3065	25	350	350.47	250	229.8	4310
25	350	351.06	125	109.8	3773	25	350	349.89	125	110.4	5301
25	350	345.2	63	56	4332	25	350	348.71	63	57.4	6691
25	350	345.78	63	60	4271	25	350	349.89	63	61.6	5517
25	350	347.54	999	957.6	2189	25	350	348.71	999	950.4	2724
25	350	348.13	500	490	2585	25	350	349.89	500	487.2	3251
25	350	349.3	250	223.6	3026	25	350	350.47	250	225.2	3832
25	350	348.71	125	109	3728	25	350	350.47	125	114.8	4651
25	350	348.13	63	57.2	4319	25	350	351.64	63	56.6	4347
25	350	349.89	63	60	4433	25	350	350.47	63	58.4	4507
25	350	349.3	999	961.6	1499	25	350	348.13	999	948.8	2574
25	350	349.89	500	484	1755	25	350	348.71	500	490.4	3025
25	350	351.06	250	229.6	2179	25	350	351.64	250	224.8	3644
25	350	349.3	125	111.4	2536	25	350	349.89	125	116.8	4259
25	350	349.89	63	58.6	2410	25	350	346.95	63	55.8	3710
25	350	349.3	63	61.4	2905	25	350	349.3	63	58.4	4609
35	150	149.45	999	952.8	973.9	35	150	148.27	999	975.2	1028
35	150	150.62	500	513.2	1258	35	150	149.45	500	523.2	1210
35	150	151.2	250	269.8	1482	35	150	150.62	250	284	1523
35	150	148.86	125	163.8	2160	35	150	151.2	125	166	1833
35	150	151.79	63	110.4	2899	35	150	150.62	63	102.8	1804
35	150	148.27	63	86.6	2761	35	150	149.45	63	132.8	1741
35	150	150.62	999	947.2	832.3	35	150	149.45	999	940	872
35	150	150.62	500	517.2	1109	35	150	151.79	500	491.2	1077
35	150	150.62	250	288.8	1489	35	150	151.2	250	254.8	1460
35	150	150.62	125	162.8	2284	35	150	150.62	125	161.4	1843
35	150	147.1	63	98.6	2690	35	150	150.03	63	95.6	2714
35	150	152.38	63	97.4	1825	35	150	151.2	63	103.2	1935
35	150	148.86	999	975.2	508.3	35	150	150.03	999	970.4	1100
35	150	151.2	500	488.4	641.8	35	150	152.96	500	490	1341
35	150	149.45	250	274.2	867.8	35	150	150.03	250	294.4	1657
35	150	150.03	125	163.8	1299	35	150	152.38	125	179.8	2210
35	150	154.72	63	93.8	1389	35	150	151.2	63	104.4	931.6
35	150	150.03	63	118.4	1098	35	150	151.2	63	119.6	2371

Summary table Section D 7 yr (Poor condition)
Shoulder, SH (Emergency Lane, EL)

Temp	Target Force	Actual force	Target pulse width	Actual pulse width	Resilient modulus
[°C]	[N]	[N]	[ms]	[ms]	[MPa]
5	2100	2085.2	999	916.8	10283
5	2100	2092.3	500	466	11242
5	2100	2094.6	250	233.6	12370
5	2100	2097.5	125	115	13372
5	2100	2095.2	63	56.2	12907
5	2100	2091.1	63	54	13298
5	2100	2087	999	906.4	8062
5	2100	2094.6	500	468	8844
5	2100	2094.6	250	233	9529
5	2100	2094.6	125	110.2	9931
5	2100	2096.9	63	55.8	9824
5	2100	2097.5	63	53.4	10277
5	2100	2084.1	999	920	9719
5	2100	2092.8	500	468	10611
5	2100	2096.4	250	240.8	11485
5	2100	2098.1	125	114.2	12379
5	2100	2100.5	63	55.8	11916
5	2100	2096.9	63	53.2	13047
15	700	694.5	999	932.8	5288
15	700	699.78	500	454.4	5936
15	700	699.78	250	226	6763
15	700	700.36	125	114	7416
15	700	696.26	63	58	6192
15	700	695.09	63	57.8	8287
15	700	697.43	999	926.4	5233
15	700	698.6	500	456	5796
15	700	699.19	250	224.6	6414
15	700	698.6	125	108.4	7197
15	700	693.91	63	56.2	8018
15	700	699.78	63	58.2	8208
15	700	697.43	999	932	4655
15	700	698.02	500	451.6	5264
15	700	698.02	250	224.8	5983
15	700	697.43	125	112.8	6470
15	700	702.12	63	56	6176
15	700	697.43	63	56	7294
25	350	348.13	999	951.2	2389
25	350	348.13	500	486.8	2799
25	350	352.23	250	234.2	3497
25	350	349.3	125	121.6	4057
25	350	347.54	63	55.6	4584
25	350	347.54	63	58.2	4123
25	350	348.13	999	949.6	2032
25	350	347.54	500	484.8	2423
25	350	349.3	250	229.8	2908
25	350	351.06	125	110.6	3310
25	350	349.89	63	57.2	2493
25	350	349.3	63	58.6	3787
25	350	346.37	999	941.6	2140
25	350	349.3	500	490.8	2650
25	350	348.71	250	230	3113
25	350	349.89	125	108.6	3776
25	350	347.54	63	55.8	4195
25	350	350.47	63	60.2	4199
35	150	148.27	999	508.8	1206
35	150	147.69	500	481.6	1569
35	150	149.45	250	275.2	1830
35	150	151.2	125	156	2248
35	150	147.1	63	101.2	2299
35	150	150.62	63	119.8	2540
35	150	150.62	999	970.4	1204
35	150	148.86	500	505.6	1455
35	150	152.38	250	293.6	1735
35	150	148.86	125	155.2	2052
35	150	148.27	63	108.8	2227
35	150	149.45	63	116.2	2397
35	150	149.45	999	988.8	1003
35	150	148.27	500	504	1231
35	150	152.38	250	270.8	1607
35	150	152.38	125	151	1913
35	150	147.69	63	91.6	1847
35	150	148.27	63	129.8	1107

Section D 7 yr (Poor condition)
Slow Lane, SL

Temp	Target Force	Actual force	Target pulse width	Actual pulse width	Resilient modulus
[°C]	[N]	[N]	[ms]	[ms]	[MPa]
5	2100	2083.5	999	905.6	9113
5	2100	2095.2	500	470.4	10120
5	2100	2094.6	250	231.2	11143
5	2100	2096.4	125	113.4	11626
5	2100	2096.4	63	56.8	11858
5	2100	2097.5	63	54.4	7174
5	2100	2087	999	900.8	8060
5	2100	2095.2	500	463.2	8918
5	2100	2094	250	236.4	10009
5	2100	2095.8	125	110.8	10893
5	2100	2098.7	63	55.8	10630
5	2100	2095.8	63	54.2	11477
5	2100	2085.2	999	924.8	10824
5	2100	2092.8	500	469.6	11817
5	2100	2094	250	241	12616
5	2100	2096.9	125	116.2	13286
5	2100	2098.7	63	55	12332
5	2100	2095.8	63	53.4	12865
15	700	696.84	999	937.6	4575
15	700	697.43	500	472.8	5124
15	700	697.43	250	225.4	5940
15	700	698.6	125	116.4	6833
15	700	689.81	63	55.8	7677
15	700	699.78	63	55.4	7743
15	700	696.26	999	938.4	6364
15	700	699.78	500	458.4	7218
15	700	699.19	250	225.2	8671
15	700	694.5	125	118.4	10058
15	700	699.19	63	55.8	8926
15	700	694.5	63	55.6	9128
15	700	695.09	999	932.8	5409
15	700	699.19	500	460.8	6128
15	700	698.02	250	224.8	6853
15	700	698.6	125	119.2	7573
15	700	699.78	63	55.6	7600
15	700	695.67	63	55.6	8500
25	350	349.89	999	953.6	2228
25	350	348.13	500	480.8	2564
25	350	349.89	250	228.6	3017
25	350	348.71	125	123.4	3616
25	350	348.13	63	56	2770
25	350	349.3	63	58	3081
25	350	346.95	999	945.6	2138
25	350	347.54	500	482	2522
25	350	346.95	250	249.2	2954
25	350	346.95	125	125.6	3453
25	350	346.37	63	55.2	3757
25	350	349.89	63	56.4	4135
25	350	350.47	999	944.8	2463
25	350	352.23	500	490.8	2971
25	350	350.47	250	225.2	3571
25	350	348.13	125	112.6	4374
25	350	345.2	63	56.2	4513
25	350	346.95	63	59.2	4832
35	150	149.45	999	984.8	596.4
35	150	149.45	500	501.6	842
35	150	150.03	250	297	1123
35	150	150.62	125	170.8	1517
35	150	151.79	63	119.8	2048
35	150	149.45	63	142.2	1349
35	150	148.86	999	955.2	801.8
35	150	150.03	500	506.8	981.6
35	150	151.2	250	261.4	1269
35	150	150.62	125	192.2	1743
35	150	148.27	63	117.2	2977
35	150	150.03	63	96.6	1736
35	150	150.62	999	949.6	872.1
35	150	148.86	500	490.8	1204
35	150	150.03	250	271.4	1518
35	150	150.03	125	161.6	2093
35	150	149.45	63	122.6	3392
35	150	151.79	63	125	2453

Summary table Section E 12 yr (Good condition)
Shoulder, SH (Emergency Lane, EL)

Temp	Target Force	Actual force	Target pulse width	Actual pulse width	Resilient modulus
[°C]	[N]	[N]	[ms]	[ms]	[MPa]
5	2100	2085.8	999	910.4	9477
5	2100	2092.8	500	444.8	10174
5	2100	2096.4	250	233	9638
5	2100	2094	125	111.6	10054
5	2100	2095.2	63	56	9732
5	2100	2092.3	63	54.4	9891
5	2100	2087	999	918.4	6840
5	2100	2092.8	500	468	7423
5	2100	2096.9	250	240.6	3248
5	2100	2096.9	125	117.6	4181
5	2100	2095.2	63	56.4	2484
5	2100	2094.6	63	53.8	2728
5	2100	2087	999	901.6	9490
5	2100	2091.1	500	460	10296
5	2100	2095.2	250	231.4	10871
5	2100	2093.4	125	111	10796
5	2100	2096.9	63	55	5249
5	2100	2095.8	63	53.8	5933
15	700	696.84	999	933.6	3938
15	700	699.78	500	456.8	4275
15	700	701.53	250	230.6	4748
15	700	695.67	125	118	5188
15	700	695.09	63	57.8	5909
15	700	702.71	63	55.8	5560
15	700	696.84	999	926.4	5621
15	700	696.84	500	460.4	6222
15	700	699.19	250	231.8	6760
15	700	696.84	125	120.6	7106
15	700	690.4	63	55.4	7185
15	700	701.53	63	56.2	8023
15	700	695.09	999	932	6079
15	700	696.84	500	455.2	6658
15	700	698.02	250	226.6	7416
15	700	695.67	125	121.2	7916
15	700	695.09	63	56.8	7946
15	700	697.43	63	55.8	8470
25	350	348.13	999	950.4	2794
25	350	348.71	500	478.4	3114
25	350	348.13	250	228	3526
25	350	351.06	125	114	3803
25	350	346.37	63	56.6	3090
25	350	348.13	63	59.4	3473
25	350	349.3	999	952	2722
25	350	348.13	500	492.4	3039
25	350	348.71	250	227.8	3417
25	350	349.89	125	108.8	3710
25	350	349.3	63	56.6	4094
25	350	348.13	63	60.4	4484
25	350	348.71	999	956	2077
25	350	347.54	500	486.8	2330
25	350	350.47	250	237.6	2617
25	350	348.13	125	115.4	2932
25	350	348.71	63	56.4	2398
25	350	349.89	63	57.8	3325
35	150	148.27	999	952	1422
35	150	148.27	500	486	1669
35	150	151.2	250	270.6	1927
35	150	150.62	125	159.2	2409
35	150	151.79	63	107.8	2710
35	150	149.45	63	106.6	2537
35	150	148.86	999	934.4	869
35	150	150.03	500	498.8	1562
35	150	150.62	250	278.6	1588
35	150	148.86	125	167	2350
35	150	151.2	63	110.6	2304
35	150	150.03	63	94.8	885.8
35	150	148.27	999	956.8	1749
35	150	151.79	500	544.4	1894
35	150	151.2	250	301.2	1954
35	150	151.2	125	158	1088
35	150	147.69	63	79.6	507
35	150	148.86	63	87.4	2051

Section E 12 yr (Good condition)
Slow Lane, SL

Temp	Target Force	Actual force	Target pulse width	Actual pulse width	Resilient modulus
[°C]	[N]	[N]	[ms]	[ms]	[MPa]
5	2100	2088.2	999	900.8	7746
5	2100	2093.4	500	462.8	8751
5	2100	2094.6	250	230.4	9877
5	2100	2096.4	125	109.8	10728
5	2100	2092.3	63	55.8	11705
5	2100	2094.6	63	54	11439
5	2100	2086.4	999	906.4	8633
5	2100	2094	500	468	9661
5	2100	2092.3	250	240.4	10744
5	2100	2094.6	125	114.2	11801
5	2100	2098.7	63	55.8	12450
5	2100	2091.7	63	53.8	11934
5	2100	2085.8	999	913.6	10067
5	2100	2093.4	500	462.8	10986
5	2100	2092.3	250	237.8	12373
5	2100	2093.4	125	111	11185
5	2100	2098.7	63	54.8	6210
5	2100	2094.6	63	54.6	5803
15	700	696.84	999	931.2	4340
15	700	696.84	500	452	4890
15	700	698.02	250	228.2	5599
15	700	696.84	125	114.2	6483
15	700	701.53	63	55.2	7530
15	700	699.19	63	55.4	7578
15	700	696.26	999	941.6	4702
15	700	697.43	500	464.4	5450
15	700	700.95	250	243.2	6314
15	700	699.78	125	110	7228
15	700	695.67	63	55.6	8178
15	700	698.6	63	56.4	8248
15	700	697.43	999	936	3927
15	700	700.36	500	457.6	4713
15	700	696.84	250	223	5589
15	700	698.6	125	112.2	6589
15	700	700.36	63	55.4	7294
15	700	698.6	63	56.6	6800
25	350	348.13	999	950.4	2329
25	350	351.06	500	494.8	2830
25	350	350.47	250	229.2	3626
25	350	349.89	125	127.6	4457
25	350	349.3	63	54.6	3513
25	350	349.3	63	60.2	4479
25	350	348.71	999	946.4	1978
25	350	348.71	500	486	2366
25	350	348.71	250	228.2	2839
25	350	348.71	125	112.8	3563
25	350	346.37	63	56.6	3165
25	350	351.64	63	59	3720
25	350	348.13	999	958.4	1744
25	350	349.89	500	491.2	2123
25	350	349.3	250	226.2	2735
25	350	346.95	125	115.4	3486
25	350	342.85	63	56.2	3623
25	350	348.13	63	58	3937
35	150	147.69	999	924.8	746.3
35	150	148.86	500	498.8	932
35	150	150.03	250	275.8	1232
35	150	151.2	125	184	1617
35	150	152.38	63	104.2	1889
35	150	152.38	63	102.6	1769
35	150	151.2	999	991.2	617.2
35	150	150.62	500	510.4	786.9
35	150	150.03	250	275.6	1060
35	150	153.55	125	170.4	1495
35	150	151.79	63	104	1693
35	150	150.03	63	115.8	1370
35	150	150.62	999	968	558.8
35	150	148.86	500	497.6	683.7
35	150	149.45	250	259.6	933.2
35	150	150.62	125	176.4	1080
35	150	150.03	63	92.2	786.4
35	150	151.79	63	110.6	1146

Summary table Section F 12 yr (Poor condition)
Shoulder, SH (Emergency Lane, EL)

Temp	Target Force	Actual force	Target pulse width	Actual pulse width	Resilient modulus
[°C]	[N]	[N]	[ms]	[ms]	[MPa]
5	2100	2085.2	999	902.4	11275
5	2100	2092.8	500	460	11937
5	2100	2095.2	250	229.8	12644
5	2100	2095.8	125	110.4	11187
5	2100	2094.6	63	55.6	10486
5	2100	2094	63	54.2	10461
5	2100	2084.6	999	912	10987
5	2100	2092.8	500	463.2	11841
5	2100	2094	250	237.2	12752
5	2100	2095.2	125	109.6	12091
5	2100	2095.2	63	53.8	9072
5	2100	2094.6	63	54	11633
5	2100	2086.4	999	910.4	8163
5	2100	2094	500	464.8	8972
5	2100	2096.9	250	236.8	9586
5	2100	2095.2	125	110.4	10169
5	2100	2095.2	63	55.4	10264
5	2100	2098.1	63	53.4	9144
15	700	698.02	999	931.2	7340
15	700	698.02	500	452	7995
15	700	699.78	250	225.4	8768
15	700	696.84	125	110.6	7714
15	700	692.16	63	56.8	4308
15	700	698.6	63	56.2	8354
15	700	696.26	999	932	6771
15	700	699.19	500	457.6	7309
15	700	696.84	250	225.6	7803
15	700	699.19	125	114.4	7827
15	700	701.53	63	55	6513
15	700	699.78	63	55.4	5690
15	700	697.43	999	938.4	6191
15	700	698.02	500	473.2	6737
15	700	698.02	250	245	7359
15	700	696.84	125	122	7744
15	700	695.67	63	55	7763
15	700	697.43	63	55	8297
25	350	348.71	999	938.4	3871
25	350	351.06	500	492.8	4324
25	350	352.23	250	227.8	4971
25	350	348.71	125	112.8	4182
25	350	342.85	63	55.6	1386
25	350	349.3	63	60	3434
25	350	348.71	999	945.6	3951
25	350	348.13	500	477.2	4402
25	350	354.57	250	229.8	5175
25	350	350.47	125	109.8	5839
25	350	349.89	63	57.6	6515
25	350	346.95	63	61	6302
25	350	348.71	999	950.4	3824
25	350	348.71	500	473.6	4426
25	350	351.06	250	233.8	5052
25	350	349.3	125	109.8	5233
25	350	352.82	63	58.2	4891
25	350	349.3	63	60.6	4991
35	150	148.86	999	959.2	1319
35	150	150.03	500	492.8	1685
35	150	150.62	250	279.2	2074
35	150	150.62	125	163.2	2406
35	150	150.03	63	109.4	1805
35	150	151.79	63	104.8	1931
35	150	149.45	999	988.8	1853
35	150	151.2	500	518	2265
35	150	152.38	250	289	2710
35	150	151.79	125	175.4	3109
35	150	150.03	63	115	3354
35	150	150.62	63	111.6	3100
35	150	149.45	999	976.8	1432
35	150	150.03	500	530	1682
35	150	150.62	250	276.2	1989
35	150	149.45	125	193	2296
35	150	151.2	63	99	2322
35	150	149.45	63	114.8	2574

Section E 12 yr (Poor condition)
Slow Lane, SL

Temp	Target Force	Actual force	Target pulse width	Actual pulse width	Resilient modulus
[°C]	[N]	[N]	[ms]	[ms]	[MPa]
5	2100	2085.8	999	923.2	11611
5	2100	2092.8	500	464.8	12398
5	2100	2095.2	250	243.2	13080
5	2100	2092.8	125	113.6	13604
5	2100	2096.4	63	56.2	13401
5	2100	2098.7	63	53.6	12079
5	2100	2087.6	999	917.6	7652
5	2100	2095.2	500	462.4	8207
5	2100	2095.8	250	230.6	8771
5	2100	2094	125	115.8	9408
5	2100	2092.3	63	53.4	8215
5	2100	2092.8	63	54	8118
5	2100	2086.4	999	915.2	11235
5	2100	2095.2	500	462	12123
5	2100	2096.9	250	235.8	12854
5	2100	2095.2	125	111.6	12580
5	2100	2097.5	63	55	10626
5	2100	2093.4	63	53.8	10379
15	700	695.67	999	925.6	6993
15	700	698.02	500	449.2	7490
15	700	700.36	250	223.8	8072
15	700	696.84	125	110.4	9039
15	700	702.12	63	56	8417
15	700	700.36	63	56	8827
15	700	696.26	999	927.2	5468
15	700	697.43	500	465.6	5999
15	700	699.78	250	228.2	6637
15	700	697.43	125	110.8	6964
15	700	693.91	63	55.8	5353
15	700	698.6	63	56.4	6706
15	700	696.26	999	931.2	4393
15	700	695.67	500	451.6	4740
15	700	696.84	250	232	5370
15	700	698.02	125	120.6	6134
15	700	697.43	63	55.2	6257
15	700	697.43	63	55.6	6071
25	350	347.54	999	941.6	3329
25	350	349.3	500	480.4	3827
25	350	349.3	250	234.4	4578
25	350	348.71	125	112.4	7647
25	350	352.23	63	57.2	2730
25	350	349.3	999	932.8	3288
25	350	349.89	500	498.4	3889
25	350	350.47	250	227.4	4413
25	350	349.3	125	110.2	4862
25	350	351.06	63	56.6	4165
25	350	353.4	63	61	4841
25	350	349.89	999	949.6	3620
25	350	347.54	500	490.4	4184
25	350	351.64	250	227.8	4883
25	350	349.3	125	109.4	5962
25	350	349.3	63	56	6524
25	350	349.89	63	61.4	6409
35	150	150.62	999	986.4	1567
35	150	150.03	500	492	1798
35	150	150.03	250	284	2138
35	150	150.03	125	169.2	2553
35	150	150.62	63	100.4	2784
35	150	151.2	63	101.8	3208
35	150	148.86	999	953.6	1265
35	150	150.62	500	534.8	1525
35	150	151.2	250	296	1862
35	150	151.79	125	184.2	2106
35	150	150.03	63	122.8	1143
35	150	152.38	63	126.6	2017
35	150	148.86	999	965.6	1091
35	150	148.86	500	493.2	1378
35	150	152.96	250	273.2	1720
35	150	149.45	125	175.4	2187
35	150	151.79	63	100	1169
35	150	147.1	63	108	2243

Curriculum Vitae

Name Eyassu Tesfamariam Hagos
Date of birth November 23, 1968

Educational background

2000 – 2002 Master of Science degree (MSc.) in Transport and Road Engineering at Delft University of Technology (TU Delft) / International Institute for Infrastructural, Hydraulic, and Environmental Engineering (UNESCO-IHE), the Netherlands.
Thesis: Characterization of Polymer Modified Bitumen (PMB).

1987 – 1990 Bachelor of Science degree (BSc.) in civil engineering at Faculty of Technology, Addis Ababa University, Ethiopia.

Working experience

2003 - 2008 PhD Researcher at the Road and Railway Engineering section of Delft University of Technology (TU Delft), The Netherlands.
Title: The Effect of Aging on Binder Properties of Porous Asphalt Concrete.

2002 - 2003 Acting Manager, Adigrat road maintenance district office - Ethiopian Roads Authority (ERA), Ethiopia.

1997 - 2000 Acting Project Manager, Alula Aba-Nega and Axum airport runway construction projects (ERA), Ethiopia.

1995 - 1997 Project Engineer, Alula Aba-Nega airport runway construction project (ERA), Ethiopia.

1993 - 1994 Highway Engineer, Planning and programming division of ERA, Ethiopia.

1992 - 1993 Engineer under training (ERA), Ethiopia.

PROPOSITIONS

1. Aging is the dominant factor determining raveling of porous asphalt concrete. The effect of moisture is only secondary.
2. From a practical point of view, field aging of the binder in porous asphalt concrete can not be simulated in the laboratory.
3. Porous asphalt concrete should not be used in areas with extreme temperatures.
4. The Dutch specification for porous asphalt concrete should significantly be improved to address the huge variability of performance in the field.
5. Aging of a human body does not necessarily result in aging of the mind (spirit), which makes it unique from aging of materials.
6. The world knows the truth about Africa, but not the whole truth.
7. Developing countries need to invest primarily in education and health sectors to improve the livelihood of their people for sustainable long term investment on development.
8. Western politics towards the developing world is dictated by own interests resulting in hypocrisy and lack of long term vision (commitment).
9. African leaders fail to create peace in the continent because they wish to protect their grip in power.
10. In doing my PhD, I realized that I knew less as I learned more.
11. PhD's at Delft University of Technology should give due credit to the coffee machines for their splendid contribution at work for "gratis".
12. Success is a journey not a destination... [Arthur Robert Ashe, Jr.]

These propositions are considered opposable and defensible and as such have been approved by the promotor, Prof. dr. ir. A.A.A. Molenaar.

STELLINGEN

1. Veroudering is de dominante factor voor rafeling van zeer open asfaltbeton. Het effect van vocht is van secundair belang.
2. Praktisch gezien kan de veroudering van zeer open asfaltbeton zoals die in de praktijk optreedt niet in het laboratorium worden gesimuleerd.
3. Toepassing van zeer open asfaltbeton in gebieden met extreme temperaturen moet sterk worden ontraden.
4. Om de grote spreiding in het praktijkgedrag van zeer open asfaltbeton te verminderen dienen de Nederlandse specificaties voor dit type asfalt sterk te worden verbeterd.
5. De veroudering van een menselijk lichaam leidt niet noodzakelijkerwijs tot veroudering van de geest, en dat is uniek vergeleken met de veroudering van materialen.
6. De wereld kent de waarheid over Afrika, maar niet de hele waarheid.
7. Voor een duurzame ontwikkeling van het welzijn van de bevolking zouden ontwikkelingslanden primair moeten investeren in de onderwijs- en gezondheidssector.
8. De politiek van westerse landen ten opzichte van ontwikkelingslanden wordt gedreven door eigenbelang, resulterend in hypocrisie en een gebrek aan lange termijn visie.
9. Omdat zij hun machtspositie wensen te beschermen, slagen Afrikaanse leiders er niet in om vrede op het continent te bewerkstelligen.
10. Tijdens mijn promotie-onderzoek heb ik mij gerealiseerd dat ik minder weet als ik méér leer.
11. Promovendi aan de Technische Universiteit Delft zouden de koffiemachines dankbaar moeten zijn voor hun geweldige bijdrage “om niet” aan het werk.
12. Succes is een reis, geen bestemming... [*Arthur Robert Ashe, Jr.*]

Deze stellingen worden oponeerbaar en verdedigbaar geacht en zijn als zodanig goedgekeurd door de promotor, Prof. dr. ir. A.A.A. Molenaar

